Nearshore effects of submerged breakwaters

Laboratory experiments in a wave basin and 2DH numerical modeling.

Volume I: Analysis

L. Torrini

Simualtion D3 - Average Water Level

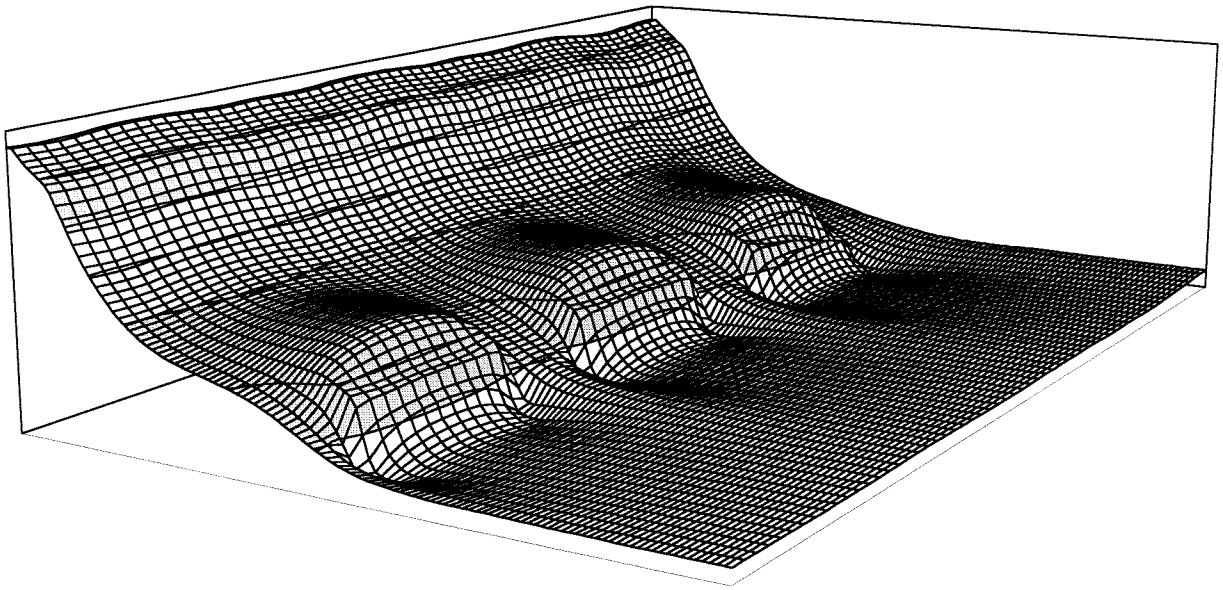

Master Thesis
October 1997

Nearshore effects of submerged breakwaters

Laboratory experiments in a wave basin and 2DH numerical modeling.

Volume I: Analysis

L. Torrini

Master Thesis
October 1997

Delft University of Technology
Faculty of Civil Engineering

Politecnico di Milano
Facolta` di Ingegneria Ambientale

Supervision:

Dr. Ir. J. van de Graaff
Dr. Ir. J. A. Roelvink
Ir. S. C. van der Biezen
Dr. Ir. G. Passoni

Abstract

This master thesis is a contribution to the Dynamics of Beaches project, which is a part of the EU funded Human Capital and Mobility program (HCM).

In this study, the 3D-effects of detached segmented submerged breakwaters, in the nearshore zone, primarily on the hydrodynamic processes and only secondarily on the morphodynamics, are investigated. First the results of previous laboratory experiments, performed in a wave basin by Delft University of Technology, are discussed. After that, the outcomes of different series of simulations with the 2DH version of the numerical model DELFT3D (Delft2D-MOR), developed by Delft Hydraulics, are analysed. The primary aim of these simulations is to investigate whether the model is able to reproduce the basin experiments. The secondary aim is to analyse the effects of different submerged breakwaters configurations on the hydrodynamic processes.

From the laboratory experiments, it resulted that the submerged breakwaters induce wave breaking and consequently wave energy dissipation. The effect of the submerged breakwaters, in dissipating wave energy, weakens as the wave height becomes small compared to the submergence of the crest of the structures.
A water volume is transported over the submerged breakwaters shorewards. Then a longshore current in the direction of the gaps develops, due to a longshore gradient in the average water level sloping down from the submerged breakwaters to the gaps. A strong off-shore current through the gaps can be observed. In comparison with the tests without submerged breakwaters, a larger amount of sediment from the shoreface is transported seawards through the gaps.
From the experiments, it seems that the overall effects of segmented submerged breakwaters are more harmful than beneficial. Although the basin condition is different from a prototype condition, the use of segmented submerged breakwaters as a protection tool for sandy coast should be carefully studied.

Comparing Delft2D-MOR output with the basin experiments, some positive conclusions can be drawn. In the area close to the submerged breakwaters, the numerical model correctly reproduces the current field and the pattern of the average water level. In agreement with the measurements, sediment is transported seawards through the gaps.
Nevertheless, some discrepancies with the measurements are found. Erosion at the lee side of the submerged breakwaters is overestimated. This is due to the high dissipation concentrated in this area and to the low resolution of the computational grid. Furthermore, the retreat of the shoreline is not modelled, yielding an unrealistic trough at the shoreline. Improvements to Delft2D-MOR are requested mainly in the area landwards of the submerged breakwaters.

The flow field has been analysed while enlarging the exposure ratio (ratio of gap width to the sum of submerged breakwater length and gap width) artificially from zero (one single breakwater, no gap) to unity (no submerged breakwater).

In the region around the submerged breakwaters, the longshore and cross-shore currents first increase, until an exposure ratio of approximately two third is reached, then a constant decrease can be observed. Since sediment transport and current field are closely correlated, the presence of gaps seems to be more harmful than the situation without submerged breakwaters.
By decreasing the off-shore distance of the structures, the efficiency in dissipating energy seems to be reduced.

Acknowledgements

I would like to express my deep gratitude to Dr. Ir. Jan van de Graaff for his guidance and his advises with respect to the contents as well as to the organizational aspect of this thesis.
I am sincerely grateful to Ir. Stephan van der Biezen for his time and for many helpful discussions.
I am indebted to Dr. Ir. Dano Roelvink. Thanks to him, I did not get lost in the labyrinth of the numerical model Delft2D-MOR.

A special thank to Dr. Ir. Giuseppe Passoni for his encouraging support and constructive comments.

I greatly appreciated the cooperation with Jasper Schaap. He encouraged me during his graduation and he kept encouraging me also later.

My heartfelt gratitude is for my parents. They support me throughout my whole study and in particular during my graduation abroad.

At last a special thank to Ari for his patience and support. He helped me to get through this long year. Thank you!

Table of Contents

Volume I: Analysis

Volume II: Appendices

1. INTRODUCTION

1.1 Submerged breakwaters

Beaches can be considered as the natural defence of the inland. The problem of preventing the erosion of sandy beaches is of particular interest for many countries where the coasts are densely populated. The gradient in the longshore sediment transport is considered one of the main factors of the retreat of the shoreline. Considering the sediment balance of a part of the coast (see Figure 1.1-1), if more sediments are transported away than into this part, the total amount of the sediment will decrease yielding the dangerous phenomenon mentioned above.

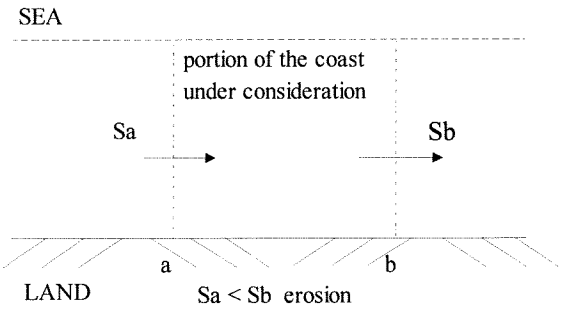

Figure 1.1-1 Transport mass balance

One approach for shoreline stabilization is the adoption of detached submerged breakwaters located outside or inside the surf zone. These structures present less environmental impacts than other methods as emerged breakwaters or seawalls due to the fact , for instance, that they allow better water exchange between the inner and the outer zones of them. The required stability is lower than at non-overtopped structures, since wave energy can pass over the crest, yielding lower wave forces on the armour layer of the seaward slope. Besides, in comparison with artificial beach nourishments, they are less expensive.

However, the existing knowledge about the effects of these constructions is still very limited.

This study intends to improve the knowledge about the influence of discontinuous submerged breakwaters on the hydrodynamics. The results presented in this report derive from the analyses of data obtained by laboratory experiments and by using a numerical model.

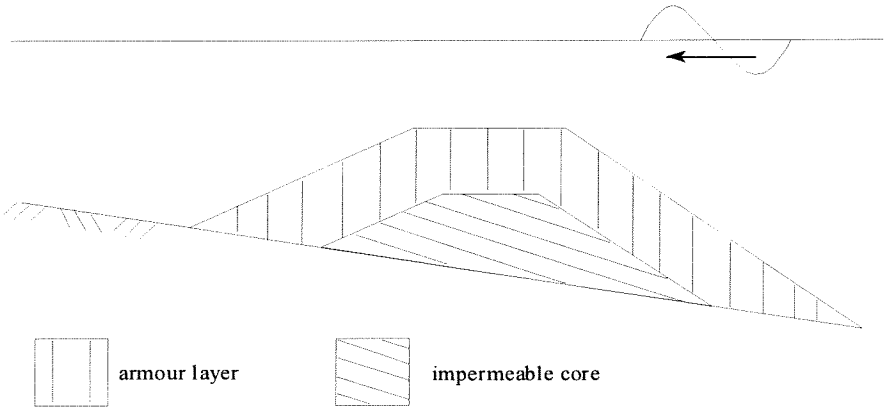

Figure 1.1-2 Submerged breakwater

1.2 The Dynamics of Beaches project

This work is a contribution to the Dynamics of Beaches project, which is a part of the Human Capital and Mobility program (HCM). The subject of this project is the research into the physical processes involving the nearshore region.

Six European Universities are cooperating in this scheme:

I. Aristotele University of Thessaloniki (Greece)
II. University of Ghent (Belgium)
III. University of Liverpool (United Kingdom)
IV. University College of Cork (Ireland)
V. Delft University of Technology (The Netherlands)
VI. University Politecnico de Catalunya (Spain)

Different areas have been investigated by means of experiments conducted in four of the Universities mentioned above. The tests concerned:

- Hydrodynamics: water motion
- Morphodynamics: bed and suspended transport and bottom profile development
- Structural effects: hydrological and morphological effects of the submerged breakwater on the inshore zone

This study deals with the outcomes of the laboratory experiments carried out at the Delft University of Technology. They consist of 3D movable bed tests in a wide basin with regular unidirectional waves.

1.3 Object of the study

- The primary aim of this work is to estimate the 3D effects of the submerged breakwaters on hydrodynamics. In order to do this, first the outcomes of laboratory experiments, carried out with different wave heights and different breakwater configurations, are analysed. To calculate the average water level, time series of the surface elevation are used.
  By comparing the development in time of the bottom profile to the different pattern of the average water level, the behaviour of the wave set-up is investigated.
  Since the experiments were performed mainly to analyse the morphological effect of submerged breakwaters, the hydrodynamic measurements were not very detailed over the whole basin. Therefore, in order to supply extra data a numerical model named DELFT3D, developed at Delft Hydraulics, is implemented.

- The secondary aim is to investigate the influence of the ratio between the length of the submerged breakwater and the width of the gap (the so-called exposure ratio) on the hydrodynamics. For this purpose, a series of simulations is carried out by means of the numerical model DELFT3D.

- The last aim of this work is to analyse the hydrodynamic effect of different off-shore distances of the submerged breakwater from the mean shoreline. This is obtained by means of the numerical model DELFT3D.

1.4 General layout of the report

This section concerns a brief review of the contents of this study.

The report consists of two volumes. The first volume (Volume I: Analysis) deals with the text of the work.
The second volume (Volume II: Appendices) contains the graphics of the outcomes and a brief description of the used numerical model. The text of the first volume, when it is necessary, refers to the graphics and to the description presented in the second volume.

The contents of this volume (Volume I: Analysis) are described in the following.

Chapter 2 describes the layout of the laboratory experiments performed at the Delft University of Technology. A short description of the wave basin and of the equipment used for the tests is presented.

Chapter 3 gives a brief review of the basic theory of the nearshore circulation.
Some knowledge about the purpose and the influence of the submerged breakwater on the inshore zone is illustrated.

In Chapter 4 the measured wave set-up is discussed. A short description of the program DASY*Lab*, used to calculate the average water level from the raw wave signal recorded during the laboratory experiments, is presented.

Chapter 5 concerns a brief description of the numerical model Delft2D-MOR.

In Chapter 6 the calibration of HISWA wave parameters is discussed.

Chapter 7 deals with the outcomes of the simulations carried out with a fixed bed. The analysis of the results follows a brief description of the input of the numerical model. The calculated wave set-up and current field are compared with the measurements.

In Chapter 8 the outcomes of the simulations performed with a movable bed are discussed. The hydrodynamic aspect of the results is described in more detail compared with the morphodynamics. The measurements are taken as a reference for the comparison with the computations.

In Chapter 9 the simulations carried out with different submerged breakwater configurations are analysed. First different ratios of submerged breakwater length to gap width are investigated, then the off-shore distance of the submerged breakwater from the mean shoreline has been changed.

Finally, in Chapter 10 some conclusions are drawn and recommendations for further research are made.

2. LAYOUT OF THE TESTS

2.1 Introduction

The set-up of the experiments had to meet general standards within the framework of the Dynamics of Beaches project.
The 3D tests should be comparable to the 2DV tests which were already done (see Claessen and Groenewoud (1995)), therefore the experimental 2DV set-up was taken as an example.
Three different series of experiments have been made, viz.:

A - without breakwaters
C - with one breakwater split up in two parts of 12 m and 6 m, with a 3 m gap in between
D - with one breakwater split up in three parts of 6 m each, with gaps of 3 m

Each series can be divided again in three, according to the different wave heights used.
The initial bottom profile and the design of the submerged breakwater are the same for each experiment.
Each experiment lasted 7.5 hours divided in four time intervals:

Interval 1 :	0.0 - 0.5	h	0.5 hours
Interval 2 :	0.5 - 1.5	h	1 hours
Interval 3 :	1.5 - 3.5	h	2 hours
Interval 4 :	3.5 - 7.5	h	4 hours

Table 2.1-1 shows the wave conditions used for the tests.

Test Series	Wave Height [m]	Wave Period [s]
A1, C1, D1	0.08	1.55
A2, C2, D2	0.10	1.55
A3, C3, D3	0.12	1.55

Table 2.1-1 Wave conditions

2.2 Laboratory of Fluid Mechanics at the Delft University of Technology

The wave basin

To carry out the experiments, use was made of the equipment of the Laboratory of Fluid Mechanics at the Delft University of Technology. The dimension of the basin can be seen in the Figure 2.2-1.
The basin was supplied with the wave paddles extended over the entire width, in order to generate regular unidirectional waves.
In the lowest part of the basin a concrete 1:13 slope was built to guarantee the stability of the breakwaters. Landward of the submerged breakwaters a 1:15 slope of sand constituted the area investigated by the tests.

Both the shorter sides of the basin consisted of brick walls.
The first series of tests were carried out without breakwaters in order to obtain a reference for the tests with breakwaters.
For the second series of tests a breakwater split up in two parts of 12 m and 6 m with a gap of 3 m in between was placed in the basin. The last series of tests were carried out by means of a breakwater split up in three parts of 6 m each with 3 m of gaps.
For each tests, the still water level is equal to 0.57 m at the wave generator.
The layout of the two configurations is illustrated in Figure 2.2-2.

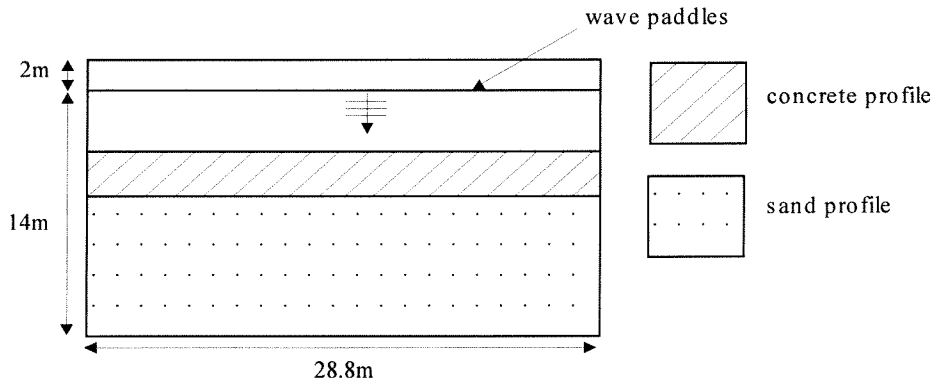

Figure 2.2-1 Layout of the basin (Delft)

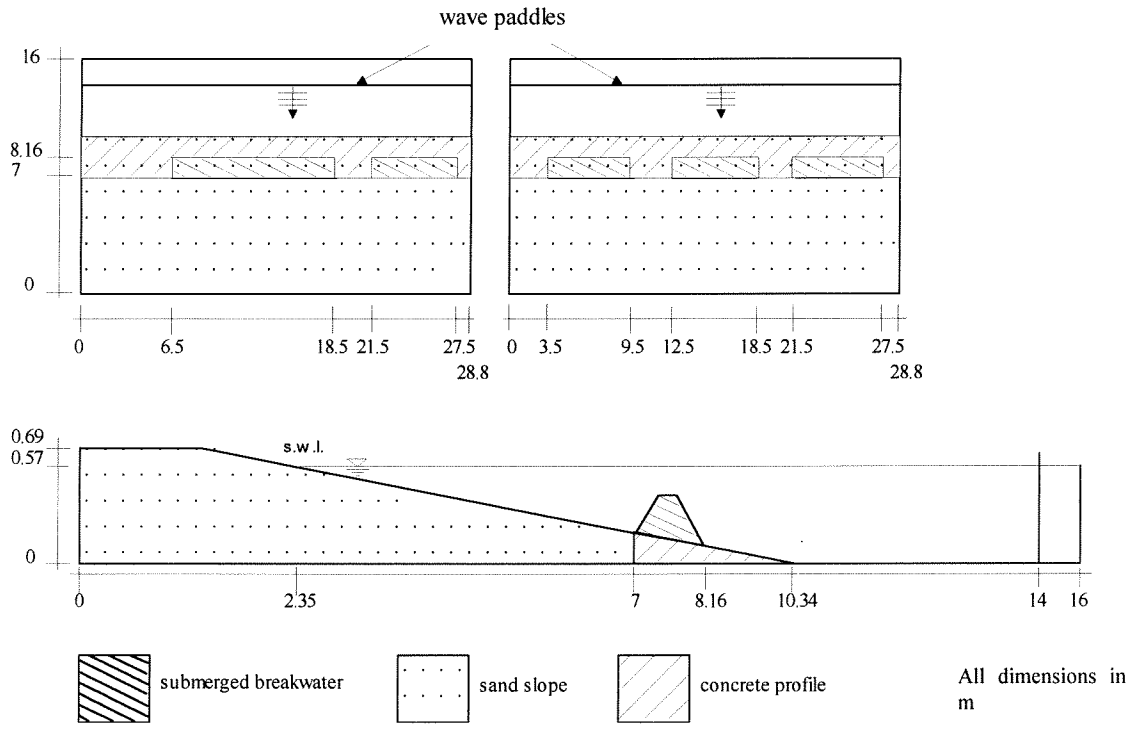

Figure 2.2-2 Plan view & Cross-section of the two configurations (Delft)

The submerged breakwater

The design of the breakwater was made by the University of Ghent. According to this, the construction was statically stable with a permeable core, although for simplicity an impermeable core was built. Van der Meer & Daemen (1994) and Davier and Kriebel (1992) demonstrated that the permeability of the structure (underneath the armour layer) did not show significant influence on the stability of the structure itself.

For the impermeable core 18 triangular prefab concrete elements were used. The armour layer consisted of 2 layers of stone based on the formula of Van der Meer which is not exact, but on the safe side.
Characteristics of the armour layer for the prototype breakwater:

- average rock mass: W_{50} = 1416 kg
- dimension: D_{n50} = 0.812 m
- rock density ρ = 2650 kg/m^3

In order to conform to the scale of the model of 1:15 a D_{n50}= 0.05 m was used which complied with the stability condition. In Figure 2.2-3 the cross-section of the breakwater built for the experiments is shown.

Scale of the
breakwater 1:15

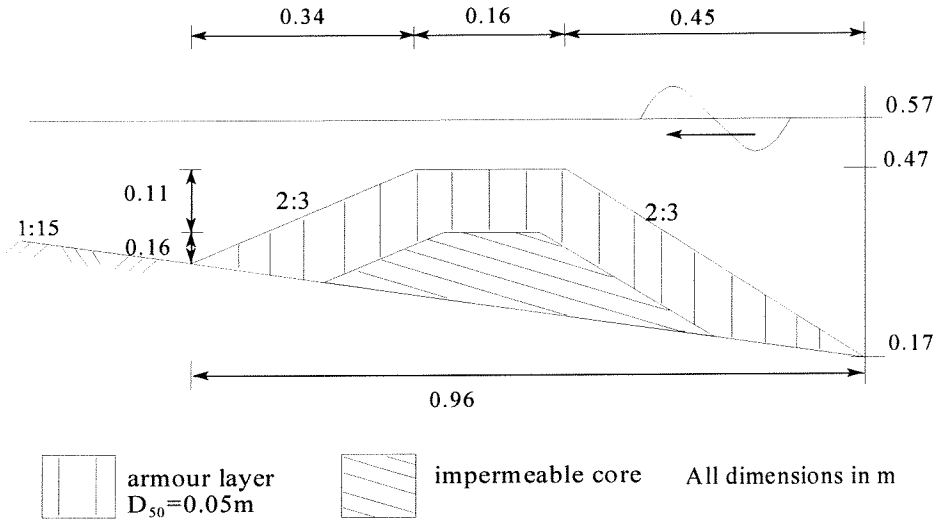

Figure 2.2-3 Scale model of the submerged breakwater

The scale of the model

The initial slope of the sand profile had to be 1:15, therefore, at the end of every experiment, time was employed to restore the above mentioned slope. The ratio between bed transport and suspension transport was supposed to be close to the value in the prototype situation. Because of this, the sand which was used had a D_{50} of 75 μm. This diameter is quite small in comparison with the sand which normally constitutes beaches. On the other hand, by using scaled down wave parameters but unscaled sand parameters, the decrease in the wave energy would cause less sediment transport in comparison with bed transport. Besides, the aim of the tests was not to represent the proper scale relationships according to any prototype, therefore, not many efforts were made in this direction.

The instruments

To carry out the measurements, use was made of a movable bridge extended over the entire width of the basin. All the equipment was positioned on it, except for two wave probes placed in fixed positions in the corners of the basin.

By moving the bridge it was possible to analyse every cross-section. In Figure 2.2-4 the location of the equipment can be seen and in Figure 2.2-5 a picture of the basin is shown.
The measurements concerned the bottom profile, the flow velocity and the wave height.
In order to register all the data in a personal computer, the analogue output signals coming from the equipment had to be digitized by an analogue-digital converter.
This section deals with the equipment without going into specific details. For further information about this subject, reference is made to De Later (1996).

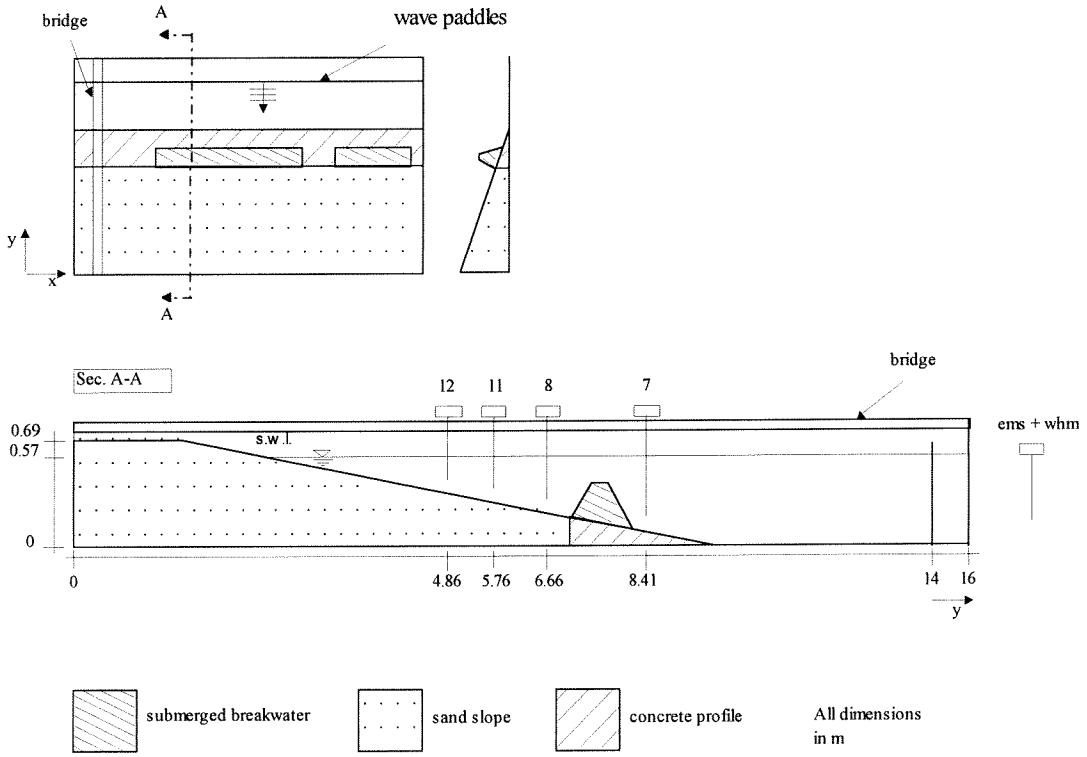

Figure 2.2-4 Location of the equipment

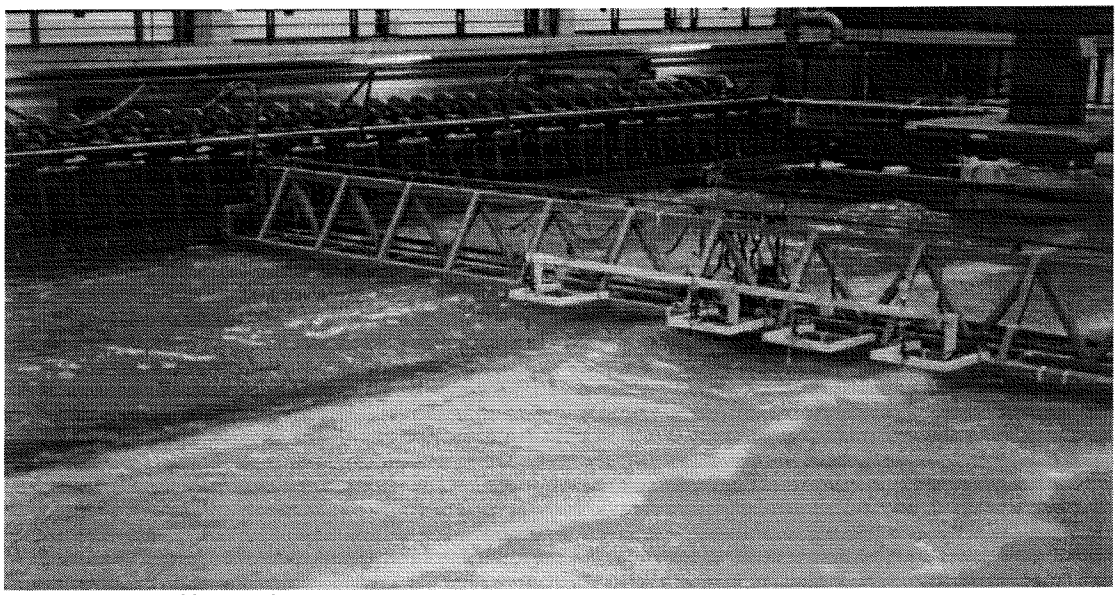

Figure 2.2-5 Delft wave basin

The PROFO

The instrument used for the bottom profile measurements was an Electrical Profile Follower (PROFO). It is based on the appreciable difference of the electric conductivity between water and bed material. By means of a servomechanism, the tip of the probe is maintained at a constant distance above the bed. The profo was placed on a trolley which could be moved over the bridge in a horizontal direction with a constant speed, following in this way the profile of the bed continuously.

The instrument consists of a probe made of stainless-steel completely insulated dipped vertically into the water. The compensation electrode is constituted by a stainless-steel ring interrupting the insulation about 15 mm from the tip of the needle. The measuring electrode is placed at the tip, completely insulated.

Considering the electrodes on the needle and the plate-electrode (the bed of the basin) in the fluid, the electrical resistance between them is a function of the area of the electrodes and the conductivity of the fluid. If the area between the measuring electrode and the non-conductive bed decreases, the resistance of the conductive fluid increases rapidly. A potentiometer mounted on the probe registers this difference and restores the needle to its original position. The accuracy of the probe is of 0.2 mm.

Calibration of the profo

The calibration of the instrument had to be made every day. It did not have a warming-up period. A special step-wise construction was made to calibrate it and was put under water. The profo was positioned above each step and the output signal (Volts) was registered. Once the vertical position of the calibration construction was measured by using a gauge, the relation between the output signal and the vertical position itself could be determined.

The EMS

In attempt to measure the fluid velocities, use was made of Electromagnetic fluid-velocity meters (EMS). The longshore and the cross-shore current could be determined. A magnetic field was generated by a pulse current through a small coil inside the body of the sensor. The voltages produced by the conductive fluid moving across the magnetic field are sensed by two pairs of diametrically opposed platinum electrodes. These voltages are proportional to the sine and cosine of velocities parallel to the plane of the electrodes.

The EMS works until a distance of approximately 5 mm above the bottom and in a range variable from 0 to ± 1 m/s or from 0 to ± 5 m/s. The maximum error is ± 1% of the selected full scale with respect to calibrated conditions. The zero-flow stability is better than 0.01 m/s per day.

The velocity data

Four EMS were mounted on the bridge on steady positions. Therefore, the velocities were measured for every experiment at the same y-coordinates.

The y-positions were: y = 4.86 m, 5.71 m, 6.66 m, 8.41 m (see Figure 2.2-4) in accordance with 2DV flume tests, which were also carried out by Delft University of Technology.

The first three locations were situated landward of the breakwaters while the last was positioned seaward, in order to measure currents around the breakwater.

Due to the shallow water it was impossible to measure more landward than y = 4.86 m.
The cross-sections measured were the same for the A series of tests as for C series, while they were different for D series:

- Tests A & C x = 3 m, 6.5 m, 12.5 m, 20 m, 24.5 m
- Test D x = 12.5 m, 14 m, 15.5 m, 17 m, 18.5 m, 20 m

During the tests four different depths were supposed to be measured, but because of bottom changes during the tests, it was sometimes only possible to carry out measurements in the two highest positions only.
To be able to analyse the measurement it was necessary to register for at least 4 minutes. Every measurement of a cross-section (wave heights and current velocities) took about 5 minutes and at the end the velocity meters were put in the new position.
It has to be said that some measurements resulted not to be accurate because the EMS1 (y = 4.86 m) and the EMS2 (y = 5.71 m) touched the bottom profile due to its development in time.

Calibration of the EMS
The calibration of the EMS was made previously by Delft Hydraulics. It had a warming-up period of at least half an hour. A standard calibration formula was used for the velocity meters, therefore, the calibration factors were not computed. The offset in x-direction and in y-direction was derived by means of a zero-measurement at the beginning of every time interval.

The wave probe
The wave heights were measured by means of a wave probe. The instrument is composed of two parts: a gauge with an integral pre-amplifier and a separate main-amplifier. A small box contains the pre-amplifier. Under this box two parallel stainless-steel roods constitute the gauge.
By knowing that the electric resistance measured between the two rods is inverse proportional to the specific conductivity of the water, the wave height could be determined.
A platinum reference-electrode was installed between the lower tip of the two rods to avoid the effect of conductivity fluctuations.
The main amplifier was supplied with several ranges from 0.05 m to 0.5 m. The error of each range was less than ± 0.5 %. The interference between several probes working simultaneously could be neglected for distances larger than 0.2 m. Sometimes the immersion of the gauge probably changed after the calibration leading to results visually out of range.

The wave height measurements
Six wave probes were used during the experiments. Two of them were positioned steadily in the corners of the basin, in front of the wave generator. The other four probes were situated on the bridge, in line with the EMS. Therefore, wave heights and current velocities were measured simultaneously for each cross-section. Every 5 minute a new series of measurements was registered.

Calibration of the wave probes

The wave probes were calibrated every day after a warming-up period of half an hour. The following procedure was adopted for the calibration:

1. The platinum reference-electrode must be positioned at least 0.04 m under the zero-position, i.e. the lowest expected water level.
2. The pointer of the indicating meter of the main amplifier must indicate the centre-scale position corresponding with 0.000 Volt output.
3. Five different immersion-depths were measured (see Table 2.2-1).
   For y = 6.66 m, 8.41 m and for the corners the depths were: -0.1 m, -0.05 m, 0 m, +0.05 m, +0.1 m.
   For y = 5.71 m, 4.86 m the depths were: -0.05 m, -0.025 m, 0 m, +0.025 m, +0.05 m.
   Nine measurements were carried out changing the immersion of the wave probe. These different signals were used for the calibration.
   A linear relation exists between the signals and the position.
   The calibration determines the relation (direction coefficient) between these magnitudes.
4. The average direction coefficient was determined (Sum/8).
5. The average of the three values, obtained for the zero-position, was taken as the offset.
6. All the signals of the wave probes were recorded by means of a data-acquisition program called Dasy*Lab*. The calibration was complete when the calibration factors were installed into this program.

Immersion-depth	**signal** [Volt]	**direction coefficient** 0.05/ difference signal [m/Volt]
zero-position	a	
+0.05	b	0.05/(b-a)
+0.1	c	0.05/(c-b)
+0.05	d	0.05/(d-c)
zero-position	e	0.05/(e-d)
-0.05	f	0.05/(f-e)
-0.1	g	0.05/(g-f)
-0.05	h	0.05/(h-g)
zero-position	i	0.05/(i-h)

Table 2.2-1 Immersion depth for the wave probes calibration

3. REVIEW OF RELEVANT THEORIES

3.1 Introduction

In this chapter a brief review of the basic theory of the nearshore circulation is given, in order to supply the reader with a support to understand the arguments will be discussed later more easily.

The basic assumption of the following theories is irrotational flow which implies that there are no internal shear stresses.

The fundamental equations for unsteady irrotational flow in the vertical plane (see Figure 3.2-1) are the continuity equation and the Euler equation of motion, which yield the Bernoulli equation:

$$-\frac{\partial \phi}{\partial t}+\frac{1}{2}\left(\frac{\partial \phi}{\partial x}\right)^2+\frac{1}{2}\left(\frac{\partial \phi}{\partial z}\right)^2+\frac{P}{\rho}+gz=0 \qquad (3.2.1\text{-}1)$$

where ϕ = potential function
P = pressure
g = acceleration of gravity
ρ = fluid density

The Section 3.2 reviews the basic equations about regular waves and in the Section 3.3 irregular waves will be examined.

3.2 Regular waves and linear theory

In nature waves are neither regular nor sinusoidal. However, the results obtained by the study of this type of water waves are very useful due to the relative simplicity of this theory, and to the reasonable similarity to reality.

The simplest theory used to describe these waves is the linear or Airy theory. According to this theory, the wave profile is simplified to a linear sinusoidal wave form.

As an example of more complex and more accurate theories, the non-linear theory can be mentioned, as the higher order Stockes theories. Both linear and non-linear theories belong to the small-amplitude wave theory. They are not accurate in shallow water, when h/L is very small (the definition of the symbols is explained in Figure 3.2-1). To overcome this, special wave theories have been developed, as, for instance, the cnoidal wave theory. This theory belongs to the finite-amplitude wave theories.

The equations described in the following are based on the linear theory.

The non-linear terms $(\partial\phi/\partial x)^2$ and $(\partial\phi/\partial z)^2$ in the Equation (3.1-1) can be neglected, yielding the linear Bernoulli equation:

$$-\frac{\partial \phi}{\partial t}+\frac{P}{\rho}+gz=0 \qquad (3.2.1\text{-}1)$$

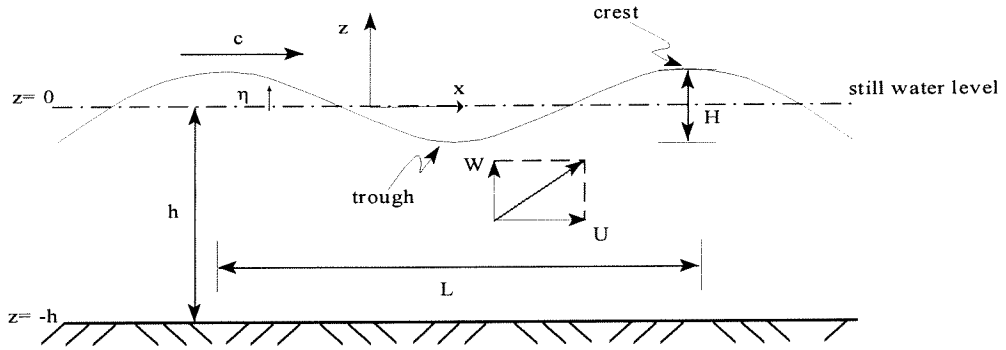

Figure 3.2-1 Definition of the symbol

3.2.1 Fluid particle velocities

Consider the potential function ϕ:

$$\phi = c\frac{H}{2}\frac{\cosh[k(h+z)]}{\sinh[kz]}\sin(\omega t - kx) \qquad (3.2.1\text{-}1)$$

where
- c = ω/k = wave celerity
- ω = 2π/T = angular frequency
- k = 2π/L = wave number
- T = wave period
- L = wave length
- H = wave height
- h = water depth to still water surface
- z = vertical coordinate (see Figure 3.2-1)
- x = horizontal coordinate (see Figure 3.2-1)

By taking the derivatives of the Equation (3.2.1-1) the horizontal and vertical fluid velocities can be obtained:

$$U = \frac{\omega H}{2}\frac{\cosh[k(z+h)]}{\sinh[kh]}\cosh(\omega t - kx) \qquad (3.2.1\text{-}2)$$

$$V = \frac{\omega H}{2}\frac{\sinh[k(z+h)]}{\sinh[kh]}\sinh(\omega t - kx) \qquad (3.2.1\text{-}3)$$

where
- U = horizontal fluid velocity at depth z below surface, at distance x and at time t
- W = vertical fluid velocity at depth z below the surface, at distance x and at time t
- H = wave height
- ω = angular frequency
- t = time

These equations show the local fluid velocity components any distance (z + h) above the bottom. The following features can be pointed out (see Figure 3.2.1-1):

- the orbit described in each point by the velocity vector ($\vec{v}$) is elliptical
- the horizontal and vertical velocities are 90° out of phase
- the maximum positive horizontal velocity (U) occurs under the wave crest
- the maximum horizontal velocity (U) in the negative direction occurs under the wave trough
- the vertical velocity (W) is maximum upward at the zero-downward crossing of the wave profile
- the vertical velocity (W) is minimum downward at the zero-upward crossing of the wave profile
- the horizontal velocity (U) is zero at the point of zero elevation of the water level
- the vertical velocity (W) is zero under the wave crest and the wave trough
- the fluid velocity near the bottom is essentially horizontal ($W \approx 0$).

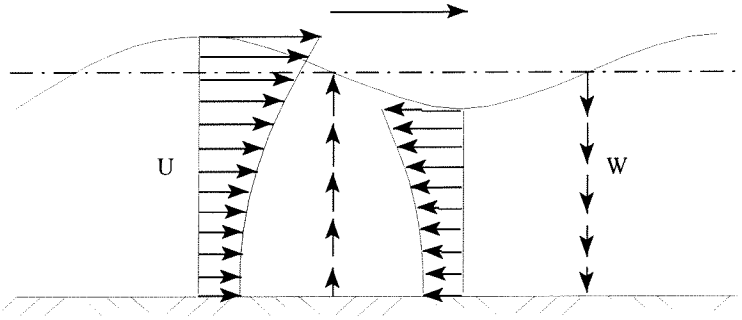

Figure 3.2.1-1 Local fluid velocities

3.2.2 Water particle displacements

Water particles generally move in elliptical paths in shallow water and in circular paths in deep water (see Figure 3.2.2-1). If the mean particle position is considered to be at the centre of the ellipse or circle, than vertical particle displacement with respect to the mean position cannot exceed one-half the wave height (see Figure 3.2.2-2). Considering the instantaneous particle position x + A, z + B, the displacement component (A,B) can be obtained by integrating the velocity with respect to time:

$$A_{x,z,t} = \int U_{x+A,z+B}\,dt \qquad (3.2.2\text{-}1)$$

$$B_{x,z,t} = \int W_{x+A,z+B}\,dt \qquad (3.2.2\text{-}2)$$

Since the wave height is supposed to be small, A and B can be neglected in $U_{x+A,z+B}$ and in $W_{x+A,z+B}$ with respect to x and z. Thus, substituting Equations (3.2.1-2) and (3.2.1-3) and integrating, gives:

$$A = \frac{H}{2}\frac{\cosh[k(z+h)]}{\sinh[kh]}\sinh(\omega t - kx) \qquad (3.2.2\text{-}3)$$

$$B = \frac{H}{2} \frac{\cosh [k(z+h)]}{\sinh [kh]} \cosh (\omega t - kx) \qquad (3.2.2\text{-}4)$$

where A = horizontal fluid particle displacement at depth z below the water surface, at distance x and at time t

B = vertical fluid particle displacement at depth z below the water surface, at distance x and at time t

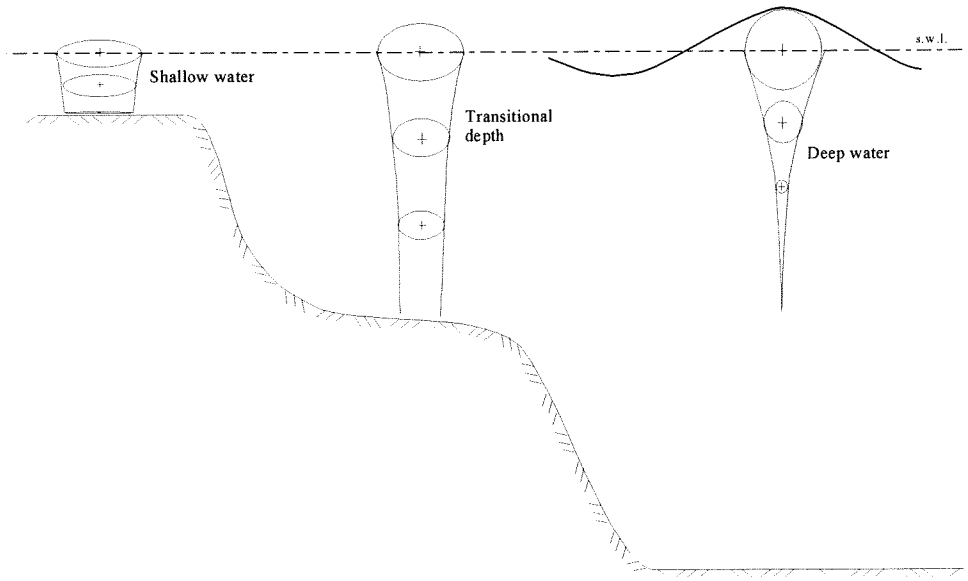

Figure 3.2.2-1 Orbital motion in shallow and deep water

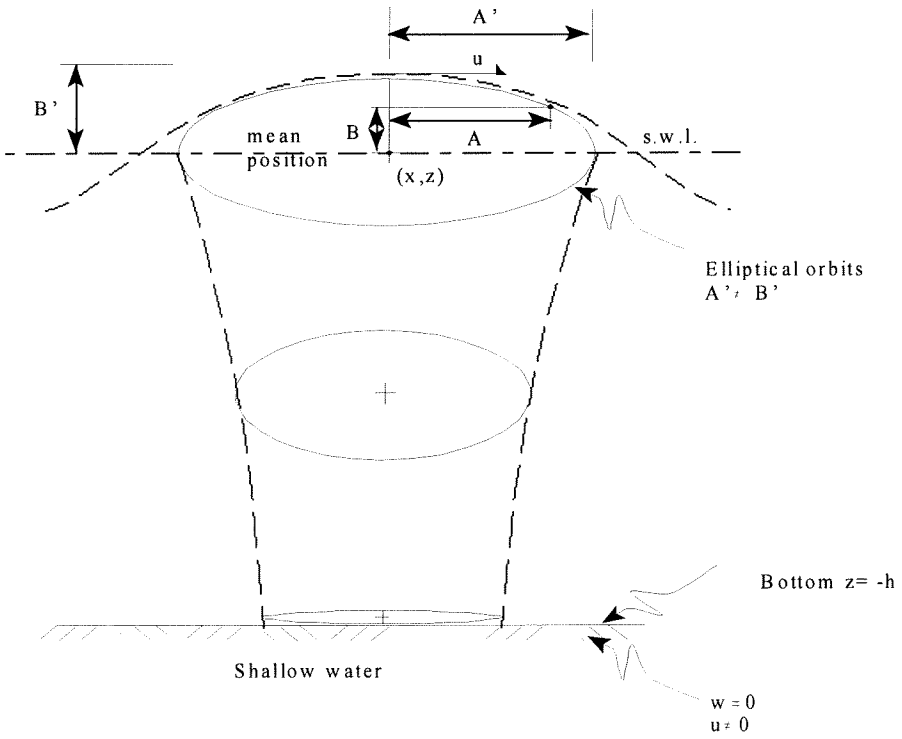

Figure 3.2.2-2 Water particle displacement from mean position for shallow water

3.2.3 Mass transport

Non-breaking waves

Mass transport is a non-linear effect because the equations involved contain terms of H^2 (square wave height). Nevertheless these equations can be obtain by means of the Airy wave theory.

The fluid particles do not describe exactly closed orbital trajectories in case of small-amplitude (sinusoidal) surface waves propagating in a perfect non-viscous (irrotational) oscillatory flow (see Figure 3.2.3-1). The particles have a second-order Lagrangian velocity ('Stokes' drift U_s) in the direction of wave propagation, due to the fact that the horizontal orbital velocity increases with height (z) above the bed (see sketch in Figure 3.2-1 for the definition of the symbols). Therefore, a particle at the top of an orbit beneath a wave crest is faster in the forward direction than it is in the backward direction at the bottom of the orbit beneath a wave trough.

For waves propagating in a horizontally unbounded domain, the depth-integrated mass flux (m^2/s) yields:

$$M_s = \int_{-h}^{0} \overline{U_s}(z)\,dz = g\frac{1}{8}\frac{H^2}{c} \qquad (3.2.3\text{-}1)$$

where
- M_s = mass flux in a Lagrangian way
- $\overline{U_s}$ = Stokes drift velocity determined by applying linear wave theory and averaging over the wave period
- H = wave height
- c = wave celerity

For waves propagating in a horizontally bounded (e.g. a wave flume) domain it is appropriate impose a condition of zero mass flux ($M_s = 0$) at each location (x).

The mass flux (m^2/s) at a fixed location (x) in an unbounded domain can be determined in an Eulerian way:

$$M_e = \frac{1}{T}\int_0^T \int_{-h}^{\eta} U(t,z)\,dz \qquad (3.2.3\text{-}2)$$

where
- M_e = mass flux
- T = wave period
- U = instantaneous horizontal velocity at height z
- η = water surface elevation displacement from the mean water level

In the region between the wave crest and trough of sinusoidal waves, an asymmetry of horizontal velocity indicates that more fluid moves in the wave direction under the crest than in the trough region. Under the wave trough level of a sinusoidal wave, the time-averaged value of the horizontal velocities in a fixed point is zero.

Applying the linear wave theory for small amplitude sinusoidal waves, yields:

$$M_e = g\frac{1}{8}\frac{H^2}{c} \qquad (3.2.3\text{-}3)$$

The Lagrangian and the Eulerian method yield the same depth-integrated mass transport, while the vertical distribution of the mass transport velocities is different for both methods.

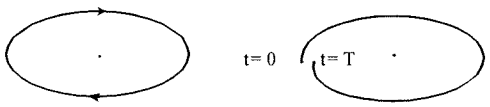

Figure 3.2.3-1Closed and non-closed particle orbits

For real fluids with viscosity ν, there is a time-averaged net downward transfer of momentum into the boundary layer by viscous diffusion ($\overline{\nu \partial U/\partial z}$), causing a mean Eulerian flow ($\overline{U_e}$) in addition to the Lagrangian Stokes drift (Longuet-Higgins (1953)).
The mean Eulerian flow can be seen as the mean velocity of the orbit centres.
The total mass transport velocity is defined as:
$\overline{U}_m = \overline{U_e} + \overline{U}_s$
Figure 3.2.3-2 shows the velocity profile over a smooth plane bottom according to Longuet-Higgins.

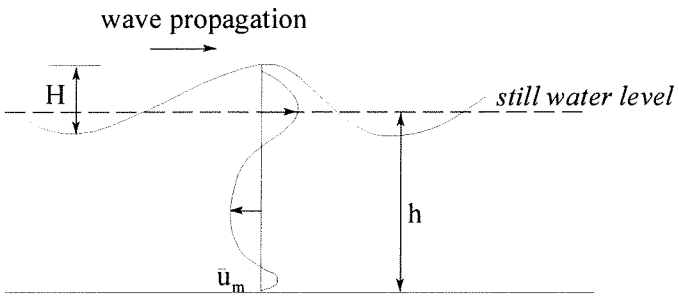

Figure 3.2.3-2 Mass transport in non-breaking waves

Breaking waves
Mass transport is also generated by breaking waves. Above the trough level there is a net mass transport in onshore direction which can be estimated (see Steetzel (1993) and Svendsen (1984)) as:

$$M = g\frac{1}{8}\frac{H_{rms}^2}{c} + Q_b K_r \rho \frac{H_{rms}^2}{T_p} \qquad (3.2.3\text{-}4)$$

where
- M = the mass flux
- H_{rms} = the rms-wave height
- Q_b = portion of breaking waves
- K_r = dimensionless quotient of roller area and H^2_{rms}
- T_p = peak wave period

In Equation (3.2.3-4), the additional term on the right side is due to the effects of wave breaking.
Figure 3.2.3-3 shows the velocity profile for a two dimensional situation (e.g. a wave flume). The return current, also called the undertow, is represented by the mean

velocity below the wave trough ($\bar{u}_{m,off}$), flowing in the opposite direction of the wave propagation.

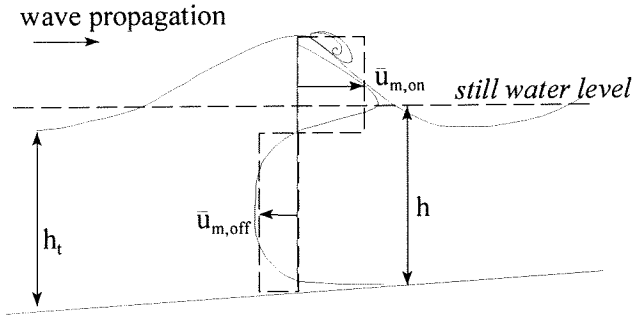

Figure 3.2.3-3 Mass transport in breaking waves

3.2.4 The governing equations of the nearshore circulation

The two-dimensional problem considered is sketched in Figure 3.2.4-1, which also explains the definition of variables.
The equations to be satisfied are based on the principle of the hydrodynamics of conservation of mass, momentum and energy, integrated over depth and averaged over a wave period T.

Conservation of mass
The general conservation of total mass per unit area reads:

$$\frac{\partial \rho(h_0+b)}{\partial t} + \frac{\partial \overline{M}_i}{\partial x_i} = 0 \qquad i = 1, 2 \qquad (3.2.4\text{-}1)$$

where (1, 2) = horizontal co-ordinates (x, y)
b = mean surface elevation
$\overline{M}_i$ = time averaged mass flux

Horizontal momentum equation
The horizontal momentum reads:

$$\frac{\partial S_{xx}}{\partial x} = -\rho g(h_o + b)\frac{\partial b}{\partial x} \qquad (3.2.4\text{-}2)$$

where b = mean surface elevation
S_{xx} = radiation stress

The so-called radiation stress represents the net (time averaged) force the waves exert on a water column. The radiation stress concept will be discussed further in the Section 3.2.5.
In Equation (3.2.4-2) the mean bed shear stress has been neglected, due to the fact that this term is mainly relevant for sediment transport which is not an argument of this section.

The energy equation
The energy equation for wave motion only (neglecting the current terms), is:

$$\frac{\partial E_f}{\partial x} = D \tag{3.2.4-3}$$

where E_f = mean energy flux
D = gain in energy ($D < 0$ for dissipation)

The definition of E_f is:

$$E_f = \overline{\int_{-h_0}^{h+b} [P_D + \frac{1}{2}\rho(u^2 + v^2 + w^2)]u \, dz} \tag{3.2.4-4}$$

where P_D = dynamic pressure

The dynamic pressure, defined on the basis of the local mean water depth, yields:

$$P_D = \rho g(z - b) + P \tag{3.2.4-5}$$

where P = absolute pressure

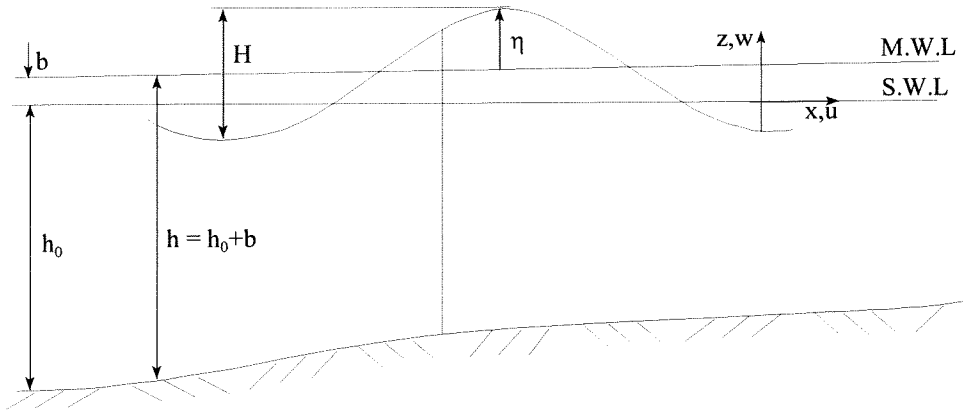

Figure 3.2.4-1 Definition sketch

3.2.5 The radiation stress and the wave-induced water level variation

Waves influence the average condition of the flow in which they propagate. The passage of the crest and of the trough causes fluctuation in the time-averaged values of pressure and velocity (see Figure 3.2.5-1). By integrating these values over the depth, a positive result is found, which means that the waves cause a positive contribution to the mass and to the momentum balance in the horizontal direction. The effect of the mass transport is balanced by an undertow, while the wave-induced contribution to the mean balance of momentum can be observed in an increase of the local average water level. This phenomenon is explained by the theory of the "radiation stress" developed by Longuet-Higgins and Stewart. In the following only a brief discussion is given (see Van der Velden (1995) and Van Rijn (1990)).
It is generally accepted that linear wave theory does not properly describe the radiation stress in the surf zone. Other theories have been used, as the solitary wave theory, cnoidal wave theory or hyperbolic wave theory, but they do not work properly either.

Due to this, the linear wave theory, which is the most easily accessible, will be used in the present section.

Waves normal to coastline (no current)

Considering the momentum balance in x-direction, which is the wave propagation direction (see Figure 3.2.5-1):

$$\frac{\partial}{\partial t}(\rho U) = -\frac{\partial}{\partial x}(P+\rho U^2) - \frac{\partial}{\partial y}(\rho UV) - \frac{\partial}{\partial z}(\rho UW) \qquad (3.2.6\text{-}1)$$

where U = instantaneous velocity in x-direction
V = instantaneous velocity in y-direction
W = instantaneous velocity in z-direction
P = absolute pressure
ρ = fluid density

In the following the time averaging is defined by $\overline{\quad}$, i.e.:

$$\overline{\quad} = \frac{1}{T}\int_0^T dT \qquad (3.2.6\text{-}2)$$

where T = wave period

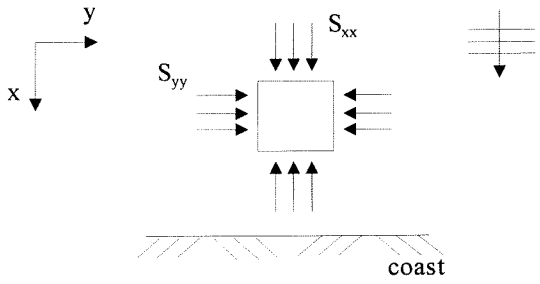

Figure 3.2.6-1 Radiation stress for normal approaching waves

In reality, the radiation stress is neither a true stress (force per area, N/m^2), nor a true force (force per unit length, N/m), but a force over the entire depth.
The components of the radiation stress are defined as the integral over a wave period T, over the depth (z = -h to z = η) of the momentum balance (Equation 3.2.5-1), minus the hydrostatic fluid pressure in the absence of waves (see Figure 3.2.5-2 for the definition of the reference frame):

$$S_{xx} = \overline{\int_{-h}^{\eta}(P + \rho U^2)dz} - \int_{-h}^{0} P_0 dz \qquad (3.2.6\text{-}3)$$

$$S_{xy} = \overline{\int_{-h}^{\eta}(\rho UV)dz} \qquad (3.2.6\text{-}4)$$

where P_0 = hydrostatic fluid pressure at height z below surface

The hydrostatic contribution is equal to:

$$\int_{-h}^{0} P_0 dz = \int_{0}^{h} \rho g z \, dz = \left(\frac{1}{2}\right)\rho g h^2 \qquad (3.2.6\text{-}5)$$

The component S_{xy} is zero when the waves are propagating normal to the coast (V=0).

The same procedure applied to the y-direction leads to the S_{yy}:

$$S_{yy} = \overline{\int_{-h}^{\eta} (P + \rho V^2) dz} - \int_{-h}^{0} P_0 dz \qquad (3.2.6\text{-}6)$$

The unit of measure is Newton per unit width (N/m).
By means of using linear theory the radiation stress, in case of waves propagating normal to the coastline (V=0), can be expressed as follows:

$$S_{xx} = (2n - \frac{1}{2})\frac{1}{8}\rho g H^2 = (2n - \frac{1}{2})E \qquad (3.2.6\text{-}7)$$

$$S_{yy} = (n - \frac{1}{2})\frac{1}{8}\rho g H^2 = (n - \frac{1}{2})E \qquad (3.2.6\text{-}8)$$

$$S_{xy} = 0 \qquad (3.2.6\text{-}9)$$

where $n = \frac{1}{2}\left[\frac{1+(2kh)}{\sin(2kh)}\right]$ = ratio of group velocity and phase velocity

H = wave height

$E = \frac{1}{8}\rho g H^2$ = wave energy

In deep water, by means of the usual approximations (n=1/2), the radiation stress becomes:

$$S_{xx} = \left(\frac{1}{2}\right)E \qquad (3.2.6\text{-}10)$$

$$S_{yy} = 0 \qquad (3.2.6\text{-}11)$$

In shallow water (n=1):

$$S_{xx} = \left(\frac{3}{2}\right)E \qquad (3.2.6\text{-}12)$$

$$S_{yy} = \left(\frac{1}{2}\right)E \qquad (3.2.6\text{-}13)$$

The radiation stresses are influenced by the wave height, via the wave energy. In deep water this is the only influencing factor, while in transitional water depth the water depth, h, the wave length, λ , or simply n are also important. In shallow water, it

seems that the radiation stress depends only upon the wave energy, however, the wave energy itself is very dependent upon the water depth when wave breaking occurs.

Considering waves propagating in a domain with constant depth and assuming no energy losses (constant wave height). The radiation stress components S_{xx} and S_{yy} are constant, which means that there is no change of momentum.

Wave set-down in non-breaking waves

The equations previously written are approximately valid in case of a bottom profile gradually varying. By balancing the forces acting on the fluid in x-direction, the following equation is derived:

$$\frac{dS_{xx}}{dx} + g(h+h')\frac{dh'}{dx} = 0 \qquad (3.2.6\text{-}14)$$

where S_{xx}= radiation stress
h = still water level
h' = water level variation with respect to the still water level

The previous equation shows that the gradient of the radiation stress is balanced by the gradient of the hydrostatic pressure due to the average water level variation.

By using the energy flux balance, neglecting dissipation effects (d(Ecn)/dx = 0) and h' << h, Equation (3.2.5-14) can be integrated over the offshore zone, with the initial condition h' = 0 in deep water, yielding:

$$h' = -\frac{kH^2}{8\sinh(2kh)} \qquad (3.2.6\text{-}15)$$

where H = local wave height
k = $\frac{2\pi}{L}$ = wave number
L = local wave length
h = local mean water depth

Approaching the breaker line, S_{xx} increases causing a positive gradient in the radiation stress ($\frac{dS_{xx}}{dx} > 0$). According to the relation:

$$\frac{dS_{xx}}{dx} = -\rho g(h+h')\frac{dh'}{dx} > 0 \qquad (3.2.6\text{-}16)$$

it follows that:

$$\frac{dh'}{dx} < 0 \qquad (3.2.6\text{-}17)$$

Therefore, Equation (3.2.5-15) yields a set-down of the average water level (h' decreases).

Equation (3.2.5-15) is valid up to the breaker line. Further landward, the assumption of negligible energy dissipation is not reliable. Measurements of h' are in good agreement with the predicted value, apart from close to the breaker line.

Adopting the approximation valid for the shallow water, the wave height at the breaker point can be determined as follows (with the breaking condition $H_{br} = \gamma h_{br}$):

$$h'_{br} \cong -\frac{1}{16}\frac{H_{br}^2}{h_{br}} \cong -\frac{1}{16}\gamma H_{br} \qquad (3.2.6\text{-}18)$$

where h'_{br} = water level variation with respect to the still water level at the breaker line
H_{br} = wave height at the breaker line
h_{br} = local mean water depth at the breaker line
$\gamma = H_{br} / h_{br}$ = breaker coefficient ($\cong 0.8$ for spilling breakers)

Predicted h'_{br}-values are however often approximately 50% smaller than h'_{br}-measured values.

Wave set-up in breaking waves

In the surf zone, with breaking waves, the shallow water approximation yields the relation:

$$S_{xx} = \frac{3}{2}E \qquad (3.2.6\text{-}19)$$

Assuming valid the relation $H(y) = \gamma(h(y) + h'(y))$ with γ constant, the following equation is defined:

$$S_{xx} = \frac{3}{2}E = \frac{3}{16}\rho g H^2 = \frac{3}{16}\rho g \gamma^2 (h + h')^2 \qquad (3.2.6\text{-}20)$$

Approaching the coast, S_{xx} decreases due to the decrease in the water depth h, yielding a negative gradient in the radiation stress ($\frac{dS_{xx}}{dx} < 0$).

For Equation (3.2.5-14) to be satisfied, the average water level increases (h' rises), i.e.:

$$\frac{dS_{xx}}{dx} = -\rho g(h+h')\frac{dh'}{dx} > 0 \qquad (3.2.6\text{-}21)$$

which implies

$$\frac{dh'}{dx} > 0 \qquad (3.2.6\text{-}22)$$

This phenomenon is called wave set-up.

Substitution of Equation (3.2.5-20) in the momentum equation (3.2.5-14), yields:

$$\frac{d}{dx}\left(\frac{3}{8}\gamma^2(h+h')+h'\right)=0 \tag{3.2.6-23}$$

which means:

$$\frac{3}{8}\gamma^2(h+h')+h'=const.=K \tag{3.2.6-24}$$

By applying the boundary conditions at the breaking line, with simple mathematical passages the value of the constant K can be determined ($K = 5/16\gamma H_{br}$). With this result, from the relation (3.2.5-24) it follows that:

$$h'=\frac{5}{16}\gamma H_{br}-\frac{3}{8}\gamma H \tag{3.2.6-25}$$

The maximum value is obtained for H = 0 (see Figure 3.2.5-2):

$$h'_{\max}=\frac{5}{16}\gamma H_{br} \tag{3.2.6-26}$$

The total variation Δh' of the average water level in the surf zone can be determined by balancing the forces over the entire breaker zone (see Figure 3.2.5-3):

Hydrostatic Force + Radiation Stress = Hydrostatic Force along the bottom

$$\frac{1}{2}\rho g h_{br}^2+\frac{3}{16}\rho g\gamma^2 h_{br}^2=\frac{1}{2}\rho g h_{br}\left(h_{br}+Dh'\right) \tag{3.2.6-27}$$

$$\Delta h'=\frac{3}{8}\gamma^2 h_{br}=\frac{3}{8}\gamma H_{br} \tag{3.2.6-28}$$

The Equation (3.2.5-24) can be expressed also as follows:

$$h'=\frac{\frac{5}{16}\gamma H_{br}-\frac{3}{8}\gamma^2 h}{1+\frac{3}{8}\gamma^2} \tag{3.2.6-29}$$

which shows a linear water level rise in the surf zone in case of a plane sloping bottom.

The wave set-up is a phenomenon due to the action of many waves acting for a sufficient period to guarantee an equilibrium condition (~ 1 hour). Wave groups move a great amount of water towards the coast, but part of it returns seaward during intervals between different wave groups.
If the wave conditions change along the coast, the wave set-up varies consequently. The different wave conditions can be determined by refraction or diffraction or, as in the situation analysed in this report, by the presence of discontinuous barriers as

submerged breakwaters. The variation in the water level between points on the coast causes pressure gradients along the shoreline. An important contribution to the longshore current is constituted by this pressure gradient.

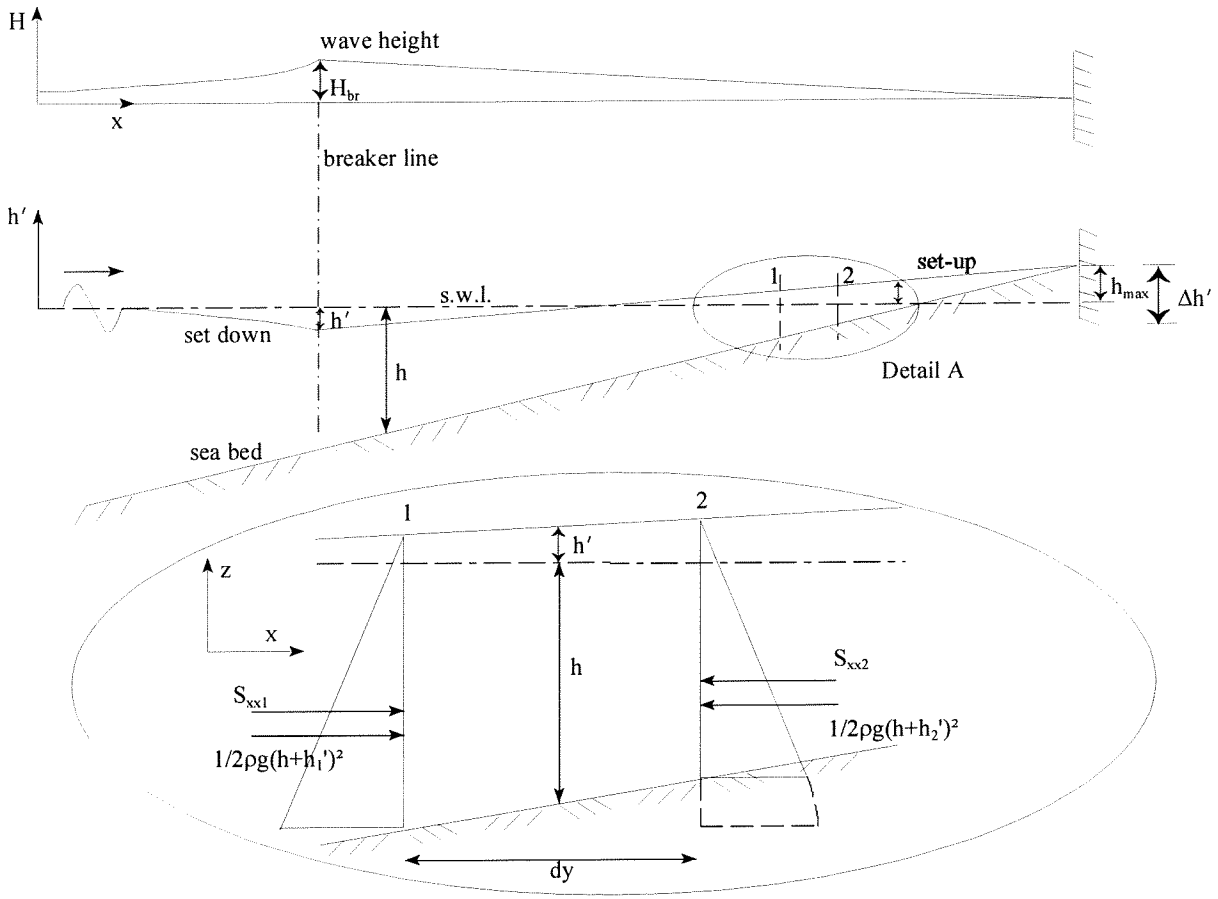

Figure 3.2.6-2 Wave-induced water level variation & radiation component S_{xx}

3.2.6 Contribution of regular waves and current

The previous sections dealt with the characteristic of waves alone. Very often a current is flowing in the direction of or at an angle to the wave propagation. The presence of a current influence the wave characteristic as, in their turn, waves affect certain current characteristics.

A current following the waves enlarges the wave length and reduces the wave height. A current opposing the waves yields an increased wave height and a decreased wave length which entails that the wave is steepened.

The wave frequency will change since the wave celerity will change. The wave celerity, in the absence of current, reads:

$$c = \frac{\omega}{k} \qquad (3.2.6\text{-}1)$$

where c = wave celerity
ω = wave frequency
k = $2\pi/\lambda$ = wave number

For currents and waves c will change in c', which reads:

$$c' = c + V_{//} \tag{3.2.6-2}$$

where $V_{//}$ = current velocity component in the direction of the wave propagation

The frequency will change in ω', given by:

$$\omega' = c'k = (c + V_{//})k = \omega + kV_{//} \tag{3.2.6-3}$$

The term $kV_{//}$ is often called the Doppler effect.

Laboratory experiments show a distinct influence of the waves on the current velocity profile. Figure 3.2.6-1 presents current velocities over the water depth measured with and without waves.
The most remarkable effects are:

- a decrease of near-bed velocities in case of a following current as well as in case of an opposing current
- an increase of near-surface velocities in case of an opposing current, whereas a slightly decrease in case of a following current
- the effects are most noticeable in case of relatively large waves in combination with weak current

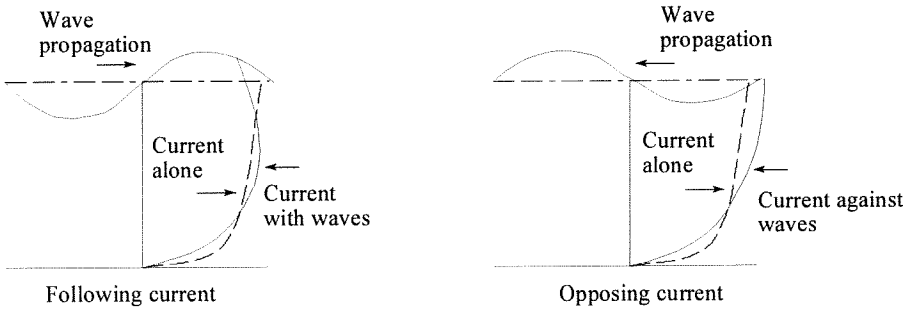

Figure 3.2.6-1 Influence of waves on current velocity profile

3.3 Nearshore currents

Nearshore currents in the littoral zone are predominantly wind and wave-induced motions superimposed on the wave-induced oscillatory motion of the water. The net motions have generally low velocities, nevertheless, they are important on determining littoral transport since they transport whatever sand is moved by the wave-induced water motion.

Wave-induced water motion

In idealised deep water waves, water particles have a circular motion in a vertical plane perpendicular to the wave crest. This motion does not reach deep enough to affect sediment on the bottom. Towards shallower water, where waves are affected by the bottom, the circular motion turns into elliptical, and water at the bottom begins to move. In shallow water, the ellipses elongate into nearly straight lines.

At breaking, particle motion becomes more complicated, but even in the surf zone the water moves forward and backward in paths that are mainly horizontal, with brief but intense vertical motions as the breaker crest passes.
Since the wave-induced water particle motion is the main cause for the sediment to move, it is useful to know the length of the elliptical path traveled by the water particles and the maximum velocity and acceleration obtained during this orbit.
For sediment transport the shallow water condition is the most important. Assuming the small-amplitude theory, the horizontal length of the path moved by the water particle as a wave passes in shallow water is approximately:

$$2A = \frac{HT\sqrt{gd}}{2\pi d} \qquad (3.3\text{-}1)$$

where 2A = horizontal length of the path
H = wave height
T = wave period
d = water depth

The maximum horizontal water velocity reads

$$u_{max} = \frac{H\sqrt{gd}}{2d} \qquad (3.3\text{-}2)$$

The term under the radical is the wave speed in shallow water.

Fluid motion in breaking waves
During most of the wave cycle in shallow water, the particle velocity is approximately horizontal and constant over the depth, although at the moment of breaking, there is a significant vertical velocity as water is brought into the crest of the breaker.
The maximum particle velocity under a breaking wave is approximated by the solitary wave theory to be:

$$u_{b\,max} = C = \sqrt{g(H+d)} \qquad (3.3\text{-}3)$$

where H + d = distance measured from the crest of the breaker to the bottom

Fluid motions at breaking cause most of the sediment transport in the littoral zone. The bottom velocities and turbulence at breaking stir up more bottom sediment in comparison with currents in the surf zone, which are normally characterised by velocities too low to move sediment at rest. The suspended sediment can now be transported in the surf zone.

Onshore-Offshore currents
Water in the nearshore zone is divided by the breaker line into two distinct water masses between which there is only a limited exchange of water.
Some of the mechanisms for the exchange are the mass transport velocity in shoaling waves, the wind-induced surface drift, the wave-induced set-up, the currents induced by irregularities on the bottom, the rip currents and the density currents.

The resulting flows are significantly influenced by, and act on, the hydrography of the surf and nearshore zones.

Wind and wave induced water drift, pressure gradients at the bottom due to set-up, density differences due to suspended sediment and temperature and other mechanisms produce patterns of motion in the surf zone that require continued observation to detect.
Diffuse return flows can be visible in aerial photos as fronts of turbid water moving seaward from the surf zone.

Rip currents are the mechanism most noticeable of the exchange between offshore and the surf zone. Rip currents are concentrated jets that carry water seaward through the breaker zone. When long, high waves produce wave set-up on the beach, the resulting rip currents are more intense. In addition to rip currents, there are other localised currents directed seaward from the shore. Some are due to concentrated flows down gullies in the beach face, and others can be attributed to the interaction of waves and edge wave phenomena.

The Longshore current
The longshore current flows parallel to the shoreline and is limited mainly between the zone of the breaking waves and the shoreline. Most longshore currents are generated by the longshore component of motion in waves obliquely approaching the coast.
The situation analysed in the report is characterised by waves perpendicularly approaching the coast. Due to the tips of the submerged breakwaters the waves diffract causing a variation in the direction of propagation. However, it is observed that the order of magnitude of the diffraction is small and consequently the longshore component of the resulting motion is small as well. Besides, in literature, diffraction is hardly mentioned concerning the effects of a submerged breakwater.
In case of a non-uniform coast, additional driving forces are generated due to the variations in wave conditions and wave set-up. The presence of submerged breakwaters will also cause additional wave height and direction changes. In the previous section the wave set-up has been examined. The water level variation with respect to the still water level (h') was found to be dependent on the wave height H and in general it is also dependent on the angle φ for oblique approaching waves. If the wave height and the angle vary along the coast, due for instance to the presence of obstacles, like submerged breakwaters, the wave set-up and the wave set-down consequently vary, resulting in a slope of the average water level along the coast ($\partial h'/\partial y$, where y is the direction of the axis parallel to the shoreline). The resultant water surface slope will supply an additional driving force for the longshore current computations.
A further additional contribution follows from a gradient in the normal stress acting on a plane perpendicular to the shoreline (S_{yy}). The additional driving force will be proportional to $\partial S_{yy}/\partial y$ which is dependent on both $\partial\varphi/\partial y$ and $\partial H/\partial y$.
In case of a non-uniform coast, the nearshore current system, consisting of longshore currents, onshore and off-shore directed currents (rip currents), can be determined by the continuity equations and motion equation, including the wave-induced

components related to mass flux and to momentum flux. The interaction between the waves and the current often is neglected.

3.4 On the submerged breakwater

In a coastal area where tide excursions are limited, submerged breakwaters can be used to protect the beaches from the strong eroding wave action.
Submerged breakwaters are statically stable structures characterised by the crest usually below low-tide levels. They are generally shore-parallel and built nearshore, where bottom induced changes occur in wave parameters.
The main purpose of these structures is to reduce the offshore sediment movement. However, they can also interrupt the onshore movement caused by 'beach building' waves. They are also used to protect and stabilise beach nourishment works. A submerged breakwater allows better water exchange between the inner and outer zones of it reducing the waterlogging area compared to the emerging breakwater's.
In the presence of a submerged breakwater the hydrodynamics and the morphodynamics change remarkably. Wave heights are reduced passing over the structure as well as the wave velocities, but the effects on waves are relatively small compared with the reduction caused by emerged breakwaters.
Laboratory experiments performed in a wave flume, show that the submerged breakwater is an excellent holding tool for the sand contained in the surf zone (Chiaia (1992)), although they did not reduce the retreat of the shoreline. Nevertheless, the wave eroding action on the emerged beach is notably attenuated.
The submerged breakwater's net effect on onshore-offshore transport processes has not been quantitatively established. Consequently, it is not known whether the submerged breakwater's overall effect is beneficial or harmful (U.S. Army Corps of Engineers (1994)).
With reference to Figure 3.4-1, the following parameters are the most commonly used in submerged breakwaters' studies: the crest width B, the crest height of the structure h_c, the water depth h in front of the breakwater, the freeboard R_c, which is defined as the difference h_c - h, the nominal diameter of armour layer stones, the incident wave height H_i, the reflected wave height H_r and the transmitted wave height H_t. An important coefficient to be taken into account when discussing transmission energy is the transmission coefficient K_t, defined as the ratio between the transmitted wave height and the incident wave height ($K_t = H_t/H_i$). Moreover, also the reflection coefficient must be considered, which reads as the ratio between the reflected wave height and the incident wave height ($K_r = H_r/H_i$).
Dissipation of energy in the presence of submerged breakwaters depends on many factors as the crest width, the freeboard, the ratio of breakwater length to gap width, the permeability of the structures.
Waves approaching the coast increase due to the wave shoaling phenomenon. Waves are affected by the bottom when the water depth becomes less than approximately half the wave length. At a certain water depth the wave height or the wave steepness becomes so large that the wave breaks, causing wave energy dissipation. Submerged breakwaters force breaking of incoming waves and dissipate effectively the wave energy.
Hattori and Sakai (1994) highlight the influence of the return flow over the crest upon the incoming waves. Permeability of the structure plays an important role in reduction

of the strength of this return flow yielding changes in the breaker height and breaking position as well as the breaker type.
Large scale vortices are generated by the breaking waves (Petti et al. (1994)). These vortices play an important role in sediment transport since sediment particles can be trapped in them thereby loosing their normal settling rate.
Dean et al. (1995) pointed out that the crest height and the offshore distance of the submerged breakwaters are two important aspects in the design of the structure. If the crest height is too low, so much water is allowed to flow over the breakwater that resulting longshore current flows will outweigh the benefit of a small reduction in wave height and cause beach erosion landward of the breakwater. Moreover, the longshore currents are inversely proportional to the offshore distance of the structure.

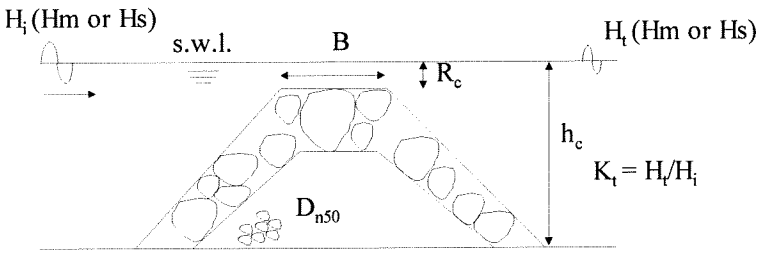

Figure 3.4-1 Governing variables related to wave transmission

Set-up behind submerged permeable breakwaters
For a deeply submerged breakwater, where no energy dissipation is considered, an analytical first order solution of set-up has been given by Longuet-Higgins (1967). Considering the conservation of vertical momentum flux above the still water level, it yields:

$$P = \frac{H_I^2 k_1}{8 \sinh 2k_1 D_1} - \frac{H_T^2 k_2}{8 \sinh 2k_2 D_2} \qquad (3.4\text{-}1)$$

where
P = set-up behind the submerged breakwater
H^2_I = sum of the square of the incident and reflected wave heights
H_T = transmitted wave height
k = wave number
D = water depth

The numerical subscripts denote parameters before (1) and behind (2) the submerged breakwater.
A simple derivation of P utilises the set-down of the mean water level $\underline{\eta}$, attendant with the shoaling of the water waves:

$$\underline{\eta} = \frac{H^2 k}{8 \sinh 2kD} \qquad (3.4\text{-}2)$$

At a breakwater, the set-down due to the incident and reflected waves is necessarily different from the set-down behind the structure due to the transmitted waves, since the wave heights and the water depth will not be the same. The difference in the two set-downs is the set-up P.

Dalrymple and Dean (1971) have shown that the increased water level can be predicted reasonably well considering the momentum flux and the mass transport over the breakwater. For the set-up on a submerged breakwater on which the waves are breaking, two contributions to the total pile-up must be considered: the momentum flux contribution and the continuity pile-up, caused by the wave-induced overtopping flow of water and return flow over and through the breakwater.

Circulation and modified currents

If the breakwater crest is low enough to allow overtopping, water carried over the breakwater will raise the water level behind it, causing flow around the breakwater. In the case of multiple breakwaters, overtopping generates a net seaward flow of water through the gaps.

Seelig and Walton (1980) developed a simple theory in the case of segmented submerged breakwaters. Water is transported over the structure until either a gap or the breakwater ends are reached. Then the impounded water is released to the offshore region. According to Seelig and Walton's approach it is possible to estimate the strength of the seaward flowing currents.

To reduce return currents the crest elevation may be raised, the gaps between the segments may be enlarged or the permeability of the structure may be increased.

Laboratory experiments with segmented submerged breakwaters pointed out the importance of the ratio between the breakwater length and the gap width upon the wave transmission and sediment transport (Sawaragi (1992)).

A strong return flux through the breakwater gap develops which carries sediment offshore and reduces the sand level behind the structure.

Effect on longshore transport

The effect of submerged breakwaters on longshore sediment transport is in general smaller than the emerging breakwaters'. The efficiency depends on the angle under which waves approach the structures. In cases of a small breaking wave angle, the presence of submerged breakwaters effect rather significantly the longshore sediment transport.

4. RESULTS OF THE WAVE SET-UP MEASUREMENTS

4.1 General introduction

In this chapter the measurements of the average water level carried out from the laboratory experiments are discussed.
Section 4.2 briefly describes the program DASY*Lab*, a program designed for data-acquisition and data-processing. It was used to calculate the average water level from the recorded signals during the experiments.
In the other sections, the tests are analysed separately. Only a qualitative analysis is presented. The description of each test is accompanied by a series of plots, which shows the development of the averaged water level. The reader is suggested to consult the appropriate appendix, to better understand the analysis of the results.

4.2 DASY*Lab*

4.2.1 Introduction

The output signal made by the wave probes was more or less in the form of a sine because regular waves were generated during every experiment. It was necessary to average this raw signal to be able to analyse the development of the wave set-up in space and in time. In order to do this, use was made of a program called DASY*Lab*.
Each position was measured for more than ten times. The three minutes recordings were gathered in several files by DASY*Lab* and could also be reproduced or replayed in the computer program itself.
DASY*Lab* is a data acquisition, process control, and analysis system. In spite of its complexity and high performance, DASY*Lab* can be used easily. A measuring, process control, or a simulating task can be set up directly on a PC screen by selecting and connecting modular elements. Several module functions are provided by DASY*Lab*. To assess the average water level use was made of a sequence of mathematical functions, which will be briefly explained in the following.

4.2.2 The program

The average water level is determined by means of the cumulative timely average of the signal recorded during the test. In Figure 4.2.2-1 a DASYLab worksheet shows the sequence of the modules used.

- Read Data: this module represents the operation of reading the files which contain the output signals of the wave probes.
- Raw signal: the output signal before any operation is shown on a graph for each wave probe.
- Scaling: due to the small order of magnitude of the wave set-up it was necessary to change the scale of the output signal from cm into mm. This result was obtained by simply multiplying the raw signal by 10.
- Average: this module calculate the cumulative average of the raw signal over a fixed number of samples, determining the average water level.

- Probe07, Probe08, Probe09, Probe011, Probe012, Probe013: the results of the cumulative averages are written in different files referring to the different wave probes. In this way it was possible to know which wave probes the average water level refers to.

The other modules represent specific operations performed in order to comply the program requirements, therefore they are not dealt with in this occasion.
For further detail, reference is made to the DASY*Lab* manual.

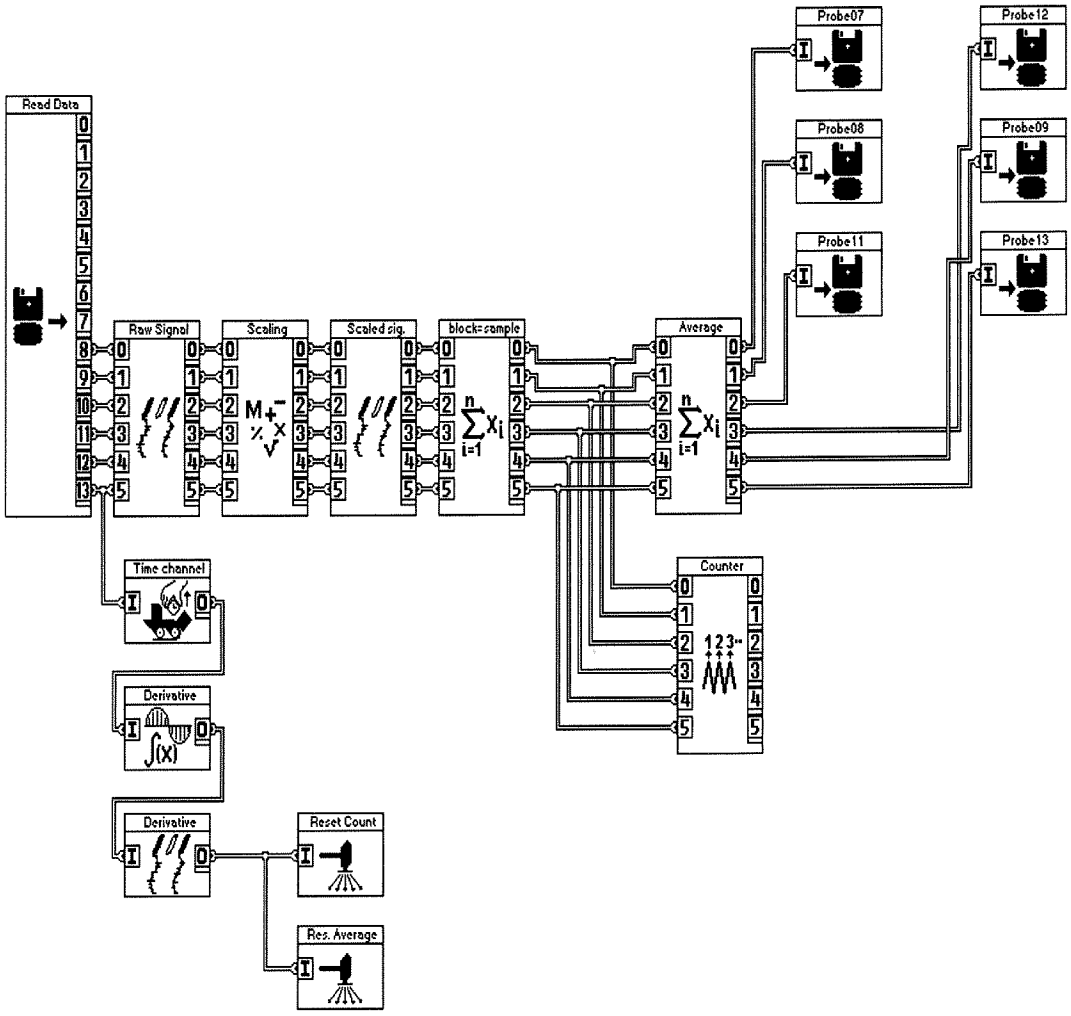

Figure 4.2.2-1 DASY*Lab worksheet*

4.3 Results

4.3.1 Introduction

Towards the breaker line and in the surf zone, the average water level varies due to the gradient in the radiation stress.
Higher waves are more affected by the submerged breakwater, whereas small waves pass unhindered. Therefore, in the case of waves high enough to sense the presence of the structure, a longshore variation in the pattern of the wave set-up could be observed between the zone landward of the breakwater and the zone in line with the gap. This

average water level gradient constituted a positive contribution to the longshore current.
The different cross-sections were measured in order to point out the influence of the submerged breakwaters on the wave heights and consequently on the average water level.
Since the bottom profile varies during the experiments as a consequence of the sediment transport, the average water level did not stay constant. Therefore, attention was paid to the variation of the values in every cross-section.
For each test, the still water level is equal to 570 mm at the wave generator.
Some measurements were visually out of range and they have been neglected in further analyses. Probably in those cases, the vertical position of the measurement equipment had been changed after calibration.
No measurements were carried out between the shoreline and y = 4.86 m (see Figure 2.2-4), hence no evolution of the average water level in this part of the basin is available. Each cross-section is handled separately if clear differences in the average water level between them are found.

4.3.2 TEST A - without submerged breakwaters

Layout

Measured cross-sections: x = 3 m, 6.5 m, 12.5 m, 20 m, 24.5 m.
Figure 4.3.2-1 shows the basin and the measured cross-sections (dotted lines).

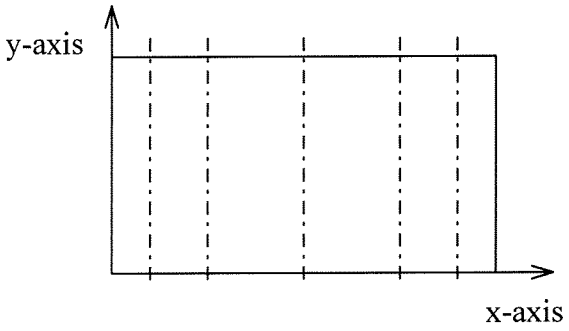

Figure 4.3.2-1 Layout Test A

TEST A1, H = 0.08 m
Graphics: Appendix A1, from A1-1 to A-15
Interval 00:00 - 07:30

Since there are not submerged breakwaters, every cross-section shows the same average water level development.
The regular waves break always at the same line, causing a trough in the bottom profile around y = 4 m, which is more landwards than the last measured position. Therefore, it is not possible to analyse the wave set-up.
The wave height in this test is small in comparison to the water depth, consequently the bottom profile has not undergone many changes during the whole experiment. As a consequence of this, the average water level shows almost the same behaviour during the 7.5 hours of wave action (test duration).
During the whole experiment, the order of magnitude of the wave set-down is approximately 4 mm for each cross-section.

TEST A2, H = 0.10 m
Graphics: Appendix A2
Interval 00:00 - 00:30
Cross-section x = 3 m
Graphic: A2-1.
The bottom profile has hardly changed after half an hour and the average water level presents a set-down towards the breaker line, around y = 4.3 m, of approximately 4 mm.

Interval 00:30 - 01:30
Cross-sections x = 6.5 m, 12.5 m, 20 m, 24.5 m
Graphic: from A2-2 to A2-5.
The wave height is bigger than the previous experiment (A1, H = 0.08 m) and the bottom profile is clearly influenced at the end of the second interval. A pronounced trough is developed around y = 4.5 m and the average water level shows a set-down towards the breaker line located around y = 5.5 m. The order of magnitude of the set-down is about 6 mm for every cross-section, apart from cross-section x = 6.5 m (Graphic A2-2). In this cross-section, the pattern of the average water level seems to be uniformly shifted upwards, probably due to a variation in the vertical position of the measurement equipment after calibration. Landwards of the breaker line, the beginning of the wave set-up can be seen.

Interval 01:30 - 03:30
Graphics: from A2-6 to A2-10.
During this interval, the bottom profile does not show many changes in the whole basin. The trough appears to be less pronounced and the bar is increased, causing the beginning of the wave set-up more seaward.

Interval 03:30 - 07:30
Cross-sections x = 3 m, 6.5 m
Graphics: A2-11, A2-12.
A wave set-down of approximately 4 mm develops towards the breaker line around y = 6 m. However, compared with the other cross-sections, it seems that the mean water level pattern is shifted uniformly upwards. An explanation for this might be the influence of the side of the basin on the wave field.

Cross-sections x = 12.5 m, 20 m, 24.5 m
Graphics: form A2-13 to A2-15.
During this interval, according to the changed bottom profile, which shows a more pronounced bar, the wave set-up is more evident. The order of magnitude of the wave set-down is about 6 mm for every cross-section.

TEST A3, H = 0.12 m
Graphics: Appendix A3
Interval 00:00 - 00:30
Cross-section x = 3 m
Graphic: A3-1.
Half an hour after the start of the experiment, the bottom profile already presents a marked trough around y = 4.5 m. The average water level shows a set-down, towards this point, of approximately 5 mm.

Interval 00:30 - 01:30
Graphics: from A3-2 to A3-5.
During this interval, the development of the bottom profile is almost the same for each cross-section. Consequently, the pattern of the average water level in the whole basin does not change in the whole basin. The average water level decreases towards the trough, positioned around y = 4.5 m. The wave set-down is of approximately 5 mm.
Considering the development in time of the average water level at the position y = 5.76 m (shorewards, next to the last one), for every cross-section a constant increase can be seen, which might be due to a downwards shift of the measurement equipment during the experiment.

Interval 01:30 - 03:30
Graphics: from A3-6 to A3-10.
The bottom profile has undergone small changes compared to the previous interval. The bar, which has become more pronounced induces breaking more seawards and the beginning of the wave set-up can be seen around y = 5.7 m.

Interval 03:30 - 07:30
Graphics: from A3-11 to A3-15.
In the last 4 hours, the bottom profile has been changing quite significantly. At the end of the 7.5 hours of the experiment it can be noticed that the bar is increased and stretched more seaward. Due to this change, the waves break sooner and the average water level starts rising around y = 6.6 m instead of y = 5.7 m of the previous interval. The order of magnitude of the wave set-down is approximately 50 mm, which is clearly too big. Probably in this case, the vertical position of the wave probes changed after calibration.

4.3.3 TEST C - two submerged breakwaters

Layout
Two submerged breakwaters of 12 m and 6 m each, with a gap of 3 m in between.
Measured cross-sections:

x = 3 m	in the gap between the right side of the basin and the longer breakwater
x = 6.5 m	in the left corner of the longer breakwater
x = 12.5 m	behind the middle of the longer breakwater
x = 20 m	in the middle of the gap between the two breakwaters
x = 24.5 m	behind the middle of the shorter breakwater.

Figure 4.3.3-1 shows the basin, the submerged breakwaters and the measured cross-sections (dotted lines).

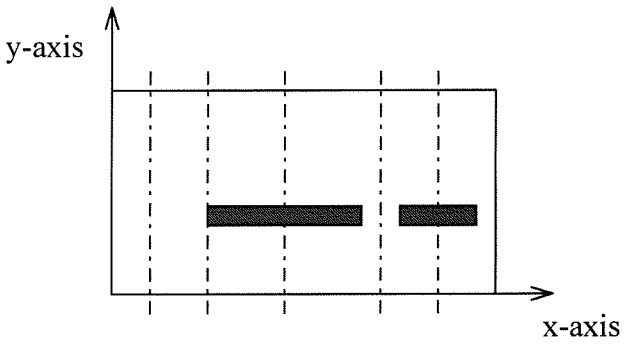

Figure 4.3.3-1 Layout Test C

TEST C1, H = 0.08 m
Graphics: Appendix B1
Interval 00:00 - 00:30
Cross-section x = 3 m
Graphic: B1-1.
The bottom profile hardly changes after the first half hour of the experiment. Approaching the coast, the average water level shows a wave set-down of approximately 4 mm.

Interval 00:30 - 01:30
Graphics: from B1-2 to B1-6.
Due to the small wave height compared to the water depth, the presence of the submerged breakwaters seems not to have much influence on the wave field. However, a slight set-up can be seen in line with the crest of the submerged breakwaters (graphics B1-4 and B1-6). Then, the average water level shows a wave set-down towards the shore line of approximately 2 mm.
The cross-section x = 6.5 m (graphic B1-3), is probably influenced by the large gap and shows a constant wave set-down towards the breaker line of approximately 2 mm.
In the cross-section x = 3 m (graphic B1-2), without submerged breakwaters, a wave set-down towards the breaker line, located around y = 5.5 m, can be seen. Also in this case, the order of magnitude is approximately 2 mm. The cross-section x = 20 m (graphic B1-5) shows a bigger wave set-down (about 4 mm). In the cross-section (x = 3 m), the strong return current, flowing through the gap, probably influences the incoming waves.

Interval 01:30 - 03:30
Cross-sections x = 3 m, 20 m
Graphics: B1-7, B1-10.
In the cross-section x = 3 m (graphic B1-7), at the end of the third interval, a large amount of sediment has been transported seaward by the action of the waves, causing a pronounced bar that influences the average water level. The wave set-up begins around y = 5.7 m.
After 3.5 hours of wave action, the bottom profile presents hardly any changes in the cross-section x = 20 m (graphic B1-10). The behaviour of the average water level is,

however, different in comparison to the situation in the previous interval. An early wave set-up around y = 5.7 m can be seen in the last time series, probably due to the increase of the return flow during the third interval.
In the cross-sections x = 3 m, the order of magnitude of the wave set-down is approximately 2 mm, while in the other (x = 20 m) the wave set-down is bigger (about 5 mm).

Cross-sections x = 6.5 m, 12.5 m, 24.5 m
Graphics: B1-8, B1-9, B1-11.
The bottom profile does not change much from the situation of the previous interval.
The cross-section x = 12.5 m (situated behind the middle of the larger breakwater, graphic B1-9) presents more irregularities than the other cross-sections. This pattern is probably due to the strong longshore current behind the longer breakwater, which develops even with a small wave height. The average water level presents a gentle set-up landwards of the submerged breakwater followed by a steep set-down approaching the breaker line. The cross-section x = 24.5 m (graphics B1-11), behind the smaller breakwater, has also a rather irregular bottom profile and the average water level shows the same behaviour.
The cross-section x = 6.5 m (graphic B1-8) presents a linear wave set-down which starts seawards of the submerged breakwater and extends towards the breaker line around y = 4 m. This cross-section is located at the tip of the structure and it is influenced by the larger gap.
The wave set-down for every cross-section is approximately 4 mm.

Interval 03:30 - 07:30
Cross-sections x = 3 m, 20 m
Graphics: B1-12, B1-15.
The bottom profile presents an increase of the bar due to the sediment transport in the longshore direction from behind the two breakwaters. At the end of the last interval, the water depth seaward of the bar decreases due to a downslope translation of the bar and consequently the wave set-up starts more seaward, around y = 6.6 m. The pattern of the average water level is approximately the same for both cross-sections. The order of magnitude of the wave set-down is smaller for the cross-section in line with the larger gap (about 3 mm) (graphic B1-12), than for the other (approximately 5 mm). An explanation for this might be the stronger return current in the larger gap (x = 3 m), influencing the incoming waves.
Comparing the mean water level development in the case with and without submerged breakwaters (graphics A1-11 and A1-14), some differences can be highlighted. Without breakwaters, during the whole experiment, only a wave set-down was measured, which means that dissipation occurs only closer to the shoreline than the last measurement location. On the contrary, with breakwaters, breaking occurs also at a greater distance from the shoreline, because of smaller water depth in the gaps. Therefore, when waves finally break on the shore, less energy is dissipated with a beneficial effect on the shoreline. Nevertheless, it seems that the retreat of the shoreline is not smaller in the case with submerged breakwaters, probably due to the great amount of sediment transported in cross-shore direction by the return current flowing through the gaps.

Cross-sections x = 6.5 m, 12.5 m, 24.5 m
Graphics: B1-13, B1-14, B1-16.
Hardly any changes are visible in the bottom profile, apart from the cross-section x = 12.5 m (graphic B1-14) where it appears that a considerable amount of sediment is transported in longshore direction towards the gaps. Therefore, the overall behaviour of the average water level does not change from the former interval, apart from cross-section x = 12.5 m. Here, the wave set-up is more pronounced behind the submerged breakwater, followed by a steep wave set-down of about 4 mm.
During the whole experiment, a longshore gradient, sloping down from the middle of the submerged breakwaters towards the gaps, can be seen. At the left side of the basin, due to the larger gap, this gradient is smaller than at the right side. At the beginning of the test, the difference is more pronounced than after 7.5 hours, in agreement with the development of the bottom profile.

TEST C2, H = 0.10 m
Graphics: Appendix B2
Interval 00:00 - 00:30
Cross-section x = 3 m
Graphic: B2-1.
After half an hour the bottom profile did not change remarkably.
The average water level shows a wave set-down of approximately 3 mm towards the breaker line, around y = 4.5 m.
The measurement at y = 6.66 m (the second position shorewards), seems to be unreliable.

Interval 00:30 - 01:30
Cross-sections x = 6.5 m, 12.5 m, 24.5 m
Graphics: B2-2, B2-3, B2-5.
At the end of the second interval, the cross-section x = 6.5 m (graphic B2-2) has a pronounced trough around y = 4 m. Passing over the crest of the submerged breakwater, the mean water level rises, followed by a wave set-down, starting around y = 6.6 m. The order of magnitude of the wave set-down is approximately 4 mm.
The other cross-sections present a less marked trough situated more landward and a wave set-down starting around y = 5.7 m. The difference in the average water level between the two sides of the submerged breakwater is for every cross-section about 3 mm.

Cross-sections x = 20 m
Graphic: B2-4.
This cross-section, in line with the smaller gap, has a deep trough around y = 4 m and an early wave set-up can be seen, followed by a wave set-down towards the breaker line. The order of magnitude of the set-down is approximately 5 mm.
The same cross-section, in the situation without submerged breakwaters (graphic A2-4), shows a more pronounced bar, which induces breaking more seawards. After 1.5 hours, the reduced wave energy, due to the presence of the submerged breakwaters, seems to have a beneficial effect on the sediment transport in cross-shore direction, which appears to be less than in the case without submerged breakwaters. However, this situation inverts after 3.5 hours of simulated wave action.

Interval 01:30 - 03:30

Cross-section x = 3 m

Graphic: B2-6.

After 3.5 hours, the pattern of the bottom in the larger gap shows a characteristic ogee-shape. At the beginning of the interval, the average water level starts rising rather seaward, around y = 5.7 m, while at the end of the 3.5 hours, only a wave set-down, of approximately 6 mm, can be seen. Compared with the cross-sections analysed in the previous interval, the wave set-up is more gentle.

In the case without submerged breakwater (graphic A2-6), only a wave set-down can be seen and less amount of sediment is transported seawards. The strong return current which develops through the larger gap, seems to have a damaging effect on the shoreline.

Cross-sections x = 6.5 m, 12.5 m, 24.5 m

Graphic: B2-7, B2-8, B2-10.

The bottom profile has not undergone many changes and the pattern of the average water level remains almost the same as the previous interval. The order of magnitude of the wave set-down (about 2 mm) is smaller than the previous interval. In this case, it seems that the measured positions shifted uniformly downwards after calibration.

Cross-section x = 20 m

Graphic: B2-9.

At the end of the interval, a pronounced trough can be noticed around y = 4 m. This is probably due to the strong return current which flows back through the gaps. The sediment, brought in suspension by breaking, is transported seawards.

The last time series presents a wave set-up starting around y = 5.7 m, according to the changed bottom profile. Also in this case, the wave set-up is more gentle compared to the cross-sections in line with the submerged breakwaters.

In the situation without submerged breakwaters, the bottom profile does not show a trough close to the shoreline (graphic A2-9). The presence of the submerged breakwater influences the behaviour of the average water level in the gap.

Interval 03:30 - 07:30

Cross-section x = 3 m

Graphic: B2-11.

At the end of the last interval, the bar is shifted more seaward and the average water level starts rising around y = 6.6 m. The wave set-down is approximately 3 mm.

This situation is rather similar to the situation without submerged breakwater, although it is the results of different processes. The influence of the structures on the larger gap seems to weaken during the experiments.

Cross-section x = 6.5 m, 24.5 m

Graphic: B2-12, B2-15.

The bottom profile hardly changes from the situation in the former interval.

Consequently, the pattern of the average water level shows the same behaviour and also the wave set-down is of the same order of magnitude.

Cross-section x = 12.5 m
Graphic: B2-13.
A considerable amount of sediment has disappeared, transported in longshore direction towards the gaps. The average water level rises landward of the submerged breakwater and decreases towards the breaker line in the same position as the previous interval. The entire shape shifts downward in accordance with the downward shift of the profile. The order of magnitude of the wave set-down (approximately 2 mm) does not increase much, compared to the previous interval.

Cross-section x = 20 m
Graphic: B2-14.
The trough has almost disappeared and an amount of sediment is settled seaward, which has been transported towards the gap from behind the two submerged breakwaters.
The seaward settlement of sediment causes a seaward shift of the start of the wave set-up, towards a position around y = 6.6 m.
During the last interval, the differences between the situation with and without submerged breakwaters (graphic A2-14) become less noticeable. However, the sediment transported is greater in the case with submerged breakwaters and the retreat of the shoreline is larger.

Summarising, during the whole experiment, a longshore gradient in the mean water level, sloping down towards the gaps, can be seen. In agreement with the development of the bottom profile, the longshore differences in the average water level between the gap and the submerged breakwaters become less pronounced during the last interval.

TEST C3, H = 0.12 m
Graphics: Appendix B3
Interval 00:00 - 00:30
Cross-section x = 3 m
Graphic: B3-1.
Already after half an hour a rather considerable amount of sediment is transported seaward, causing a pronounced bar. Following the development of the bottom profile, the first time series show a wave set-down (approximately 2 mm) towards the breaker line, situated more landward than the last measured position, which is at y = 4.86 m.
The average water level seems not to be influenced by the submerged breakwater (large gap).
The last time series present a wave set-up already at y = 6 m, where the waves start breaking. In this case, the wave set-down is about 3 mm.

Interval 00:30 - 01:30
Cross-section x = 6.5 m
Graphic: B3-2.
This cross-section is situated at the tip of the longer submerged breakwater. Due to the strong longshore current which develops behind the breakwater towards the gaps, the bottom profile presents more irregularities than the profile of the cross-section situated in the middle of the breakwater.

After half an hour of wave action, the wave set-down still appears landward of the breakwater, but later the average water level shows only a linear wave set-up, approaching the shoreline.

Cross-sections x = 12.5 m, 24.5 m
Graphics: B3-3, B3-5.
The waves start breaking on the top of the breakwaters and keep on breaking approaching the coast. Due to the development of the waves the average water level begins rising in front of the breakwater towards the shore line. The gradient in the mean water over the longer submerged breakwater (graphic B3-3) is bigger (approximately 8 mm), than over the shorter breakwater (graphic B3-5), where it is approximately 4 mm. This is probably due to the return current which flows back through the gap, influencing the wave field at the tip of the submerged breakwater (x = 24.5).

Cross-section x = 20 m
Graphic: B3-4.
At the end of the second interval, the bottom profile presents the characteristic ogee-profile shifted seaward.
The average water level shows a set-down (about 5 mm) approaching the breaker line, around y = 5.7 m and a wave set-up landward. More seawards, the average water level is influenced by the submerged breakwater.

Interval 01:30 - 03:30
Cross-section x = 3 m
Graphic: B3-6.
During this interval, the bottom profile has not been changing much. It can be noticed that the average water level starts rising around y = 6.6 m, in line with the bar in the bottom profile. The order of magnitude of the wave set-up is approximately 8 mm. The wave set-down is about 5 mm.

Cross-section x = 6.5 m
Graphic: B3-7.
The bottom profile does not change much, apart from the increased sediment settled close to the submerged breakwater. The average water level presents an early wave set-up followed by a short set-down, finishing with a wave set-up approaching the shoreline. This pattern can be explained by the fact that the waves start breaking over the crest of the breakwater, stop breaking landwards of it, due to the water depth which is still high and they start breaking again when the water depth becomes shallower.

Cross-sections x = 12.5 m, 24.5 m
Graphics: B3-8, B3-10.
After 3.5 hours hardly any changes in the bottom profile can be seen. The average water level shows an early, rather steep wave set-up around the breakwater, followed by a wave set-up with a smaller gradient.

Cross-section x = 20 m
Graphic: B3-9.
The bottom profile has not undergone many changes and the behaviour of the average water level presents the same pattern as the former interval. The order of magnitude of the wave set-down does not change either.

Interval 03:30 - 07:30
During this interval, the measurement equipment probably moved downwards. Therefore, the pattern of the average water level, compared to the previous interval, appears to be shifted upwards.
Cross-section x = 3 m
Graphic: B3-11.
A considerable amount of sediment has been transported partly towards the left side wall of the basin (facing the wave generator) and partly seawards, causing the increase of the bar. According to the changes in the bottom profile, the wave set-up is shifted from y = 6.6 m more landward, towards a position around y = 5.7 m. The order of magnitude of the wave set-down does not change much during the interval, remaining approximately 5 mm.
During the whole experiment, in this cross-section, the average water level shows the same behaviour as in the situation without submerged breakwaters (graphics A3-1, A3-6, A3-11). Nevertheless, the amount of sediment transported seawards, in the latter case, is smaller than in the situation with breakwaters. With submerged breakwaters, the retreat of the shoreline is much larger, due to the strong return current flowing through the gap.

Cross-section x = 6.5 m
Graphic: B3-12.
A retreat of the shoreline can be noticed, caused by the longshore and cross-shore sediment transport. The pattern of the mean water level is almost the same as the one of the previous interval.

Cross-section x = 12.5 m
Graphic: B3-13.
Comparing the bottom profile at the end of 3.5 hours to the one at the end of 7.5 hours of wave action, shows that a considerable amount of sediment has been transported in the longshore direction. The wave set-up becomes less steep at the end of the interval, due to the deeper water depth.

Cross-section x = 20 m
Graphic: B3-14.
The bottom profile has been changing considerably during the last interval and at the end of 7.5 hours, it can be noticed that the pronounced trough has almost disappeared. After 6 hours of experiment, the breaker line is shifted seaward and this causes a wave set-up starting around y = 6.7 m, while at the beginning of the interval the average water level starts rising around y = 5.7 m. The wave set-down is approximately 2 mm.
The comparison between this situation and the situation without submerged breakwaters shows the same behaviour of the average water level, although the retreat of the shoreline is much more pronounced in this case.

Cross-section x = 24.5 m
Graphic: B3-15.
A retreat of the shoreline, together with a sediment transport in cross-shore direction, can be seen. Due to the generation of a bar, the average water level shows a set-up starting before the breaker line which keeps on rising towards the shoreline.

For each interval, a longshore gradient in the average water level, sloping down from the middle of the submerged breakwaters towards the gaps, can be seen. At the left side of the basin, due to the less influence of the submerged breakwater in the middle of the larger gap, this gradient is steeper than in the right side. During the experiment, in agreement with the changed bottom profile, the longshore differences in the mean water level become less pronounced.
With respect to the previous experiments (C2), the same pattern of the average water level shifted upwards can be seen, due to the higher wave height.

From the comparison between the situation with and without submerged breakwaters it results that the effects of the structures are not beneficial, since a greater amount of sediment is brought from the shoreline into the basin.

4.3.4 TEST D - three submerged breakwaters

Layout

Three submerged breakwaters of 6 m each with gaps of 3 m.
Measured Cross-sections:

x = 12.5 m		in the left corner of the centre submerged breakwater
x = 14 m		behind the centre submerged breakwater
x = 15.5 m		behind the middle of the centre submerged breakwater
x = 17 m		behind the centre submerged breakwater
x = 18.5 m		in the right corner of the centre submerged breakwater
x = 20 m		in the gap

Figure 4.3.4-1 shows the layout of the basin, the submerged breakwaters and the measured cross-sections (dotted lines).

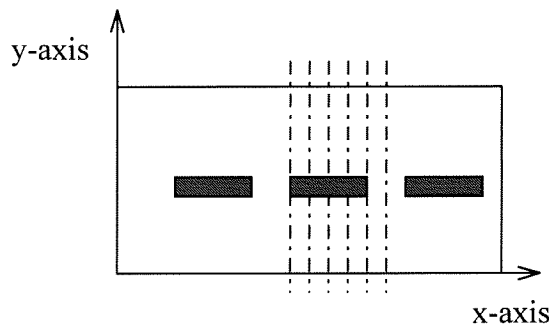

Figure 4.3.4-1 Layout Test D

TEST D1, H = 0.08 m
Graphics: Appendix C1
Interval 00:00 - 00:30
Cross-section x = 12.5 m
Graphic: C1-1.
The wave height is too small to cause clear changes in the bottom profile only after half an hour of wave action. The average water level shows that the breakwater is not 'felt' by the waves which pass over it unaltered. Because of probe locations, only a wave set-down towards the breaker line can be seen. Its order of magnitude is approximately 5 mm.

Interval 00:30 - 03:30
Graphics: from C1-2 to C1-6.
The behaviour is approximately the same for each cross-section. The bottom profile hardly changes. A little amount of sediment is transported seaward. The pattern of the average water level shows a clear set-down towards the breaker line. For the cross-sections in line with the submerged breakwaters (graphics from C1-2 to C1-5), the order of magnitude of the wave set-down is approximately 3 mm. In the cross-section in line with the gap (graphic C1-6), the wave set-down is around 4 mm.
Hardly any changes in the average water level in longshore direction are noticeable.

Interval 03:30 - 07:30
Graphics: from C1-7 to C1-12.
The pattern of the bottom profile after 7.5 hours of wave action (graphic C1-12), shows that sediment is transported towards the gap. The average water level presents no changes during the whole experiment, due to the small height of the waves.
In the cross-section x = 20 m (graphic C1-12), located in the gap, the wave set-up during the last interval is shifted more seaward. This behaviour is due to formation in the gap of a bar, caused by the sediment transport in longshore direction, from behind the breakwaters towards the cross-section x = 20 m. In the other cross-sections, only the wave set-down of approximately 4 mm can be seen. The measurements position more seawards probably shifted upwards after calibration.
As a consequence of the different average water level in the cross-sections in line with the gap (x = 20 m) and over the submerged breakwater, a longshore gradient, decreasing from the submerged breakwaters to the gap, can be observed.
Comparing the development in time of the average water level in the cross-section x = 20 m, for the situation with and without submerged breakwaters (graphic A1-4, A1-9, A1-14), shows hardly any differences.
The presence of the submerged breakwater does not have much influence on the wave field, due to the small wave height.

TEST D2, H = 0.10 m
Graphics: Appendix C2
Interval 00:00 - 03:30
Graphics: from C2-1 to C2-12.
Since the wave is high enough to be modified by the submerged breakwater, breaking occurs passing over the structure and consequently the average water level starts rising.

The wave set-up is followed by a set-down leading to the breaker line, located around y = 4 m. The waves do not immediately react to the presence of the submerged breakwaters, but a time-lag can be seen. The wave set-up seems to be shifted landwards compared to the crest of the submerged breakwater. This behaviour is similar for every cross-section.
In the cross-section in line with a gap (graphic C2-6 and C2-12), the pattern of the average water level seems to be influenced by the presence of the submerged breakwater, showing a slight set-up.
A small longshore gradient in the average water level, decreasing from the middle of the submerged breakwaters towards the gap, can be observed.

Interval 03:30 - 07:30
Cross-sections x = 12.5 m, 14 m, 15.5 m, 17 m, 18.5 m
Graphics: from C13- to C2-18.
During this interval the bottom profile has undergone some changes. A loss of sediment can be seen in each cross-section.
Due to the changes in the bottom profile, the wave set-up has been shifting seaward. At the end of 7.5 hours, a linear set-up can be noticed, starting before the breakwaters towards the shoreline.

Cross-section x = 20 m
Graphic: C2-7.
This cross-section is situated in the middle of the gap. During this interval, the bottom profile has been changing, due to the interaction between sediment transported in cross-shore direction and the amount of sediment transported by the longshore current from behind the breakwaters to the gap.
The simultaneous presence of these two factors leads to a profile which shows a pronounced bar shifted more seaward. According to this, at the end of the last interval, the average water level starts rising more seaward than after 3.5 hours. The wave set-down is approximately 3 mm.
The comparison with the situation without submerged breakwaters (graphics A2-4, A2-9, A2-14), shows rather similar behaviour. Nevertheless, especially after 7.5 hours, it can be seen that the amount of sediment transported seawards is greater in the case with submerged breakwaters.

TEST D3, H = 0.12 m
Graphics: Appendix C3
Interval 00:00 - 00:30
Cross-section x-12.5 m
Graphic: C3-1.
Around the submerged breakwater, the average water level rises, due to the breaking of the waves on the submerged breakwater crest. The wave set-up is followed by a set-down which starts around y = 5.7, since the waves stop breaking in the lee side of the breakwaters. The breaker line is actually more landward.

Interval 00:30 - 01:30
Cross-sections x = 12.5 m, 14 m, 15.5 m, 17 m, 18.5 m
Graphics: from C3-2 to C3-6.

The bottom profile does not change much from one cross-section to another.
The behaviour of the average water level is approximately the same for this section of the basin. Landwards of the breakwater there is a steep set-up followed by a milder slope. This pattern is probably due to the fact that the waves start breaking over the breakwater crest and go on breaking towards the shore line. The different gradient of the slope is probably determined by the sudden change in the bottom profile due to the breakwater.
The difference in the average water level before and after the submerged breakwater is of the same order of magnitude (approximately 6 mm) for each cross-section.

Cross-section x = 20 m
Graphic: C3-7.
The bottom profile presents the characteristic ogee-shape. The waves break first seaward around y = 8 m and then around y = 6.6 m, due to the bar in the bed profile. An early wave set-up can be seen followed by a wave set-down and finally by the wave set-up which leads to the shore line. The order of magnitude of the wave set-down is 2 mm. Comparing this order of magnitude with the previous one (6 mm, for the cross-sections in line with the submerged breakwaters), shows that a longshore gradient in the average water level occurs, sloping down from the middle of the submerged breakwater to the gap. This matches with the pattern of current field, which details a return current flowing back through the gaps and a longshore current developing from behind the middle of the submerged breakwater to the gaps.

Interval 01:30 - 03:30
At the end of the third interval, the bottom profile is different for some cross-sections, due to the sediment transport in longshore direction.

Cross-section 12.5 m
Graphic: C3-8.
This cross-section borders an ending of the breakwater. An amount of sediment is transported towards the gap, as a consequence of the longshore current. The return current, flowing through the gap, causes the development of a bar seaward.
Due to the considerable energy loss, which occurs close to the shoreline, the average water level, right behind the submerged breakwater, decreases rather quickly towards the breaker line, around y = 4.5 m.
The wave set-down is approximately 4 mm.

Cross-sections x = 14 m, 15.5 m, 17 m
Graphics: C3-9, C3-10, C3-11.
These cross-sections are located behind the submerged breakwater and they show almost the same pattern. The bottom profile does not present a pronounced bar and the amount of sediment transported away is not much. The average water level shows a set-up, landwards of the submerged breakwater, which is not so steep as in the previous interval and a set-down towards the breaker line, around y = 4 m. The breaker line is shifted seawards, in agreement with the changes in the bottom profile. The order of magnitude of the set-down is approximately the same (2 mm) for each cross-section.

Cross-section x = 18.5 m
Graphic: C3-12.
This cross-section borders the right corner of a breakwater. The amount of sediment lost during the third interval, at this side of the breakwater, is less than at the left side of the submerged breakwater. This asymmetry in the behaviour is due to the asymmetry in the basin: the distance between the left breakwater and the left side of the basin (facing the wave generator) is 3.5 m, while the distance between the right breakwater and the right side of the basin is only 1.3 m. The longshore current behind the structures is pointed to the left. The bottom profile presents a large bar around y = 5 m. The waves do not break over the bar but landward and according to this, the average water level, after an early wave set-up passing over the breakwater, shows a set-down towards the breaker line. The order of magnitude of the set-down is 6 mm.

Cross-section x = 20 m
Graphic: C3-13.
After 3.5 hours, the bottom profile presents a pronounced trough around y = 5 m and a considerable amount of sediment settled seaward which forms a bar. According to the changed profile, the average water level shows a set-up starting more seaward, around y = 6.6 m.
The wave set-down is approximately 4 mm.

Interval 03:30 - 07:30
Cross-section x-12.5 m
Graphic: C3-14.
This cross-section, which borders the left corner of a submerged breakwater, shows a different bottom profile compared to the other cross-sections over the same submerged breakwater (x = 14 m, 15.5 m, 17 m and 18.5 m). The profile presents many irregularities due to the interaction of the current around the breakwater ending, and the incoming waves. A considerable amount of sediment has settled next to the structure. Due to the development of the bottom profile during the interval, the average water level shows different patterns.
For the first 2.5 hours, the average water level presents a set-up around the crest of the submerged breakwater, followed by a set-down, approximately 5 mm, towards the breaker line.
Later, the breaker line is shifted more seaward because the set-up begins around y = 5.7 m and the set-down is now approximately 3 mm.
At the end of the 7.5 hours, the waves start breaking before the submerged breakwater and keep on breaking towards the shore line. According to this, the average water level presents a linear wave set-up starting around y = 8.5 m. The difference in the average water level from the positions seawards and landwards of the submerged breakwater is approximately 2 mm.

Cross-sections x = 14 m, 15.5 m, 17 m
Graphics: C3-14, C3-15, C3-16.
These cross-sections (in line with the submerged breakwater) present almost the same behaviour of the previous interval. A set-up due to the submerged breakwaters can be seen, followed by a set-down leading to the breaker line around y = 4 m. The order of

magnitude of the wave set-down (approximately 4 mm) is bigger than the one of the previous interval, probably due to the shift of the breaker line more seawards.

Cross-section x = 18.5 m
Graphic: C3-16.
For this cross-section, the last interval does not produce many changes in the bottom profile and the average water level shows almost the same pattern of the former interval. The wave set-up starts around the breakwater followed by the wave set-down approaching the breaker line around y = 4 m. Only the last time series shows a wave set-up starting more seawards.
The order of magnitude of the wave set-down is the same of the previous interval (approximately 6 mm).

Cross-section x = 20 m
Graphic: C3-17.
The bottom profile does not change remarkably. The pattern of the average water level and the order of magnitude are almost the same as the ones of the former interval.
Comparing the development in time of the average water level in this cross-section, for the situation with and without submerged breakwaters (graphics A3-4, A3-9, A3-14), shows rather similar behaviour. The wave set-up starts almost at the same position, but the order of magnitude is smaller with submerged breakwaters. After 7.5 of wave action, indeed, the bottom profile shows a milder slope and less sediment is transported seawards. This phenomenon might be due to the reduced wave energy over the whole basin, caused by breaking over the submerged breakwater.

The average water level decrease in longshore direction from the middle of the submerged breakwater towards the gap. The gradient is rather pronounced, which means that a strong current develops around the tip of the submerged breakwater.

4.4 Conclusions and recommendations

The measurements made during the experiments are concentrated around the submerged breakwater, in a band of 3.55 m, from y = 8.41 m to y = 4.86 m. This is, for most of the profile shapes, the part of the cross-shore section just before the breaker line. Therefore, the measurements mainly give information on the influence of the submerged breakwaters on the wave set-down landwards of the structures.
Since only few cross-sections in the basin and few positions in each section were measured, the data set available is not detailed enough to give a 3D 'picture' of the wave set-up in the basin. Moreover, it appears to be necessary having data also in the area closest to the shoreline. Therefore, further laboratory experiments with more detailed measurements would be useful, in order to supply these extra data.
Up to now, very little can be said about the pattern of the wave set-up in the basin and about the influence of the submerged breakwaters on it.
However, comparing the different measured cross-sections highlights that a longshore gradient in the average water level, sloping down towards the gaps, occurs behind the submerged breakwaters. This gradient leads to longshore current towards the gaps.

Considering the pattern of the mean water level around the crest of the submerged breakwaters, it seems that there is a time-lag between the moment of waves pass over the crest of the breakwaters and the moment of breaking occurs.
From the comparison between the experiments without (A1, A2, A3) and with two submerged breakwaters (C1, C2, C3), it is not clear whether the effects of the submerged breakwaters are beneficial or detrimental, since the retreat of the shoreline was more pronounced in the latter case. However, with three submerged breakwaters, especially in the case with a higher wave height (D3), the sediment transport in the cross-section in line with a gap seems to be reduced, due to the decreased wave energy and so less retreat of the shoreline was observed.
When observing the wave energy spectrum during the experiments, it is seen that in addition to the peak at the frequency corresponding to the time period of 1.55 second, an other peak develops at a lower frequency, which entails the presence in the basin of waves of longer period than the one generated by the wave generator. The long wave amplitude is amplified in shallow water due to a 'resonance' situation. Therefore, the measured average water level can be influenced by the long waves generated within the basin.
Since standing waves are logically generated in the basin (see Sand (1982)), further research is recommended upon this subject in order to highlight the influence of these lower frequency waves on the average water level.

5. THE NUMERICAL MODEL DELFT3D

5.1 Introduction

The influence of submerged breakwaters upon the average water level and the current field has been investigated by means of the numerical model DELFT3D. This program is able to simulate two-dimensional (2D, depth-averaged) and three dimensional (3D) phenomena in which the horizontal scales are larger than their vertical length scales. The present work has been carried out using a 2D application which is called Delft2D-MOR, in the following.
Waves, currents and bottom changes are strongly correlated and influence each other. Therefore, the program consists of separate modules for the physical processes connecting together in various combinations.
Delft2D-MOR is created to model irregular waves, whereas the experiments made at the Delft laboratory were carried out with regular waves. Hence, before going ahead with the calculations, it has been necessary to calibrate the wave parameters to describe the wave field as close as possible to a regular wave field.
A further problem which had to be solved is the fact that diffraction is not modeled by the program. To go round this obstacle, use is made of the directional spreading of wave energy, which will be briefly described in the Appendix D.
Since the input values for the calculations are based upon the layout adopted for the experiments, additional complications are generated due to the small dimensions of the involved magnitudes (wave heights, wave period, dimension of the basin, etc.). This circumstance entails the assumption of orders of magnitude for some parameters which have not literature references.
In this chapter the general structure of the Delft2D-MOR modelling system will be presented together with the separate modules. Delft2D-MOR stands for the part of DELFT3D modeling system suitable for morphological application.
A brief description of the programs used within the modules will be presented in the related appendices. Further detail can be found in Delft Hydraulics (1996a).

5.2 Delft2D-MOR

The modelling system Delft2D-MOR simulates physical processes by a mathematical model. The available physical processes account for one or more of the following physical effects and for their interactions:

- waves
- flow
- sediment transport
- bed level variations

The modeling system describes the development in time of the physical process, starting from a given initial state.
The mathematical model description consists of equations for a 2DH area.

5.3 The combined model

Two different module combinations have been used in the computation of the wave set-up, as it is shown in Figure 5.3-1.

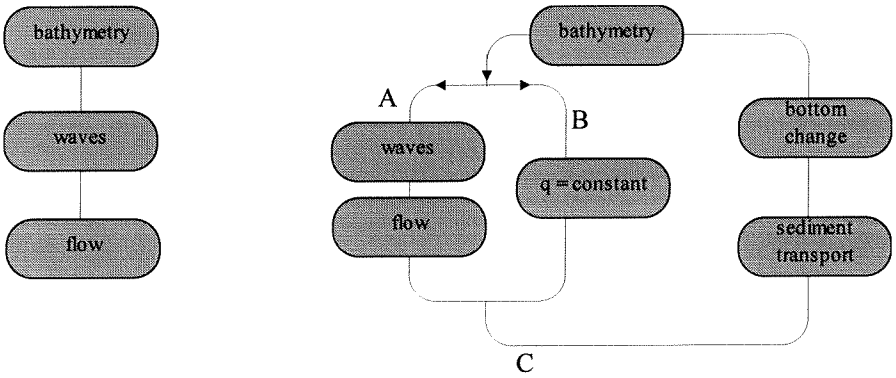

Figure 5.3-1 Different module combinations used in the computation

The first combination of the modules has been used on the assumption that the bottom profile is fixed during the calculations.
Once the bathymetry is given, the wave computation starts. The resulting wave-induced forces serve as input for the flow module.
Since nothing changes in the input bottom profile, there is no need to restart the simulation, which stops after the flow computation.

The second scheme does take into account bottom changes, therefore, the sediment transport module and the bottom module must be included in the simulation. Two different main routes (A and B) are presented for the computation of the bed level changes. If there is no information available on the waves and flow field, first a wave and flow computation have to be made on the initial bathymetry (route A). These computations are made on the assumption that the bottom level is invariant during the wave and flow computation.
The next step is the determination of the sediment transport rate (route C). At the end of one cycle the computed bottom changes are superimposed to the original bathymetry. After this the next cycle starts.
If wave and flow information are available, then the route B is followed under the following assumption. It is assumed that for small change of the bottom level the wave height and flow pattern remain constant. This results in a simple computation of the new flow velocities, by dividing the constant flow rate by the new depth values.
By means of this "continuity correction" the computation time reduces considerably.

The routes which should be followed in the program must be specified by a user-supplied process tree.
The process tree is built from the bottom up. First it starts with the elementary subprocesses, which contains the actual calls to the modules. Higher processes are built up by combining elementary processes. A process and a lower process are linked by a "branch" and the processes themselves are called "nodes".
A branch is a controller for the node below it, which means that it determines whether the subprocess has to be activated or not.

The execution of a simulation is now the climbing up and down the branches of the tree. Starting from the top it is checked whether the node below at the left side has to be executed. This procedure is repeated downwards until it can not go further.
An example of a tree structure is given in Figure 5.3-2. The numbering is from the left to the right, starting with all the end nodes and going back up to the root node.

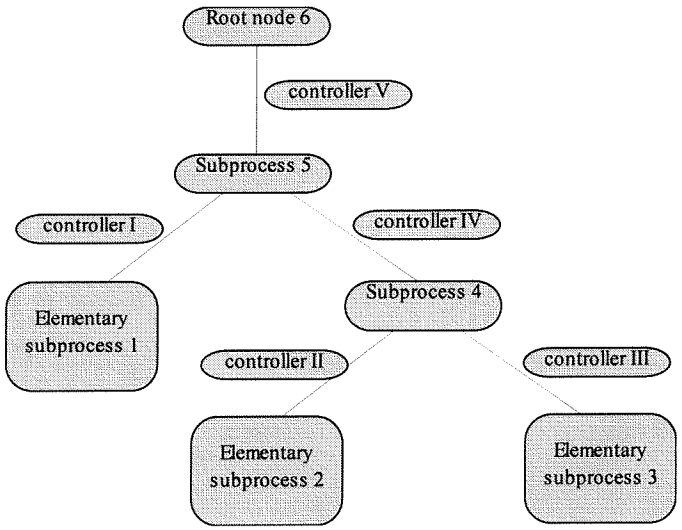

Figure 5.3-2 Example of a tree structure

5.4 Data communication

Relevant data used by the various modules are stored in a communication file. This file has a nefis structure (NEutral FIle System). By means of a communication file all inter-module data exchange takes place.

5.5 The Morsys module

The control module morsys steers the execution of the processes within Delft2D-MOR program. In the input file used by morsys (morf.*case*) reference is made to the input files of the modules to be called:

md-wave.*case*	for the wave module (WAVES)
md-flow.*case*	for the flow module (TRISULA)
md-tran.*case*	for the transport module (TRSTOT)
md-bott.*case*	for the bottom change module (BOTTOM)

5.6 The wave module WAVES

The wave module is the physical subprocess module which simulates the propagation of waves and gives as a result, the distribution of wave parameters and current-driving terms.
Due to the very significant role of waves within the morphological evolution of a coastal area it is important predicting the wave field well. Waves stir up the bottom material and bring it into suspension. Moreover, they are responsible for currents yielding the sediment transport.

The wave module makes use of the HISWA model (see Appendix D). HISWA, which stands for HIndcast Shallow water WAves, is a numerical model for prediction of stationary, short-crested waves in shallow water (Holthuijsen et al., 1989).

General structure

The input and output of the wave modules are defined by the user by means of switches.
These switches determine the way the bottom depth, water level and current velocity are taken into account by the module.
In Appendix D an example of an input file for the wave module is presented.
The succeeding procedure is generally followed. Every time the process tree starts the wave module, the bottom and flow data are read from a user-specified file (in general the communication file). Since the flow data computed by TRISULA is available on a staggered grid (Appendix E), the data must be interpolated onto the HISWA input grid. Next the HISWA computation can be executed, followed by the interpolation of the results back onto the TRISULA grid.

5.7 The flow module TRISULA

The flow module is the physical subprocess module which simulates the non-steady flow and water level variation from a tidal, a wave or meteorological forcing. The flow module in Delft2D-MOR consists of the Delft3D-FLOW model (in the following called TRISULA as it was formerly known).
TRISULA allows a 2D-horizontal or a 3D flow field computation, including the effects of waves, wind and density differences. Within DELF2D-MOR the 2DH version of the flow simulation field is available.
The bottom profile will be assumed fixed. The module reads the wave parameters from the communication file of WAVES.
In Appendix E a brief description of TRISULA is given.

Communication file

The TRISULA module writes to the communication file the water level, discharge components and velocity components.

5.8 The transport module TRSTOT

The transport module determines the sediment transport using the time-dependent flow and wave field. The magnitude of the sediment transport will be computed by means of a selected sediment transport relation. In the present study Bijker's formula is used. This formulation does take into account a bed load and a suspended load component of the total sediment transport.
In Appendix F a short description of Bijker's formula can be found .

5.9 The bottom module BOTTOM

The bottom module calculates the bottom changes from the transport rates following from the transport module. The new bottom profile is superimposed to the original bathymetry. A description of the procedure used is given in Appendix G.

6. CALIBRATION HISWA WAVE PARAMETERS

6.1 Introduction

The following chapter will present a brief review of the wave parameters' calibration, for further details reference is made to Schaap (1997).
In HISWA the effect of breakwaters and other obstacles are modelled. Nevertheless, the energy dissipation induced by the obstacles is not used to generate current, but is simply "taken out" from the further calculations. Therefore, the result current field is not accurate behind an obstacle. To be able to reasonably describe the current field, the submerged breakwaters have to be represented as variations in the bottom profile. This choice entails that the energy dissipation over the breakwater has to be modelled by means of the breaking parameters, instead of the transmission coefficient K_t.
The assumption of non-physical values for some of the wave parameters are therefore inevitable.

6.2 Wave height

As input value for the incident wave height, HISWA requires the significant wave height, which is a statistic parameter defined as the average height of the one-third highest waves. This value is not proper for describing a monochromatic wave field.
Since monochromatic waves and irregular waves are very different phenomena, the most satisfactory way to relate their height parameters seems to depend on the particular application (Shore Protection Manual (1984)).
In the situation analysed a rational approach is to equate the average total wave energy in both monochromatic and irregular wave trains. For sinusoidal, non-breaking waves it reads:

$$H = \frac{H_{m0}}{\sqrt{2}} \qquad (6.2\text{-}1)$$

where H = monochromatic wave height
H_{m0} = significant wave height of irregular waves

In deep water H_{m0} is approximately equal to H_s, whereas in shallow water and for breaking waves, the difference between H_{m0} and H_s can be 30%.
A precise computation of the relationship in shallow water is much more difficult. Therefore, equation (6.2-1) is considered a reasonable approximation.
The work presented in this report deals mainly with the wave set-up, as already said before. The wave set-up is a phenomenon involving the action of a train of many waves. Considering an irregular wave field, it is necessary to select which wave height has to be used to calculate the wave set-up. The very high waves in the spectrum are too infrequent to make a significant contribution in establishing wave set-up. For this reason, the use of the significant wave height H_s is recommended (Shore Protection Manual (1984)).
If the wave energy, dissipation and, hence, driving forces are to be represented, H_{rms} value ($H_{rms} = H_{m0}/\sqrt{2}$) gives the best representation.

In HISWA the wave height H = 0.12 m has been modelled as H_s = 0.17 m.

6.3 Directional spreading (DSPR)

DSPR is an acronym for directional spreading. This function enables the simulation of the phenomenon of diffraction which is not modeled by HISWA (see Appendix D).
To choose a magnitude for the directional spreading, another computer model, named CREON, is used as a reference. CREON, developed by Delft University of Technology and Rijkswaterstaat, is able to model both regular and irregular waves and does take into account diffraction.
Contrary to the situation with emerged breakwaters, in the case of submerged breakwaters, diffraction is not one of the most important phenomena. The outcome of the calibration confirms this, leading to a rate of directional spreading which is rather small.

The result of the calibration yields a directional spreading of 10.2 degrees (ms = 30).

6.4 Breaking parameters

The breaking parameters which have to be set after calibration are the deep water breaking index γ_d, the shallow water breaking index γ_s and the dissipation coefficient α.
The calibration is based on the assumption that the chosen parameters would be considered correct if the wave field generated by HISWA satisfactory correspond to the measured wave field.
The shallow water breaking index γ_s is defined as the ratio between the maximum wave height H_m, which can exist at the given depth, and the water depth h (H_m/h). By modifying this coefficient the maximum wave height H_m changes consequently. This variation yields the shifting offshore or onshore (decreasing or increasing of γ_s respectively) of the breaker line.
The dissipation coefficient α determines directly the magnitude of the wave dissipation (see Equation D.2-3). Therefore, by increasing this coefficient the bottom induced wave breaking increases.
The calibration shows that a better accuracy in modelling of the dissipation at the submerged breakwater (high values of α), causes small inaccuracies in reproducing the wave field farther behind the obstacle and vice versa.
At the first instance the choice of the coefficients is mainly due to the fact that this study deals with the effects of a submerged breakwater on hydrodynamics (and morphodynamics). Moreover, the wave field further behind the breakwaters has not been measured and the actual knowledge about the developing of the wave heights close to the shoreline is very little. Consequently, there are not many data available for calibration purpose in this region.
For these reasons it seems wiser to model the dissipation at the submerged breakwater as accurate as possible and thus chose high values of α.

The result of the calibration yields γ_d = 1.0, γ_s = 2.0, α = 8.

Especially $\gamma_s = 2$ and $\alpha = 8$ are, in fact, completely out of reasonable range ($\gamma_s \approx 0.8$ and $\alpha \approx 1$ are usual).

Figure 6.4-1 show the comparison between HISWA calculation and measured wave heights in a cross-section with breakwater, while in Figure 6.4-2 a cross-section without breakwater can be seen (from Schaap (1997)).

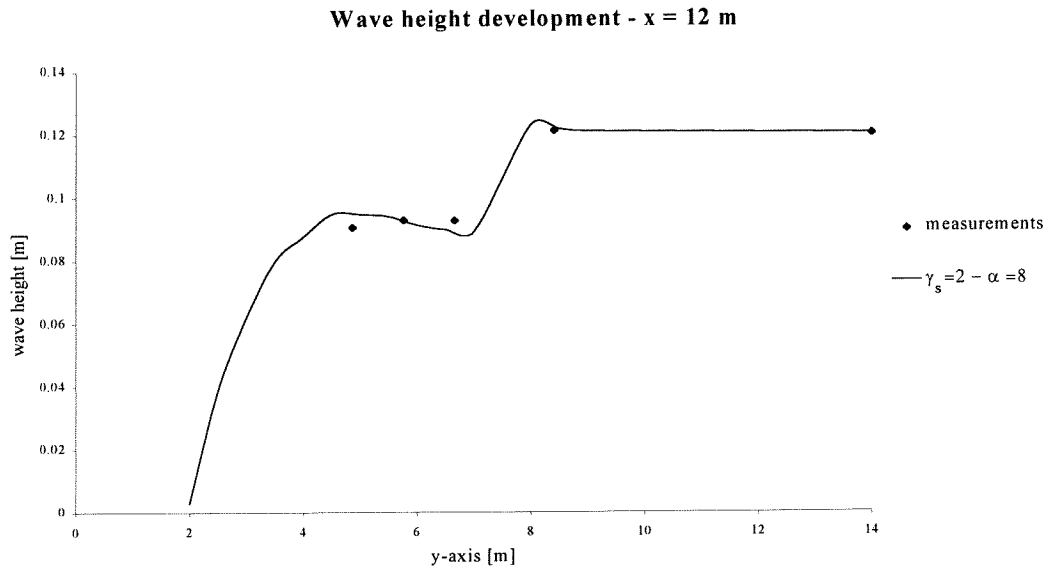

Fig. 6.4-1 Wave height comparison between measurements and HISWA computation - cross-section in line with a submerged breakwater (from Schaap (1997))

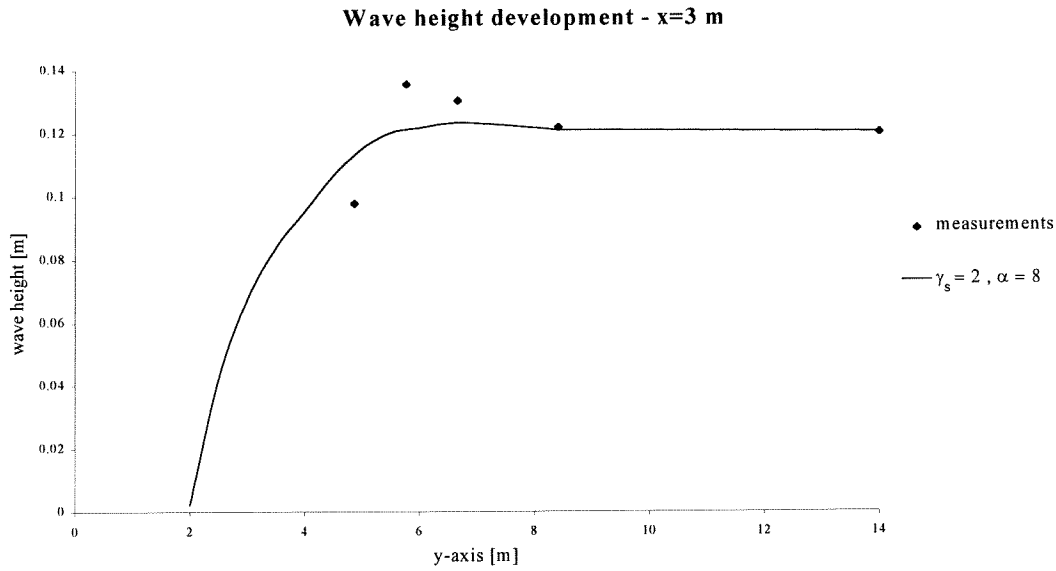

Fig. 6.4-2 Wave height comparison between measurements and HISWA computation - cross-section in line with a gap (from Schaap (1997))

7. 2DH SIMULATION, FIXED BOTTOM PROFILE

7.1 Introduction

The first set of simulations is carried out on the assumption that the bottom profile is invariant during the calculation.
The simulations described in the following are performed with regular, normal incident waves. The layout of the calculations is based on the configurations of the experiments described in Chapter 2, Section 2.1.2. Three series of simulations are carried out (see Table 7.1-1).

Wave period	Wave height	No breakwater A	Two breakwaters C	Three breakwaters D
T = 1.55 s	H = 0.08 m	A1	C1	D1
T = 1.55 s	H = 0.10 m	A2	C2	D2
T = 1.55 s	H = 0.12 m	A3	C3	D3

Table 7.1-1 Wave condition used for the simulation

The first sections will describe the input used for the computations. After this, the results of the simulations will follow.

7.2 The process tree

The process tree presented in Figure 7.2-1 is used in order to determine the wave field. The process to be simulated, represented by the root node number 4, exists in one execution of subprocess 3. Subprocess 3 is simulated by the wave module (HISWA). The flow module (TRISULA) is executed as a stand alone module, using the wave field generated by the process tree.
First a wave computation is made by executing one time (stop criterion of controller I) the wave module. The communication file so created will be read by the flow module. TRISULA will start each time until a stationary flow field is reached, which occurs when the change of the flow velocity is negligible.
At the end of the flow computation the wave-induced current and the wave set-up are known.
The effect of flow on waves is not taken into account.

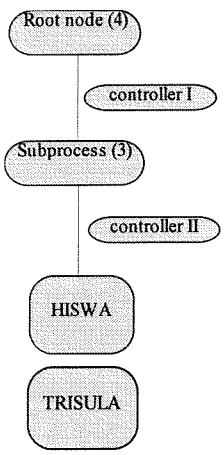

Figure 7.2-1 Used process tree

7.3 Input files

7.3.1 Wave file

The input grid

The input grid for the wave module consists of a rectangular grid with dimension 14.1 by 29.5 m, covering the entire area of interest. The shorter side is parallel to the wave propagation (the x-direction), while the longer side is parallel to the shoreline (the y-direction). The mesh sizes are 0.10 m in the x-direction and 0.50 m in the y-direction. In all grid points the bottom depth is given according to the experiment layouts. The depth values are positive downwards, the submerged breakwaters are represented by a variation in the bottom depth.

Figure 7.3-1 shows the different grids.

In this case, the x- and y-axis are respectively the y- and x-axis of the basin of the laboratory experiments.

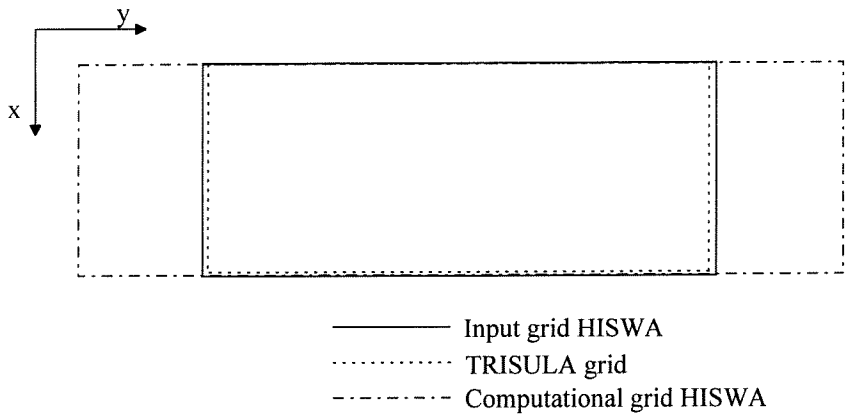

Figure 7.3-1 Different grids used for the computation

Computational grid and boundary conditions

In contradiction with the basin, along lateral sides it is necessary to implement open boundaries, since the wave model does not permit reflective boundaries along these sides. This implies that along each lateral side of the grid a region exists where the wave field is disturbed by an import of zero energy from the lateral boundaries (Figure 7.3.1-1). Therefore, the computational grid is taken, in y-direction, longer than the area of interest (the input grid).

Outside the input grid, HISWA assumes that the bottom level and the friction coefficient are identical to those at the nearest boundary of the input grid. For the current and wind velocity, 0 m/s is taken for points outside the input grid.

The mesh size in y-direction is chosen equal to the Δy of the input grid (0.50 m).

The mesh size in x-direction is now determined by both the conditions of numerical stability imposed to the HISWA computation (Appendix D, Equation D.3-1) and to the TRISULA computation (Section 7.4), i.e. Δx equal to 0.2 m.

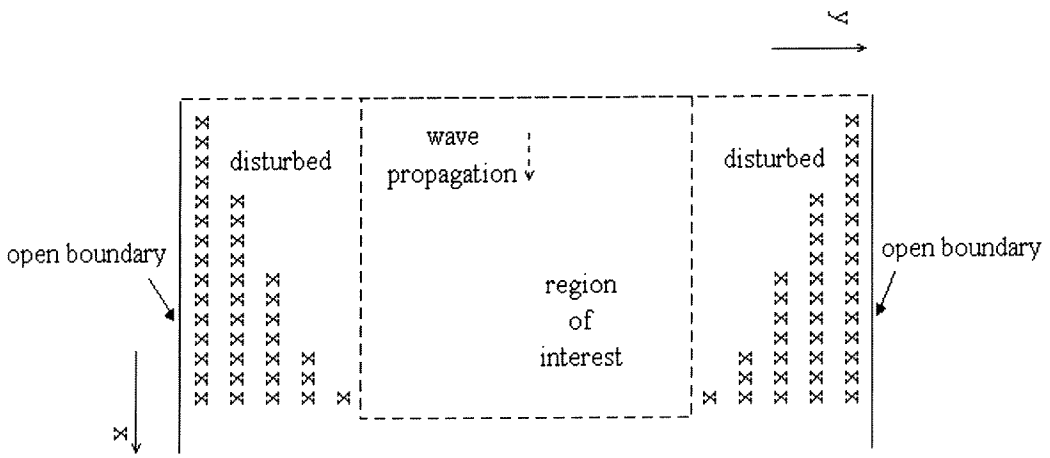

Figure 7.3.1-1 Disturbed region in the computational grid

Wave data

The wave height and the wave period in HISWA should respectively be given as the significant wave height H_s (see Chapter 6, Section 6.2) and the peak wave period T_p. According to the different experiments done, different significant wave heights are given:

$$H_s = \sqrt{2}\,H = 0.17\ m \qquad for\ H = 0.12\ m$$

$$H_s = \sqrt{2}\,H = 0.141\ m \qquad for\ H = 0.10\ m$$

$$H_s = \sqrt{2}\,H = 0.113\ m \qquad for\ H = 0.08\ m$$

The wave period is T_p = 1.55 s for every experiment and therefore, for each computation.

The waves are approaching normal to the shoreline which entails a wave direction of 0° in HISWA module.

The spreading factor ms (see Chapter 6, Section 6.2) is taken equal to 30.

Dissipation due to wave breaking

The wave-breaking induced dissipation is computed according to the energy dissipation model of Battjes and Jansen (1978).

Outside the breaker zone the wave decay is rather weak and the time-mean dissipated power D_b can be neglected entirely.

Inside the surfzone, the dissipation of wave energy in the breaking process is dominant.

The mean dissipation of breaking random waves per unit area, reads:

$$D_b = \frac{\alpha}{4}\rho g f_m Q_b H_{\max}^2 \qquad (7.3.1\text{-}1)$$

where D_b = time-mean dissipated power per unit area; the subscript b states for "breaking"-induced

α = calibrated parameter (see Chapter 6, Section 6.4)
f_m = mean wave frequency
Q_b = fraction of broken waves
H_{max} = maximum possible wave height

The fraction of broken waves reads:

$$\frac{1-Q_b}{\ln Q_b} = -\left(\frac{H_{rms}}{H_{max}}\right)^2 \qquad (7.3.1\text{-}2)$$

The maximum possible wave height reads:

$$H_{max} = \frac{\gamma_d}{k}\tanh\left(\frac{\gamma_s kh}{\gamma_d}\right)^2 \qquad (7.3.1\text{-}3)$$

where γ_d = breaker coefficient for deep water = 1
γ_s = breaker coefficient for shallow water = 2
k = wave number
h = water depth

The water level
The initial water level is taken constant and equal to the still water level. In HISWA the water level is defined relative to the horizontal plane from which the bottom depths are measured. The still water level corresponds to the value zero.

7.3.2 Flow input

Input grid
The TRISULA input grid has dimension of 14.2 m by 30 m, larger than the HISWA input grid, due to the fact that TRISULA makes use of a staggered grid (see Appendix E). The mesh sizes are equal to the HISWA's input grid (0.1 m in x-direction and 0.5 m in y-direction).

Water level
The initial water level is defined at 0 m.

Bottom friction
For a depth-averaged flow, the shear stress on the bed induced by a turbulent flow is assumed to be given by a quadratic friction factor law:

$$\tau_b = \rho\frac{g}{C_{2D}^2}|\underline{U}|^2 \qquad (7.3.2\text{-}1)$$

where C^2_{2D} = 2D-Chézy coefficient
$|\underline{U}|$ = depth-averaged horizontal velocity

The 2D-Chézy coefficient is determined according to the White-Colebrook's formulation and reads:

$$C_{2D} = 18 \log_{10}\left(\frac{12h}{k_s}\right) \qquad (7.3.2\text{-}2)$$

where h = total water depth
k_s = Nikuradse roughness length

The Nikuradse roughness length k_s is taken equal to 0.01 m to take into account the bed forms.

Eddy viscosity
A uniform horizontal eddy viscosity equal to 0.1 m^2/s is applied in the model.
Since a 2DH version of the model is used, the vertical eddy viscosity is not important.

Numerical stability
For the computational time step in TRISULA it is required that the Courant number is smaller than 10:

$$\sigma = \sqrt{gh}\frac{\Delta t}{\Delta x} \leq 10 \qquad (7.3.2\text{-}3)$$

The mesh size in x-direction Δx is equal to 0.2 m. This fact leads to have a very small time step Δt equal to 0.06 s. Nevertheless to ensure a reasonable accuracy in the computation the mesh Δx can not be chosen larger.
The computation time step is taken 2 minutes which means 200 computational steps each time the flow module is started by the process tree.

Initial and boundary conditions
To get a well-posed problem, a set of initial and boundary conditions for water levels and horizontal velocities must be specified. It is assumed that initially the model is at rest ('cold start'). The velocities are zero everywhere.
Open boundaries are introduced to obtain a limited computational area. Along the seaward boundary an open boundary is chosen characterised by a constant water level. Waves can cross open boundaries unhampered and without reflections. In a model this property must be included in the boundary conditions. A weakly reflective boundary condition is chosen in order to reduce the spin-up time of the model.
The assumption of an open boundary condition at the seaward boundary, allows water to come into the basin, in contradiction with the laboratory layout.
In order to compensate the increased average water level, which is approximately 0.01 m, the water level condition at the seaward boundary is taken equal to -0.01 m below the zero level (still water level).

Further and more detailed explanations about the module can be found in the TRISULA manual.

7.4 Results

7.4.1 Introduction

In the following sections the results of the simulations are discussed.

A description of the outcomes, performed with a wave height of 0.12 m, is detailed. In order to better understand the analysis, the reader is suggested to refer to the appropriate appendices, in which a series of figures, taken from the computations, is included. These figures are obtained by means of a graphical program named GPP, which is able to use output data of Delft2D-MOR. It has to be noticed that in these plots the axis-system has somewhat changed. The origin, which represents the seaward boundary, is equal to 100 for both the y- and x-axis.
Some Excel figures are included in the text. In this case, the orientation followed is the same of the basin of the laboratory experiment defined in Chapter 2, Section 2.2.
A qualitative comparison with the measurements, carried out during the laboratory experiments, is illustrated, presenting the possible causes for the discrepancies between simulation outcomes and measurements.
The computations performed with a wave height of 0.10 m will not be described, due to the fact that the results obtained are rather similar to the ones related to the simulation with 0.12 m wave height. The smallest wave height (H = 0.08 m) seems not to be highly influenced by the submerged breakwaters. Therefore, only the plots concerning the simulations are given in the appendices.
The stationary situation is achieved already after 2 minutes (see Figure 7.4.1-1 and Figure 7.4.1-2). After this time, the changes in the flow velocity and of the water level are already negligible. In fact, the stationary situation in the case of a rigid bed is reached even before two minutes; nevertheless, in order to avoid instability in the computations with a movable bed, the TRISULA computation lasts more than the minimum time requested to obtain a stationary field. The computation is then stopped, yielding the water level and the current field. These results are the initial states for the further simulations carried out by means of the sediment transport and bottom change modules (see Chapter 8).

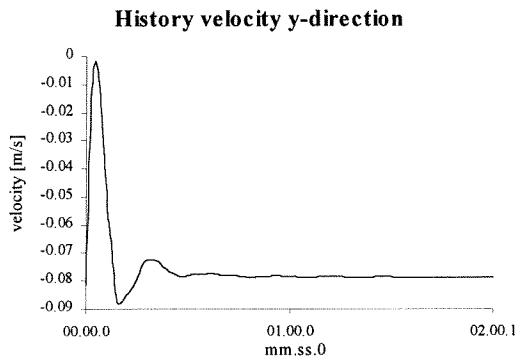

Figure 7.4.1-1 History velocity in y-direction at one location

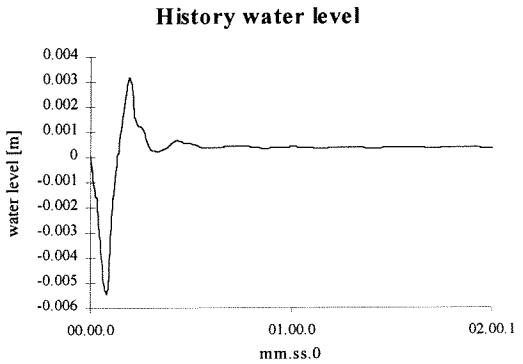

Figure 7.4.1-2 History water level at one location

Through out the following sections, 'left' and 'right' of the basin, if not otherwise specified, will be referred to while facing the shoreline.

7.5 Simulation A3 - no submerged breakwater

The figures are included in Appendix H3.

Wave field

The contour map of the initial wave field is illustrated in Figure H3-1.

Without submerged breakwaters there is no longshore variation in the wave field. Approaching the shoreline, the wave heights increase due to shoaling. This phenomenon is made more clear by the wave height distribution over one cross-section plot in Figure 7.5-1. Due to a regular wave field approaching perpendicularly to the shoreline, a shore-parallel breaker line develops. The wave height decay agree with this, showing for every cross-section the same development.
The wave force distribution plotted in Figure H3-2 confirms the regularity of the wave field, as every longshore-section is characterised by the same pattern.
The energy dissipation contour map is illustrated in Figure H3-3. Also in this case, due to the regular wave field, no longshore variations in the wave energy dissipation pattern can be seen.
When the water becomes shallower the waves start breaking inducing wave energy dissipation (see Figure 7.5-2).

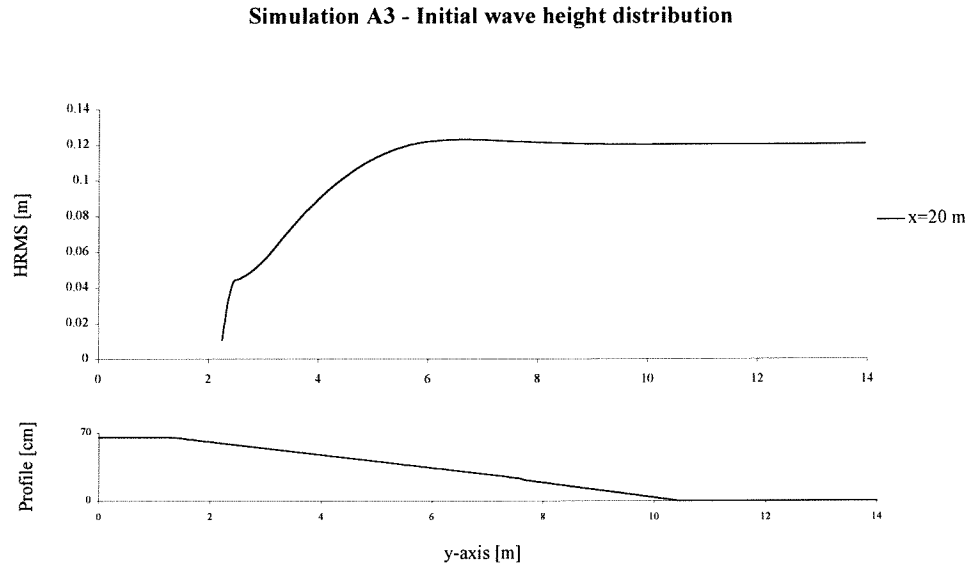

Figure 7.5-1 Initial wave height distribution over one cross-section

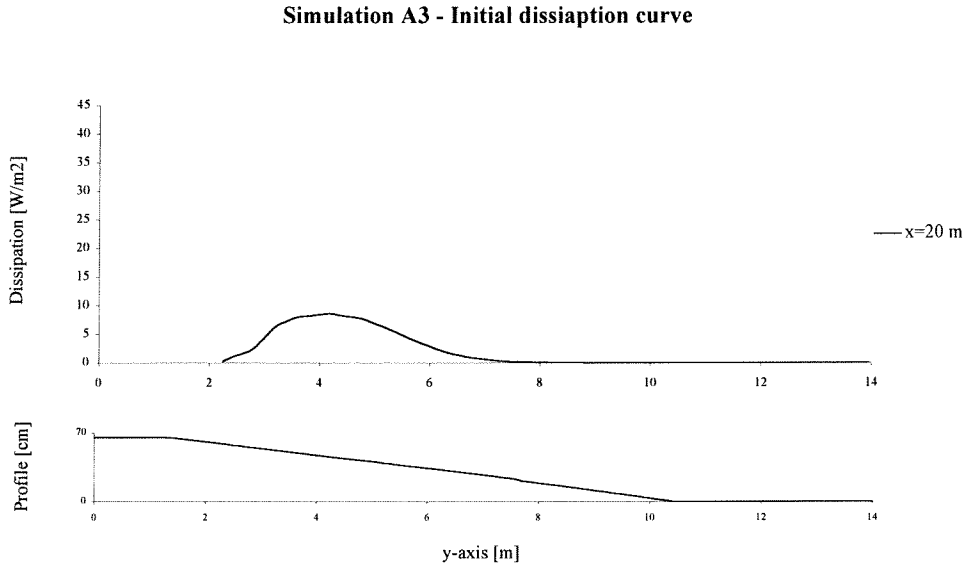

Figure 7.5-2 Initial dissipation curve over one cross-section

Initial average water level

The contour map of the initial average water level is presented in Figure H3-4. Without submerged breakwaters the average water level is uniform over the entire basin, increasing towards the shoreline, in the breaking zone.

No longshore gradient occurs in the mean water level, therefore no longshore current is generated.

In Figure 7.5-3 the development of the average water level over one cross-section is shown. The mean water level approaches the breaker line unaltered, whereas, according to the radiation stress theory, a wave set-down should be developed in this area. The explanation of this phenomenon can be sought in the way the average water level is computed by the numerical model. The driving forces of wave-induced currents and consequently the mean water level, are determined in terms of the wave energy dissipation rather than in terms of the radiation stress. In the following, a brief explanation of this approach is given. Indeed, as the radiation stress tensor can be a rapidly varying function of the spatial coordinates, numerical differentiation can lead to poor results. Moreover, a large part of the driving force per unit volume can be shown not to generate current (the irrotational part) and it is omitted from the force computation. According to Dingemans et al. (1987), the rotational part of the wave-induced force per unit mass is closely proportional to the wave energy dissipation per unit area. Furthermore, examples show that the formulation of the driving force in terms of the wave energy dissipation is more robust than the approach in which the forces are obtained by numerical differentiation of the radiation stress tensor.

Since wave dissipation occurs only in breaking phenomena, the average water level presents a horizontal profile until the breaker line and, then, it starts rising.

Flow computation

The current field is plotted in Figure H3-5. The irregularities in the flow field are probably a consequence of small inaccuracies which occur during the simulation. It has to be noticed that the order of the magnitude of the arrows plotted in Figure H3-5 is so small that the irregularities are considered negligible.

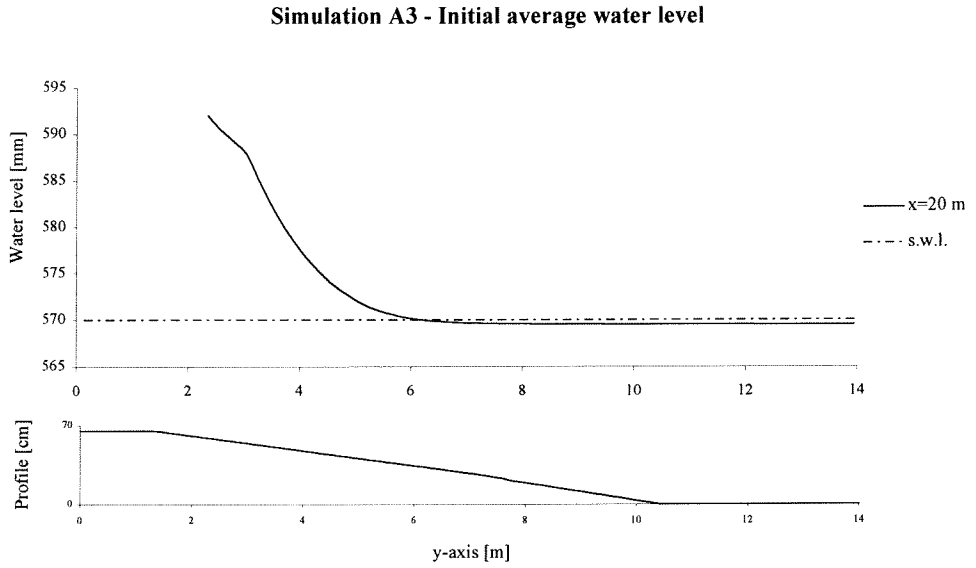

Figure 7.5-3 Initial average water level over one cross-section without submerged breakwater

7.6 Simulation C3 - two submerged breakwaters

The figures are included in Appendix I3.

Wave computation

The contour map of the initial wave field is detailed in Figure I3-1. The influence of the submerged breakwaters upon the wave height can be seen. The incoming wave starts breaking on the crest of the structure causing a decay in the wave height.

Although wave diffraction is not accounted for in the program, the use of the directional spreading seems to lead to reasonable results for the area in the lee of the breakwaters.

Since the length of the two submerged breakwaters is different, different behaviour over the two structures is to be expected. It is, indeed, interesting to observe the development of the wave heights over the longer submerged breakwater. The wave heights gradually decays from the corners to the middle of the structure, showing a rather large area in which the influence of the tips of the submerged breakwater is not felt. The wave heights are smaller compared with the area behind the shorter submerged breakwater.

The consequence of the different lengths of the structures is illustrated also in the wave height distribution details in the Figure 7.6-1. In the lee side of the longer submerged breakwater (x = 12.5 m), the wave height shows a slower increase compared to the wave height behind the shorter submerged breakwater (x = 24.5 m).

Approaching the shoreline, the presence of the structure weakens, yielding a quite uniform pattern along the coast.

The increased wave height, in the region landwards of the structures, is due to the fact that waves stop breaking. This phenomenon might be caused by a shortcoming of the wave model. As characterised by Svendsen et al. (1978), in the region right after breaking, for a horizontal distance of several times the water depth at the breaking point, a rapid transition of wave shape takes place. After that, a well-organised, quasi-steady breaking motion develops.

In HISWA the rapid transitions of wave shape in the region right after breaking is not taken into account. In fact, close behind the submerged breakwaters the bottom depth is deep enough to let waves unchanged. Since the bottom depth is the only parameter which is checked by HISWA as breaking condition, when the depth increases, the waves stop breaking, to start again closer to the shoreline.

The situation detailed above can be also observed if considering the pattern of the wave force (Figure I3-2). Just behind the submerged breakwater, the wave force reached its maximum due to the great dissipation induced by breaking. The sheltered area is characterised by wave force almost equal to zero, whereas towards the shoreline it slowly increases. The zone in line with the gap presents a homogeneous increase in the wave force approaching the coast.

In line with the gap, the wave height development presents a slight increase towards the breaker line due to shoaling, followed by a normal final decay closer to the coast, while breaking occurs. In the gap, the wave height is smaller than in the same cross-section in the situation without submerged breakwaters (see again Figure 7.5-1).

The wave height in the area close behind the submerged breakwaters is much smaller than in the area of the gaps.

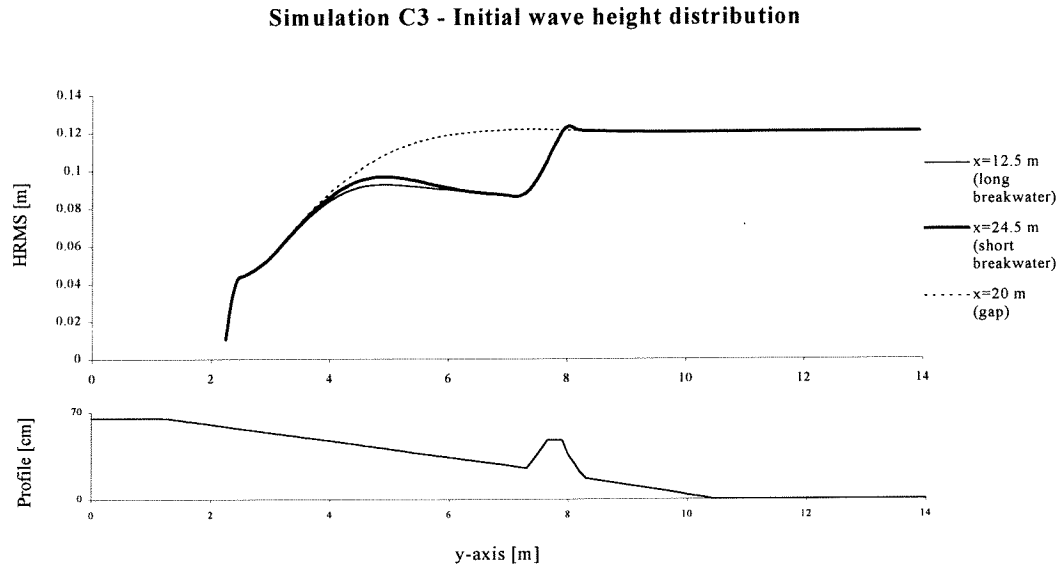

Figure 7.6-1 Initial wave height distribution over different cross-sections

The energy dissipation contour map is plotted in Figure I3-3. The maximum energy dissipation occurs over the breakwaters as Figure 7.6-2 details. The energy dissipation, in line with the longer submerged breakwater, presents a smaller increase approaching the shoreline due to the less diffraction.
In line with one gap the energy dissipation pattern shows a mild regular increase towards the breaker line.
The same amount of wave energy has to be dissipated in every cross-section. Therefore, the area under the three dissipation curves should be the same. Although from the figure it is hard to say, probably this is the case, since the development of the dissipation curve at the shoreline is not known.

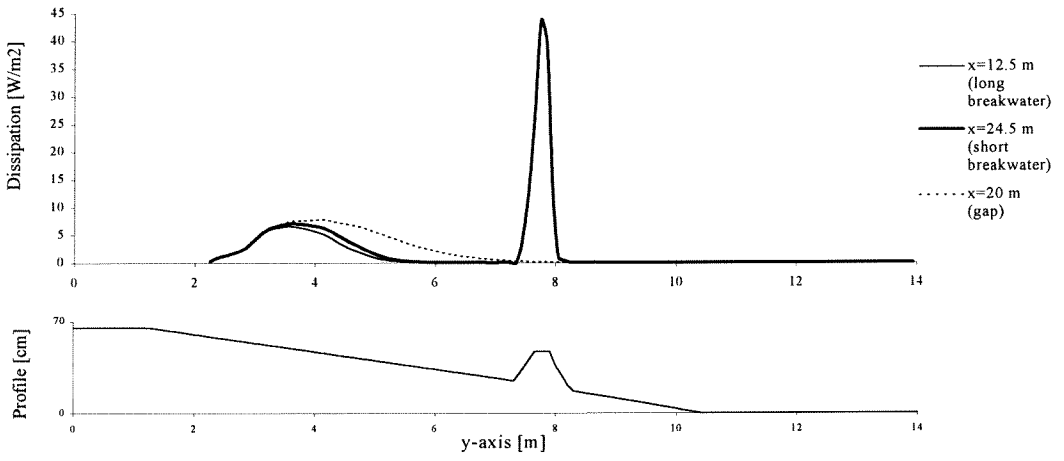

Figure 7.6-2 Initial dissipation curve over different cross-sections

Computed average water level

The contour map of the initial average water level is illustrated in Figure I3-4.

In the area seawards of the submerged breakwaters, the average water level shows a slight decrease. This phenomenon can not be called 'wave set-down', as the average water level is determined in terms of the wave energy dissipation. An explanation might be that, due to the presence of the submerged breakwater, water has to be 'forced' to flow towards the seaward side of the submerged breakwater, to be able to pass over it. As a consequence, in the area seawards of the submerged breakwaters, a gradient in the mean water level sloping down from the gaps towards the middle of the structures, occurs. The circulation cells, developed around the tips of the submerged breakwaters, confirm this circumstance.
Figure 7.6-3 shows the development of the average water level over different cross-sections. In the lee of the submerged breakwaters, the average water level remains horizontal for some distance, since waves stop breaking due to the increased water depth.
The consequence of the different lengths of the submerged breakwaters, found in the wave heights pattern, can be noticed in the average water level as well. Right landwards of the longer structure, where the influence of the diffraction is not felt, the average water level shows higher levels in comparison with the area behind the shorter breakwater.
In the gap (see also Figure 7.6-3), the average water level is influenced by the presence of the submerged breakwaters, showing a wave set-up starting later than in the case without submerged breakwaters (see Figure 7.5-3).
In comparison with the cross-sections in line with the submerged breakwaters, the mean water level rises more slowly towards the shoreline due to the influence of the mild slope of the bottom.
Closer to the shoreline the development of the mean water level is similar to the breakwater cross-section's.

Simulation C3 - Initial average water level over different cross-sections

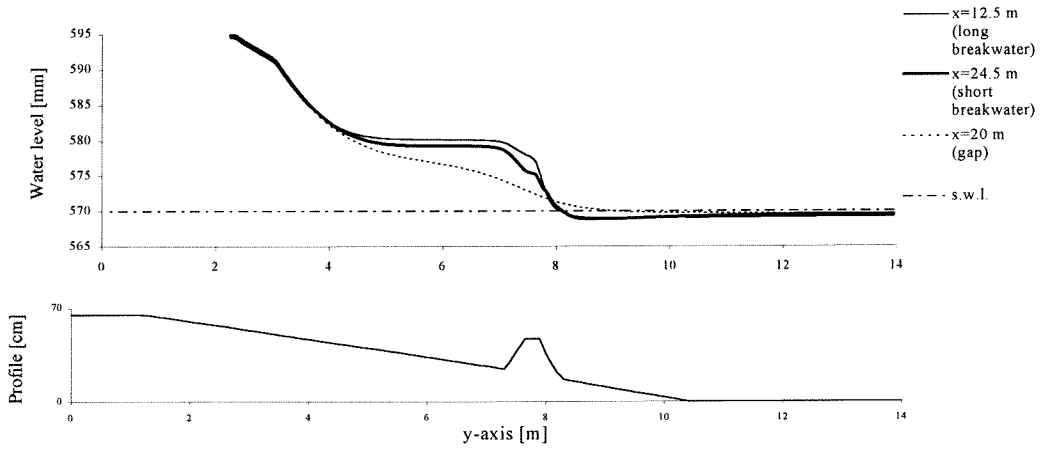

Figure 7.6-3 Initial average water level over different cross-sections

The longshore gradient in the average water level is noticeable in Figure 7.6-4. In the area close behind the submerged breakwaters the difference in the wave set-up is higher, whereas it becomes less pronounced landwards, as the influence of the structure over the waves is almost negligible.

The large gap on the right side of the basin generates a pronounced gradient in the wave set-up, sloping down towards it, which will induce a very strong current.

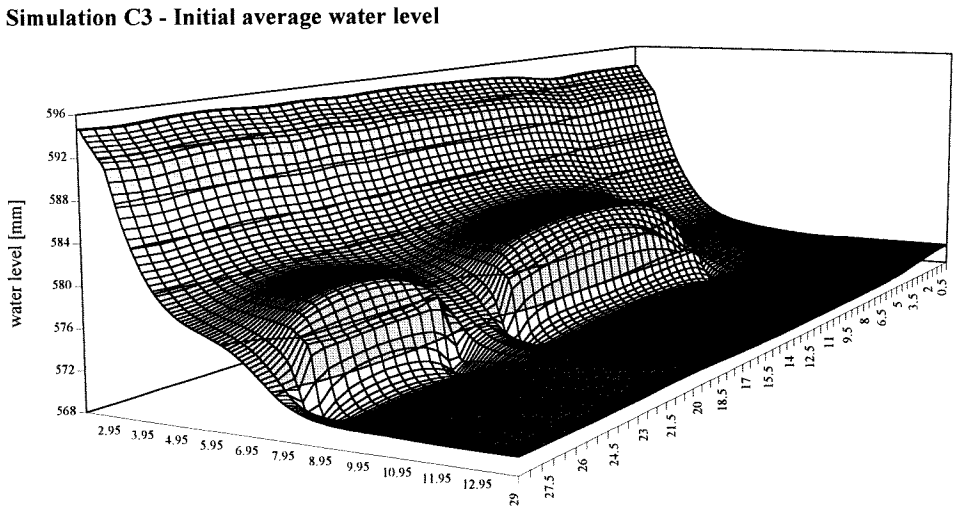

Figure 7.6-4 Simulation C3 - 3D view initial average water level

Flow computation

The initial flow field is detailed in Figure I3-5. Due to the longshore gradient in the average water level, a longshore current develops towards the gaps. Closer to the shoreline, the magnitude of the current decreases remarkably, although the influence of the longshore current is still noticeable.

Two circulation cells form around the tips of the submerged breakwaters which do agree with the flow field observed during the laboratory experiments.

In the area landwards of the submerged breakwaters, the velocities point towards the gaps, in agreement with the slope of the gradient in the average water level. Seawards of the tips of the structures, the lower mean water level induces the current towards the middle of the submerged breakwaters yielding the above mentioned circulation cells. The same pattern is noticeable in Figure 7.6-5 in which the depth-averaged velocities, measured during the first 1.5 hours of the laboratory experiment, are shown.

The different lengths of the submerged breakwaters effects also the current field, which shows smaller values landwards of the middle of the longer submerged breakwater.

Over the submerged breakwaters a strong current develops, as a consequence of the breaking, which will induce a remarkable erosion at the toe of the structures.

The gap at the right side of the basin, facing the shoreline, generates a stronger current which is matched by the pattern of the average water level.

The current is much stronger in this case than in the case without submerged breakwaters (Figure H3-5).

By analysing the average return flux illustrated in Figure I3-6 it is possible to forecast the initial development of the bottom profile. Close to the shoreline the direction of the arrows clearly indicates the presence of an offshore sediment transport. Going towards the submerged breakwaters the velocities start bending in the direction of the

gaps; this will yield a longshore sediment transport which in turn will generate a strong erosion right landwards of the submerged breakwaters. The magnitude of the return flux increases going towards the gaps.

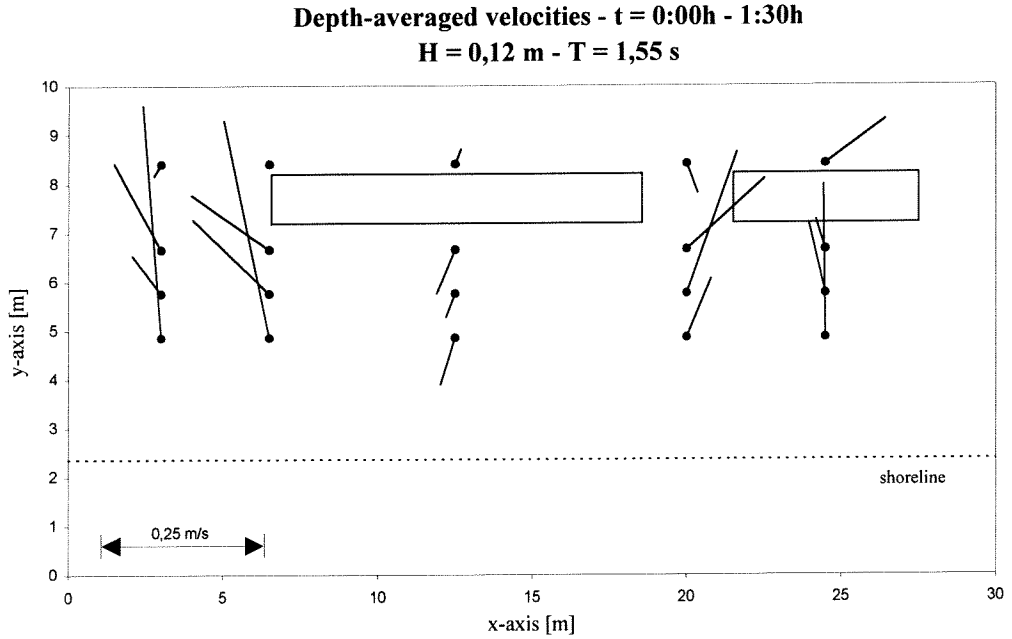

Figure 7.6-5 Test C3 - Measured depth-averaged velocities

By comparing the outcomes of this simulation with the outcomes of the simulations with smaller wave heights (cases C1 and C2, figures in Appendix I1 and Appendix I2), the patterns of the wave and the flow field and of the mean water level are approximately the same, while the order of magnitude is smaller.

7.7 Simulation D3 - three submerged breakwaters

The figures are included in Appendix L3.

Wave computation

The contour map of the initial wave field is visible in Figure L3-1. The influence of the breakwaters upon the wave height can be seen; when waves feel the breakwater they start breaking, which entails a decay in the wave heights. Close behind the structures, a decrease from the tips to the middle of the breakwaters can be seen. The influence of the submerged breakwaters weakens towards the shoreline and consequently the longshore variation in the wave heights lessens.

The wave force distribution (see Figure L3-2) shows the influence of the tips of the breakwaters on the direction of the waves. The arrows around the breakwaters slightly bend towards the middle of the structures.

The wave height distribution, detailed in Figure 7.7-1, shows the wave height decay over the cross-sections in line with one submerged breakwater (x = 15.5 m) and with one gap (x = 20 m).

Approaching the submerged breakwater, the wave height has undergone a small increase, followed by a steep decay due to breaking. In the region behind the structure, the wave height slightly increases. After that, the final decay towards the shoreline

takes place. As already explained in the previous simulation (see Section 7.6, wave computation), this evolution is probably due to a shortcoming of the wave model.
The wave height decay over the cross-section in the gap is quite different. The wave approaches the breaker line, slightly increasing its height due to shoaling. Compared to the simulation without submerged breakwaters (Figure 7.5-1), a smaller wave height can be seen, due to the influence of the submerged breakwaters.
Closer to the shoreline the waves break, yielding a slow and steady decay in the wave height.
The wave height right behind the submerged breakwater is much smaller than the wave height in the cross-section in line with the gap.

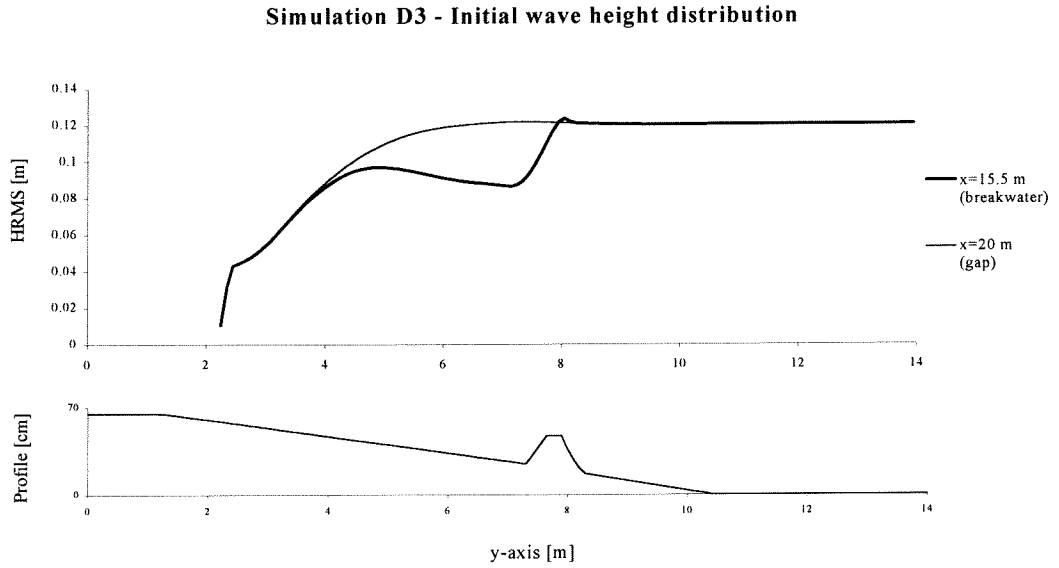

Figure 7.7-1 Initial wave height distribution over different cross-sections

The energy dissipation contour map is plotted in Figure L3-3. The maximum energy dissipation occurs over the breakwaters (see Figure7.7-2). Waves approach the submerged breakwater unaltered, therefore, no dissipation takes place in the zone seawards of the structure. The high peak in the dissipation curve corresponds to the position of the submerged breakwater, characterised by a sudden change in the bottom depth which induces breaking. Nevertheless, after this point the dissipation rapidly falls to zero which means that the waves stop breaking.
The pattern of the dissipation curve referring to the breaker line close to the coast shows a milder increase and decrease due to the breaking induced by a gentle variation of the slope.
The dissipation curve over the cross-section in the middle of one gap presents the same mild increase and decrease of the second half of the previous curve. In this case, though, the breaker line is more seaward and the dissipation is bigger.

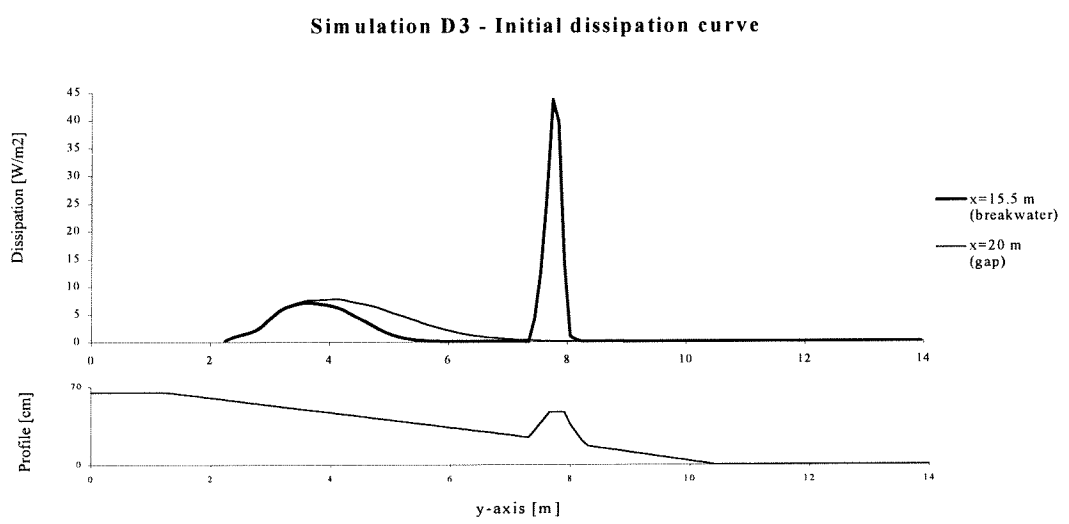

Figure 7.7-2 Initial dissipation curve over different cross-sections

Computed average water level

The contour map of the initial average water level can be seen in Figure L3-4.
Approaching the submerged breakwaters, a slight decrease can be seen, which is not due to the wave set-down, as the average water level is determined in terms of the wave energy dissipation.
Over the crest of the submerged breakwater the waves start breaking yielding an increased average water level. Close behind the structure the waves stop breaking to start again closer to the shoreline. This behaviour is reflected in the average water level, see Figure 7.7-3. After the initial increase of the mean water level, the pattern shows a horizontal line which indicates that no wave dissipation occurs (the waves stop breaking). Close to the shoreline the average water level rises, since the waves start breaking again.
In line with the gaps, the average water level presents a development quite different (see again Figure 7.7-3). The wave set-up starts more seaward, but the mean water level rises slower towards the shoreline. This phenomenon can be explained by considering the mild slope of the bottom. In the situation without submerged breakwaters (Figure 7.5-3), the average water level rises later.

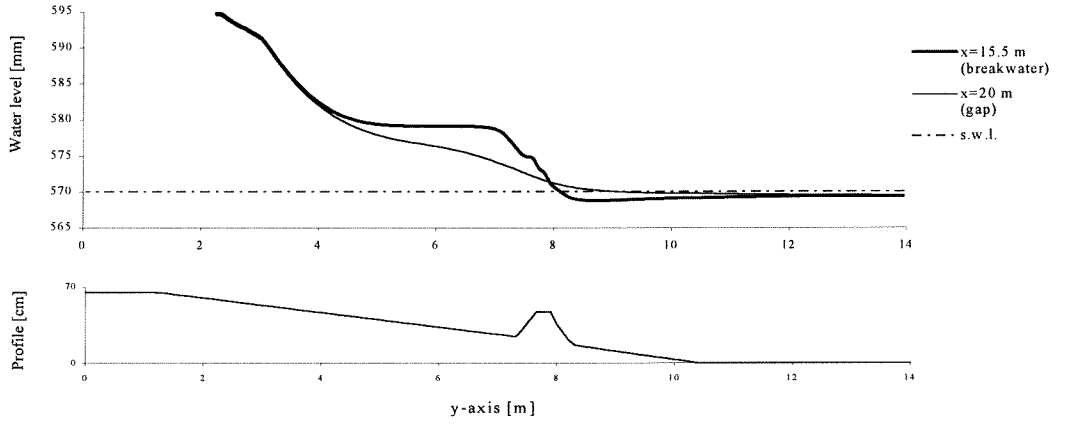

Figure 7.7-3 Initial average water level over different cross-sections

The longshore gradient in the water level is evident in Figure 7.7-4. The difference in the wave set-up is higher in the area behind the submerged breakwaters. This gradient will induce a strong longshore current pointed towards the gap (see Figure L3-5), which in turn will cause a very big sediment transport.
Closer to the shoreline the differences become smaller, since the influence of the submerged breakwaters lessens towards the coast.

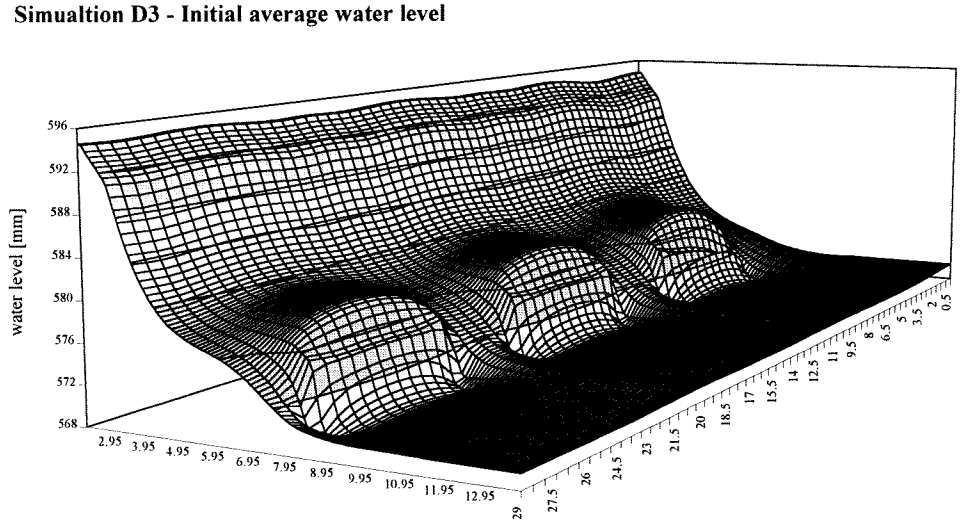

Figure 7.7-4 Simulation D3 - 3D view initial average water level

Flow computation
In the area around the tips of the submerged breakwaters two circulation cells develop (see Figure L3-5), in agreement with the flow field observed during the laboratory experiments. The gradient in the average water level is matched by the flow field. The water flows back through the gaps generating a strong current towards them. The lower average water level right seawards the submerged breakwater forces the current at the tips of the structures towards this point, generating as a result, the two circulation cells.
Towards the shoreline the current lessens. Nevertheless, a weak longshore current, pointed towards the gaps is still noticeable.
The current field is not symmetrical to the submerged breakwater due to the asymmetry of the layout of the basin. The velocities do not split up towards the gaps in the exact middle of the structures in agreement with the measured depth-averaged velocities represented in Figure 7.7-5. The larger gap at the right side of the basin creates a stronger current which forces the velocities towards this area.
The current field is stronger than the current field obtained in the simulation without submerged breakwaters (Figure H3-5).

Since the return flux is the main driving force for the sediment transport, it is possible to draw some conclusions about the development of the bottom profile from the directions and the magnitudes of the arrows plot in Figure L3-6.
In the area close to the shoreline the arrows indicate the presence of an offshore current which will cause an offshore sediment transport. Landwards of the submerged

breakwaters the velocities bend towards the gap yielding a longshore sediment transport which will induce in turn erosion at the toe of the structures.
Towards the gaps the current is stronger which will entail a large accretion in these regions.

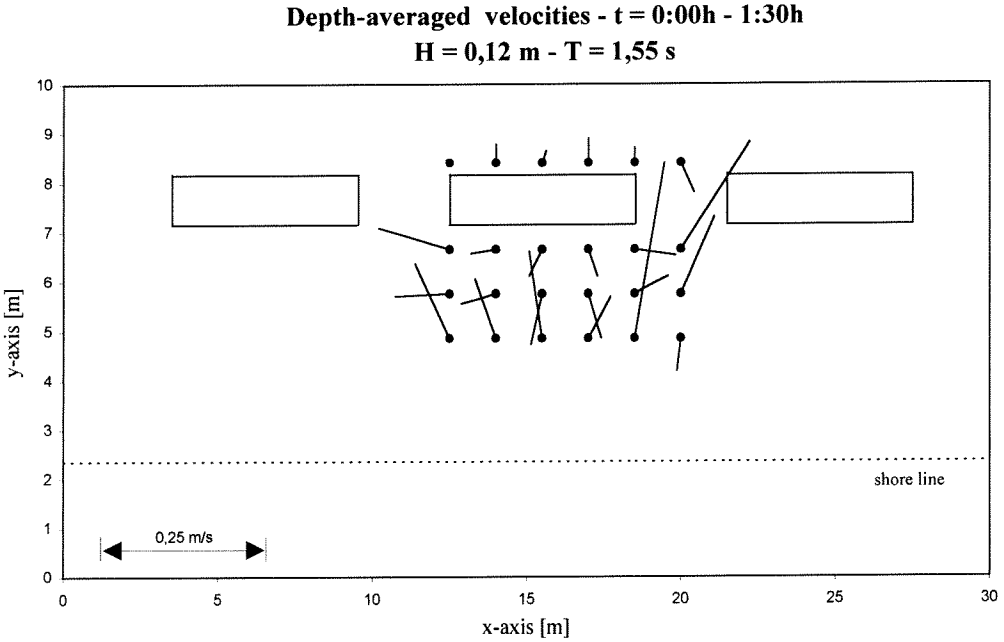

Figure 7.7-5 Test D3 - Measured depth-averaged velocities

By comparing the outcomes of this simulation with the outcomes of the simulations with smaller wave heights (cases D1 and D2, figures in Appendix L1 and Appendix L2), the patterns of the wave and flow field and of the mean water level are approximately the same, while the order of magnitude is smaller.

7.8 Conclusions and remarks

The comparison of the computation results with the measurements highlights some discrepancies in the outcomes. Multiple factors cause these differences.
Nevertheless, the pattern of the current field computed and measured is quite matching. The measurements pointed out a strong return flux generated through the gaps between the submerged breakwaters and this phenomenon does agree with the outcomes of the simulations.
The average water level is very difficult to compare due to the limited measurements and to the shortcomings of Delft2D-MOR.
Although in the simulations, waves immediately react to the presence of the submerged breakwater, whereas in reality there is a time-lag before the structure influences the wave field, the pattern of the simulated average water level around the submerged breakwaters is rather coherent with the measured one. The gradient in the longshore direction generates a strong current as it is pointed out in the test results.
In the simulations, once the waves have passed the crest of the submerged breakwaters, they immediately stop breaking. This phenomenon represents an important shortcoming of the wave module, which limits the possibility of improving

knowledge about the influence of the submerged breakwaters on the average water level in the breaker zone.
In shallow water the equipment used during the laboratory experiments is in general not able to carry out measurements, therefore, it is very important to improve the numerical model to reasonably simulate the wave pattern in this area.
It is worth to remind that the program Delft2D-MOR is still in a developing stage.

8. 2DH SIMULATION, MOBILE BOTTOM PROFILE

8.1 Introduction

In this chapter the results of the simulations, carried out with sediment transport and bottom changes included, are discussed.
The first section will deal with the Delft2D-MOR input file. After this, the results of the computations performed with three submerged breakwaters and without submerged breakwaters will be analysed.

8.2 Used process tree

The process tree used to determine the wave set-up and the bottom profile variations is presented in Figure 8.2-1.

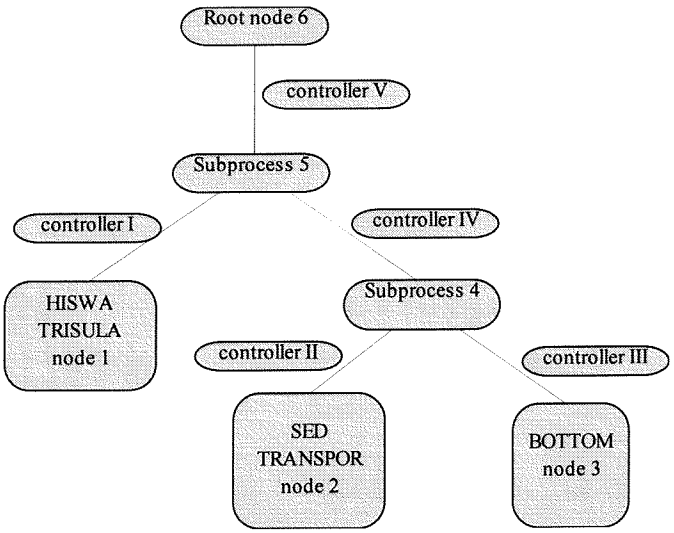

Figure 8.2-1 Used process tree

The process to be simulated here (represented by the root node 6) exists in one execution of subprocess 5. Subprocess 5, in turn, is simulated by the wave-flow module and subprocess 4. This last subprocess is alternately simulated by the sediment transport and the bottom module.
First a computation is made by executing in sequence the wave and the flow module once (stop criterion of controller I). This procedure does not differ from the one explained in the previous chapter (see Chapter 6, Section 6.2), apart from the fact that in this case the TRISULA module is run directly within the same elementary subprocess. This situation must not confuse the reader. The reason way in the previous simulations two separate modules have been used, is simply to allow the user to become more familiar with the program itself.
When, after the first computation, the wave-driven current and the wave set-up are known, the others two modules are started. The wave and flow data are now used by the sediment transport module to compute the sediment transport rate which in turn is used to update the bed-level in the bottom module.
If the specified simulation time is not yet reached (controller V), the sediment transport and the bed-level computation will be repeated maximally 30 times (controller III) with use of the "continuity correction" (see Chapter 5, Section 5.3).

After this, the simulation comes back to HISWA and TRISULA modules to update the wave and flow field.
The transport and bottom modules are executed with the automatic time step procedure described in Appendix G. Controller IV will stop the transport and bottom computation if the maximum of 30 executions or if the specified time of controller V is reached.

8.3 Input description

Since the input files concerning the wave and the flow module are the same as the ones presented in the previous chapter, the reader is referred to Chapter 7 for any details.
In the following section the input files for the transport and the bottom module will be briefly illustrated.

Transport and bottom input

Transport formula

To implement the chosen transport formula (Bijker with wave effect, see Appendix F), the user must specify the parameter b in the input file of the TRSTOT module. This parameter, in the bed load formula, depends on the relative activity of the waves (breaking or not) which is expressed in the ratio H_{rms}/h. Two values can be given to the coefficient b: one for shallow water (high values of H_{rms}/h) and one for deep water (low values of H_{rms}/h), while for the intermediate water depth, the b value is linearly interpolated. The following values refer to shallow and deep water respectively (wave height H = 0.12 m):

b = 5 $\quad H_{rms}/h \geq 0.79$

b = 2 $\quad H_{rms}/h \leq 0.08$

Furthermore, the following values are used:

d_{50}	= 75	[μm]	=	median diameter
d_{90}	= 100	[μm]	=	particle size larger than 90% of the weighted material
w	= 0.006	[m/s]	=	fall velocity of the grains
ρ_s	= 2650	[kg/m^3]	=	sediment density
ρ	= 1000	[kg/m^3]	=	water density
ϵ	= 0.4	[-]	=	porosity of bed material
ν	= 1.0e-6	[m^2/s]	=	kinematic viscosity of water
r_c	= 0.025	[m]	=	roughness length

Physical slope effect

The Bijker formula does not take into account the effect of the bed-level gradient. By means of a multiplication factor, depending on the bed-level gradient, this effect can be included. The correction term reads:

$$\alpha_s = 1 + \alpha_{bs} \frac{\partial z_b}{\partial s} \qquad (8.4.1\text{-}1)$$

The sediment transport after the correction of the physical slope is given by:

$$S = \alpha_s S' \tag{8.4.1-2}$$

where S' = [m^3/sm] = sediment transport according to the Bijker formula

The coefficient α_{bs} is assumed equal to 1.

Numerical stability
To ensure stability in the used numerical scheme for the bottom computation, numerical diffusion must be brought into it. This is obtained by introducing a slope-dependent correction term like the physical slope correction term. The stability term α_n reads:

$$\alpha_n = 1 + \alpha_{nn} \frac{\partial z_b}{\partial s} \tag{8.4.1-3}$$

The sediment transport rate will be multiplied by this expression. For the coefficient α_{nn} a number of options are available. A coefficient based on the bed level celerity $b_e S/h$ is used, in which S is the sediment transport rate, h is the water depth and b_e is a constant to be chosen properly.
The following option is used:

$$\alpha_{nn} = 0.5\alpha_{st}\left(\frac{b_e}{h}\right)dl \tag{8.4.1-4}$$

where b_e = 5.0 = power of transport relation
α_{st} = 1.0 = stability coefficient
dl = local grid cell length
h = averaged water depth over the time interval used in the bottom computation

The sediment transport including the physical slope effect and the numerical stability correction term yields:

$$S = \alpha_s \alpha_n S' \tag{8.4.1-5}$$

The computation is carried out by means of the automatic time step option (see Appendix G).
The maximum Courant number for the time step calculation is chosen equal to 0.8.

8.4 Results

The layout of the computations is shown in Table 8.4-1:

Time period	Wave height	No breakwater A	Three breakwaters D
T = 1.55 s	H = 0.1 m	A2	D2
T = 1.55 s	H = 0.12 m	A3	D3

Table 8.1-1 Wave condition used for the simulation

This section will concern only the outcomes of the simulations A3 and D3. The results of the other computations are rather similar to the previous ones, respectively. Therefore, they will be omitted in this work.
For further analysis, reference is made to Schaap (1997).
The simulations last 7.5 hours, the same as the laboratory experiments. After 7.5 hours the bottom profile of the model should have undergone the same variations as the basin bottom profile. Nevertheless, it will be noticed that the results of the simulations do show some discrepancies.
A cause for these discrepancies might be the shortcomings of the program itself.
Though the sediment transport is not a topic of this study, this aspect of the simulation will be briefly considered in the following.
A more detailed analyses about sediment transport can be found in the master thesis of Schaap (1997).
During the computations it was observed that the water depth, taken into account to determine the optimal time step (see Appendix G), was too close to the shore line, yielding a very small computational time step. In order to avoid this, the grid enclosure, used by TRISULA to limit the computation domain, is taken shorter than the bottom grid in y direction. Nevertheless, the accuracy of the simulation does not diminish since in very shallow water the equations used by the program are not valid.
The landward boundary for the flow field computation during the 7.5 hours is determined by the initial shoreline. Delft2D-MOR is not able to model the retreat of the shoreline. This shortcoming will imply inaccuracies in the outcomes, mainly influencing the sediment transport.
Through out the following sections, 'left' and 'right' of the basin, if it is not otherwise specified, will be referred while facing the shoreline.
It is not possible to draw any quantitative considerations from the outcomes due to the presence of the inaccuracies mentioned above.

8.4.1 Simulation A3 - without submerged breakwaters

Transport and bottom computation

The contour map of the initial bottom profile is plotted in Figure M1-1.
After half an hour of simulated wave action, as the initial sediment transport, which is shown in Figure M1-2, is rather small, the bathymetry does not present any significant changes (see Figure M1-3). Nevertheless, it can be seen from the increase of the 'layer' characterised by bottom depths minor than 0.3 m, that sediment is already transported seawards.
In Figure 8.4.1-1 the development of the bottom profile during the simulation is plotted. After half an hour a shortcoming of the program is already visible. The fixed location of the shoreline causes the development of a trough close to the coast, which will increase remarkably during the simulation, reaching its maximum at the end of the simulation. The bottom profile measured during the laboratory experiment, visible in Figure 8.4.1-2, shows a considerable retreat of the shore line with sediment transported seaward.
Considering the bottom profile after 1.5 hours from the beginning of the simulation showed in Figure M1-4, the sediment is transported seawards uniformly over the

whole basin. Only at the left side a longshore component in the sediment transport can be noticed, probably due to an amplification of a numerical noise.
In Figure M1-5, the contour map of the bottom profile after 7.5 hours from the beginning of the simulation can be seen. The bottom profile shows a uniform milder slope.
The interference in the left side of the basin is amplified, yielding more remarkable irregularities in the bathymetry. Nevertheless, the order of magnitude of the longshore sediment transport is still very small, see Figure M1-6. After 7.5 hours the equilibrium profile has not been reached yet, which implies that the interference, now restricted to the left side of the basin, if the wave action lasted longer, could be propagated in the whole basin, distorting the results of the simulation.

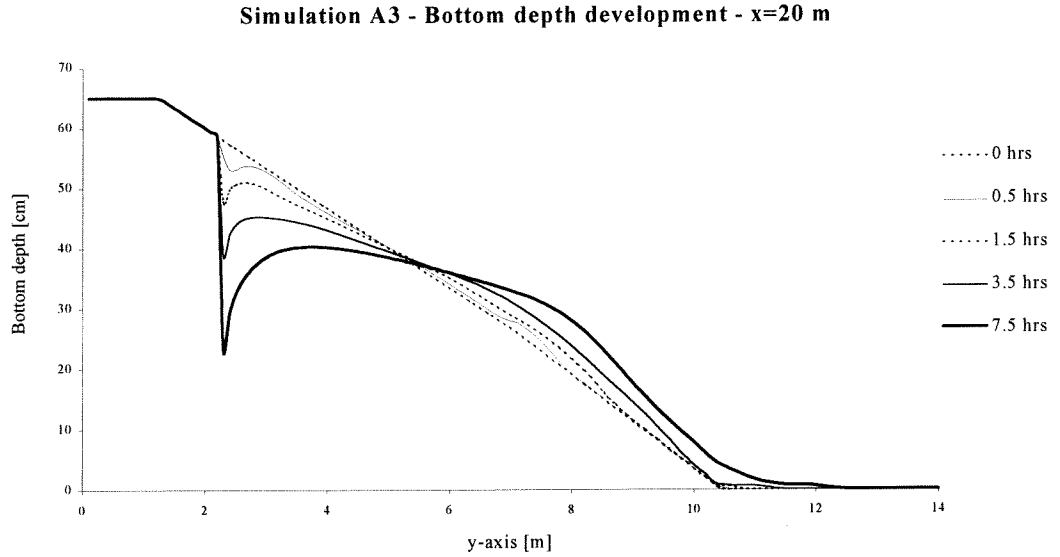

Figure 8.4.1-1 Simulation A3 - Development bottom profile over one cross-section

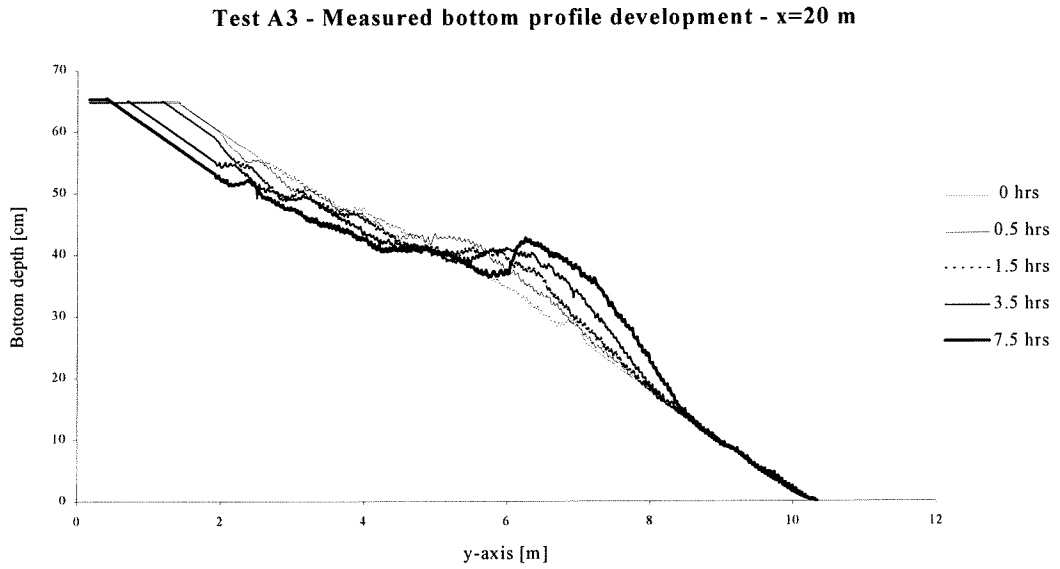

Figure 8.4.1-2 Test A3 - Development bottom profile over one cross-section

Wave computation

The computer model was run for a 7.5 hours simulation. The bottom topography changed considerably. With that bottom profile, the following results are discussed.
The contour map of the wave field after 7.5 hours of wave action is represented in Figure M1-7. Approaching the shore line, the wave height increases caused by shoaling, followed by a constant decrease started in line with the breaker line (see Figure 8.4.1-3). This pattern is the same for every cross-section due to the simualted regular wave field. An exception is represented by the area close to the left wall of the basin. Here, the behaviour of the wave height is different due to the interference caused by a numerical noise.
The wave force distribution detailed in Figure M1-8 confirms the regularity of the wave height pattern previous observed.
When the water becomes shallower, the waves start breaking. This is confirmed by the contour map of the wave energy dissipation (see Figure M1-9). In Figure 8.4.1-4 the comparison between the initial dissipation curve and the dissipation curve after 7.5 hours can be seen. The dissipation at the end of the simulation is smaller and less concentrated due to the generated bar visible in the bottom profile, which allows waves to keep on breaking towards the shore line.

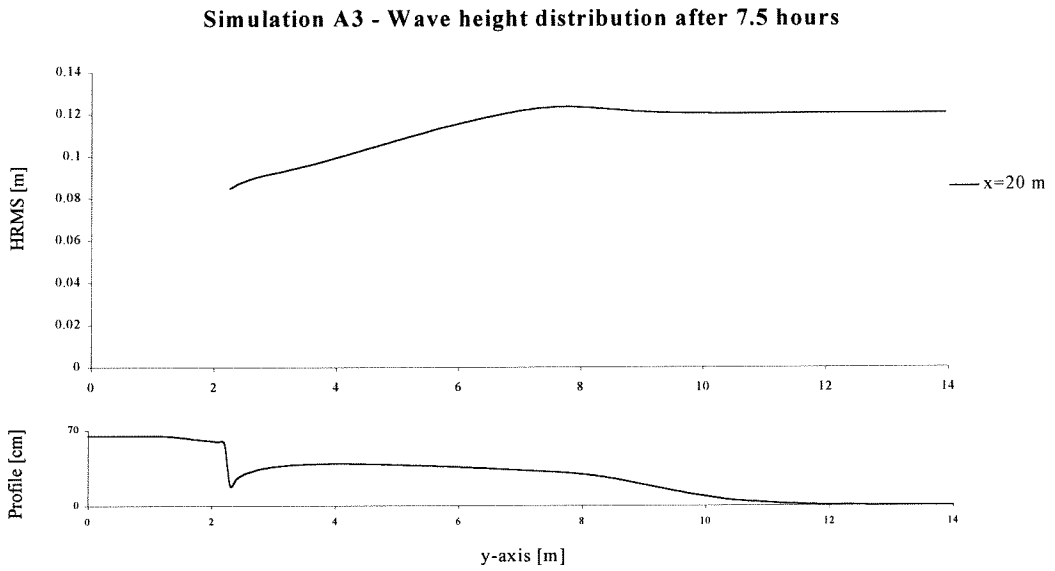

Figure 8.4.1-3 Wave height distribution after 7.5 hours over one cross-section

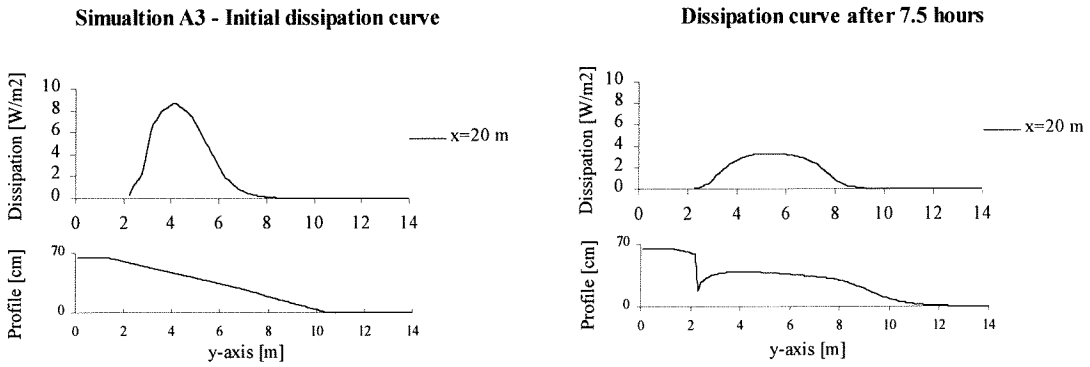

Figure 8.4.1-4 Initial distribution curve and after 7.5 hours over one cross-section

Average water level and flow computation

The contour map of the average water level after 7.5 hours of simulation is plotted in Figure M1-10.
No longshore differences in the whole basin can be observed, apart from a region in the left side of the basin, due probably to a numerical noise.
However, the distortion is very small and its influence on the outcomes over the whole basin, can be neglected.
In Figure 8.4.1-5 is shown the average water level development over one cross-section. Although the pattern does not change compared with the initial development, the magnitude of the wave set-up decreases remarkably due to the milder slope of the bottom.

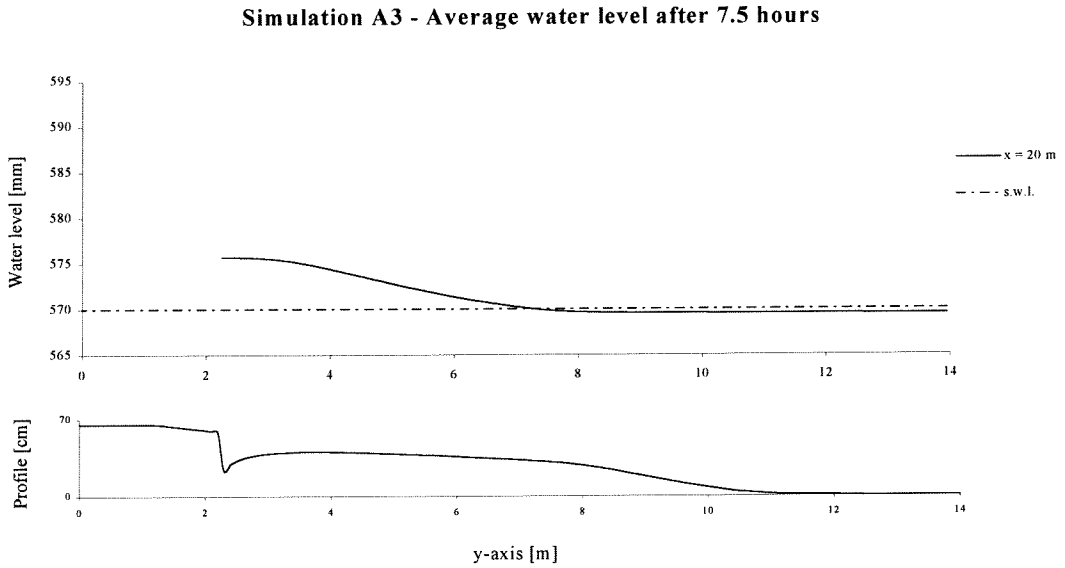

Figure 8.4.1-5 Average water level after 7.5 hours over one cross-section

8.4.2 Simulation D3 - three submerged breakwaters

Transport and bottom computation

The initial contour map of the bottom profile is represented in Figure N1-1.
After half an hour of wave action the bathymetry shows already remarkable changes (see Figure N1-2). Sediment is accumulated in the gaps between the submerged breakwaters and erosion occurs in the lee side of the structures.
The development of the bottom profile over the cross-section in line with the breakwater is illustrated in Figure 8.4.2-1.
After half an hour from the beginning of the computation, two significant shortcomings of the program are already visible. First of all, the impeded retreat of the shoreline results in the development of a trough close to the shore line. A large amount of sediment does not come into the basin from the shoreline, in contradiction with the measurements, leading to an unrealistic bottom profile evolution.
The second limitation of the program can be found in the pattern of the bottom profile right behind the submerged breakwater.
As it has been explained in the general remarks of the previous chapter (see Chapter 7, Section 7.4.2), HISWA is not able to model the quasi-steady breaking motion. This shortcoming has a big influence in the sediment transport which is very high right landwards of the submerged breakwaters (see Figure N1-3). The dissipation induced

by the breaking phenomenon over the structure does not disperse towards the coast, but it is concentrated right landwards of the submerged breakwater. Therefore, a considerable amount of sediment is brought in suspension by the waves in this area and transported by the current towards the gaps, giving as a result, a strong erosion at the toe of the submerged breakwaters in the lee side.
In Figure N1-4 this is illustrated by the bottom profile after 1.5 hours. The area eroded at the shore side of the submerged breakwater is enlarged remarkably and consequently the shoal in the gaps between the structures increases.
Close to the shore line the bathymetry does not present remarkable variations.
The contour map of the bottom profile after 7.5 hours is detailed in Figure N1-6. The erosion, in the area just behind the submerged breakwaters, is highly increased reaching the bottom of the basin in some zones. The shoal in the gaps is extremely deepened (see again Figure 8.4.2-1).
The comparison with the measured bottom profile during the laboratory experiments (Figure 8.4.2-3 and 8.4.2-4) reveals the need of improving the model mainly in the lee side of the submerged breakwater.
The 3D view of the bottom profile of the basin after 7.5 hours of simulated wave action is shown in Figure 8.4.2-5.
The development of the bottom profile in the simulation without submerged breakwater shows that the trough close to the shore line deepens faster than the trough in the simulation performed with submerged breakwater. This result agrees with the fact that the submerged breakwater influences the magnitude of the cross-shore sediment transport by reducing the wave energy.
In Figure 8.4.2-6 the contour map of the calculated erosion and accretion which occur in the basin after 7.5 hours is shown, while in Figure 8.4.2-7 the measured ones after the same interval is given. Although it is not possible to draw quantitative conclusions, it is noticeable that the model reproduces reasonably well the area where accretion occurs and overestimates the erosion.

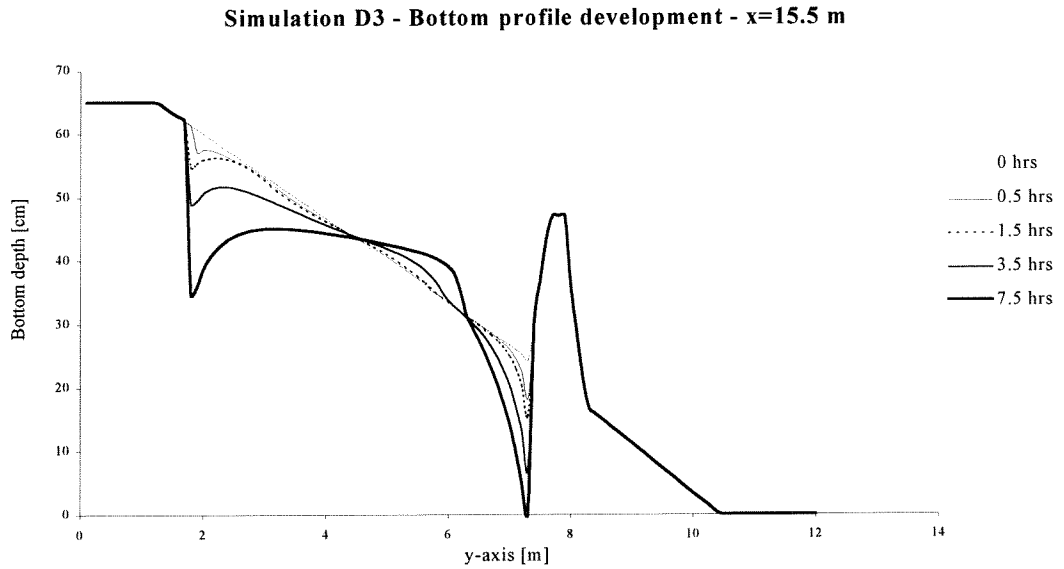

Figure 8.4.2-1 Simulation D3 - Development bottom profile over one cross-section in line with a submerged breakwater

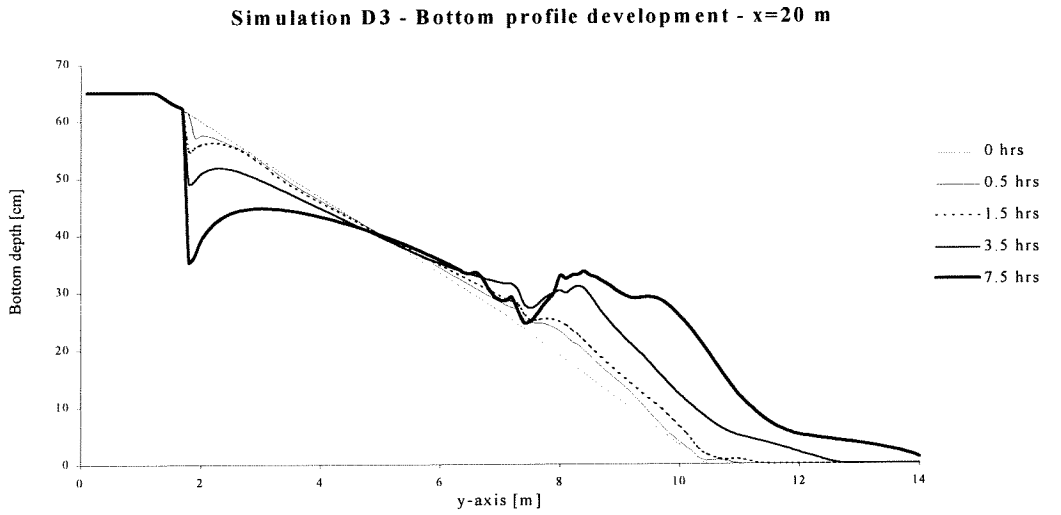

Figure 8.4.2-2 Simulation D3 - Development bottom profile over one cross-section in line with a gap

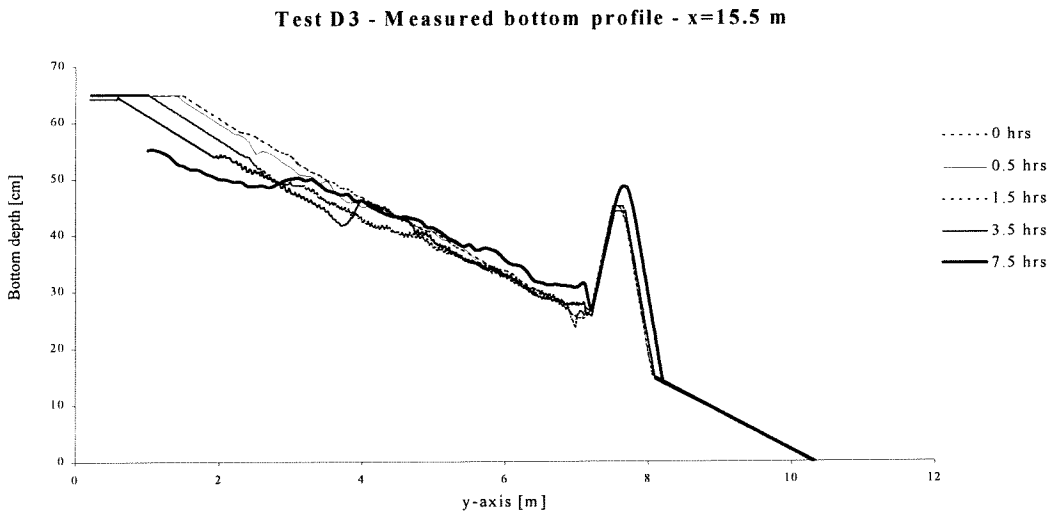

Figure 8.4.2-3 Test D3 - Development bottom profile over one cross-section in line with a submerged breakwater

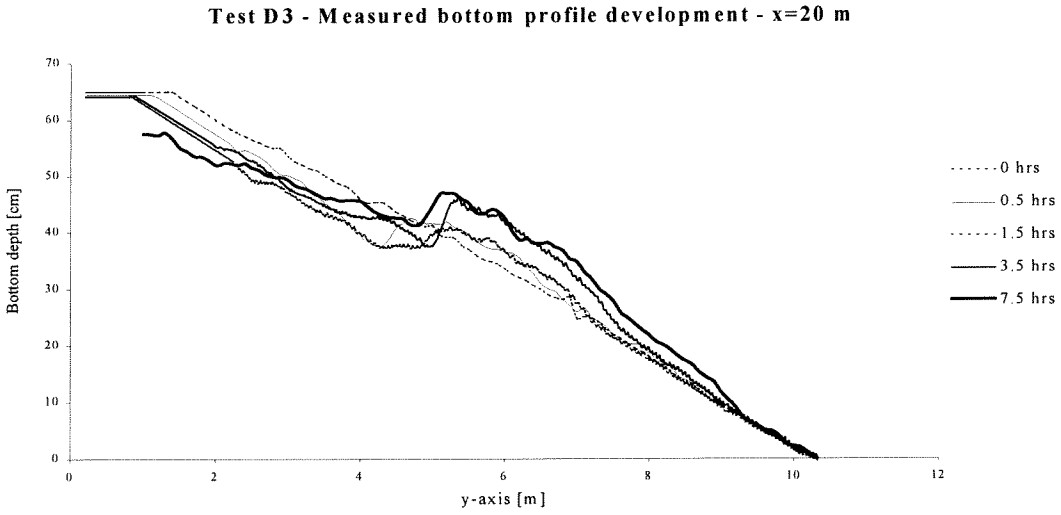

Figure 8.4.2-4 Test D3 - Development bottom profile over one cross-section in line with a gap

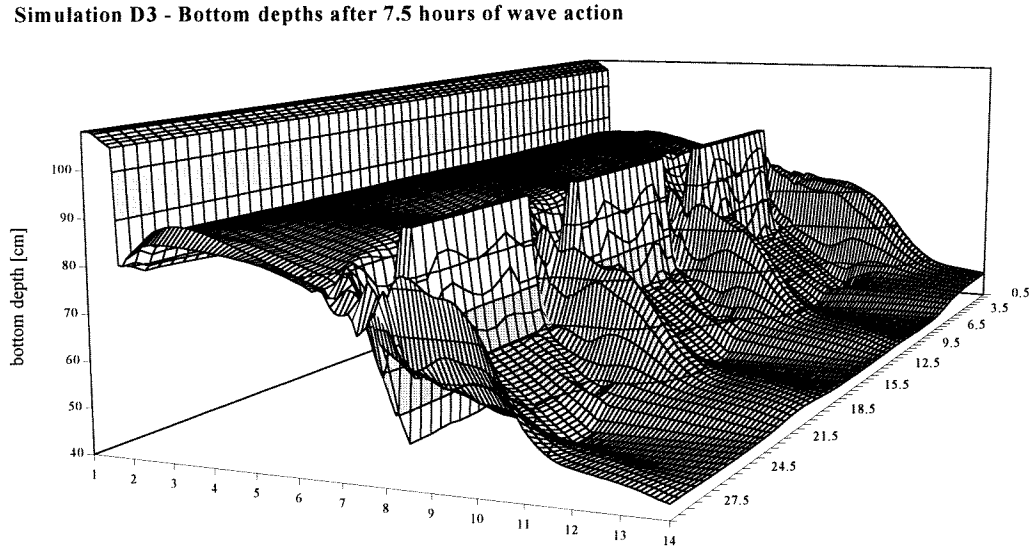

Figure 8.4.2-5 Simulation D3 - 3D view bottom depths after 7.5 hours of wave action

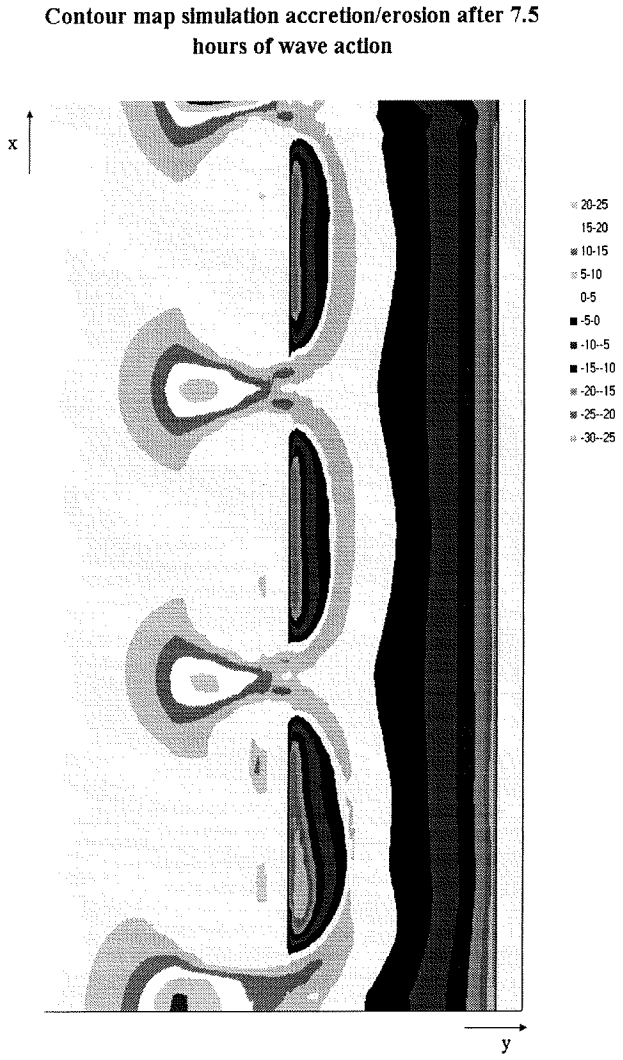

Figure 8.4.2-6 Contour map computed accretion/erosion after 7.5 hours of wave action [values in cm]

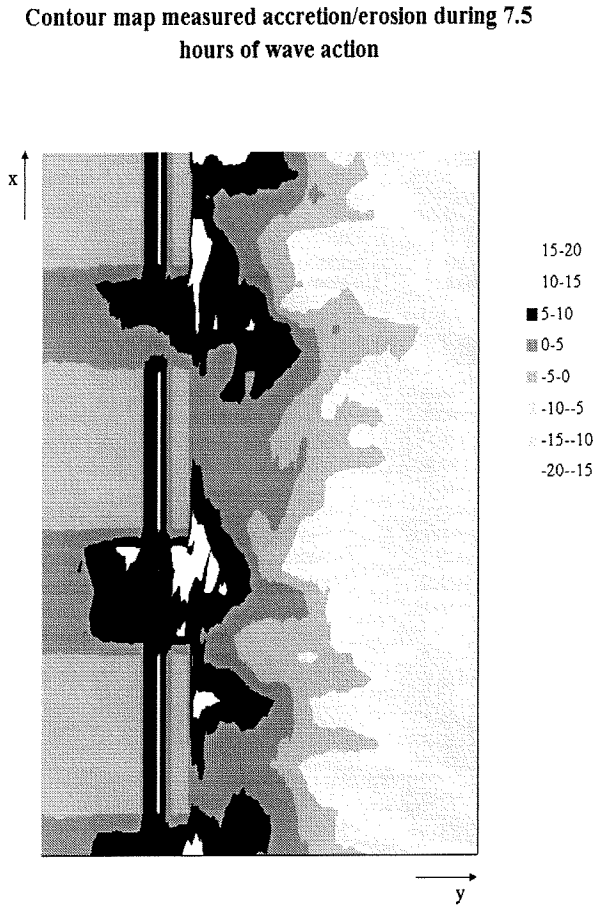

Figure 8.4.2-7 Contour map measured accretion/erosion after 7.5 hours of wave action [values in cm]

Since the bottom profile after 7.5 hours of simulated wave action shows an unrealistic pattern, it is not useful to illustrate the outcomes of the hydrodynamic processes, which are obviously not reliable.

8.5 Conclusions and remarks

In this chapter the outcomes of the simulations performed with a movable bed have been analysed.
Although some discrepancies with the results of the laboratory experiments have been highlighted, the program has been found to reasonably well reproduce the current field and the average water level in both the simulations with and without submerged breakwaters.

The simulation without submerged breakwaters underlines the need of improving the program in the area close to the shore line, since the impeded retreat of the shore line generates an unrealistic bottom profile evolution in this region.

The outcomes of the simulation with three submerged breakwaters pointed out that the sector in the lee side of the structures needs further research. In fact, due to the wave energy dissipation concentrated right behind the submerged breakwaters, an excessive erosion takes place in this area, yielding an unrealistic development of the bottom profile.

However, the average water level does show a pattern which satisfactory agrees with reality. Around the submerged breakwaters the gradient in the average water level, sloping down towards the gaps, generates a strong current towards them. Sediment transport evolves in cross-shore and longshore direction, yielding the developing of shoals in the gaps. The pattern of the flow field and the return current are in good agreement with the observed reality.
Delft2D-MOR is a very complex numerical model and its sensibility to different parameters is still under investigation.
As already said, the actual knowledge of the phenomena induced by a submerged breakwater is not thorough. Therefore, the laboratory experiments, on a scale 1:15, were made to improve this knowledge. If it was possible to give an exact interpretation of the outcomes, Delft2D-MOR could be implemented based on an accurate data set and its improvement might be less difficult. In this case, however, the discrepancies found between calculations and measurements are more complex to investigate, since it is not always evident whether they are a consequence of the shortcomings of the numerical model itself or of the inaccuracies in the data set.

9. 2DH SIMULATION, DIFFERENT CONFIGURATIONS

9.1 Introduction

The present chapter concerns the outcomes of simulations performed with different submerged breakwater configurations.
The following section explains the meaning of the terms and the symbols used in this chapter. Section 9.3 deals with the simulation set-up. In the last sections the hydrodynamic aspects of the results are discussed.

9.2 The exposure ratio

Wide gaps permit more wave energy to penetrate into the area behind both the emerged and the submerged breakwaters, thus maintaining some level of longshore sand transport. The ratio of gap width to the sum of breakwater length and gap width is called the *exposure ratio* (U. S. Army Corps of Engineers (1994)):

$$E = \frac{G}{L+G} \qquad (9.2\text{-}1)$$

where E = exposure ratio
G = gap width
L = breakwater length

The definition of the symbols are detailed in Figure 9.1-1
Experiments have been conducted in Japan on wave-induced flow patterns around a submerged breakwater with length L, gap width G and distance from the shoreline X_{off} (Sawaragi (1992)).

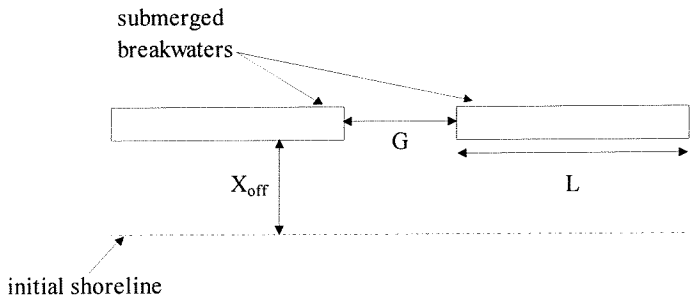

Figure 9.1-1 Definition sketch of a plane arrangement of submerged breakwaters

9.3 Simulation set-up

The domain of the computations consists of a basin based on the one used in the laboratory experiments described in Chapter 2, Section 2.1.2. The length of the basin is equal to 30 m and the width to 14.1 m. Three identical submerged breakwaters have been located at different positions on a fixed bed. The still water level is fixed to 570 mm. The submergence of the crest of the structures have been maintained equal to 0.1 m below the still water level for every simulation.
Each computation is performed with regular waves of 0.12 m high and with a wave period of 1.55 s.

The same parameters settings as the previous chapters have been used.
The process tree and the Delft2D-MOR input file, used for the simulations, are described in Chapter 7.
The first series of simulations is carried out with different exposure ratios and a distance from the shoreline equal to 6.4 m, as detailed in the Table below.

Simulation	E00	E01	E02	E03	E04	E05	E07	E09
Exposure ratio E	0.0	0.1	0.2	0.3	0.4	0.5	0.7	0.9
G [m]	0	1	2	3	4	5	7	9
L [m]	29	9	8	7	6	5	3	1
X_{off} [m]	6.4	6.4	6.4	6.4	6.4	6.4	6.4	6.4

Table 9.1-1 Simulation layout with different exposure ratios

The second series is performed with different positions of the submerged breakwaters from the shoreline and an exposure ratio equal to 0.3 (see Table 9.1-2).
The submerging of the crest has been maintained equal to 0.1 m for each simulation.

Simulation	X01	X02	X03
E	0.3	0.3	0.3
X_{off} [m]	7.45	4.30	3.00
L/X_{off}	~ 1	1< <2	~ 2

Table 9.1-2 Simulation layout with different off-shore distance X_{off}

In the following sections, the hydrodynamic aspects of the outcomes are analysed.
In order to better understand the analysis, a series of figures is included in the appropriate appendices. Some Excel figures are illustrated in the text. For both the figures in the text and in the appendices, the same criteria as the previous chapters are used.

9.4 Different exposure ratios results

Simulation E01

Figure 9.4-1 shows the layout of the simulation.

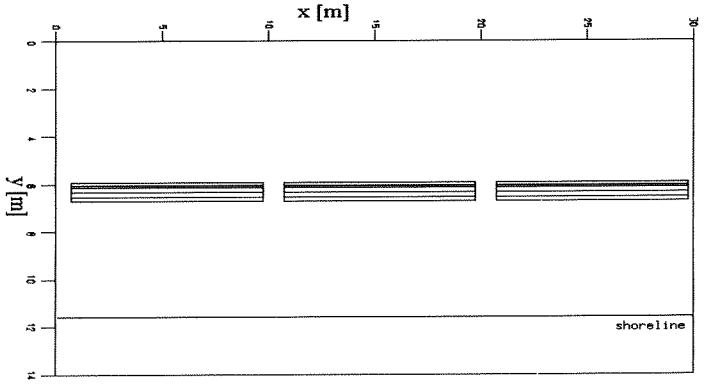

Figure 9.4-1 Simulation E01- layout

The pictures indicated with the code P01 are included in Appendix P01.

In the gaps, due to the low resolution of the TRISULA computational grid, only one grid point is computed. Therefore, the resulting flow and wave field are not very accurate.

Flow computation

The resulting flow field is given in Figure P01-1. The influence of the narrow gaps upon the current field is limited. The velocities are small over the whole basin; a slight increase is noticeable towards the gaps resulting in two weak circulation cells around the tips of the submerged breakwaters.

Figure P01-2 shows the return flow field. The current over the submerged breakwaters is pointed seawards. The magnitude of the longshore component, right behind the structures, is very small. The sediment transport, which is mainly driven by the return flow, will be predominant in the off-shore direction.

This configuration can be classified as 2D, since it is similar to the one with a single long submerged breakwater (see Figure P01-3 and P01-4).

The contour map of the wave energy dissipation shown in Figure P01-5 and P01-6 confirms this. There are hardly any longshore differences in line with the submerged breakwaters. The dissipation in the gaps is probably due to the influence of the structures and to the low resolution of the computational grid.

Computed average water level

The contour map of the average water level is given in Figure P01-7. The sudden change in the bottom depth induces breaking. The resulting wave set-up increases towards the shoreline. A longshore gradient in the average water level, decreasing from the middle of the submerged breakwaters towards the gaps, occurs. Nevertheless, due to the narrow widths of the gaps, this gradient becomes almost zero immediately landwards of the submerged breakwaters.

Figure 9.4-2 shows a 3D view of the average water level in the basin. The development of the average water level is similar to the one obtained by means of a single detached submerged breakwater (Figure 9.4-3).

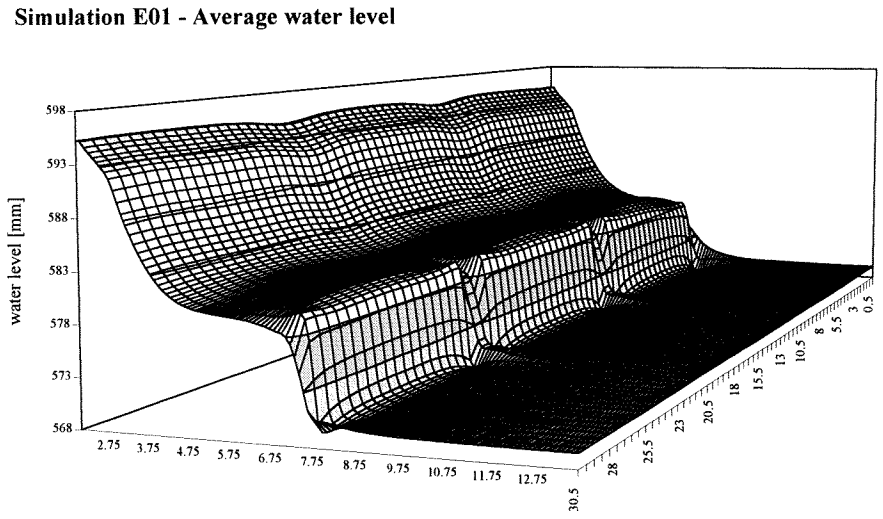

Figure 9.4-2 Simulation E01 - 3D view average water level

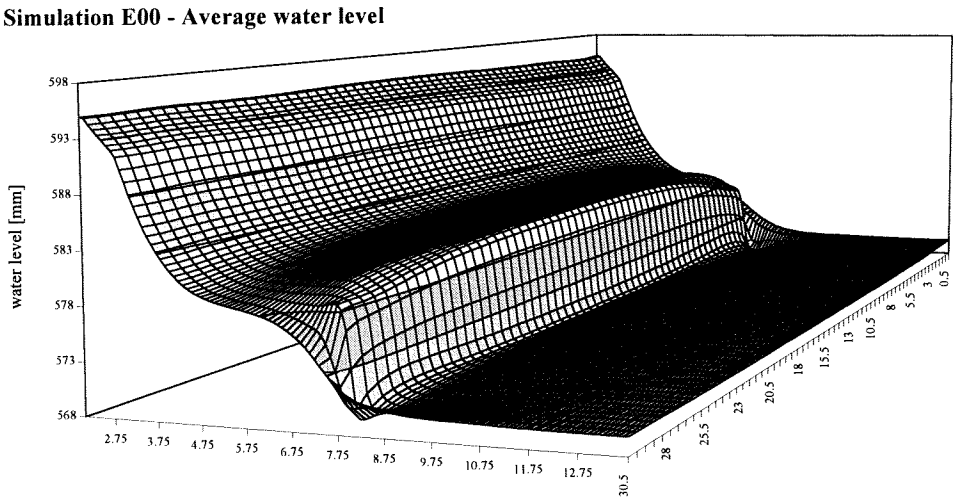

Figure 9.4-3 Simulation with one submerged breakwater - 3D view average water level

Simulation E02

Figure 9.4-3 shows the layout of the simulation.

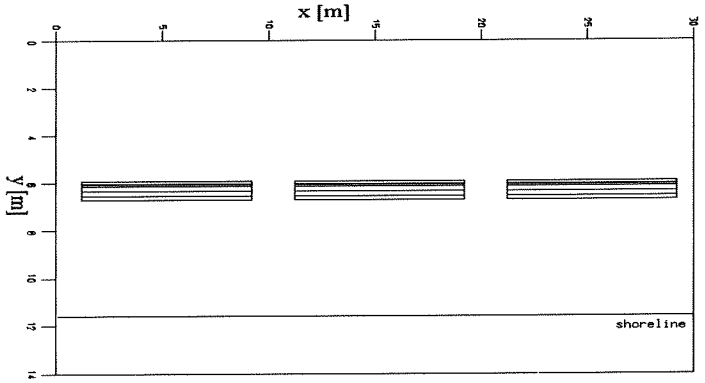

Figure 9.4-3 Simulation E02 - layout

The pictures indicated with the code P02 are included in Appendix P02.

Flow computation

The resulting flow field is given in Figure P02-1. Comparing this figure with the previous flow field, shows an increase in the velocities landwards of the submerged breakwaters and towards the gaps. The circulation cells around the tips of the structures are more pronounced.
The wider widths of the gaps cause an increased return flow field (see Figure P02-2). Over the crest of the submerged breakwaters, the current is partly pointed seawards and partly landwards, as a consequence of the enlarged influence of the gaps.

Computed averaged water level

The average water level contour map is shown in Figure P02-3. The gradient in the longshore direction, sloping down from the middle of the submerged breakwaters to the gaps, is more pronounced and a slight decrease in the water level right seawards of the structures is visible.

The 3D view of the average water level details the pattern described above (Figure 9.4-4).

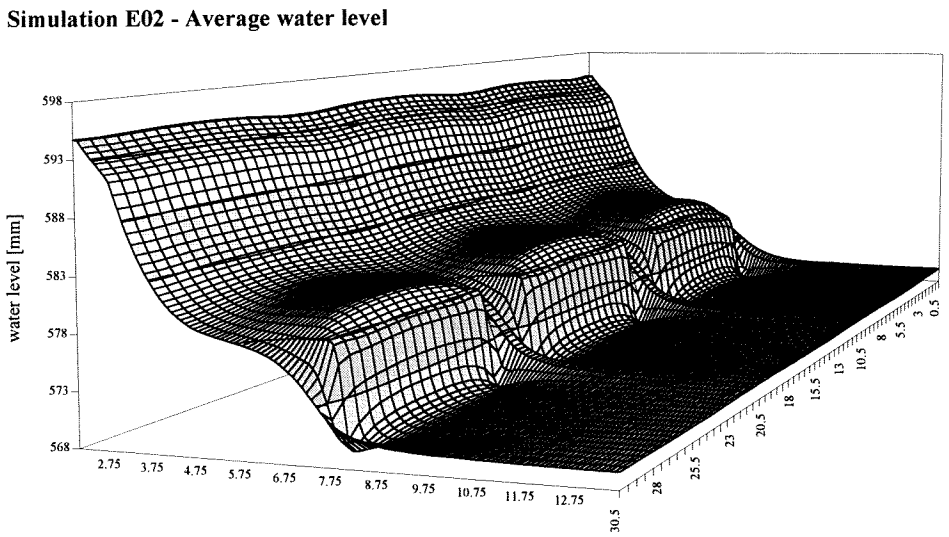

Figure 9.4-4 Simulation E02 - 3D view average water level

Simulation E03

Figure 9.4-5 shows the layout of the simulation.

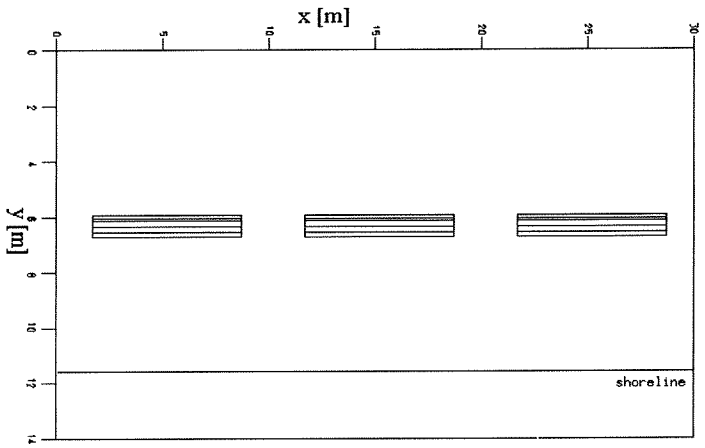

Figure 9.4-5 Simulation E03 - layout

The pictures indicated with the code P03 are included in Appendix P03.

Flow computation

The resulting flow field, given in Figure P03-1, shows some differences with the previous outcomes. A strong current evolves towards the gaps and, consequently, the velocities split up in the middle of the submerged breakwater. Two circulation cells develop around the tips of the structures. A significant longshore current occurs in the lee side of the submerged breakwaters.

The exposure ratio equal to 0.3 outlines the change between the configuration comparable with one single submerged breakwater and the multiple system configuration.

Figure P03-2 shows the return current field. The water flows back through the gaps, therefore, over the crest of the submerged breakwaters, the velocities are heading landwards.

Computed averaged water level

The contour map of the average water level is given in Figure P03-3. A longshore gradient develops in line with the crest of the submerged breakwaters, decreasing towards the gaps, and it weakens to the shoreline. Figure 9.4-6 gives a 3D view of the average water level in the basin.

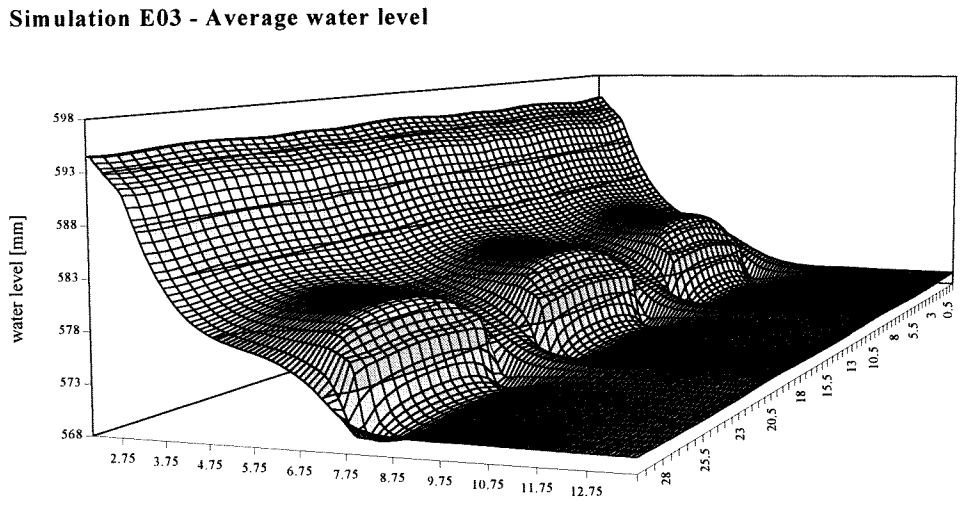

Figure 9.4-6 Simulation E03 - 3D view average water level

Simulations E04, E05, E07

By enlarging the exposure ratio from 0.4 to 0.7, the return flow through the gaps varies. First it is noticeable an increase, then, as a consequence of the reduced influence of the submerged breakwaters, the return current decreases. The evolution of the current pattern and the mean water level can be observed in the figures presented in Appendix P04, P05, P07 respectively.

Simulation E09

Figure 9.4-7 shows the layout of the simulation.

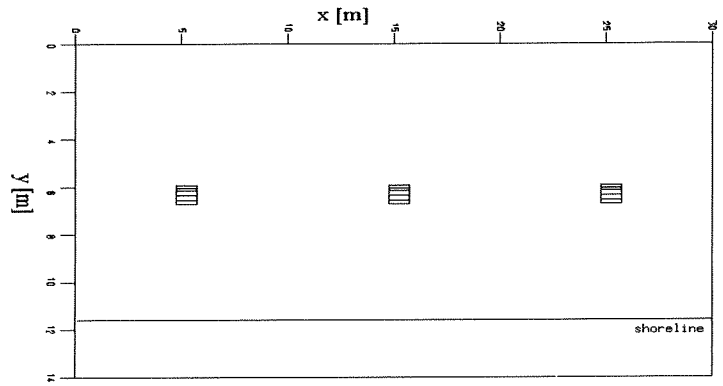

Figure 9.4-7 Simulation E09 - layout

The pictures indicated with the code P02 are included in Appendix P02.

Flow computation

The average flow field is given in Figure P09-1. Two circulation cells around the tips of the submerged breakwaters develop, although the magnitude of the velocities is very small. Higher values of the current field occur over the crest of the submerged breakwaters, pointed towards the shoreline.

The longshore current, developed landwards of the submerged breakwaters, weakens to the gaps.

The return flow field is shown in Figure P09-2. The current is dominant in the cross-shore direction and it is almost not influenced by the submerged breakwaters. The efficiency of the submerged breakwater is very small in comparison to the large width of the gaps.

Figure P09-3 shows the wave energy dissipation. Comparing this figure with the results of the previous simulations, shows that over the submerged breakwaters the order of magnitude of the dissipation does not change.

Computed averaged water level

The average water level contour map, given in Figure P09-4, shows that there are hardly any longshore variations in the mean water level. This situation is comparable with the one without submerged breakwaters.

The predominance of the gaps upon the submerged breakwaters is made more clear by the Figure 9.4-10.

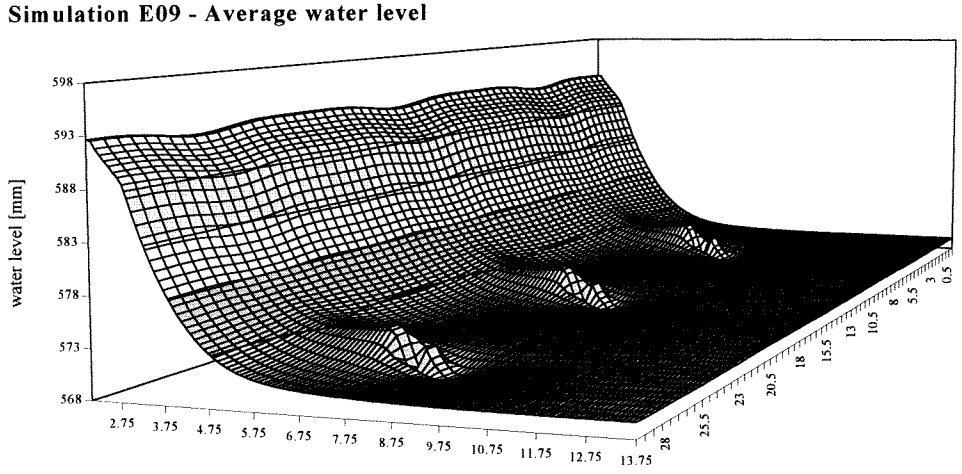

Figure 9.4-10 Simulation E09 - 3D view average water level

9.5 Results of the simulations with different X_{off}

Simulation X01 (X_{off} = 7.45 m)

The layout of the simulation can be seen in Figure 9.5-1.

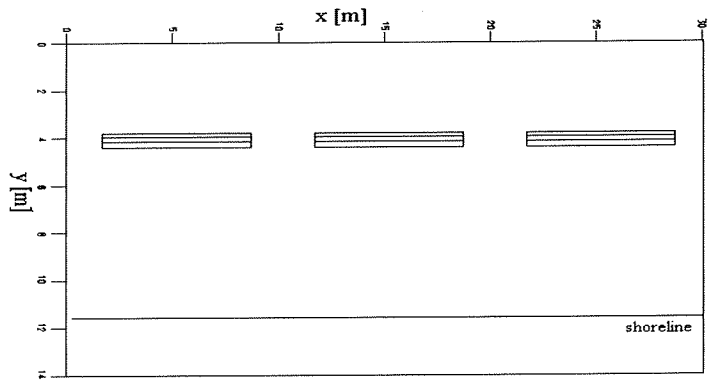

Figure 9.5-1 Simulation X01- layout

The pictures indicated with the code Q1 are included in Appendix Q1.

The submerged breakwaters are positioned at the beginning of the slope.
Figure 9.5-2 shows the development of the wave height over two cross-sections, one in line with a submerged breakwater (x = 15 m) and the other over a gap (x = 20 m). It seems that the submerged breakwater influences the evolution of the wave height over the gap.
The wave energy dissipation curve is given in Figure 9.5-3. The high value of dissipation, concentrated over the crest of the submerged breakwaters, causes the development of a strong current towards the shoreline.
In Figure Q1-1 the average flow field can be seen. The velocities are split up from the middle of the submerged breakwaters to the gaps, since a strong return flow takes place through them, yielding the evolution of two circulation cells around the tips of the structures.
The influence of the gaps weakens only very close to the shore line.
Figure Q1-1a gives a detail of the flow pattern near the coast. The velocities, headed towards the middle of the submerged breakwaters, cause two circulation cells in the opposite directions of the ones generated around the tips of the structures.
The average return flow field is plotted in Figure Q1-2. A strong return flow in off-shore direction develops close to the shoreline. An opposite current occurs behind the submerged breakwaters. The sediment transport, mainly driven by the return current, will probably be higher in a cross-shore than in a longshore direction.
Right behind the submerged breakwaters, the longshore gradient in the average water level slopes down to the gaps (see Figure Q1-3). Close to the shore line the situation reverses. The average water level is higher in the area in line with the gaps, where waves did not break yet, whereas is smaller in the lee side of the submerged breakwaters. The 3D view of the average water level, shown in Figure 9.5-4, gives prominence to this pattern.

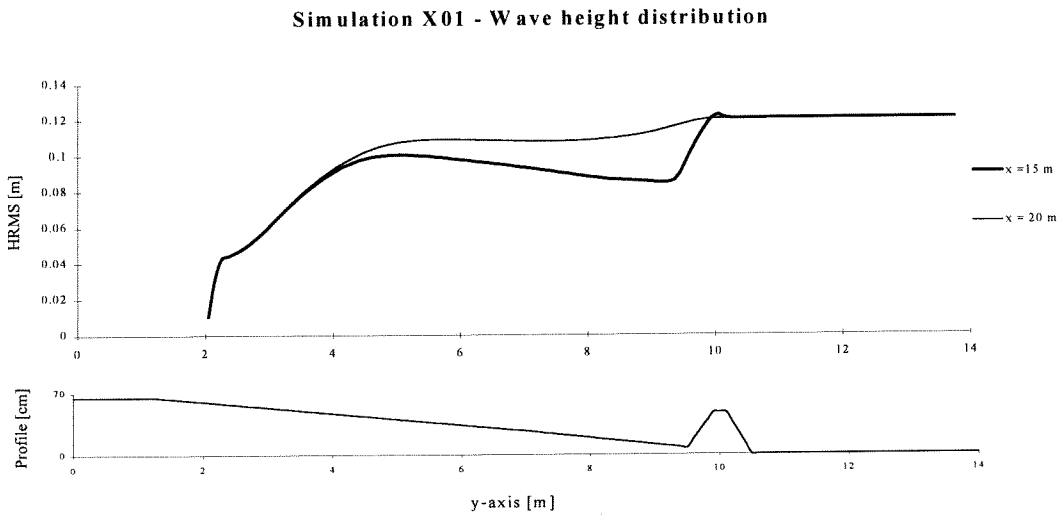

Figure 9.5-2 Simulation X01 - Wave height distribution over different cross-section

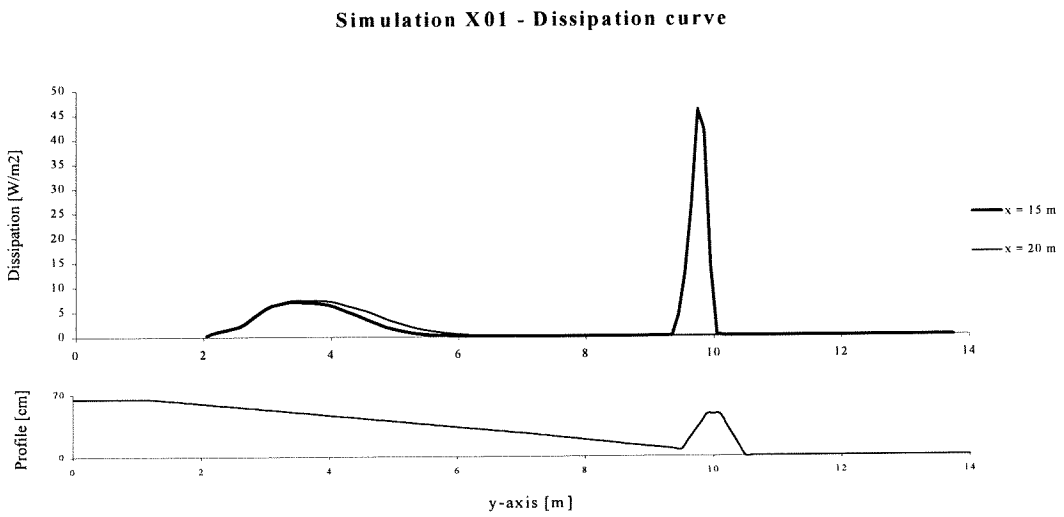

Figure 9.5-3 Simulation X01 - Dissipation curve over different cross-sections

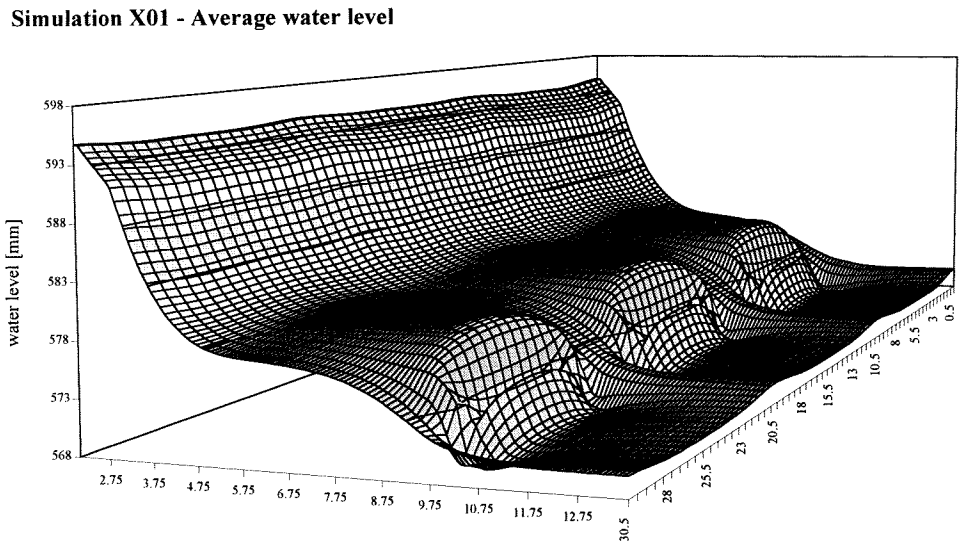

Figure 9.5-4 Simulation X01- 3D view average water level

Simulation X02 (X_{off} = 4.30 m)
The layout of the simulation can be seen in Figure 9.5-5.

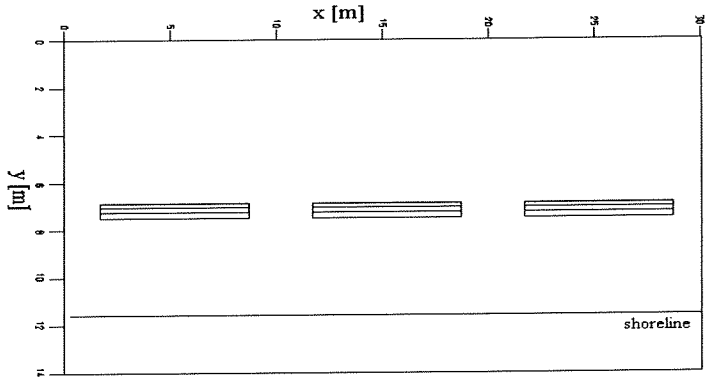

Figure 9.5-5 Simulation X02 - layout

The pictures indicated with the code Q2 are included in Appendix Q2.

The development of the wave height is given in Figure 9.5-6, where one cross-section is taken in line with the submerged breakwater (x = 15 m) and the other in line with a gap (x = 20 m). Approaching the breaker line, the wave heights increase due to shoaling.
When the structures are located closer to the shore line, the wave energy dissipation over the submerged breakwater decreases. This can be observed by comparing the dissipation curve given in Figure 9.5-7 with the dissipation curve of the previous simulation, as given in Figure 9.5-3.
One possible cause might be the different ratio between the crest width and the wave length, which influences the efficiency of the submerged breakwaters. The crest width is constant for each simulation, whereas the wave length varies along the slope.
Another explanation could be the different water depth, right seawards of the submerged breakwater. In the first case, the depth suddenly varies from 0.57 m to 0.10 m, while in the second case, it decreases from about 0.3 m to 0.10 m.
The average flow field, shown in Figure Q2-1, presents two circulation cells around the tips of the submerged breakwaters. As a consequence of the smaller dissipation, the velocities are weaker over the whole basin, compared with the previous configuration. A longshore current develops close to the shoreline, weakening from the middle of the submerged breakwaters towards the gaps.
No circulation cells develop near the shoreline.
Figure Q2-2 shows the average return flow field. Over the submerged breakwater, the return current is partly directed seawards and partly landwards. Right behind the structure, it is noticeable small velocities headed landwards.

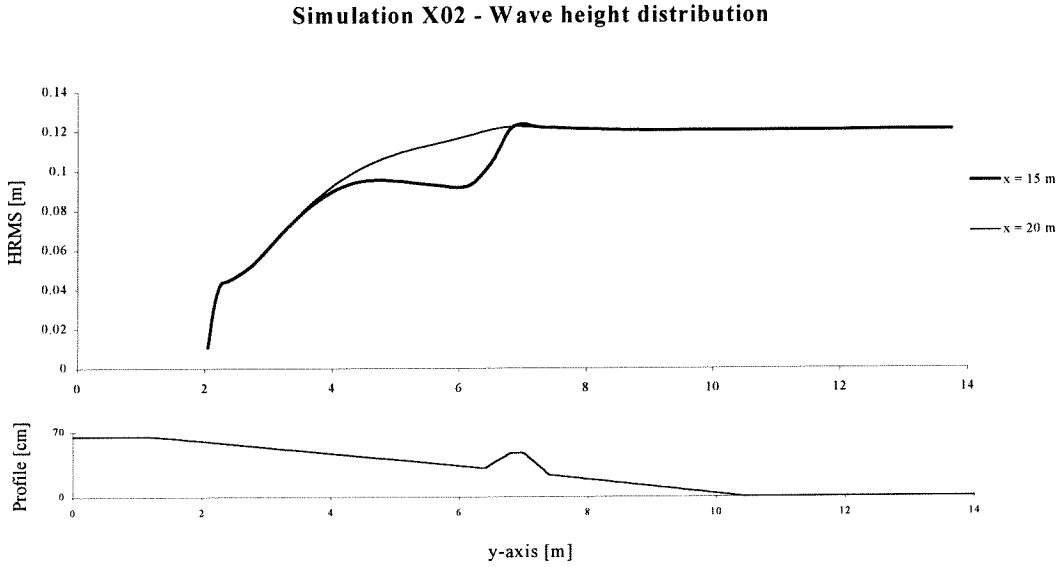

Figure 9.5-6 Simulation X02 - Wave height distribution over different cross-section

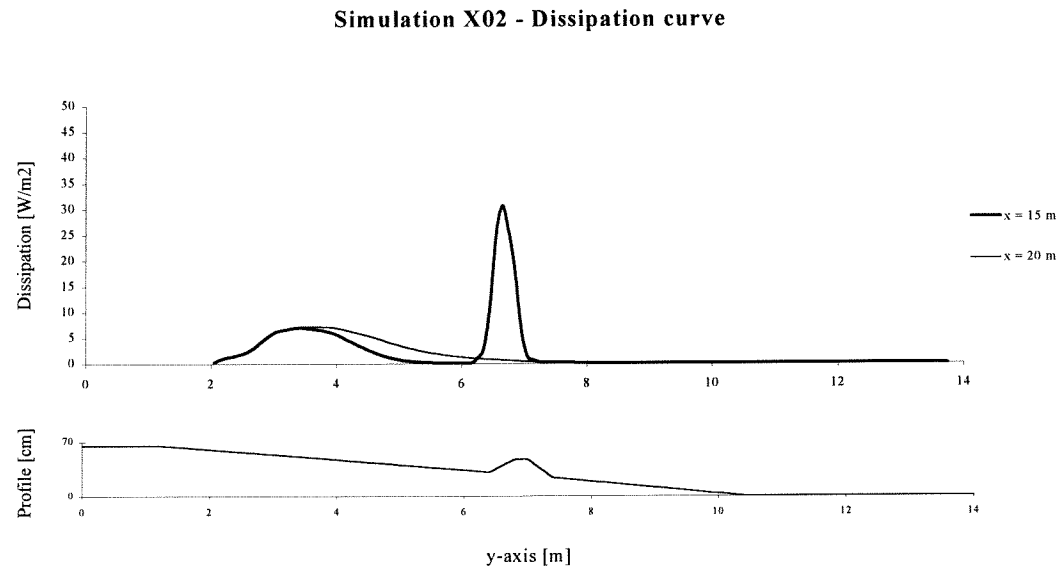

Figure 9.5-7 Simulation X02 - Dissipation curve over different cross-sections

The mean water level is given in Figure Q2-3. The gradient in the longshore direction in the area behind the submerged breakwaters is smaller, compared with the one of the previous computation and decreases towards the gaps.
Figure 9.5-8 gives a 3D view of the average water level in the basin.

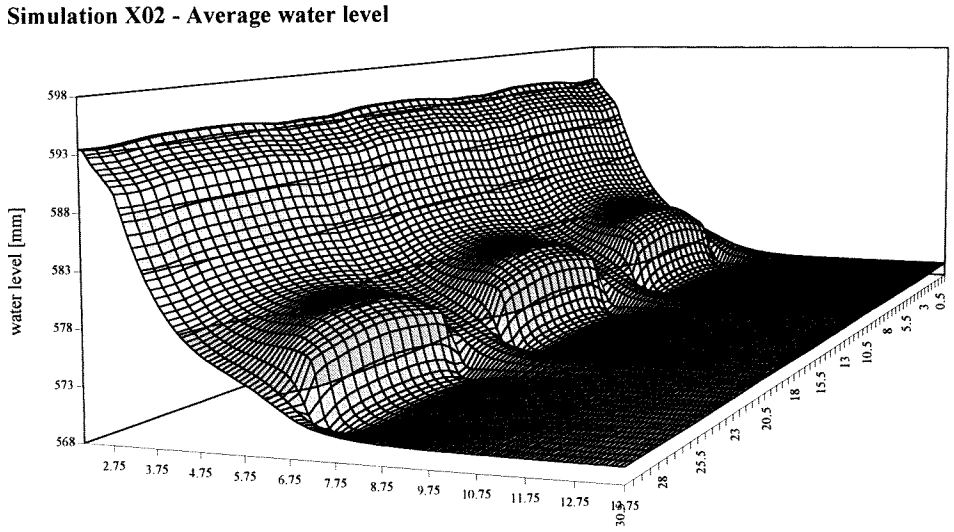

Figure 9.5-8 Simulation X02 - 3D view average water level

Simulation X03 (X_{off} = 3 m)

The layout of the simulation can be seen in Figure 9.5-9.

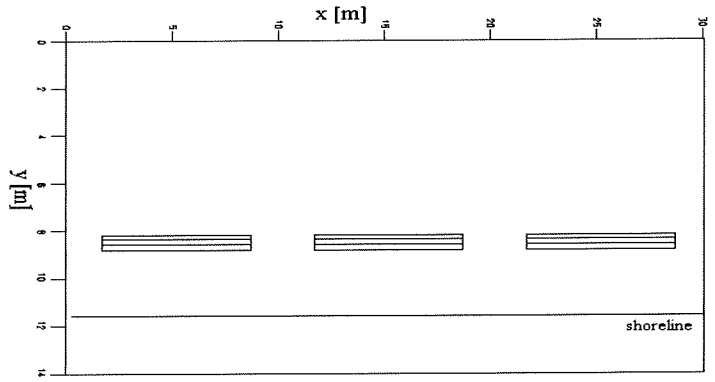

Figure 9.5-9 Simulation X03 - layout

The pictures indicated with the code Q3 are included in Appendix Q3.

The wave height development over different cross-sections is given in Figure 9.5-10. Approaching the shoreline, the wave heights increase due to shoaling.
Figure 9.5-11 shows the development of the wave energy dissipation over two different cross-section, one in line with a submerged breakwater (x = 15 m) and one in line with a gap (x = 20 m). The dissipation, induced by the submerged breakwater, is smaller compared with the results of the previous simulations. Also in this case, both the ratio of crest width to the wave length and the water depth in front of the structure are different from the ones of the previous computations.
It is interesting to notice that dissipation occurs before the structure is reached by the waves, probably due to the bottom induced breaking, since the same pattern of the dissipation curve can be seen over the gap. Then, over the crest of the submerged breakwater more breaking occurs, resulting in a peak in the dissipation curve.

The flow field is given in Figure Q3-1. Two circulation cells develop around the tips of the submerged breakwaters. Near the shoreline, a longshore current flows from the middle of the structures towards the gaps.
Figure Q3-2 shows the average return flow field. The velocities, over the submerged breakwaters, are directed seawards and only a weak longshore current develop in the lee side of the structure towards the gaps.
It seems that in this case, the efficiency of the submerged breakwaters, in reducing the off-shore sediment transport, is quite reduced.
The sediment transport will be mainly in off-shore direction, passing over the crest of the submerged breakwaters.

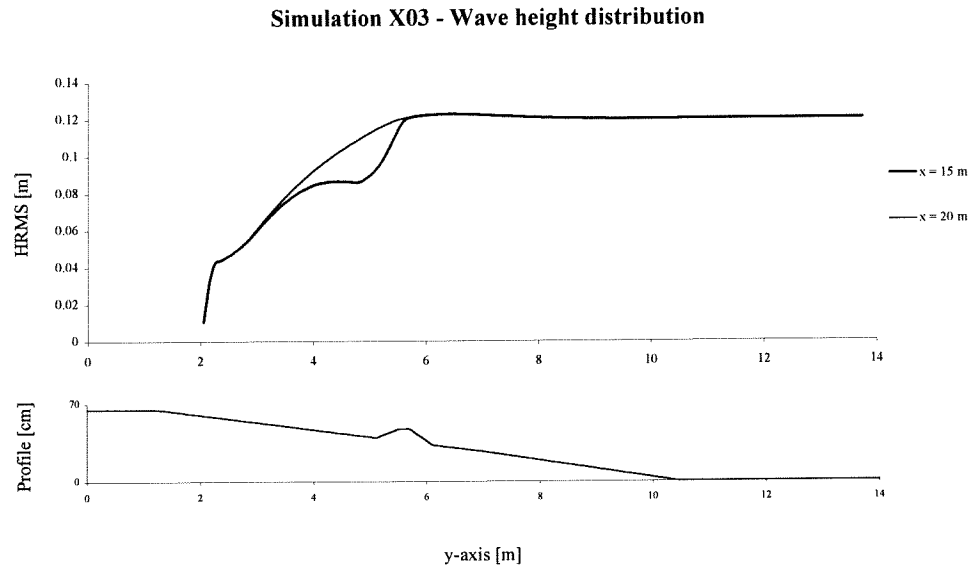

Figure 9.5-10 Simulation X03 - Wave height distribution over different cross-sections

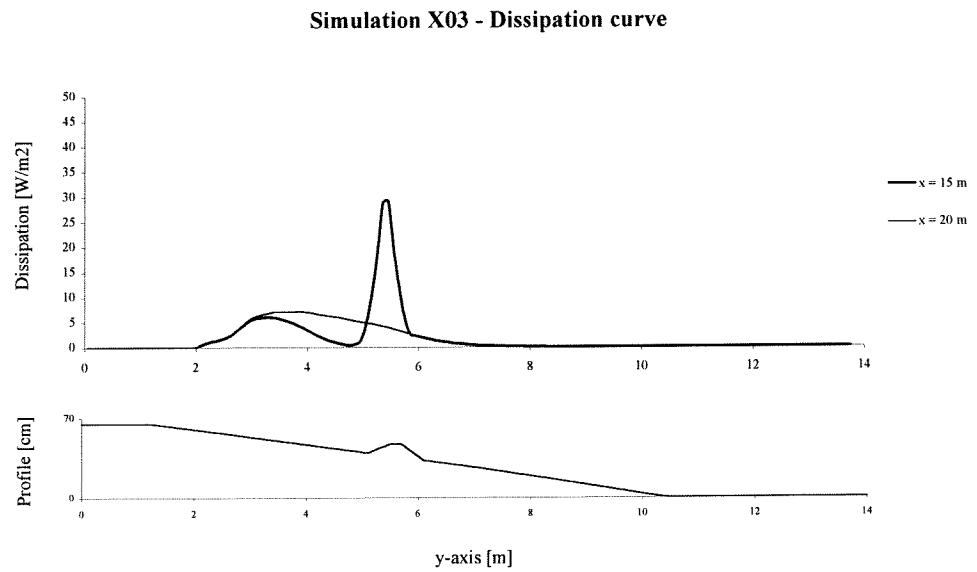

Figure 9.5-11 Simulation X03 - Dissipation curve over different cross-sections

The average water level is shown in Figure Q3-3. The longshore gradient, decreasing from the middle of the submerged breakwaters towards the gaps, is rather pronounced close to the tips of the structures and weakens rapidly towards the shoreline. This is made more clear by the 3D view of the mean water level of Figure 9.5-12.

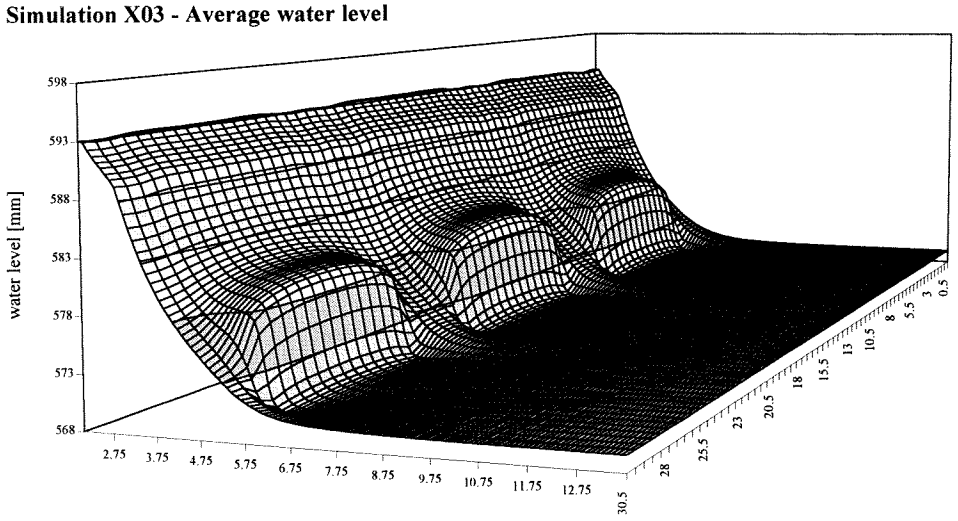

Figure 9.5-12 Simulation X03 - 3D view average water level

9.6 Conclusions and recommendations

In this chapter the effects of different submerged breakwaters configurations on the hydrodynamics have been investigated. The simulations are performed with regular, perpendicularly incident waves with a wave height H of 0.12 m and a time period T of 1.55 s.

The first series of simulations concerned different exposure ratios.
Figure 9.6-1 details the average velocity in cross-shore direction as function of the exposure ratio, in one point located in the middle of one gap. When negative values are observed, it means that the velocities are pointed seawards.
Figure 9.6-2 shows the average velocity in longshore direction as function of the exposure ratio, in one point located behind one submerged breakwater.
By enlarging the exposure ratio, starting form E = 0.0, a strong return flow through the gaps develops (Figure 9.6-1) and a longshore current takes place right behind the submerged breakwaters (Figure 9.6-2).
Both the cross-shore and the longshore current increase until an exposure ratio of approximately 0.4 has been reached and later, they decrease. It has to take into account that the exposure ratio does not vary continuously, but a step of 0.1 has been taken.
In the region around the submerged breakwaters, detached submerged breakwaters seem to have negative effects on the current field. Velocities, both the longshore and cross-shore component, result greater than the velocities in the case without submerged breakwaters and in the case with one single structure.
Beneficial effects can be observed closer to the shoreline, where the velocities and consequently the sediment transport are, in general, reduced.
When the gap width becomes too large, compared with the submerged breakwater length, the efficiency of the structures weakens.
Further research with a movable bed is suggested.

The wave energy dissipation over the submerged breakwater appears to be not affected by the different exposure ratios, which means that the wave field, landwards of the submerged breakwater, does remain constant.

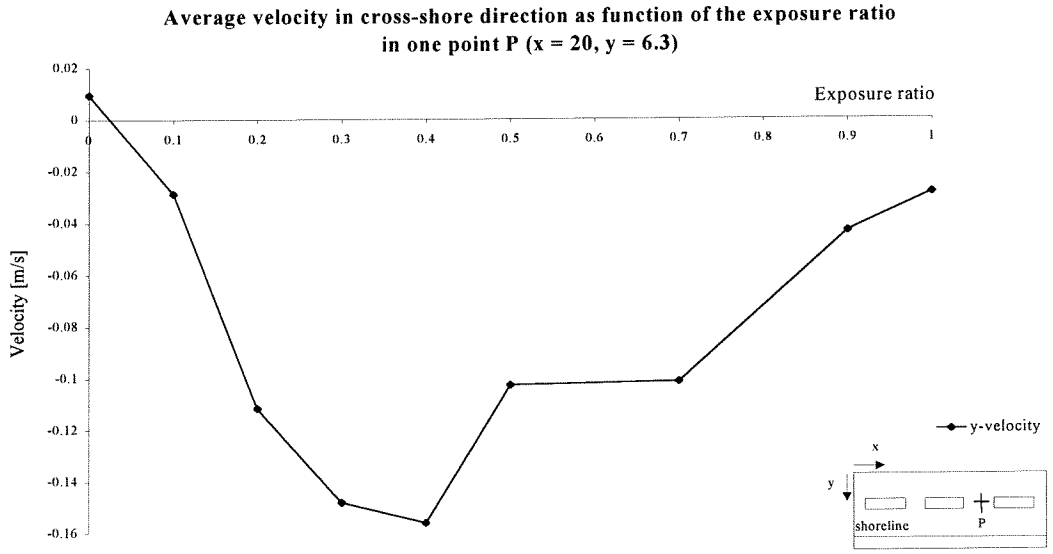

Figure 9.6-1 Average velocity in cross-shore direction as function of the exposure ratio

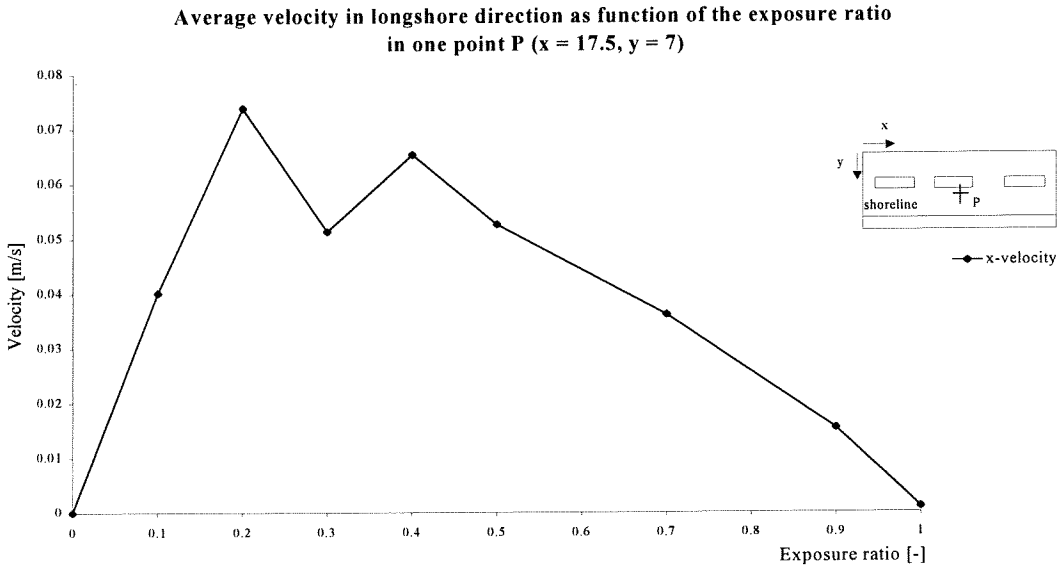

Figure 9.6-2 Average velocity in longshore direction as function of the exposure ratio

The second series of simulation was performed with different off-shore positions of the submerged breakwaters.
When the submerged breakwaters are located at the beginning of the slope (most seaward position), different circulation cells evolve: in one direction, around the tips of the submerged breakwaters, due to the velocities heading for the gaps, and in the opposite one, close to the shore line.
By decreasing the off-shore distance, it seems that the efficiency of the structure has been reduced.
Also in this case, simulations with movable bed should be carried out in order to investigate the morphological effects.

The crest width of the submerged breakwater has been maintained constant during each simulation. By varying the off-shore distance of the structures, the wave length right behind the submerged breakwater was not constant. Due to the different ratio of wave length to crest width, it was difficult to compare the outcomes of the simulations. Therefore, further investigations upon the effect of different ratio of wave length to width crest is suggested.
Furthermore, simulations with different exposure ratios coupled with different off-shore distances should be performed.

10. CONCLUSIONS AND RECOMMENDATIONS

10.1 Introduction

In this study, the 3D-effects of detached submerged breakwaters primarily on the hydrodynamic processes in the nearshore zone and only secondarily on morphological ones have been investigated.
The phenomena induced by a submerged breakwater are complex and not well-known yet. Due to this lack of knowledge, it was very difficult to correctly model the induced effects in a numerical model. Therefore, the conclusions presented in the following are to be considered only as a qualitative first step for further research.

10.2 Conclusions

Regarding the measurement data, the following can be concluded:

1. In general, the submerged breakwaters induce wave breaking and consequently wave energy dissipation.
2. Wave breaking does not occur at the crest of the structures. Instead, a time-lag can be noticed. This can be seen in the average water level, which starts rising more landwards of the submerged breakwaters. Therefore, the dissipation is concentrated closer to the coast and the resulting flow, near the shoreline, causes large sediment transport in cross-shore direction, which might increase the retreat of the shoreline itself instead of reducing it.
3. The efficiency of the submerged breakwaters, in dissipating wave energy, seems to be influenced by the submergence of the crest. In the experiments with the smaller wave heights, indeed, the wave set-up is not visible, since breaking does not occur over the crest of the submerged breakwater.
4. A longshore gradient in the average water level, sloping down from the middle of the submerged breakwaters to the gaps, is observed. The strong resulting velocities, flowing back through the gaps, cause a large amount of sediment to be transported seawards. Moreover, the longshore current, developed in the lee side of the submerged breakwaters, might increase the sediment transport in this direction.
5. From the limited laboratory experiments results, it is difficult to say whether the overall effects of the submerged breakwater are beneficial or harmful.

Regarding the numerical modeling study, the following conclusions can be drawn:

1. The outcomes of the simulations lead to some agreement with the measurements.
2. The laboratory experiments were performed by means of regular, unidirectional waves, while HISWA can only reproduce an irregular wave field. Nevertheless, from calibration is followed that a high value of the dissipation coefficient ($\alpha = 8$) yields a wave height development in good agreement with the measurements.
3. In the area close to the submerged breakwaters, the comparison between the computations and the measurements shows that the numerical model correctly reproduces the current field and the pattern of the average water level.
4. HISWA is not able to model diffraction, although in the case of submerged breakwaters with big submergence of the crest (which is the case analysed in the report), its effects can be approximated by means of the directional spreading. However, this yields some inaccuracies in the results.

5. The calculated accretion and erosion pattern at the end of 7.5 hours of wave action and the measured one show some similarities, which means that the sediment transport phenomenon is probably reproduced to some degree.
6. The return current increased remarkably while enlarging the exposure ratio.
7. By decreasing the off-shore distance, it seems that the efficiency of the structure has been reduced.

10.3 Recommendations

1. Further experiments, with different submergence of the crest, should be done.
2. In HISWA, the dissipated energy over an obstacle (if the 'obstacle function' is implemented) is only 'taken' out from the simulation and it is not used to induce wave forces and currents. In order to avoid this, the submerged breakwater is modeled as a variation in the bottom profile elevation, which entails, in turn, that the transmission relation cannot be used. Hence, the adoption of the obstacle function would be very useful.
3. HISWA is not able to model the quasi-steady breaking motion, yielding to an unrealistic pattern of the wave height behind the submerged breakwaters. Here, the waves stop breaking and shoaling occurs, while, in reality, the waves probably propagate like bores. A subject for further research might be the development of HISWA in order to reproduce this behaviour over submerged obstacles.
4. Erosion at the lee side of the submerged breakwaters is overestimated, as a consequence of the high dissipation concentrated in this area. Another reason for this might be the low resolution of the TRISULA computational grid. TRISULA calculates velocities only at 'velocity points', while interpolates them at the 'water level points'. If a velocity point is located over the submerged breakwaters, then the computed high velocity, caused by the small water depth, influences the low velocity in a water level point further behind the structure, where the water depth is higher. Better results would probably be obtained with a higher resolution of the computational grid.
5. The impeded retreat of the shoreline is a very important limitation of the program. A deep trough develops close to the shoreline, yielding to an unrealistic development of the bottom profile. Improvements of the numerical model are mainly necessary in the area landwards of the submerged breakwaters.
6. Further research, with movable bed, is recommended to improve the knowledge about the morphological effects of different exposure ratios.
7. Further research is recommended in order to analyse the influence of different off-shore distances combined with different exposure ratios.

I. References

Battjes, J. A. and Janssen, J. P. F. M. (1978)
Energy loss and set-up due to breaking of random waves. *Proc. 16th Int. Conf. Coastal Engineering,* ASCE, pp. 569-587.

Booij, N., Holthuijsen, L. H. and de Lange, P. H. M. (1992)
The penetration of short-crested waves through a gap. *Proc. 23rd Int. Conf. Coastal Engineering,* ASCE, pp. 1044-1052.

Chiaia, G., Damiani, L. and Petrillo, A. (1992)
Evolution of a beach with and without a submerged breakwater: experimental investigation. *Proc. 23rd Int. Conf. Coastal Engineering,* ASCE, pp. 1959-1971.

Claessen, E. W. M., Groenewoud M. D. (1995)
Effect of submerged breakwater on a profile development. *Master Thesis*, Delft University of Technology.

Dalrympe, A. and Dean, R. G. (1971)
Pilling-up behind low and submerged permeable breakwater. *Discussion in Journal of the Waterways, Harbour and Coastal Eng. Division,* ASCE, Vol. 97, WW2, pp. 423-427.

De Later, J. (1996)
Effect of submerged breakwaters on a beach profile exposed to regular waves in a wave basin. *Master thesis*, Delft University of Technology.

Dean, G. D., Chen, R. and Browder, A. E. (1995)
Full scale monitoring study of a submerged breakwater. *Personal communication*, Dynamic of Beaches Project.

Delft Hydraulics (1996a)
An introduction to Delft2D-Mor. *Delft Hydraulics.*

Delft Hydraulics (1996b)
Manual Delft3D-FLOW. *Delft Hydraulics.*

Dingemans, M. W., Radder, A. C. and de Vriend, H. J. (1987)
Computation of the driving forces of wave-induced currents. *Coastal Engineering 11,* pp. 539-563.

Hattori, M. and Sakai, H. (1994)
Wave breaking over permeable submerged breakwaters. *Proc. 24th Int. Conf. Coastal Engineering*, ASCE, pp. 1101-1114.

Holthuijsen, L. H., Booij, N. and Herbers, T. H. C. (1989)
A prediction model for stationary, short-crested waves in shallow water with ambient currents. *Coastal Engineering 13,* pp. 23-54.

Longuet-Higgins, M. S. (1967)
On the wave-induced difference in mean sea level between the two sides of a submerged breakwater. *Journal of Marine Research*, pp. 148-153 .

Petti M., Quinn P. A., Liberatore G. and Easson W. J. (1994)
Wave velocity field measurements over a submerged breakwater. *Proc. 24th Int. Conf. Coastal Engineering,* ASCE, pp. 525-539.

References (continues)

Sand, S. E. (1982)
Long wave problems in laboratory models. *Journal of the Waterway, Port, Coastal and Ocean Division*, ASCE, Vol. 108, No. WW4, pp. 492-503.

Sawaragi , T. (1992)
Detached breakwaters. *Proc. of the Short Course on Design and Reliability of Coastal Structures.* Design and Reliability of Coastal Structure, pp. 351-372.

Schaap, J. (1997)
Modelling the effects of submerged breakwaters in a wave basin. 2DH-simulation of tests with Delft2D-MOR. *Master thesis*, Delft University of Technology.

Seelig, W. N. and Walton, T. L. (1980)
Estimation of flow through offshore breakwater gaps generated by wave overtopping. *U. S. Army Corps of Engineers, Coastal Research Center*, Rep. No. CETA 80-8.

Shore Protection Manual (1984)
Coastal Engineering Research Center. Department of the Army. Waterways Experiment Station, Corps of Engineers, Vicksburg, Mississippi.

Steetzel, H. J. (1993)
Cross-shore transport during storm surges. *Research project.* Delft Hydraulics.

Stelling, G.S. (1984)
On the construction of computational methods for shallow water flow problems Rijkswaterstaat communications, No. 35.

Svendsen, I. A. (1984)
Mass flux and undertow in a surf zone. *Coastal Engineering 8,* pp. 347-365.

U.S. Army Corps of Engineering (1994)
Coastal Groins and Nearshore breakwaters. *Technical Eng. And Design Guides as adapted from the U.S. Army Corps of Engineers,* ASCE, No. 6.

Van der Velden, E. T. J. M. (1995)
Coastal Engineering. *Lectures notes*, Delft University of Technology, Vol. II.

Van Rijn, L. C. (1990)
Principles of fluid flow and surface waves in rivers, estuaries, seas and oceans. *University of Utrecht, Department of Physical Geography, Delft Hydraulics*, Aqua Publications.

II. Reference - Useful Background Information

If further information about the subjects discussed in the thesis is requested, the following papers might be useful.

Battjes, J.A. and Stive, M.J.F. (1985)
Calibration and verification of a dissipation model for random breaking waves. *Journal of Geophysical Research*, Vol. 90, No C5, pp.9159-9167.

Boers, M., van de Graaff, J. (1995)
Contributions to the Momentum Balance in the surf zone. *Proc. Coastal Dynamics*, ASCE, pp. 257-268.

Booij, N. and Holthuijsen, L. H. (1996)
User manual HISWA. *Delft University of Technology, Department of Civil Engineering.*

Bos, K. J. (1996)
Modelling the impact of an offshore breakwater on the shore. *Master Thesis*, Delft University of Technology.

Buhr Hansen, J. and Svendsen, I. A. (1984)
A theoretical and experimental study of undertow. *Proc. 19th Int. Conf. Coastal Engineering*, ASCE, pp. 2246-2261.

Cooker, M., Peregrine, H. (1988)
Solitary waves passing over submerged breakwaters. *Proc. 21st Int. Conf. Coastal Engineering*, ASCE, pp. 624-632.

Cruz, Eric C., Isobe, M. and Watanabe, A. (1992)
Non linear wave transformation over a submerged permeable breakwater. *Proc. 23rd Int. Conf. Coastal Engineering*, ASCE, pp. 1101-1114.

Daemen, I. F. R. and D'Angremond, K. (prof.) (1991)
Wave transmission at low-crested structures. *Master thesis*, Delft University of Technology.

Dean, R. G. (1992)
Defense of shorelines by structural approaches. *Proc. of the Short Course on Design and Reliability of Coastal Structures*. Design and Reliability of Coastal Structure, pp.285-299.

Dingemans, M. W., Stive, M. J. F., Bosma, J., de Vriend, H. J. and Vogel, J. A. (1986)
Directional nearshore wave propagation and induced currents. *Proc. 20th Int. Conf. Coastal Engineering*, ASCE, pp. 1092-1106.

Gent, M. R. A. van (1994)
The modelling of wave action on and in coastal structures. *Proc. 24th Int. Conf. Coastal Engineering*, ASCE, Ch. 125, pp. 1-15.

Gent, M. R. A. van, Tonjes, P., Petit, H. A. H. and P. van den Bosch (1994)
Wave action on and in permeable structures. *Proc. 24th Int. Conf. Coastal Engineering*, ASCE, Ch. 125, pp. 1-15.

Gent, M. R. A. van and Petit, H. A. H.(1994)
Simulations of wave interaction with coastal structures. *Delft Hydraulics Report, Hydroinformatics '94*, pp. 1-6.

Gomez Pina, G., and Valdes Fernandez de Alarcon, J. M. (1990)
Experiments on coastal protection : submerged breakwater: a way to look at the results. *Proc. 22nd Int. Conf. Coastal Engineering,* ASCE, pp. 1592-1605.

Gourlay, M.R. (1971)
Pilling-up behind low and submerged permeable breakwaters. *Discussion in Journal of the Waterways, Harbour and Coastal Eng. Division,* ASCE, Vol. 96, WW1, pp. 219-222

Gourlay, M.R. (1996)
Wave set-up on coral reefs. 1. Set-up and wave generated flow on an idealised two dimensional horizontal reef. *Coastal Engineering 27,* pp. 161-193.

Gourlay, M.R. (1996)
Wave set-up on coral reefs. 2. Set-up on reefs with various profiles. *Coastal Engineering 28,* pp. 17-55.

Hara, M., Yasuda, T. and Sakakibara, Y. (1992)
Characteristics of a solitary wave breaking caused by a submerged obstacle. *Proc. 23rd Int. Conf. Coastal Engineering,* ASCE, pp. 253-266.

Holthuijsen, L. H. and Booij, N. (1986)
A grid model for shallow water waves. *Proc. 18th Int. Conf. Coastal Engineering,* ASCE, pp. 261-270.

Kuik, A. J., van Vledder, G. Ph. and Holthuijsen, L. H. (1988)
A method for the routine analysis of pitch-and-roll buoy wave data. *Journal of physical oceanography*, Vol. 18, pp. 1020-1034.

Liberatore, G. (1992)
Detached breakwaters and their use in Italy. *Proc. of the Short Course on Design and Reliability of Coastal Structures*. Design and Reliability of Coastal Structure, pp. 373-396.

Lo, Jen-Men. (1988)
Dynamic wave set-up. *Proc. 21st Int. Conf. Coastal Engineering,* ASCE, pp. 999-1010.

Murphy, J., Lewis, A. W., Wall, C., van de Graaf, J. and van der Biezen, S. (1995)
Submerged breakwaters research in the EU human capital and mobility programme.

Nielsen, P.(1989)
Wave set-up and run-up: an integrated approach. *Coastal Engineering 13,* pp. 1-9.

Petti M., Quinn P. A., Liberatore G. and Easson W. J. (1994)
Wave velocity field measurements over a submerged breakwater. *Proc. 24th Int. Conf. Coastal Engineering,* ASCE, pp. 525-539.

Prinos, P., Arcilla, A. S., Christiansen, N., van de Graaf, J., Hogedal, M., Lewis, A., O'Connor, B., Rivero, F. and de Rouck, J. (1995)
The 'Dynamics of Beaches' Project. *Proc. Coastal Dynamics,* ASCE, pp. 571-582.

Rojanakamthorn, S., Isobe M. and Watanabe, A. (1990)
Modeling of wave transformation on submerged breakwater. *Proc. 22nd Int. Conf. Coastal Engineering,* ASCE, pp. 1060-1073.

Sawaragi, T. , Deguchi, I. And Ga-Ya Kim (1990)
Function of detached breakwater to control longshore sediment transport. *Proc. 22nd Int. Conf. Coastal Engineering,* ASCE, pp. 2603-2615.

Stive, M. J. F. (1984)
Energy dissipation in waves breaking on gentle slopes. *Coastal Engineering 8,* pp. 99-127.

Svendsen, I. A., Madsen, P. Å. And Buhr Hansen, J. (1978)
Wave characteristic in the surf zone. *Proc. 16th Int. Conf. Coastal Engineering*, ASCE, pp. 520-539.

Svendsen, I. A. (1984a)
Wave heights and set-up in a surf zone. *Coastal Engineering 8,* pp. 303-329.

Svendsen, I. A. (1984c)
Wave attenuation and set-up on a beach. *Proc. 19th Int. Conf. Coastal Engineering*, ASCE, pp. 54-69.

Svendsen, IB. A. and Lorenz, R. S. (1989)
Velocities in combined undertow and longshore currents. *Coastal Engineering 13,* pp. 55-79.

Svendsen, I. A. (1992)
Hydrodynamics of the surf zone. *Proc. of the Short Course on Design and Reliability of Coastal Structures*. Design and Reliability of Coastal Structure, pp. 109-146.

Thorntorn, E. B. (1970)
Variation of longshore current across the surf zone. *Proc. 12th Int. Conf. Coastal Engineering*, ASCE, pp. 291-308.

Van der Meer, J. W. (1991)
Stability and transmission at low-crested structures. *Publication*, No. 453, Delft Hydraulics.

Van der Meer, J. W. (1994)
Stability and wave transmission at low-crested rubble-mound structures. *Journal of Waterway, Port, Coastal and Ocean Engineering*, ASCE, Vol. 120, No. 1, pp. 1-19.

Nearshore effects of submerged breakwaters

Laboratory experiments in a wave basin and 2DH numerical modeling.

Volume II: Appendices

L. Torrini

Simualtion D3 - Average Water Level

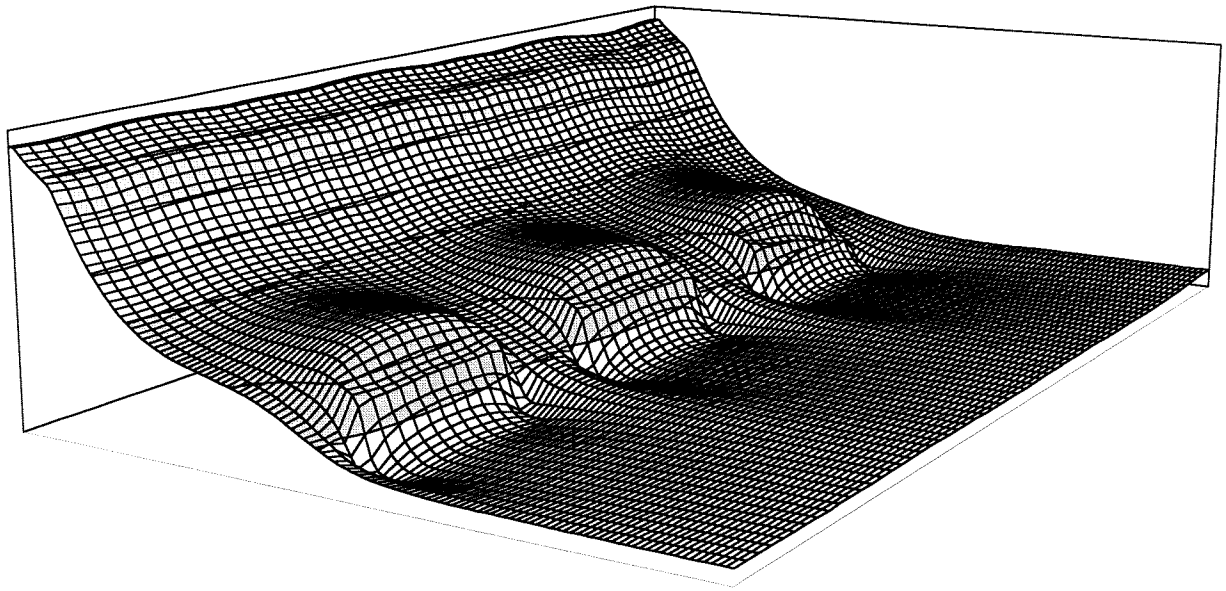

Master Thesis
October 1997

Nearshore effects of submerged breakwaters

Laboratory experiments in a wave basin and 2DH numerical modeling.

Volume II: Appendices

L. Torrini

Master Thesis
October 1997

Delft University of Technology
Faculty of Civil Engineering

Politecnico di Milano
Facolta` di Ingegneria Ambientale

Supervision:

Dr. Ir. J. van de Graaff
Dr. Ir. J. A. Roelvink
Ir. S. C. van der Biezen
Dr. Ir. G. Passoni

Table of Contents

Volume II: Appendices

Appendix A1. Graphics TEST A1 - Average Water Level

TEST A1 - cross-section x=3 m - interval 00:00 - 00:30

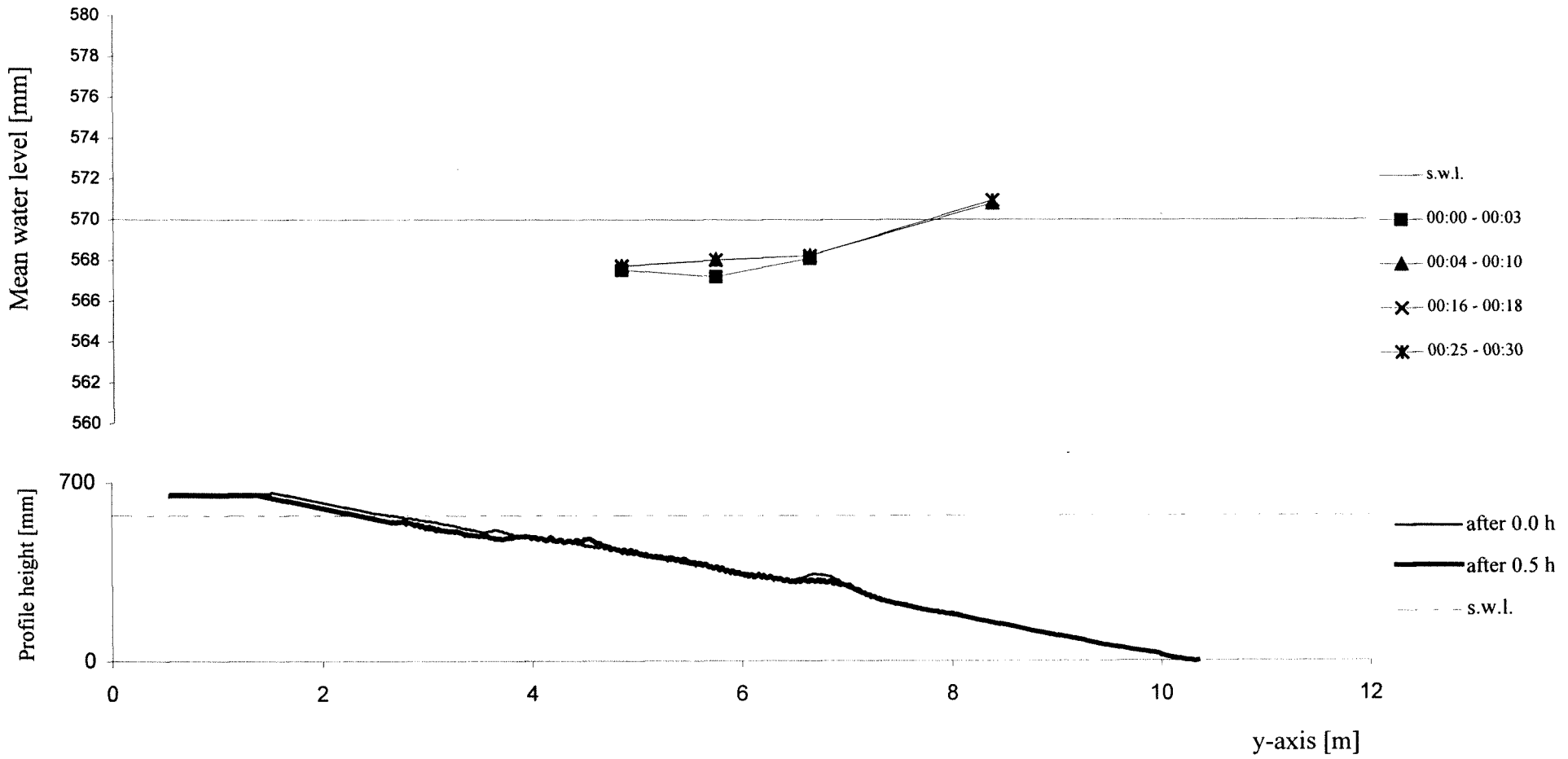

TEST A1 - cross-section x=12.5 m - interval 00:30 - 01:30

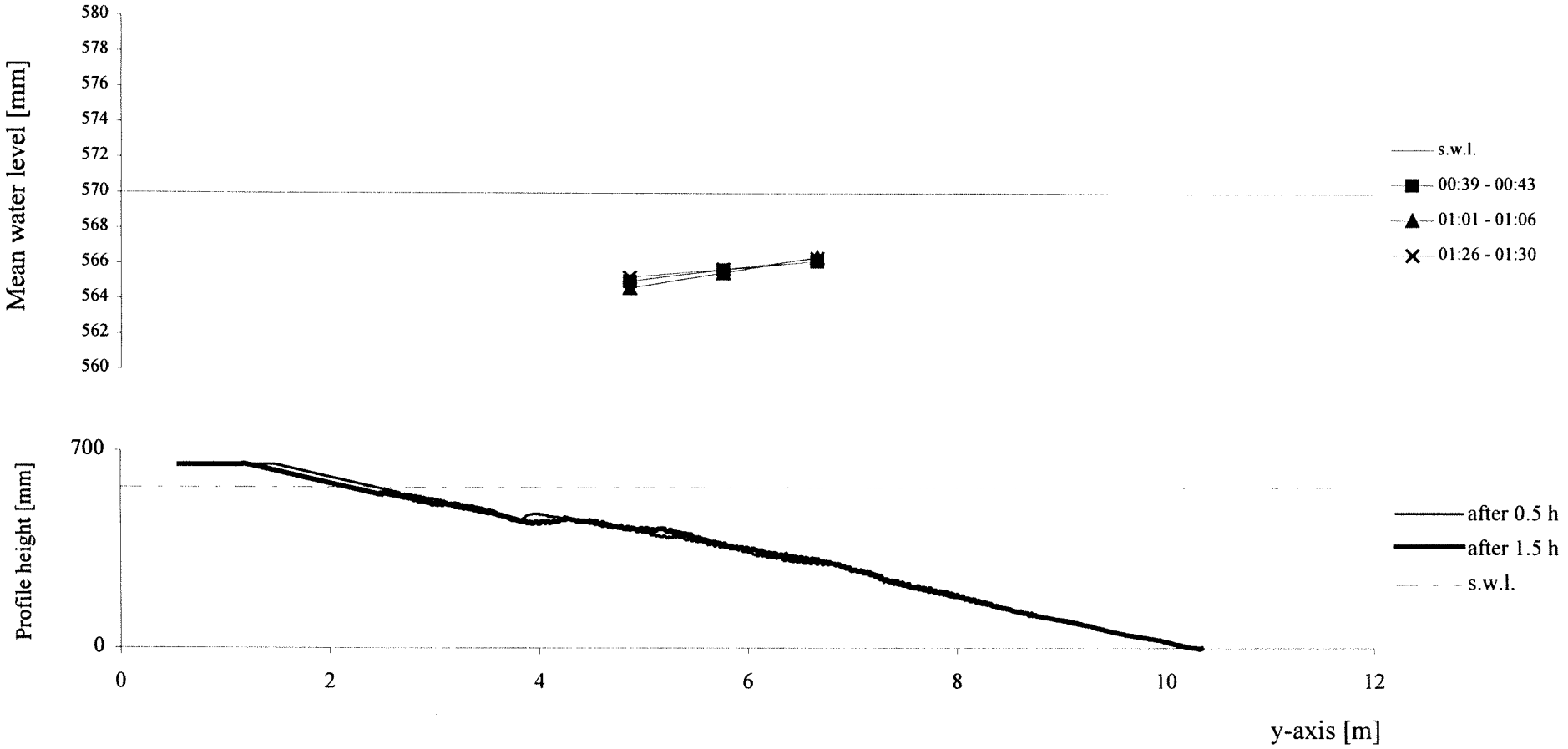

TEST A1 - cross-section x=24.5 - interval 00:30 - 01:30

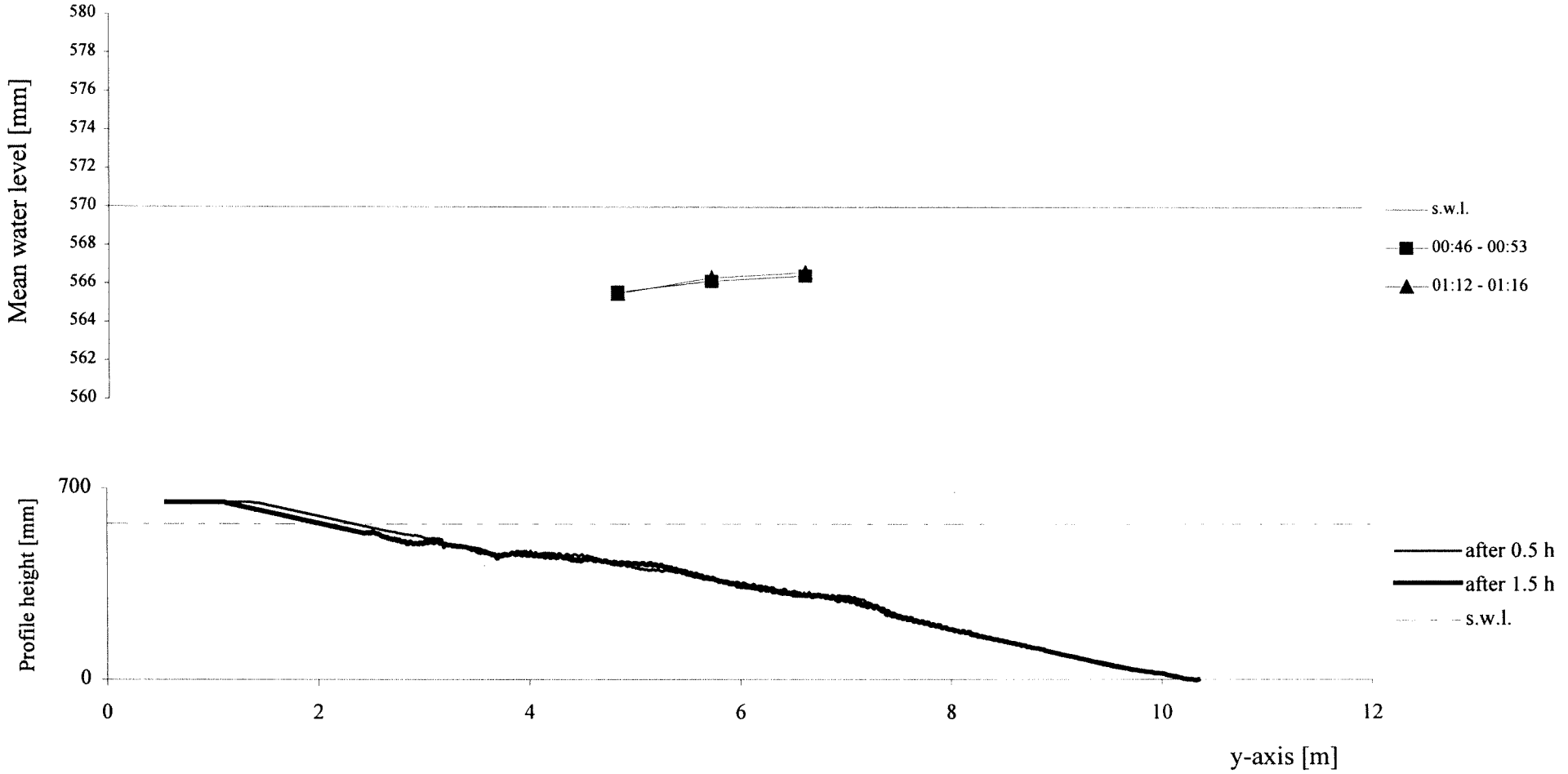

TEST A1 - cross-section x=6.5 m - interval 01:30 - 03:30

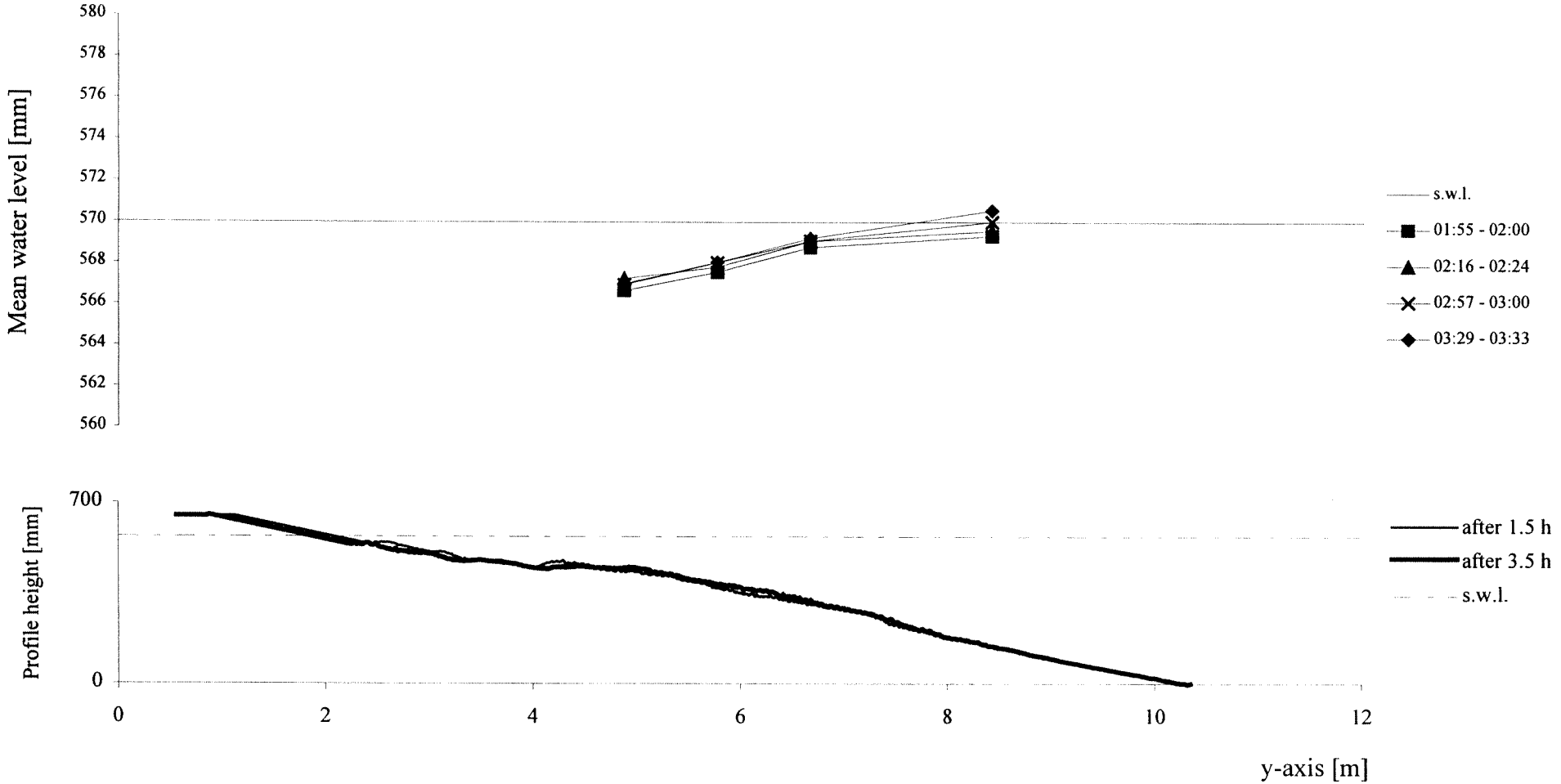

TEST A1 - cross-section x=20 m - interval 01:30 - 03:30

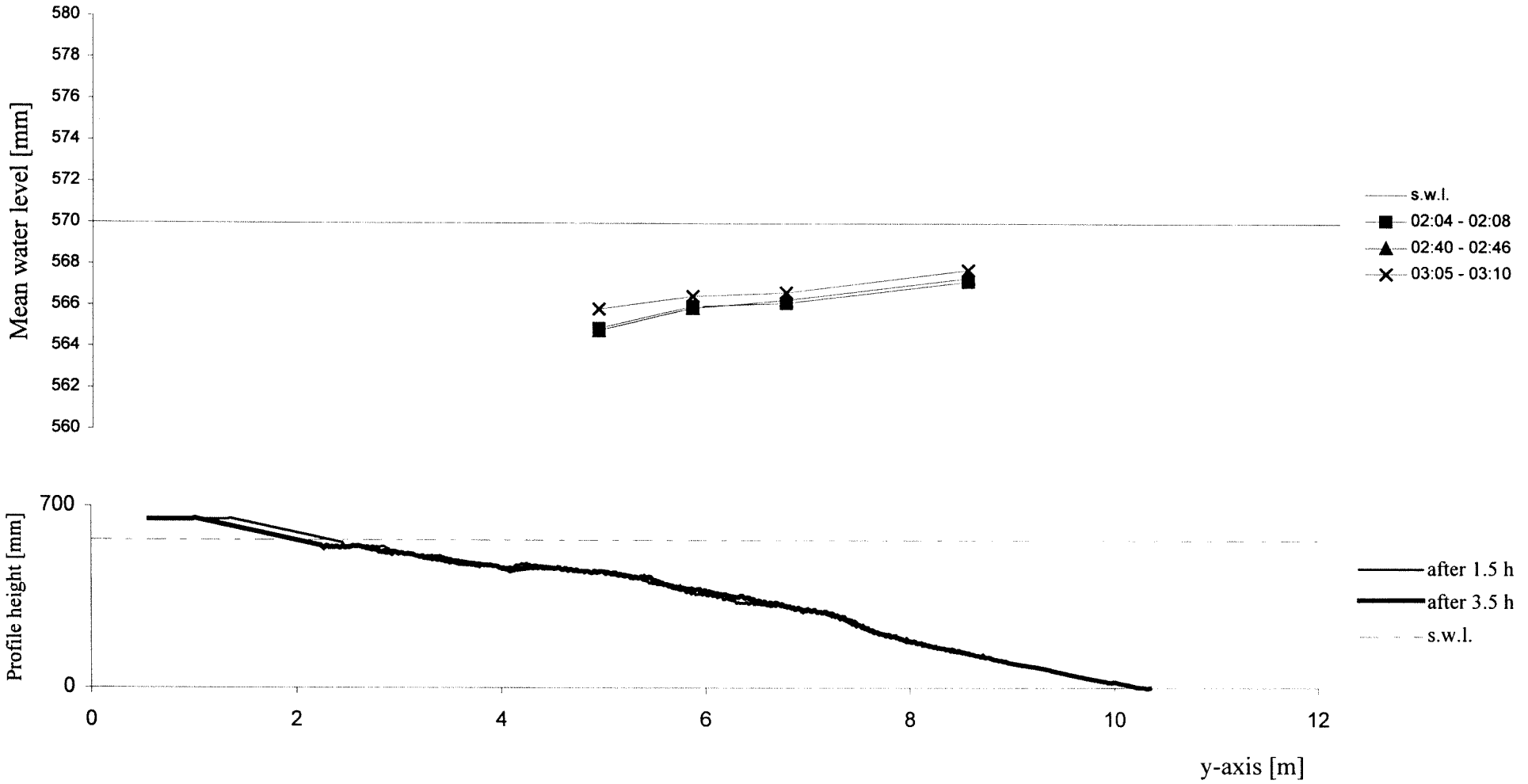

TEST A1 - cross-section x=3 m - interval 03:30 - 07:30

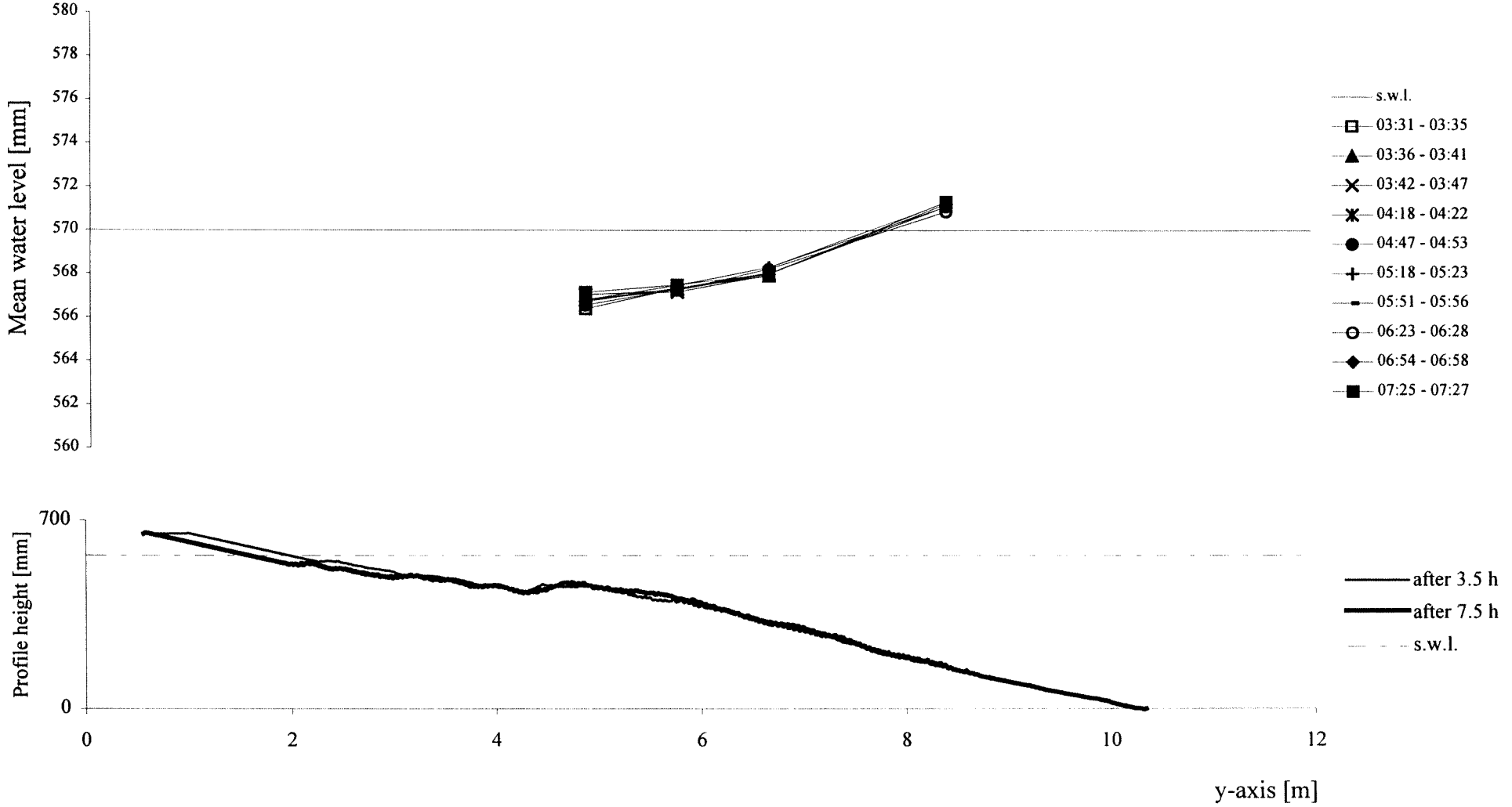

TEST A1 - cross-section x=12.5 m - interval 03:30 - 07:30

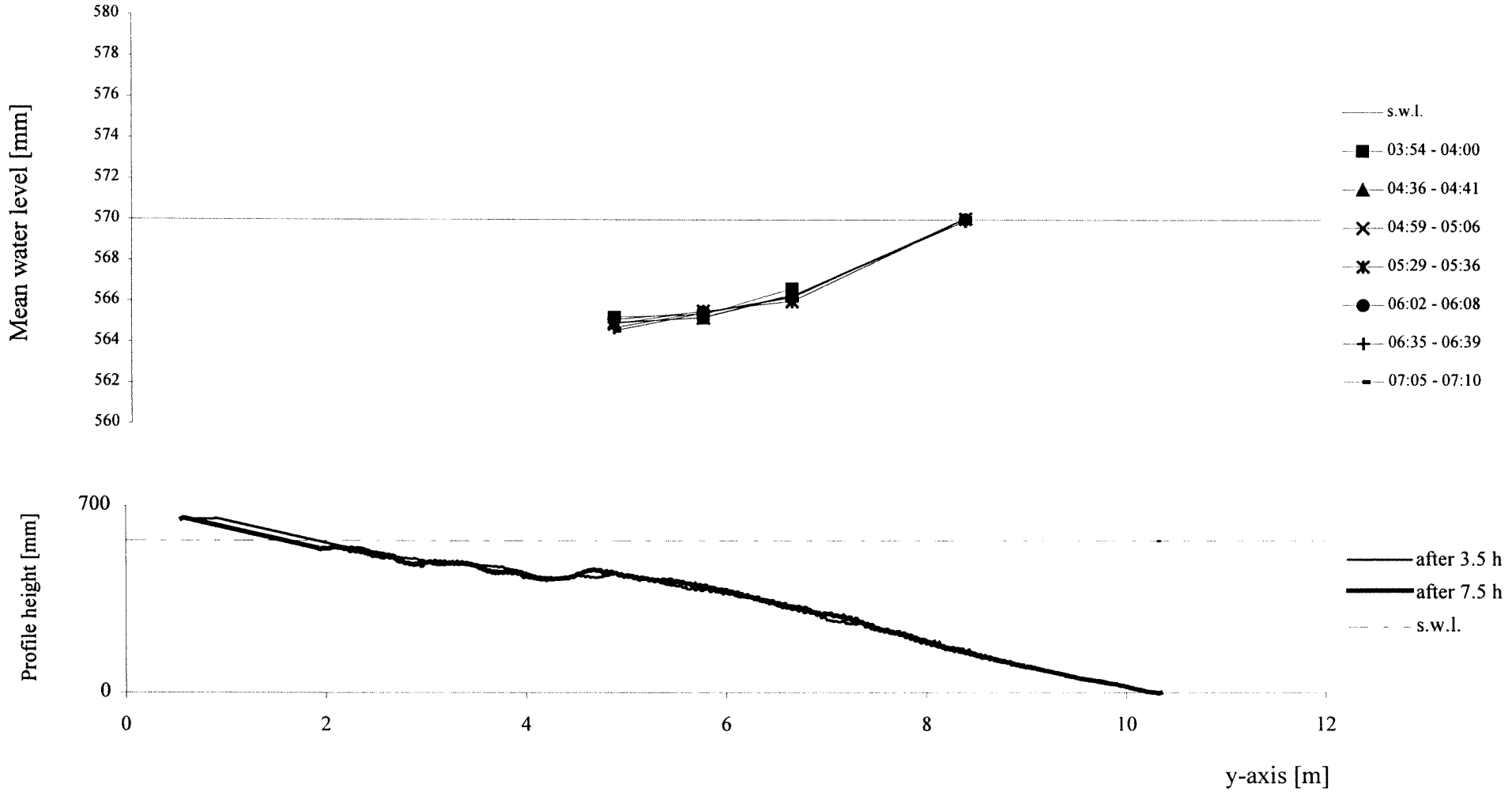

TEST A1 - cross-section x=24.5 m - interval 03:30 - 07:30

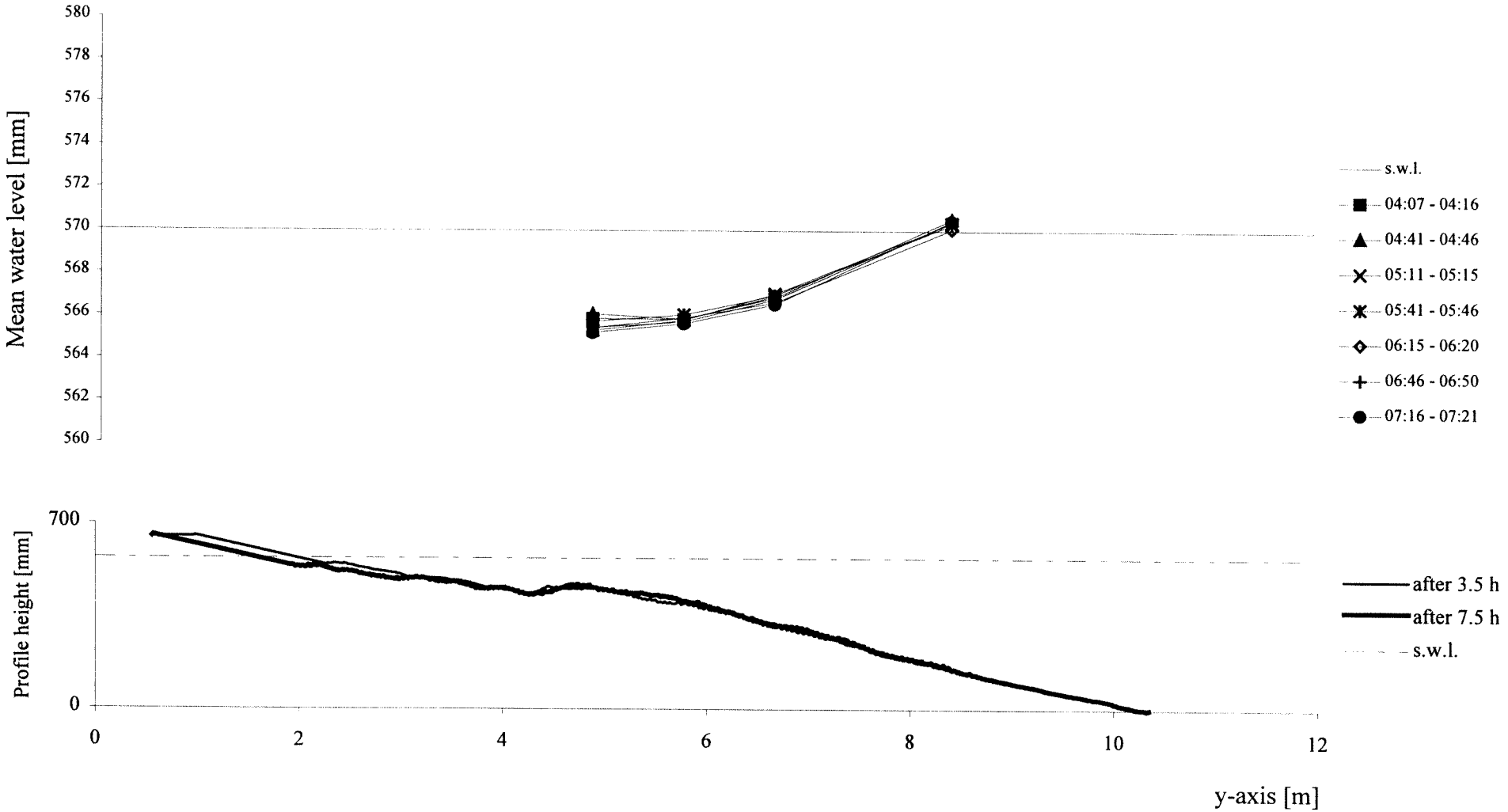

Appendix A2. Graphics TEST A2 - Average Water Level

TEST A2 - cross-section x=3 m - interval 00:00 - 00:30

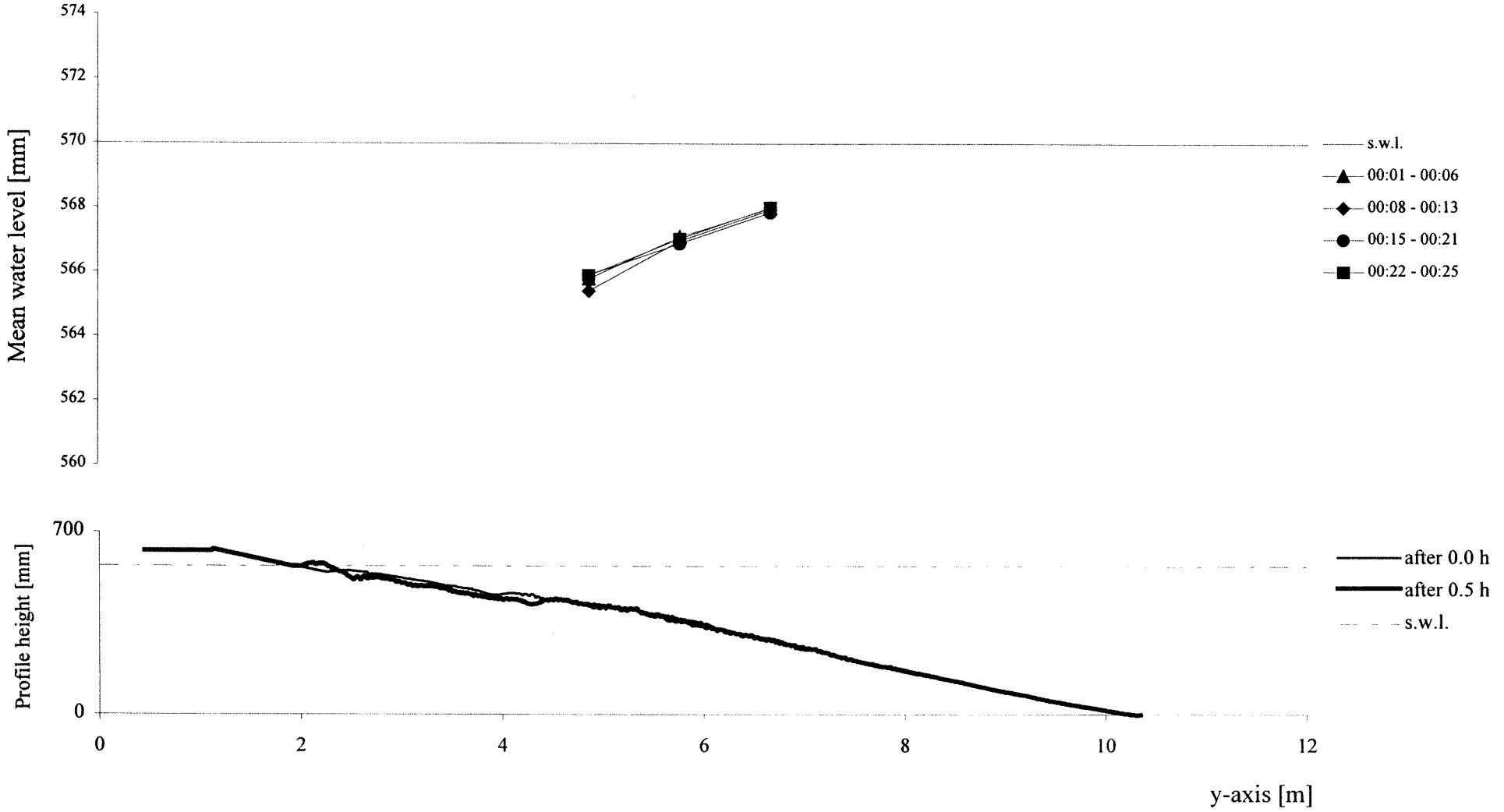

TEST A2 - cross-section x=12.5 m - interval 00:30 - 01:30

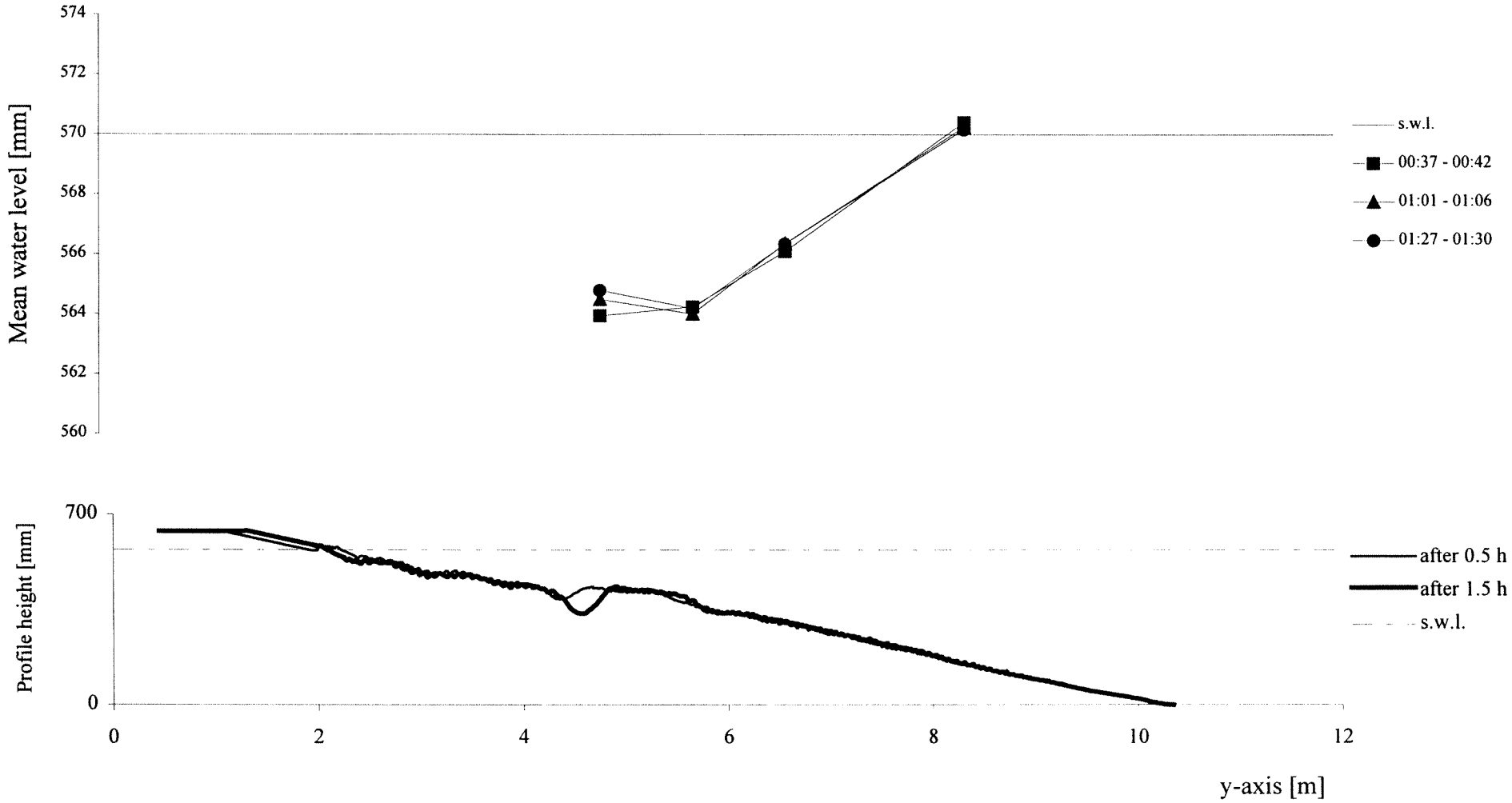

TEST A2 - cross-section x=24.5 m - interval 00:30 - 01:30

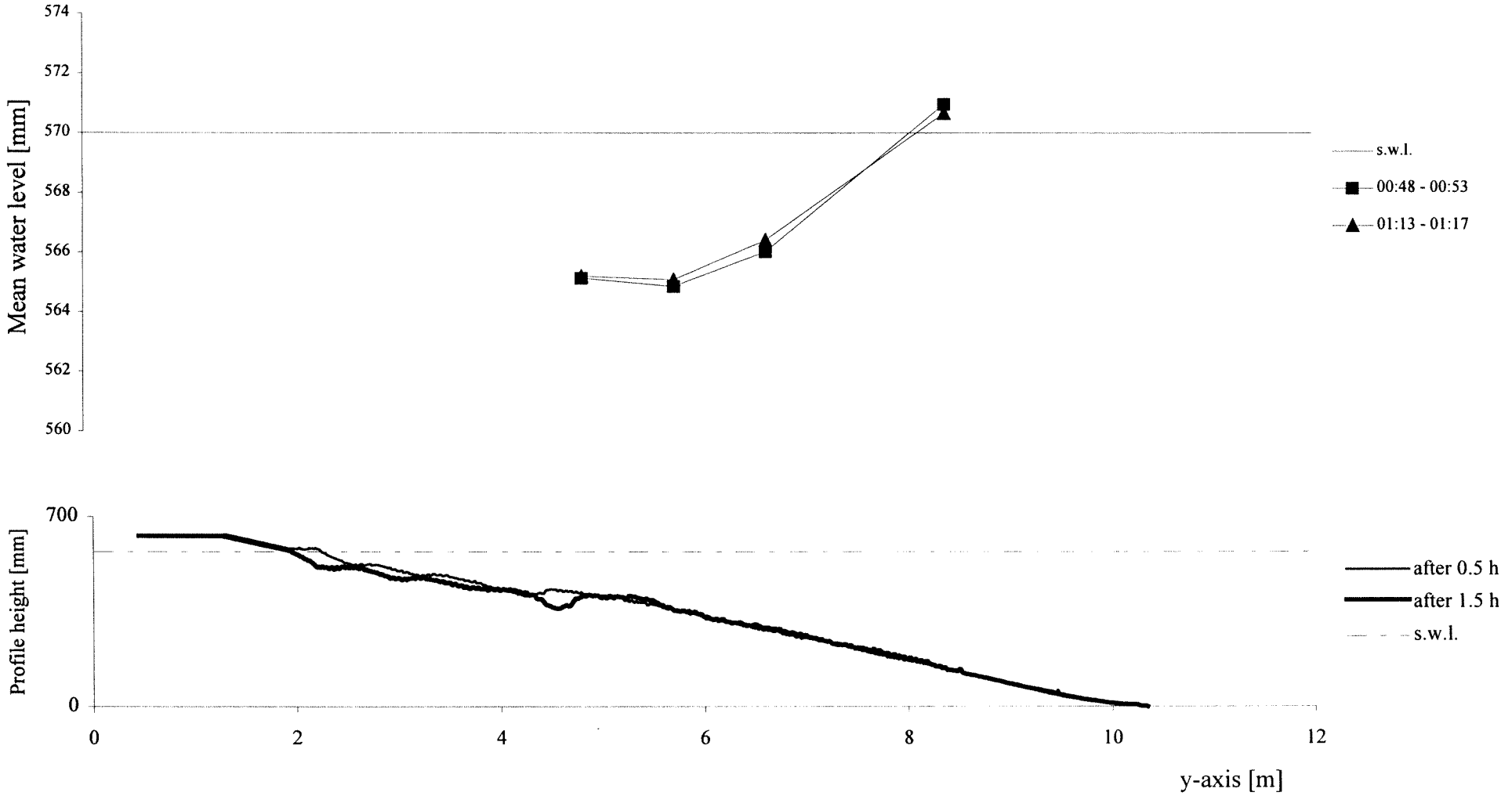

TEST A2 - cross-section x=6.5 m - interval 01:30 - 03:30

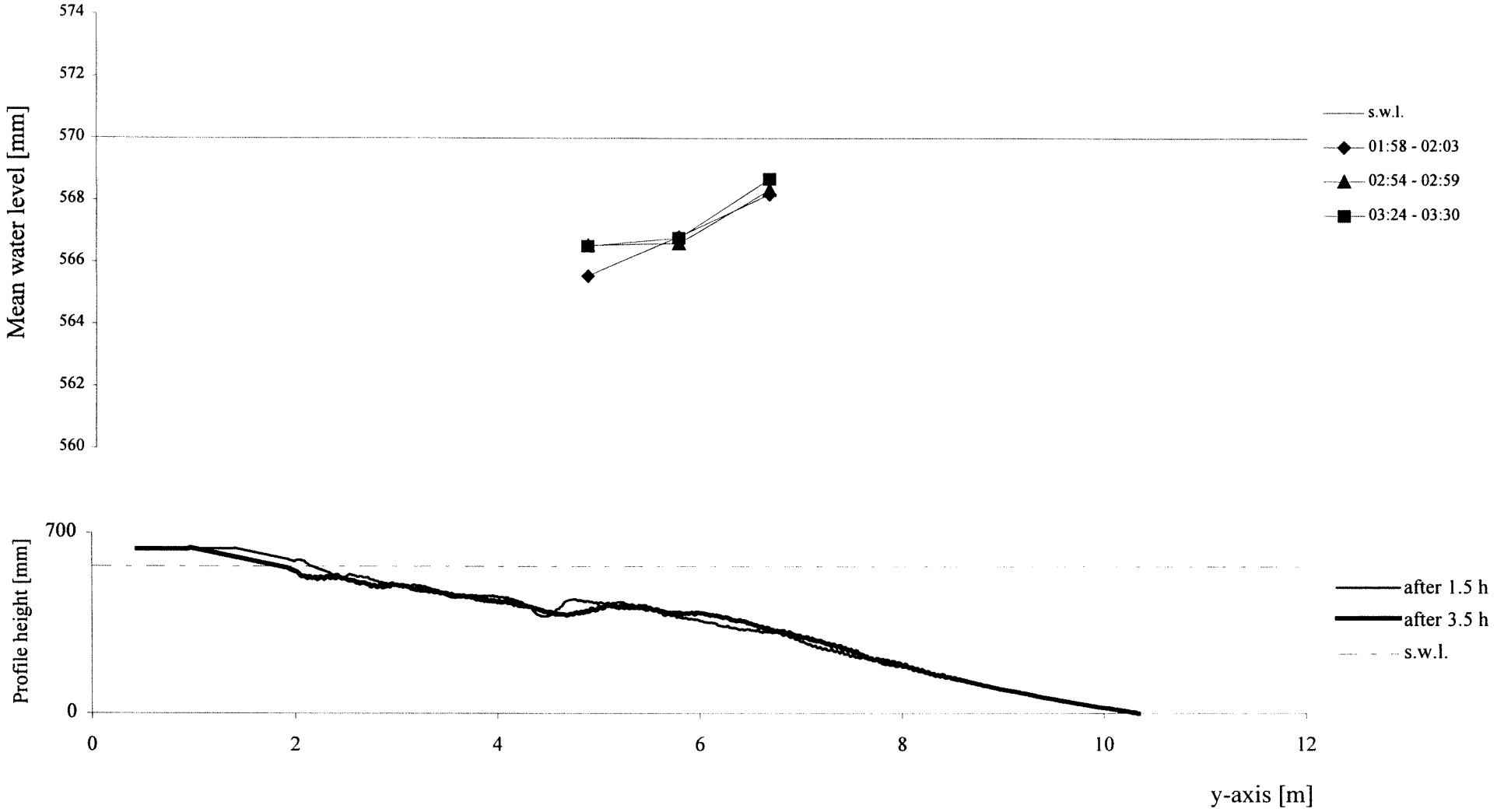

Test A2 - cross-section x=20 m - interval 01:30 - 03:30

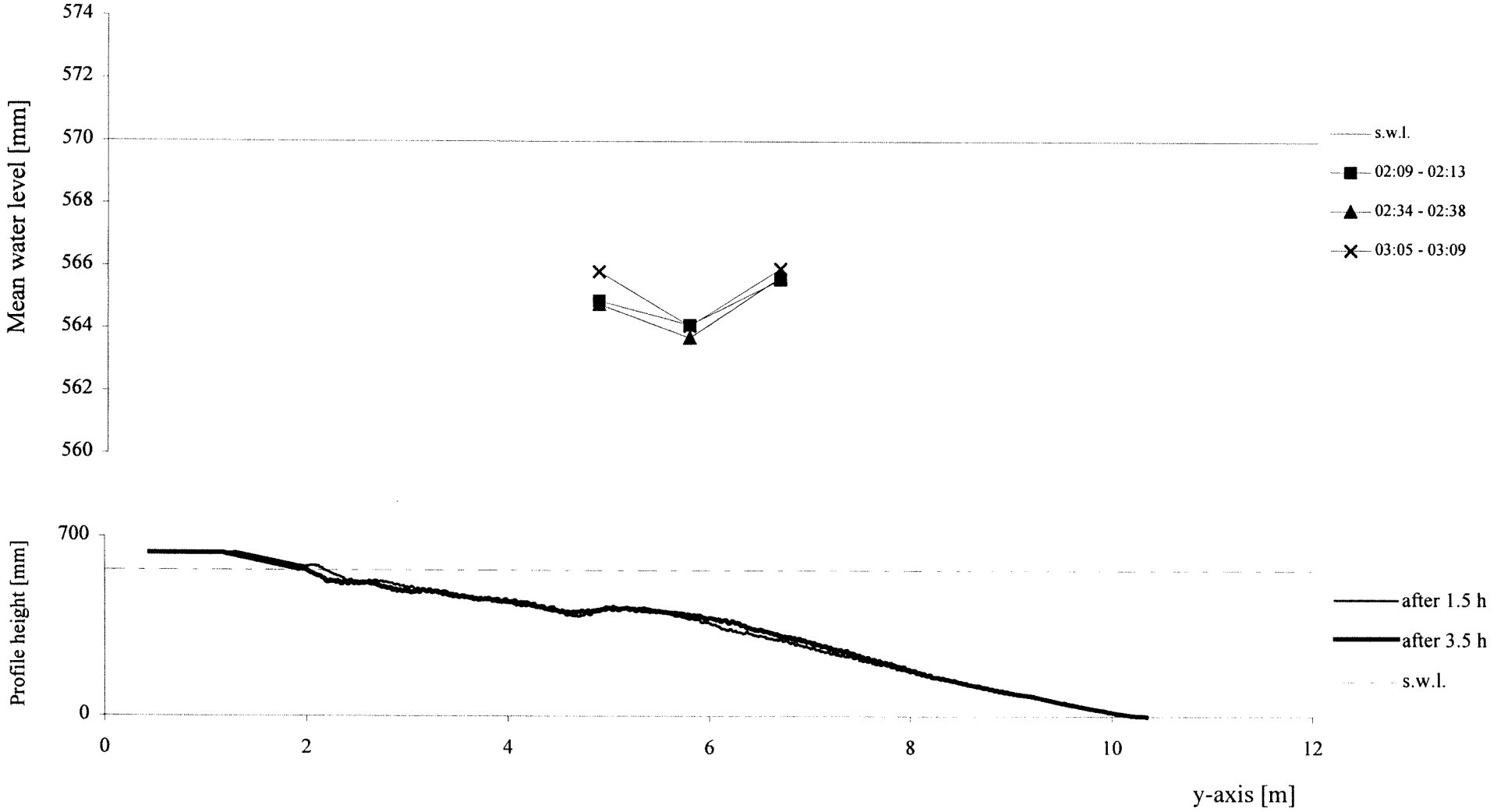

TEST A2 - cross-section x=3 m - interval 03:30 - 07:30

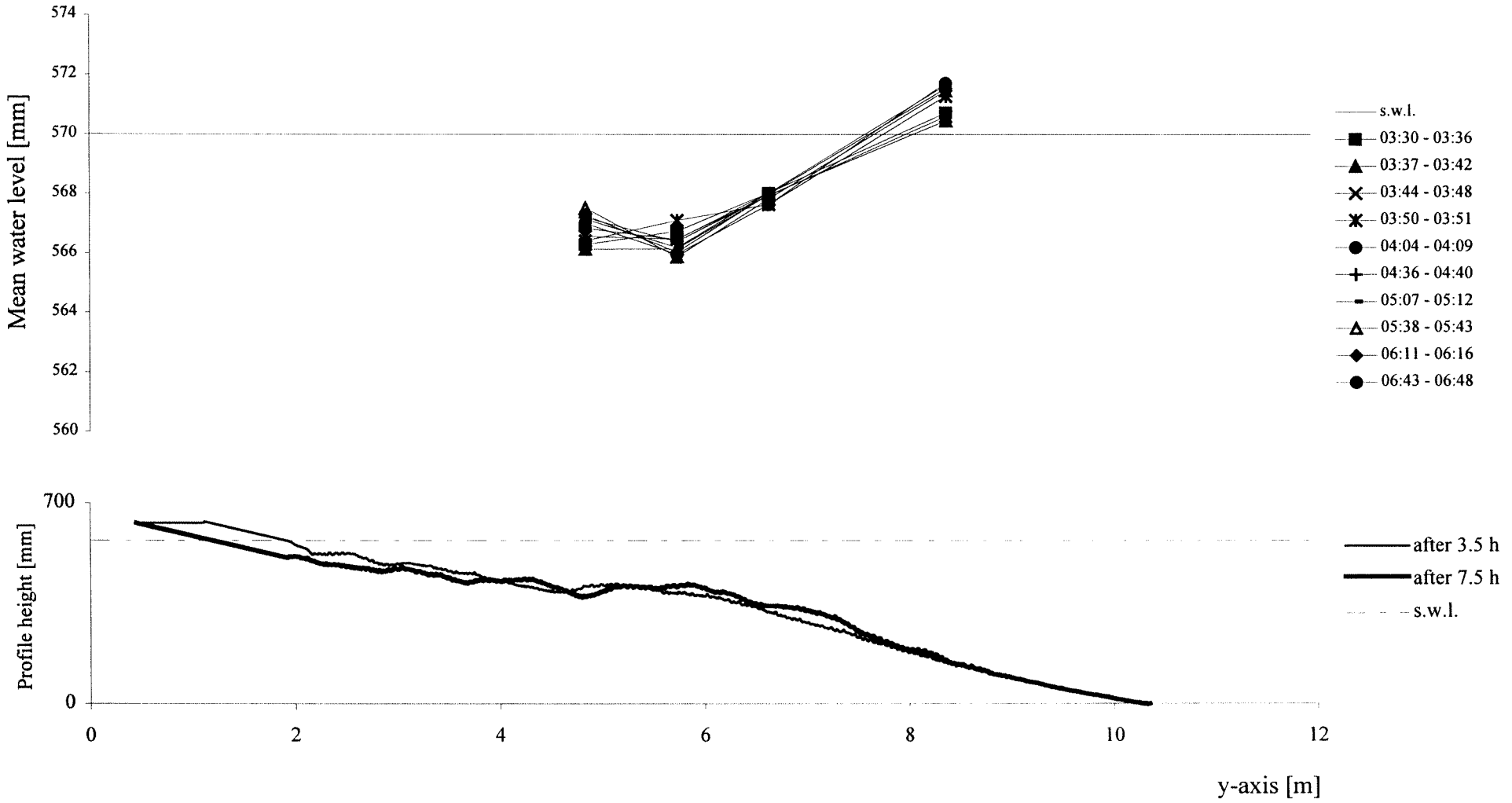

TEST A2 - cross-section x=12.5 m - interval 03:30 - 07:30

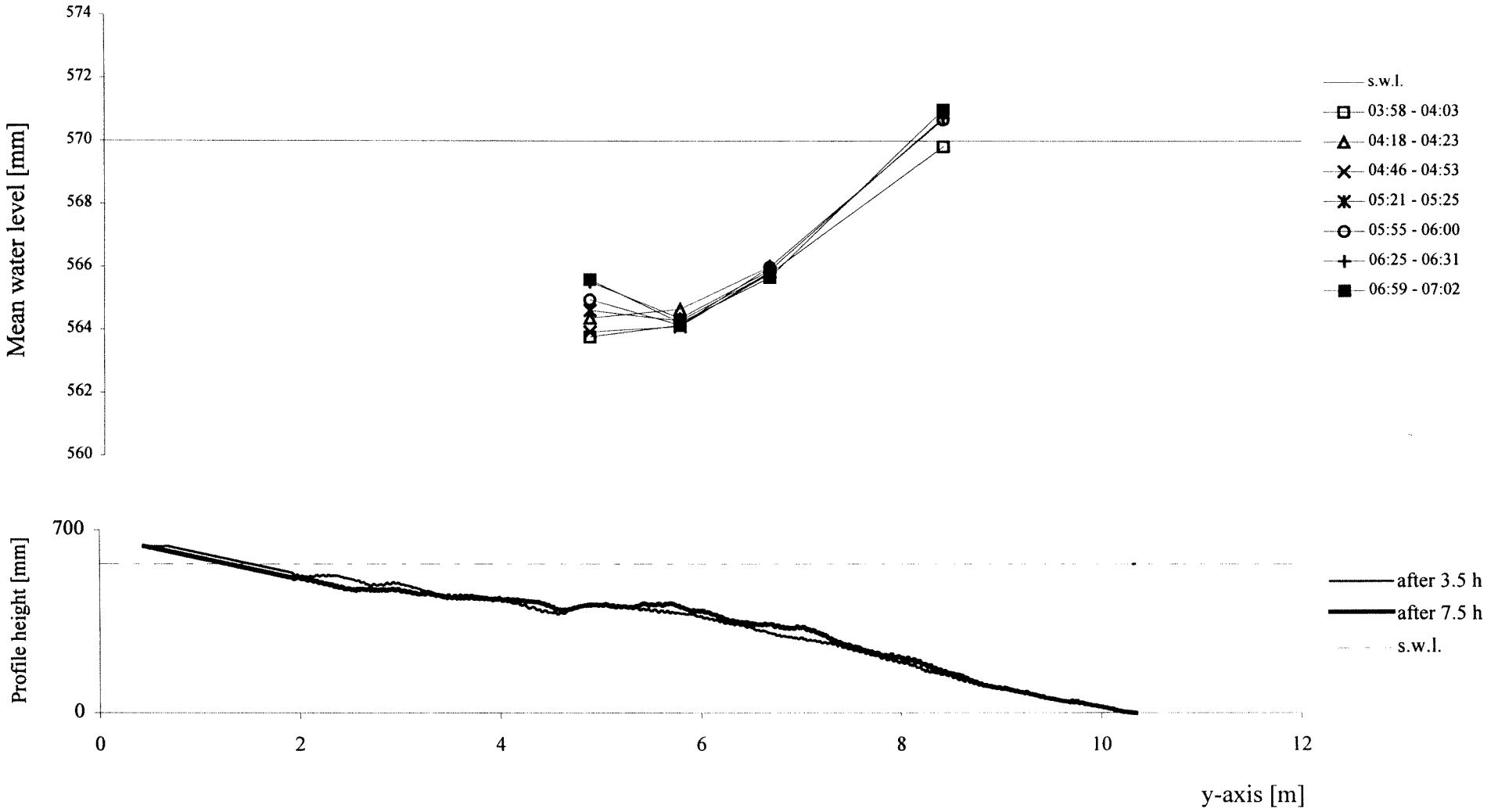

TEST A2 - cross-section x=24.5 m - interval 03:30 - 07:30

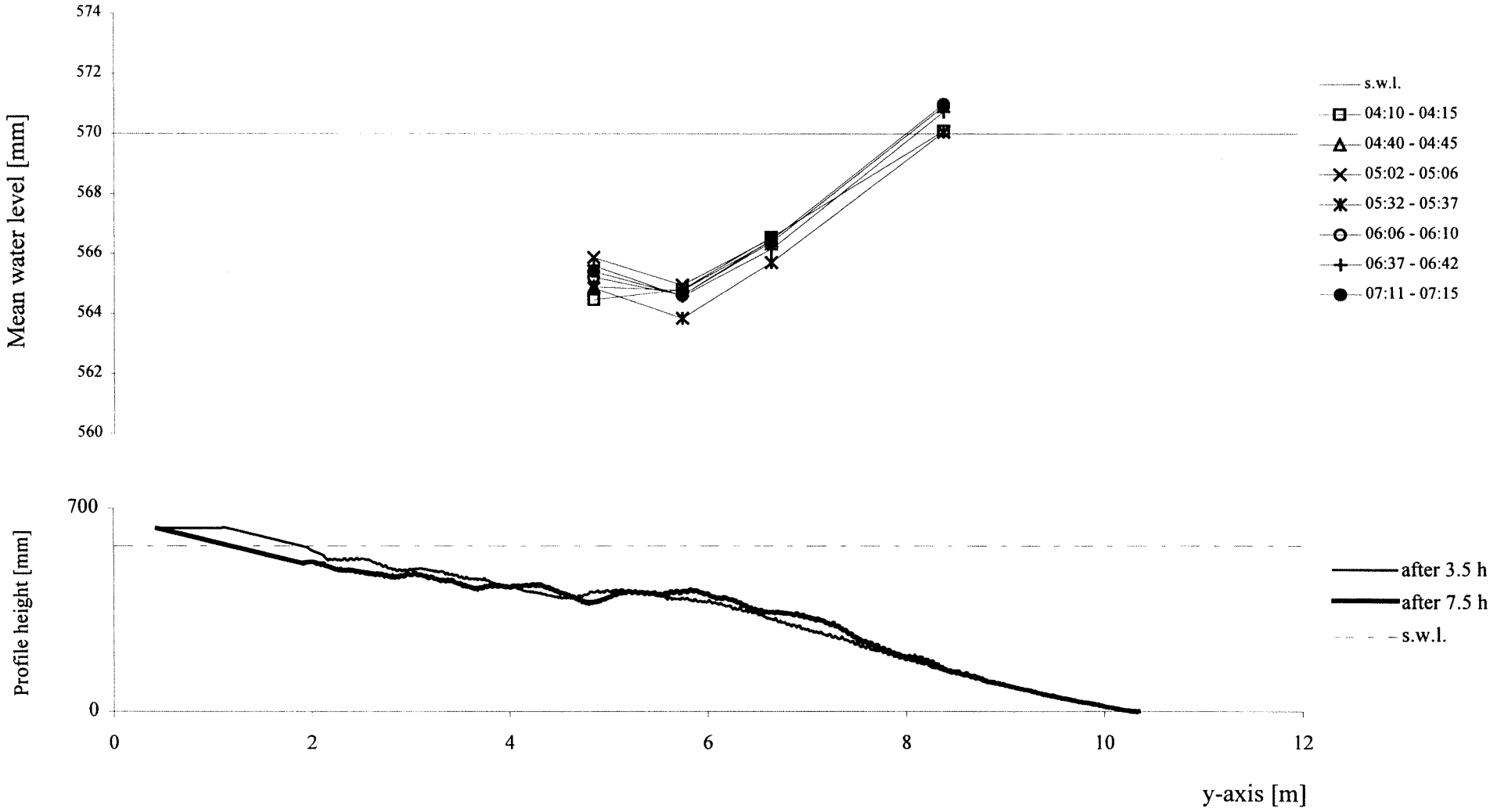

Appendix A3. Graphics TEST A3 - Average Water Level

TEST A3 - cross-section x=3m - interval 00:00 - 00:30

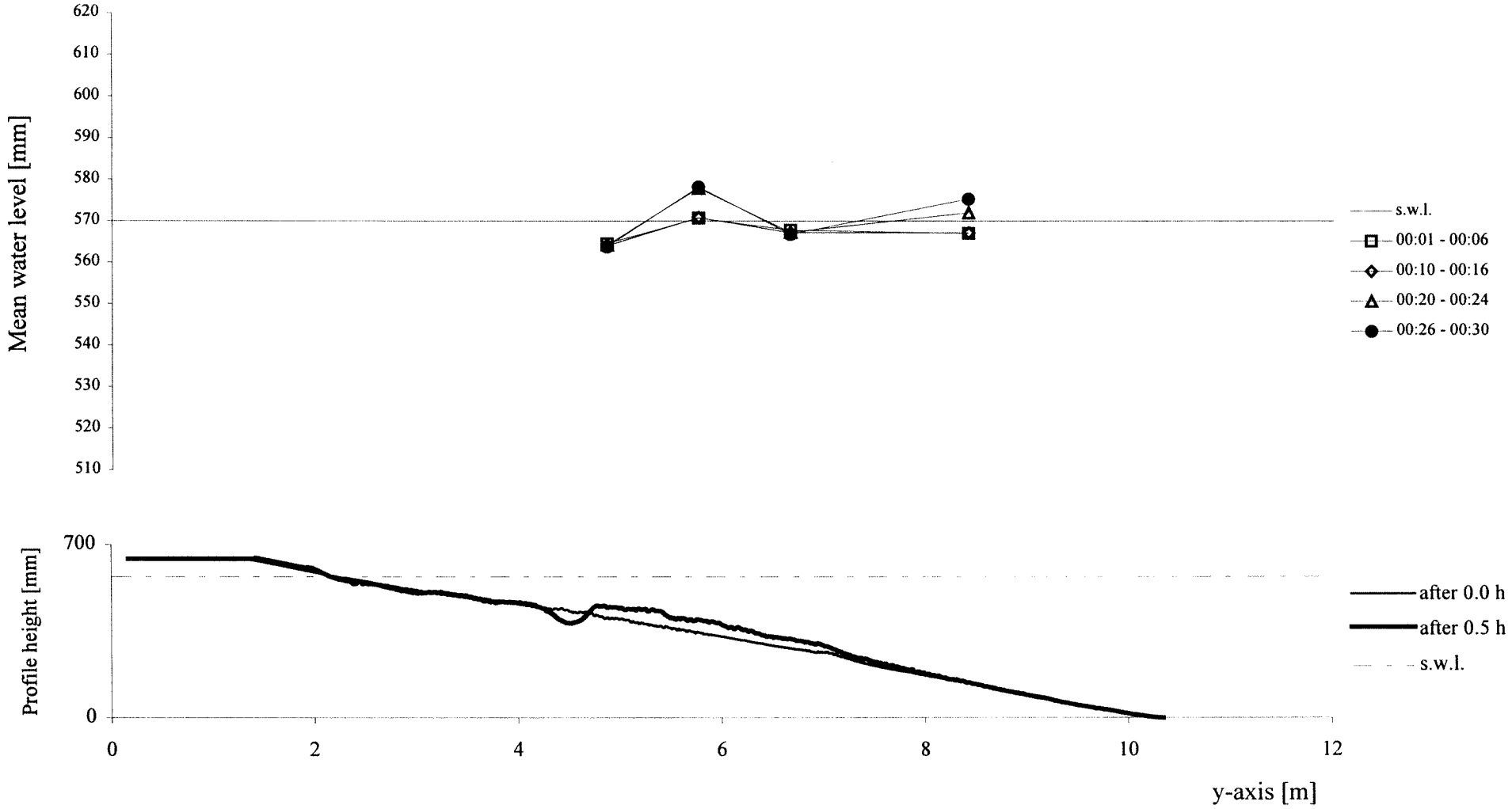

TEST A3 - cross-section x=12.5 m - interval 00:30 - 01:30

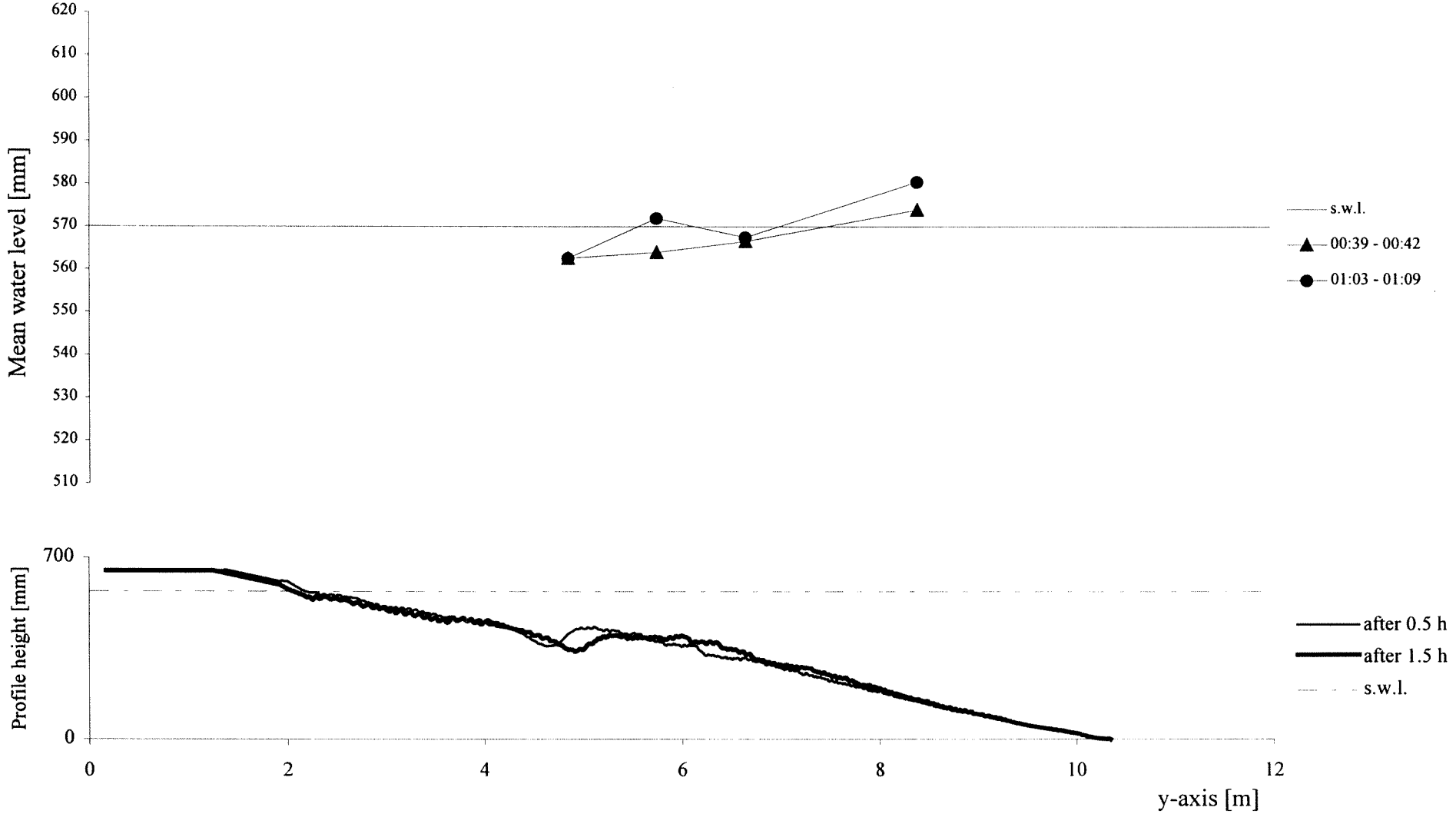

TEST A3 - cross-section x=24.5 m - interval 00:30 - 01:30

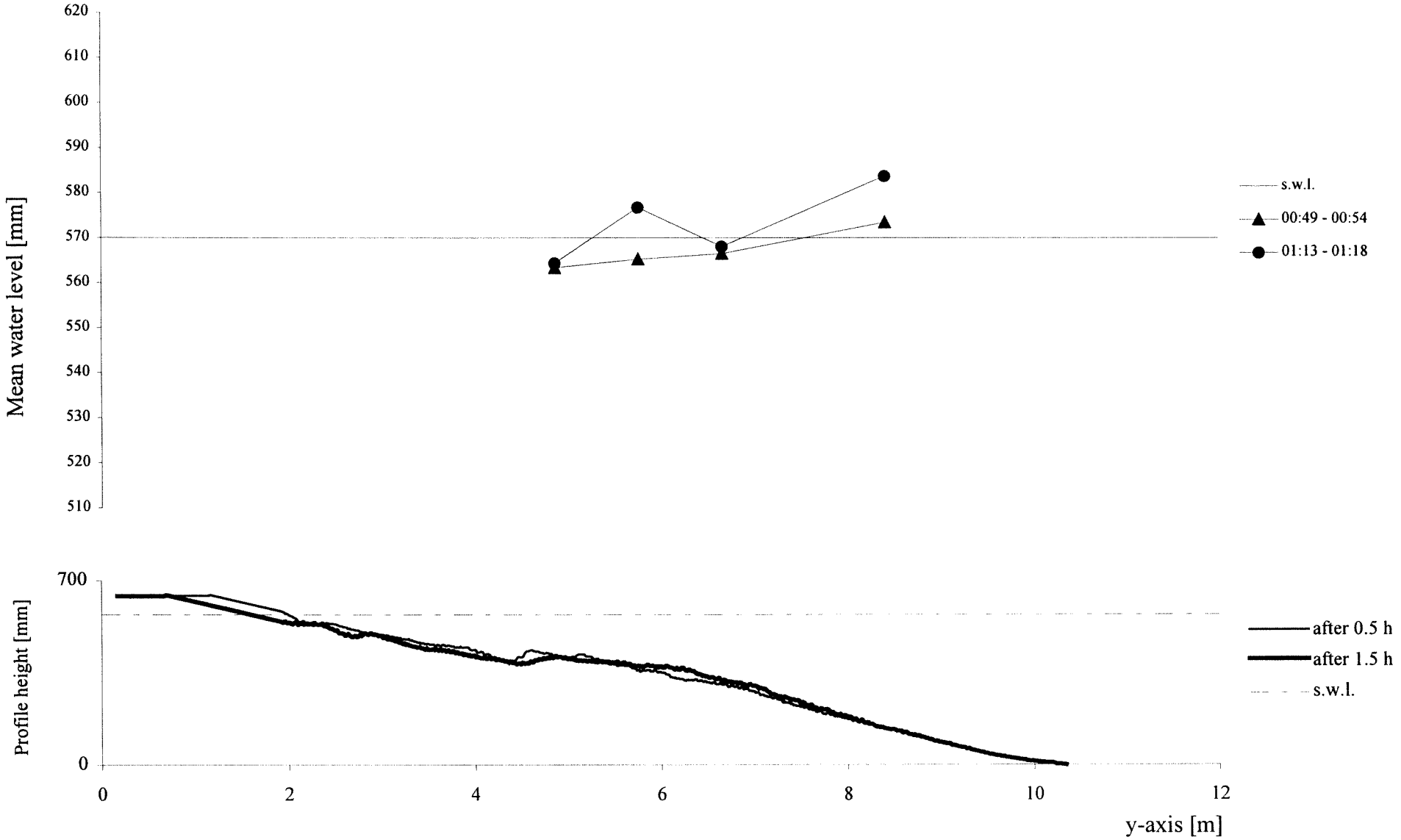

TEST A3 - cross-section x=6.5 m - interval 01:30 - 03:30

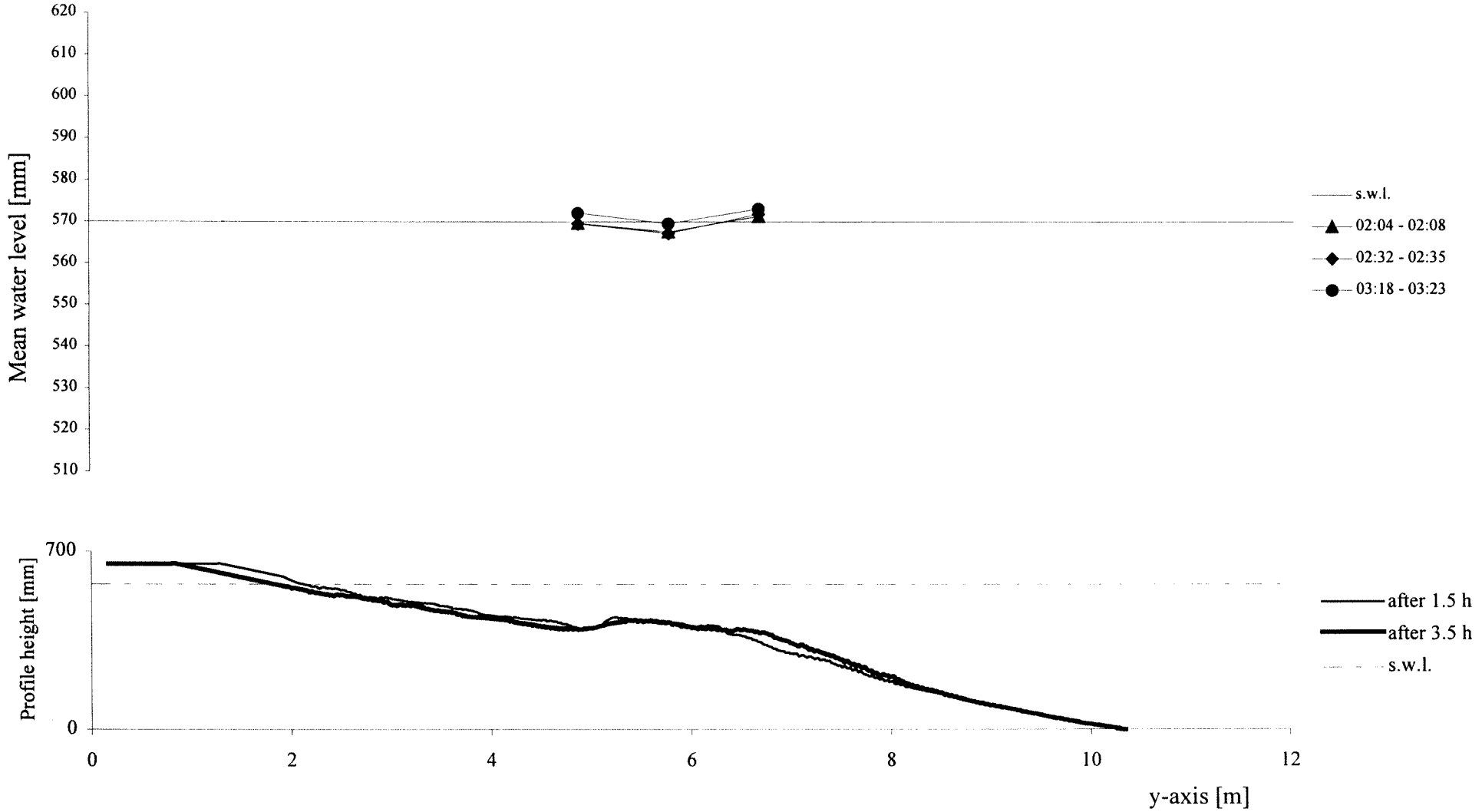

TEST A3 - cross-section x=20 m - interval 01:30 - 03:30

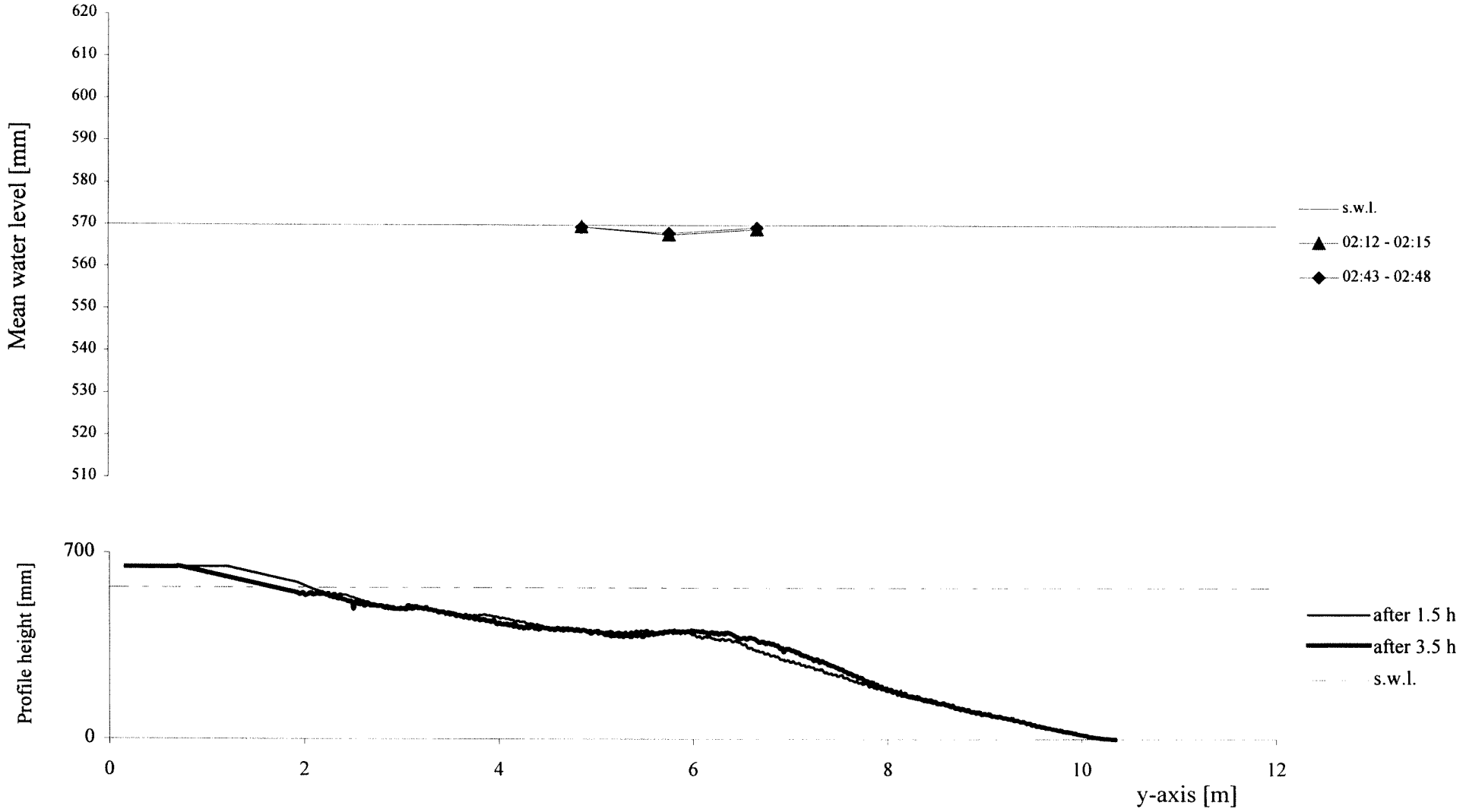

TEST A3 - cross-section x=3 m - interval 03:30 - 07:30

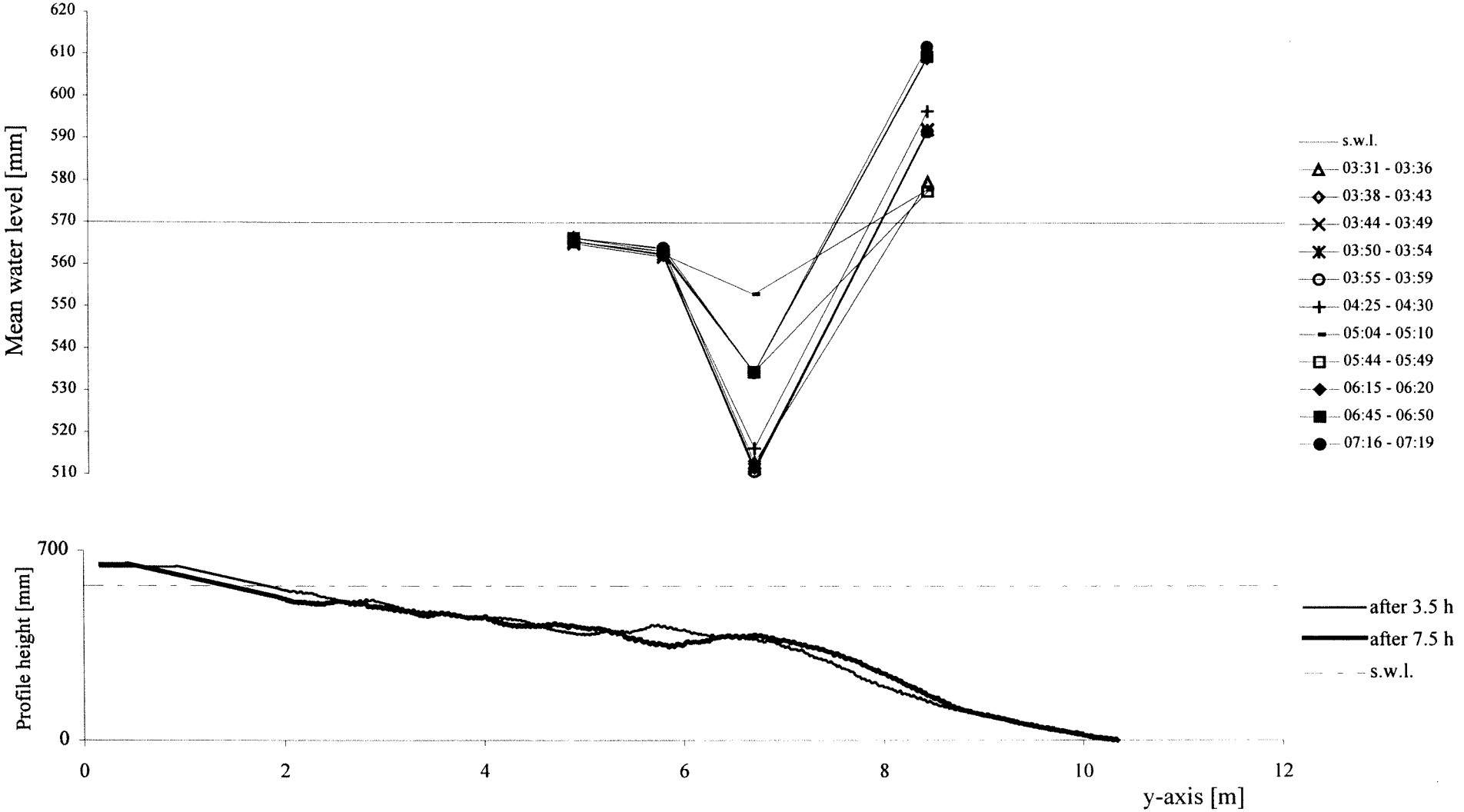

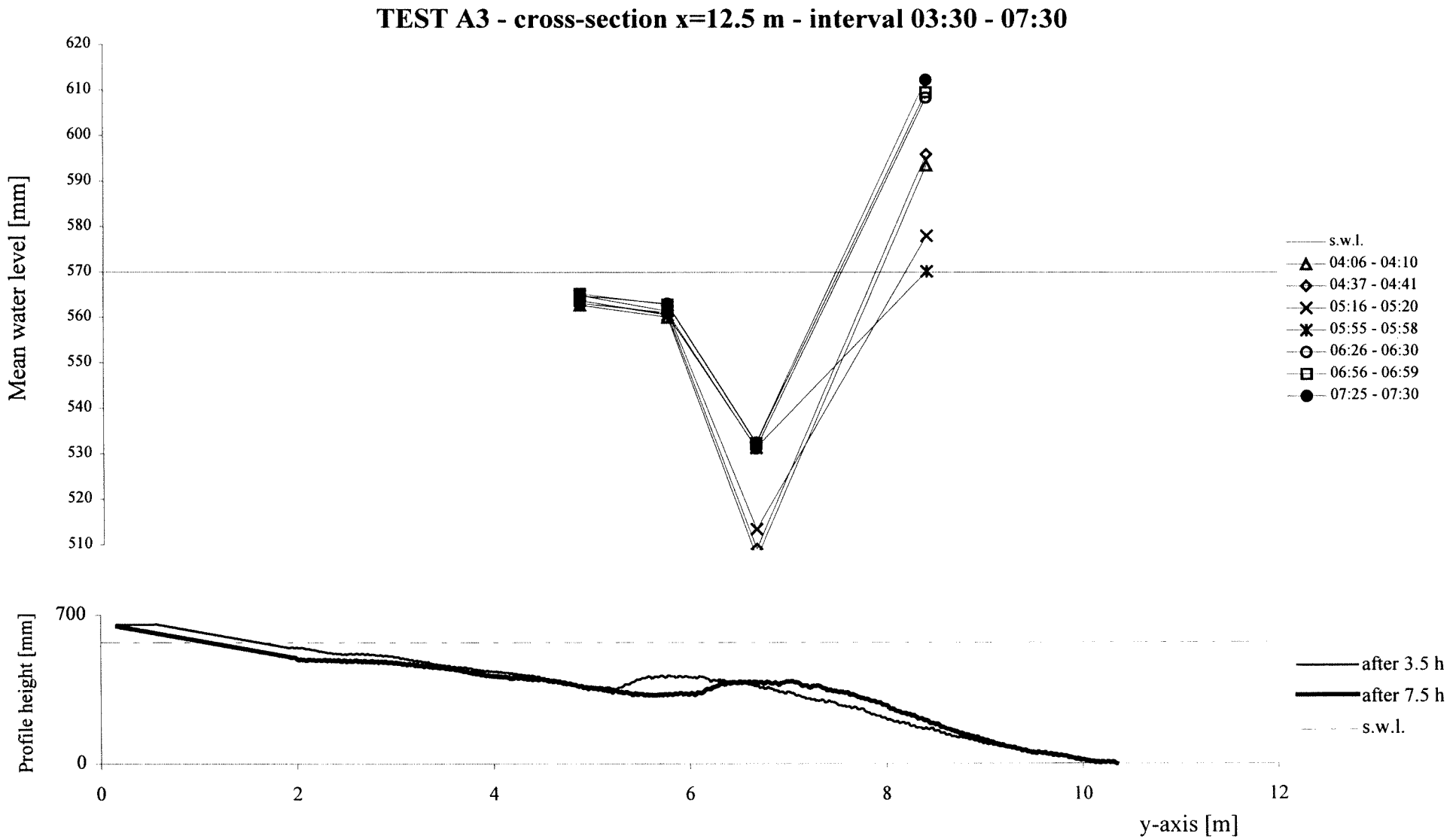
TEST A3 - cross-section x=12.5 m - interval 03:30 - 07:30
Mean water level [mm]
620
610
600
590
580
570
560
550
540
530
520
510
s.w.l.
04:06 - 04:10
04:37 - 04:41
05:16 - 05:20
05:55 - 05:58
06:26 - 06:30
06:56 - 06:59
07:25 - 07:30
Profile height [mm]
700
0
after 3.5 h
after 7.5 h
s.w.l.
0
2
4
6
8
10
12
y-axis [m]

TEST A3 - cross-section x=24.5 m - interval 03:30 - 07:30

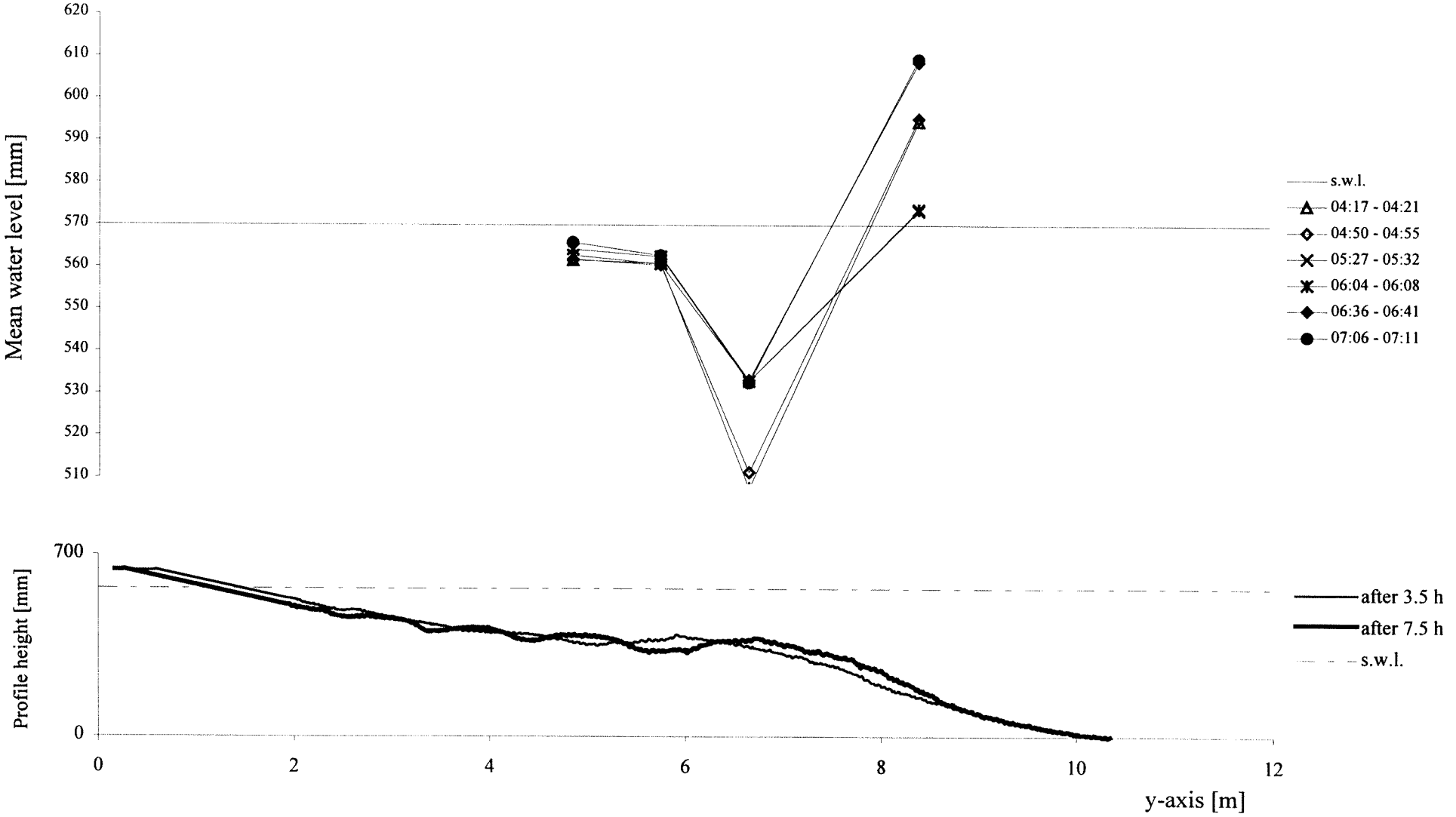

Appendix B1. Graphics TEST C1 - Average Water Level

TEST C1 - cross-section x=3 m - interval 00:00 - 00:30

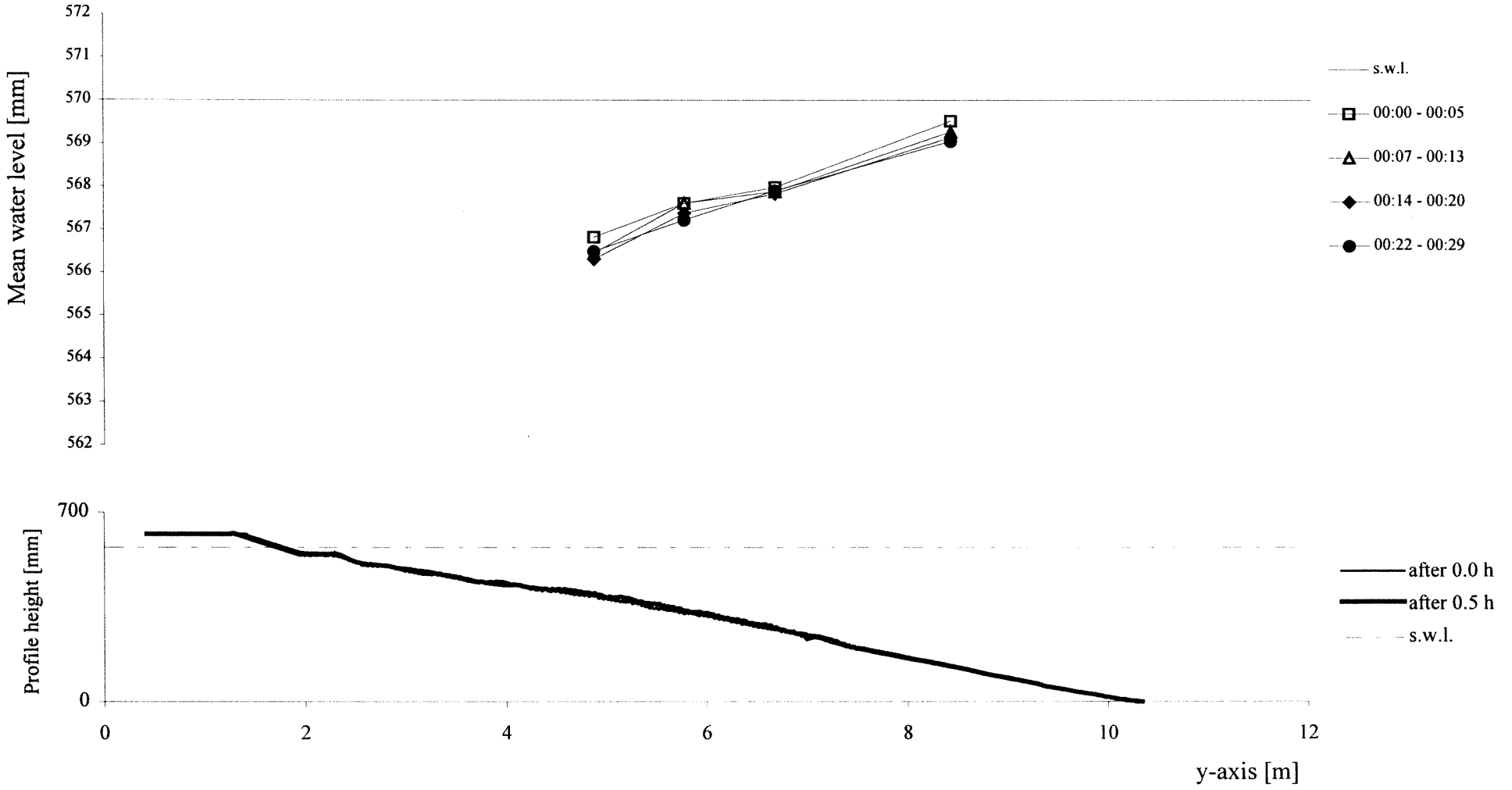

TEST C1 - cross-section x=6.5 m - interval 00:30 - 01:30

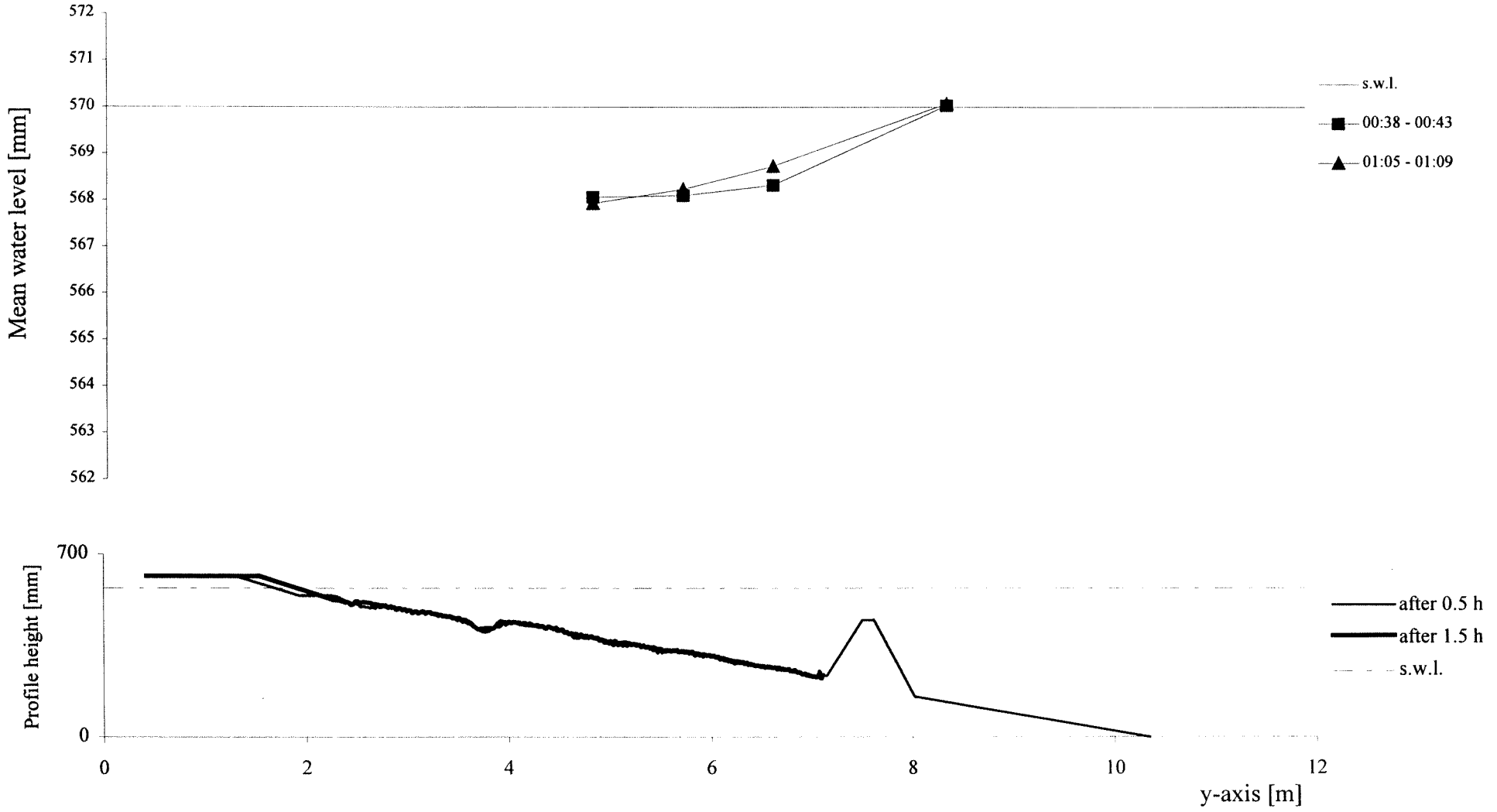

TEST C1 - cross-section x=20 m - interval 00:30 - 01:30

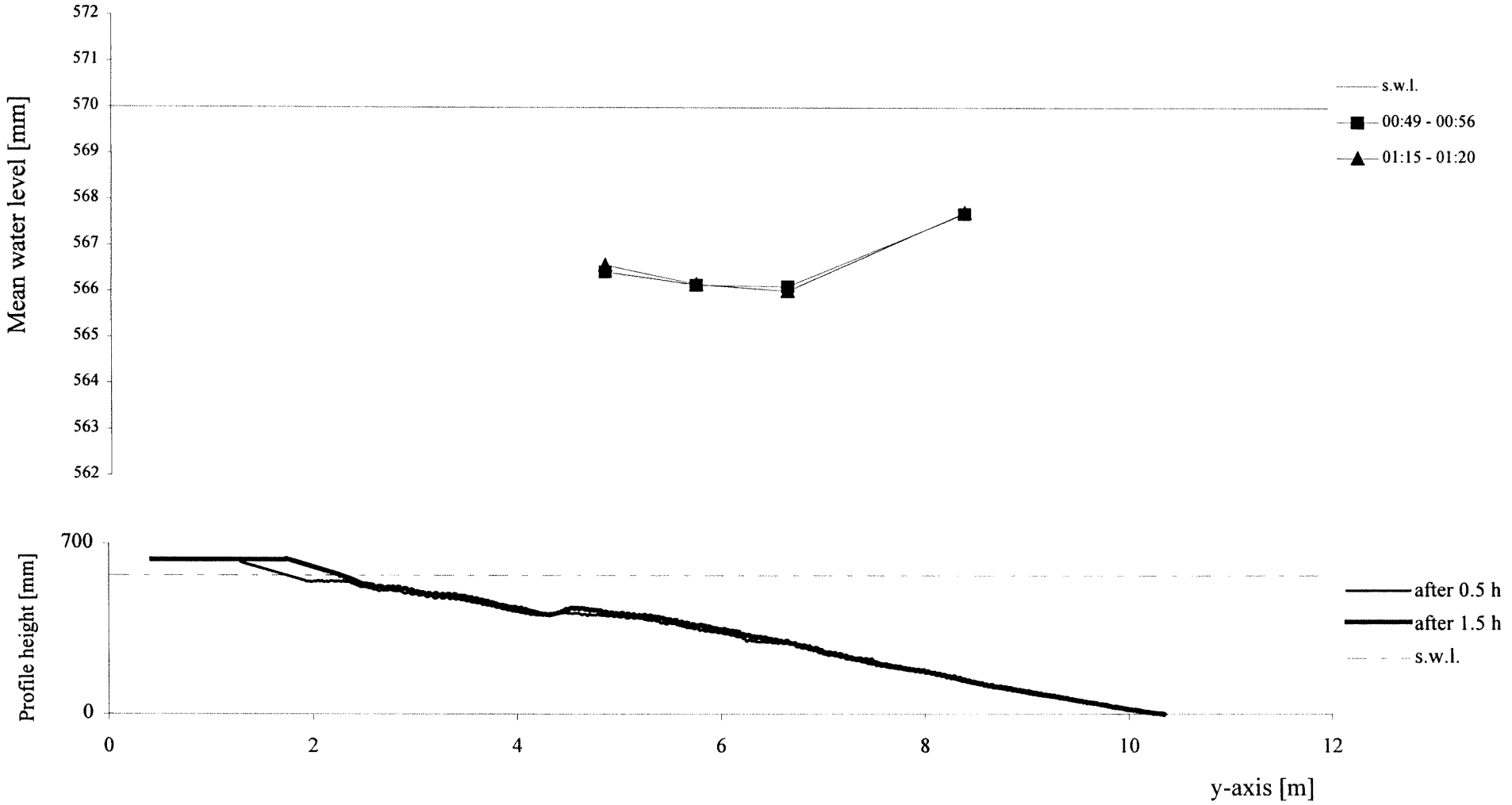

TEST C1 - cross-section x=3 m - interval 01:30 - 03:30

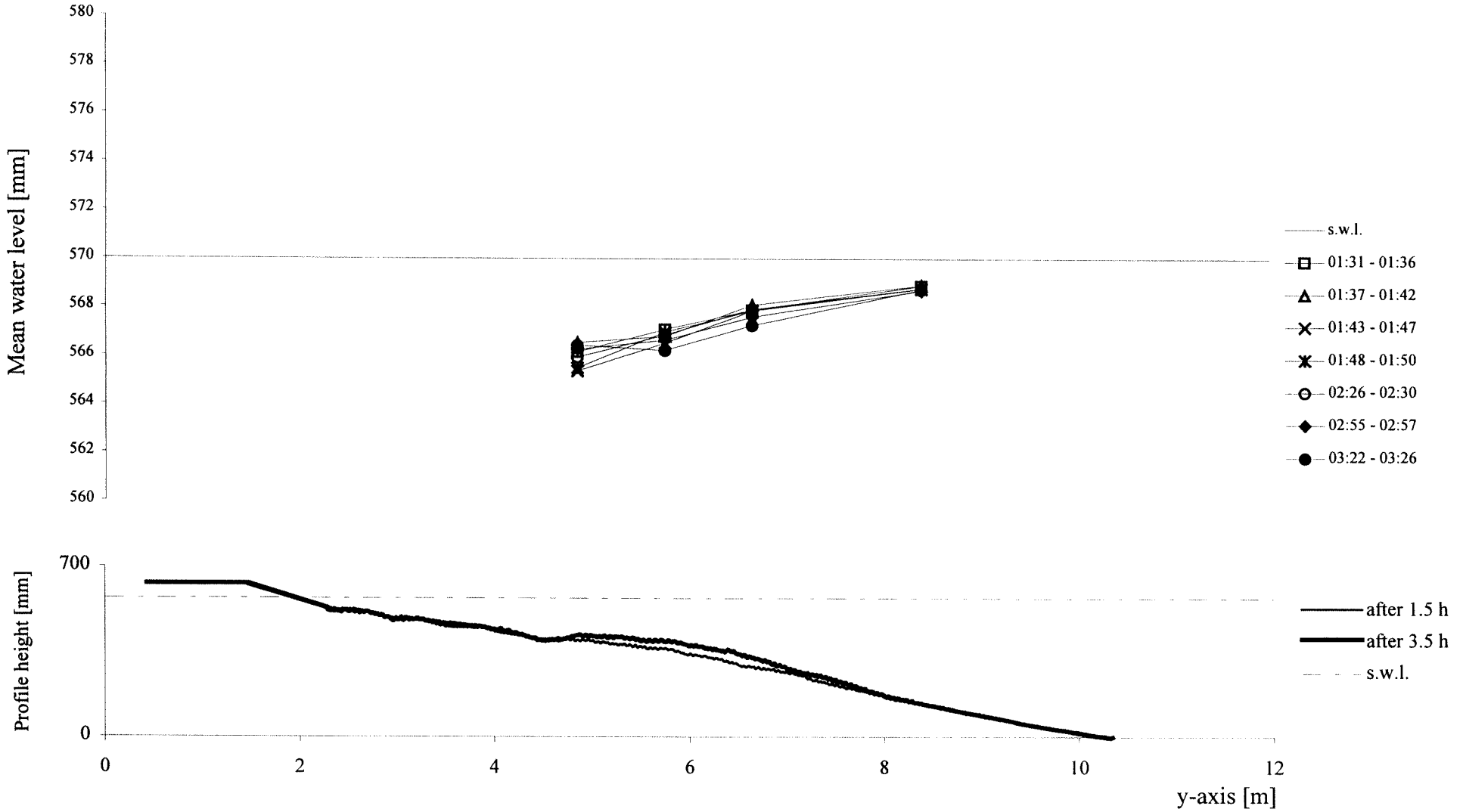

TEST C1 - cross-section x=12.5 m - interval 01:30 - 03:30

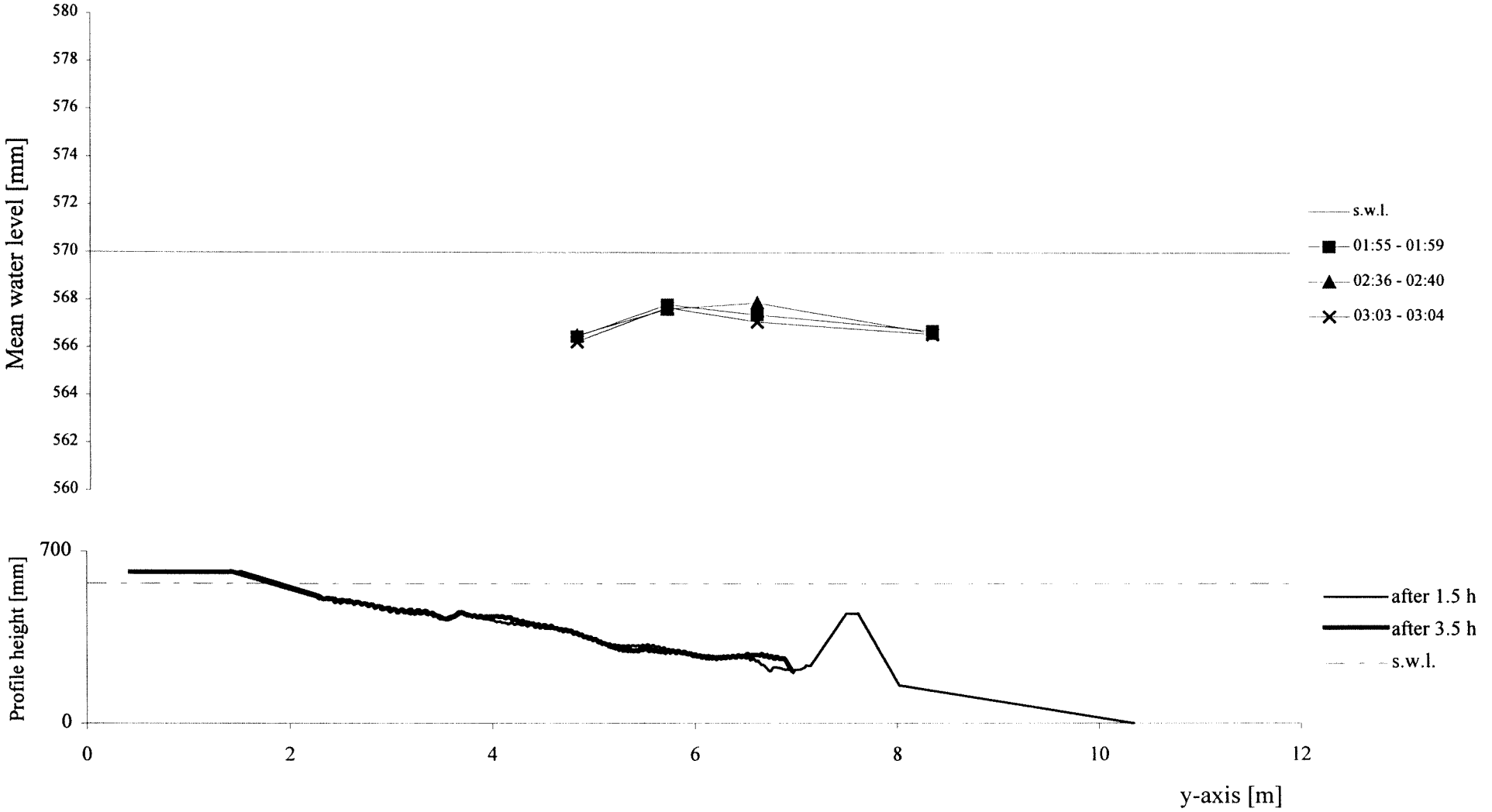

TEST C1 - cross-section x=24.5 m - interval 01:30 - 03:30

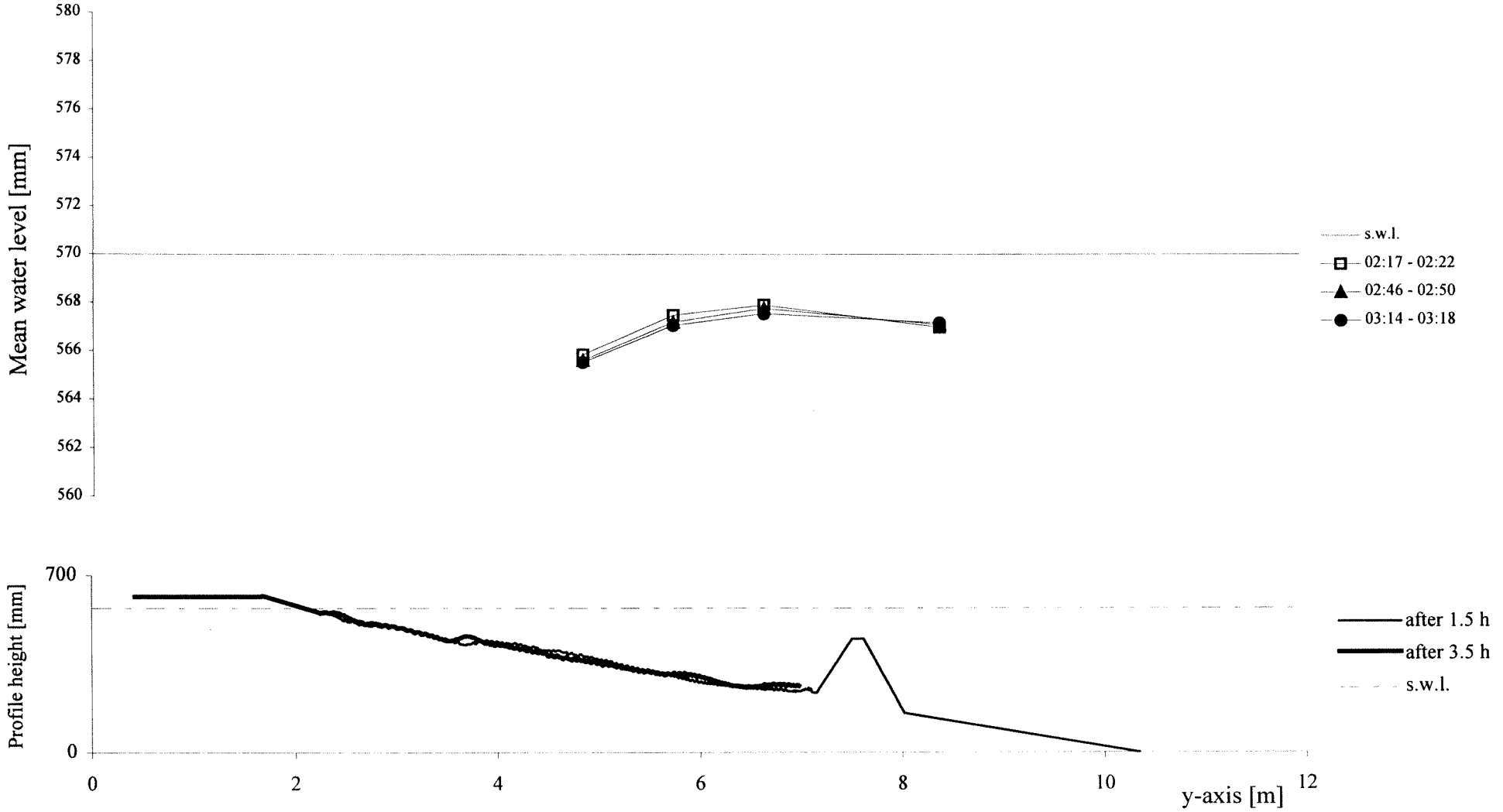

TEST C1 - cross-section x=6.5 m - interval 03:30 - 07:30

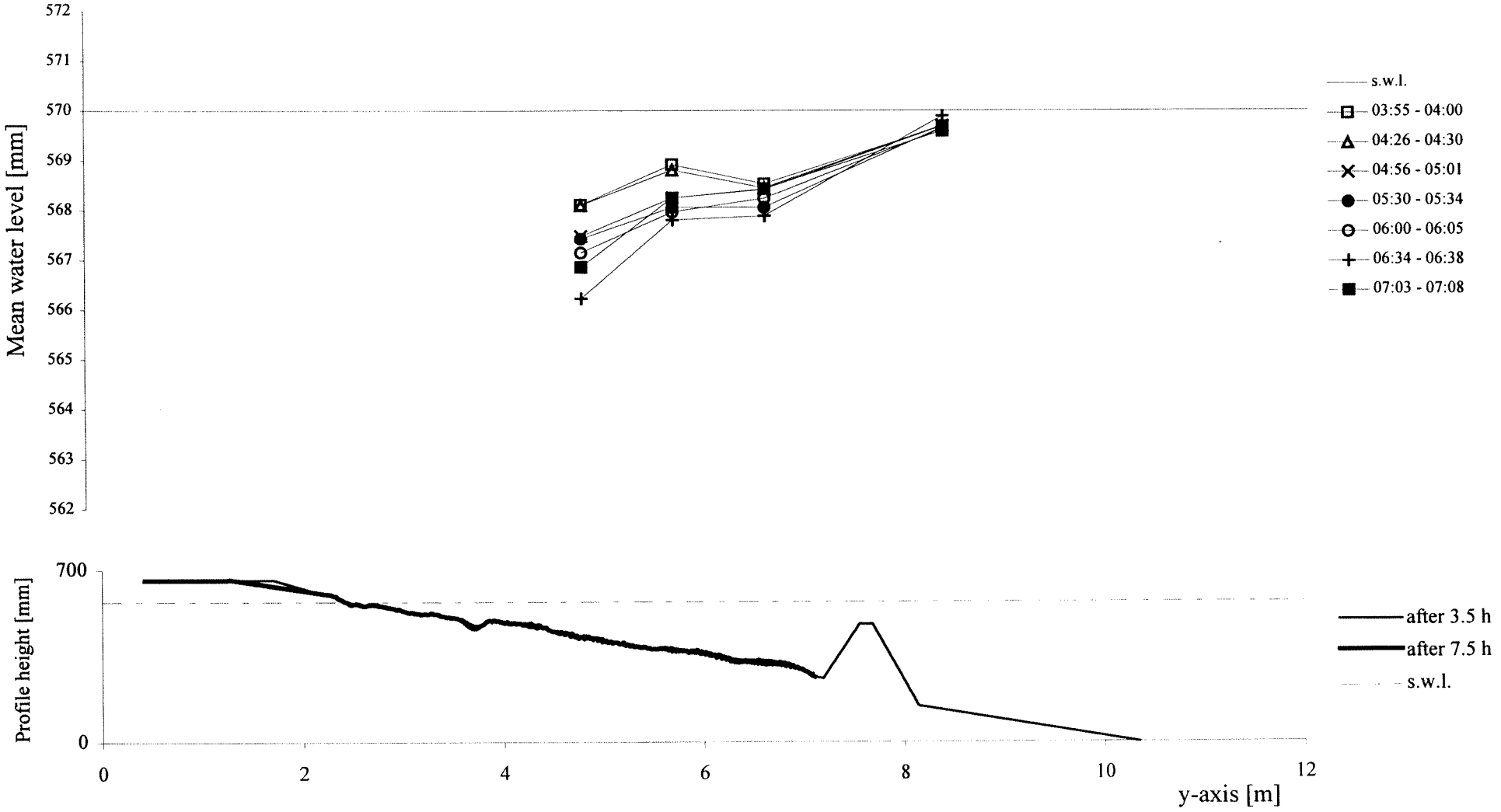

TEST C1 - cross-section x=20 m - interval 03:30 - 07:30

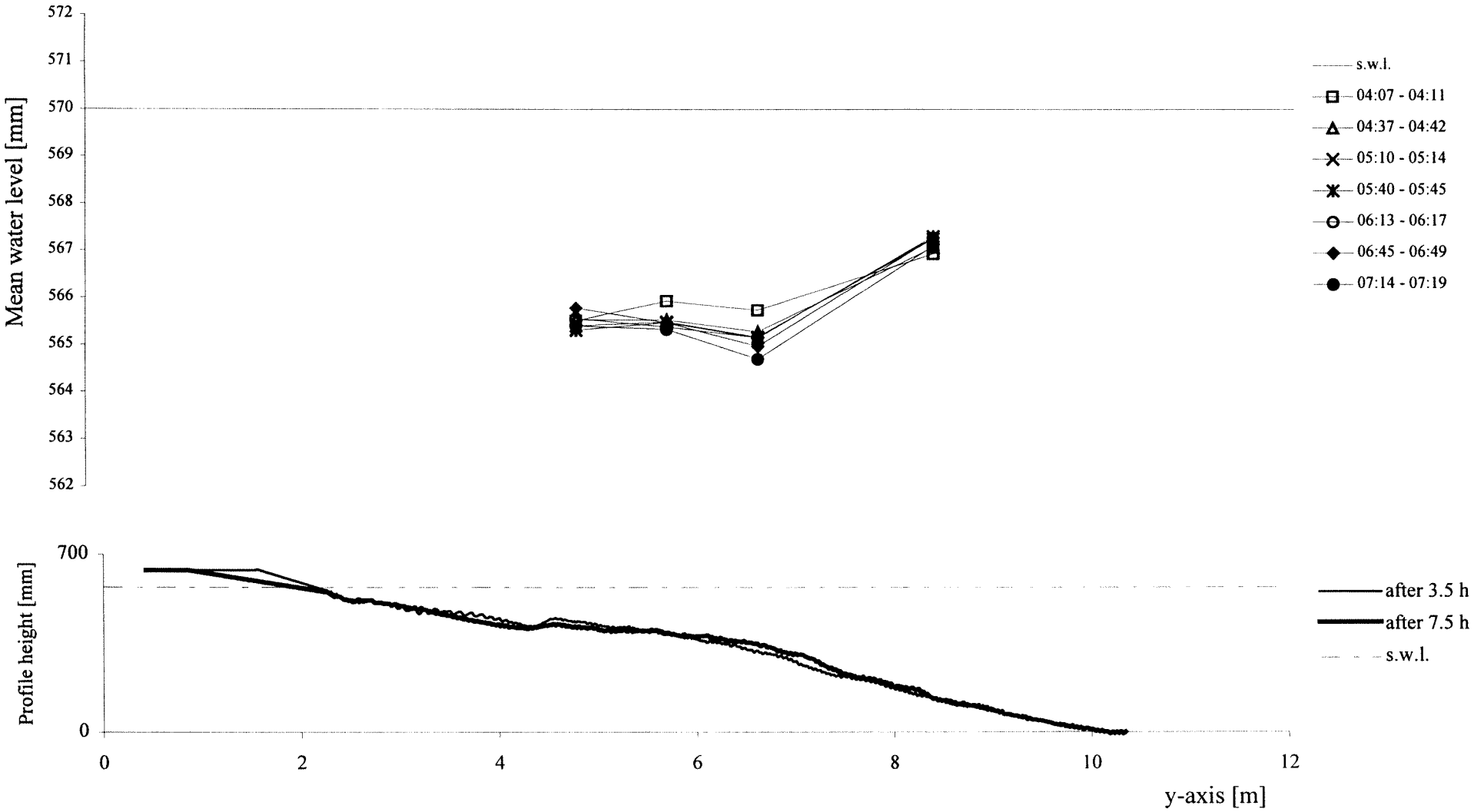

Appendix B2. Graphics TEST C2 - Average Water Level

TEST C2 - cross-section x=3 m - interval 00:00 - 00:30

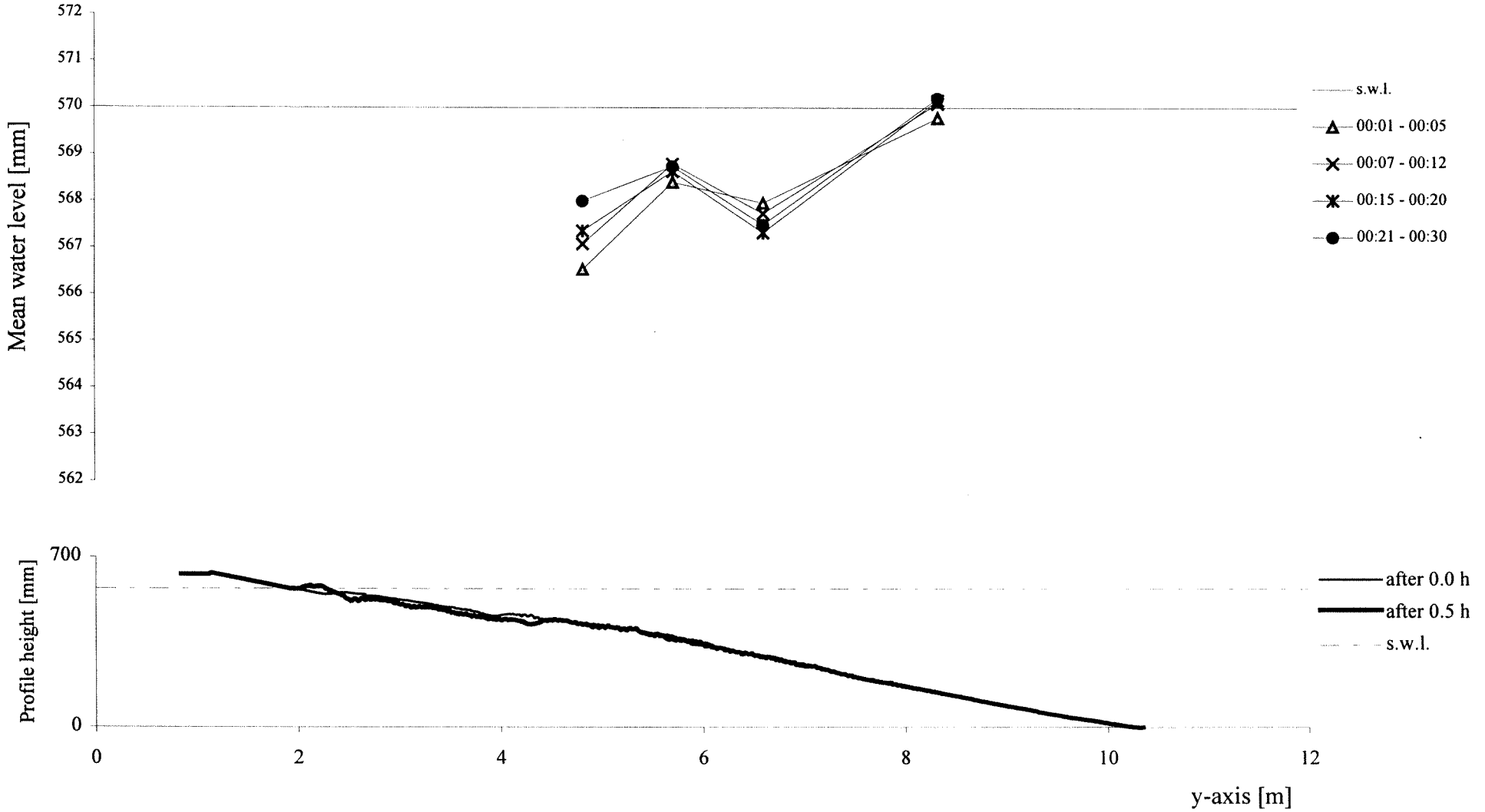

TEST C2 - cross-section x=12.5 m - interval 00:30 - 01:30

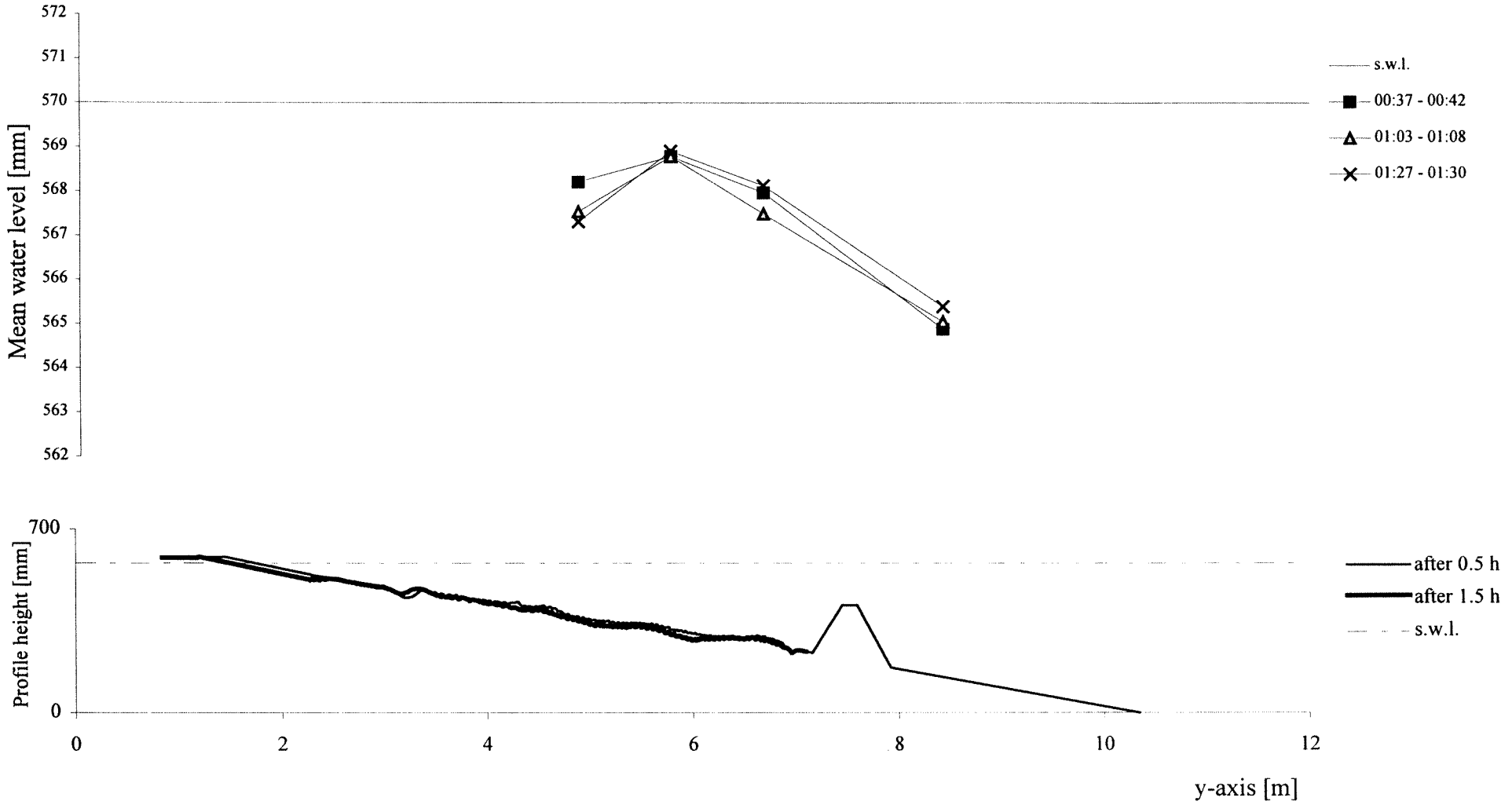

TEST C2 - cross-section x=24.5 m - interval 00:30 - 01:30

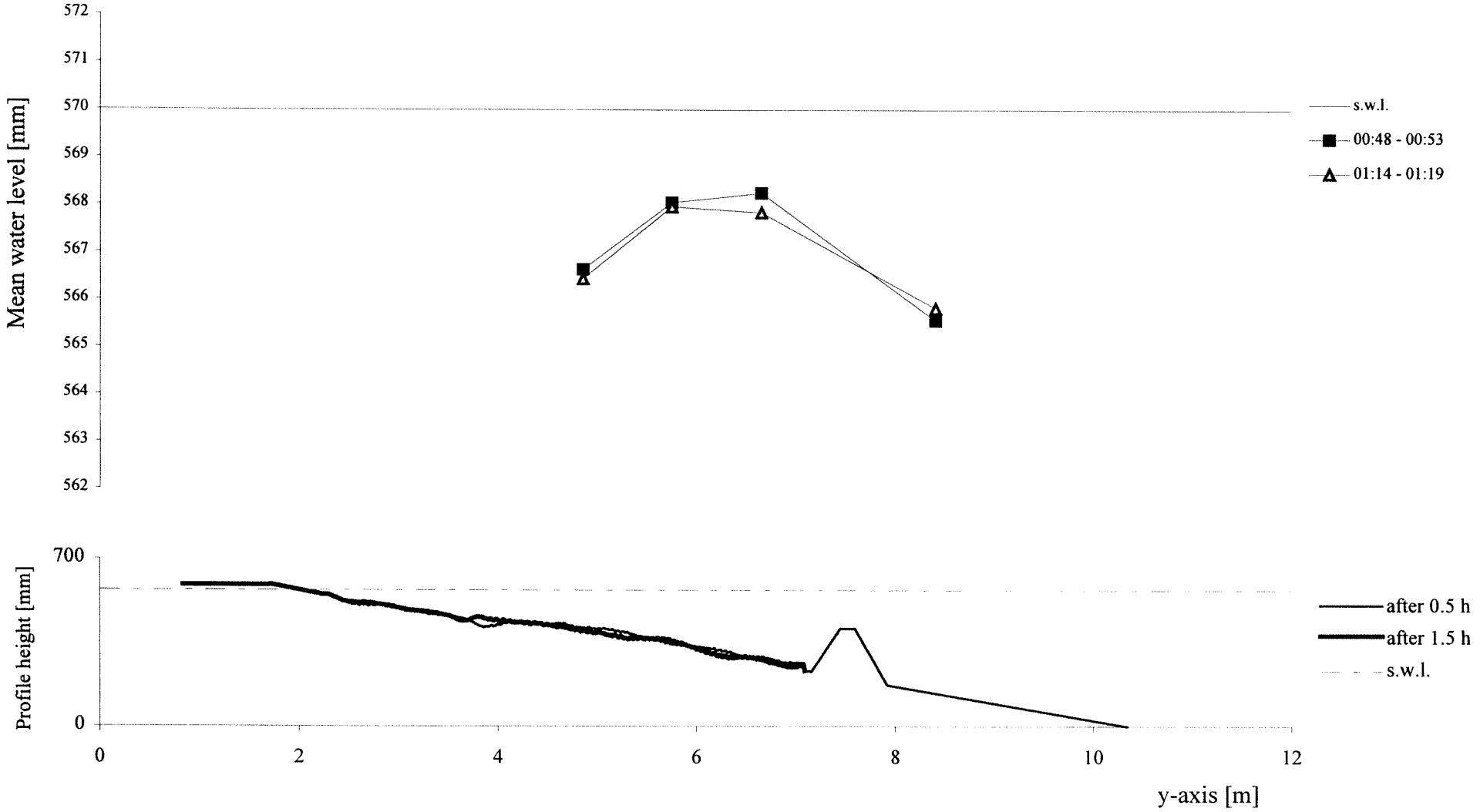

TEST C2 - cross-section x=6.5 m - interval 01:30 - 03:30

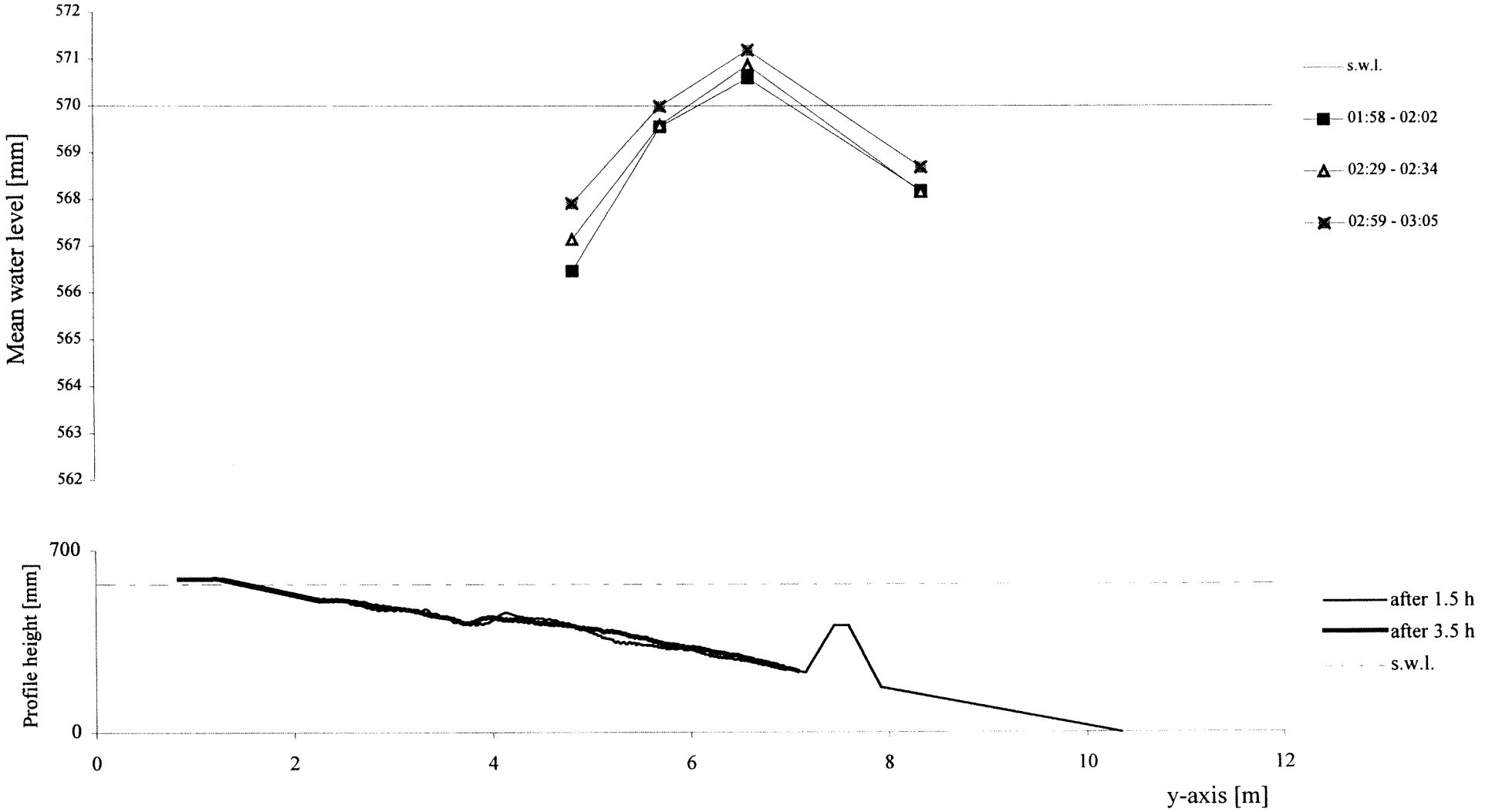

TEST C2 - cross-section x=20 m - interval 01:30 - 03:30

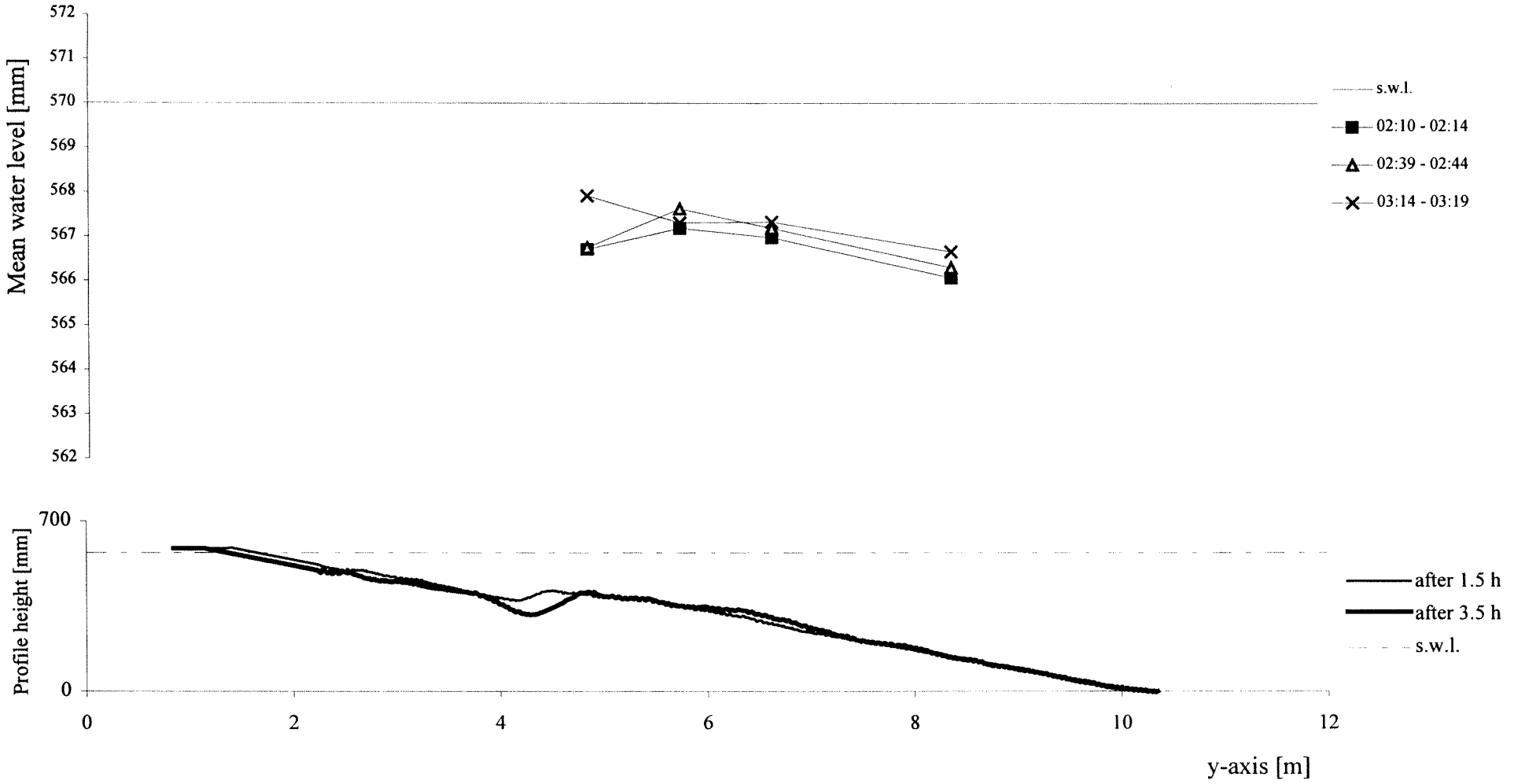

TEST C2 - cross-section x=3 m - interval 03:30 - 07:30

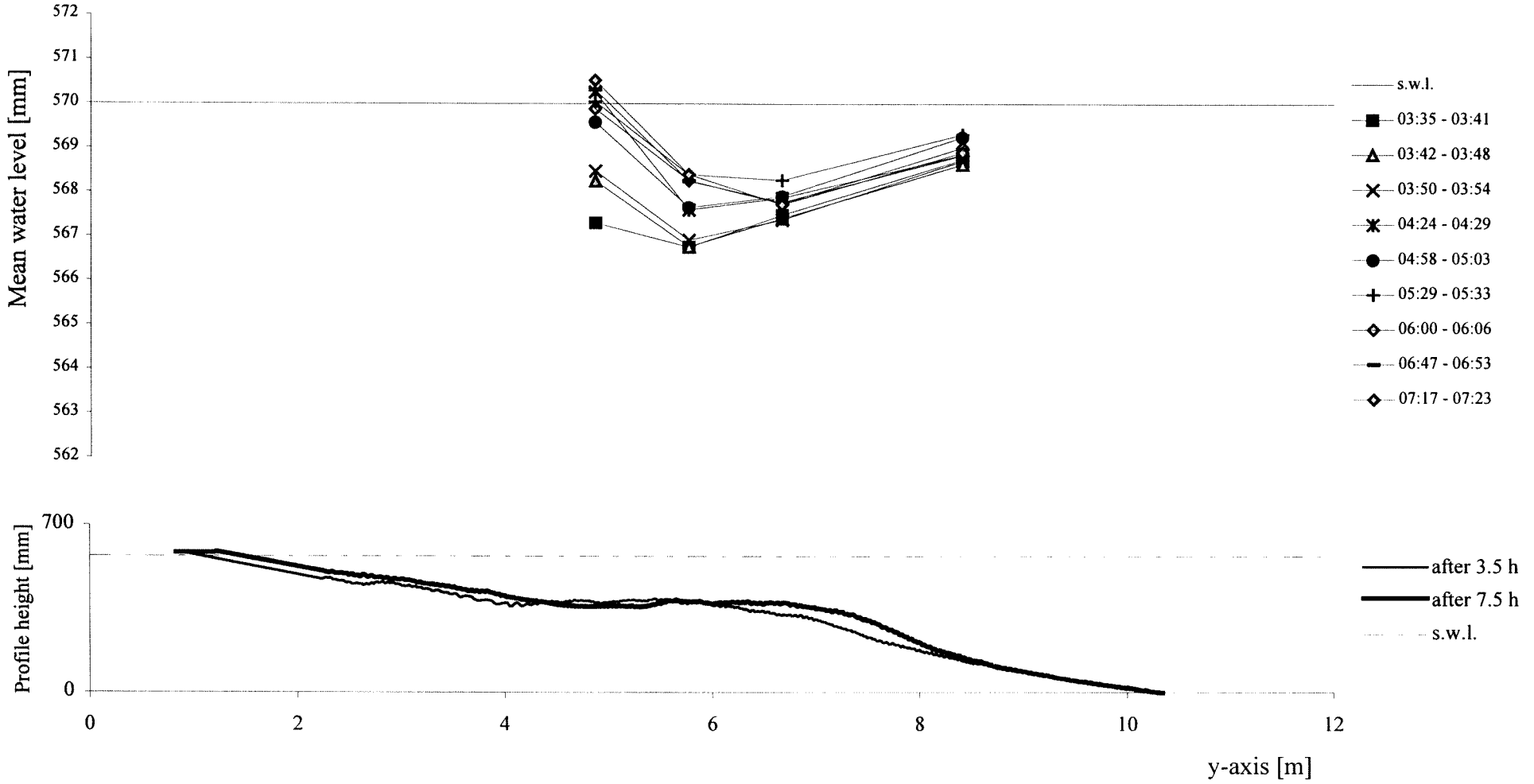

TEST C2 - cross-section x=12.5 m - interval 03:30 - 07:30

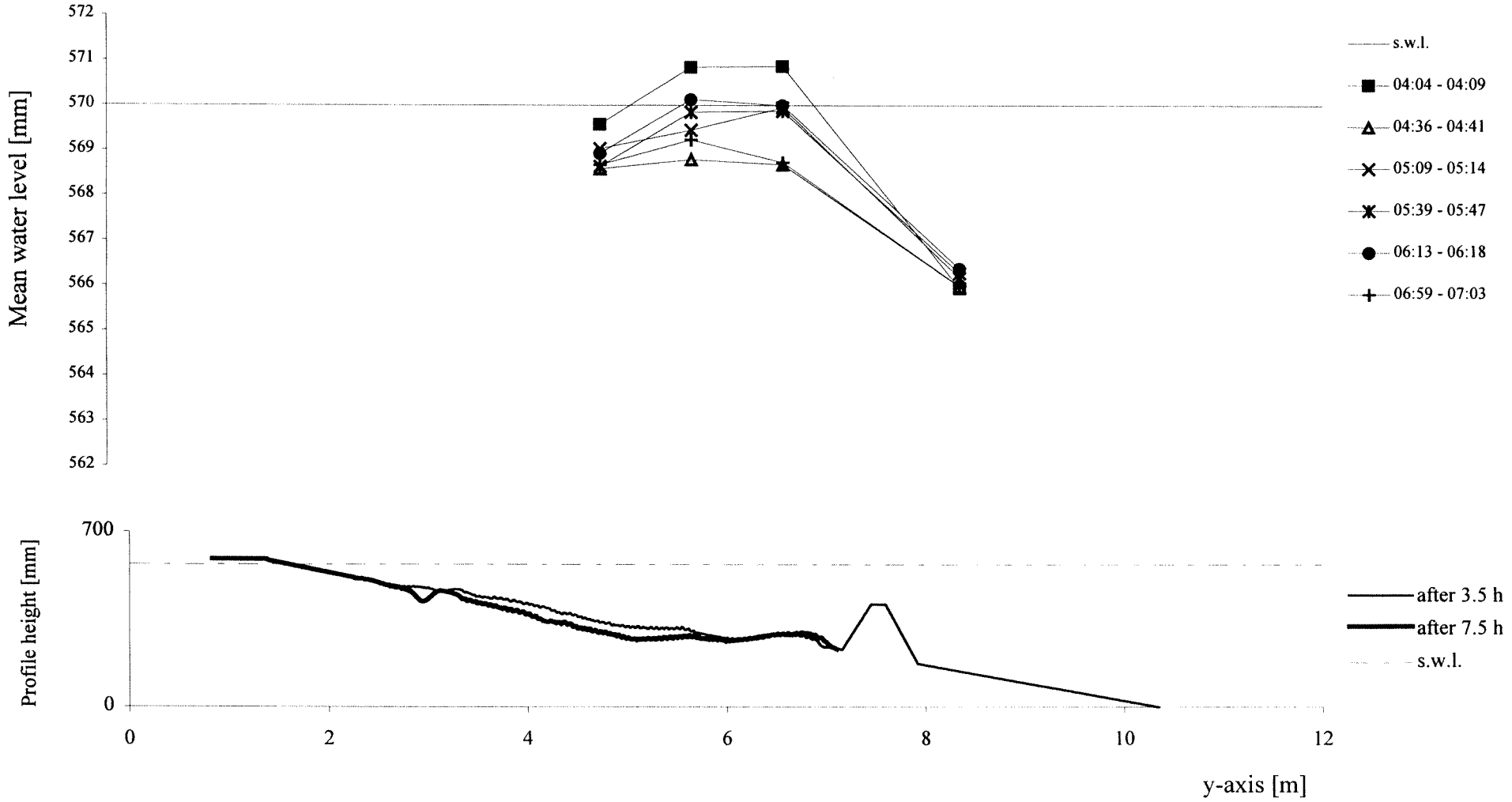

TEST C2 - cross-section x=24.5 m - interval 03:30 - 07:30

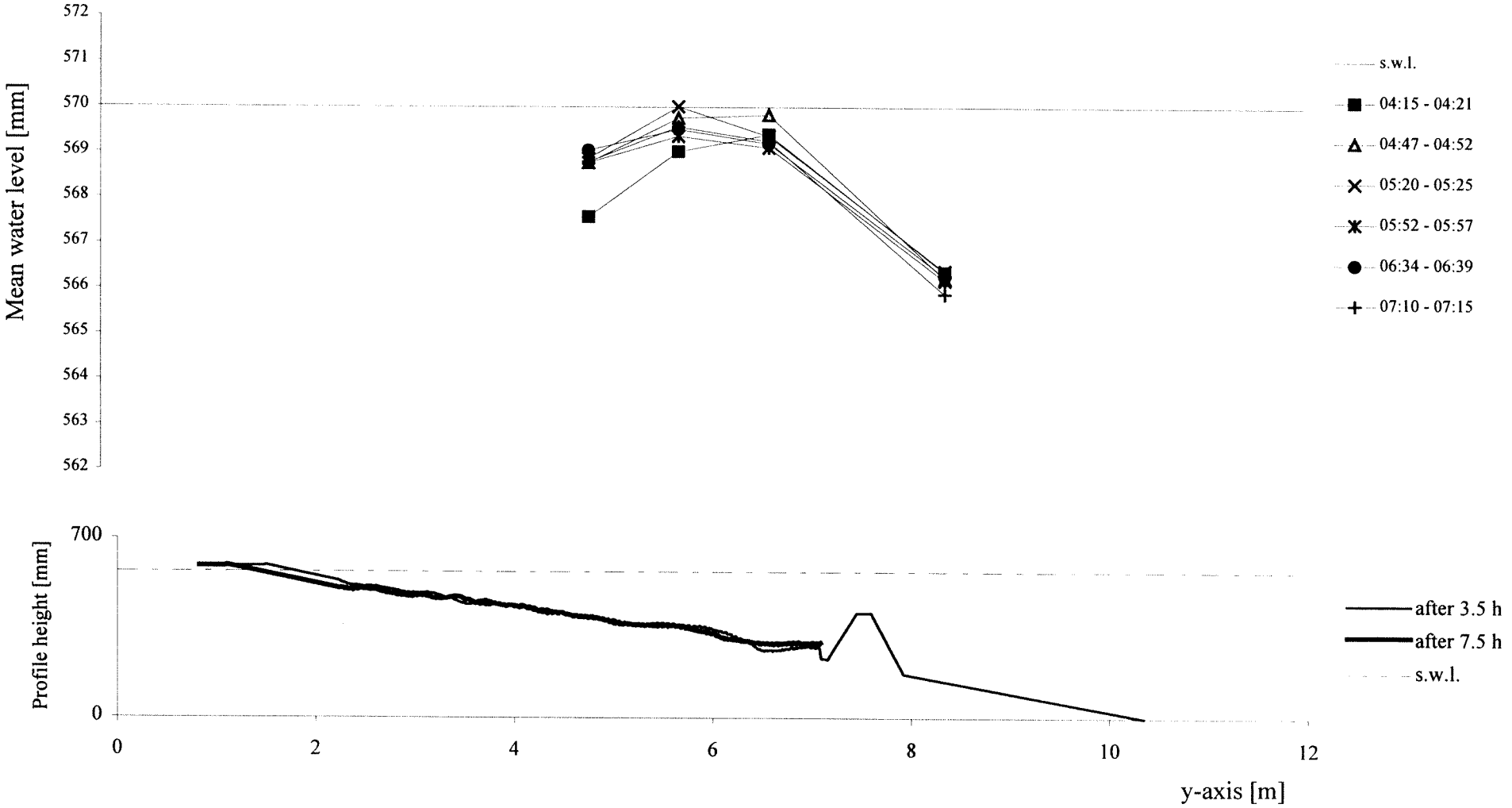

Appendix B3. Graphics TEST C3 - Average Water Level

TEST C3 - cross-section x=3m - interval 00:00 - 00:30

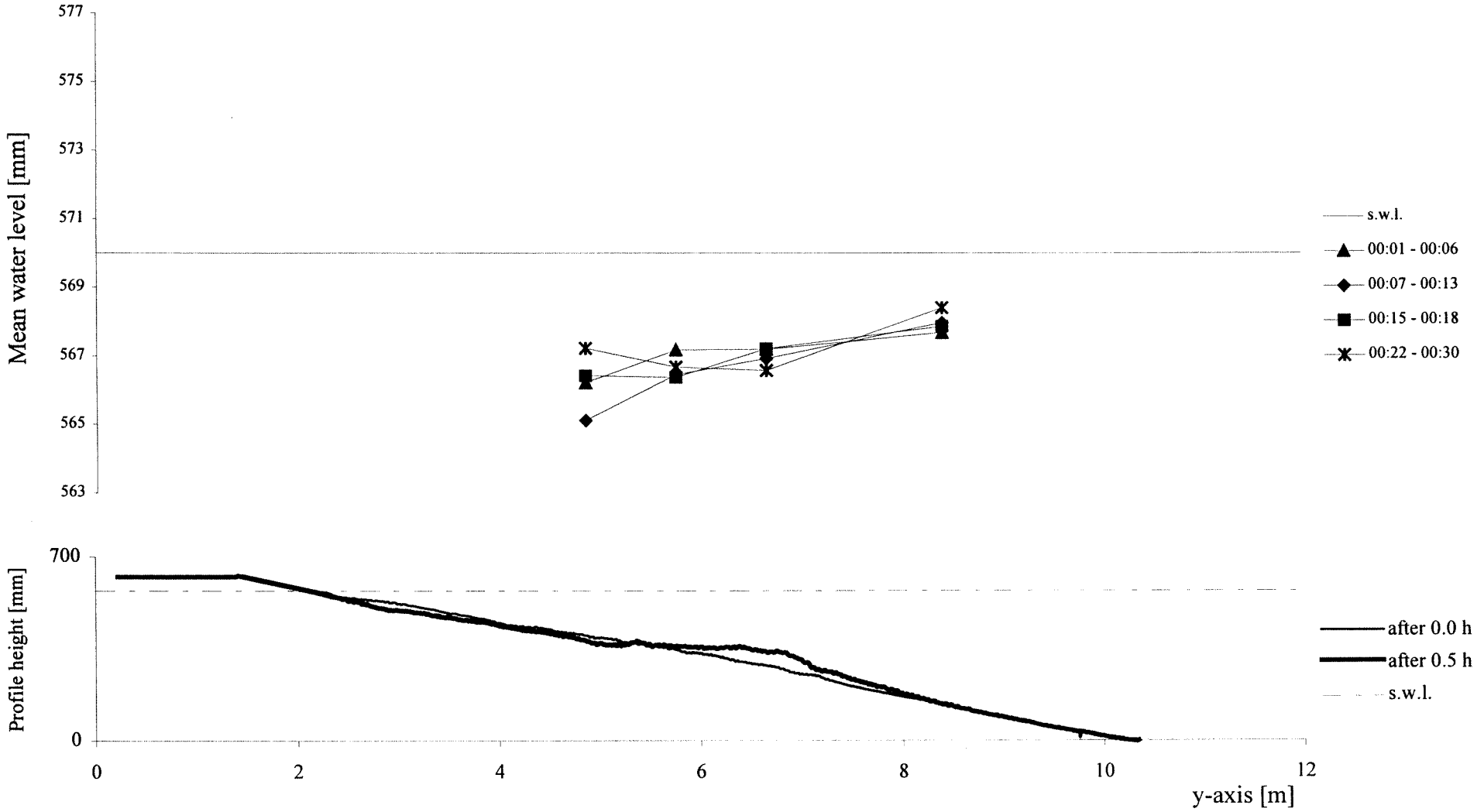

TEST C3 - cross-section x=12.5 m - interval 00:30 - 01:30

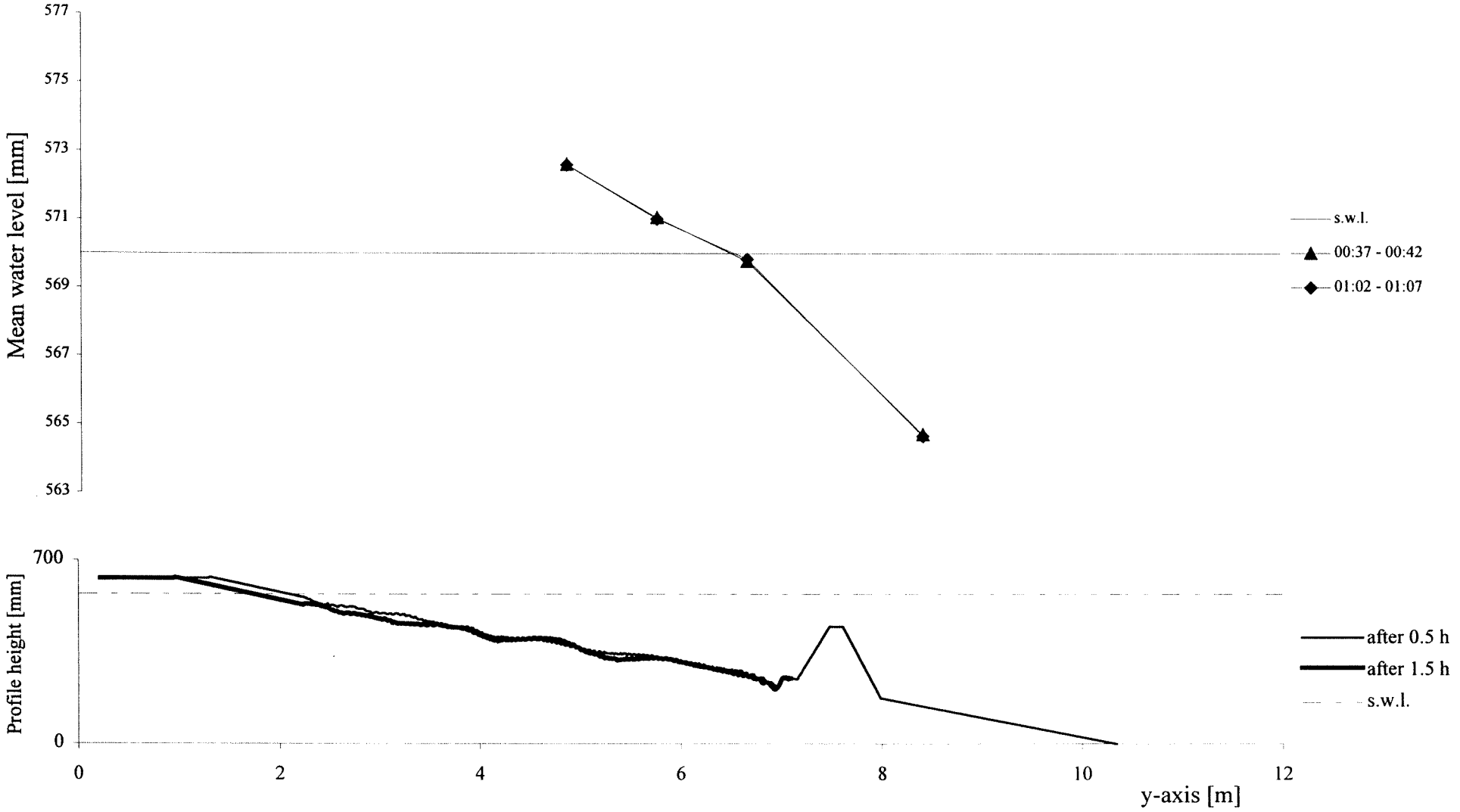

TEST C3 - cross-section x=24.5 m - interval 00:30 - 01:30

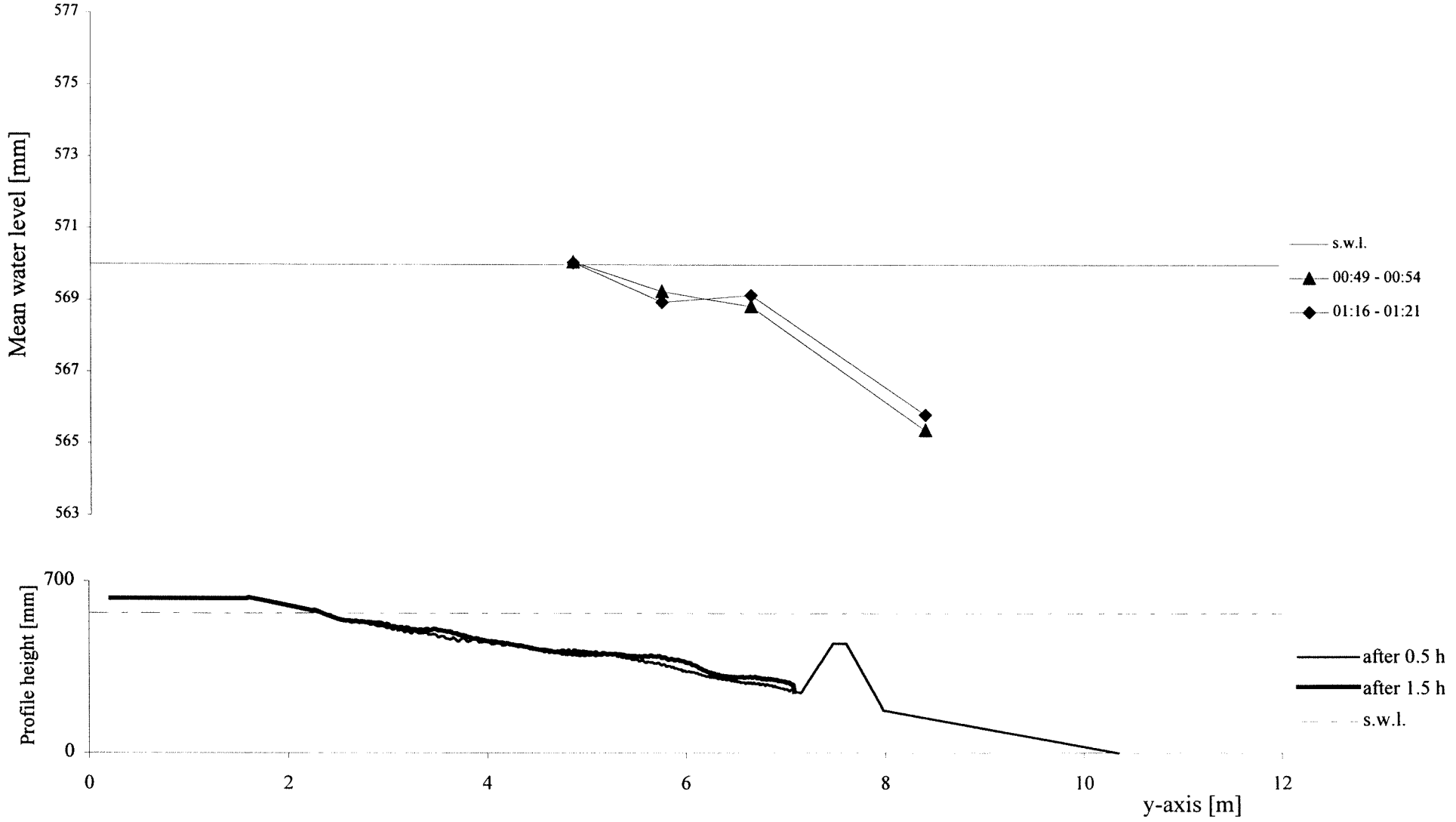

TEST C3 - cross-section x=6.5 m - interval 01:30 - 03:30

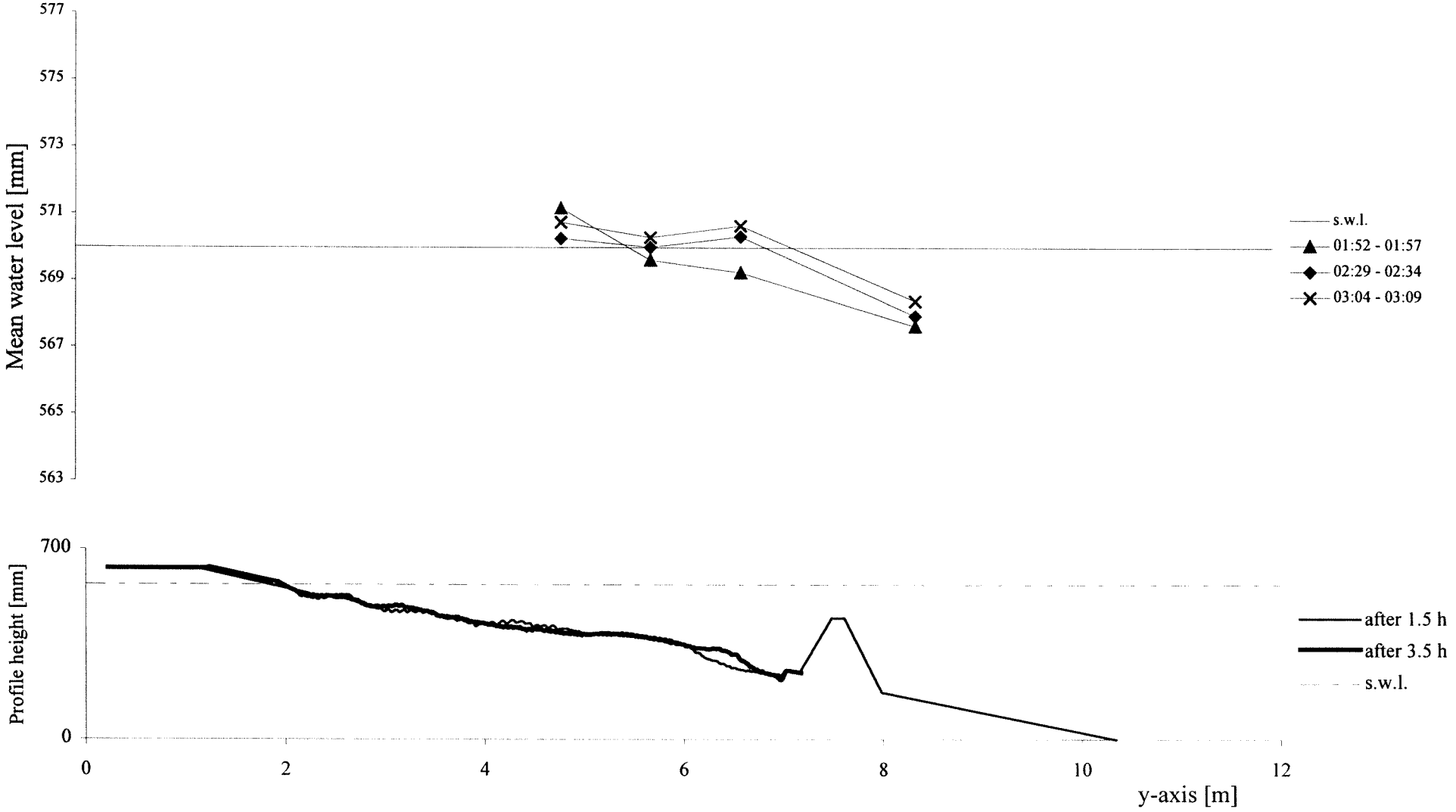

TEST C3 - cross-section x=20 m - interval 01:30 - 03:30

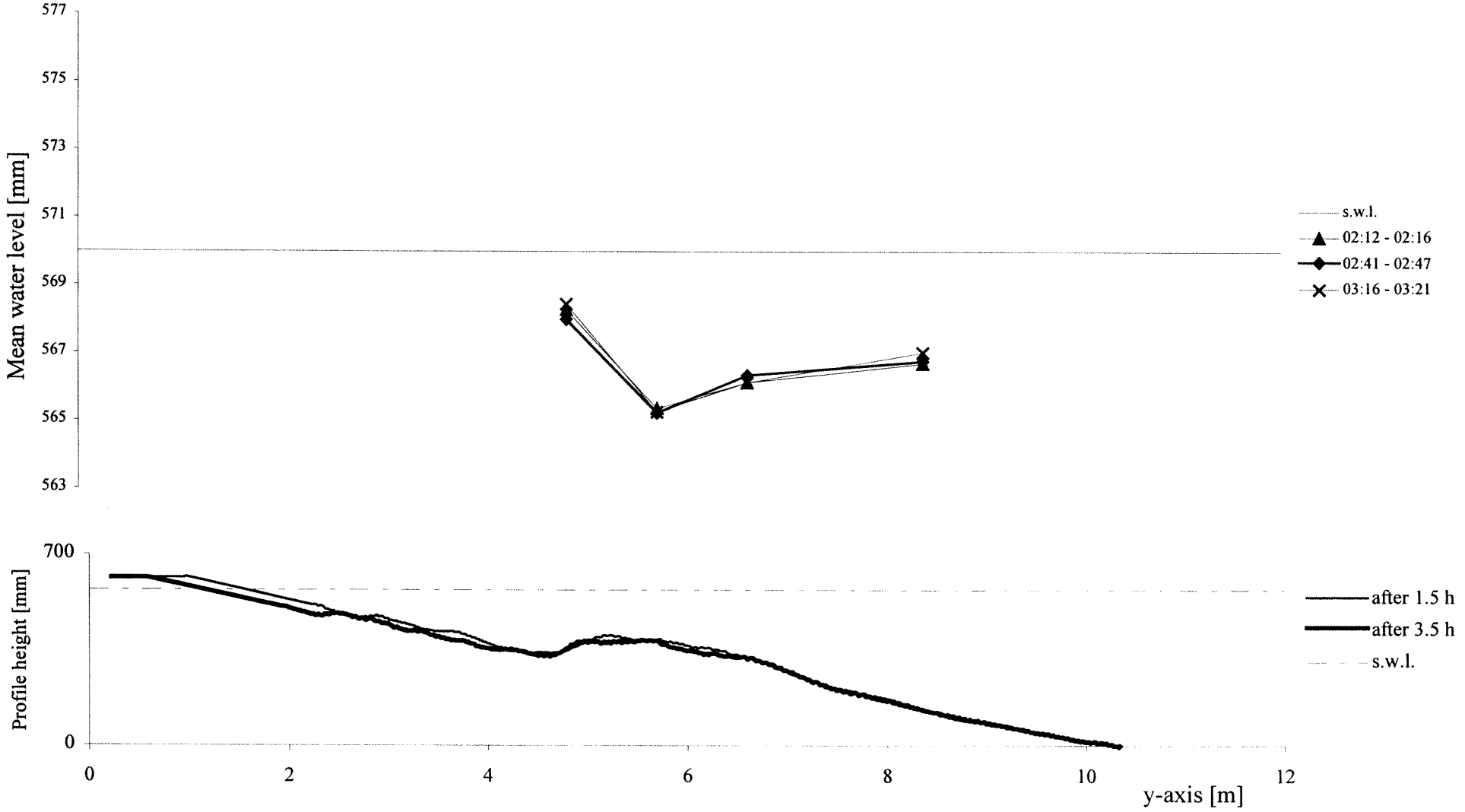

TEST C3 - cross-section x=3 m - interval 03:30 - 07:30

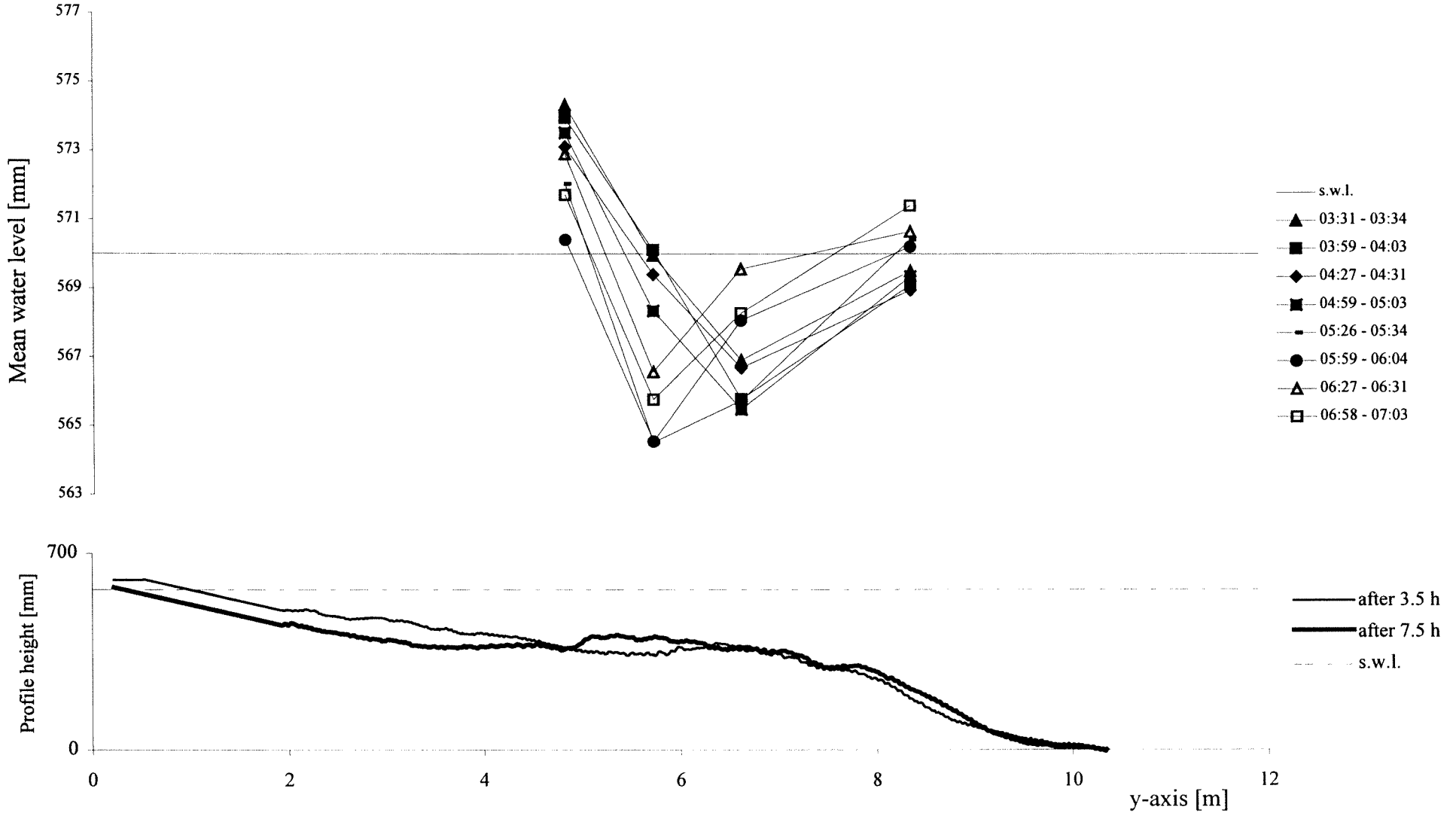

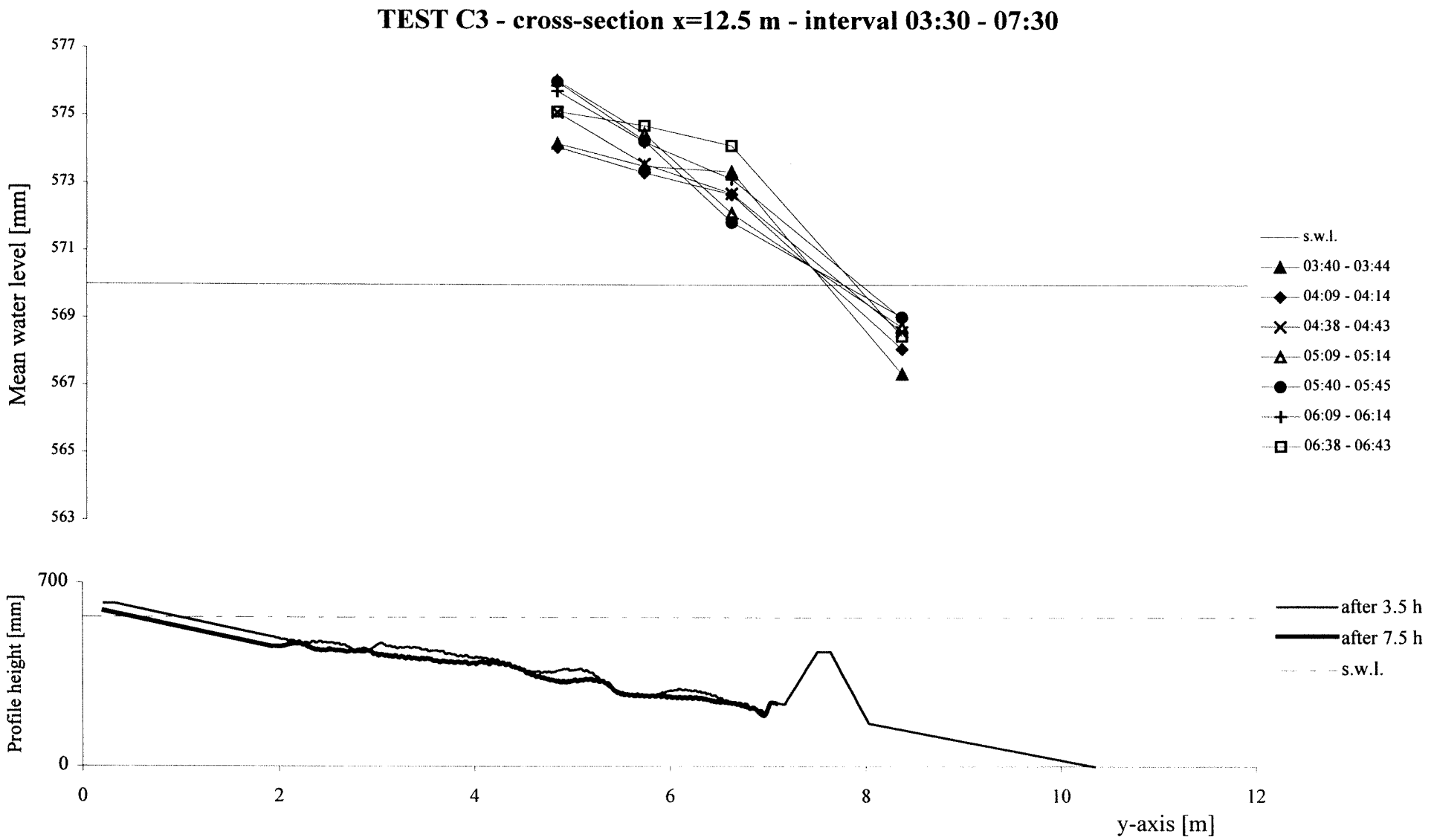
TEST C3 - cross-section x=12.5 m - interval 03:30 - 07:30
Mean water level [mm]
577
575
573
571
569
567
565
563
s.w.l.
03:40 - 03:44
04:09 - 04:14
04:38 - 04:43
05:09 - 05:14
05:40 - 05:45
06:09 - 06:14
06:38 - 06:43
Profile height [mm]
700
0
0
2
4
6
8
10
12
y-axis [m]
after 3.5 h
after 7.5 h
s.w.l.

TEST C3 - cross-section x=24.5 m - interval 03:30 - 07:30

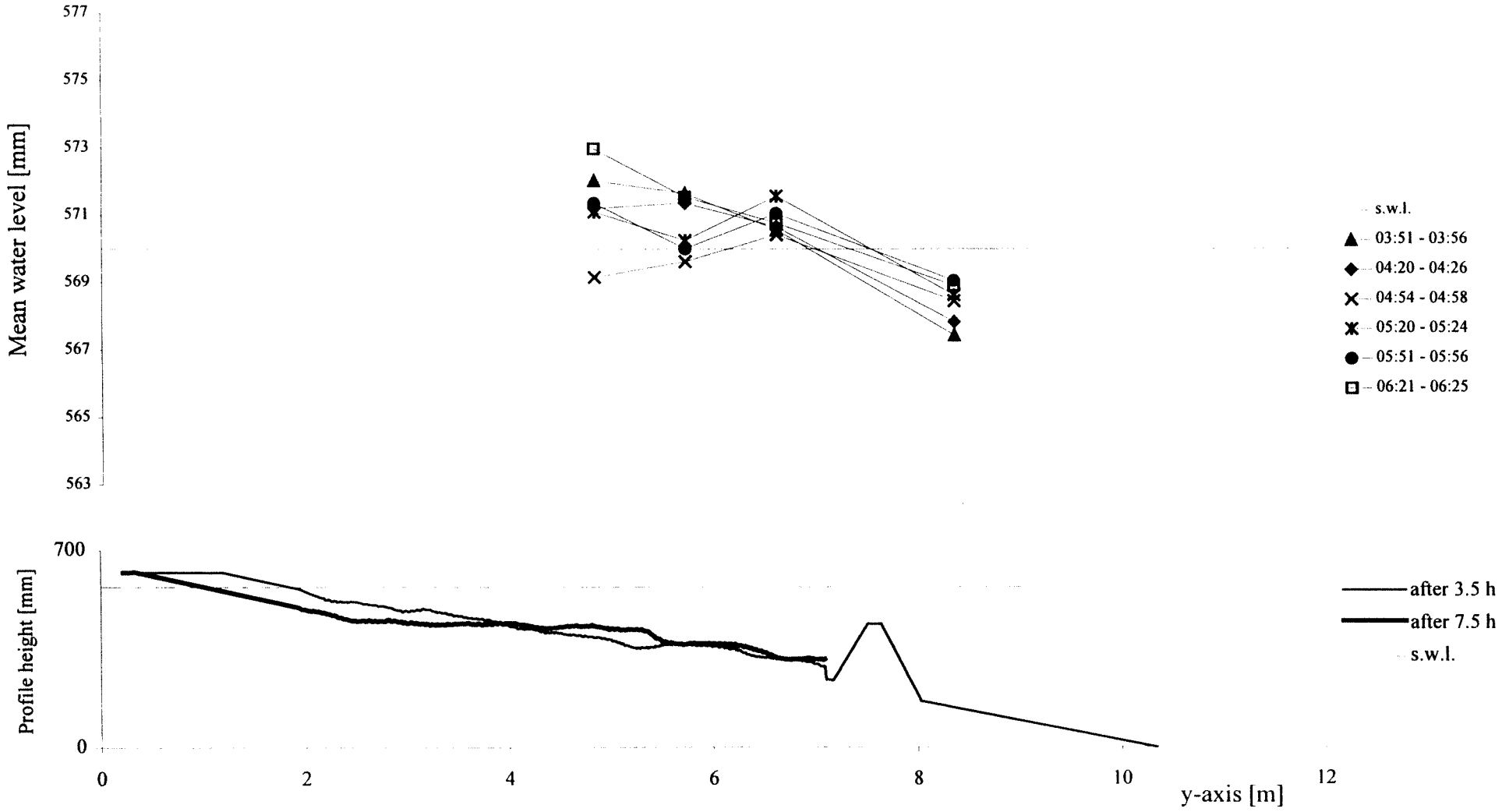

Appendix C1. Graphics TEST D1 - Average Water Level

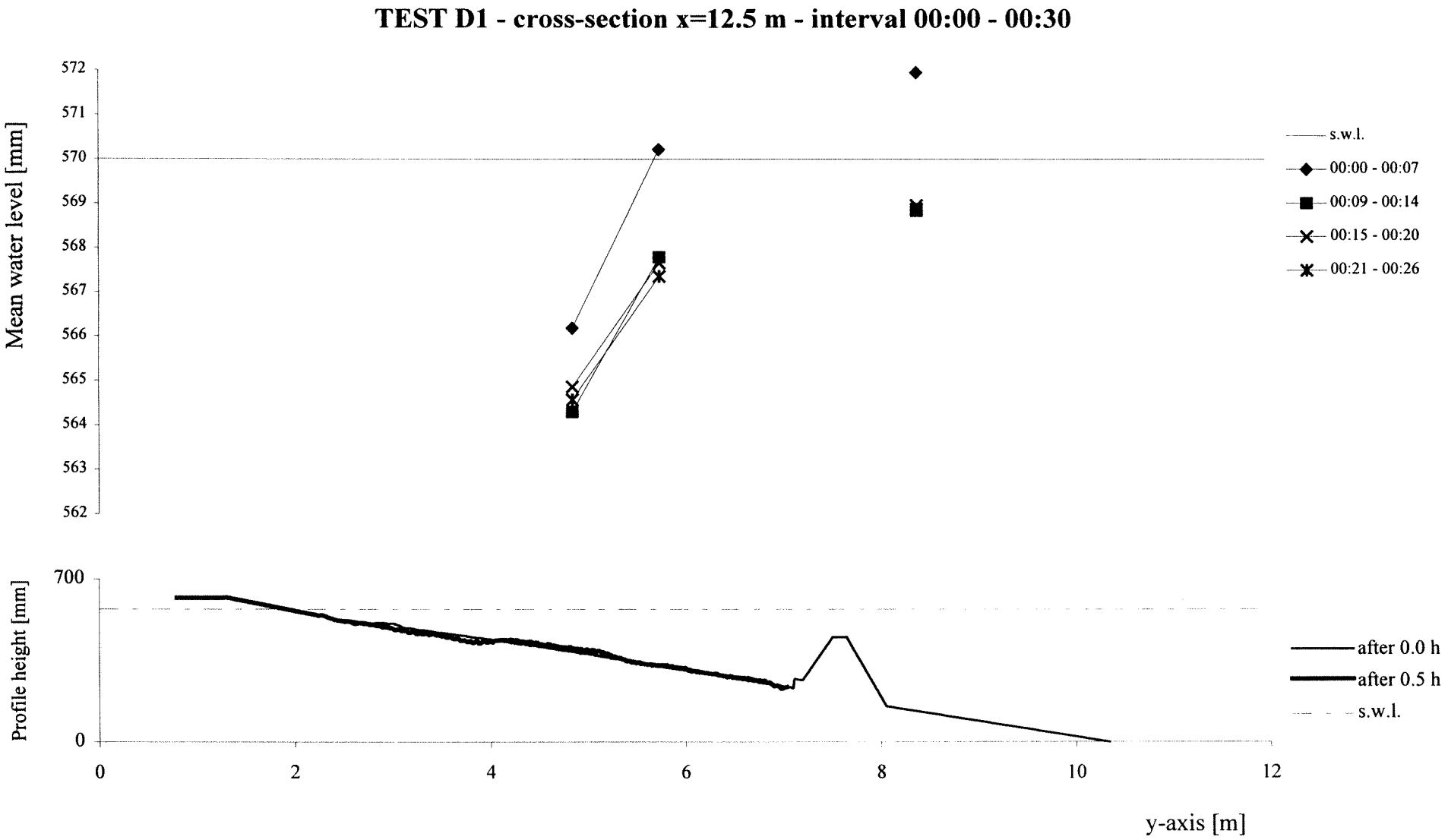
TEST D1 - cross-section x=12.5 m - interval 00:00 - 00:30
Mean water level [mm]
572
571
570
569
568
567
566
565
564
563
562
s.w.l.
00:00 - 00:07
00:09 - 00:14
00:15 - 00:20
00:21 - 00:26
Profile height [mm]
700
0
after 0.0 h
after 0.5 h
s.w.l.
0
2
4
6
8
10
12
y-axis [m]

TEST D1 - cross-section x=15.5 m - interval 00:30 - 01:30

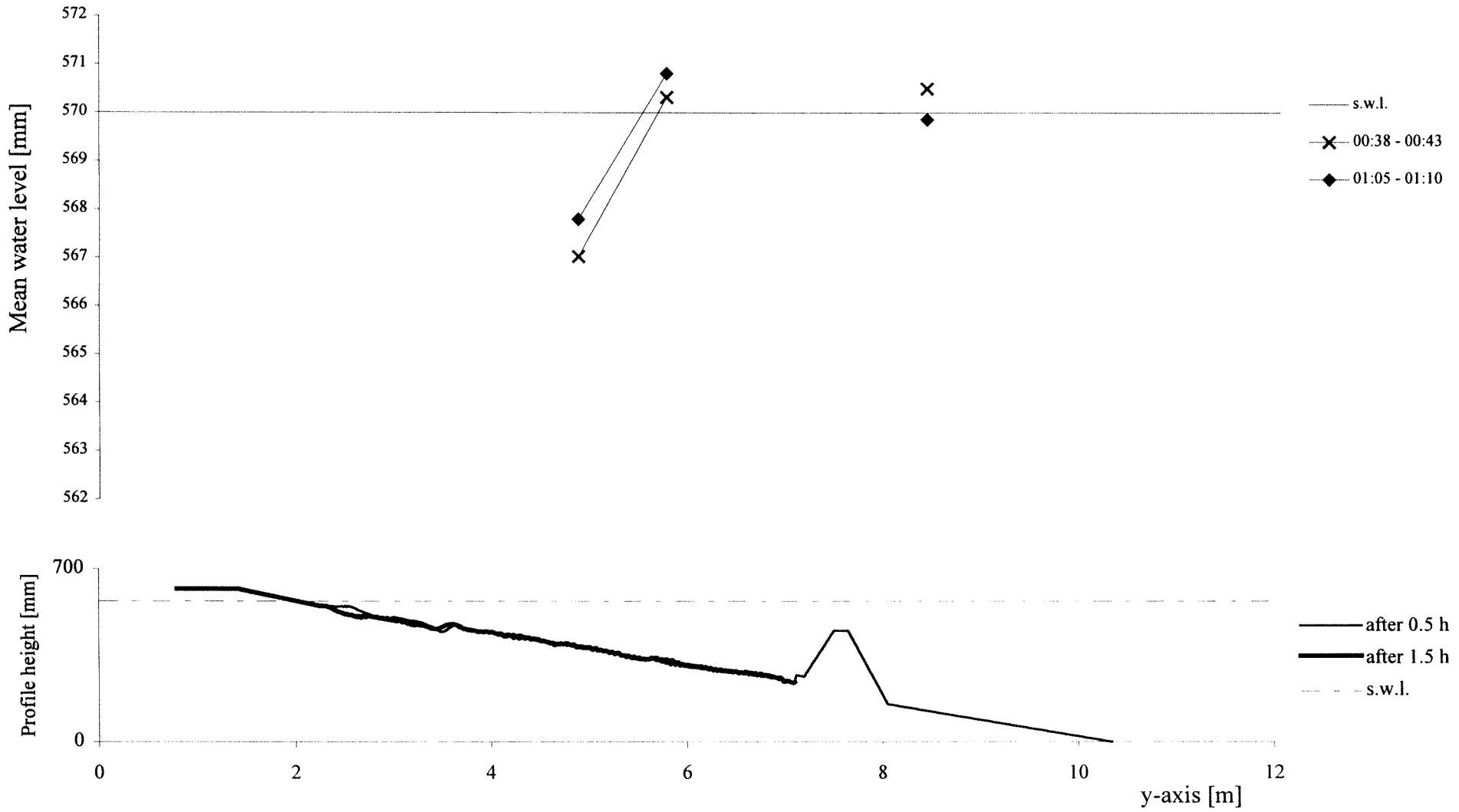

TEST D1 - cross-section x=18.5 m - interval 00:30 - 01:30

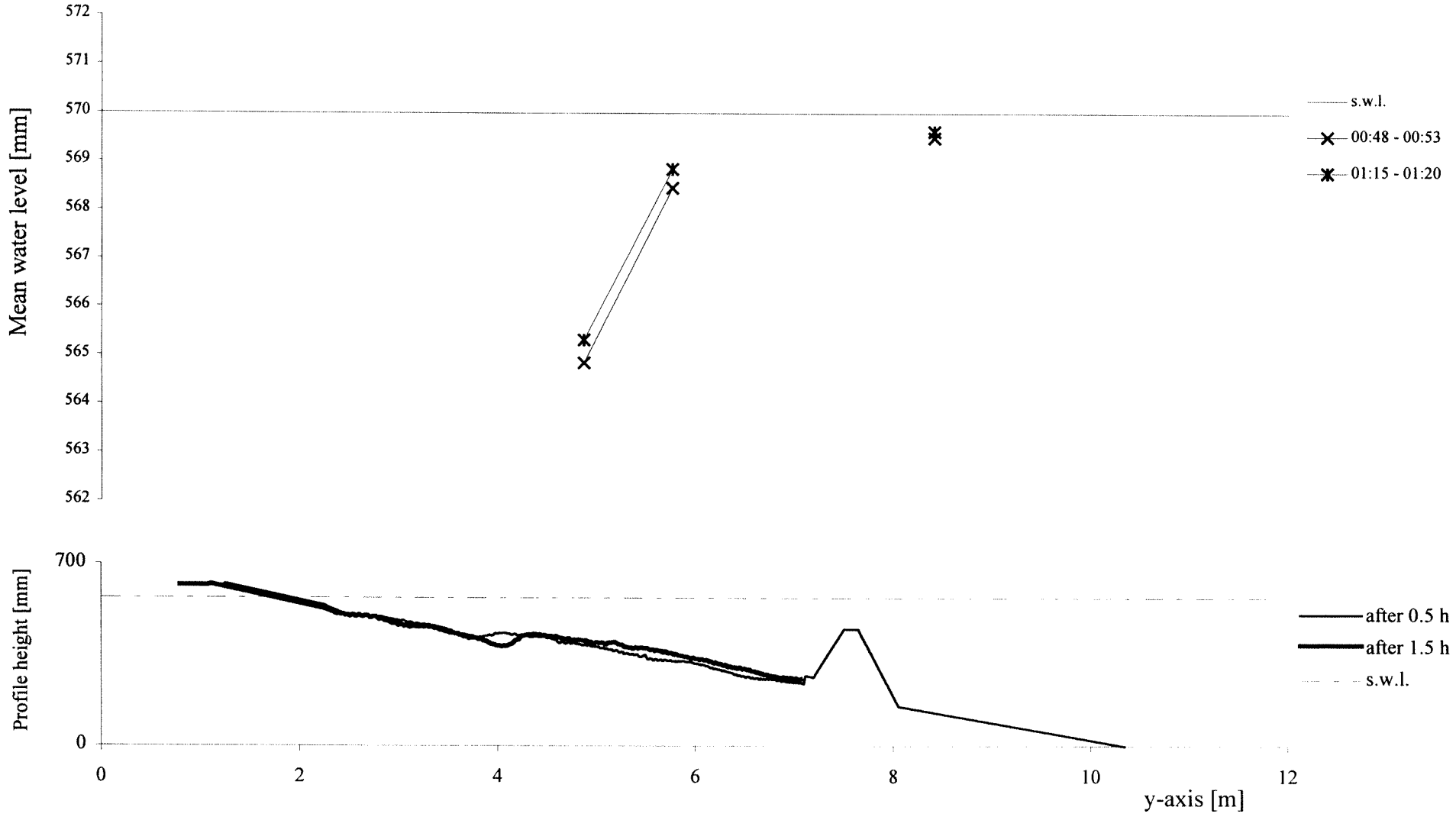

TEST D1 - cross-section x=12.5 m - interval 01:30 - 03:30

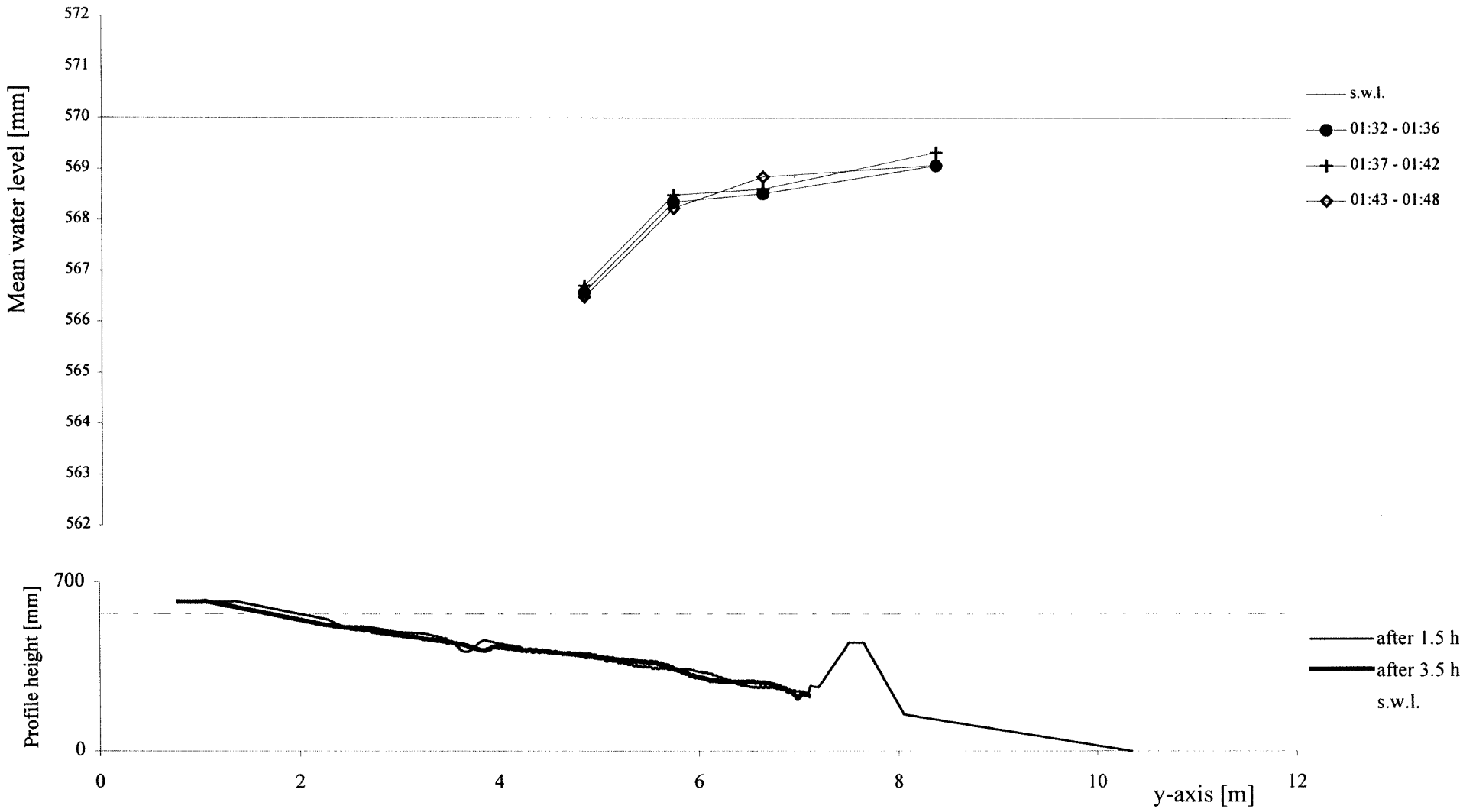

TEST D1 - cross-section x=15.5 m - interval 01:30 - 03:30

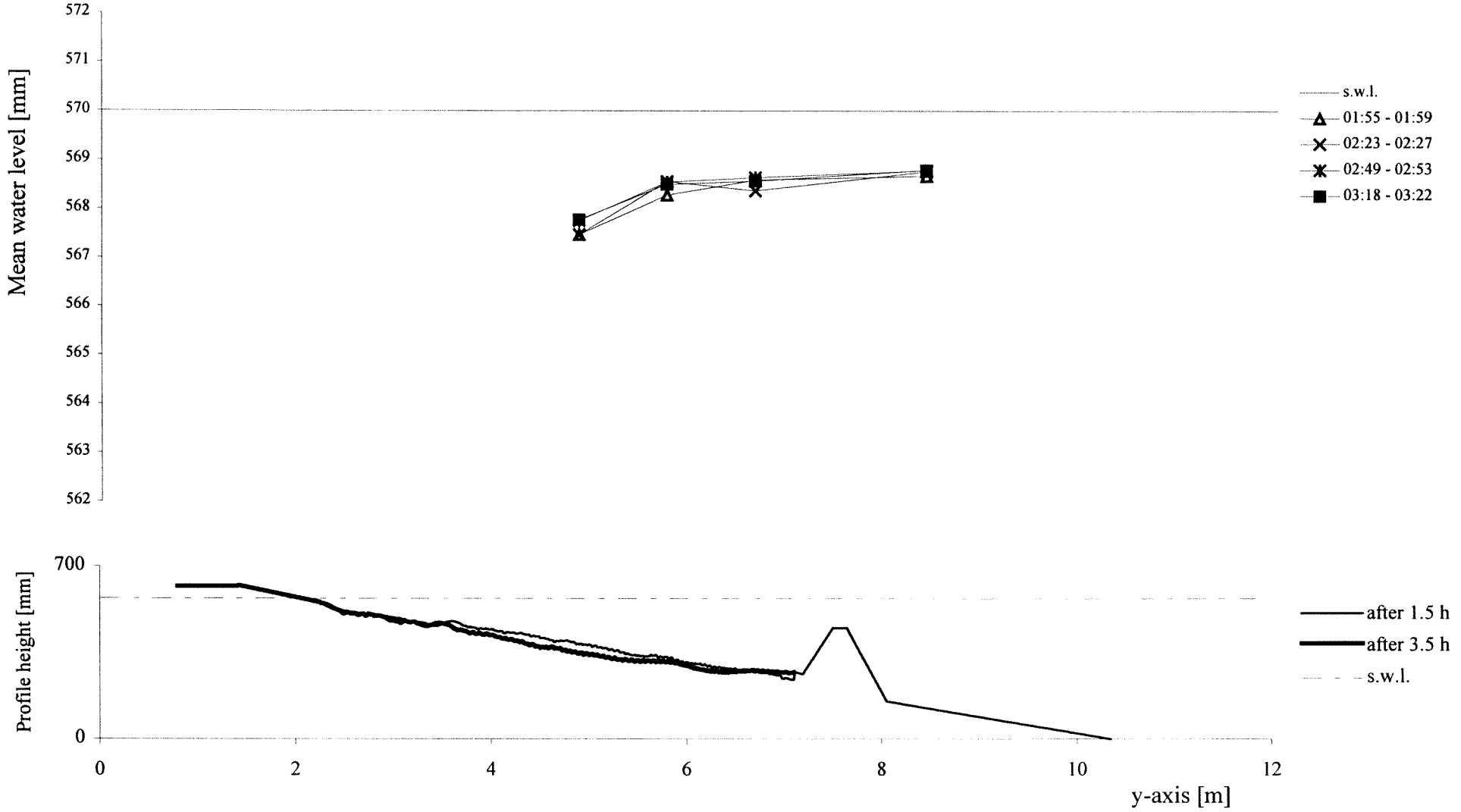

TEST D1 - cross-section x=18.5 m - interval 01:30 - 03:30

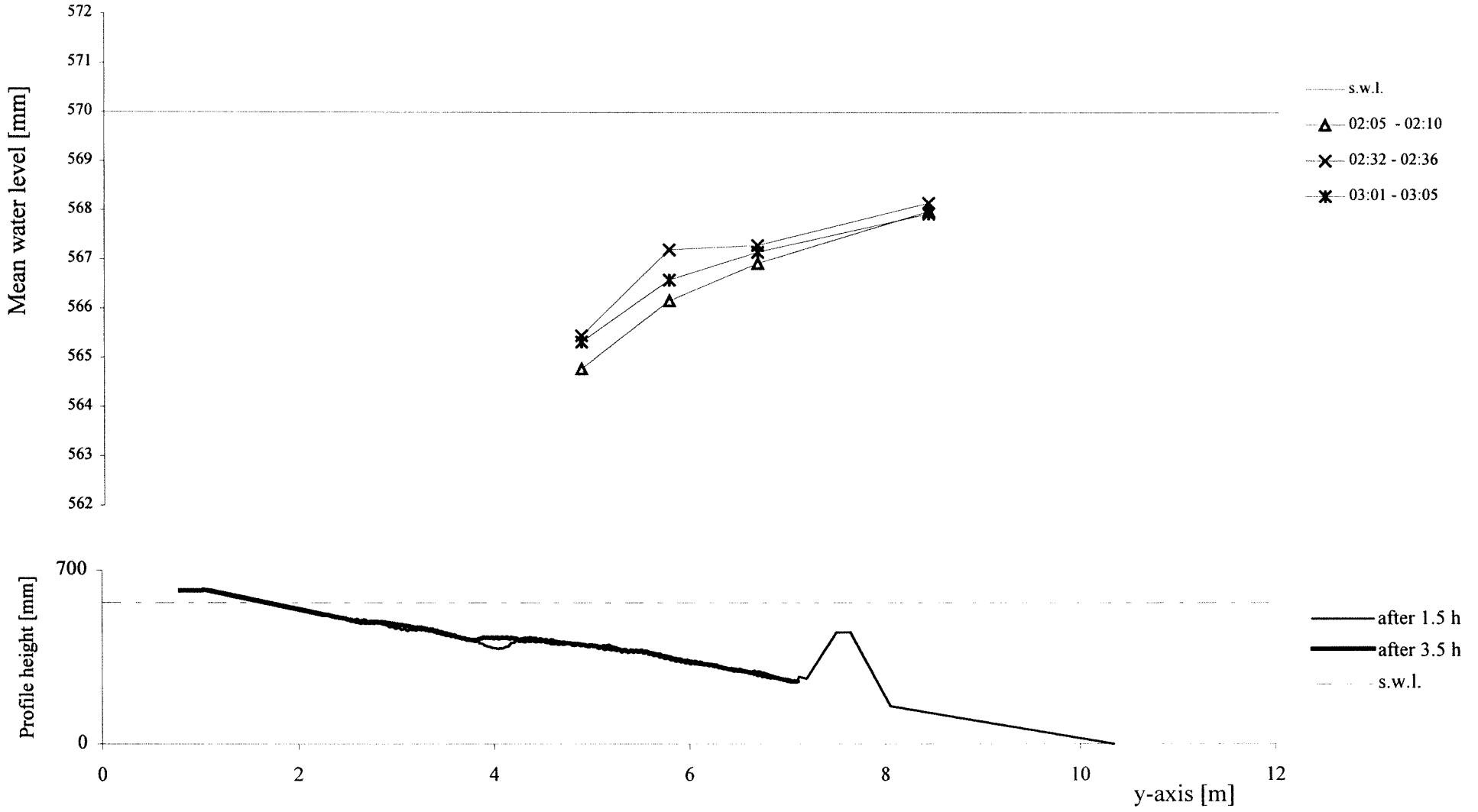

TEST D1 - cross-section x=12.5 m - interval 03:30 - 07:30

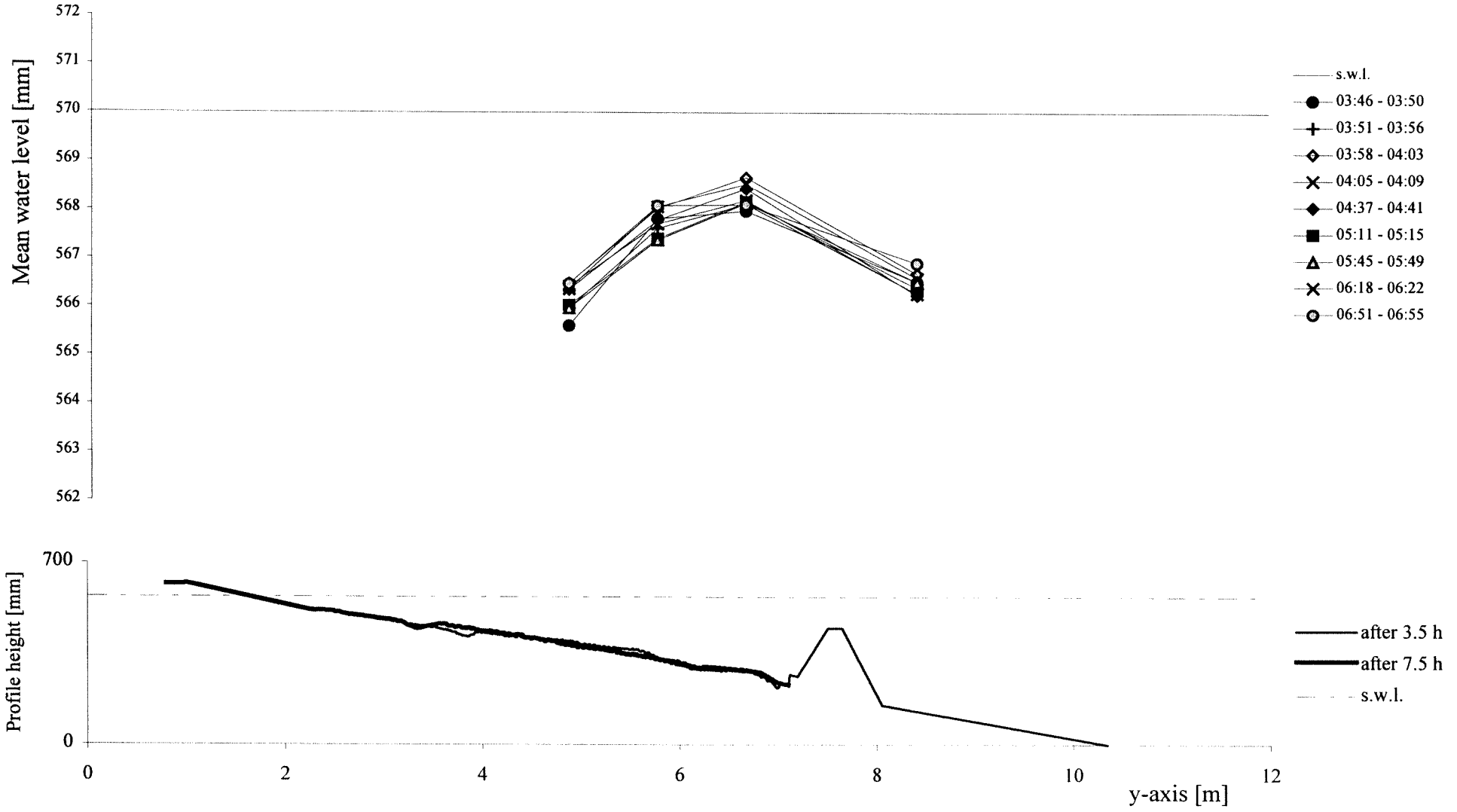

TEST D1 - cross-section x=15.5 m - interval 03:30 - 07:30

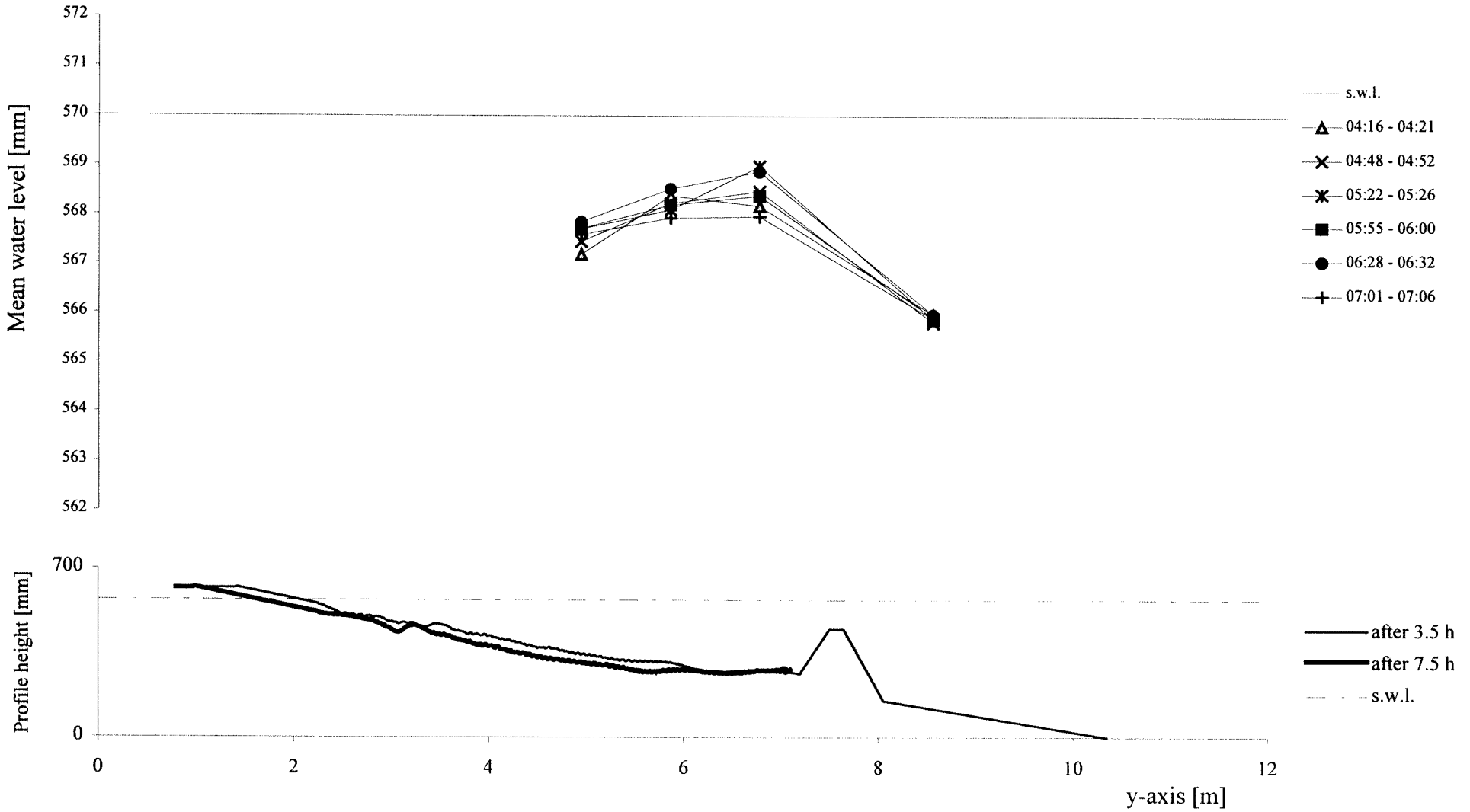

TEST D1 - cross-section x=18.5 m - interval 03:30 - 07:30

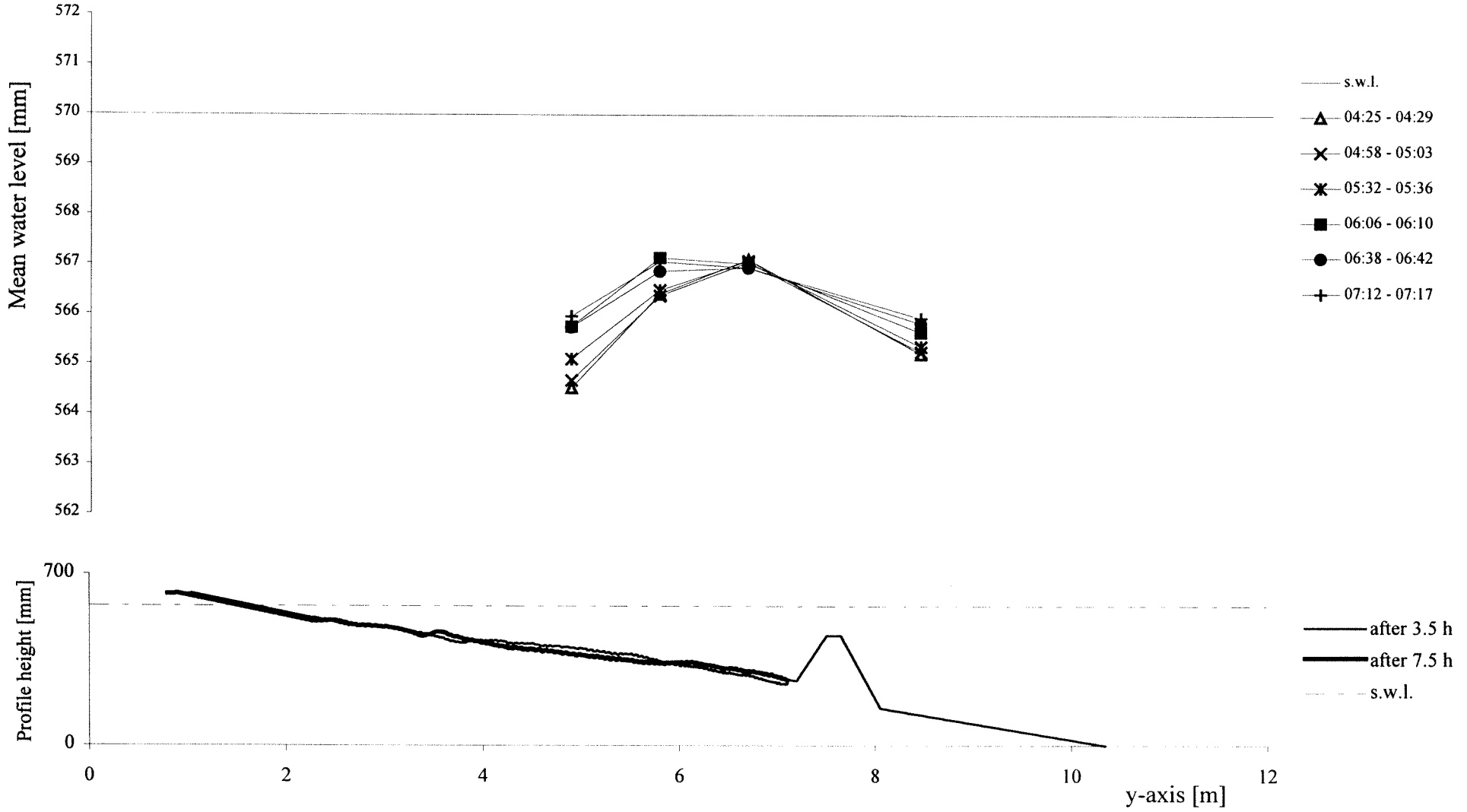

Nearshore effects of submerged breakwaters

Laboratory experiments in a wave basin and 2DH numerical modeling.

Volume II: Appendices

L. Torrini

Simualtion D3 - Average Water Level

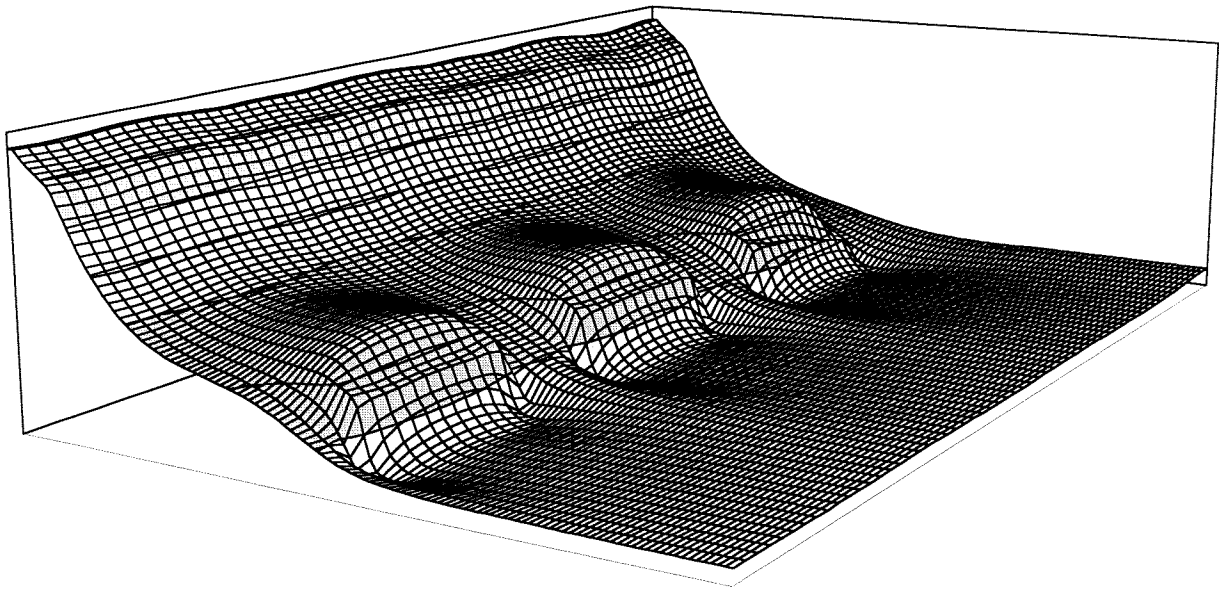

Master Thesis
October 1997

Nearshore effects of submerged breakwaters

Laboratory experiments in a wave basin and 2DH numerical modeling.

Volume II: Appendices

L. Torrini

Master Thesis
October 1997

Delft University of Technology
Faculty of Civil Engineering

Politecnico di Milano
Facolta` di Ingegneria Ambientale

Supervision:

Dr. Ir. J. van de Graaff
Dr. Ir. J. A. Roelvink
Ir. S. C. van der Biezen
Dr. Ir. G. Passoni

Table of Contents

Volume II: Appendices

Appendix A1. Graphics TEST A1 - Average Water Level

TEST A1 - cross-section x=3 m - interval 00:00 - 00:30

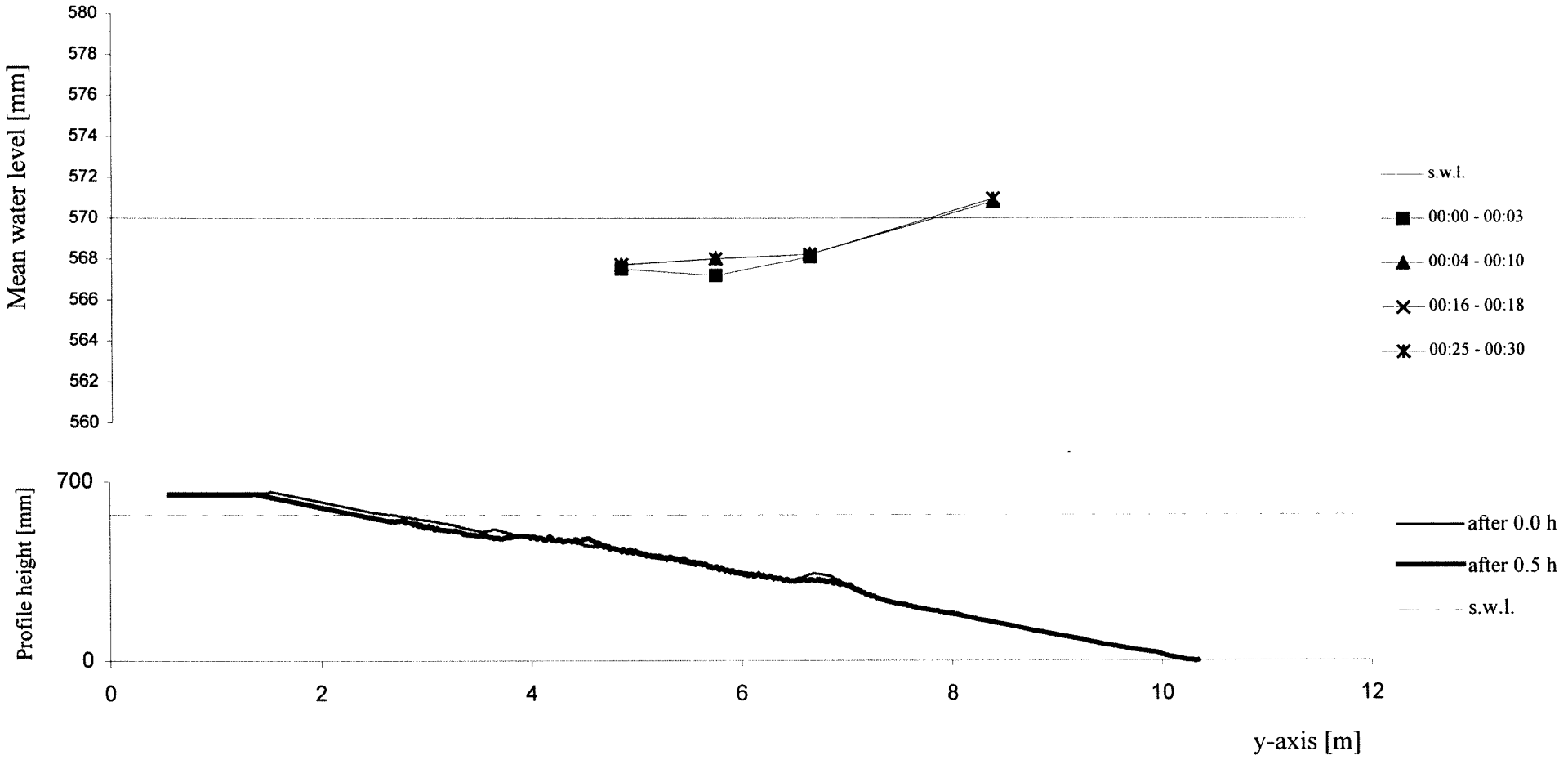

TEST A1 - cross-section x=6.5 m - interval 00:30 - 01:30

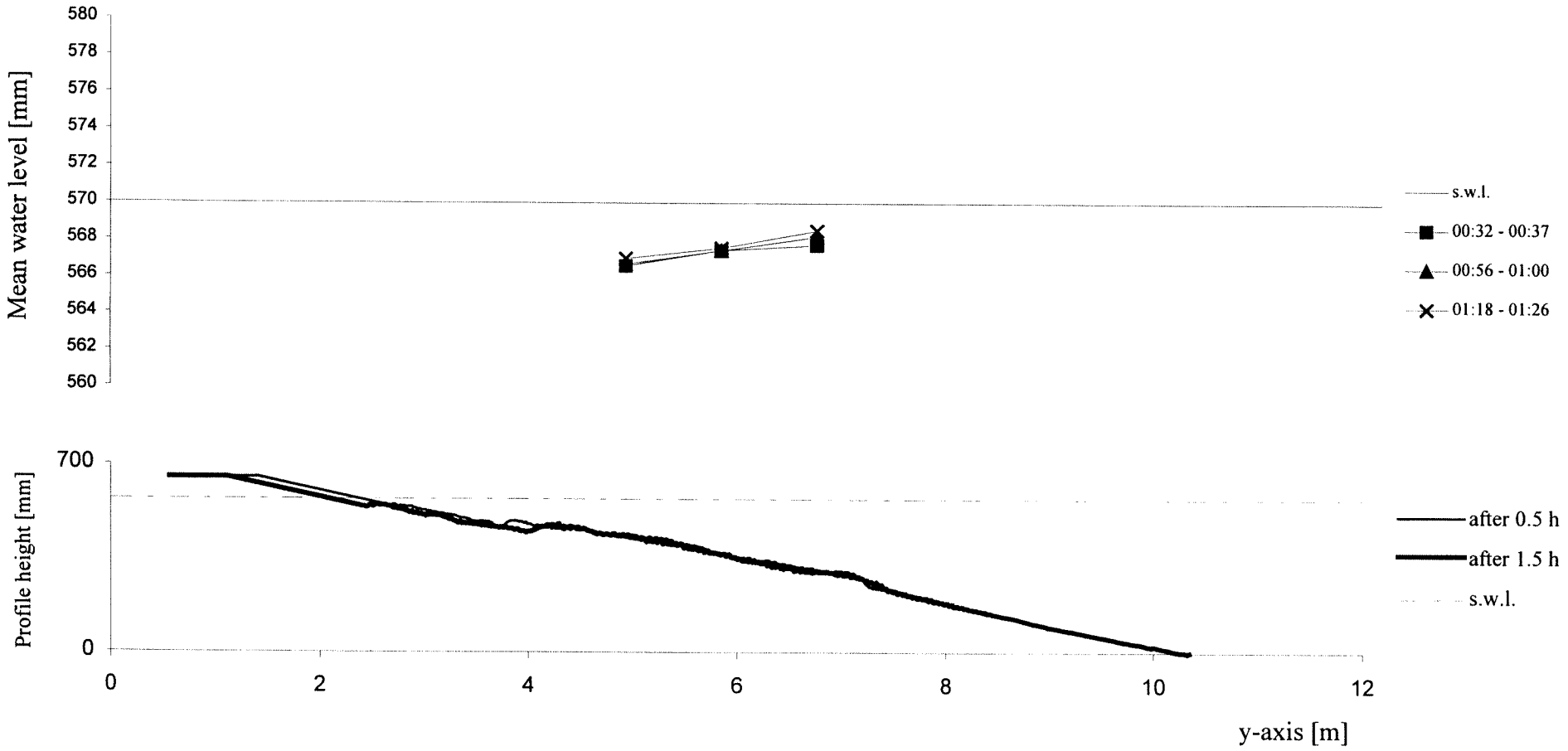

TEST A1 - cross-section x=12.5 m - interval 00:30 - 01:30

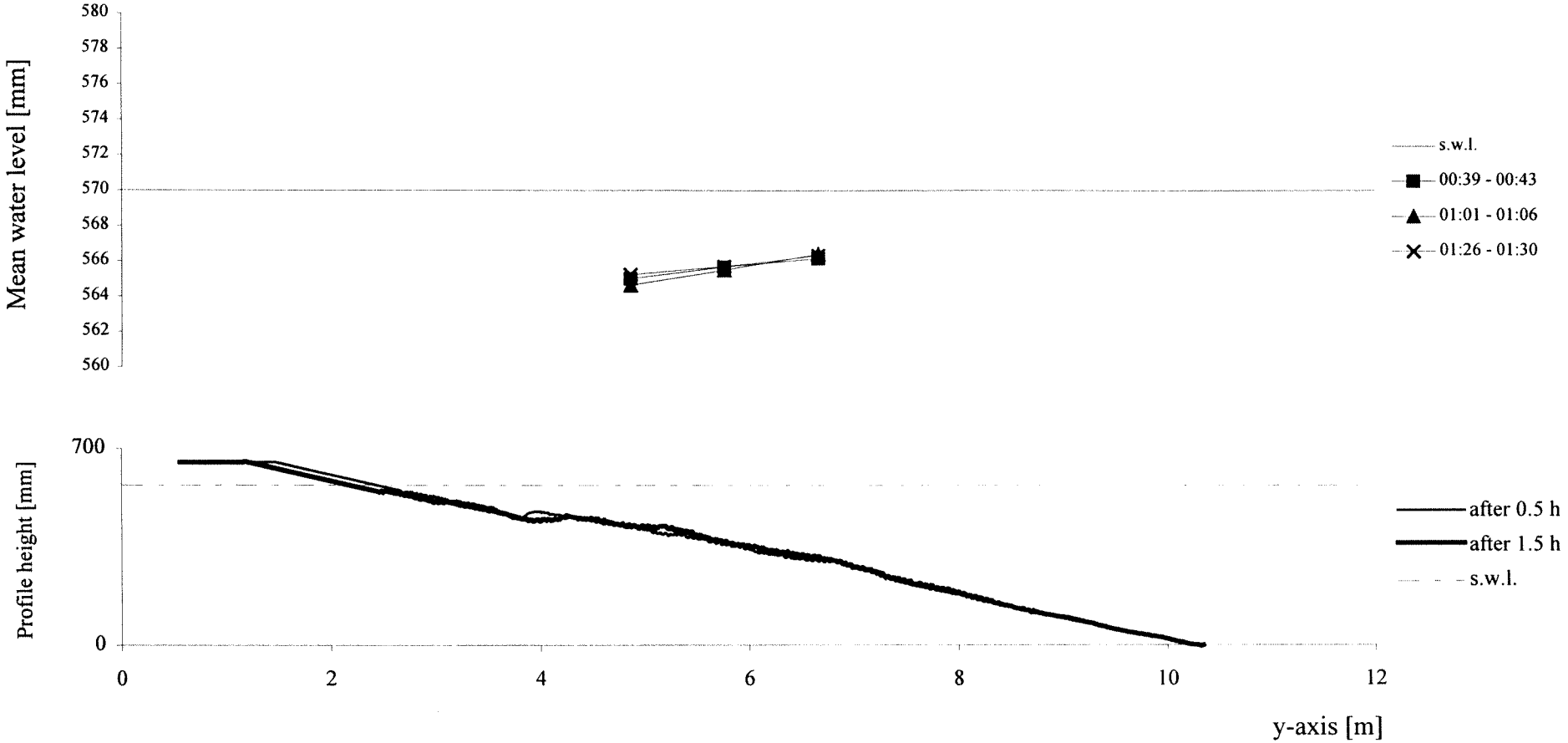

TEST A1 - cross-section x=20m - interval 00:30 - 01:30

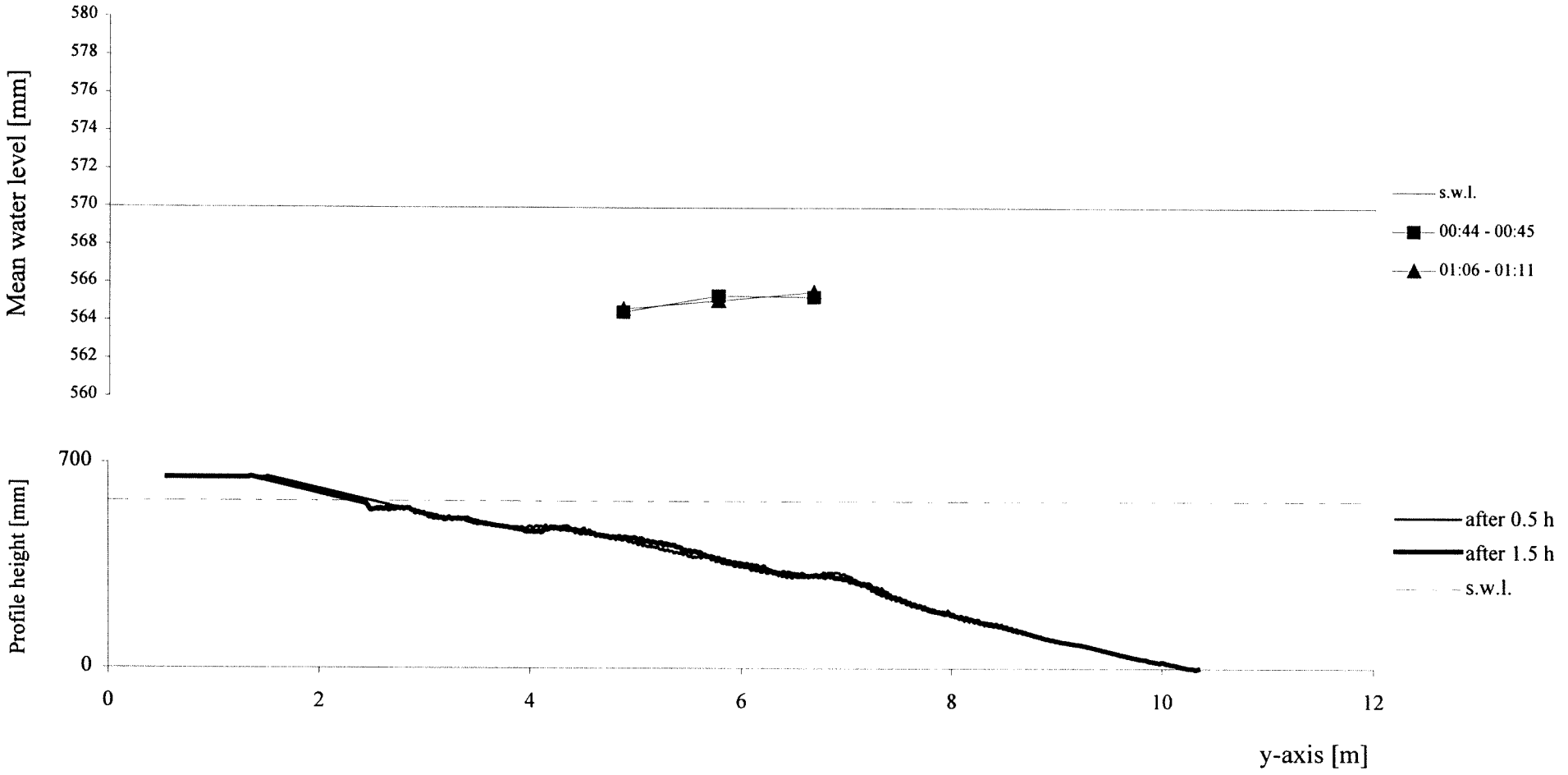

TEST A1 - cross-section x=24.5 - interval 00:30 - 01:30

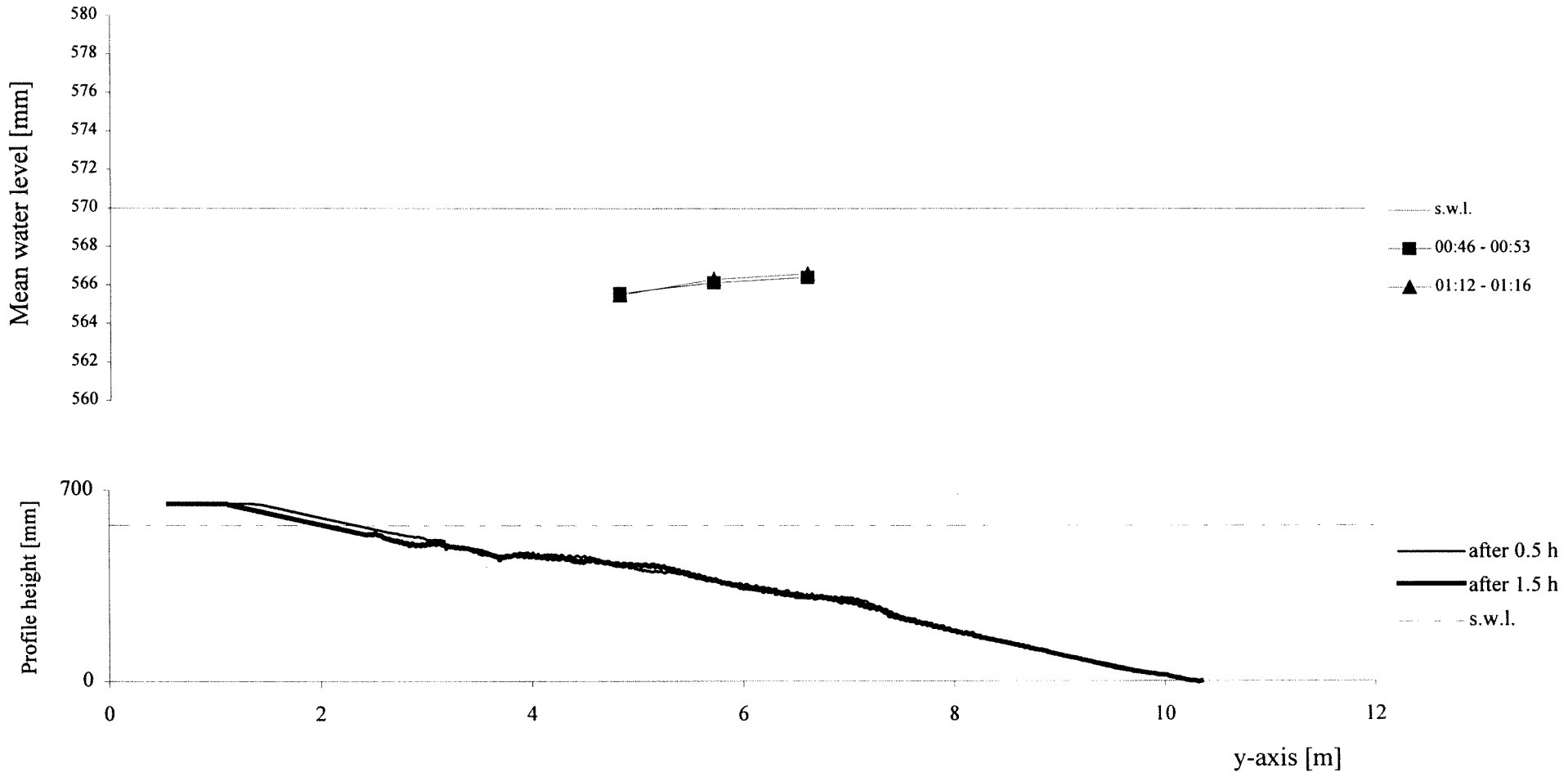

TEST A1 - cross-section x=3 m - interval 01:30 - 03:30

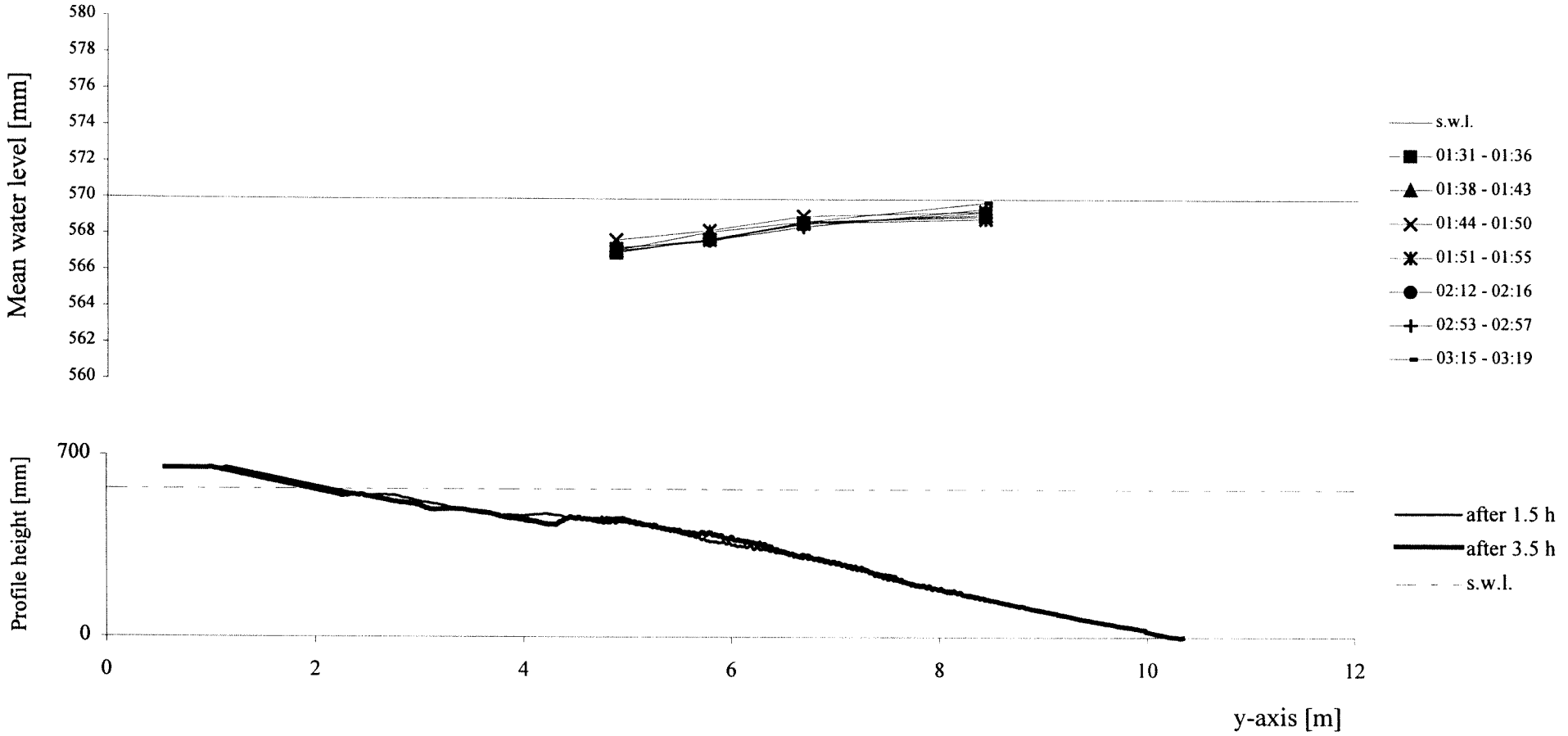

TEST A1 - cross-section x=6.5 m - interval 01:30 - 03:30

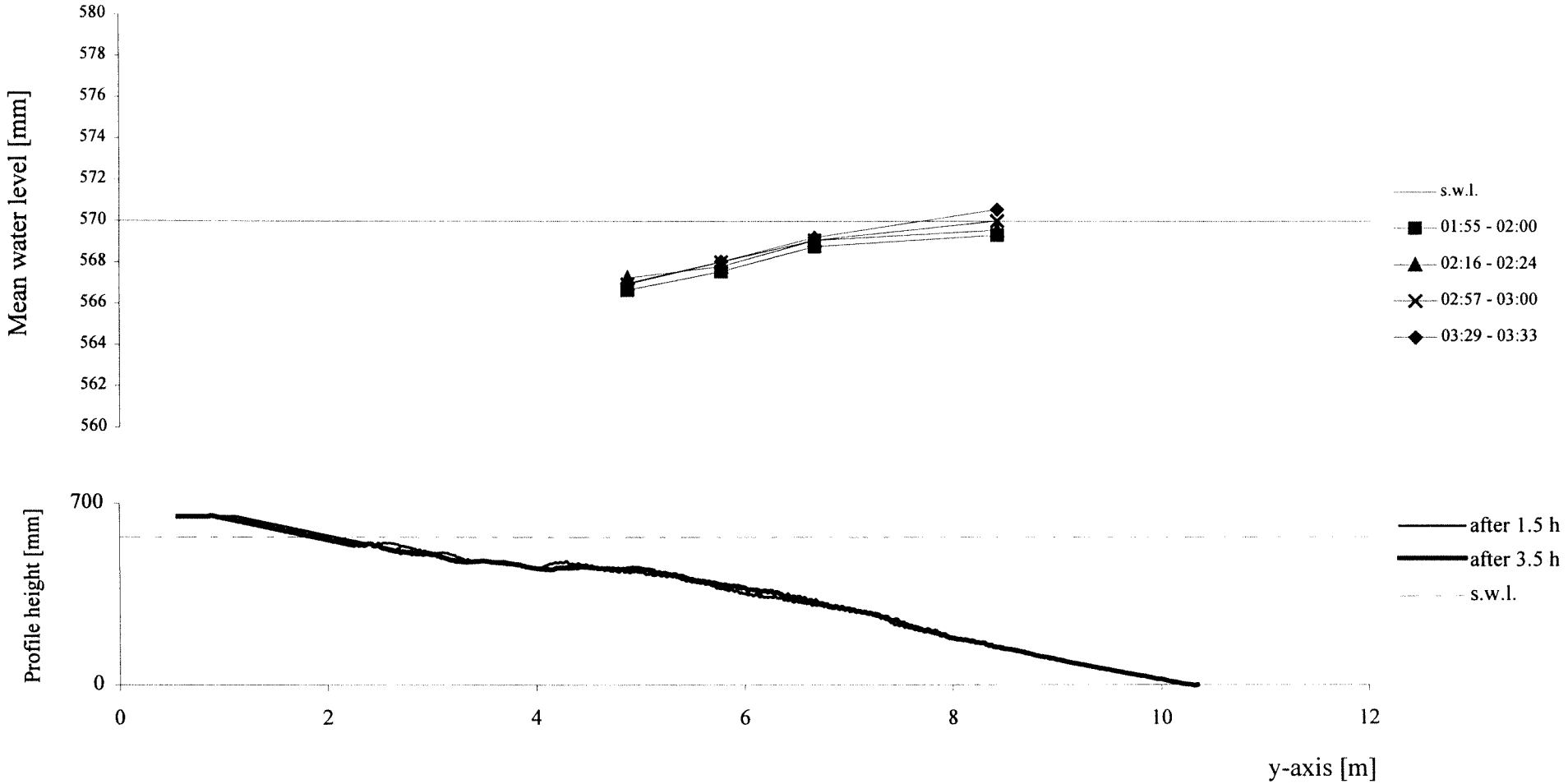

TEST A1 - cross-section x=12.5 m - interval 01:30 - 03:30

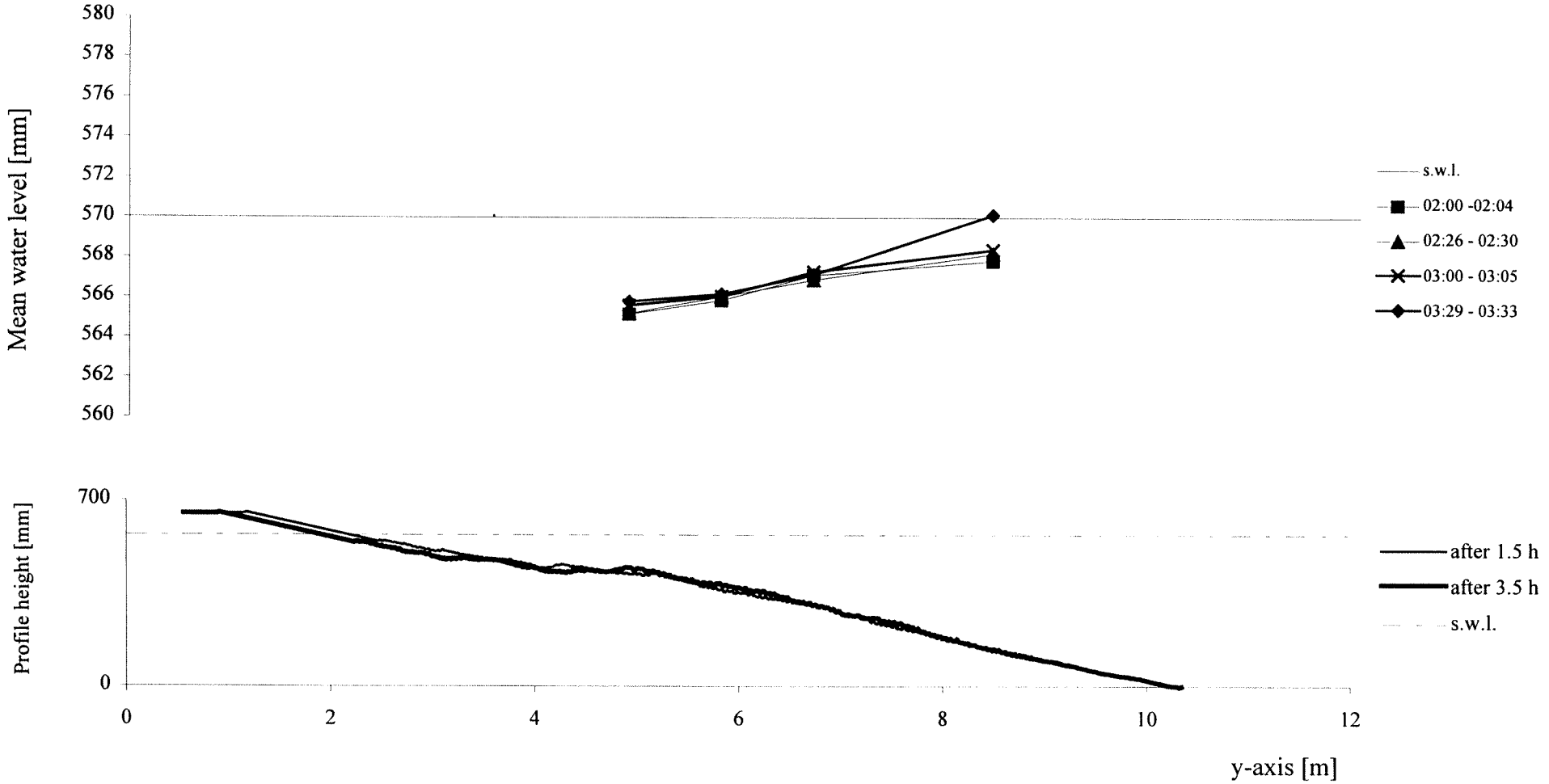

TEST A1 - cross-section x=20 m - interval 01:30 - 03:30

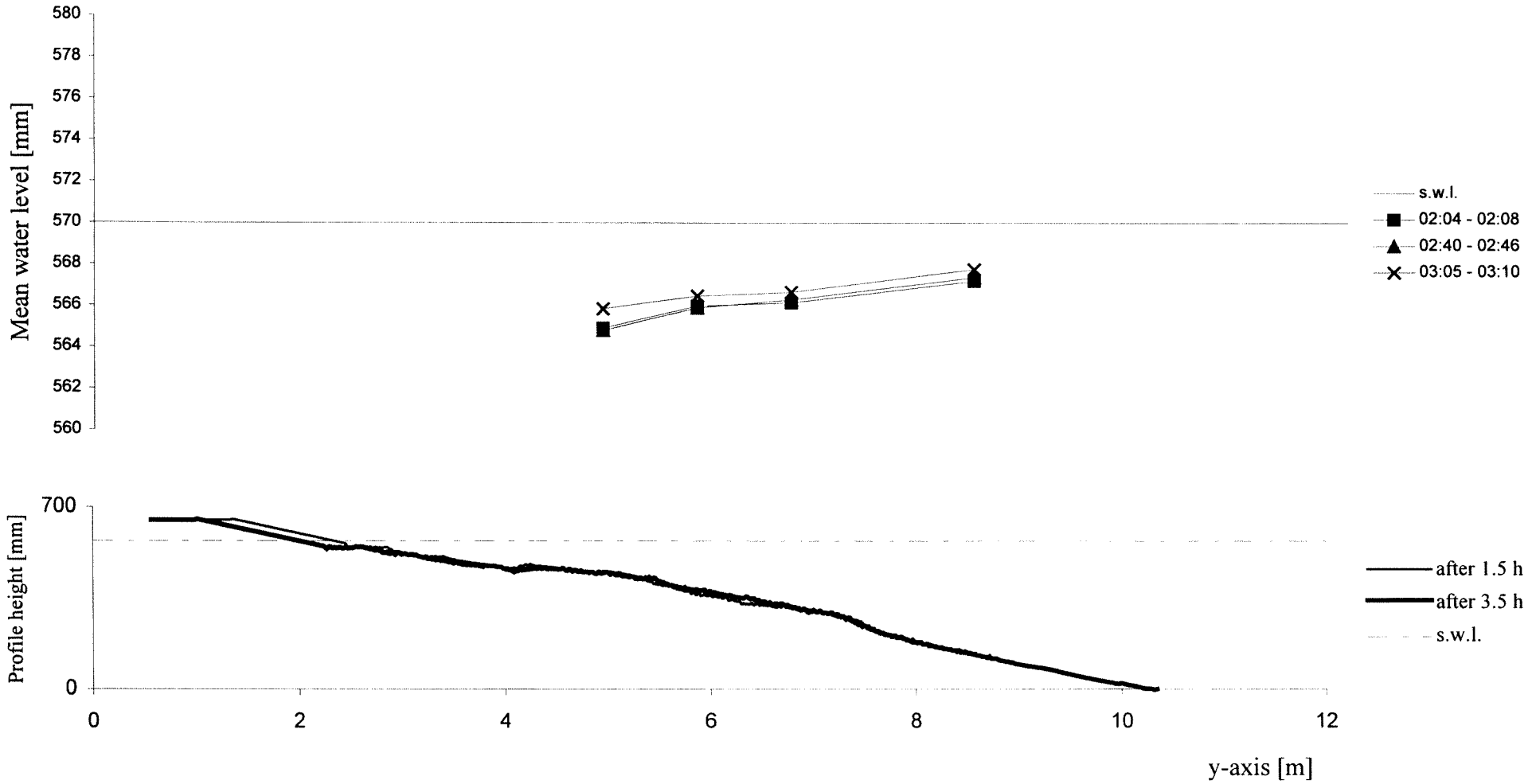

TEST A1 - cross-section x=24.5 m - interval 01:30 - 03:30

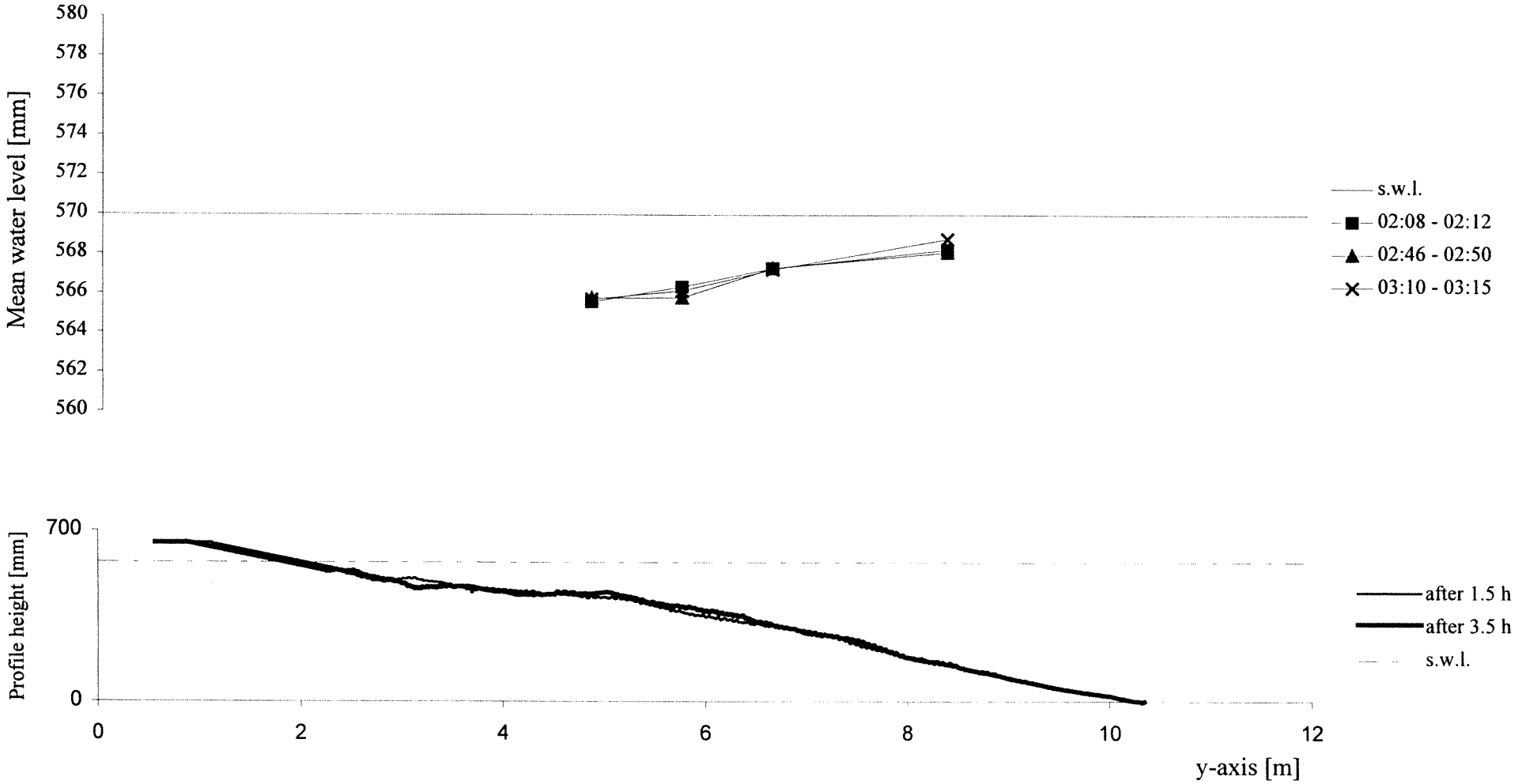

TEST A1 - cross-section x=3 m - interval 03:30 - 07:30

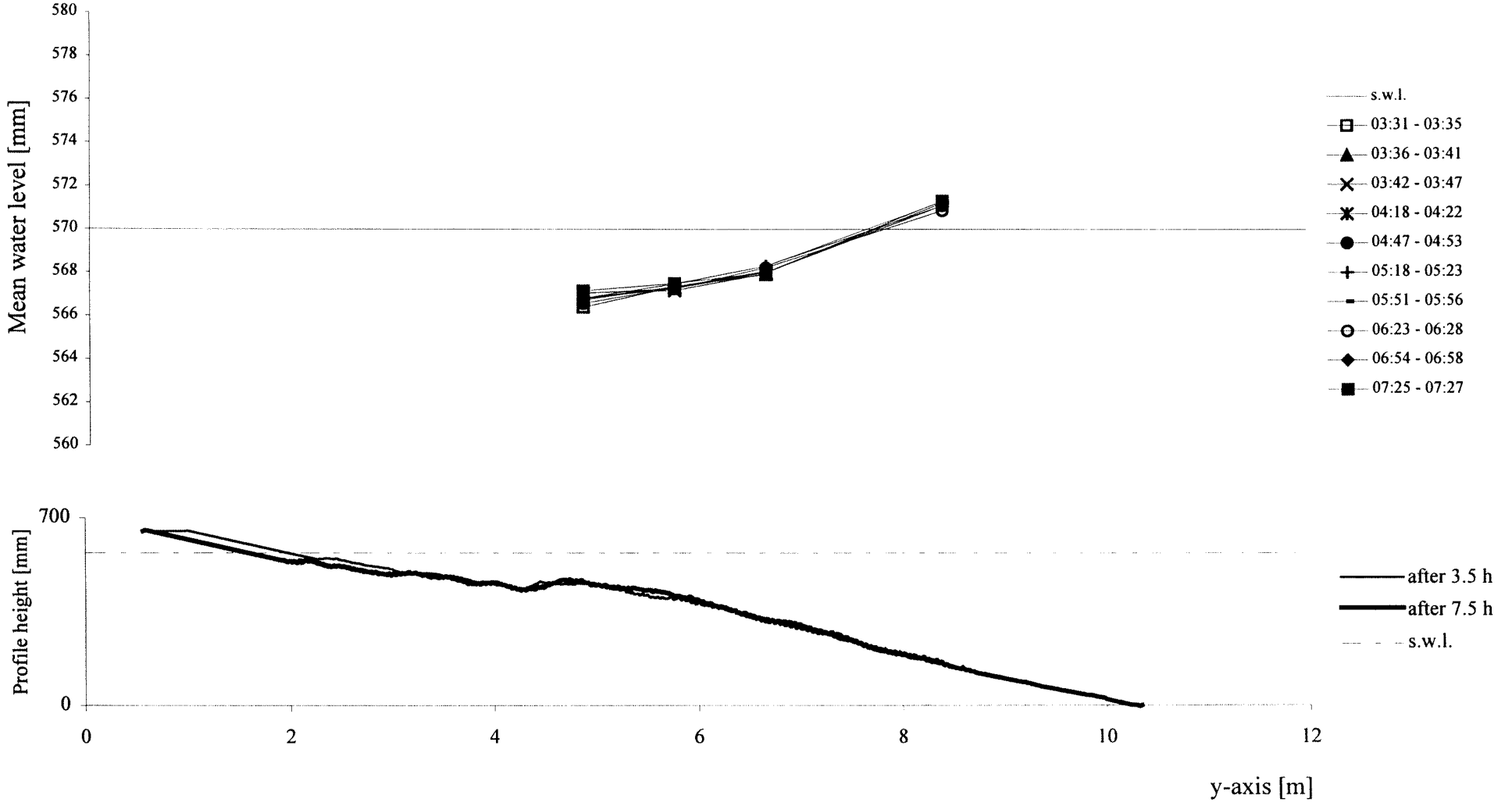

TEST A1 - cross-section x=6.5 m - interval 03:30 - 07:30

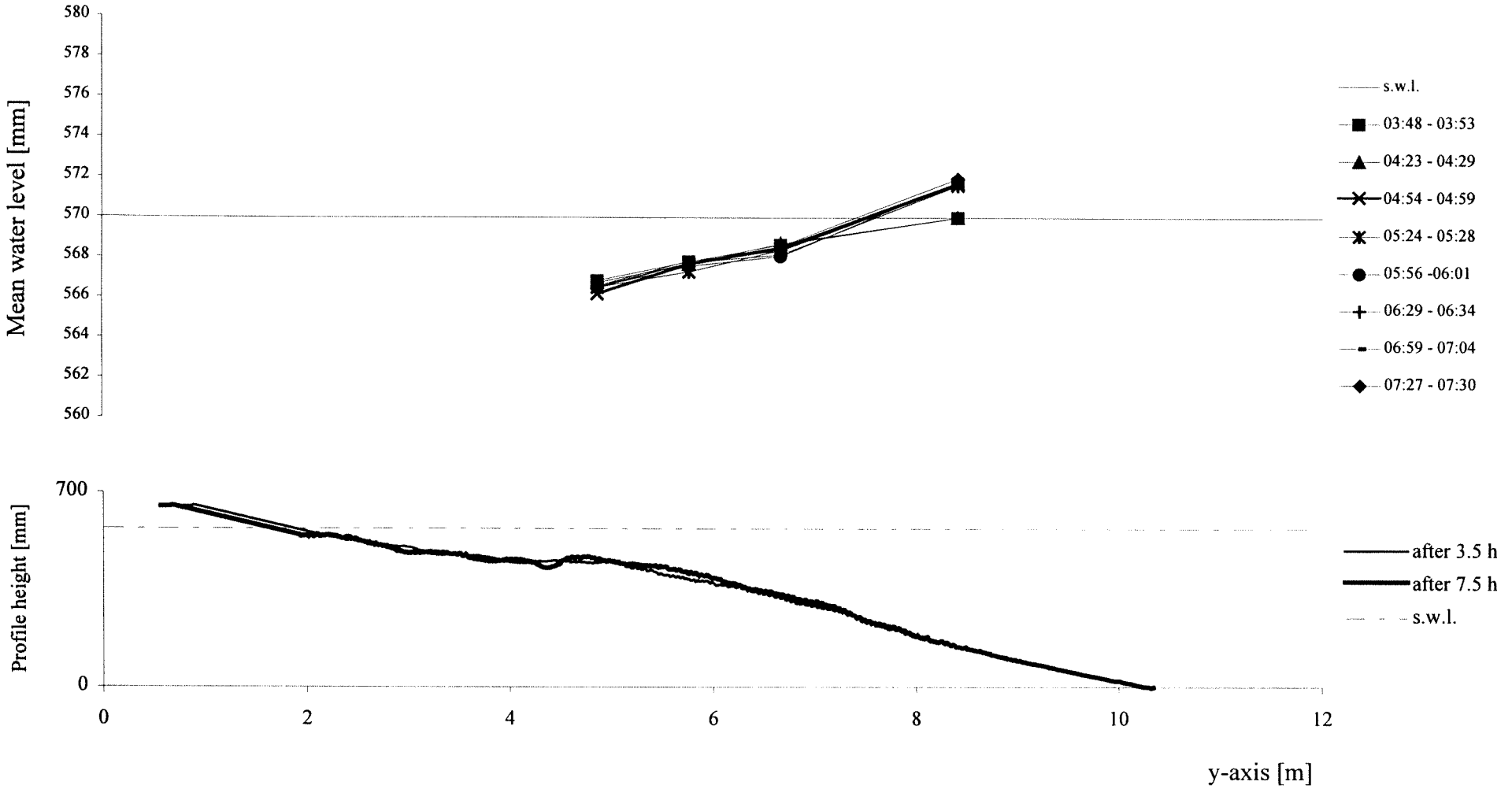

TEST A1 - cross-section x=12.5 m - interval 03:30 - 07:30

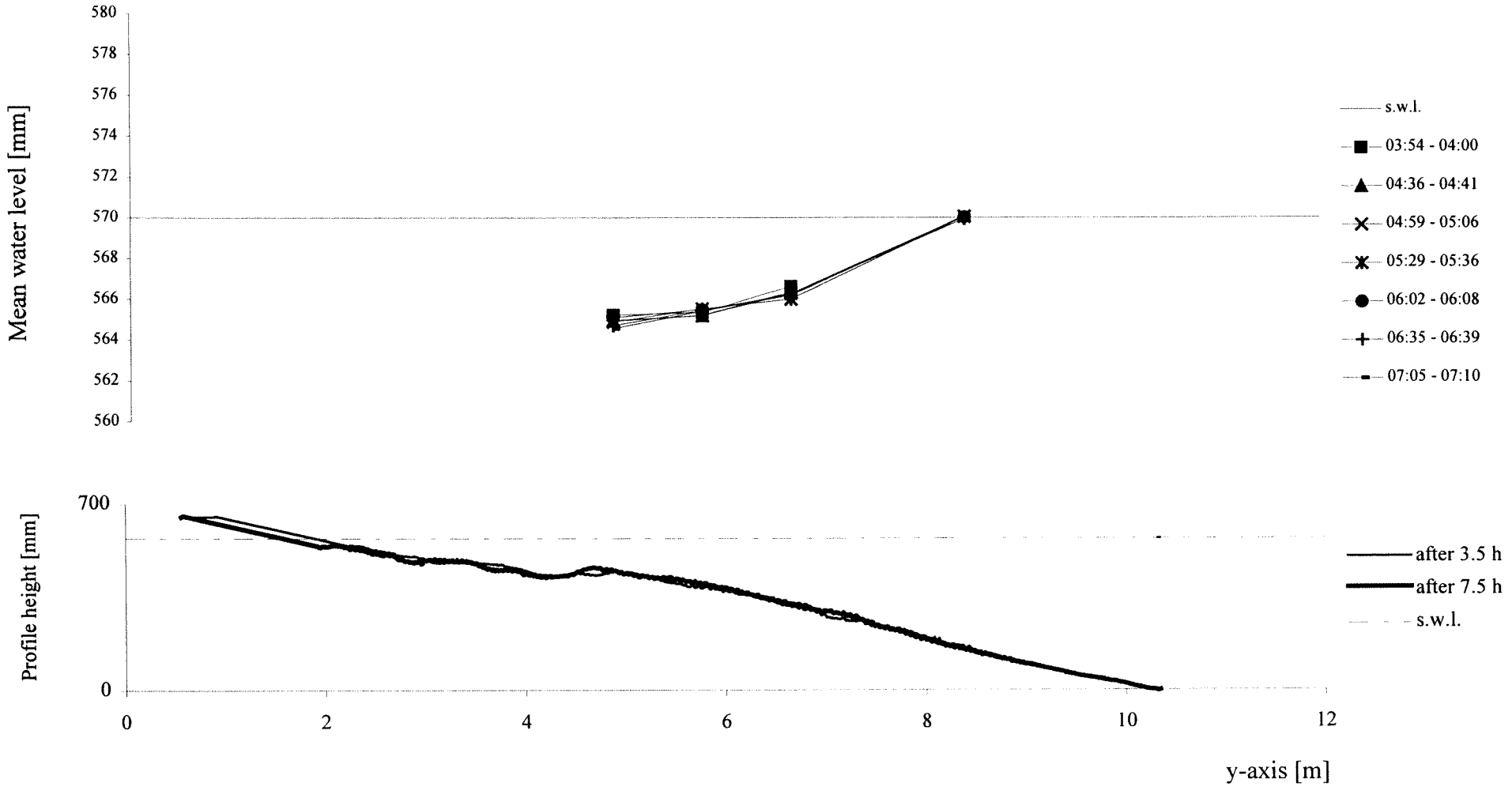

TEST A1 - cross-section x=20 m - interval 03:30 - 07:30

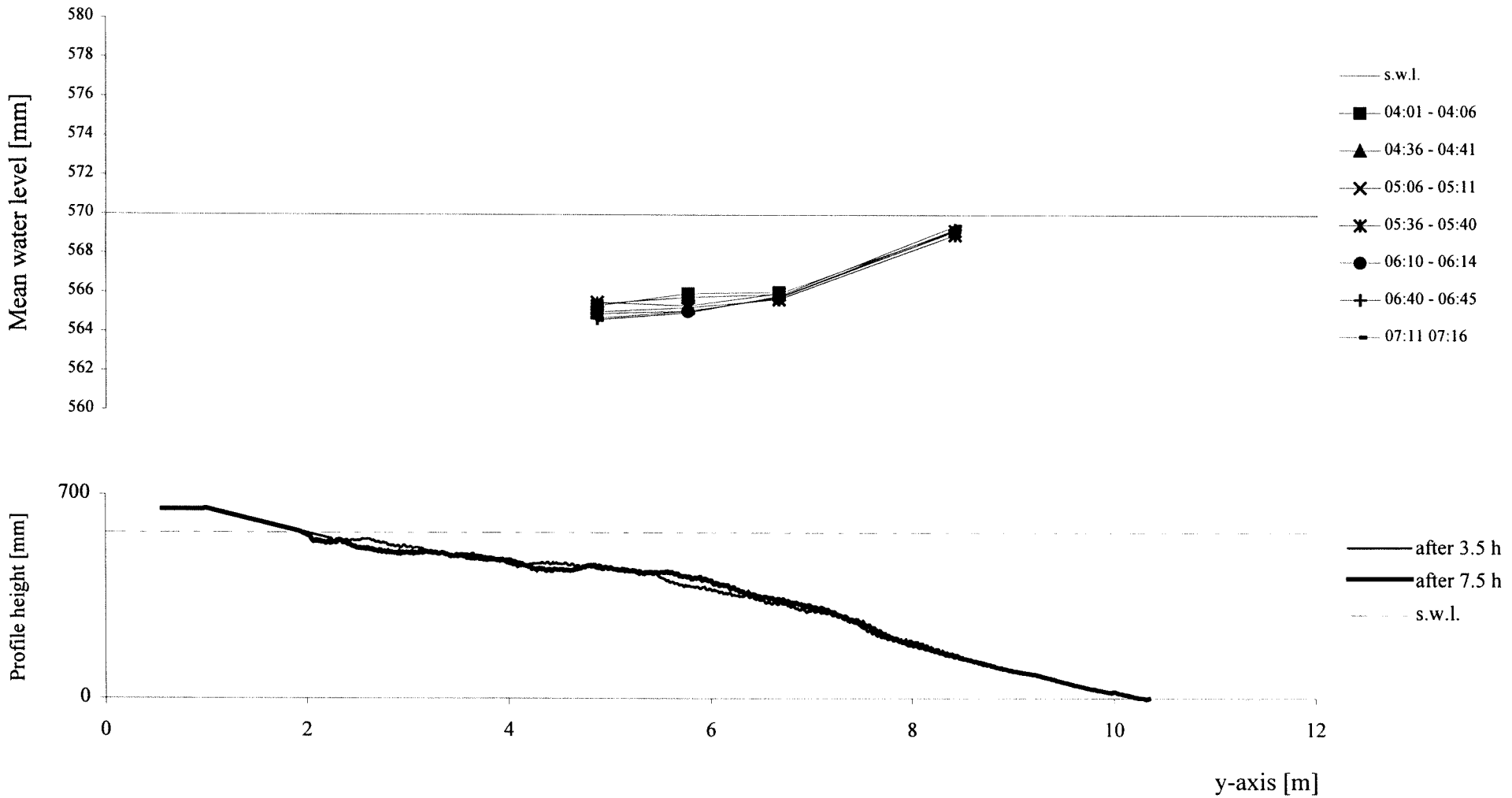

TEST A1 - cross-section x=24.5 m - interval 03:30 - 07:30

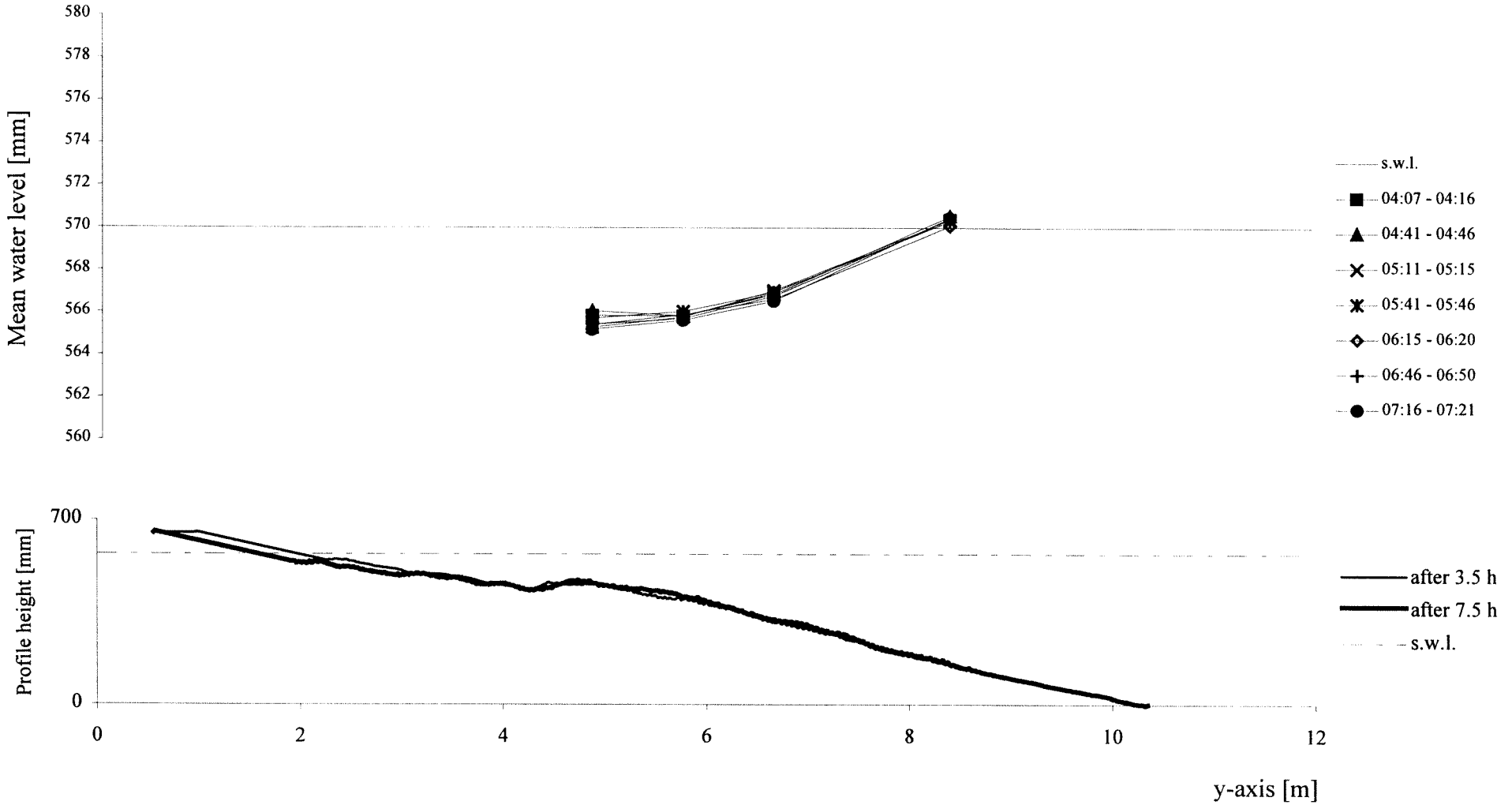

Appendix A2. Graphics TEST A2 - Average Water Level

TEST A2 - cross-section x=3 m - interval 00:00 - 00:30

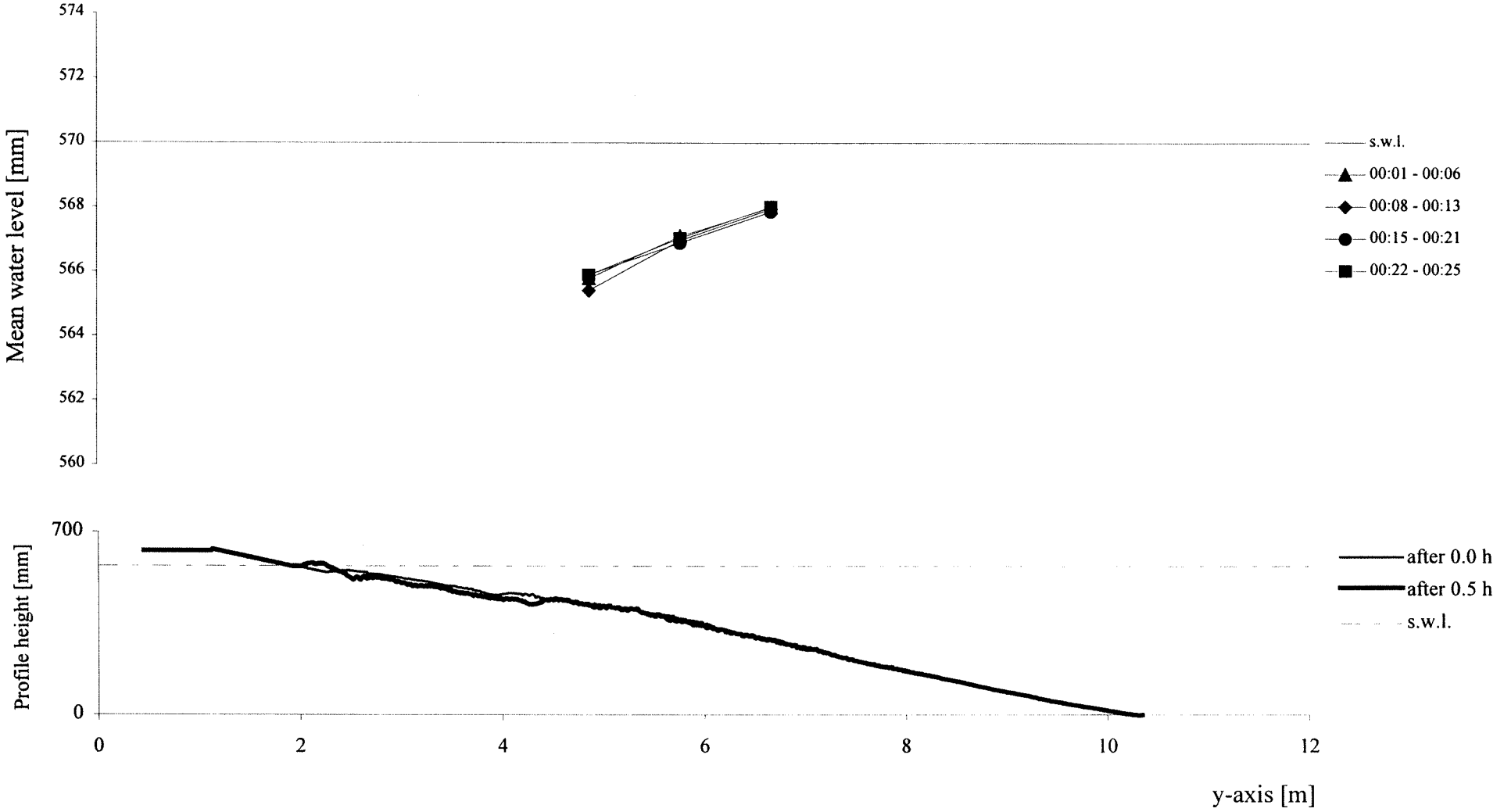

TEST A2 - cross-section x=6.5 m - interval 00:30 - 01:30

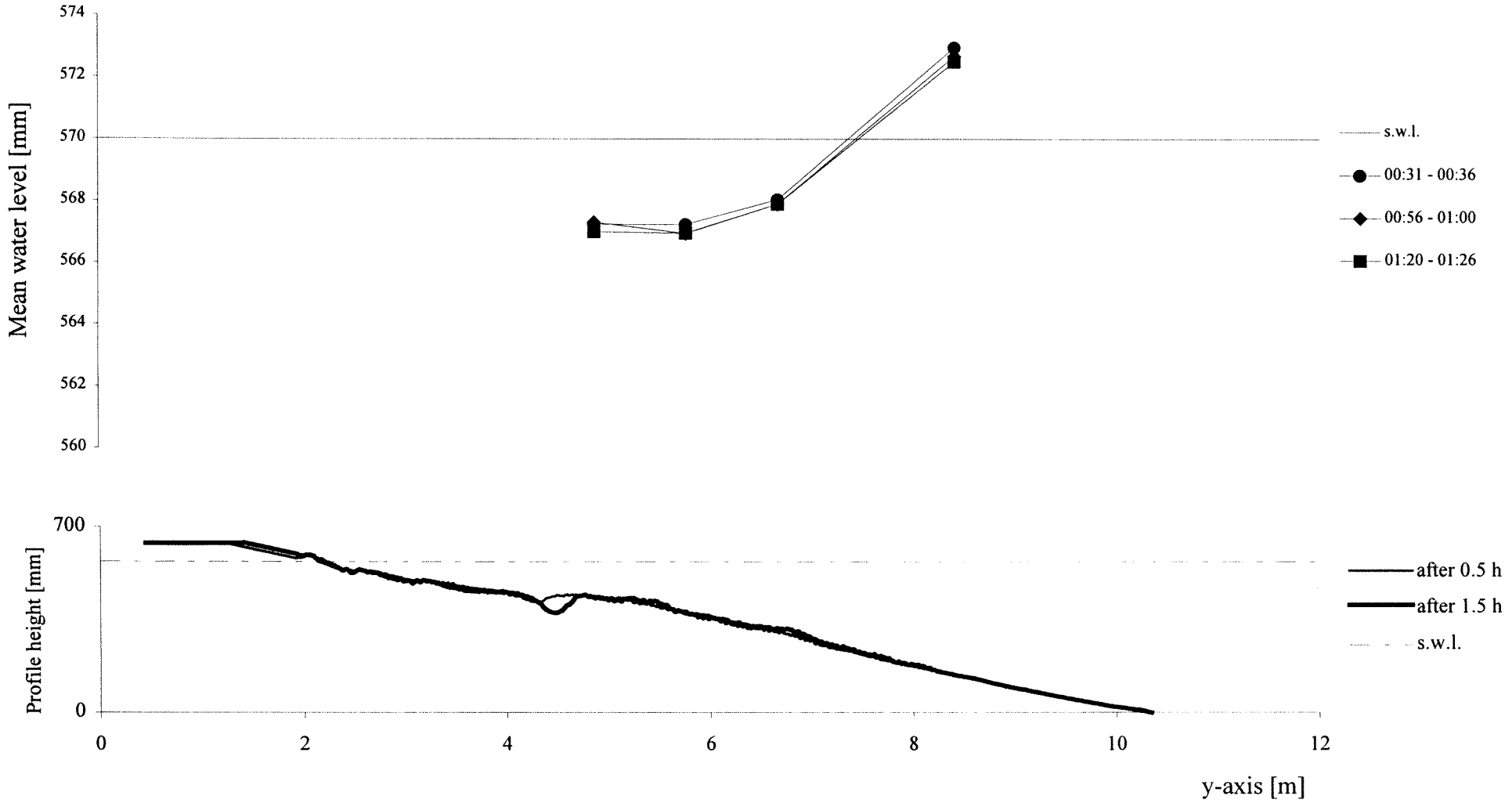

TEST A2 - cross-section x=12.5 m - interval 00:30 - 01:30

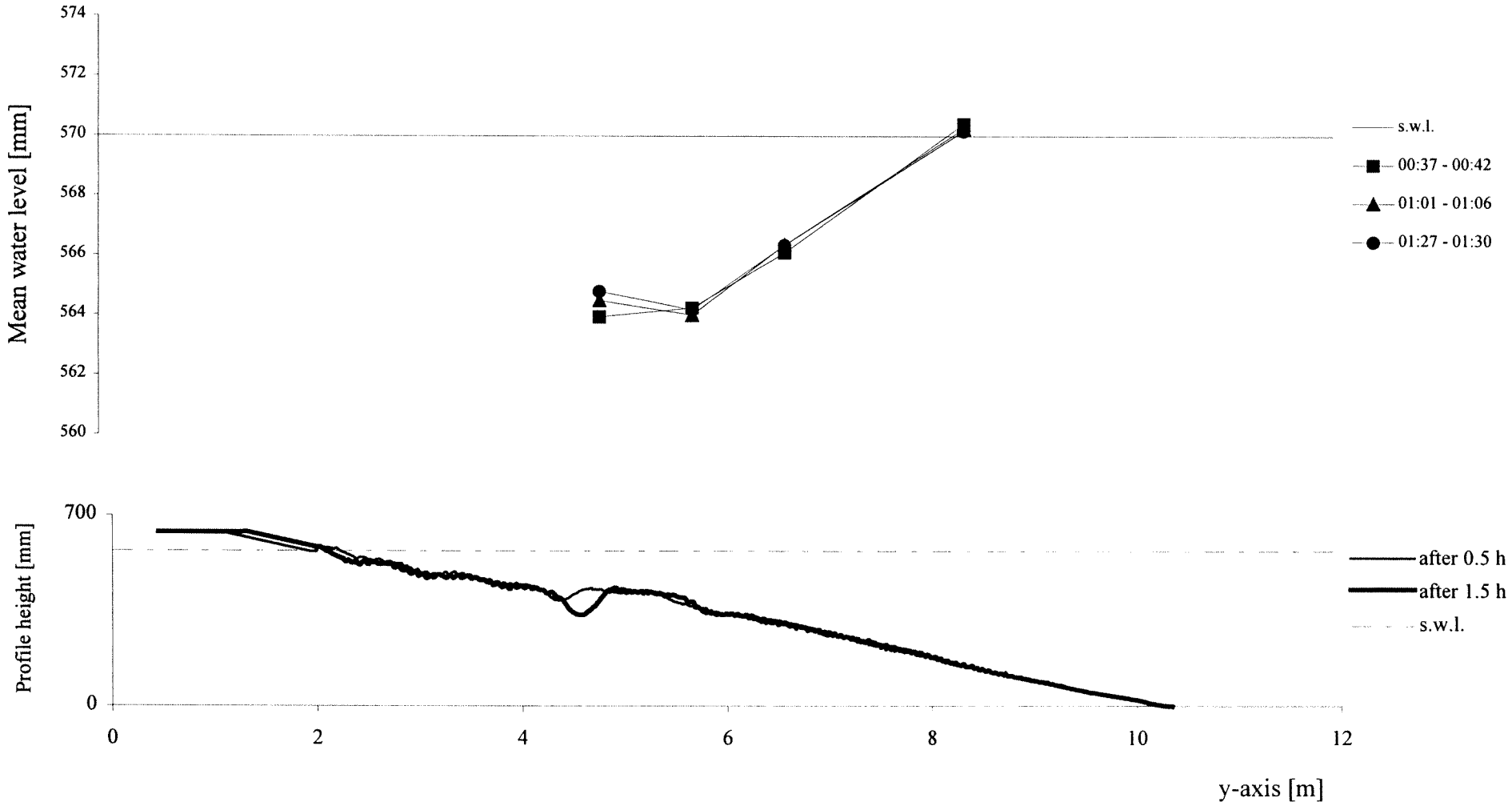

TEST A2 - cross-section x=20 m - interval 00:30 - 01:30

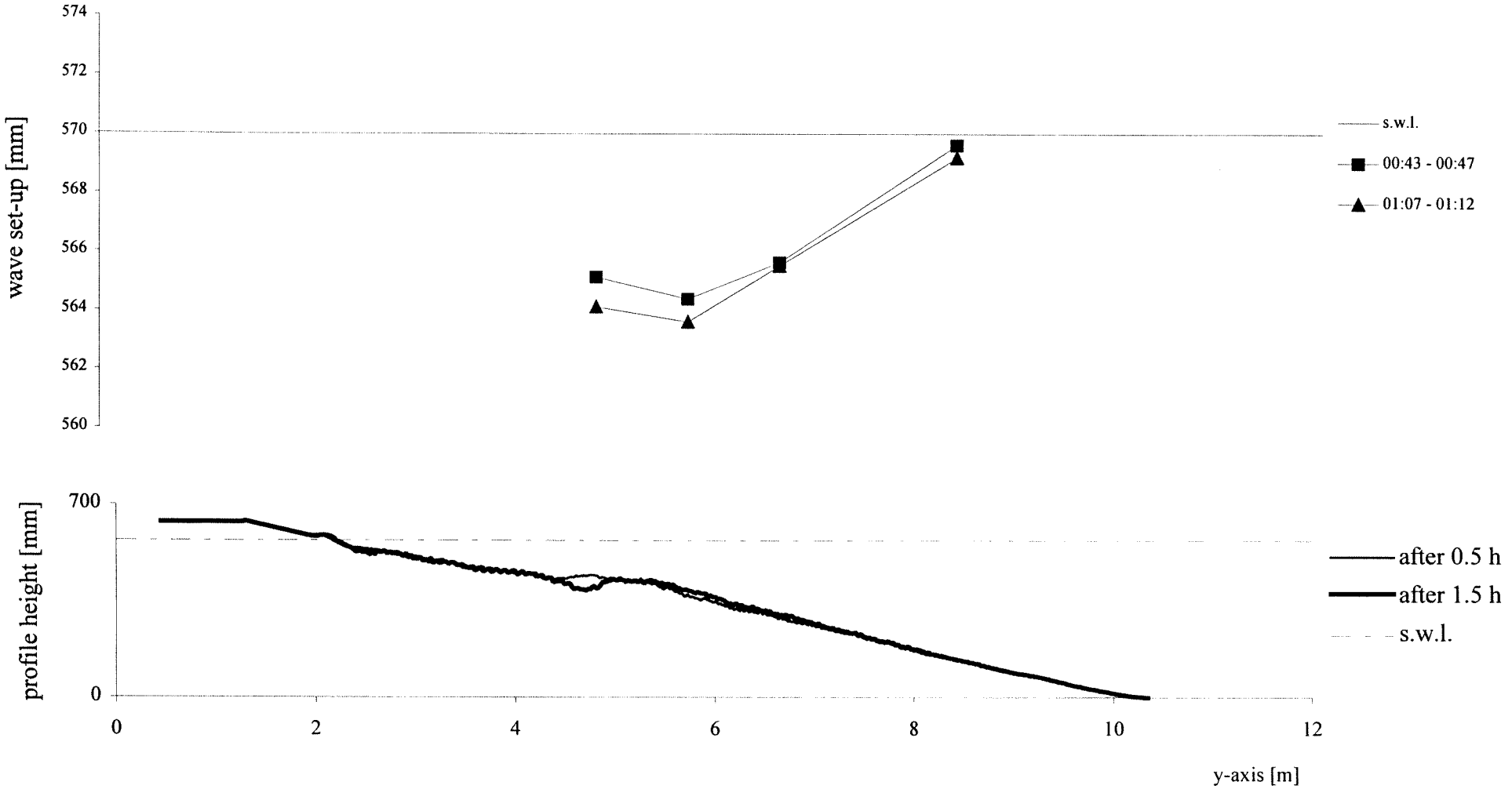

TEST A2 - cross-section x=24.5 m - interval 00:30 - 01:30

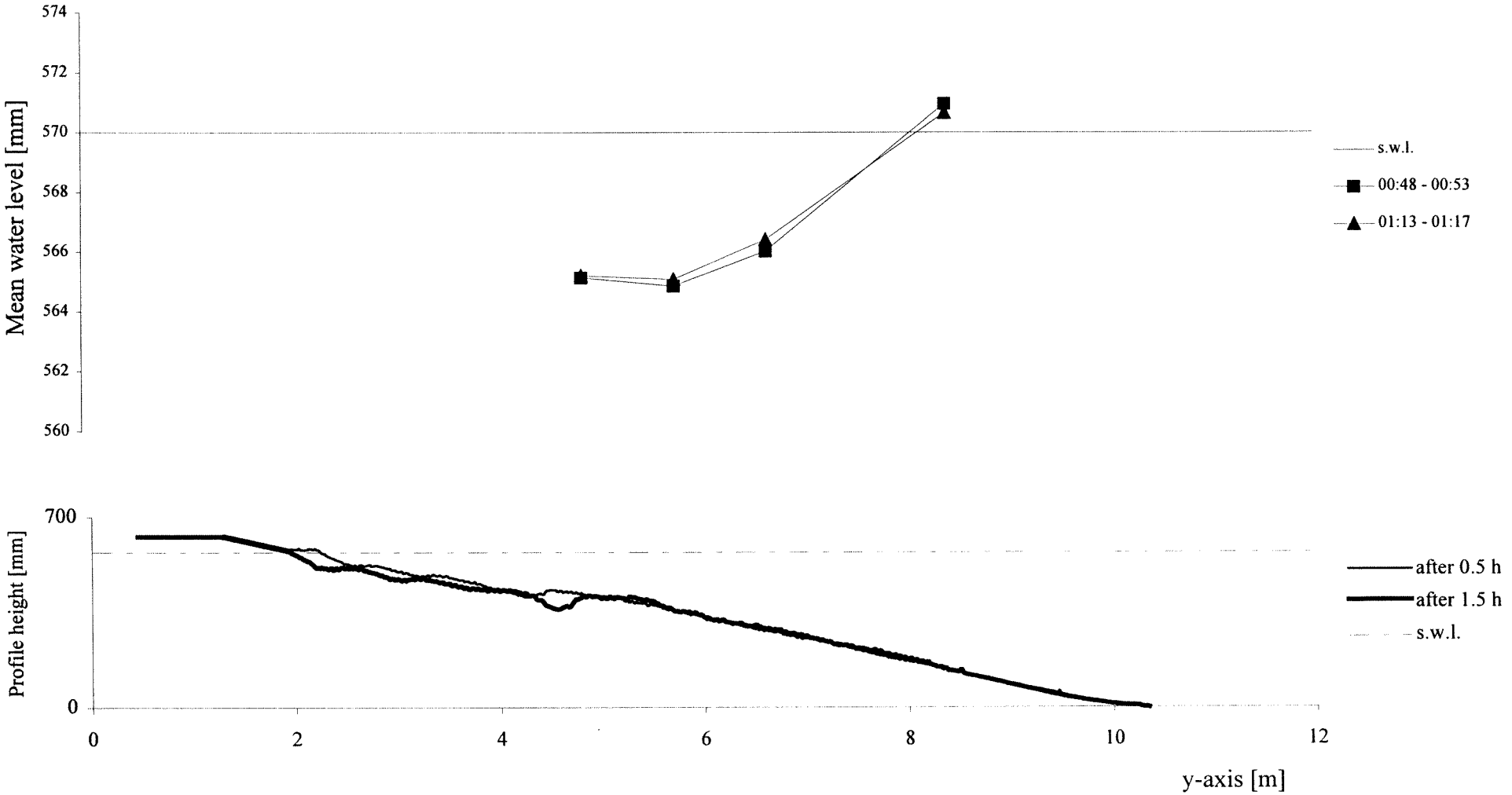

TEST A2 - cross-section x=3 m - interval 01:30 - 03:30

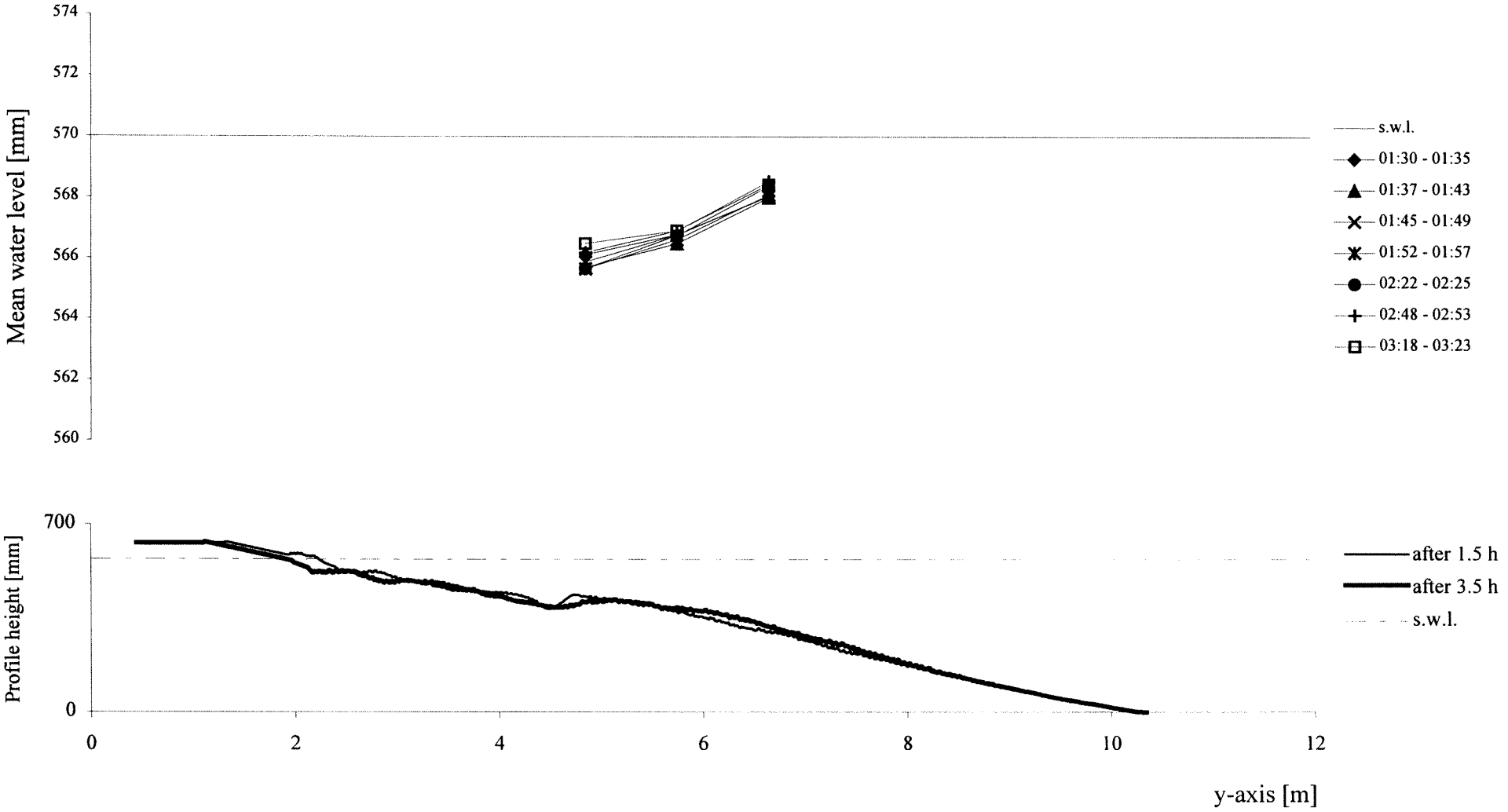

TEST A2 - cross-section x=6.5 m - interval 01:30 - 03:30

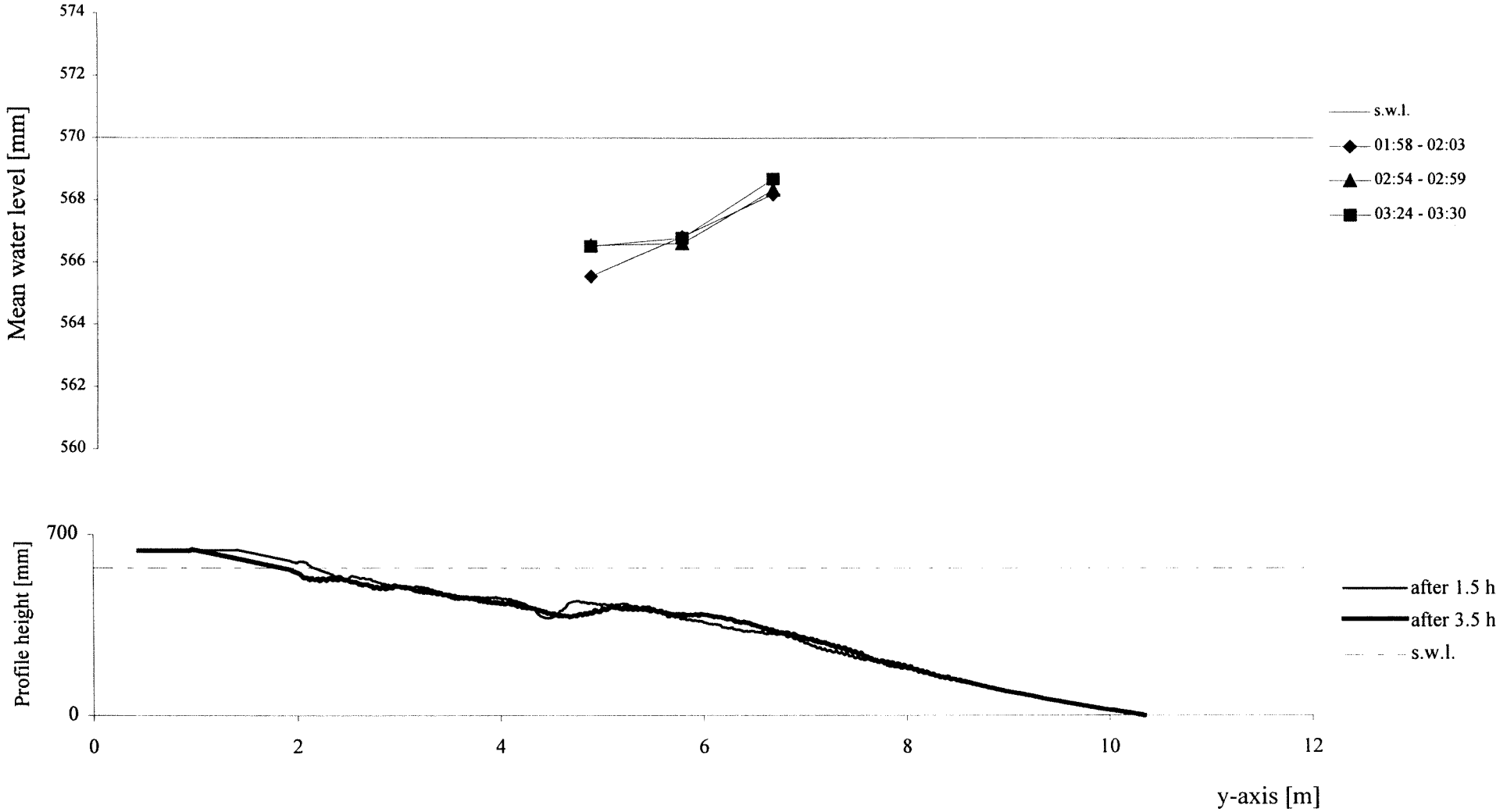

TEST A2 - cross-section x=12.5 m - interval 01:30 - 03:30

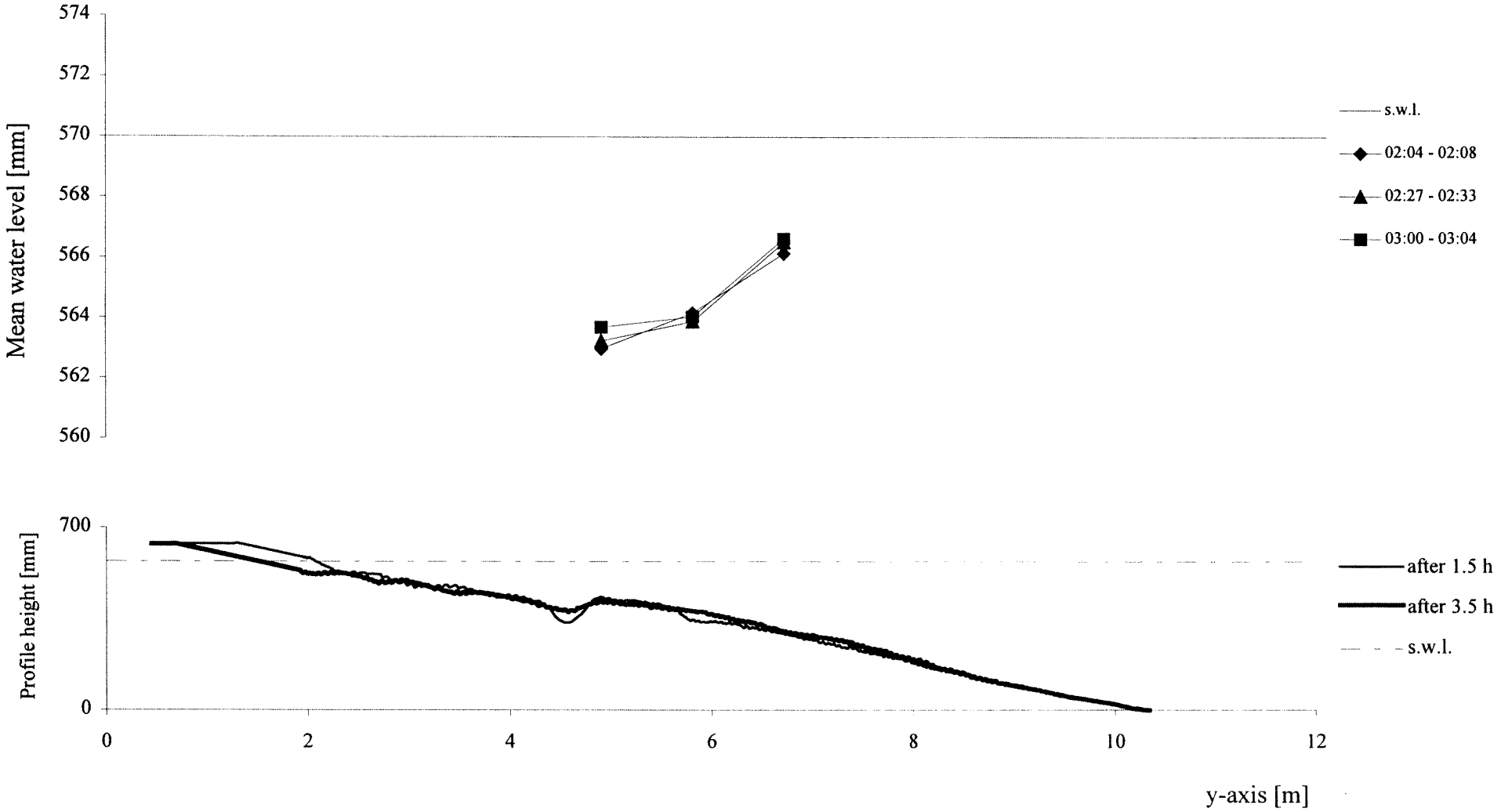

Test A2 - cross-section x=20 m - interval 01:30 - 03:30

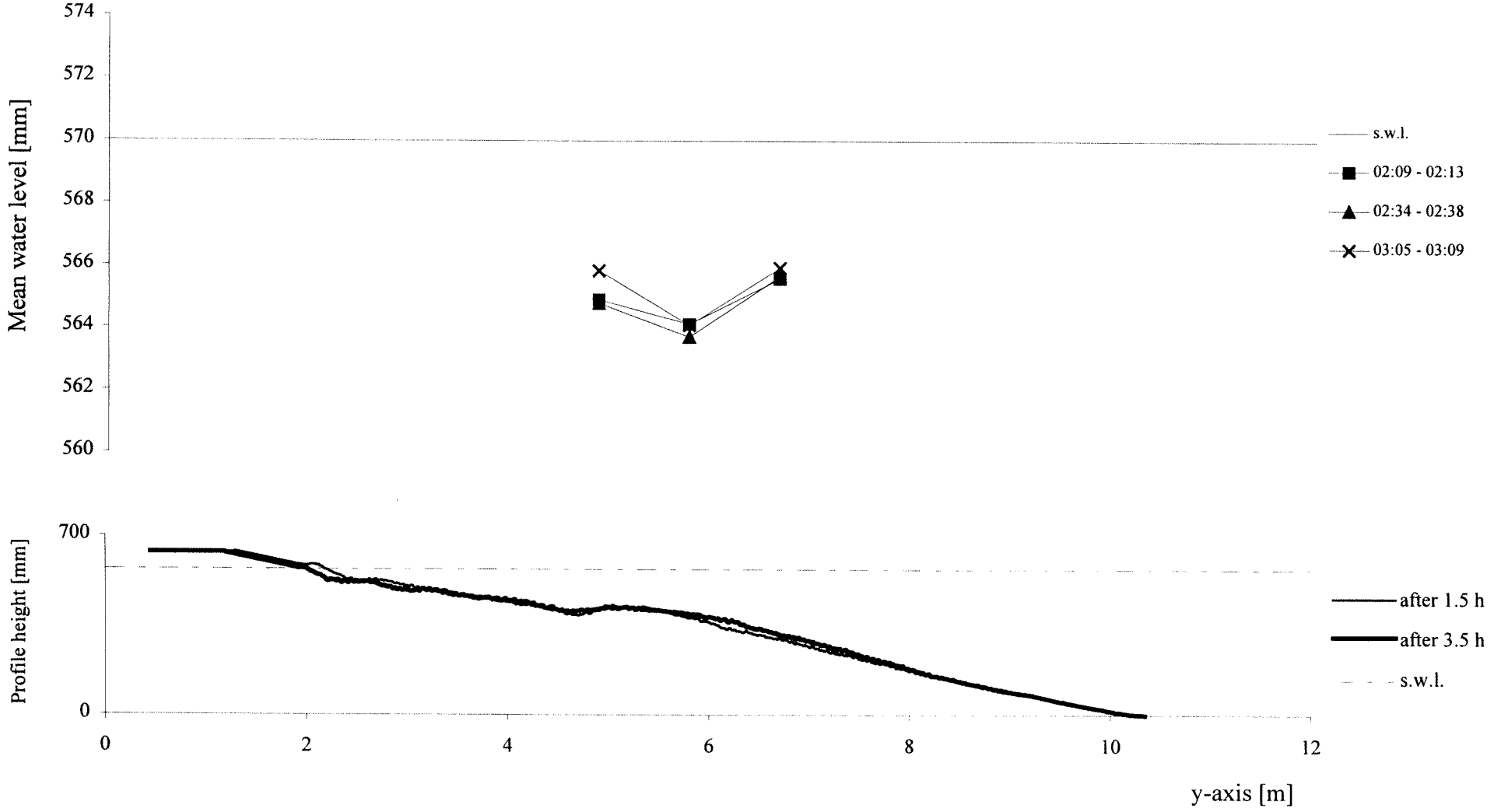

TEST A2 - cross-section x=24.5 m - interval 01:30 - 03:30

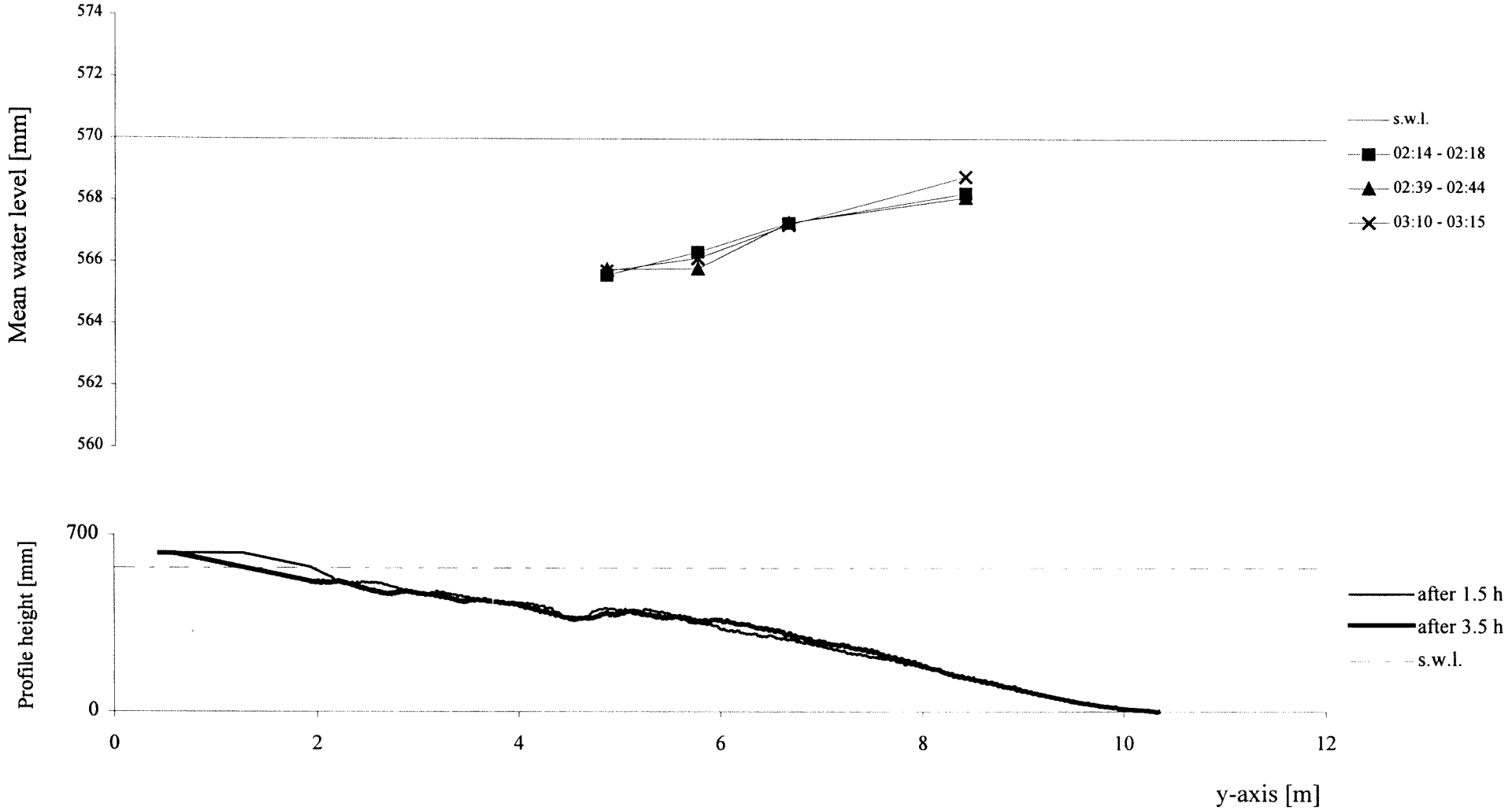

TEST A2 - cross-section x=3 m - interval 03:30 - 07:30

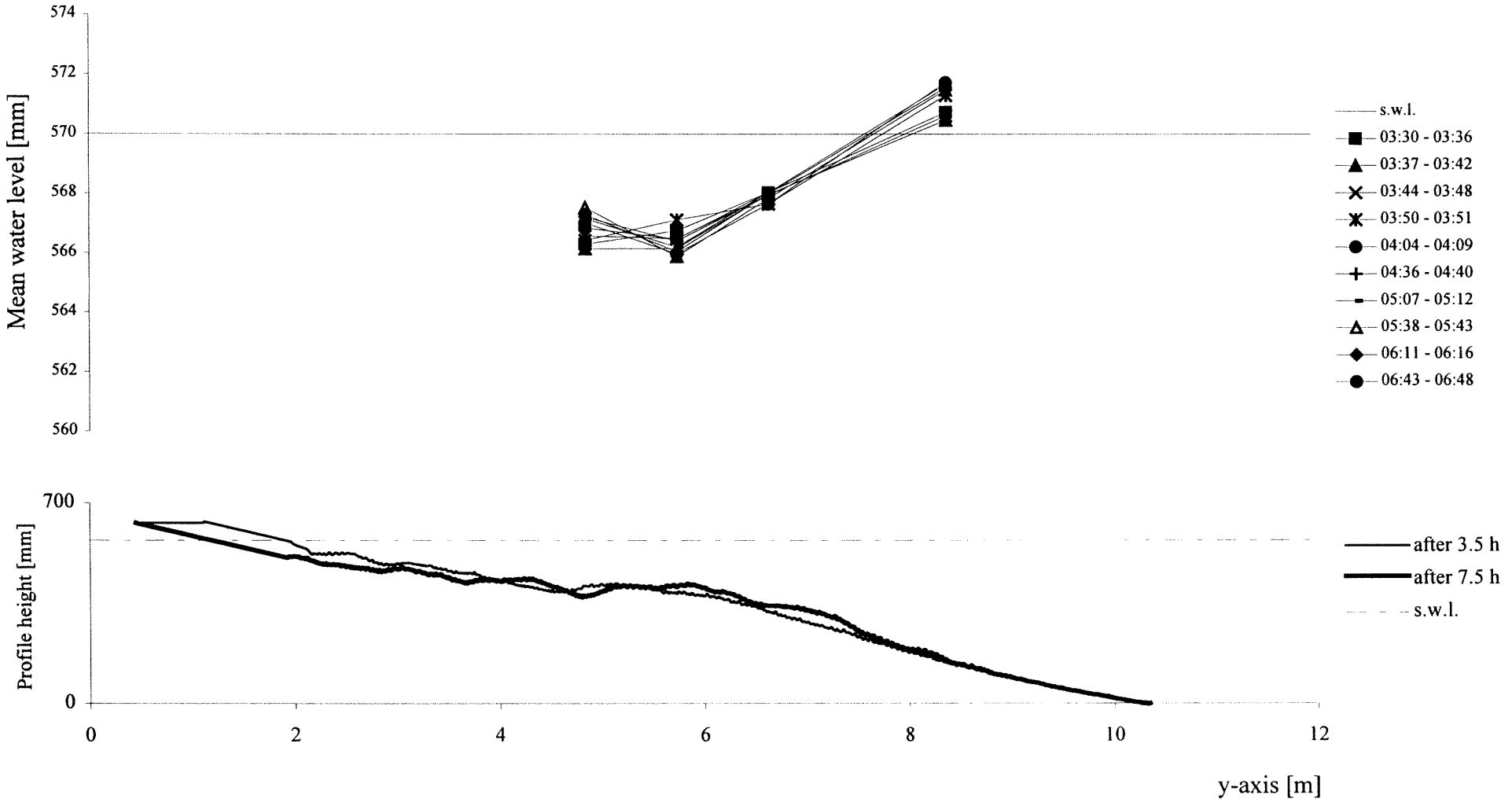

TEST A2 - cross-section x=6.5 m - interval 03:30 - 07:30

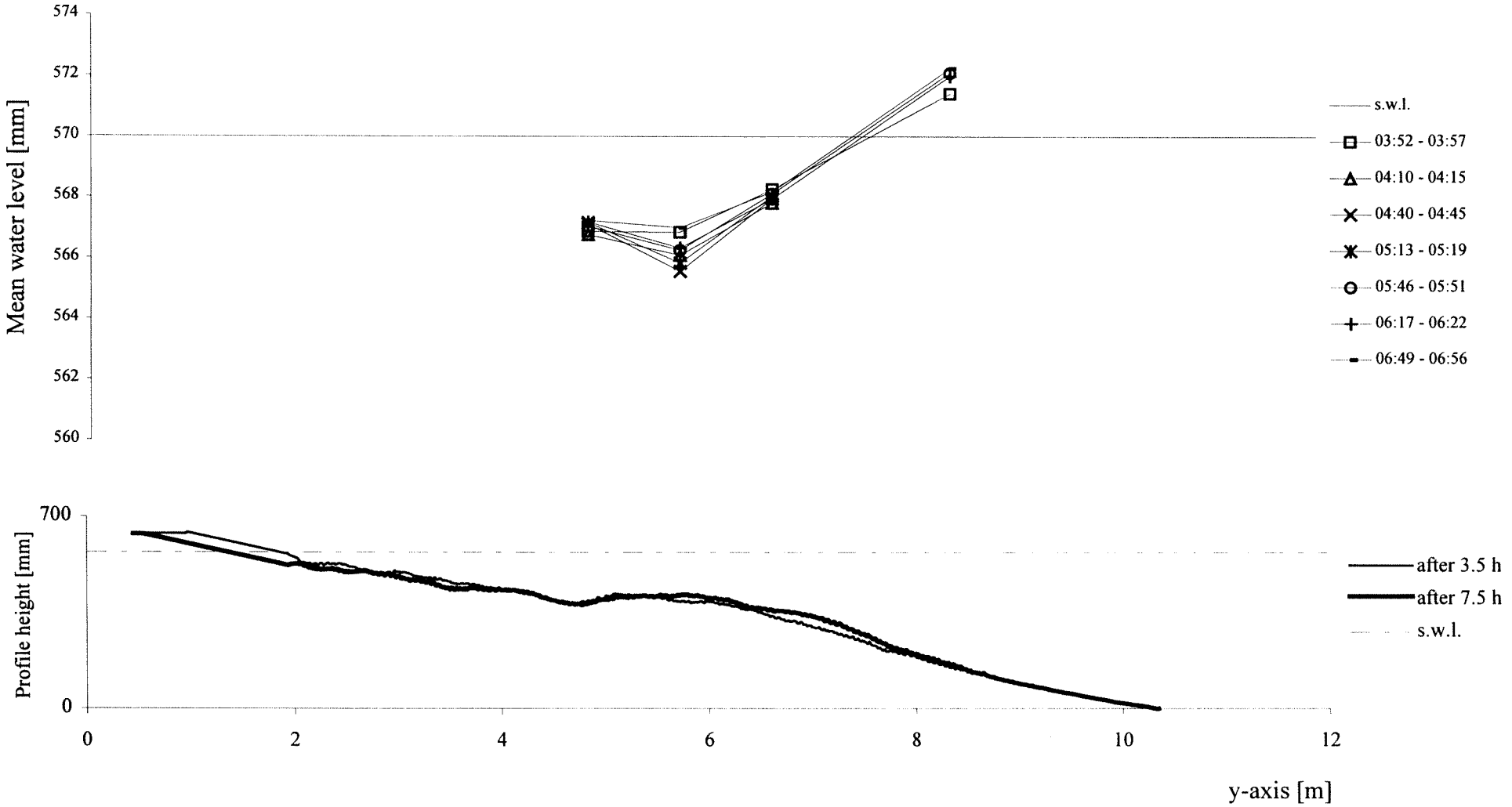

TEST A2 - cross-section x=12.5 m - interval 03:30 - 07:30

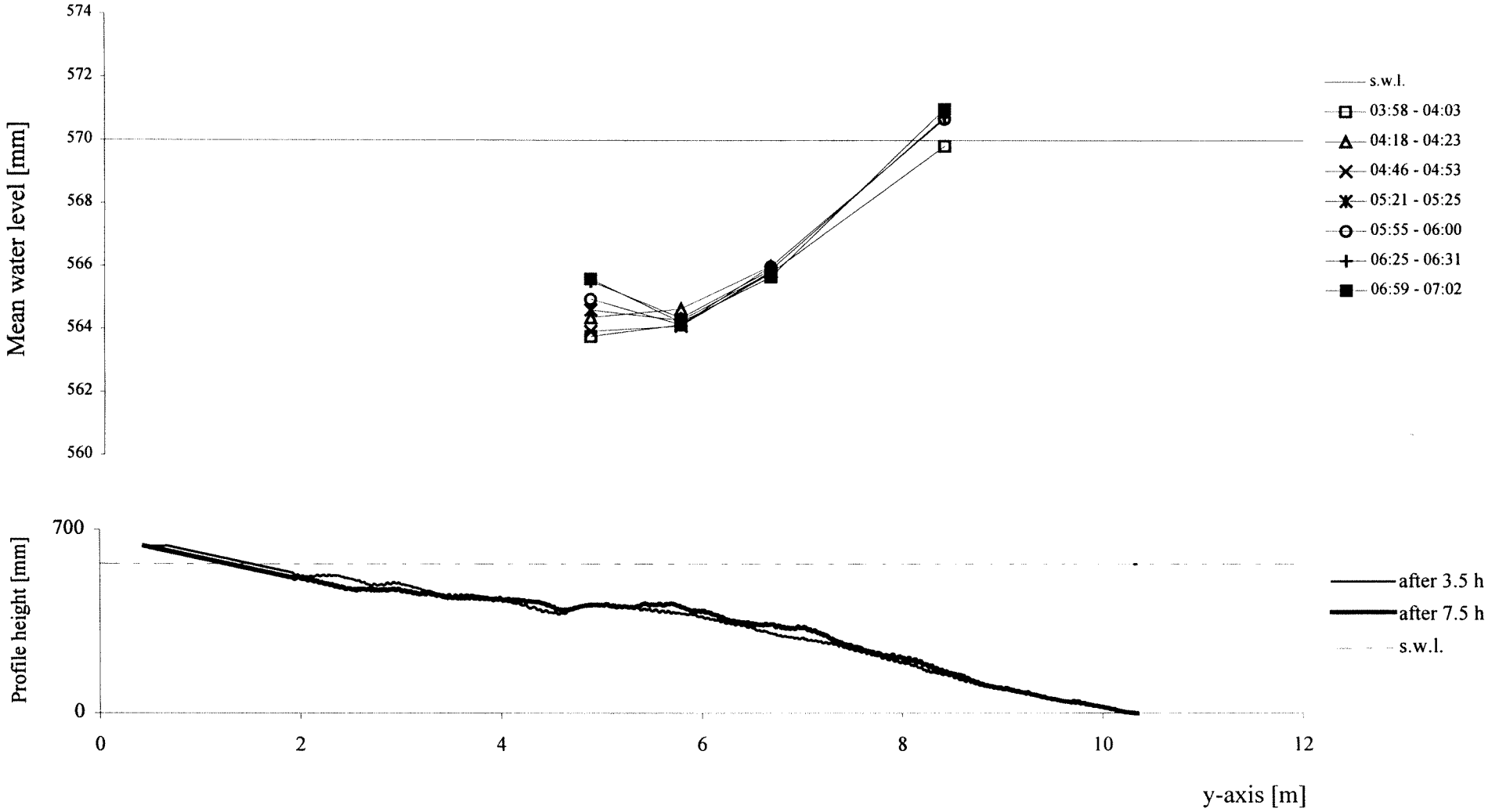

TEST A2 - cross-section x=20 m - interval 03:30 - 07:30

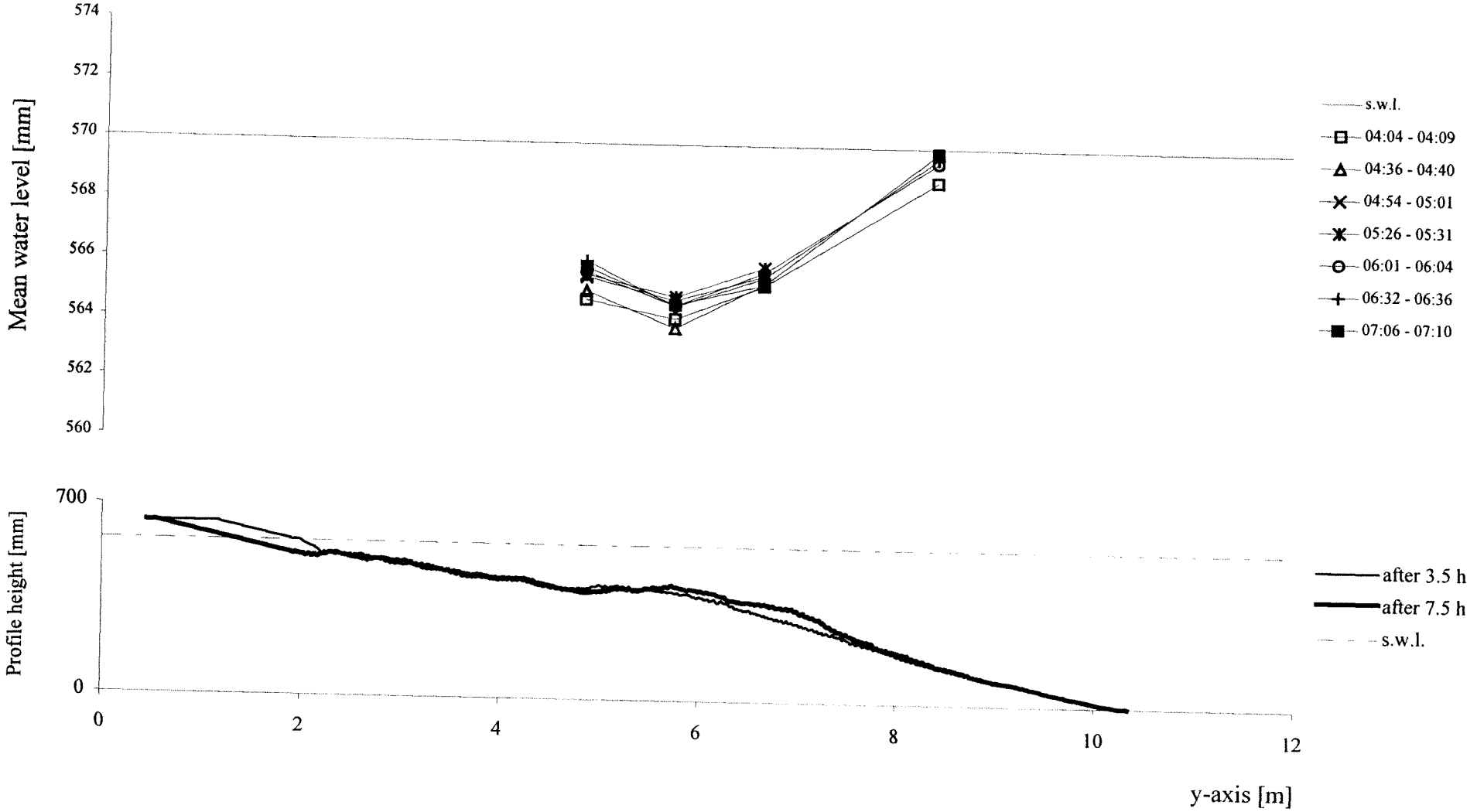

TEST A2 - cross-section x=24.5 m - interval 03:30 - 07:30

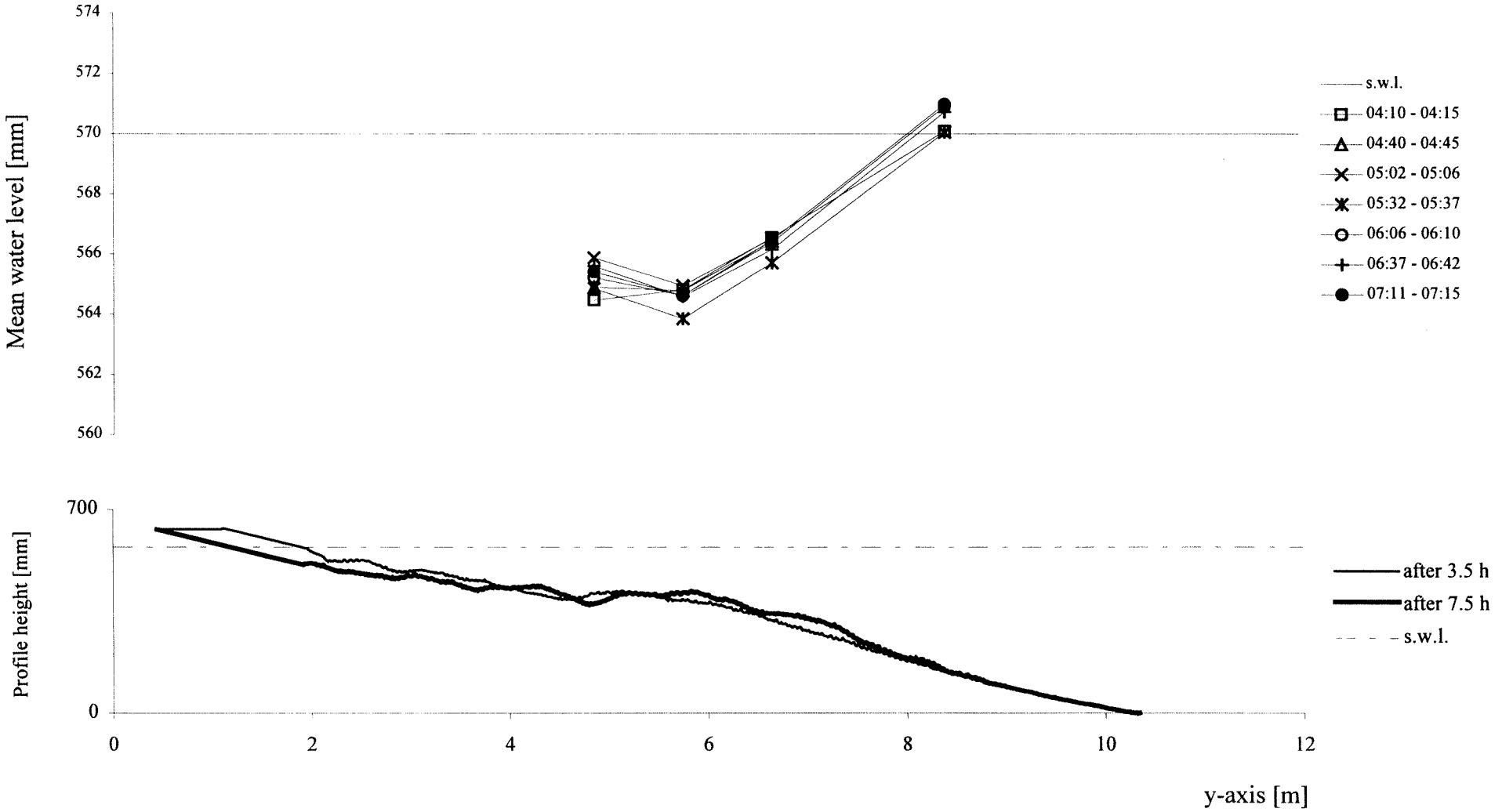

Appendix A3. Graphics TEST A3 - Average Water Level

TEST A3 - cross-section x=3m - interval 00:00 - 00:30

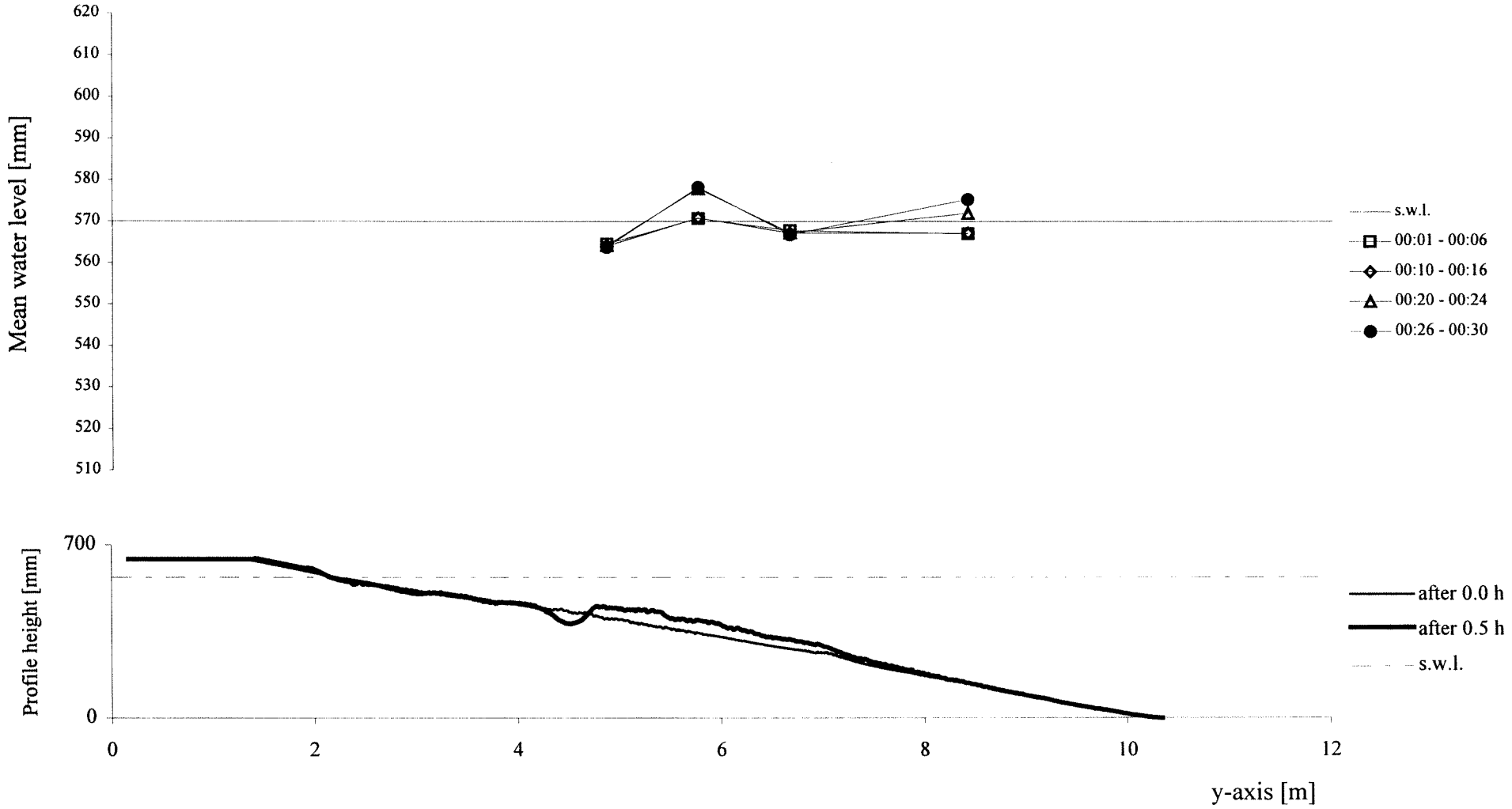

TEST A3 - cross-section x=6.5 m - interval 00:30 - 01:30

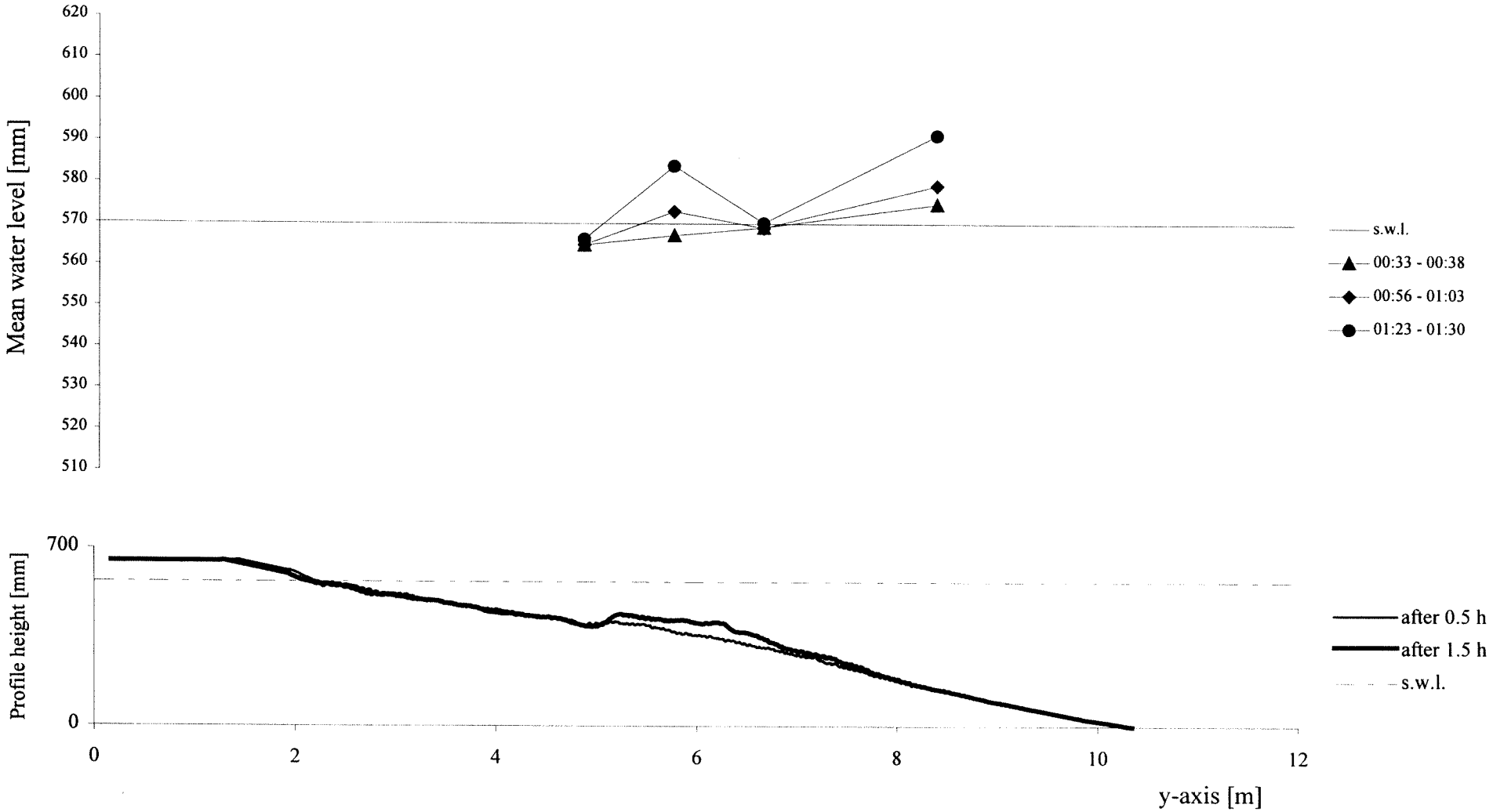

TEST A3 - cross-section x=12.5 m - interval 00:30 - 01:30

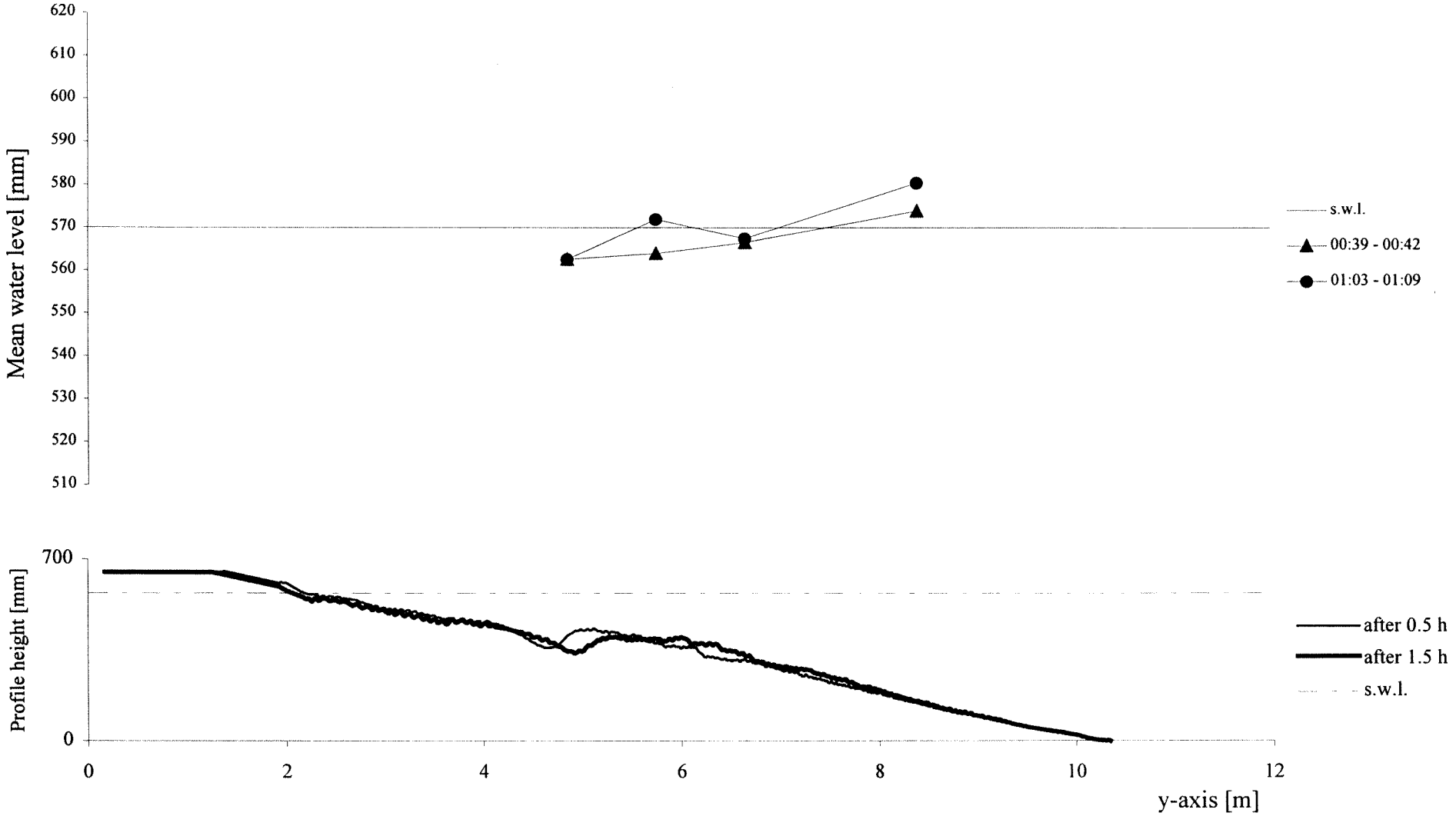

TEST A3 - cross-section x=20 m - interval 00:30 - 01:30

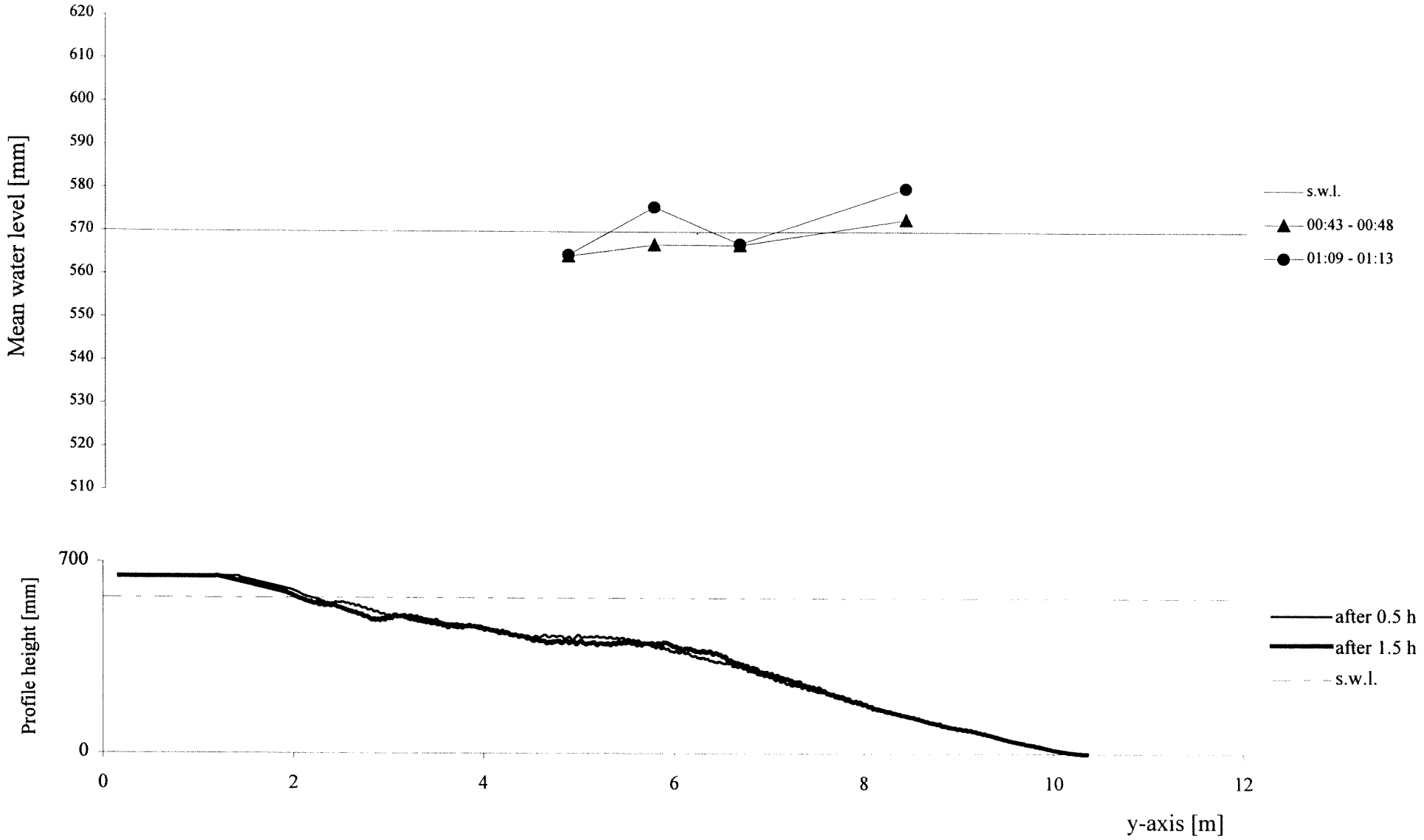

TEST A3 - cross-section x=24.5 m - interval 00:30 - 01:30

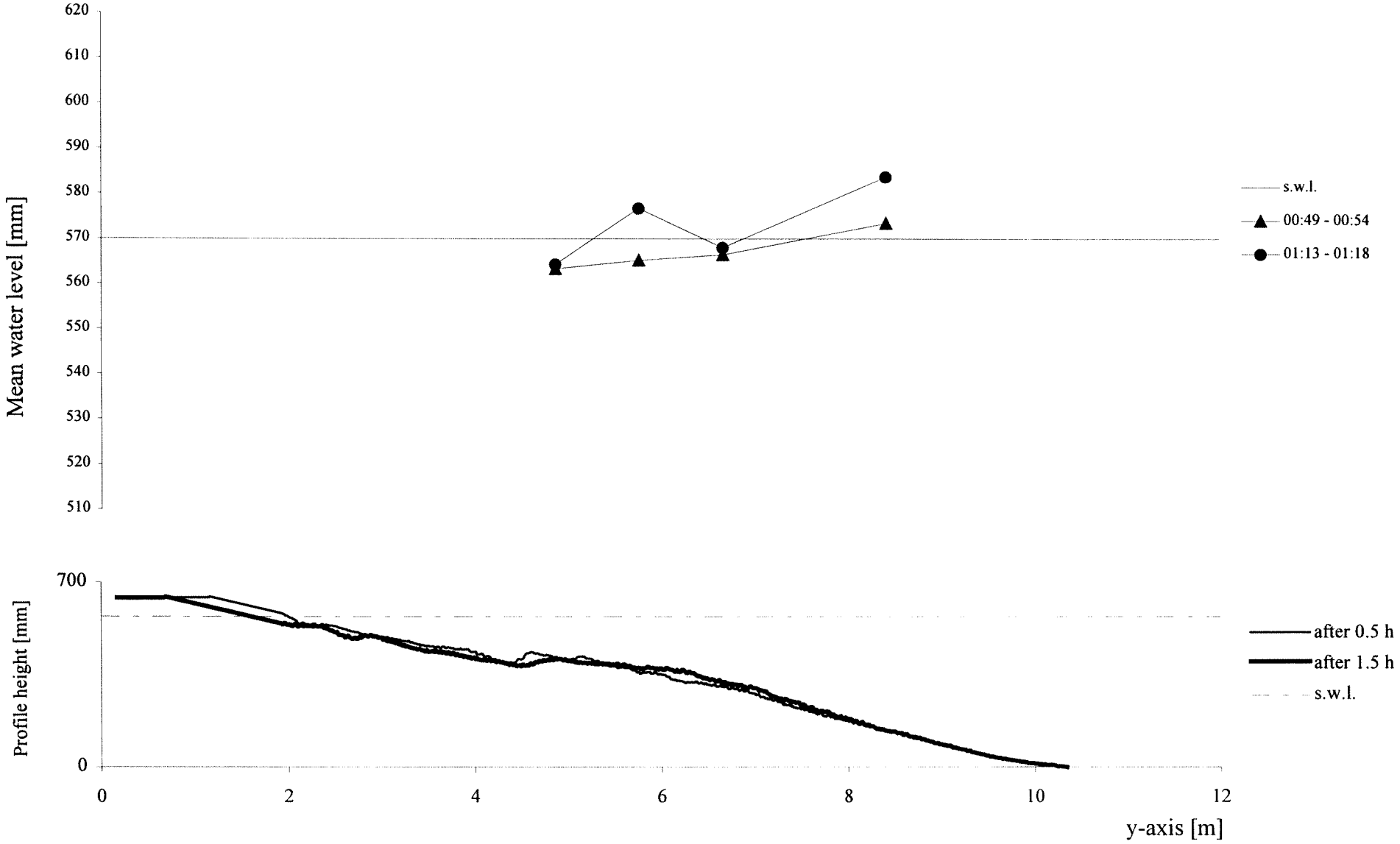

TEST A3 - cross-section x=3 m - interval 01:30 - 03:30

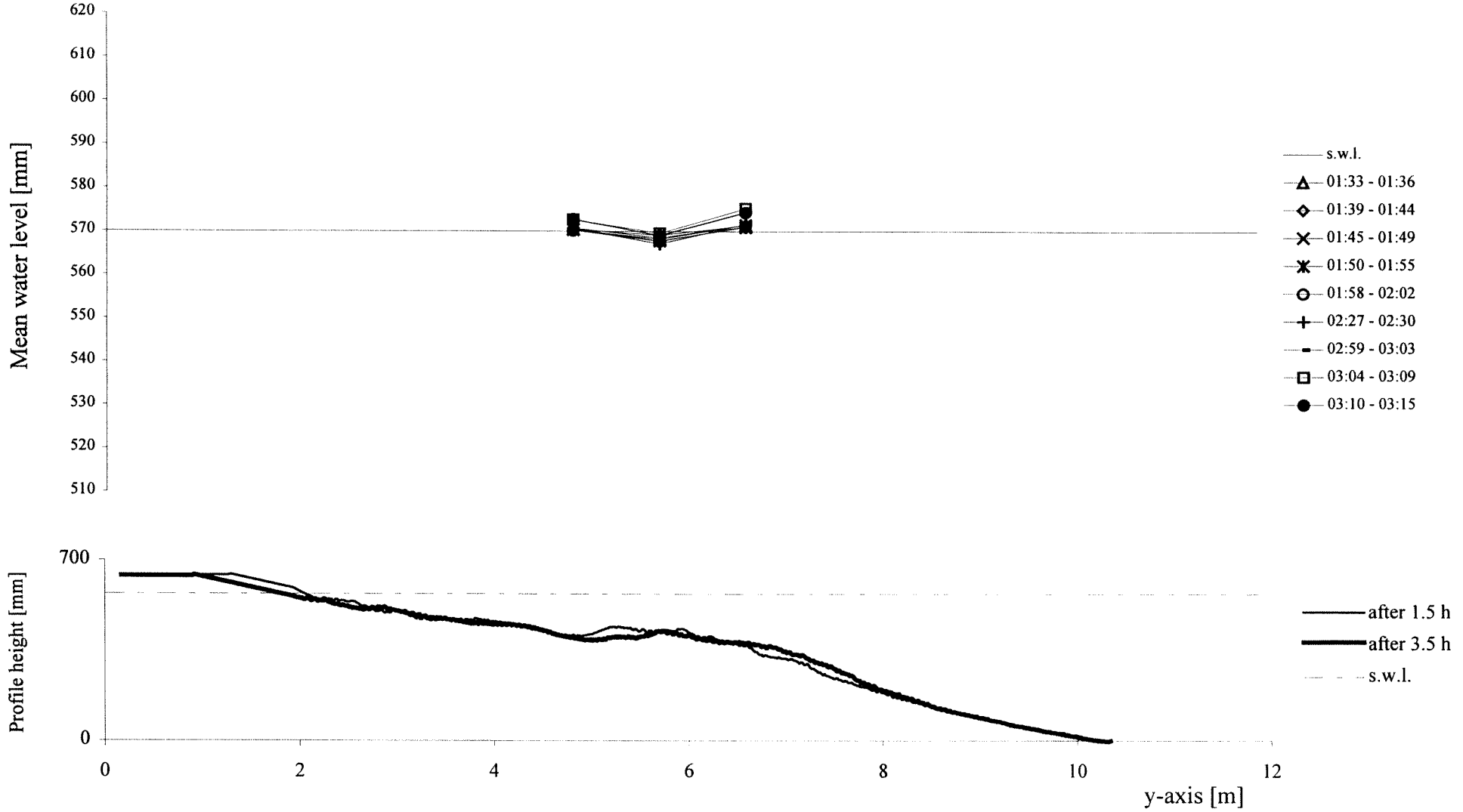

TEST A3 - cross-section x=6.5 m - interval 01:30 - 03:30

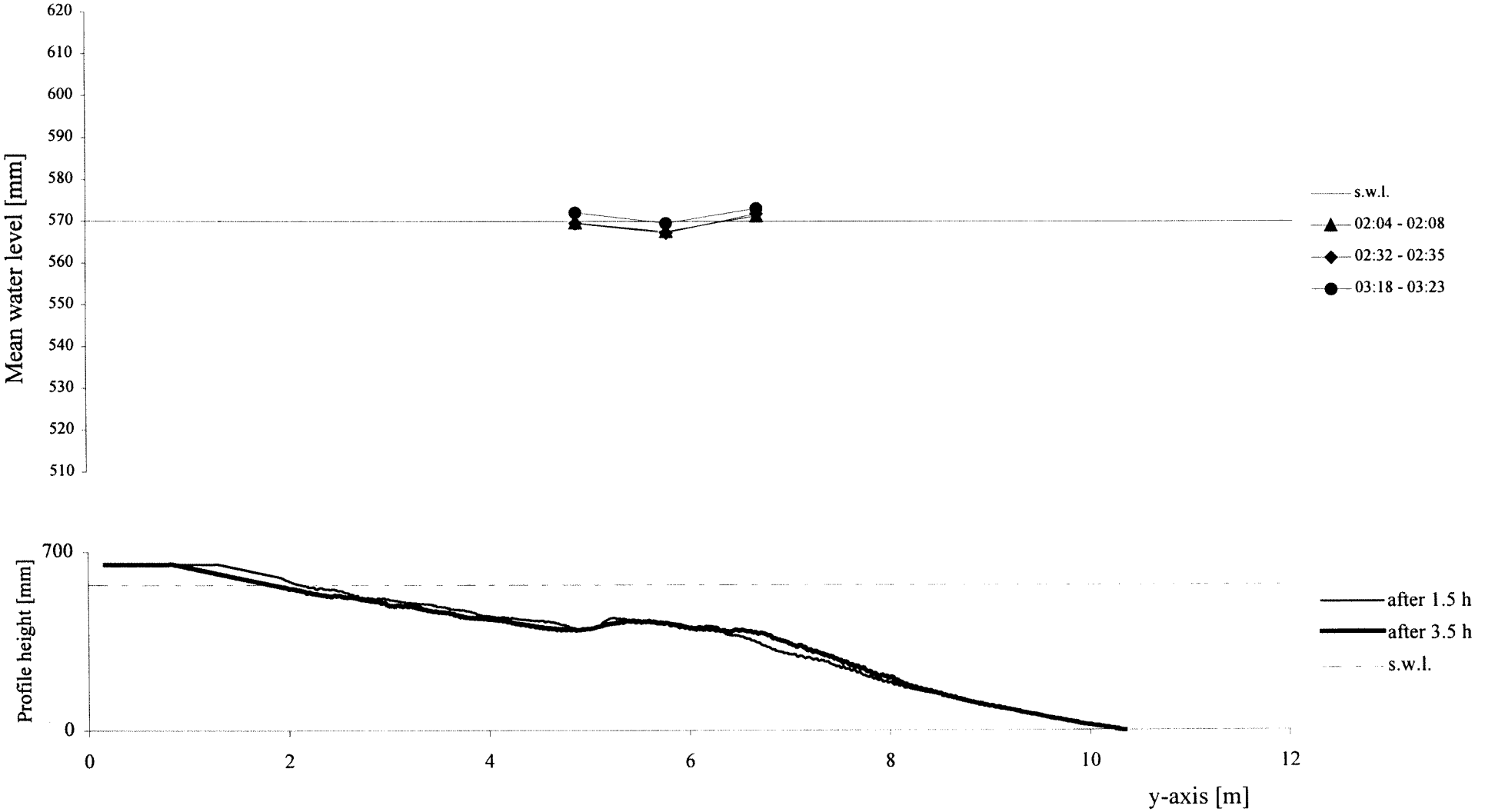

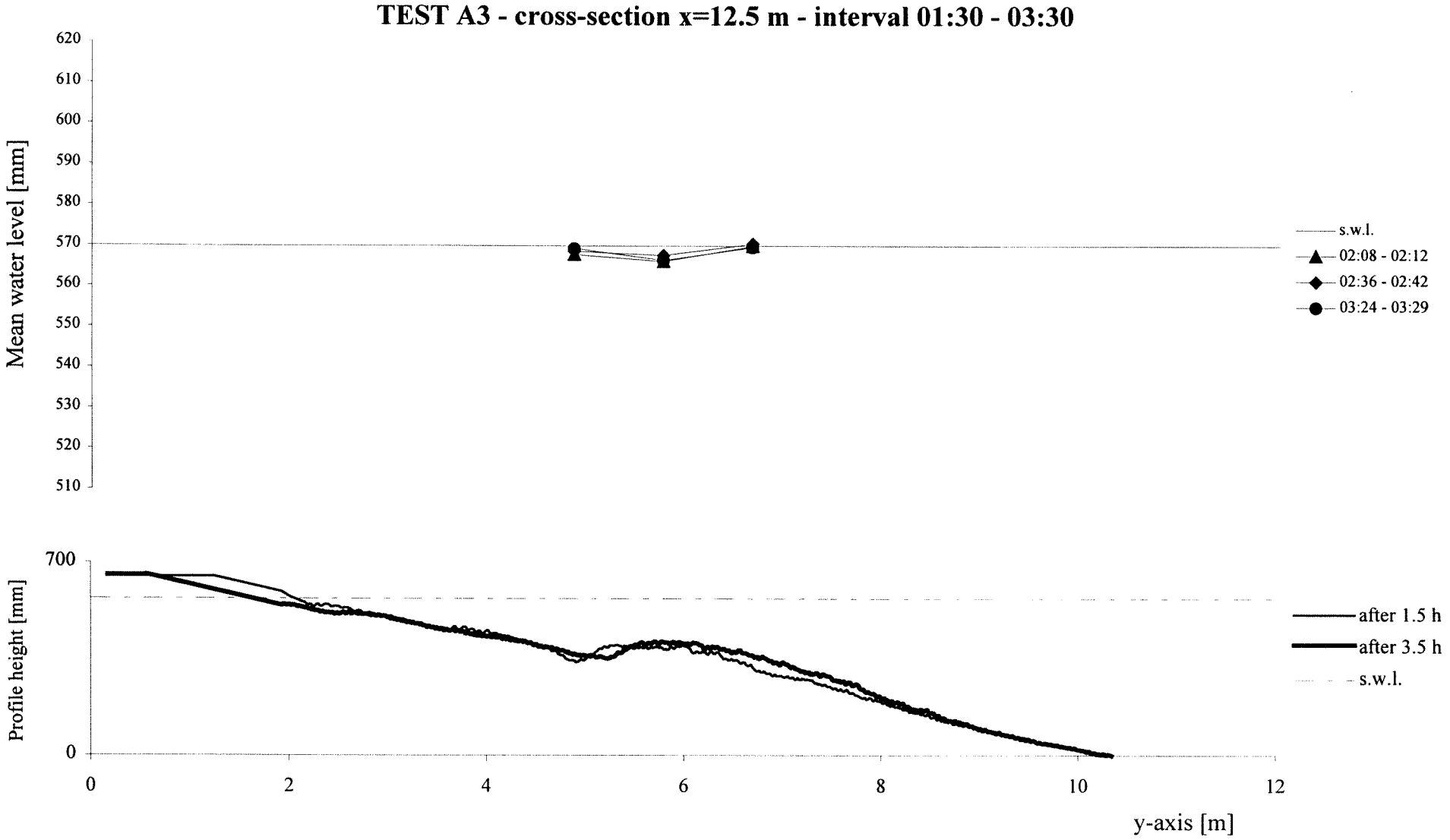
TEST A3 - cross-section x=12.5 m - interval 01:30 - 03:30
Mean water level [mm]
620
610
600
590
580
570
560
550
540
530
520
510
s.w.l.
02:08 - 02:12
02:36 - 02:42
03:24 - 03:29
Profile height [mm]
700
0
after 1.5 h
after 3.5 h
s.w.l.
0
2
4
6
8
10
12
y-axis [m]

TEST A3 - cross-section x=20 m - interval 01:30 - 03:30

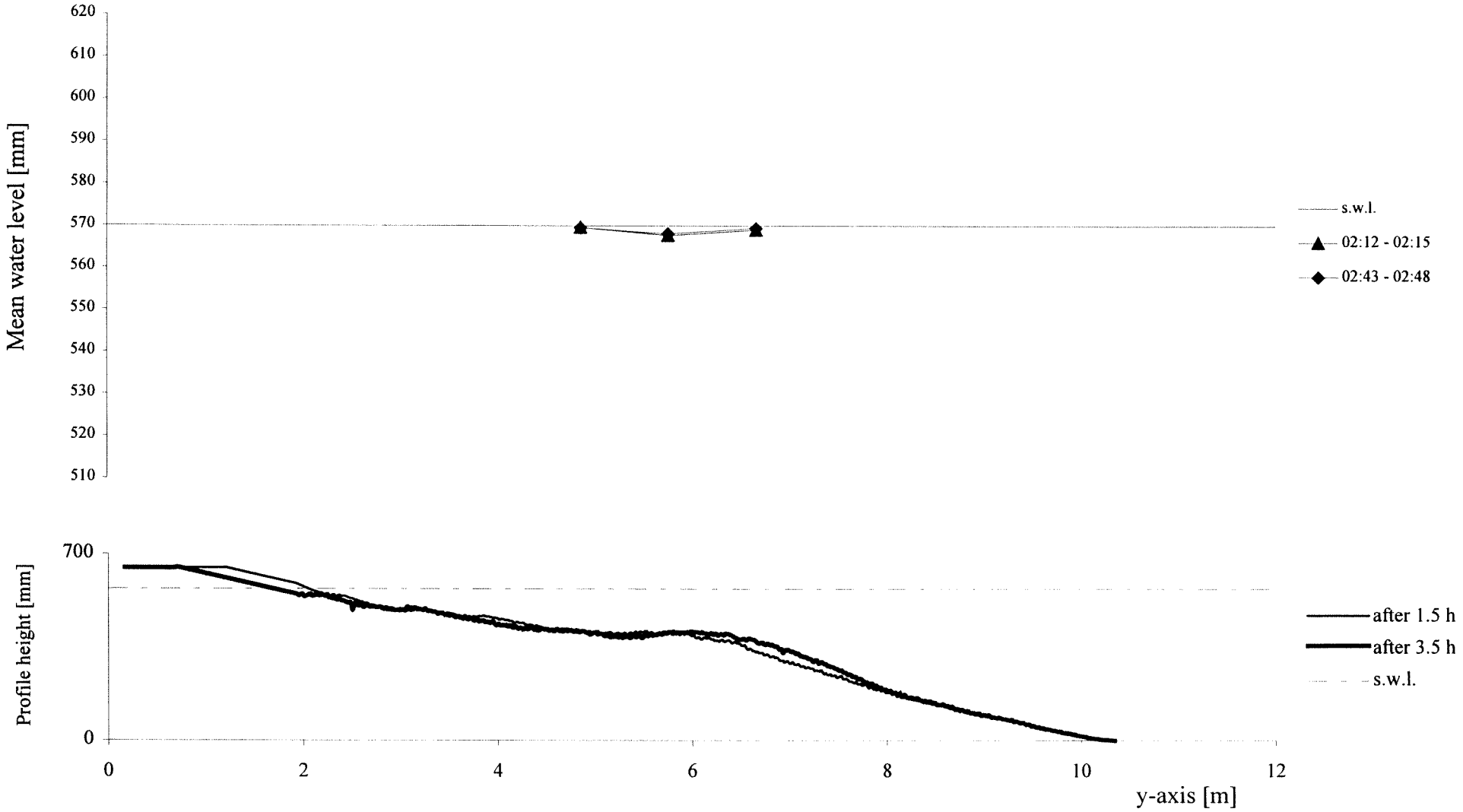

TEST A3 - cross-section x=24.5 m - interval 01:30 - 03:30

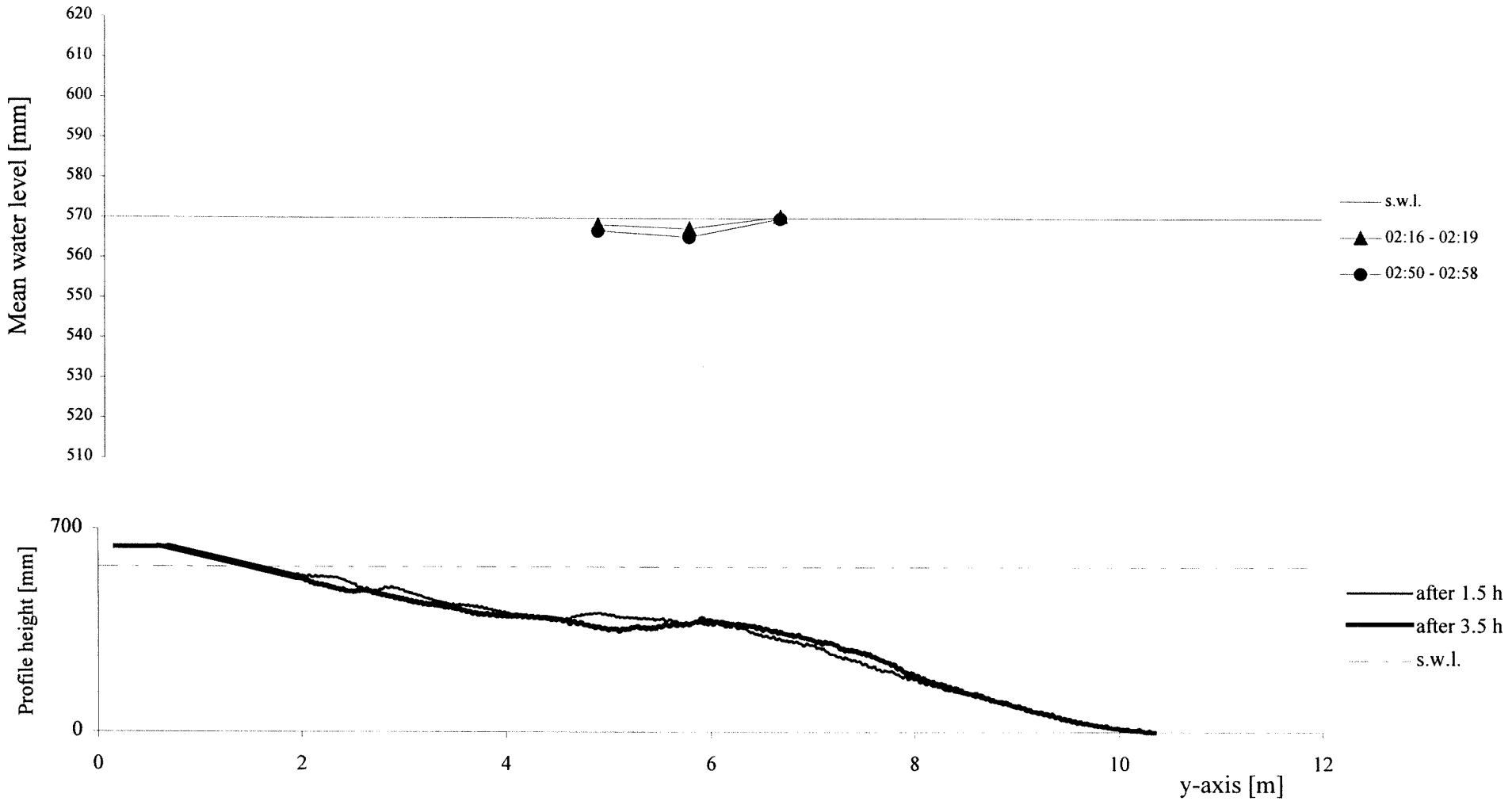

TEST A3 - cross-section x=3 m - interval 03:30 - 07:30

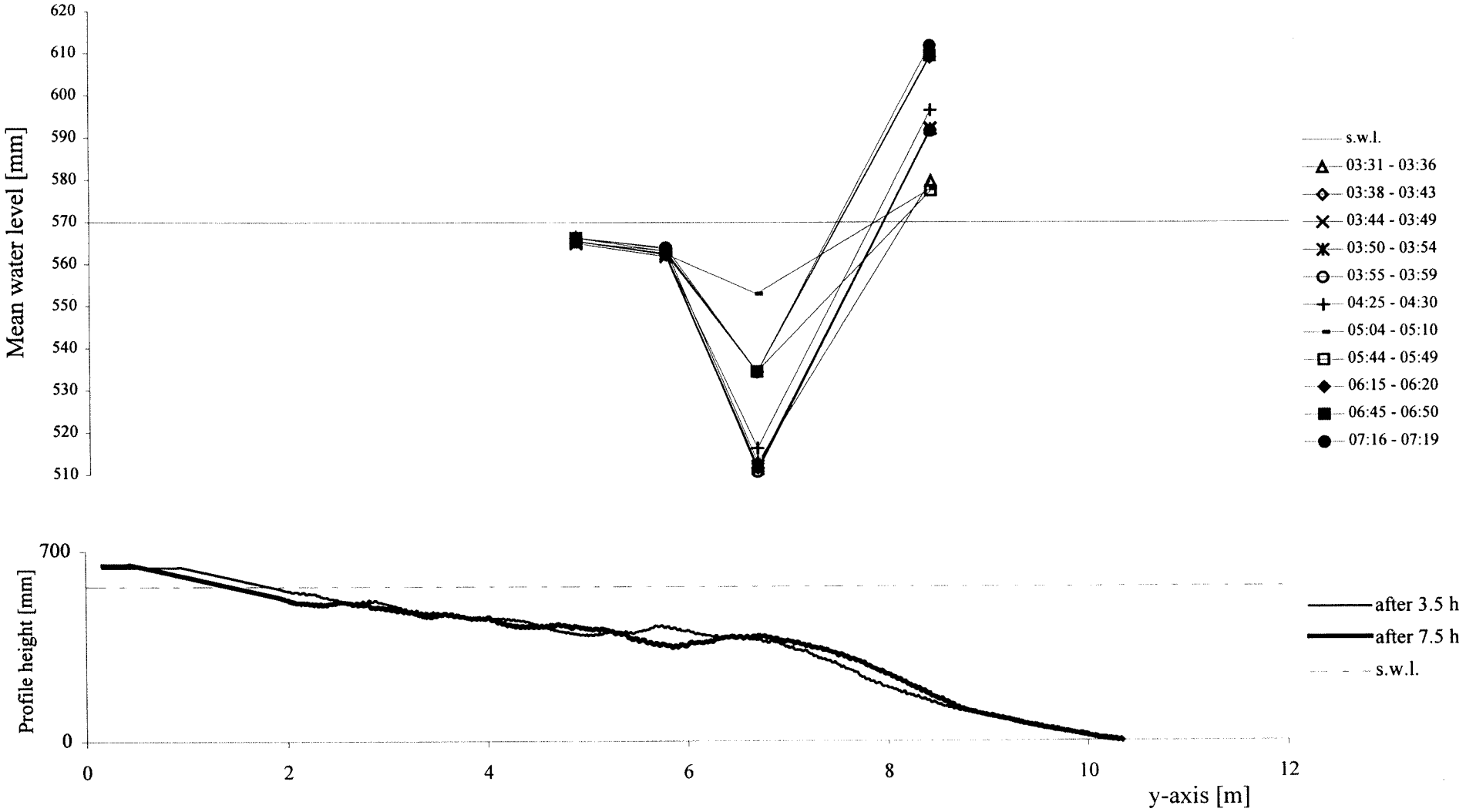

TEST A3 - cross-section x=6.5 m - interval 03:30 - 07:30

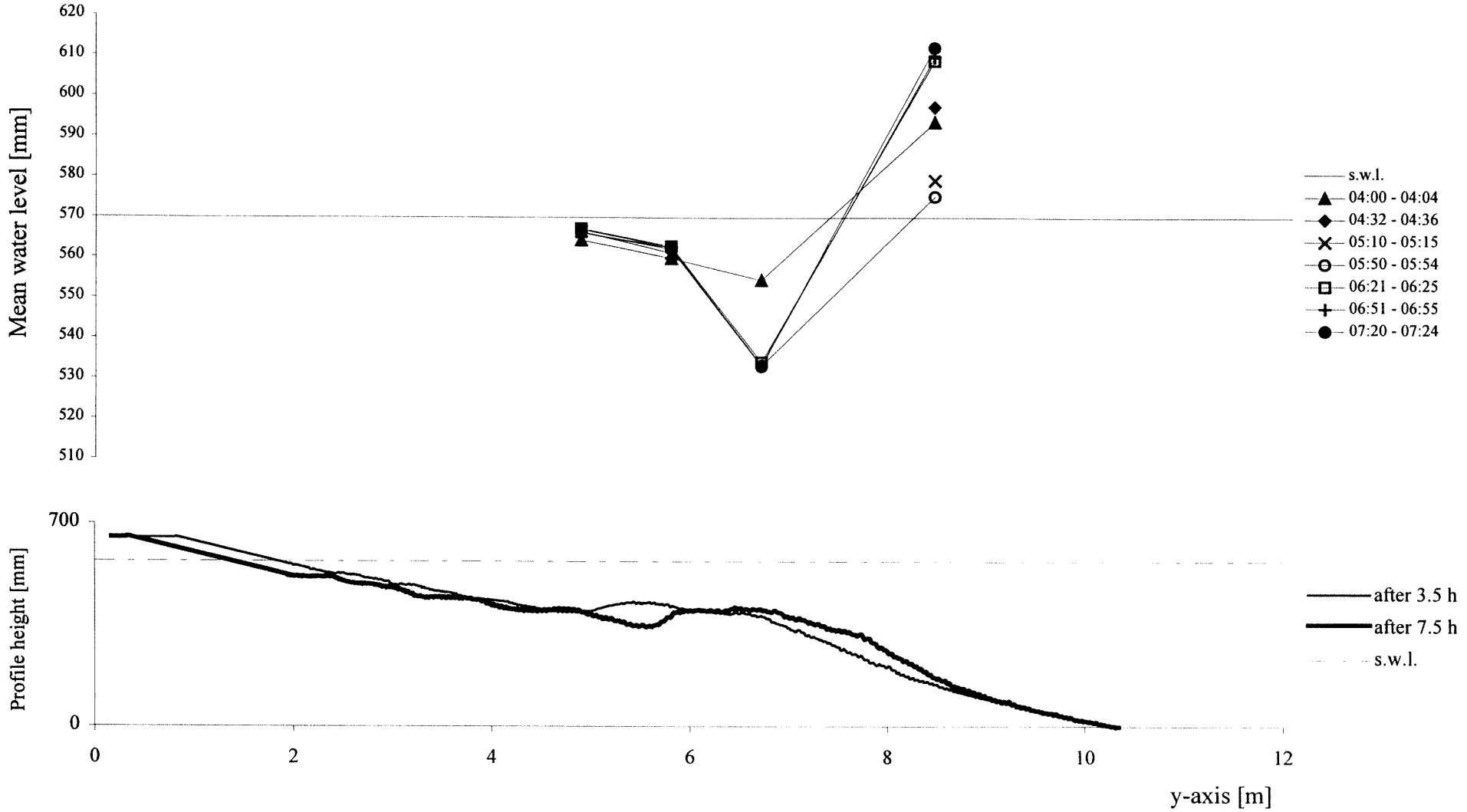

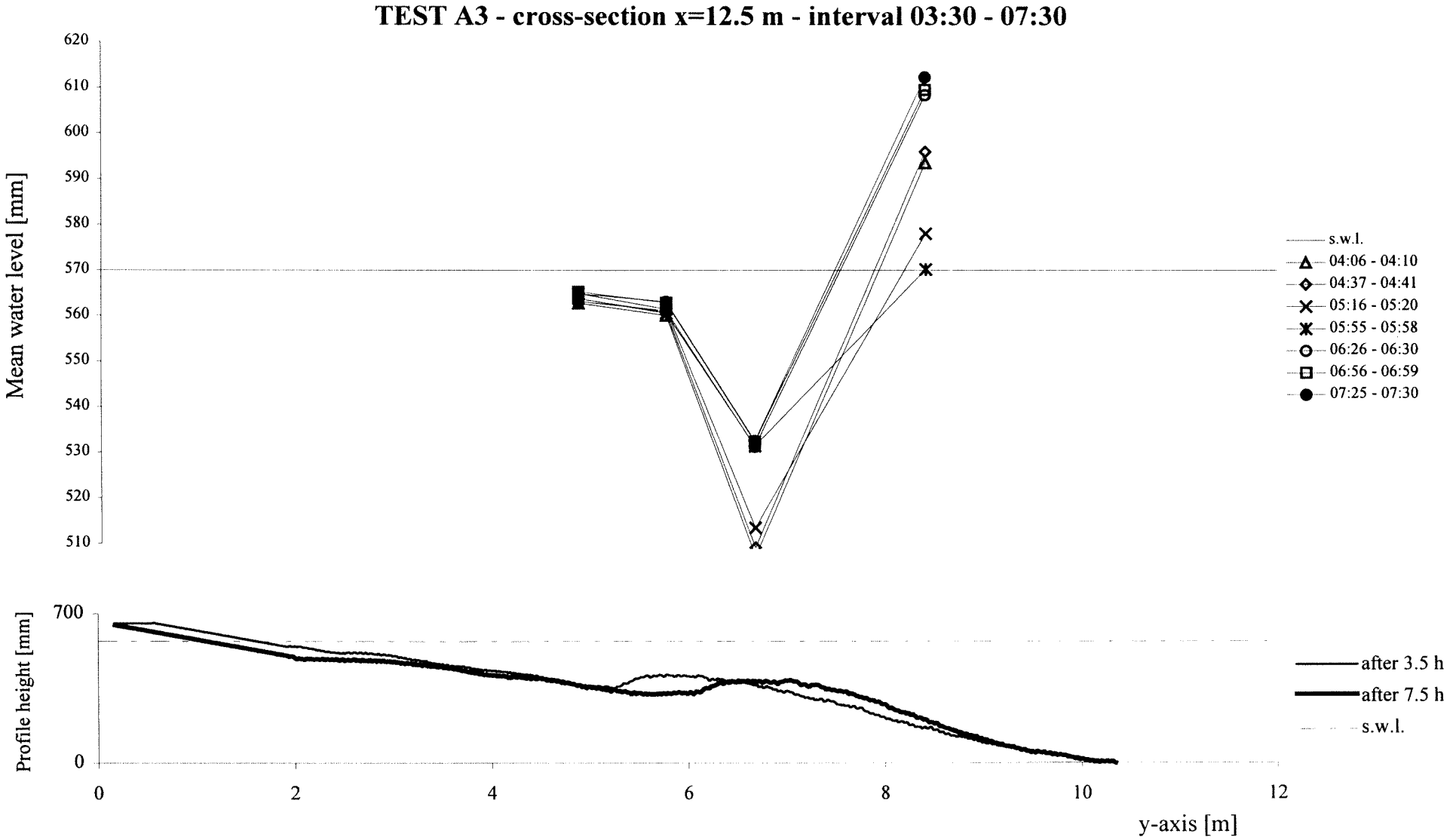
TEST A3 - cross-section x=12.5 m - interval 03:30 - 07:30
Mean water level [mm]
620
610
600
590
580
570
560
550
540
530
520
510
s.w.l.
04:06 - 04:10
04:37 - 04:41
05:16 - 05:20
05:55 - 05:58
06:26 - 06:30
06:56 - 06:59
07:25 - 07:30
Profile height [mm]
700
0
after 3.5 h
after 7.5 h
s.w.l.
0
2
4
6
8
10
12
y-axis [m]

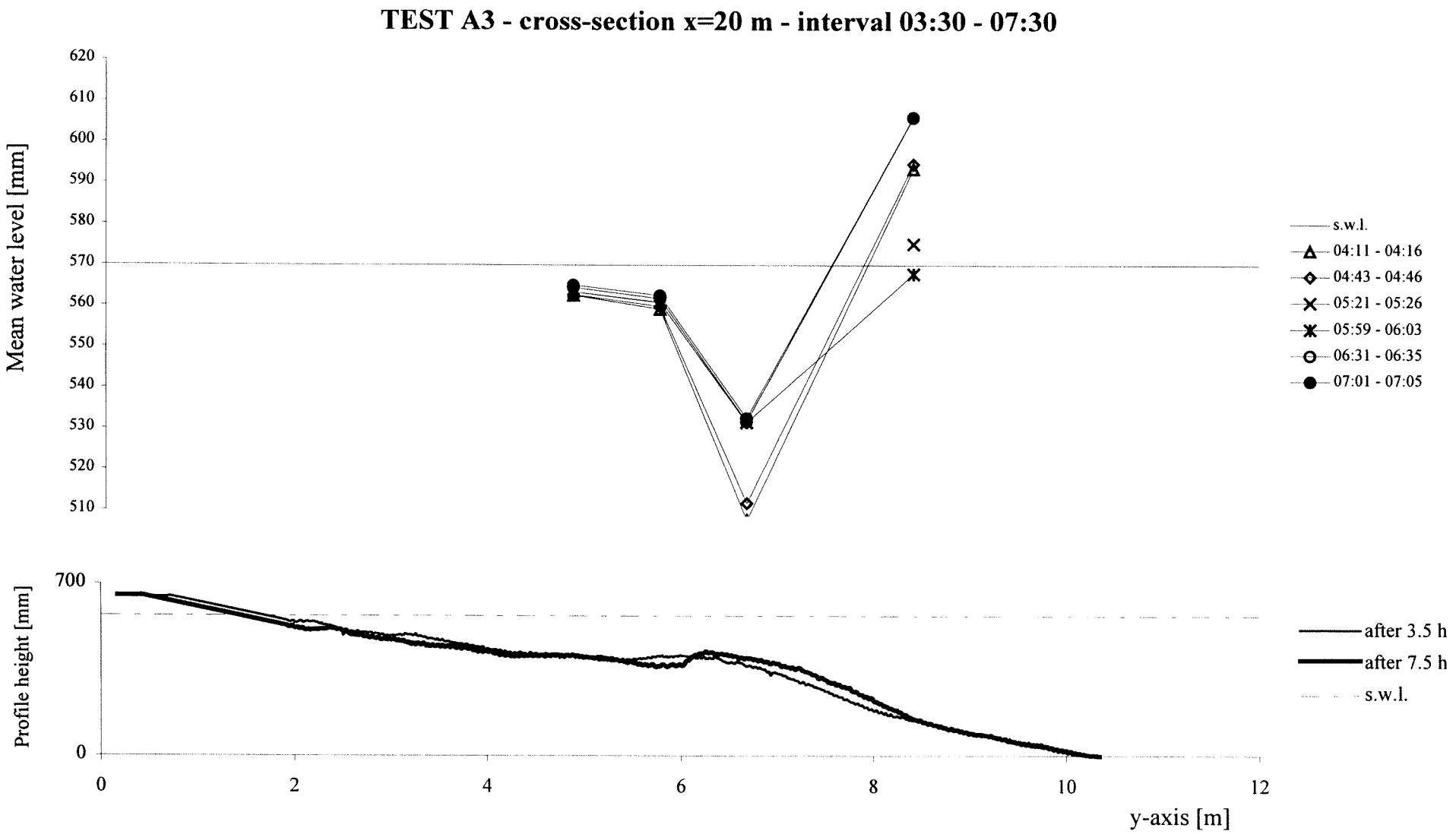
TEST A3 - cross-section x=20 m - interval 03:30 - 07:30
Mean water level [mm]
620
610
600
590
580
570
560
550
540
530
520
510
s.w.l.
04:11 - 04:16
04:43 - 04:46
05:21 - 05:26
05:59 - 06:03
06:31 - 06:35
07:01 - 07:05
Profile height [mm]
700
0
0
2
4
6
8
10
12
y-axis [m]
after 3.5 h
after 7.5 h
s.w.l.

TEST A3 - cross-section x=24.5 m - interval 03:30 - 07:30

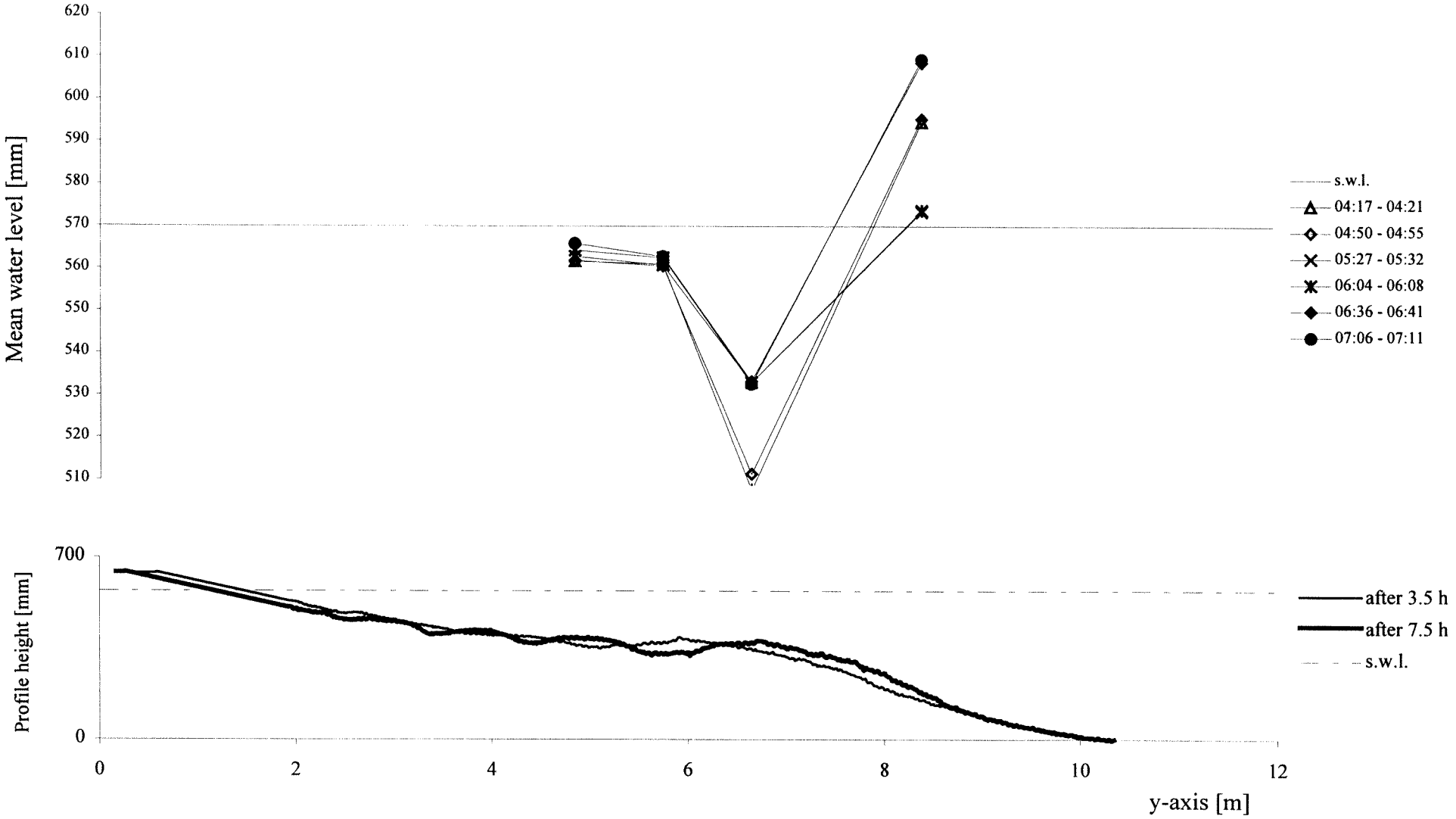

Appendix B1. Graphics TEST C1 - Average Water Level

TEST C1 - cross-section x=3 m - interval 00:00 - 00:30

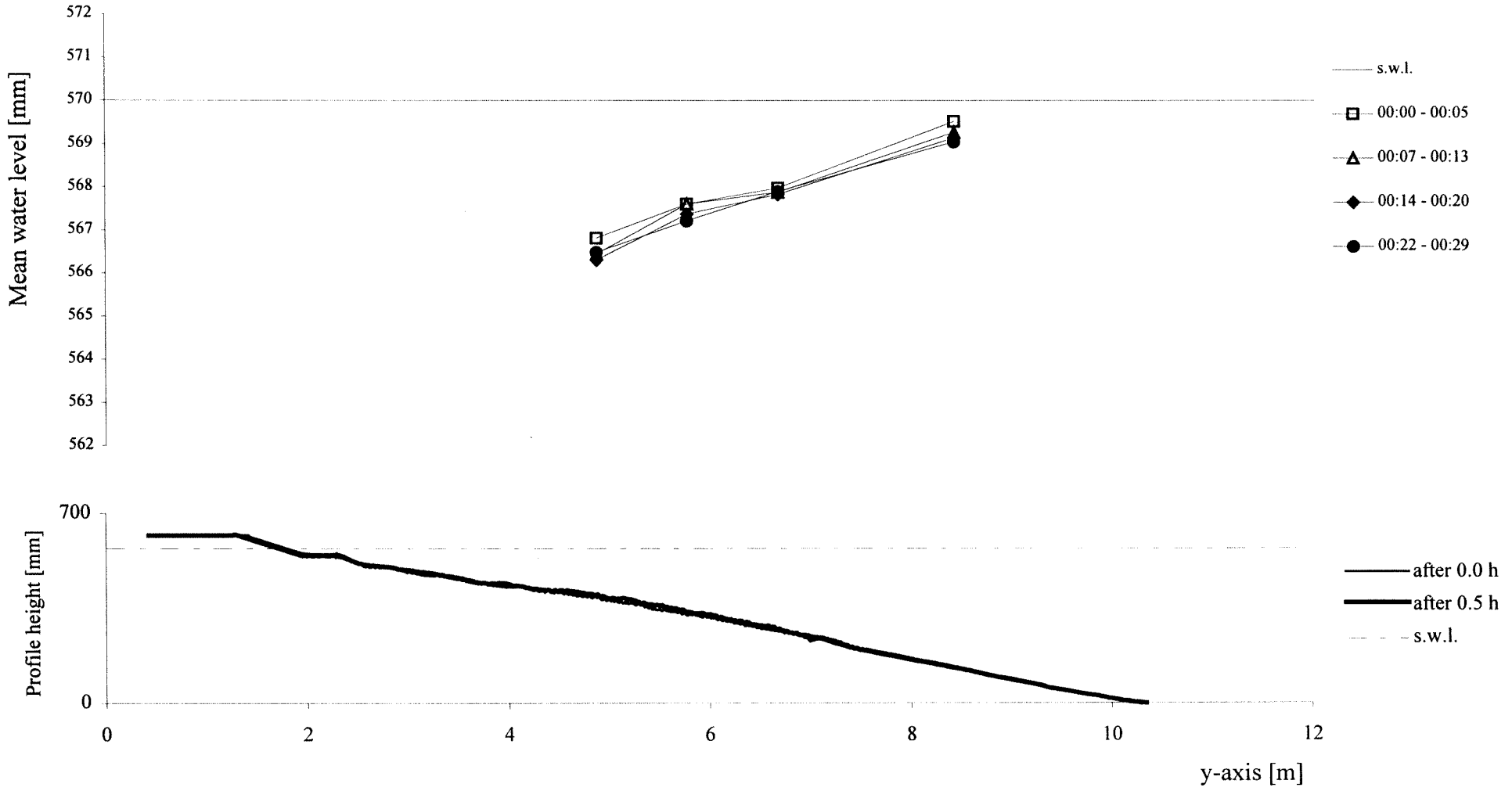

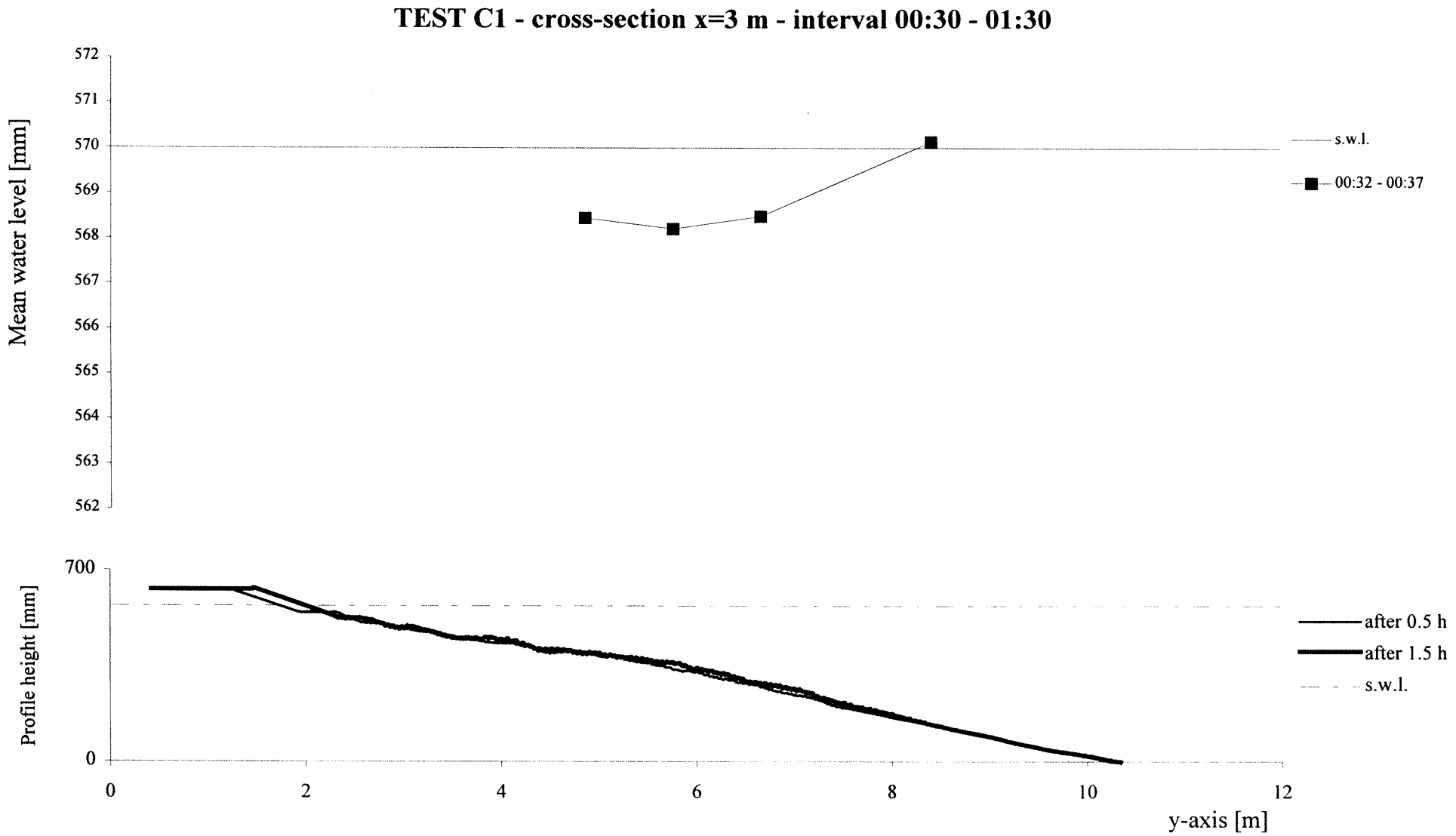
TEST C1 - cross-section x=3 m - interval 00:30 - 01:30
Mean water level [mm]
572
571
570
569
568
567
566
565
564
563
562
s.w.l.
00:32 - 00:37
Profile height [mm]
700
0
after 0.5 h
after 1.5 h
s.w.l.
0
2
4
6
8
10
12
y-axis [m]

TEST C1 - cross-section x=6.5 m - interval 00:30 - 01:30

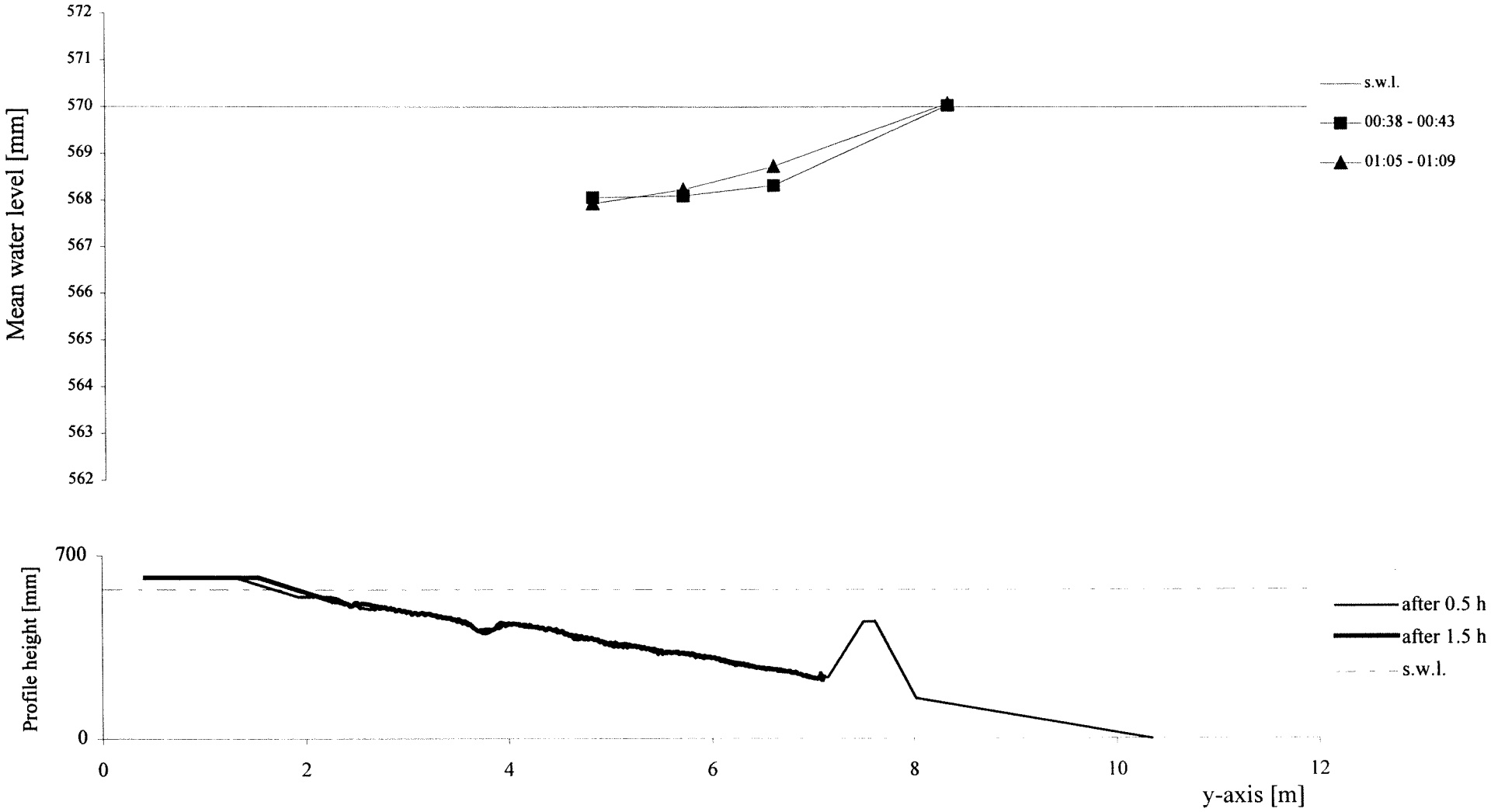

TEST C1 - cross-section x=12.5 m - interval 00:30 - 01:30

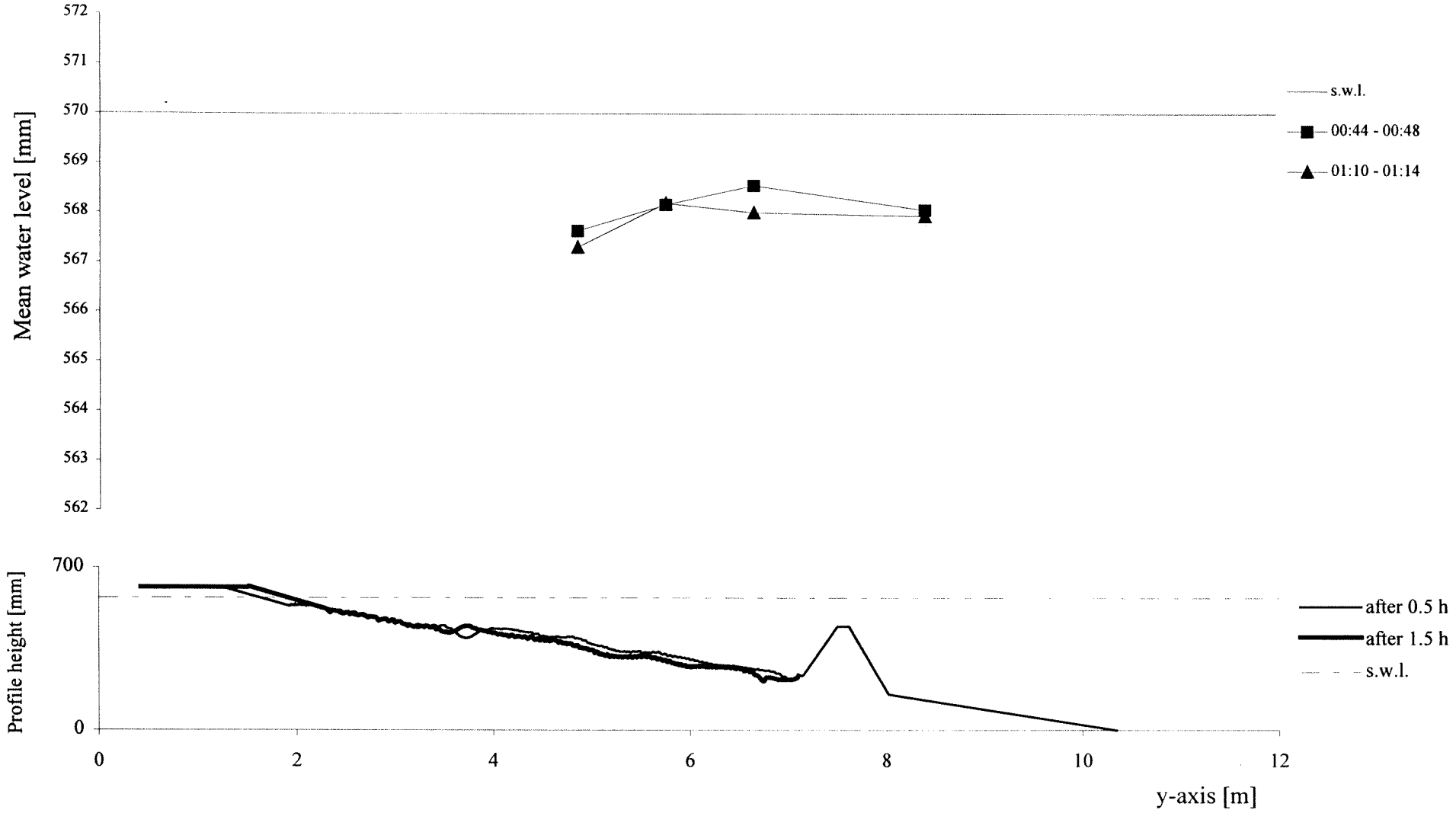

TEST C1 - cross-section x=20 m - interval 00:30 - 01:30

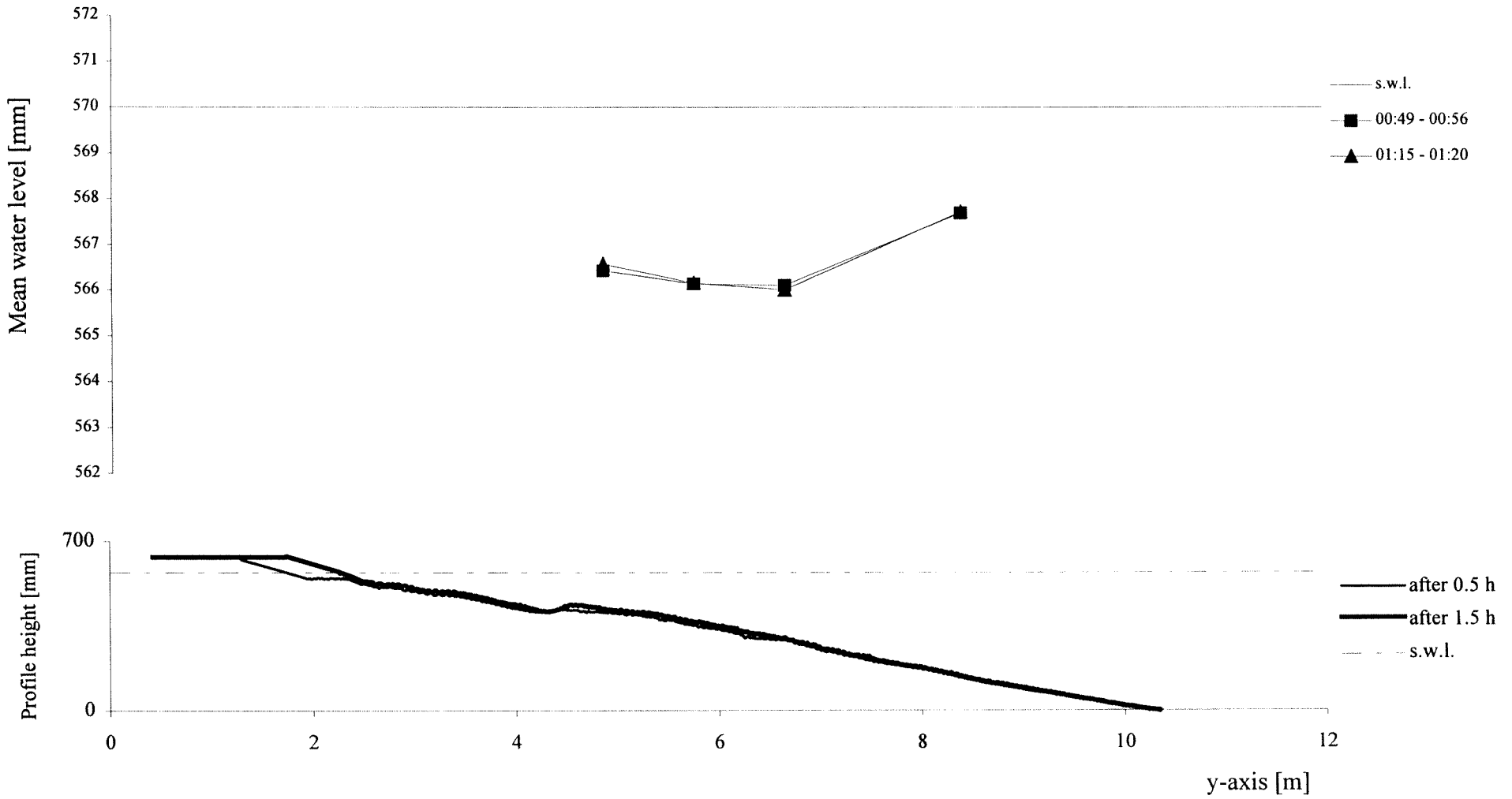

TEST C1 - cross-section x=24.5 m - interval 00:30 - 01:30

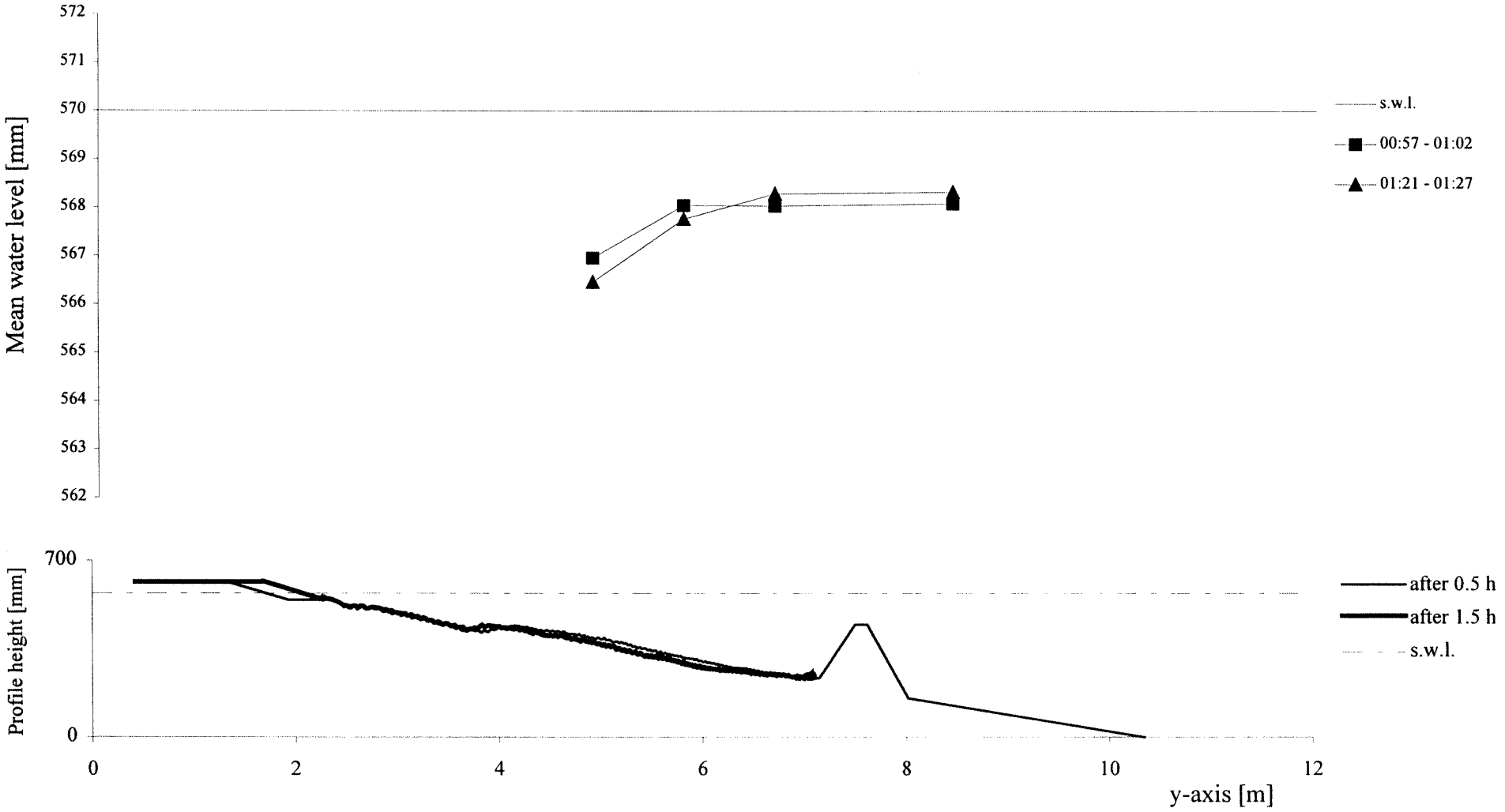

TEST C1 - cross-section x=3 m - interval 01:30 - 03:30

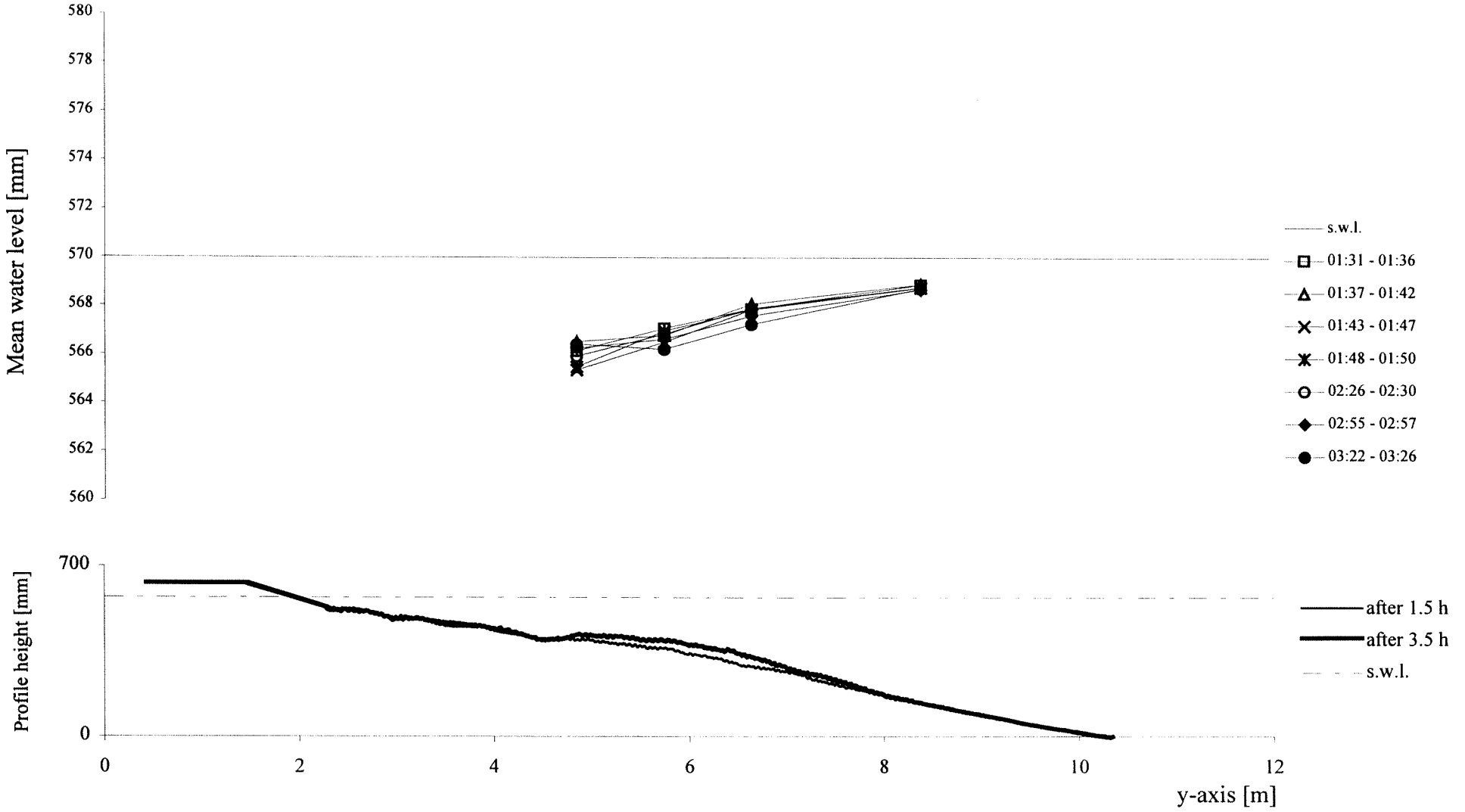

TEST C1 - cross-section x=6.5 m - interval 01:30 - 03:30

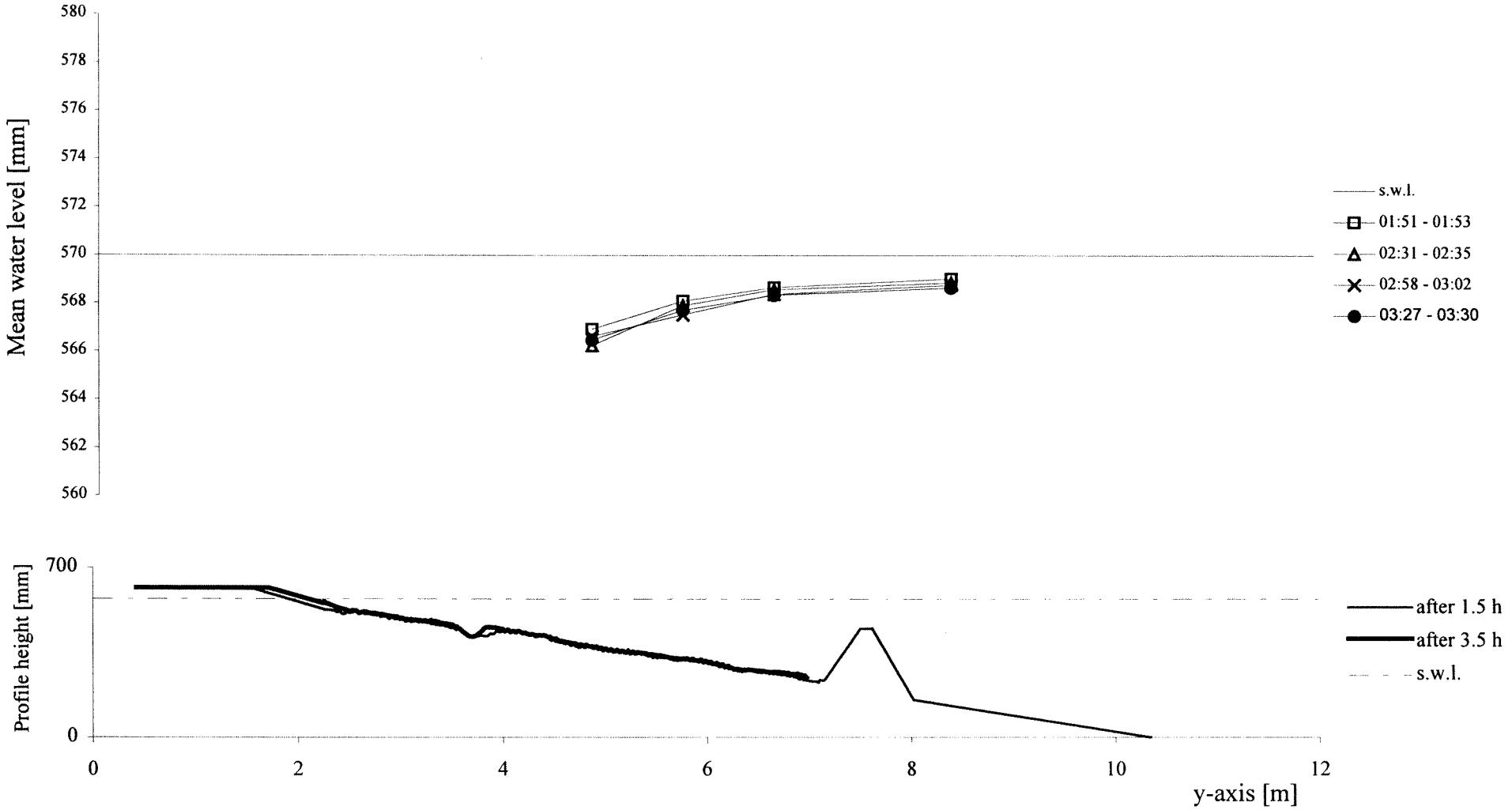

TEST C1 - cross-section x=12.5 m - interval 01:30 - 03:30

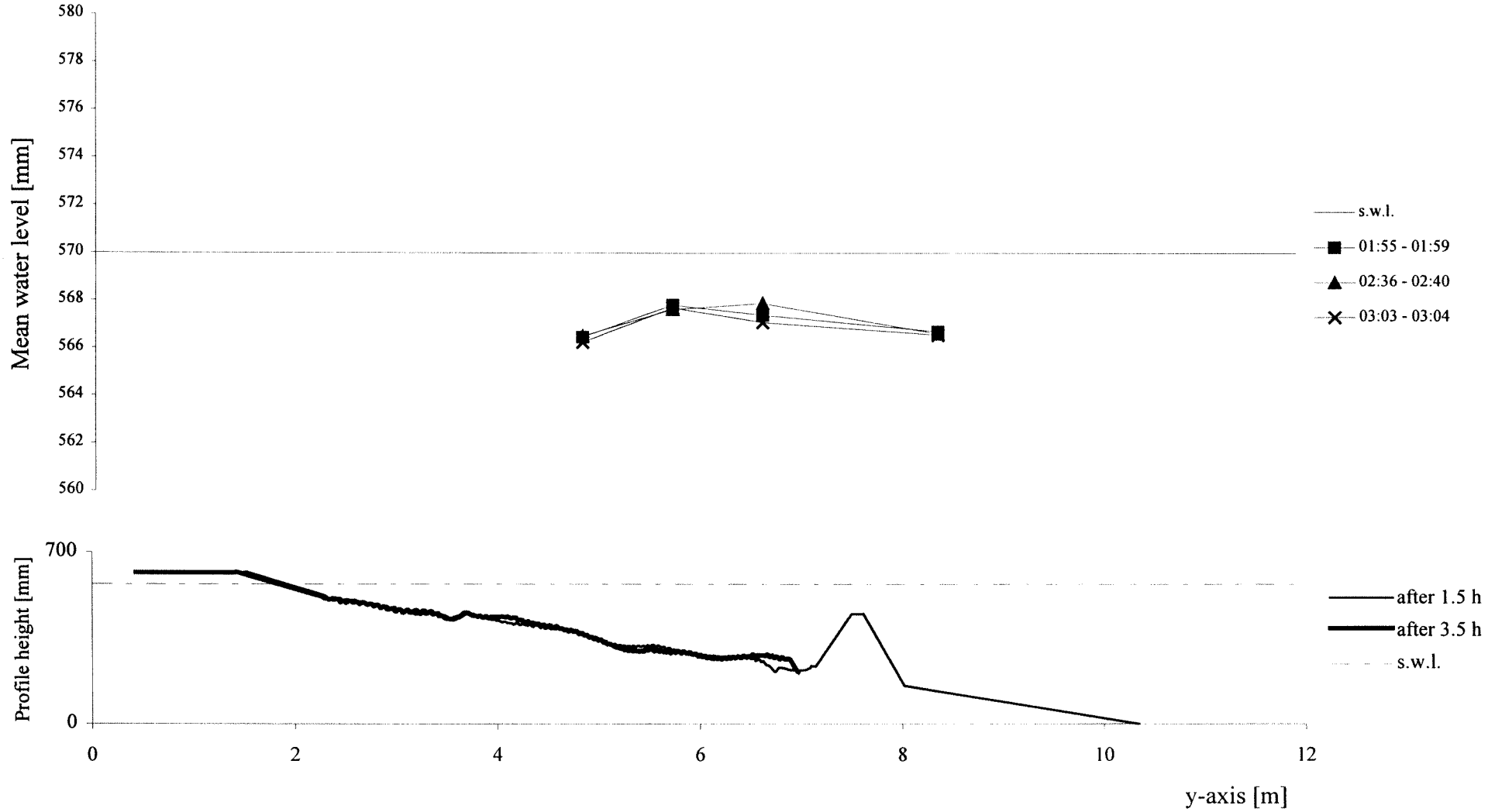

TEST C1 - cross-section x=20 m - interval 01:30 - 03:30

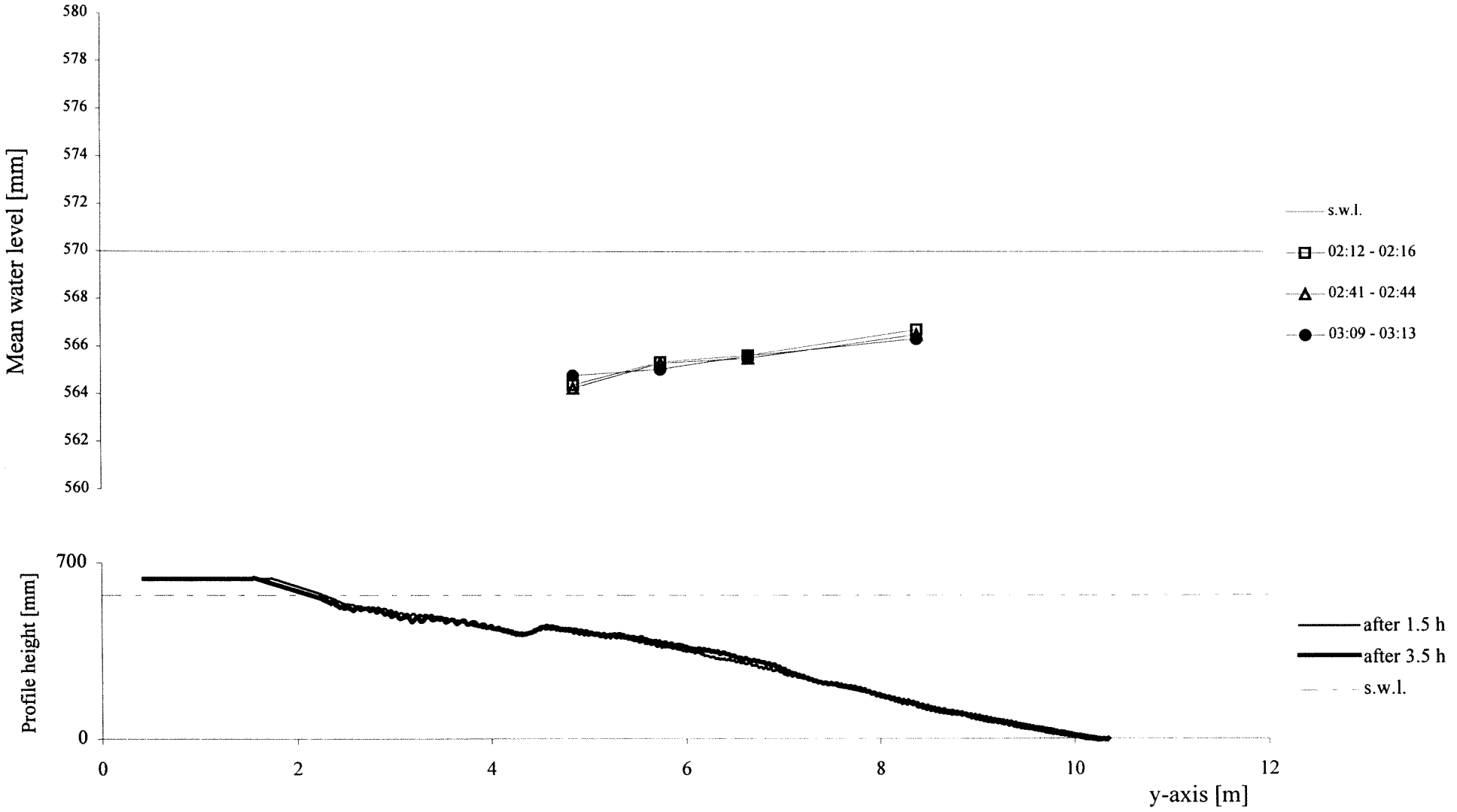

TEST C1 - cross-section x=24.5 m - interval 01:30 - 03:30

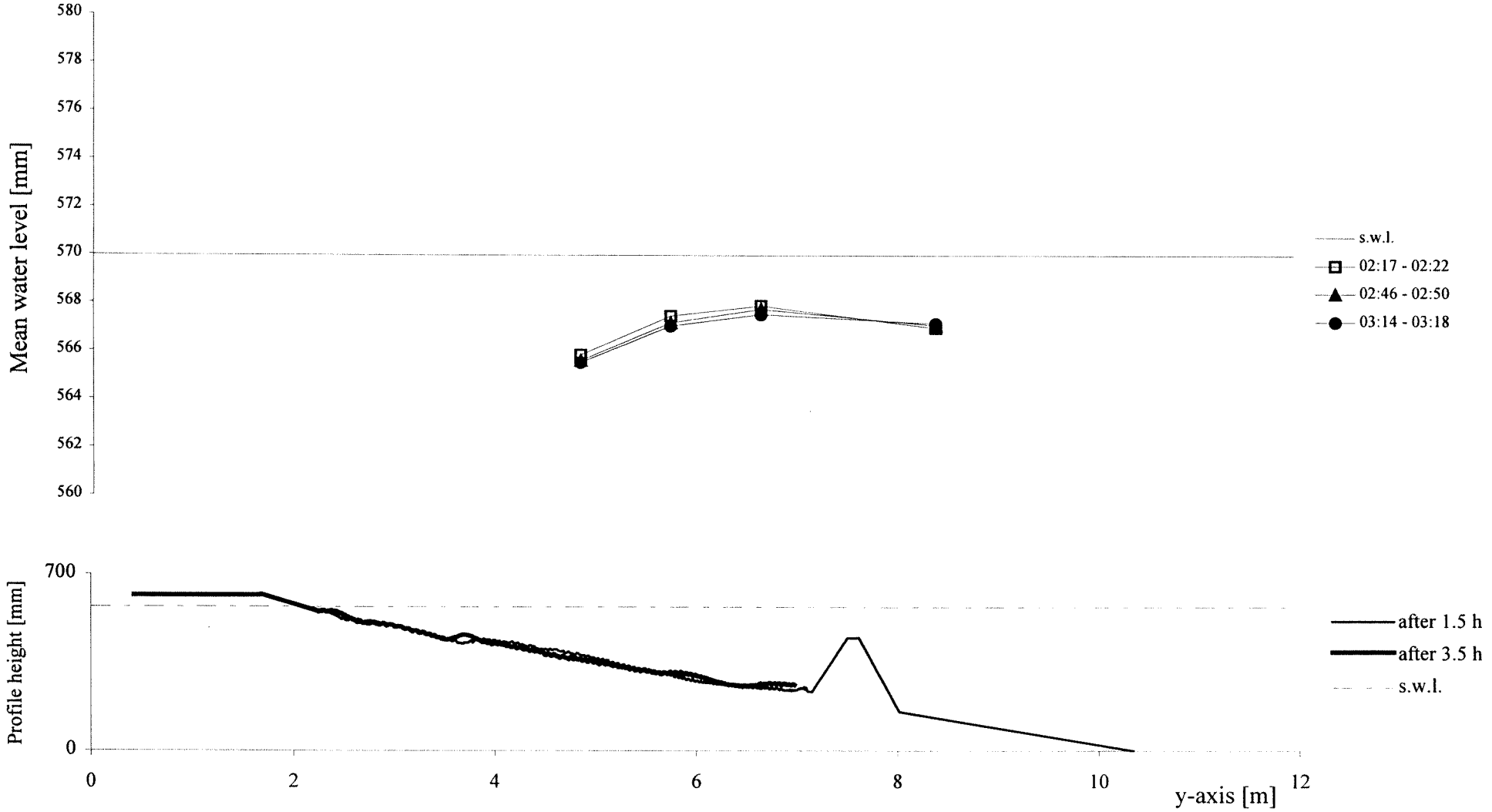

TEST C1 - cross-section x=3 m - interval 03:30 - 07:30

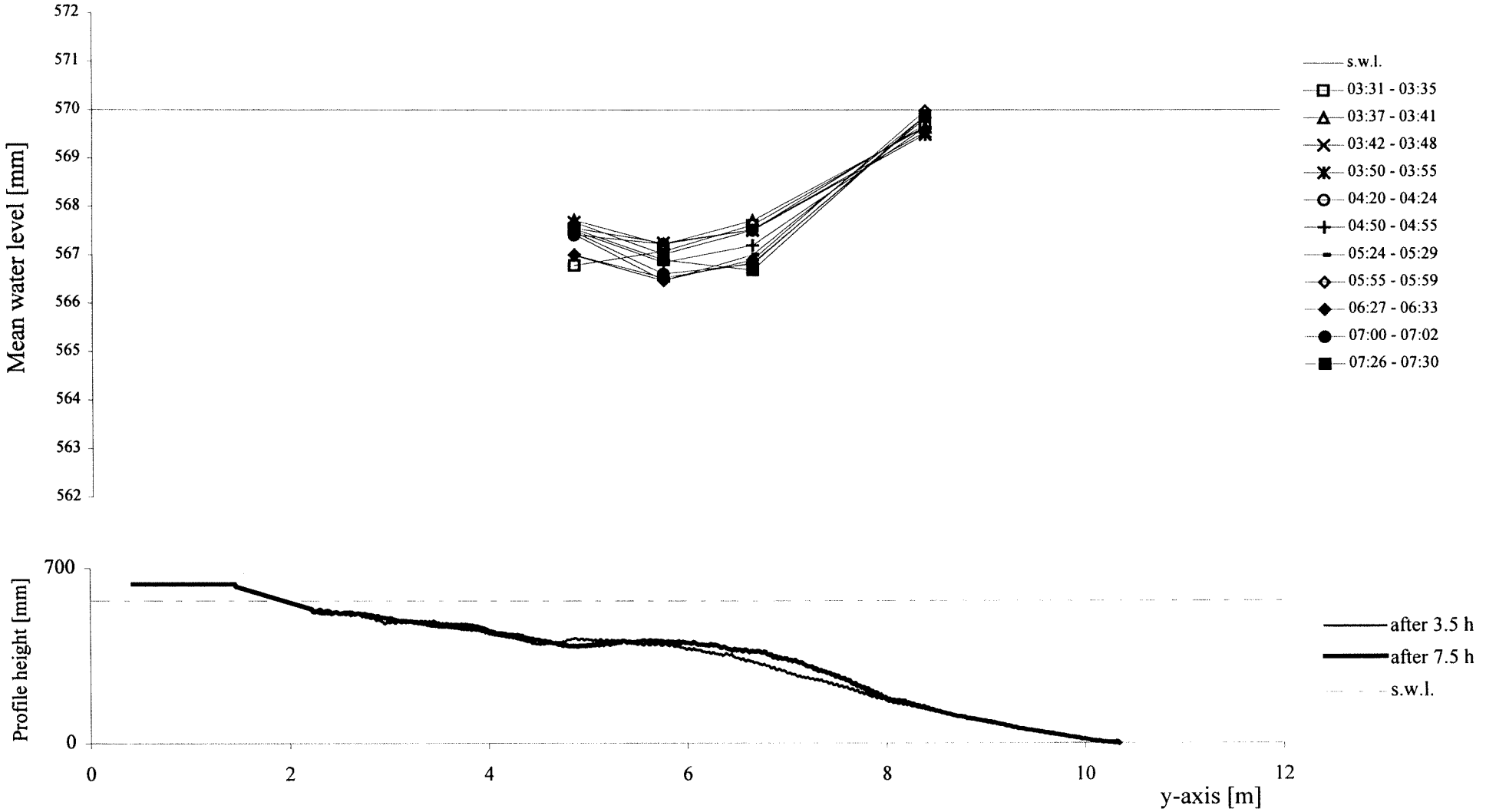

TEST C1 - cross-section x=6.5 m - interval 03:30 - 07:30

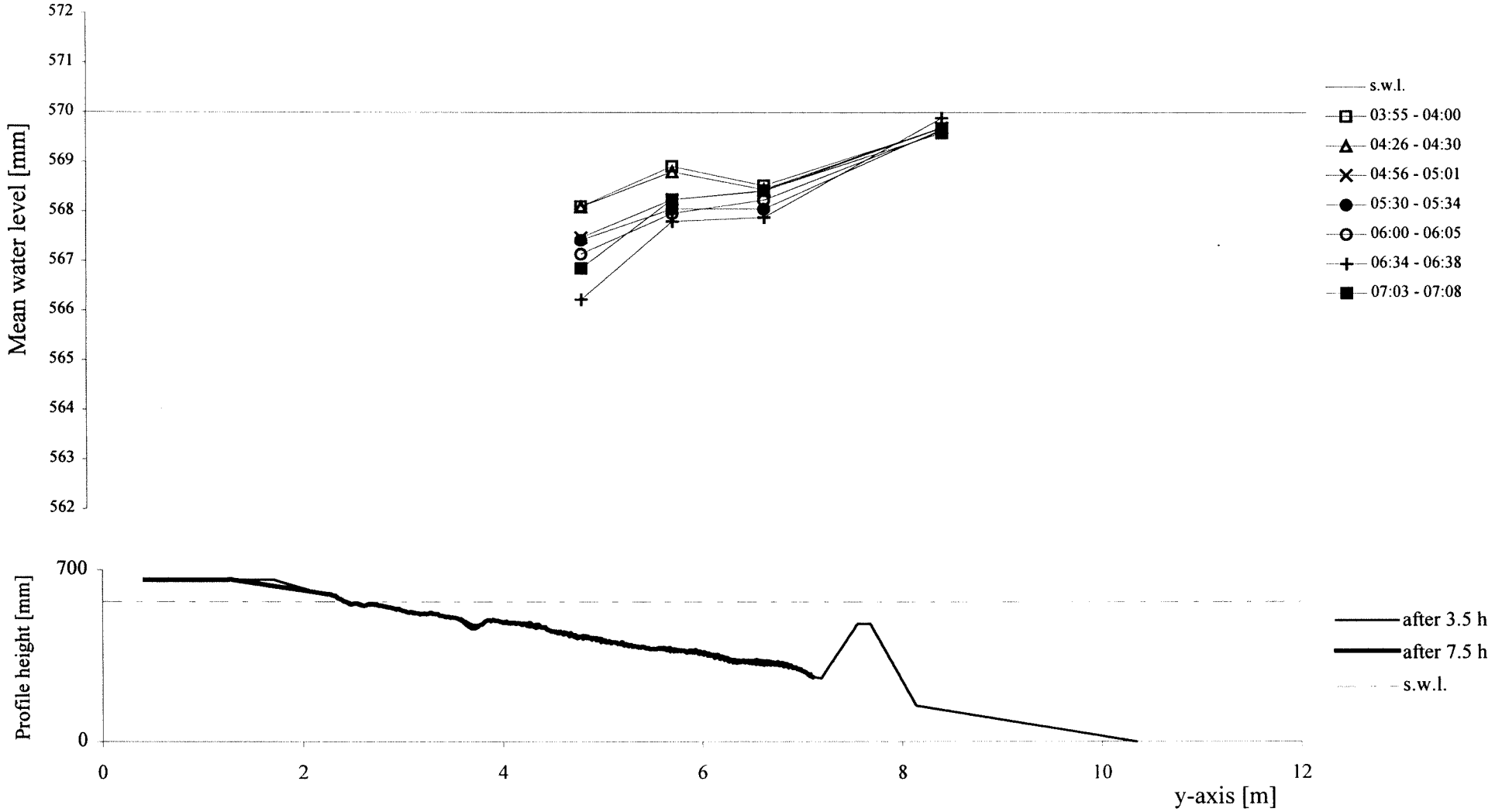

TEST C1 - cross-section x=12.5 m - interval 03:30 - 07:30

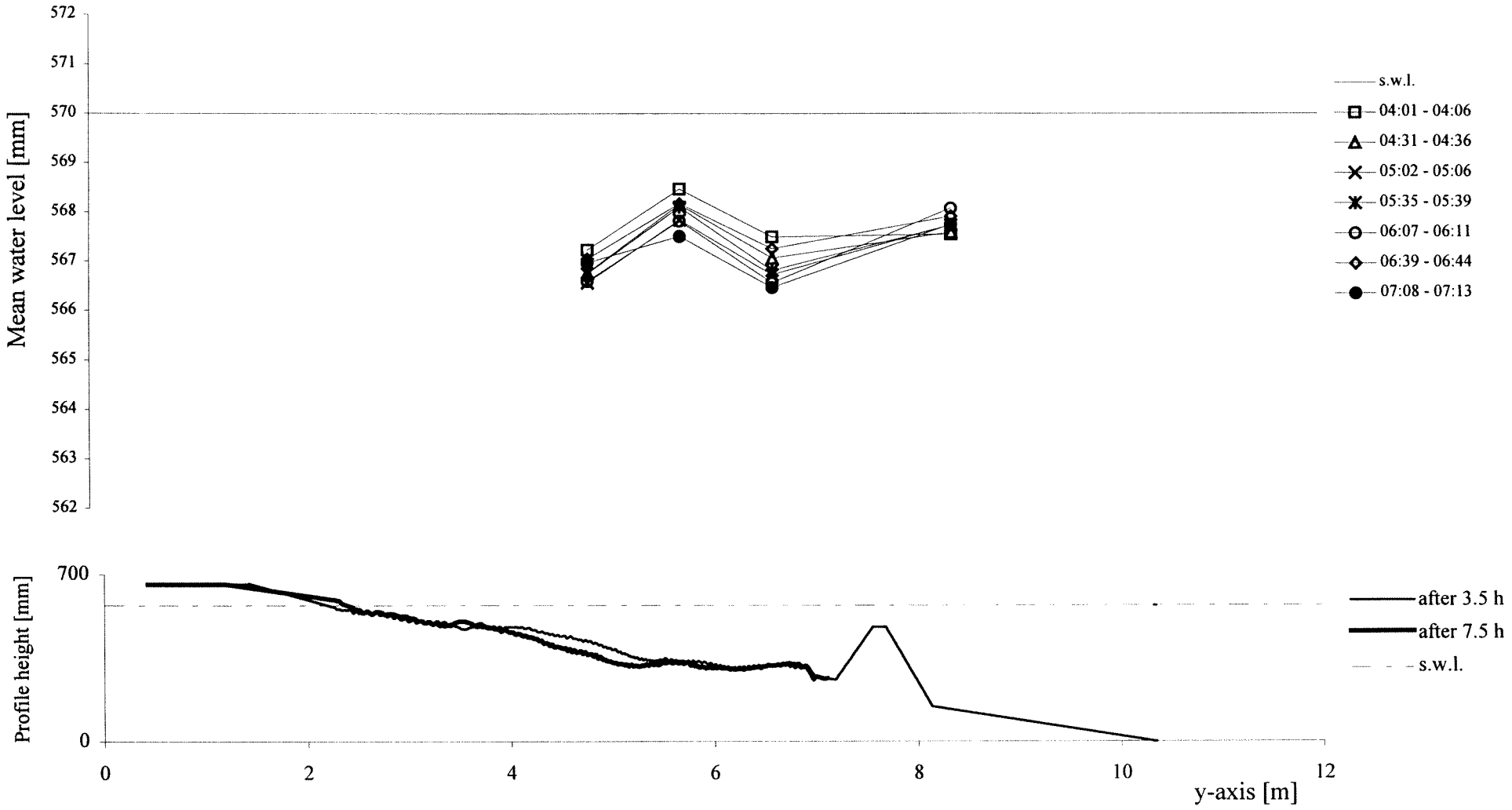

TEST C1 - cross-section x=20 m - interval 03:30 - 07:30

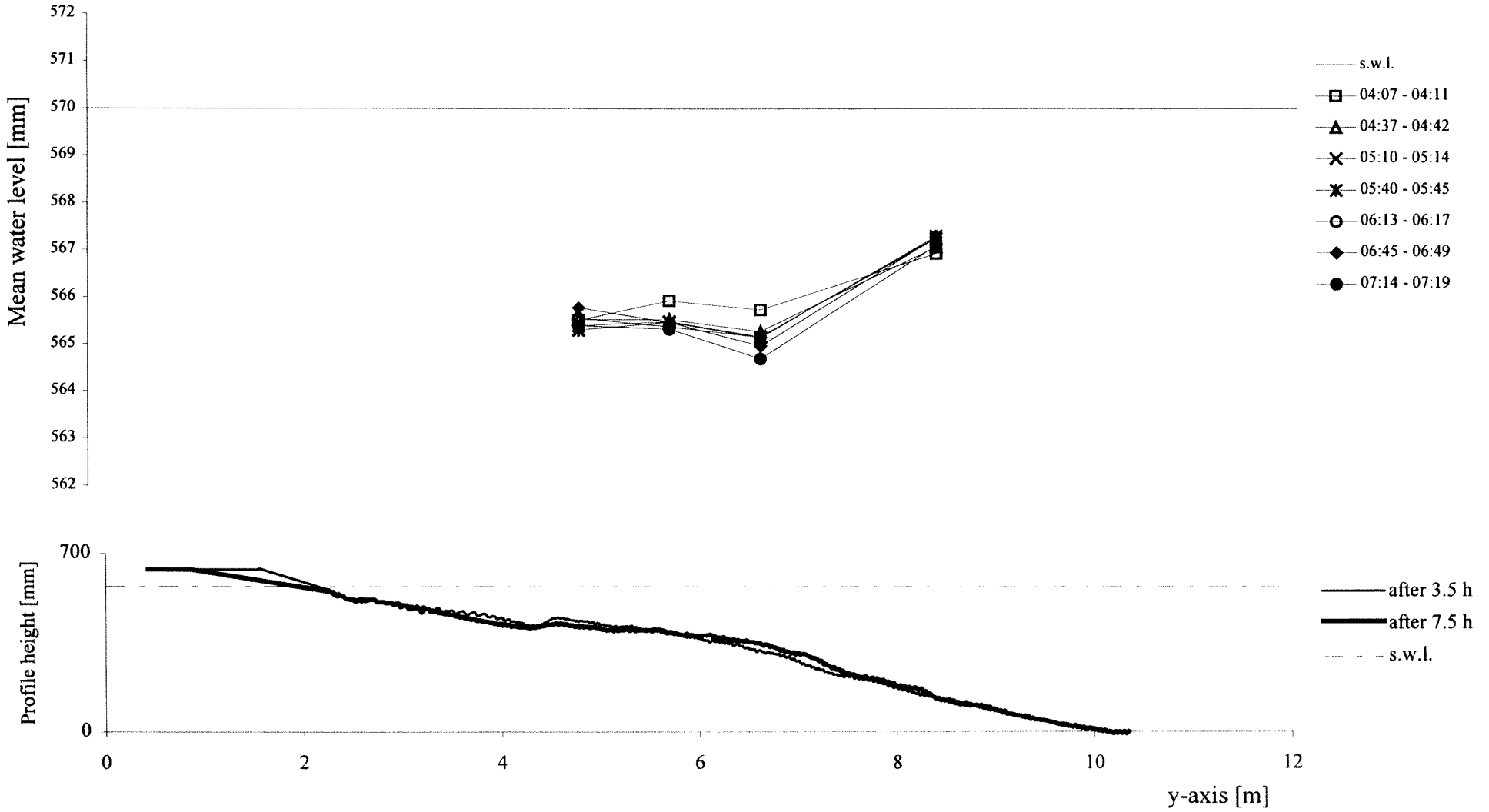

TEST C1 - cross-section x=24.5 m - interval 03:30 - 07:30

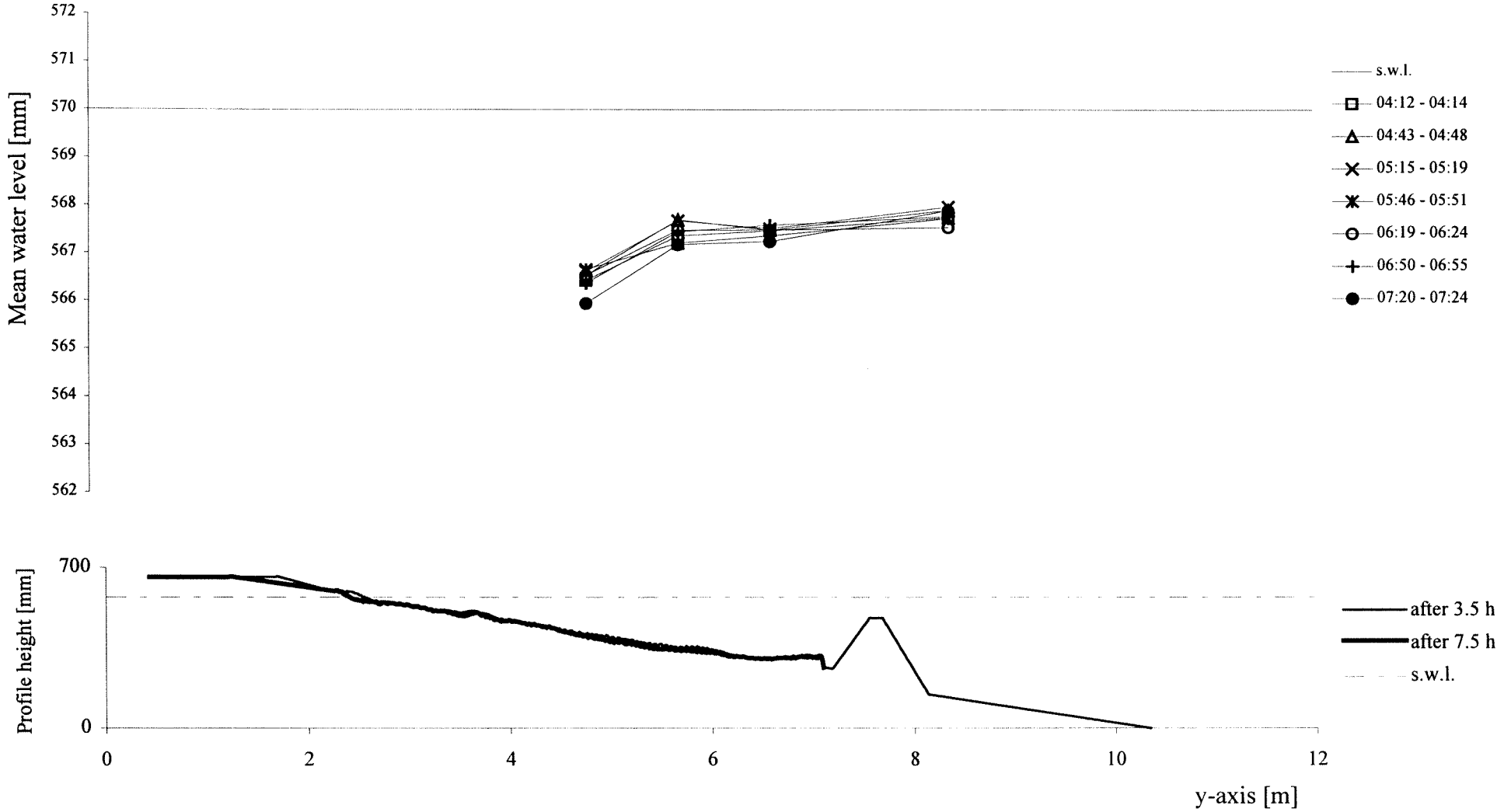

Appendix B2. Graphics TEST C2 - Average Water Level

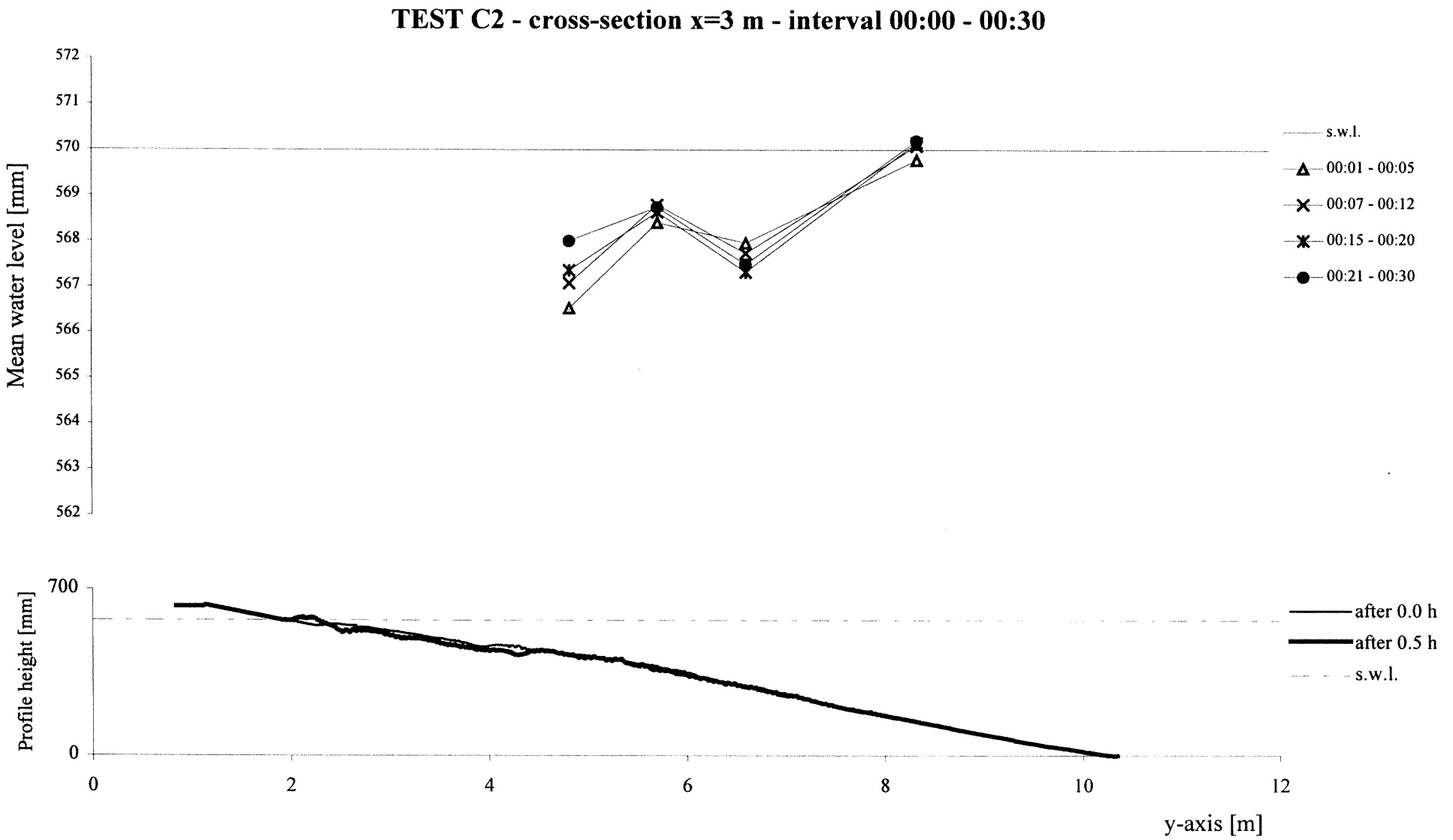
TEST C2 - cross-section x=3 m - interval 00:00 - 00:30
Mean water level [mm]
572
571
570
569
568
567
566
565
564
563
562
s.w.l.
00:01 - 00:05
00:07 - 00:12
00:15 - 00:20
00:21 - 00:30
Profile height [mm]
700
0
after 0.0 h
after 0.5 h
s.w.l.
0
2
4
6
8
10
12
y-axis [m]

TEST C2 - cross-section x=6.5 m - interval 00:30 - 01:30

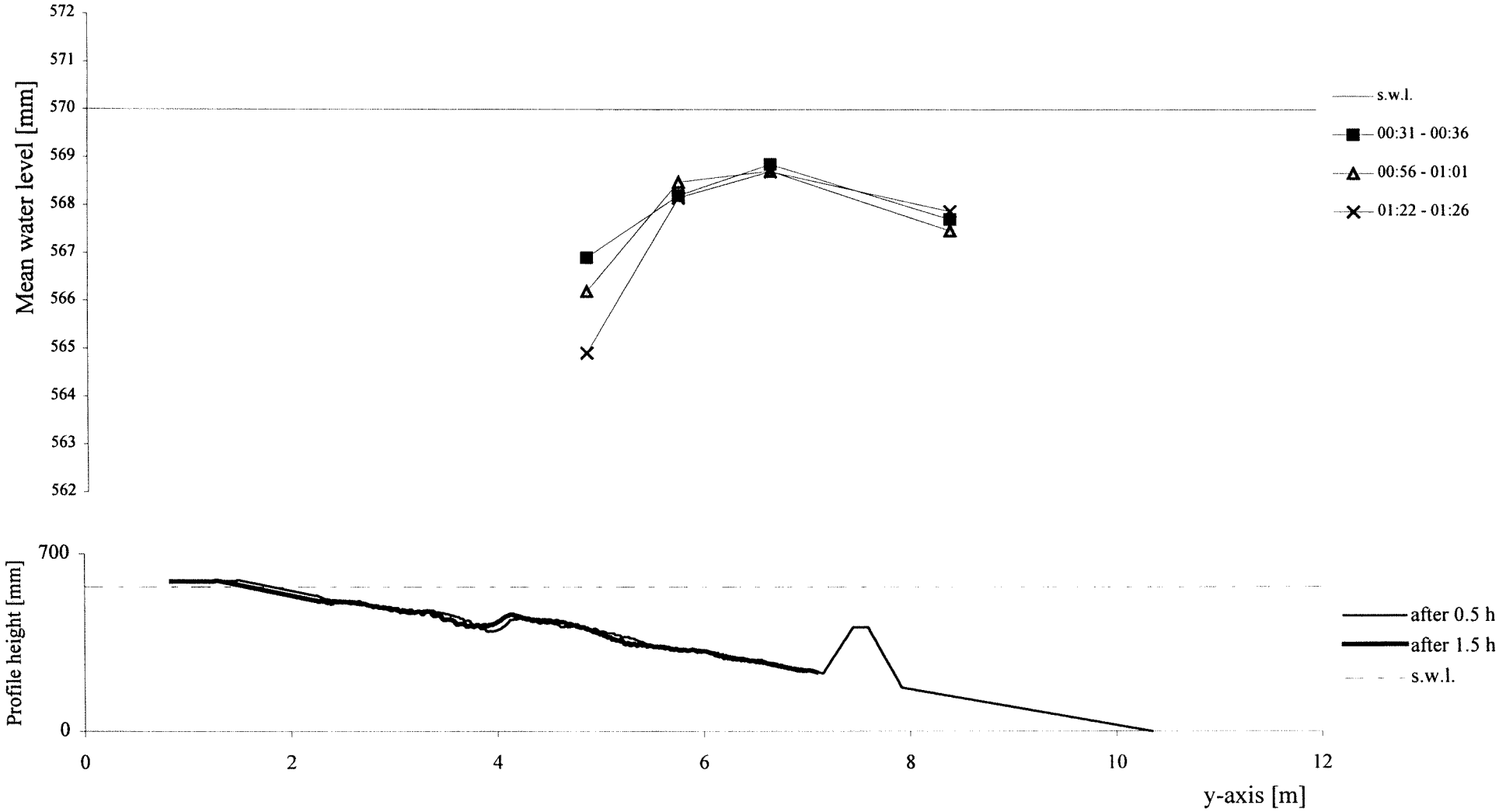

TEST C2 - cross-section x=12.5 m - interval 00:30 - 01:30

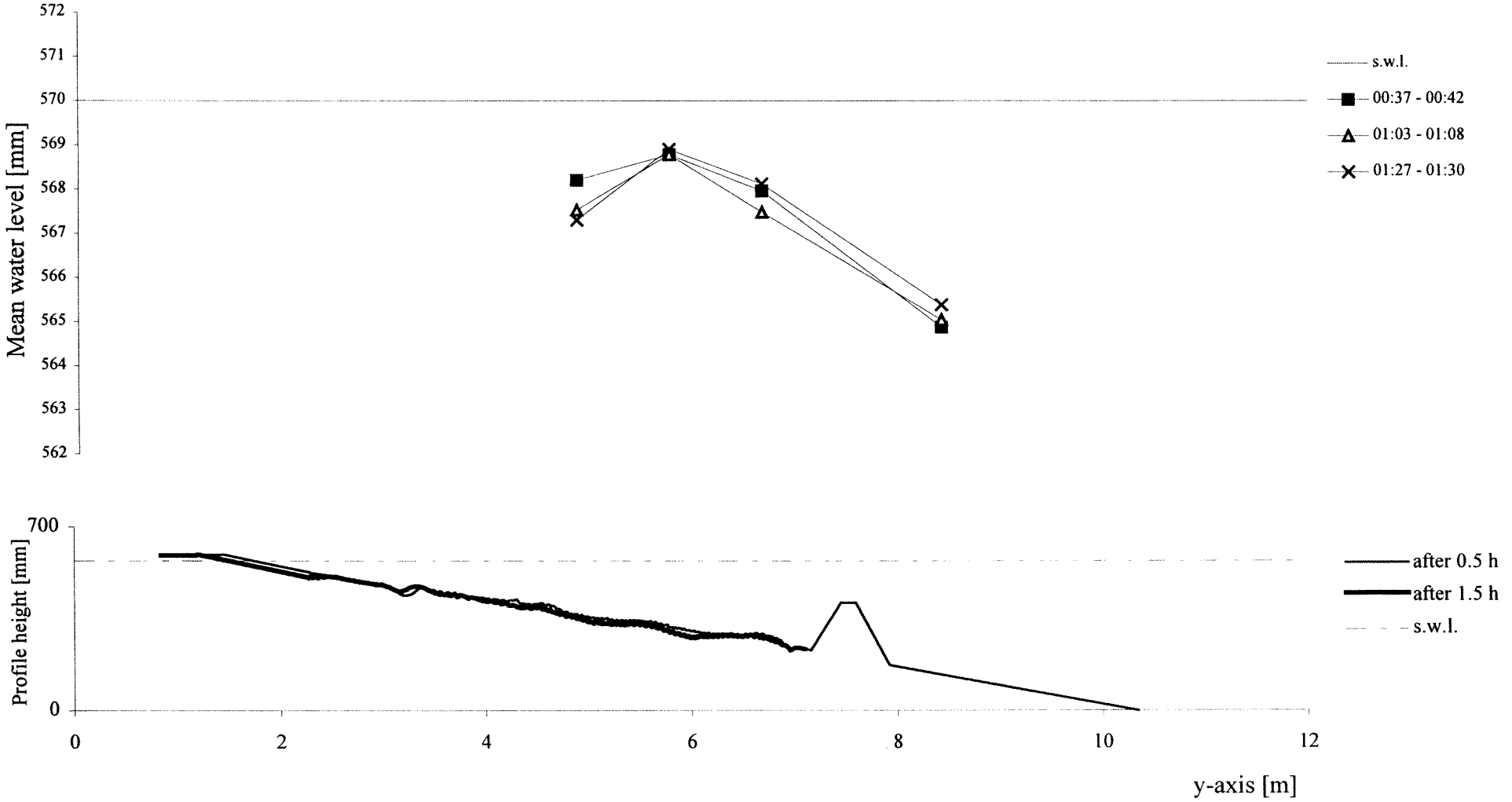

TEST C2 - cross-section x=20 m - interval 00:30 - 01:30

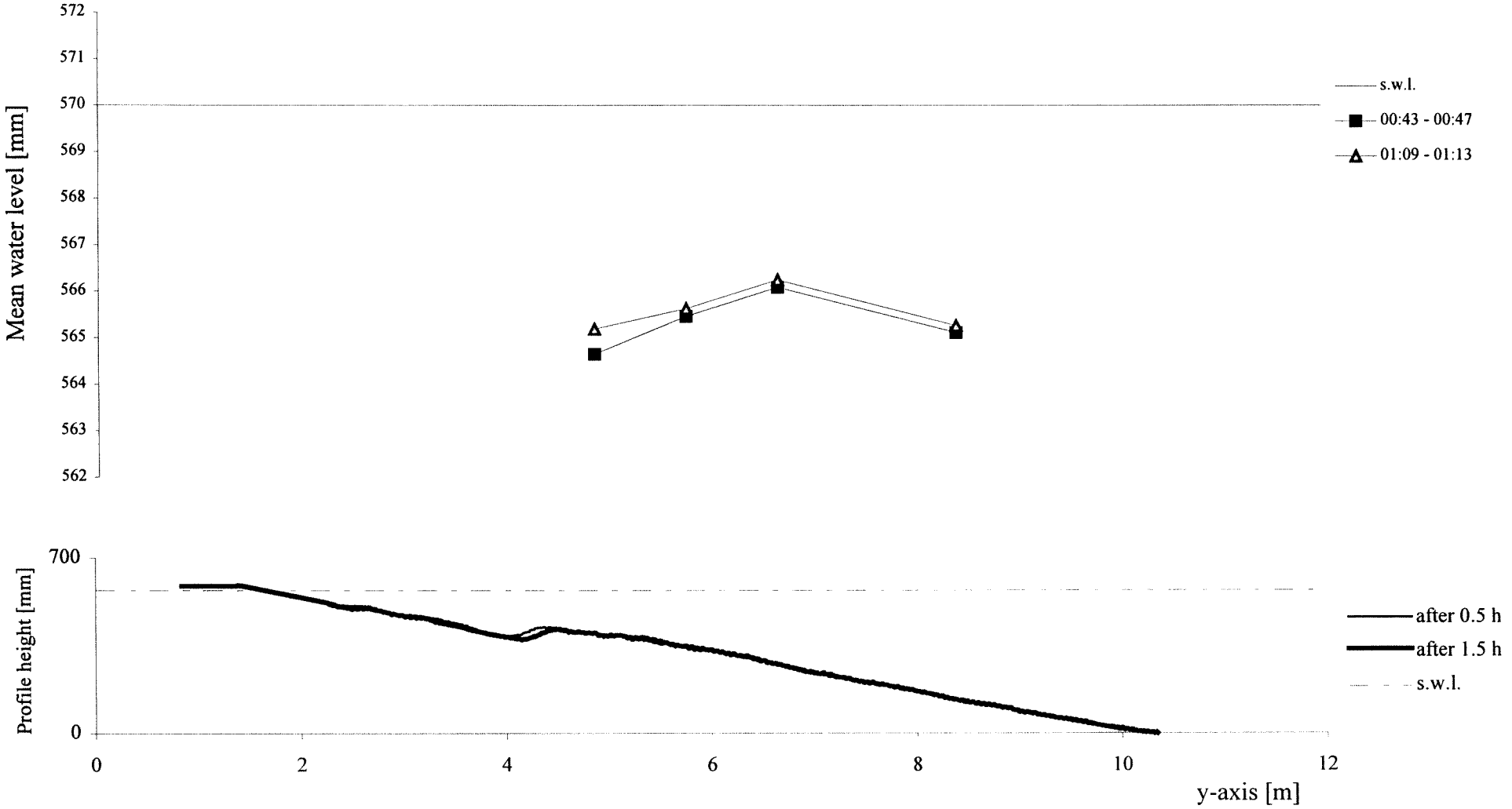

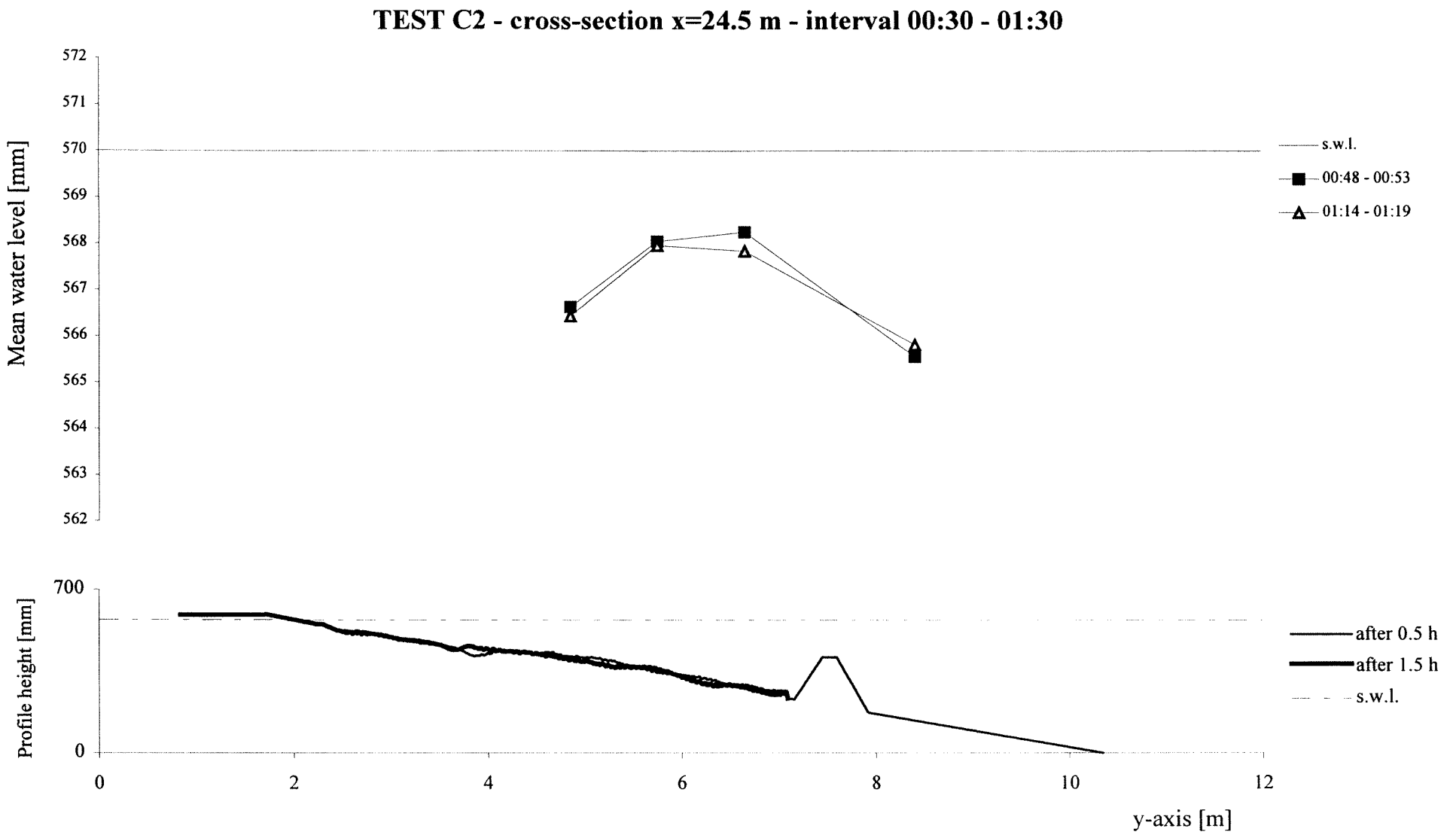
TEST C2 - cross-section x=24.5 m - interval 00:30 - 01:30
Mean water level [mm]
572
571
570
569
568
567
566
565
564
563
562
s.w.l.
00:48 - 00:53
01:14 - 01:19
Profile height [mm]
700
0
after 0.5 h
after 1.5 h
s.w.l.
0
2
4
6
8
10
12
y-axis [m]

TEST C2 - cross-section x=3 m - interval 01:30 - 03:30

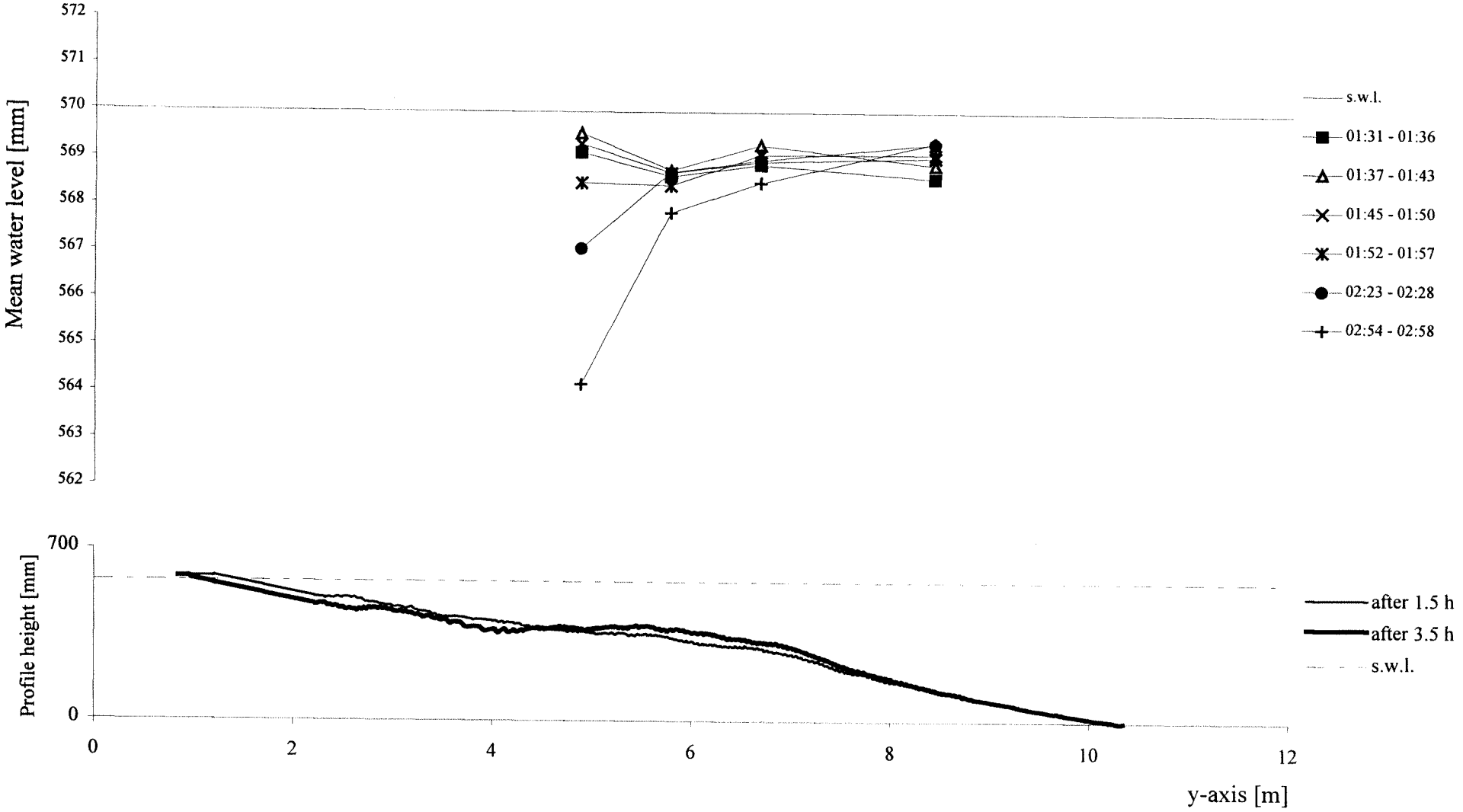

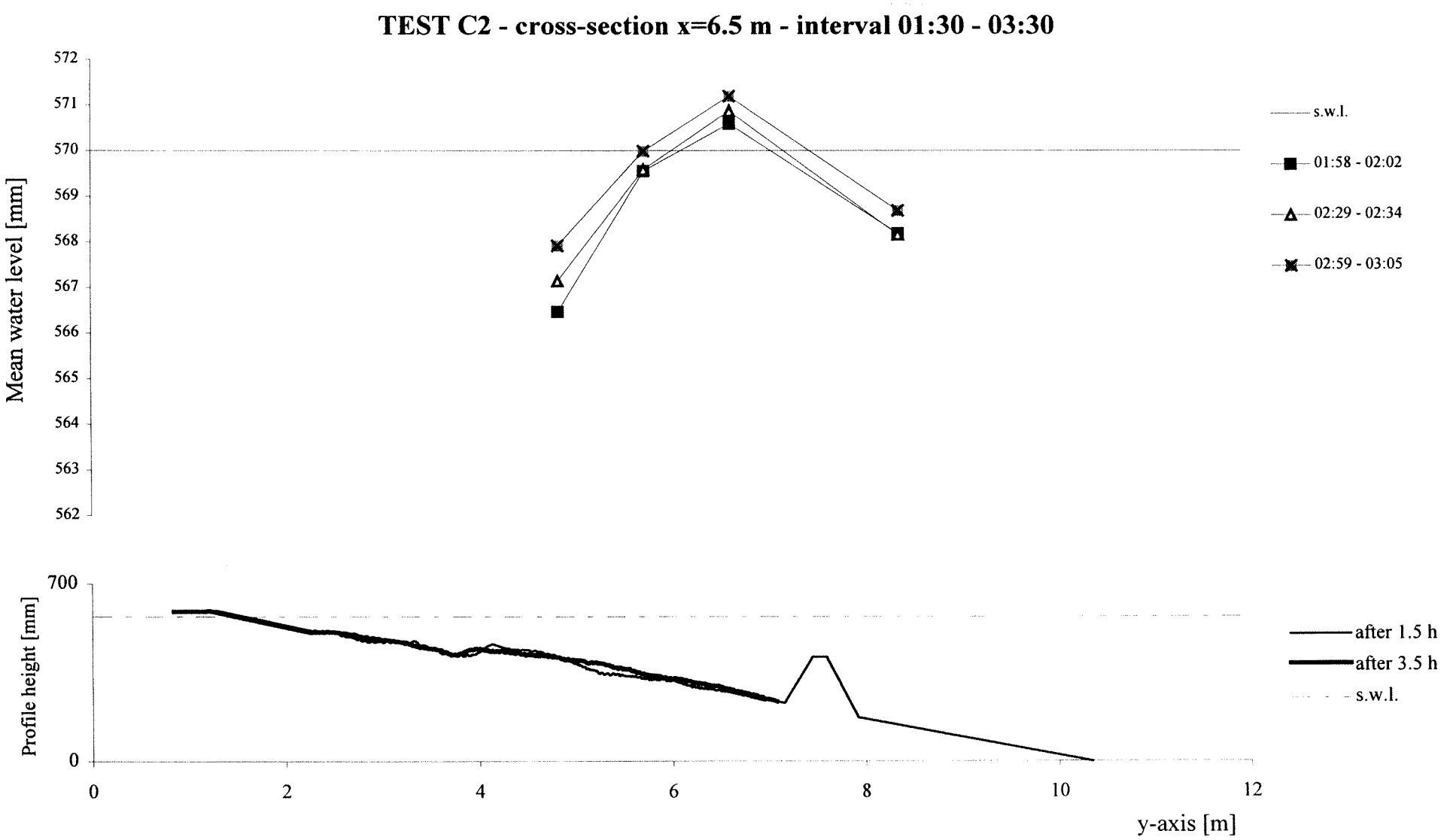
TEST C2 - cross-section x=6.5 m - interval 01:30 - 03:30
Mean water level [mm]
572
571
570
569
568
567
566
565
564
563
562
s.w.l.
01:58 - 02:02
02:29 - 02:34
02:59 - 03:05
Profile height [mm]
700
0
after 1.5 h
after 3.5 h
s.w.l.
0
2
4
6
8
10
12
y-axis [m]

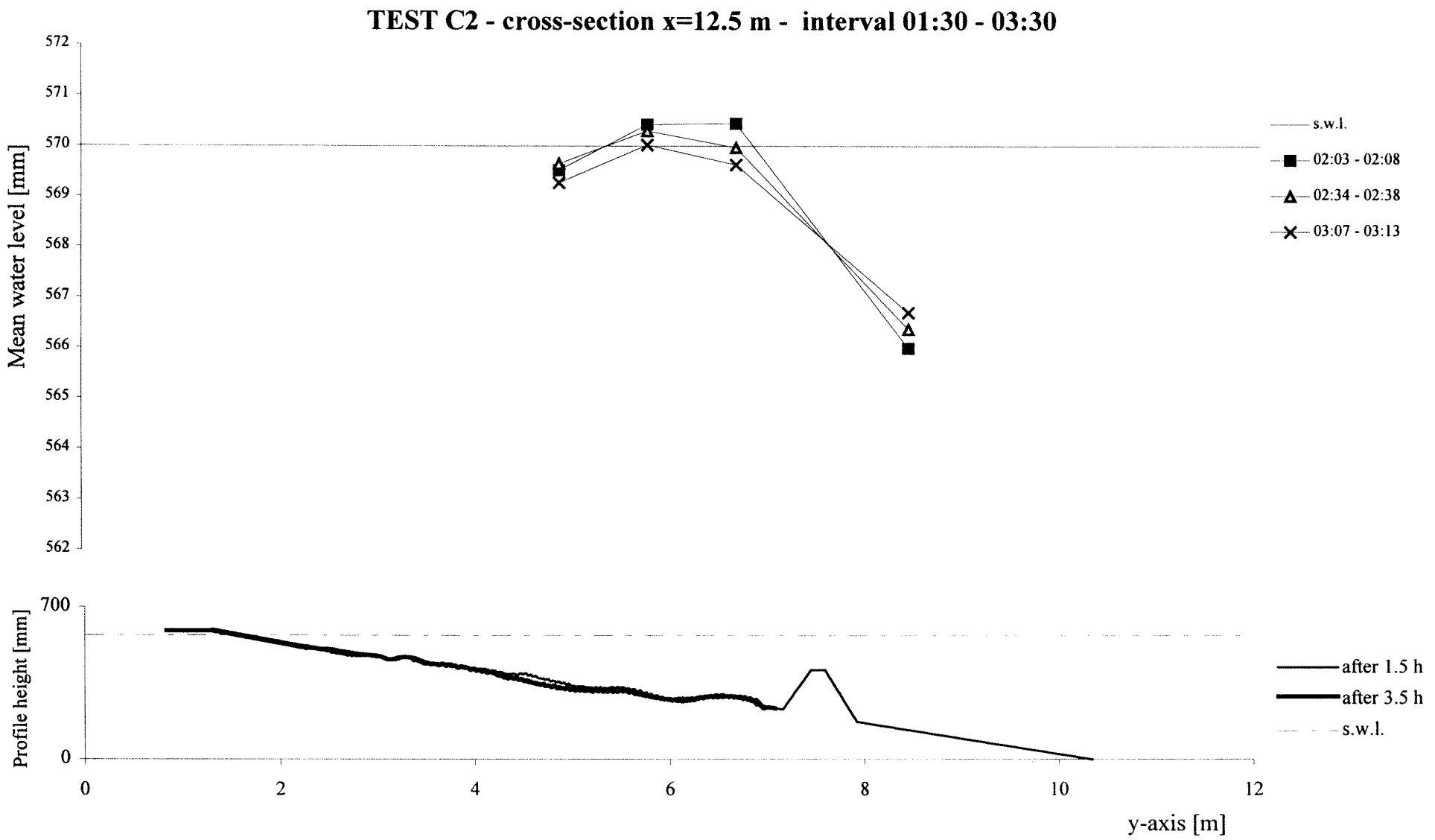
TEST C2 - cross-section x=12.5 m - interval 01:30 - 03:30
Mean water level [mm]
572
571
570
569
568
567
566
565
564
563
562
s.w.l.
02:03 - 02:08
02:34 - 02:38
03:07 - 03:13
Profile height [mm]
700
0
after 1.5 h
after 3.5 h
s.w.l.
0
2
4
6
8
10
12
y-axis [m]

TEST C2 - cross-section x=20 m - interval 01:30 - 03:30

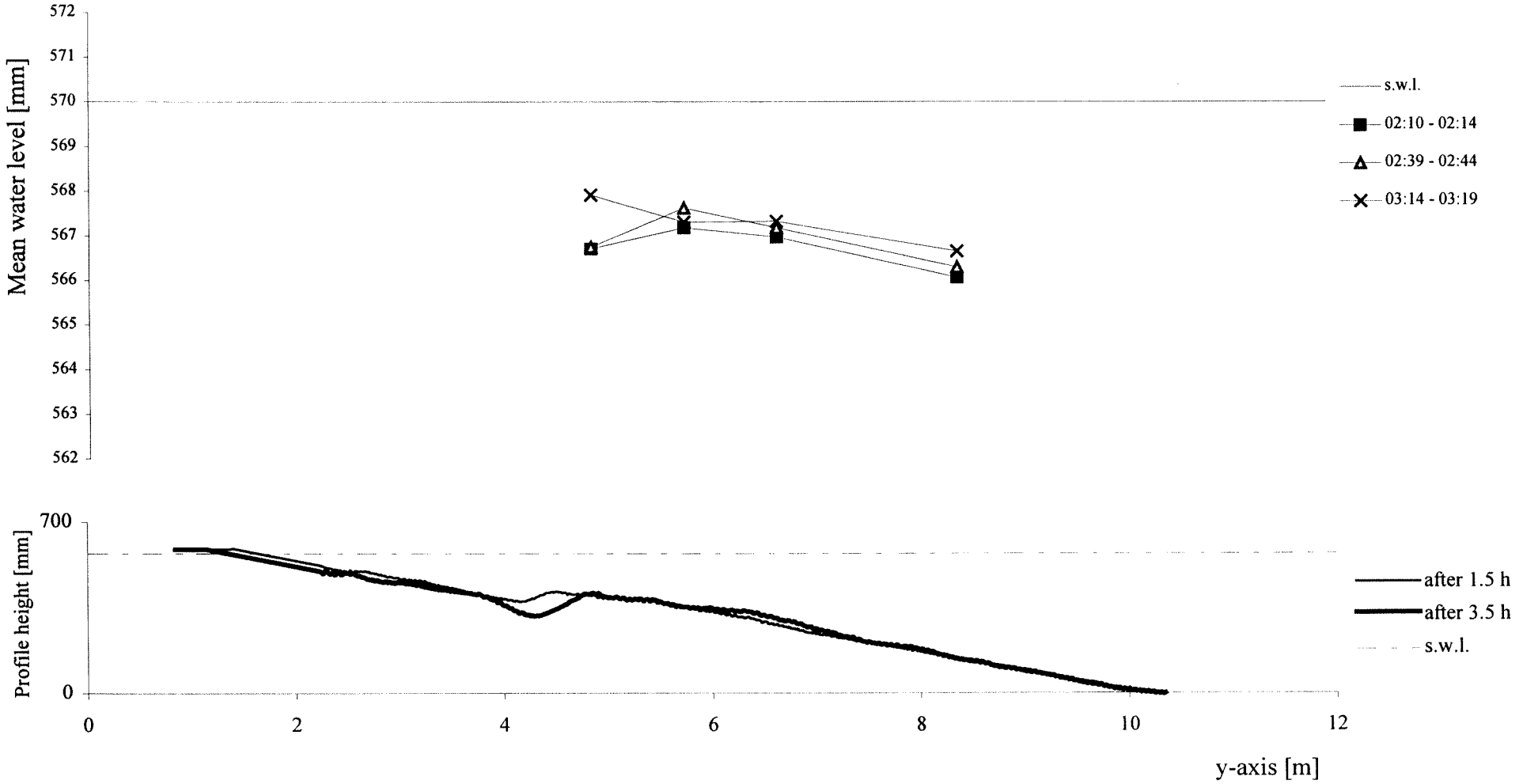

TEST C2 - cross-section x=24.5 m - interval 01:30 - 03:30

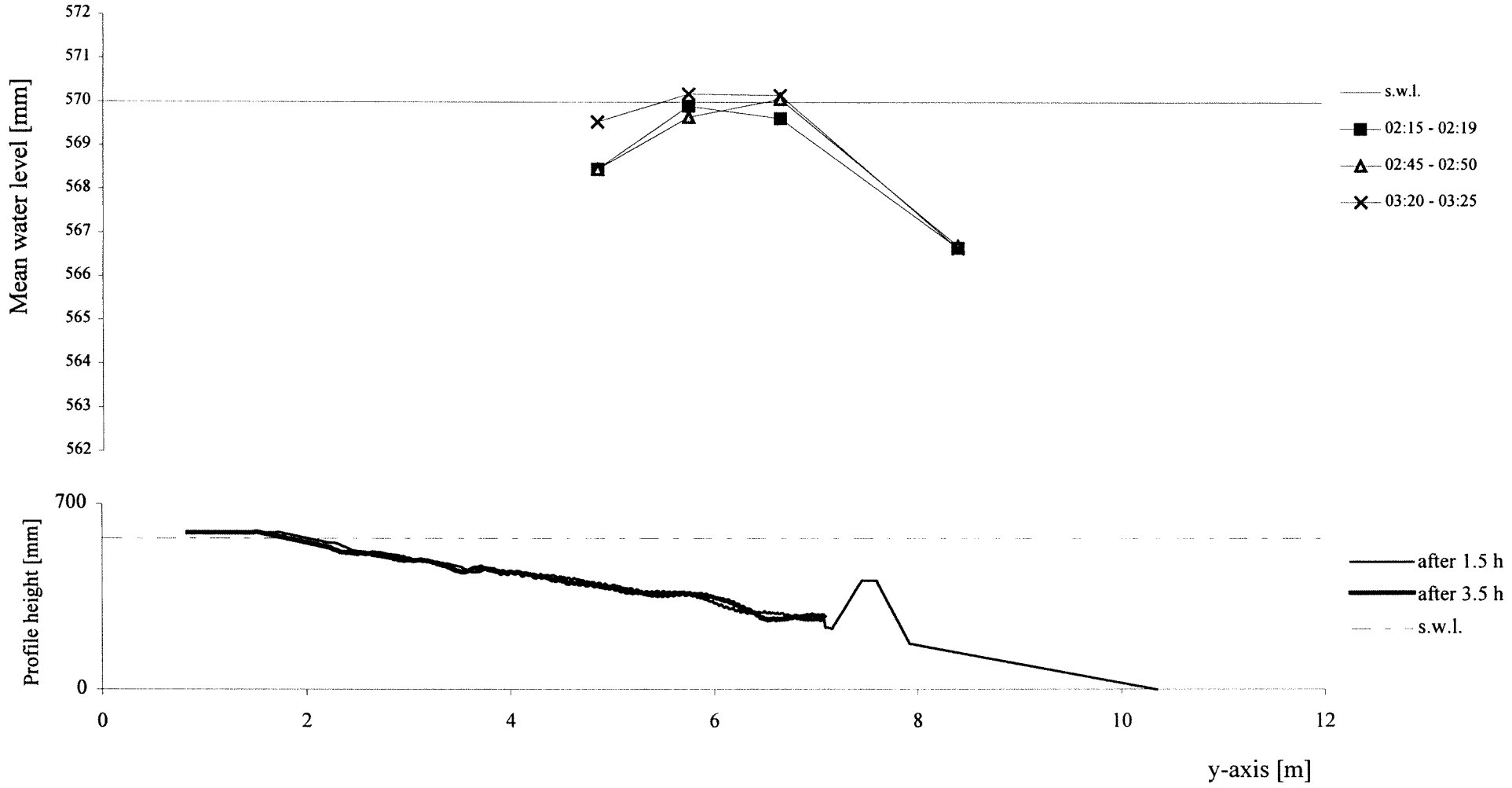

TEST C2 - cross-section x=3 m - interval 03:30 - 07:30

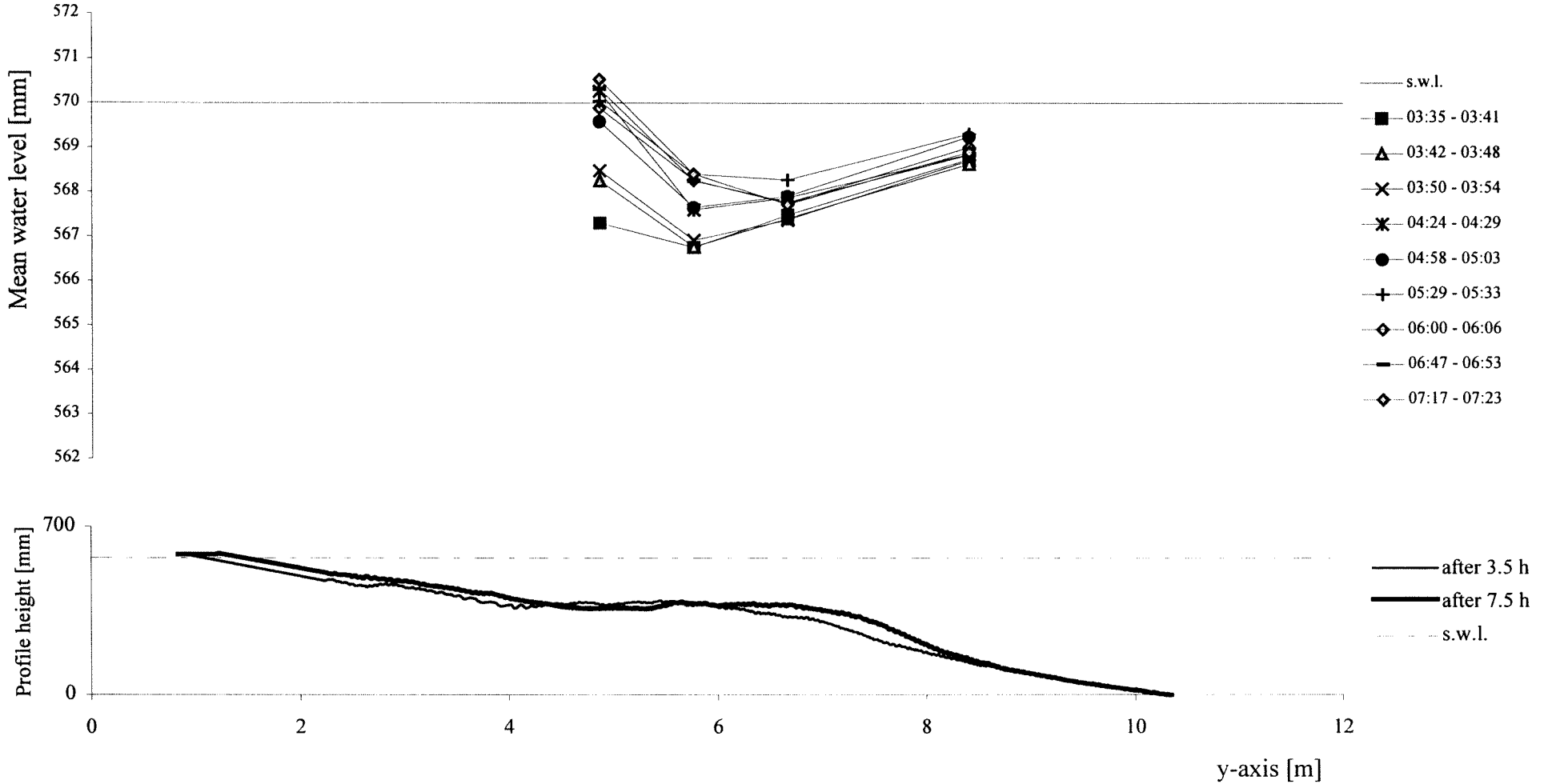

TEST C2 - cross-section x=6.5 m - interval 03:30 - 07:30

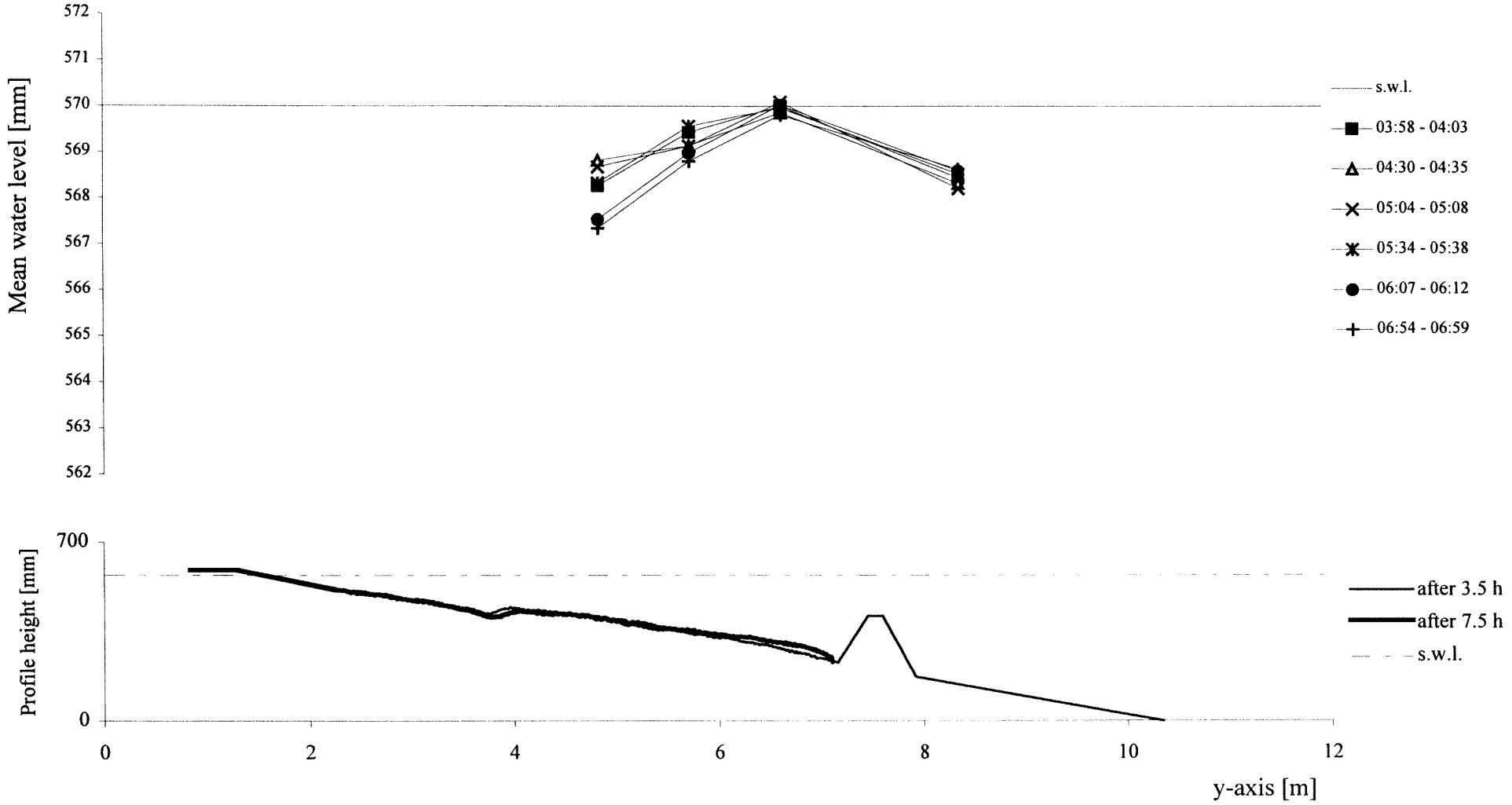

TEST C2 - cross-section x=12.5 m - interval 03:30 - 07:30

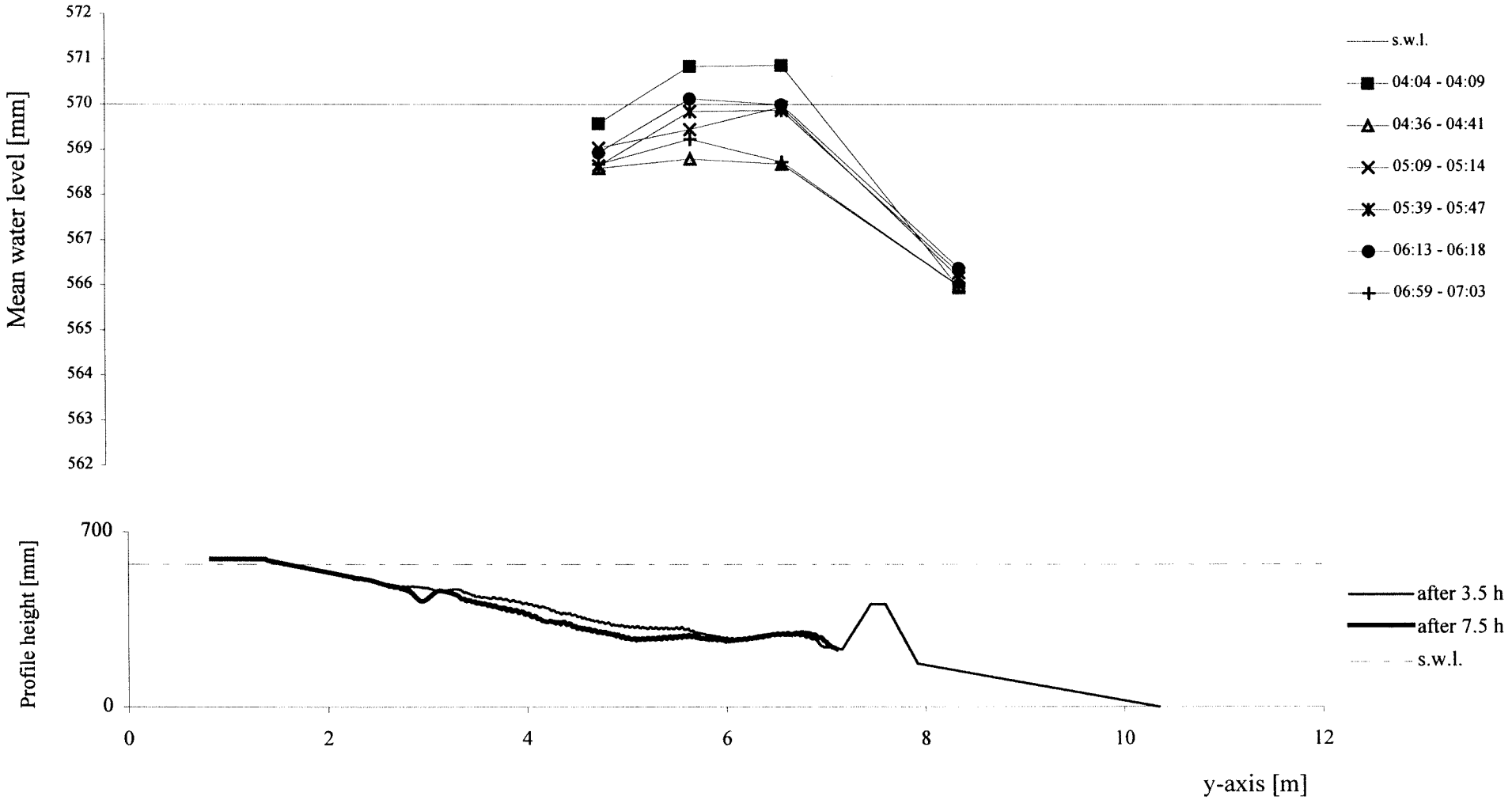

TEST C2 - cross-section x=20 m - interval 03:30 - 07:30

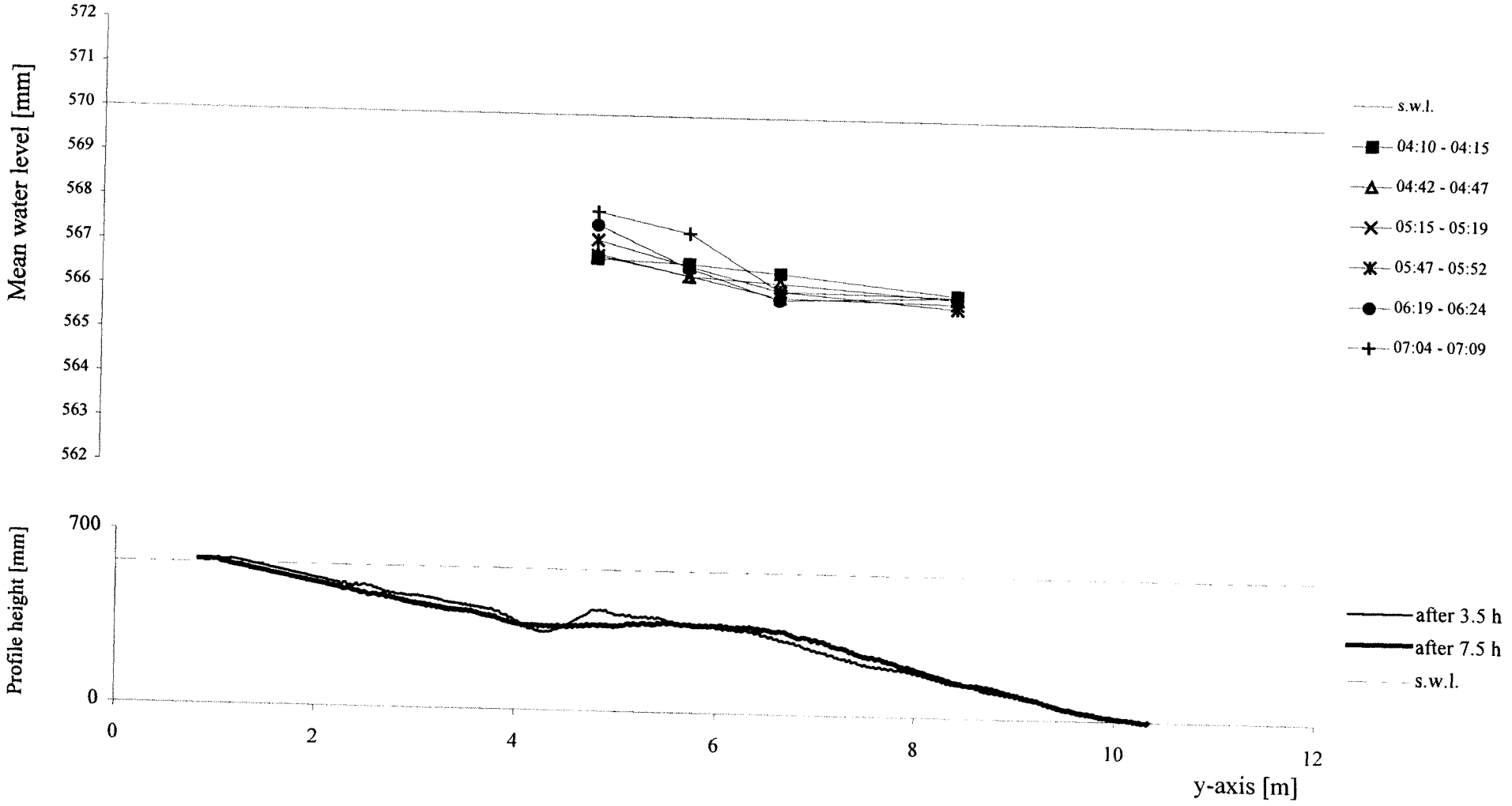

TEST C2 - cross-section x=24.5 m - interval 03:30 - 07:30

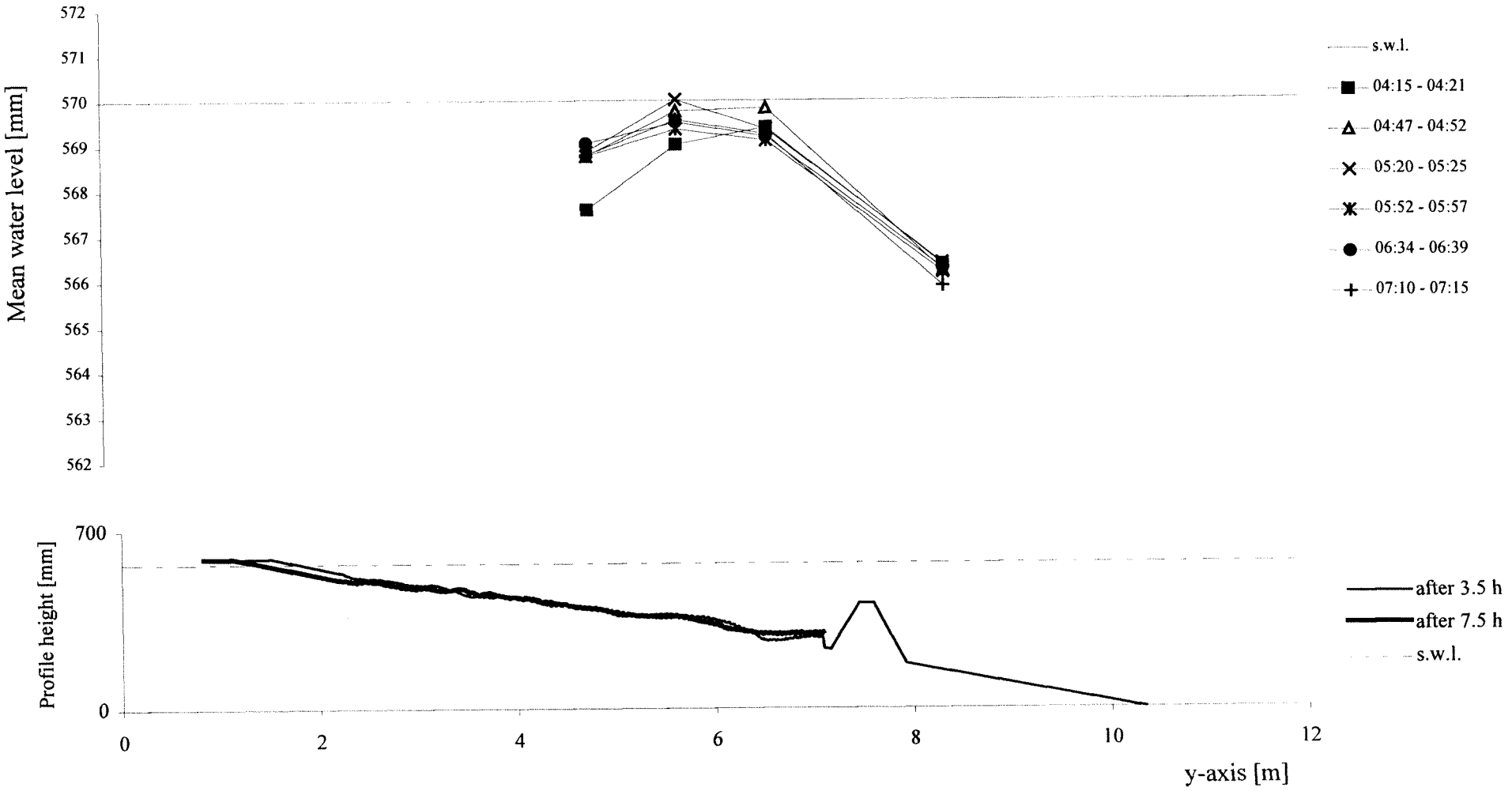

Appendix B3. Graphics TEST C3 - Average Water Level

TEST C3 - cross-section x=3m - interval 00:00 - 00:30

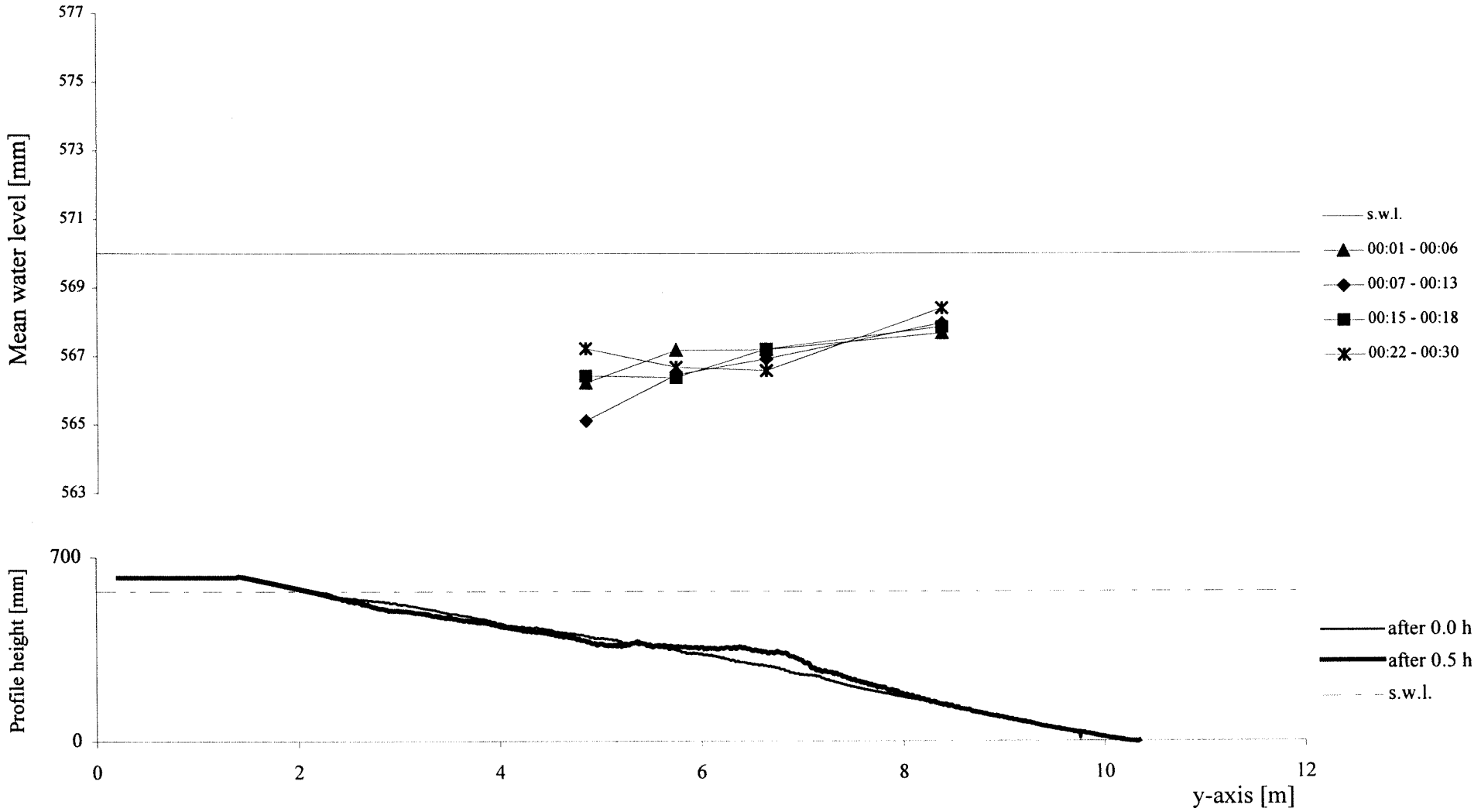

TEST C3 - cross-section x=6.5 m - interval 00:30 - 01:30

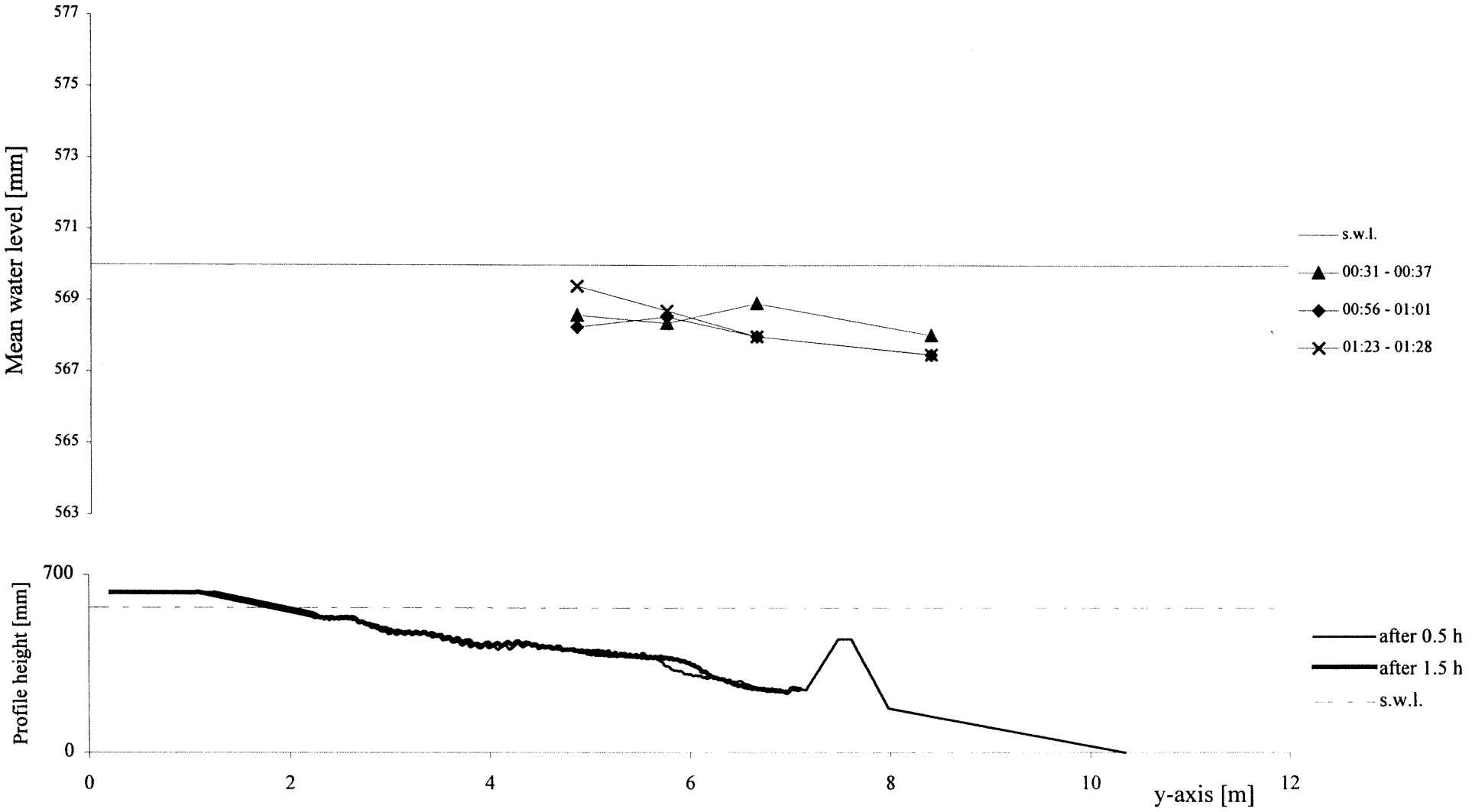

TEST C3 - cross-section x=12.5 m - interval 00:30 - 01:30

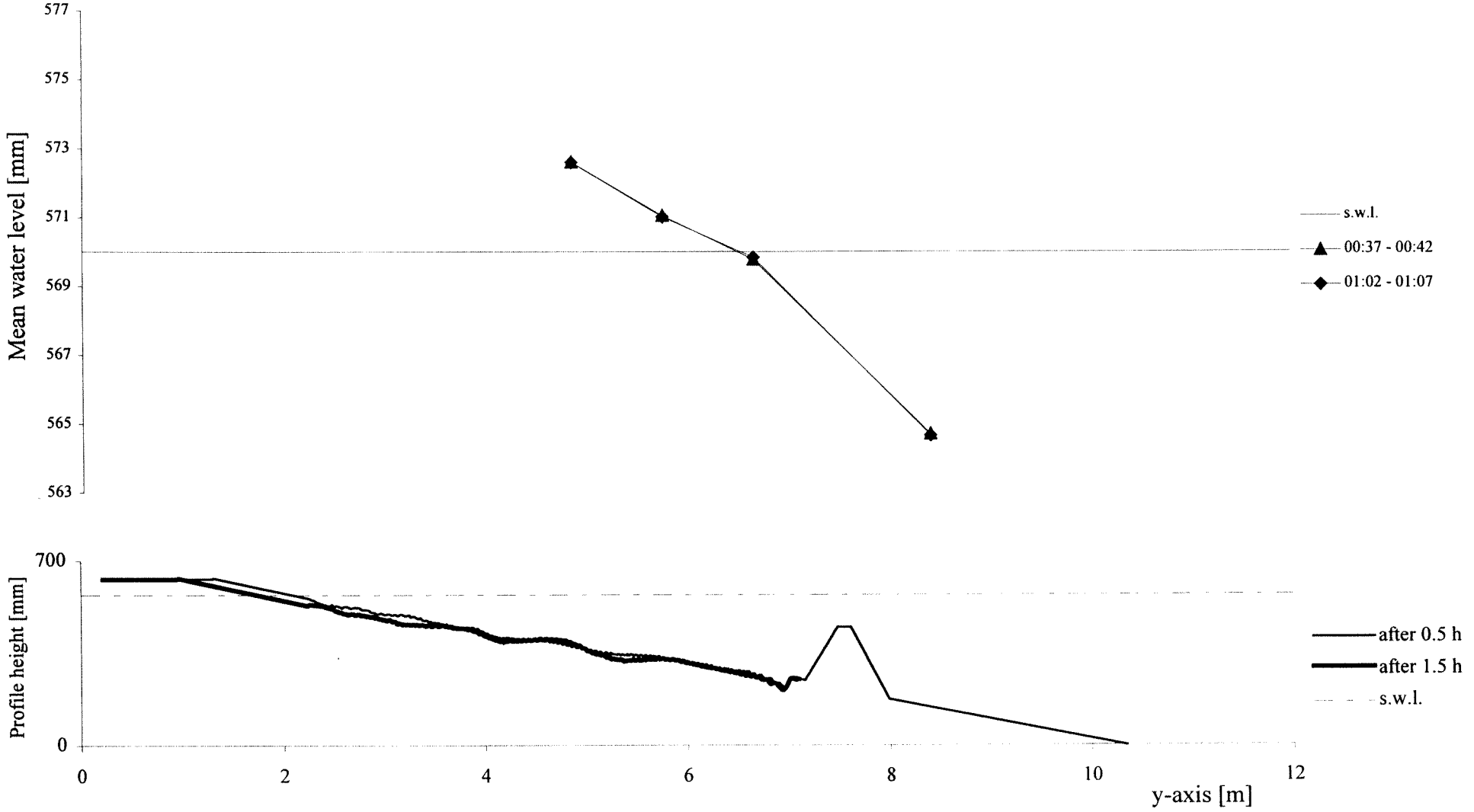

TEST C3 - cross-section x=20 m - interval 00:30 - 01:30

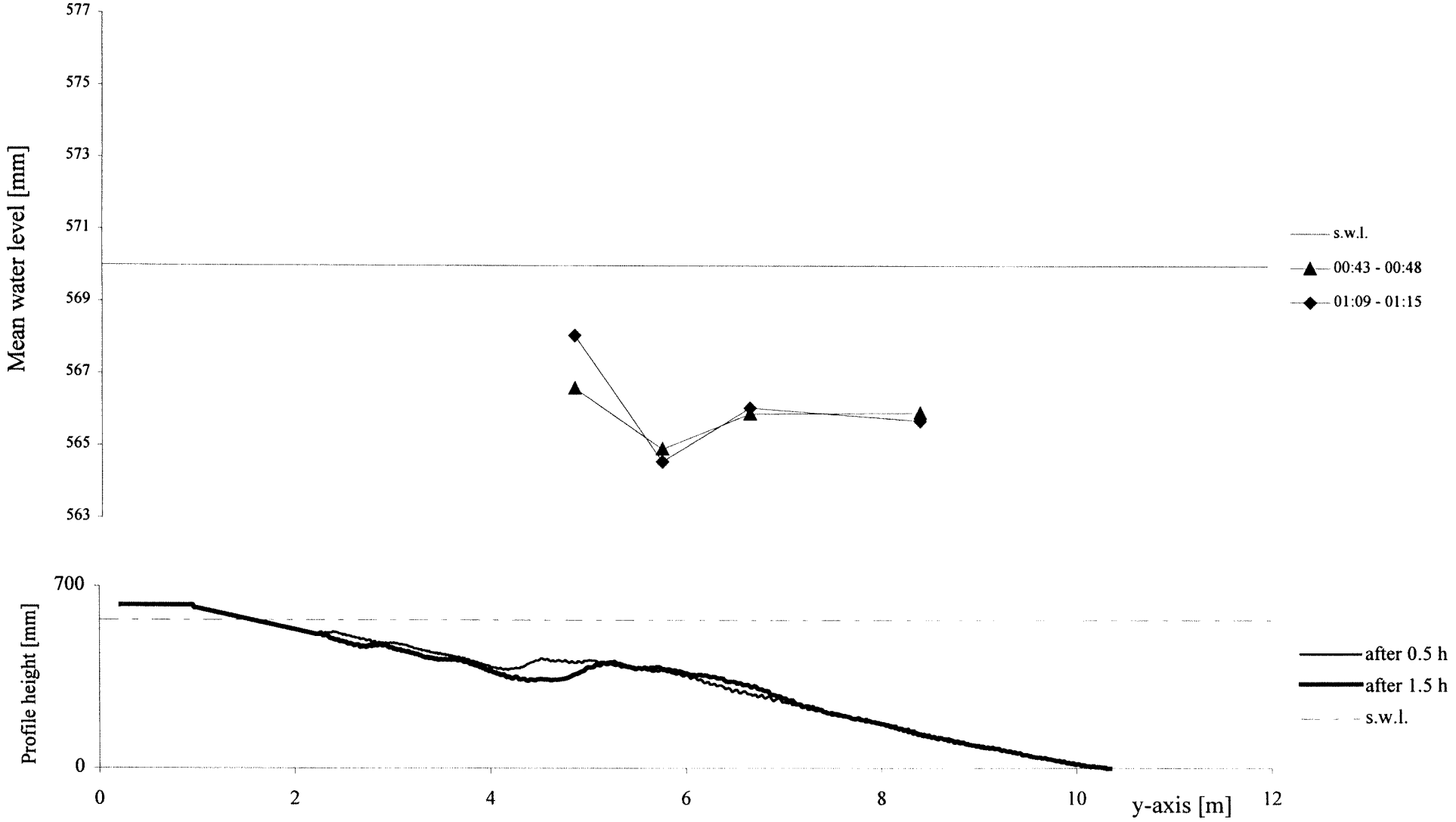

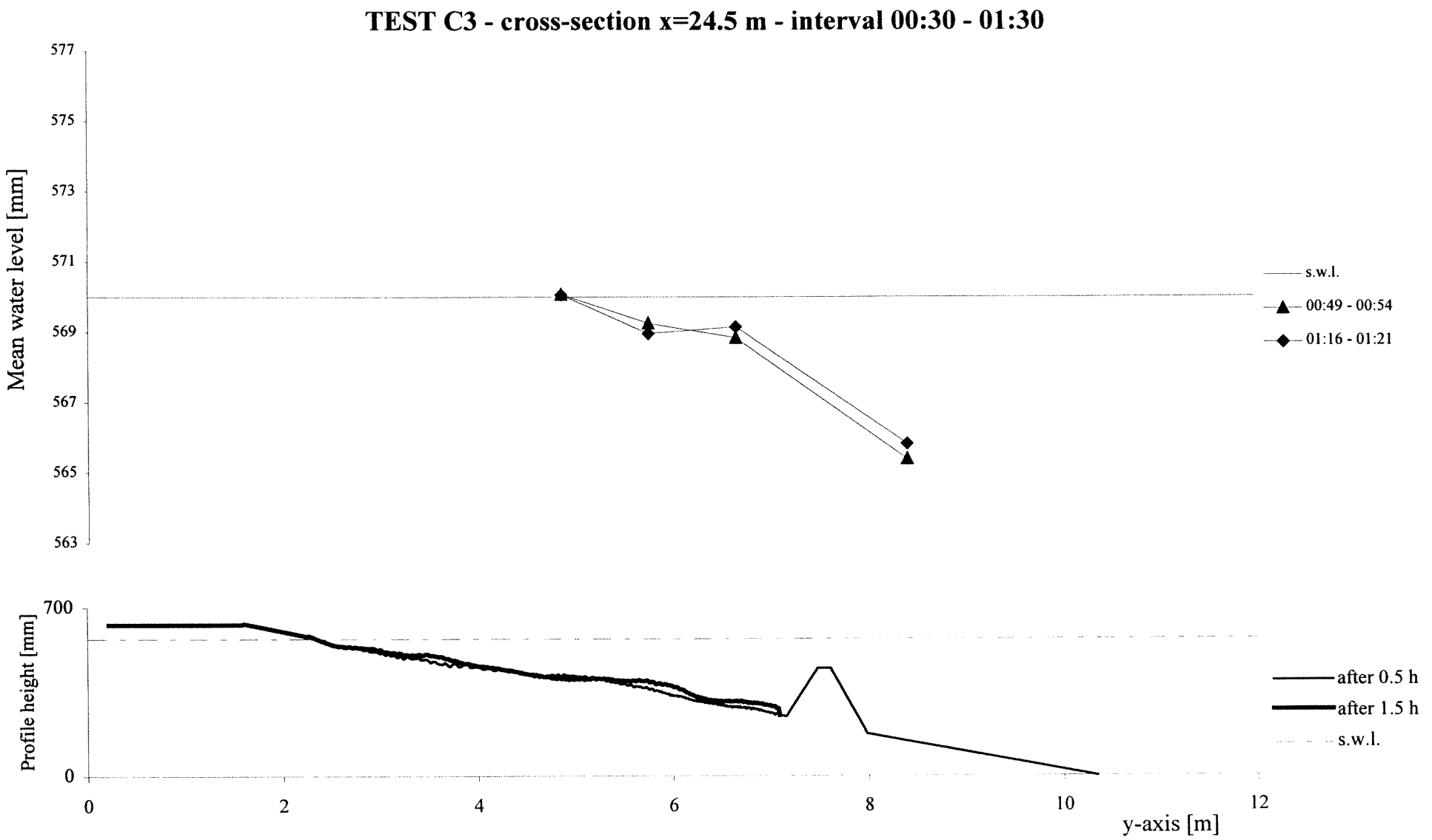
TEST C3 - cross-section x=24.5 m - interval 00:30 - 01:30
Mean water level [mm]
577
575
573
571
569
567
565
563
s.w.l.
00:49 - 00:54
01:16 - 01:21
Profile height [mm]
700
0
0
2
4
6
8
10
12
y-axis [m]
after 0.5 h
after 1.5 h
s.w.l.

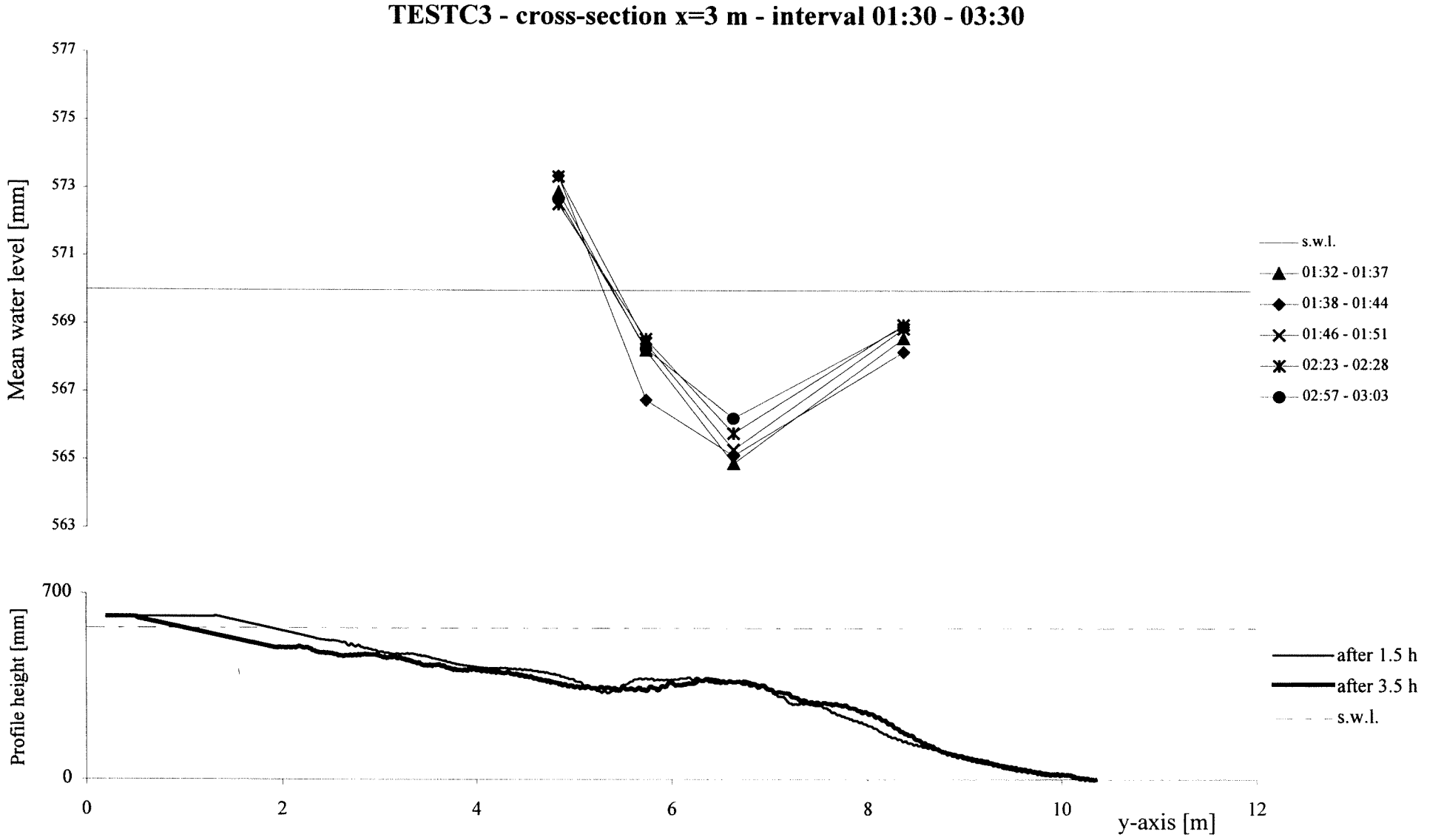
TESTC3 - cross-section x=3 m - interval 01:30 - 03:30
Mean water level [mm]
577
575
573
571
569
567
565
563
s.w.l.
01:32 - 01:37
01:38 - 01:44
01:46 - 01:51
02:23 - 02:28
02:57 - 03:03
Profile height [mm]
700
0
after 1.5 h
after 3.5 h
s.w.l.
0
2
4
6
8
10
12
y-axis [m]

TEST C3 - cross-section x=6.5 m - interval 01:30 - 03:30

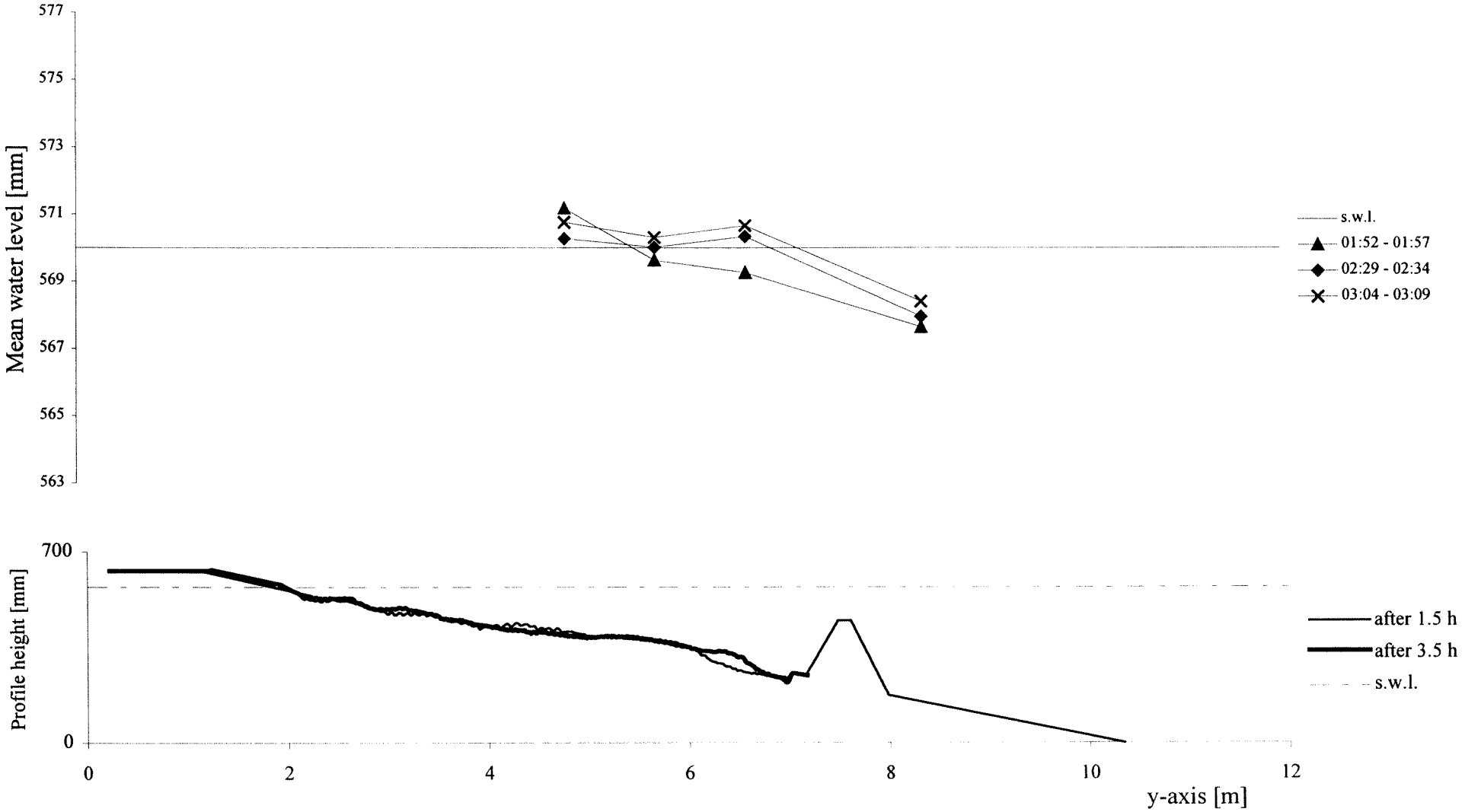

TEST C3 - cross-section x=12.5 m - interval 01:30 - 03:30

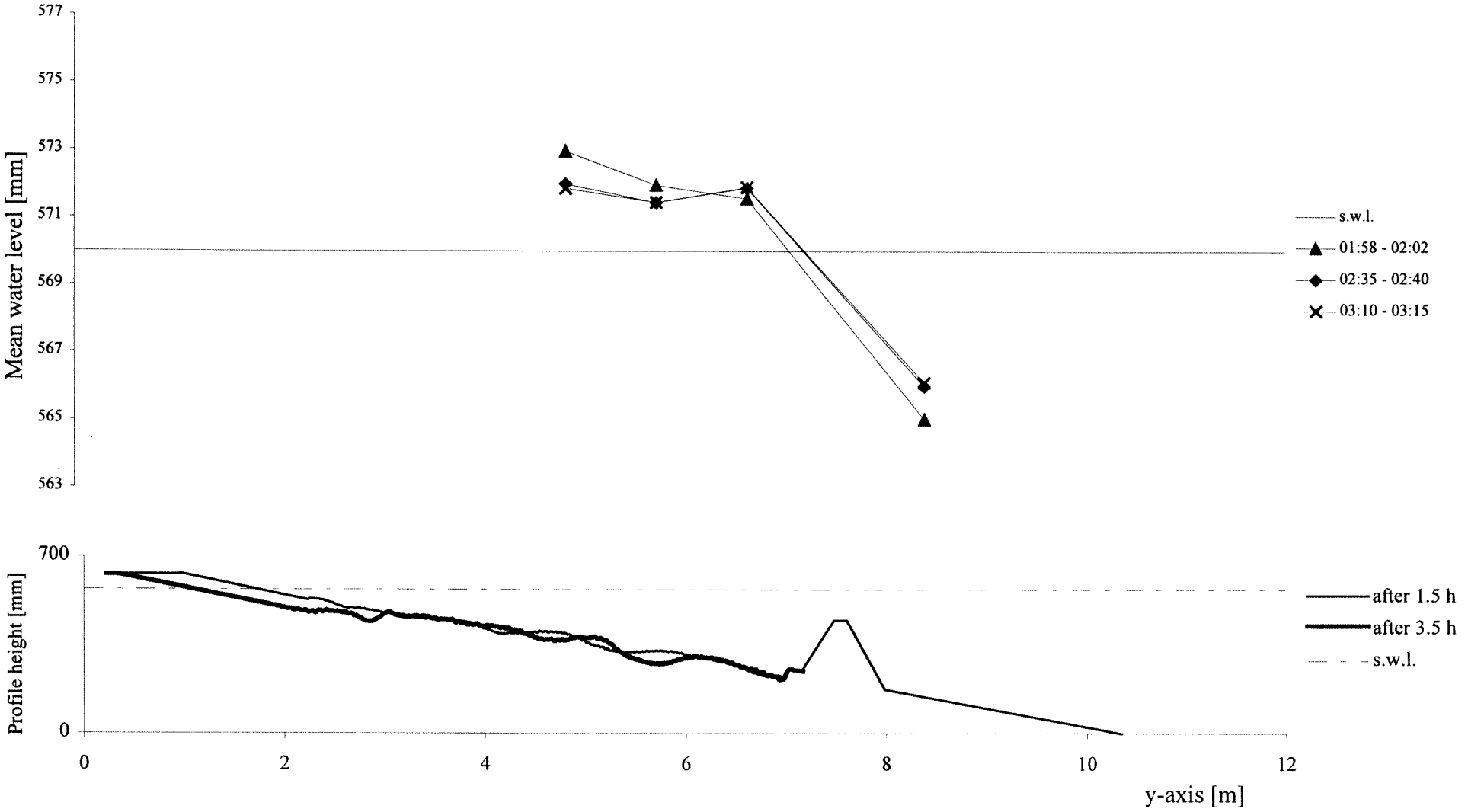

TEST C3 - cross-section x=20 m - interval 01:30 - 03:30

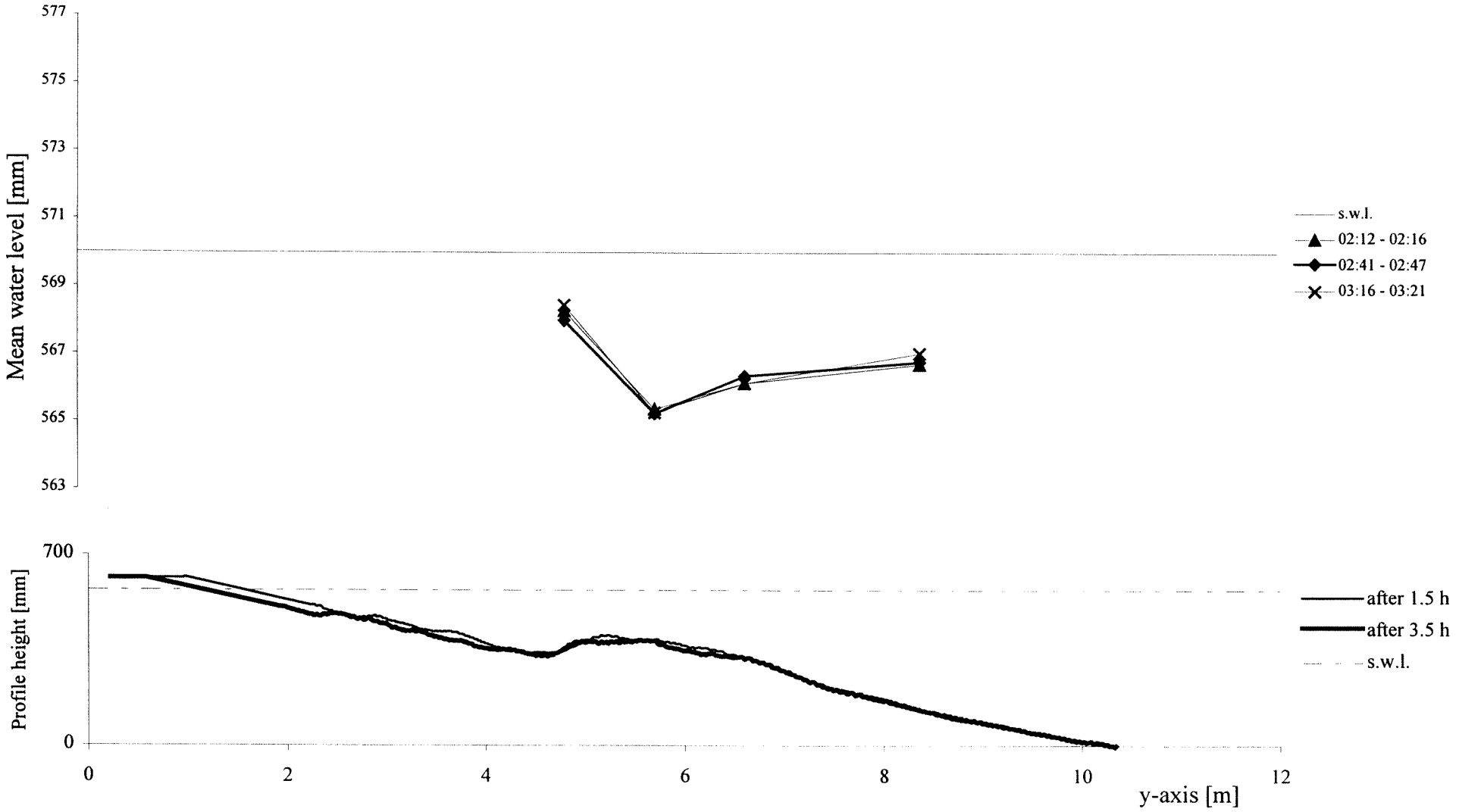

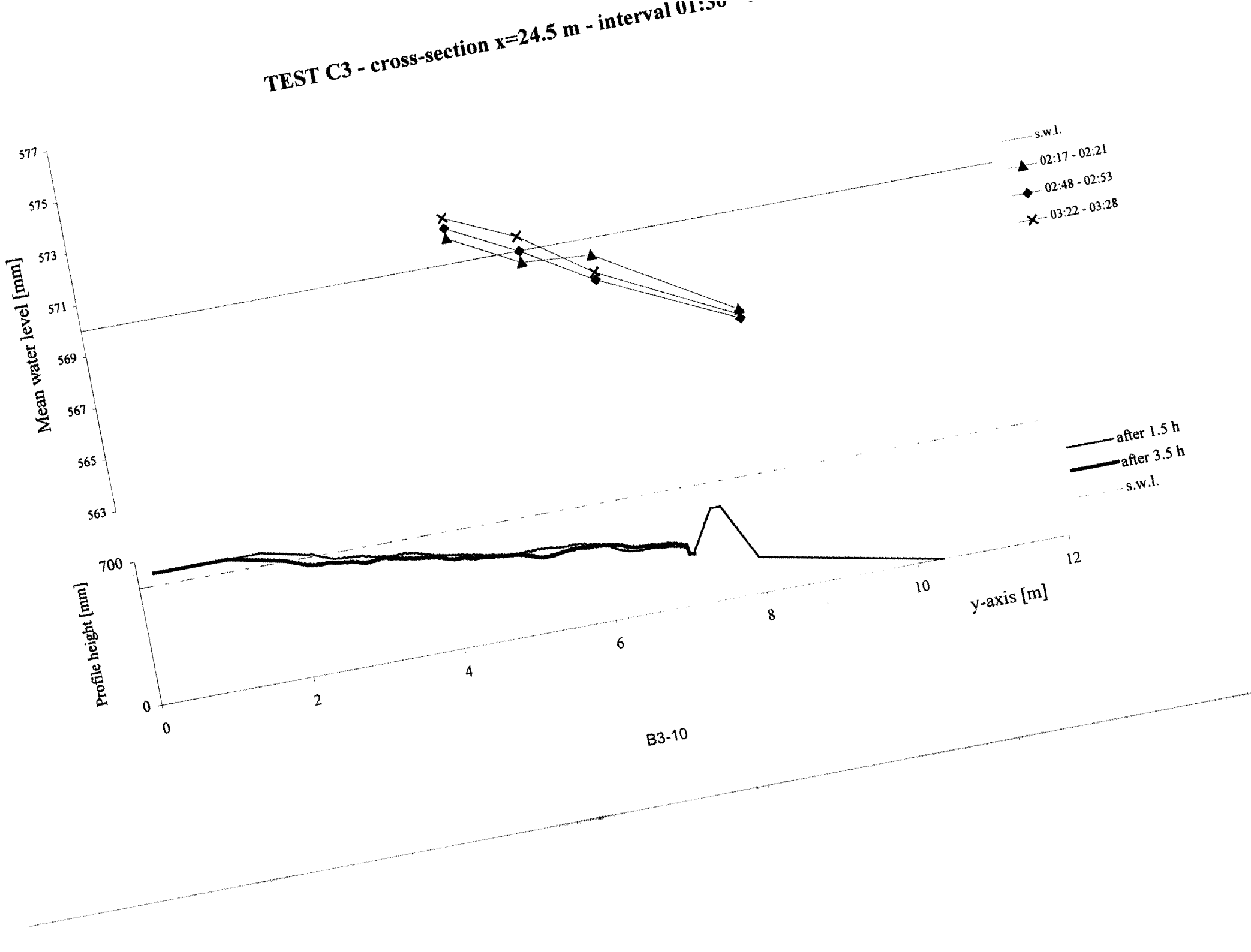
TEST C3 - cross-section x=24.5 m - interval 01:30
Mean water level [mm]
577
575
573
571
569
567
565
563
s.w.l.
02:17 - 02:21
02:48 - 02:53
03:22 - 03:28
after 1.5 h
after 3.5 h
s.w.l.
Profile height [mm]
700
0
0
2
4
6
8
10
12
y-axis [m]
B3-10

TEST C3 - cross-section x=3 m - interval 03:30 - 07:30

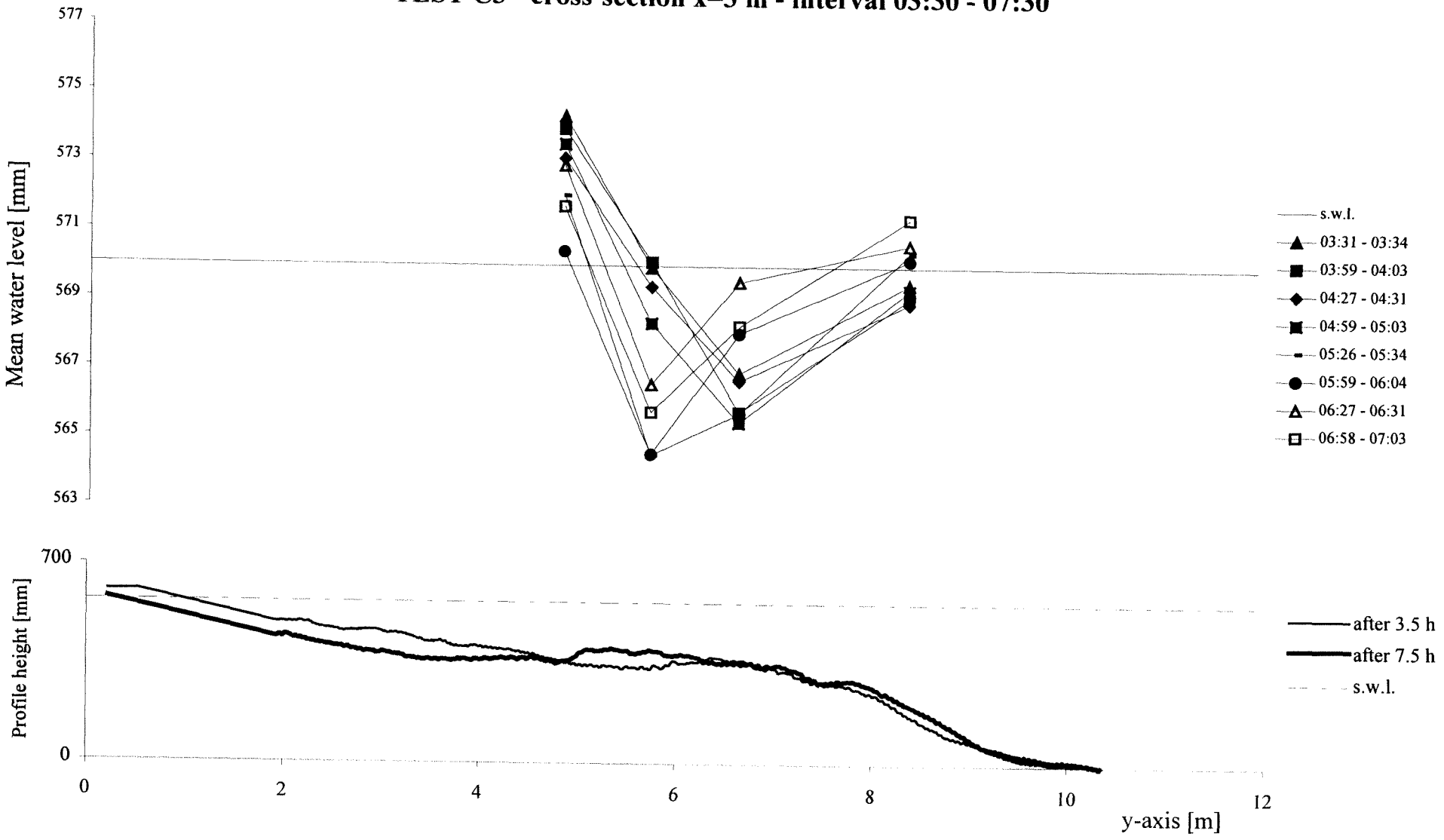

TEST C3 - cross-section x=6.5 m - interval 03:30 - 07:30

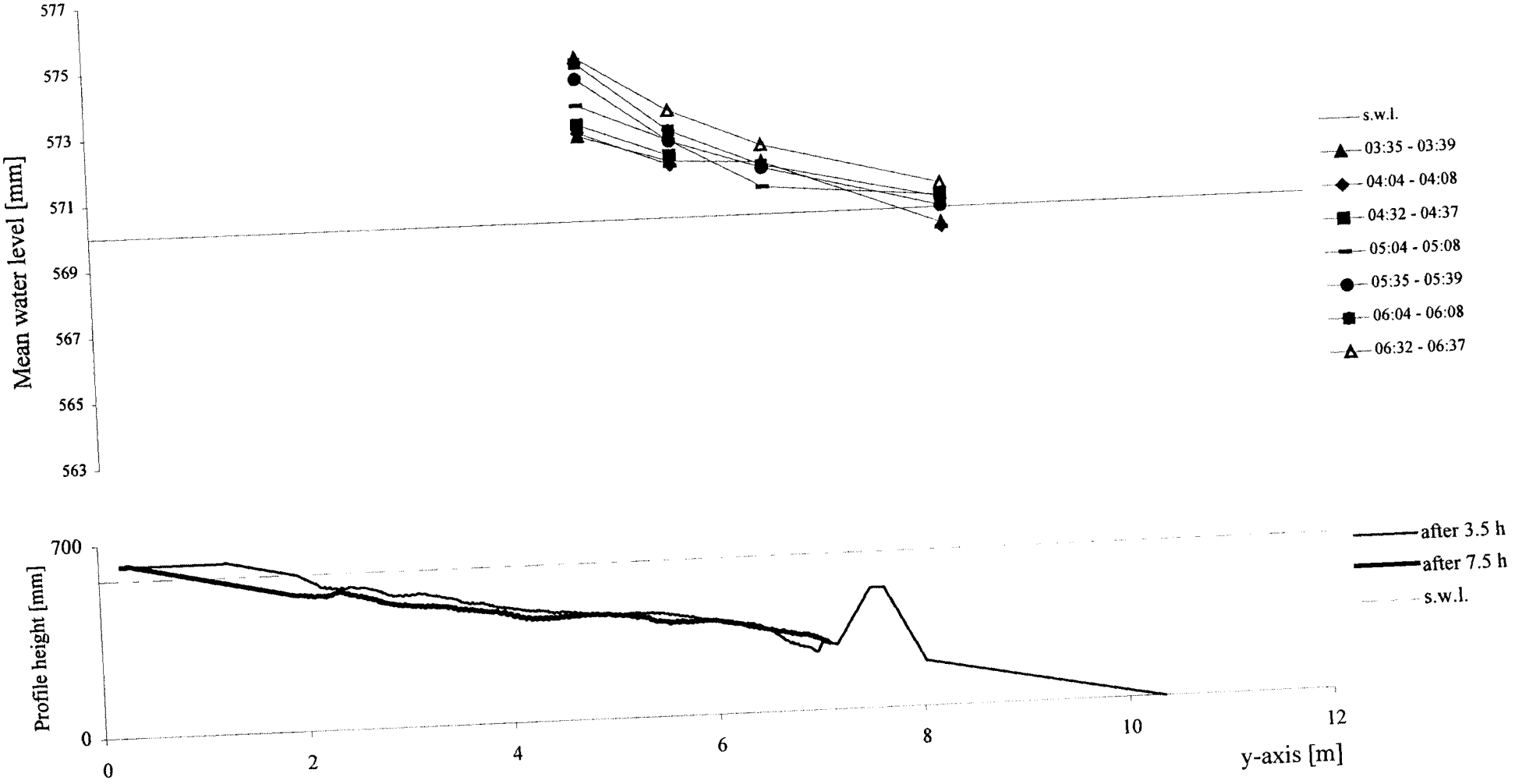

TEST C3 - cross-section x=12.5 m - interval 03:30 - 07:30

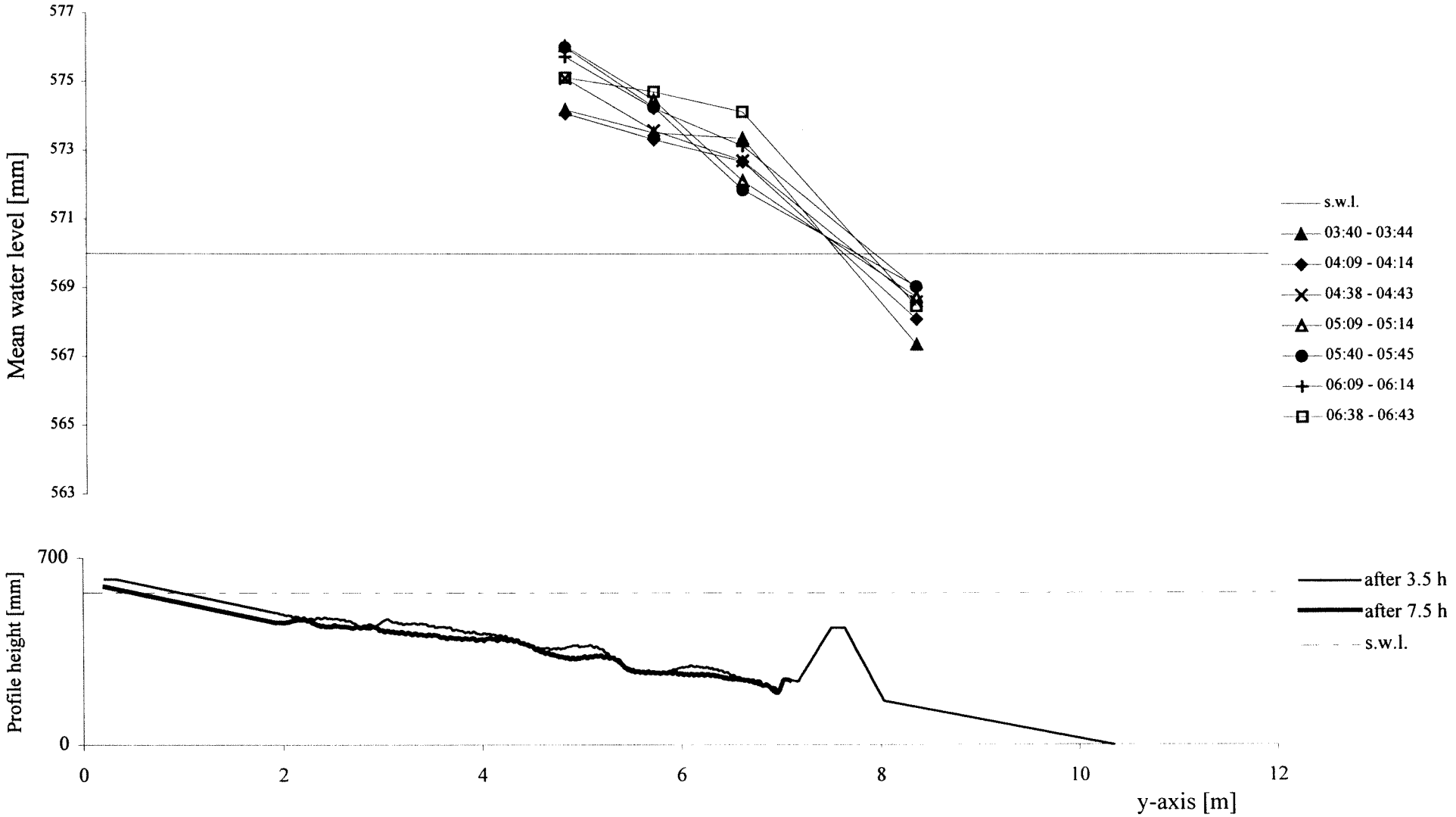

TEST C3 - cross-section x=20 m - interval 03:30 - 07:30

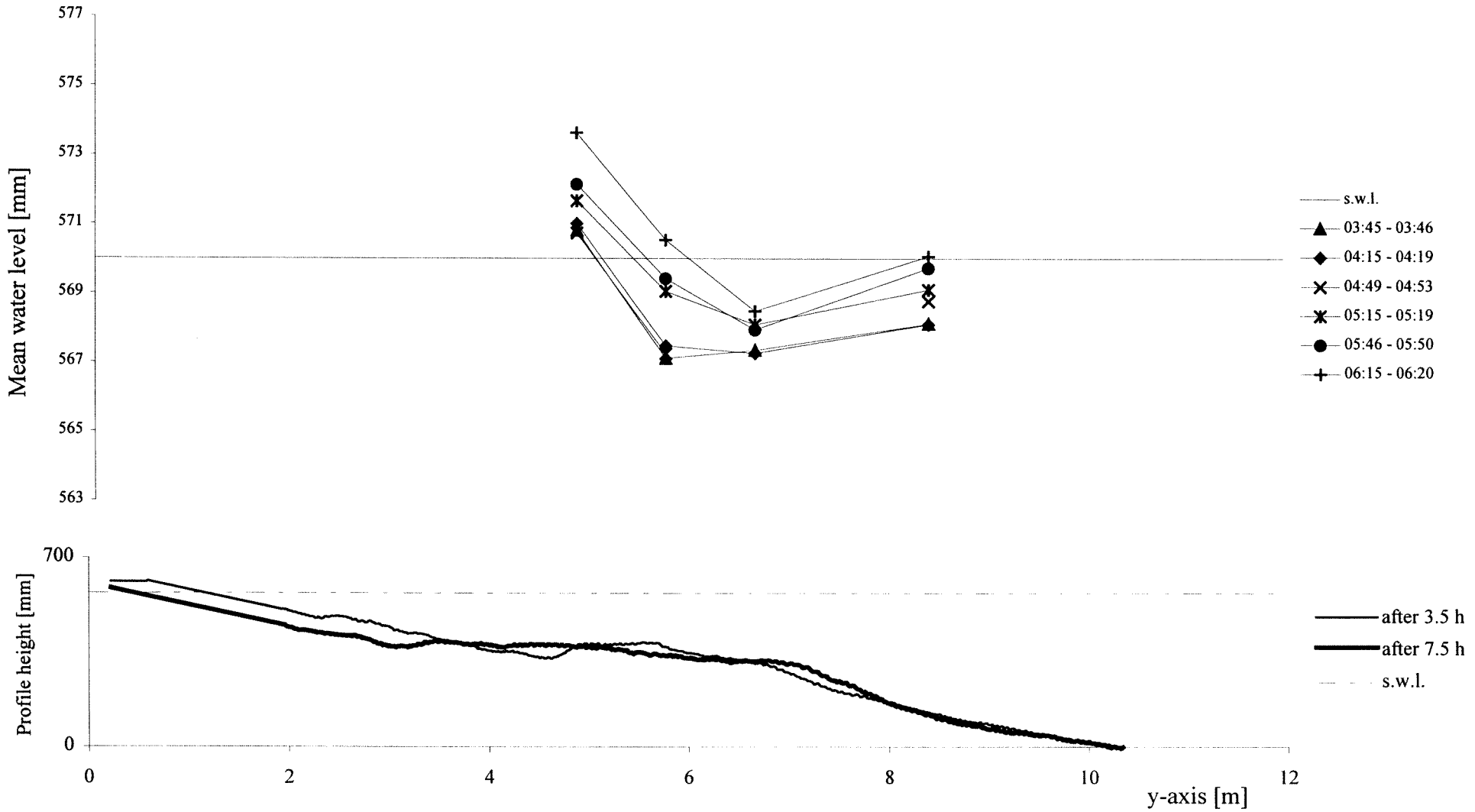

TEST C3 - cross-section x=24.5 m - interval 03:30 - 07:30

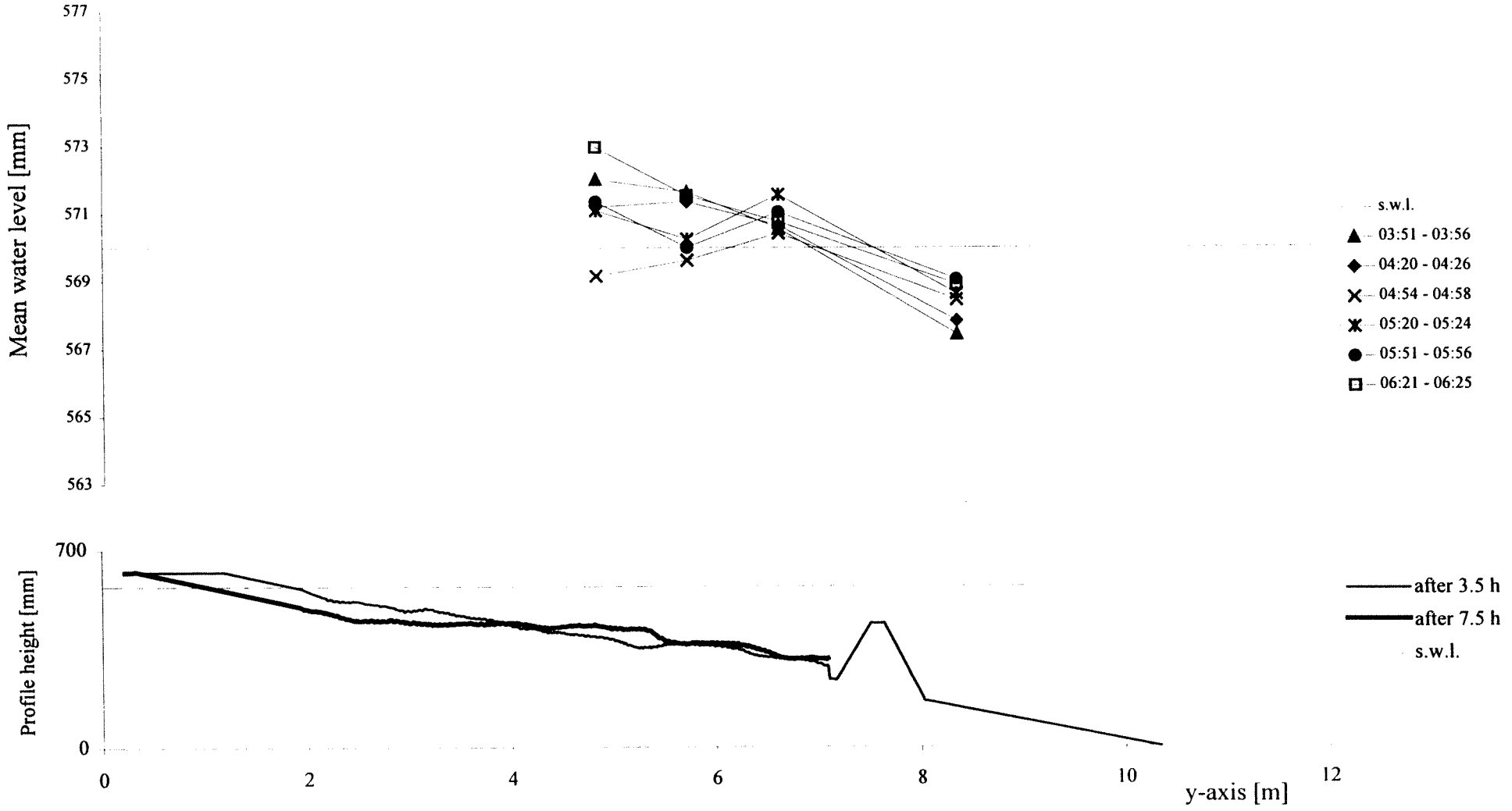

Appendix C1. Graphics TEST D1 - Average Water Level

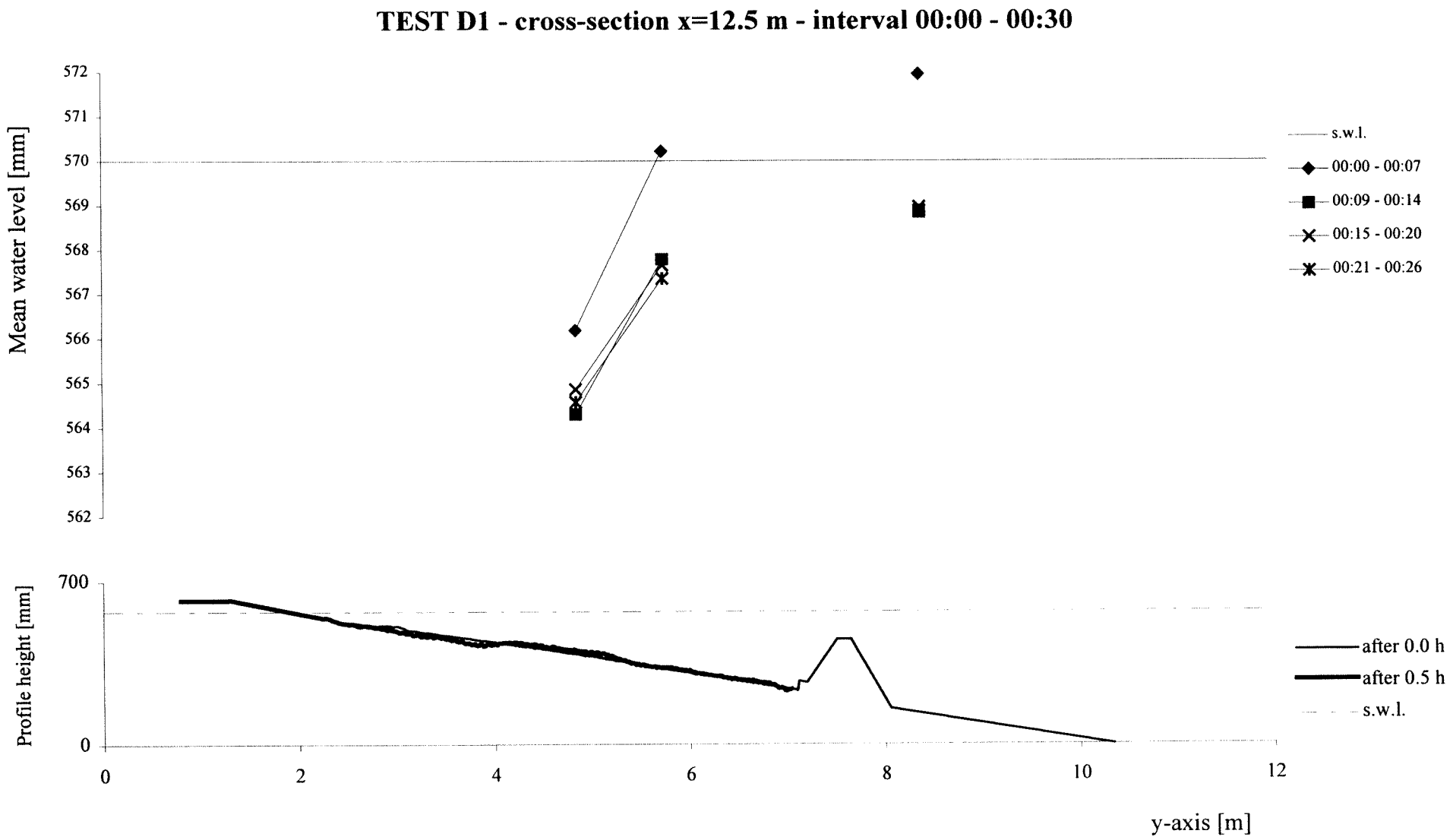
TEST D1 - cross-section x=12.5 m - interval 00:00 - 00:30
Mean water level [mm]
572
571
570
569
568
567
566
565
564
563
562
s.w.l.
00:00 - 00:07
00:09 - 00:14
00:15 - 00:20
00:21 - 00:26
Profile height [mm]
700
0
after 0.0 h
after 0.5 h
s.w.l.
0
2
4
6
8
10
12
y-axis [m]

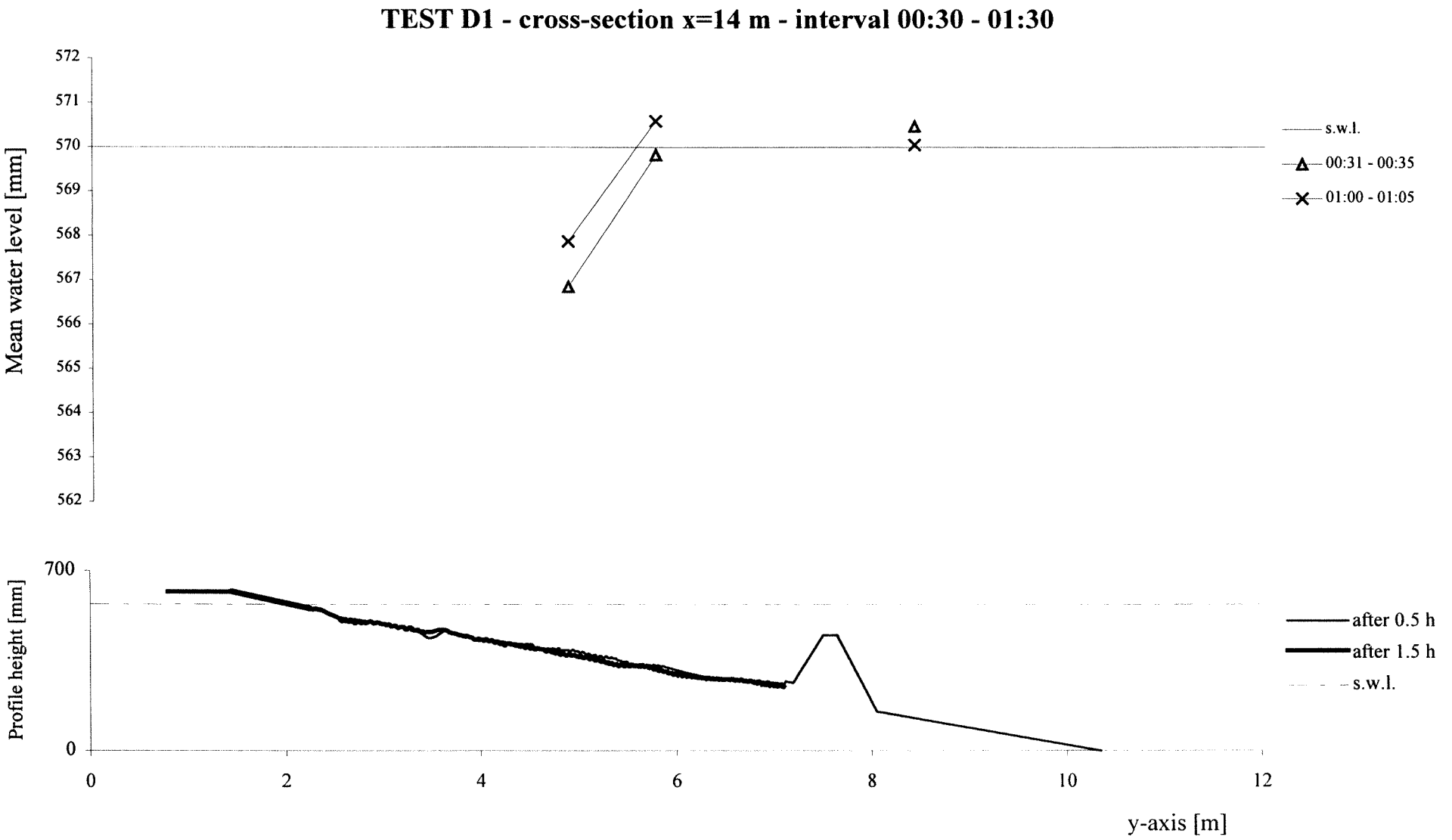
TEST D1 - cross-section x=14 m - interval 00:30 - 01:30
Mean water level [mm]
572
571
570
569
568
567
566
565
564
563
562
s.w.l.
00:31 - 00:35
01:00 - 01:05
Profile height [mm]
700
0
after 0.5 h
after 1.5 h
s.w.l.
0
2
4
6
8
10
12
y-axis [m]

TEST D1 - cross-section x=15.5 m - interval 00:30 - 01:30

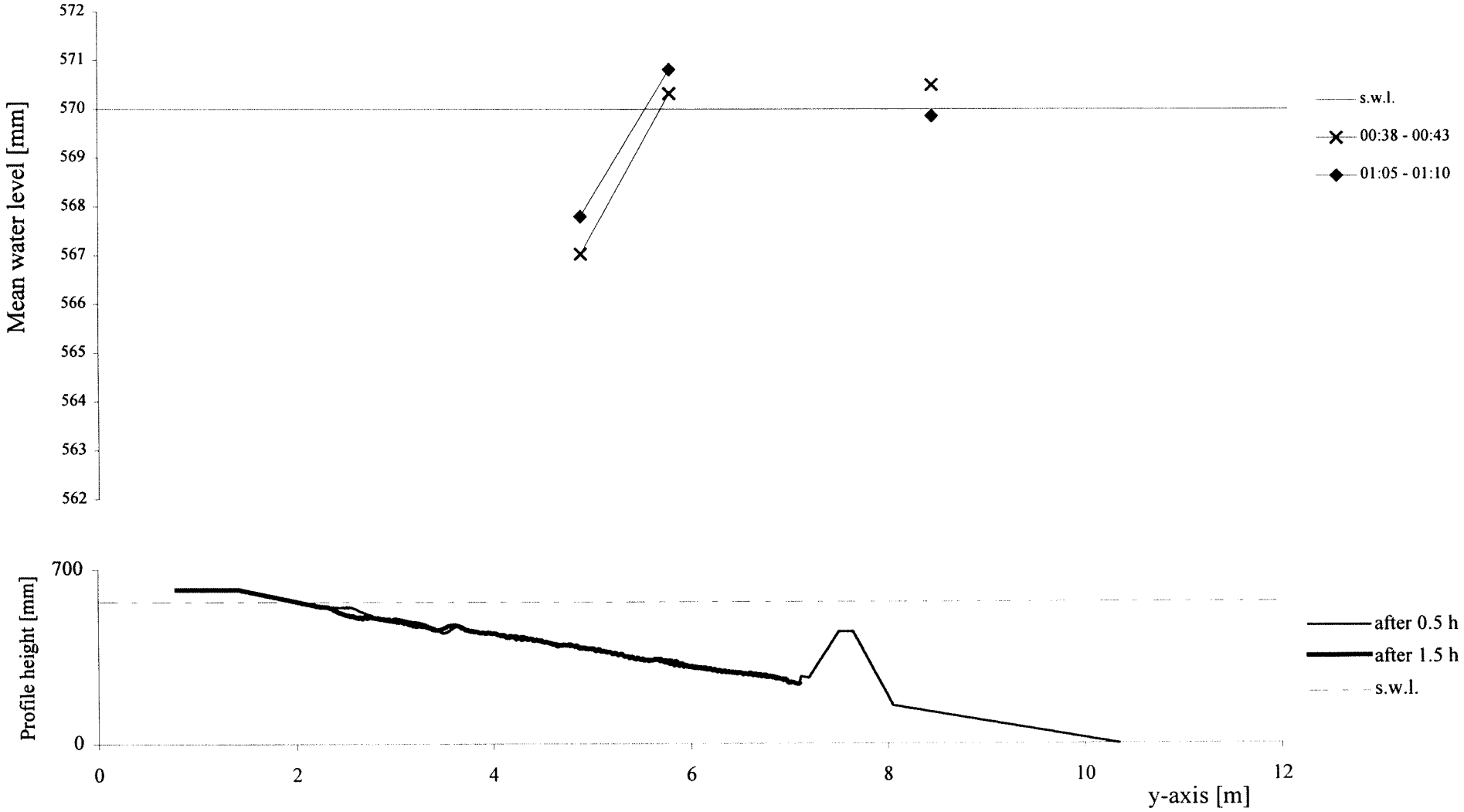

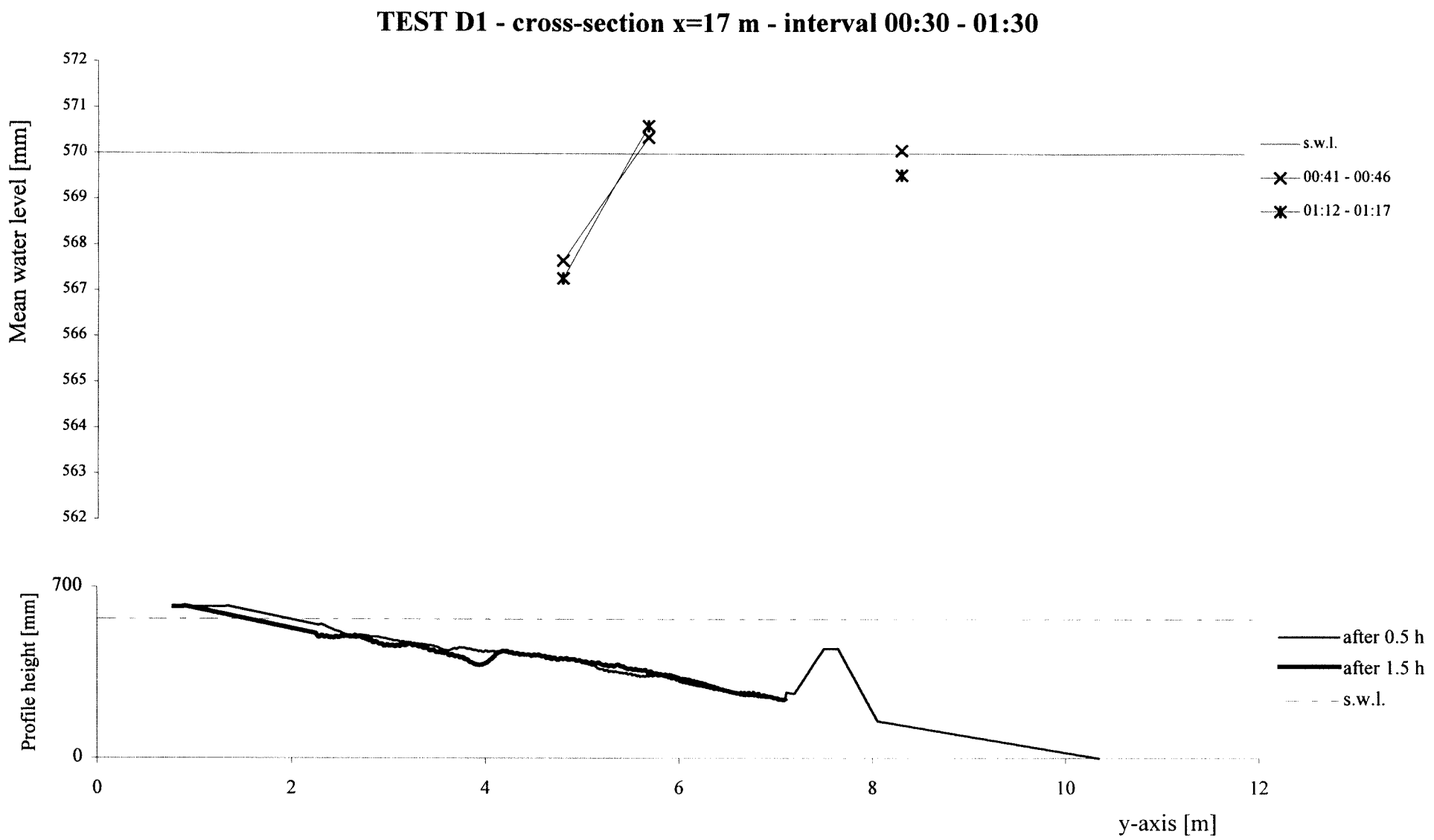
TEST D1 - cross-section x=17 m - interval 00:30 - 01:30
Mean water level [mm]
572
571
570
569
568
567
566
565
564
563
562
s.w.l.
00:41 - 00:46
01:12 - 01:17
Profile height [mm]
700
0
after 0.5 h
after 1.5 h
s.w.l.
0
2
4
6
8
10
12
y-axis [m]

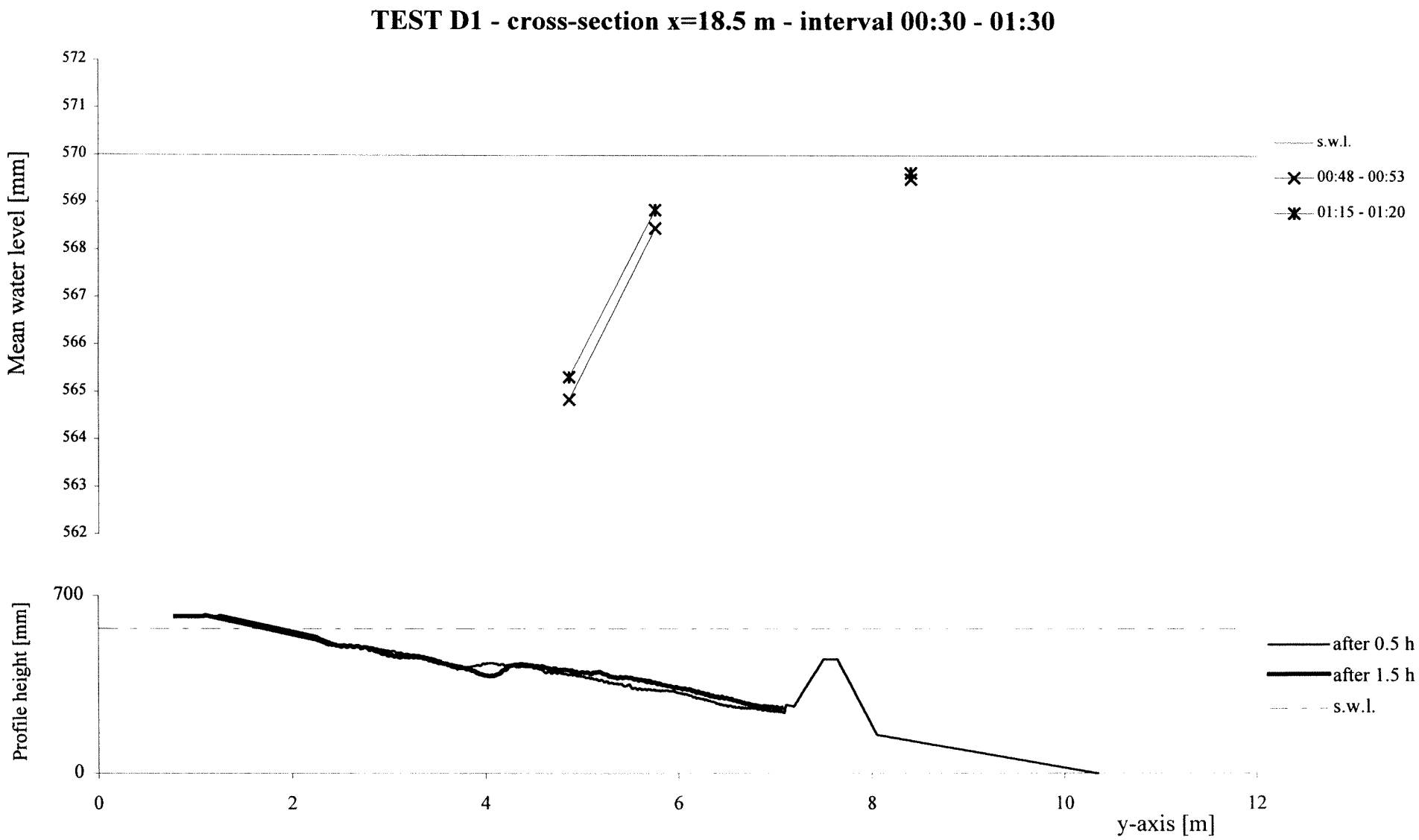
TEST D1 - cross-section x=18.5 m - interval 00:30 - 01:30
Mean water level [mm]
572
571
570
569
568
567
566
565
564
563
562
s.w.l.
00:48 - 00:53
01:15 - 01:20
Profile height [mm]
700
0
after 0.5 h
after 1.5 h
s.w.l.
0
2
4
6
8
10
12
y-axis [m]

TEST D1 - cross-section x=20 m - interval 00:30 - 01:30

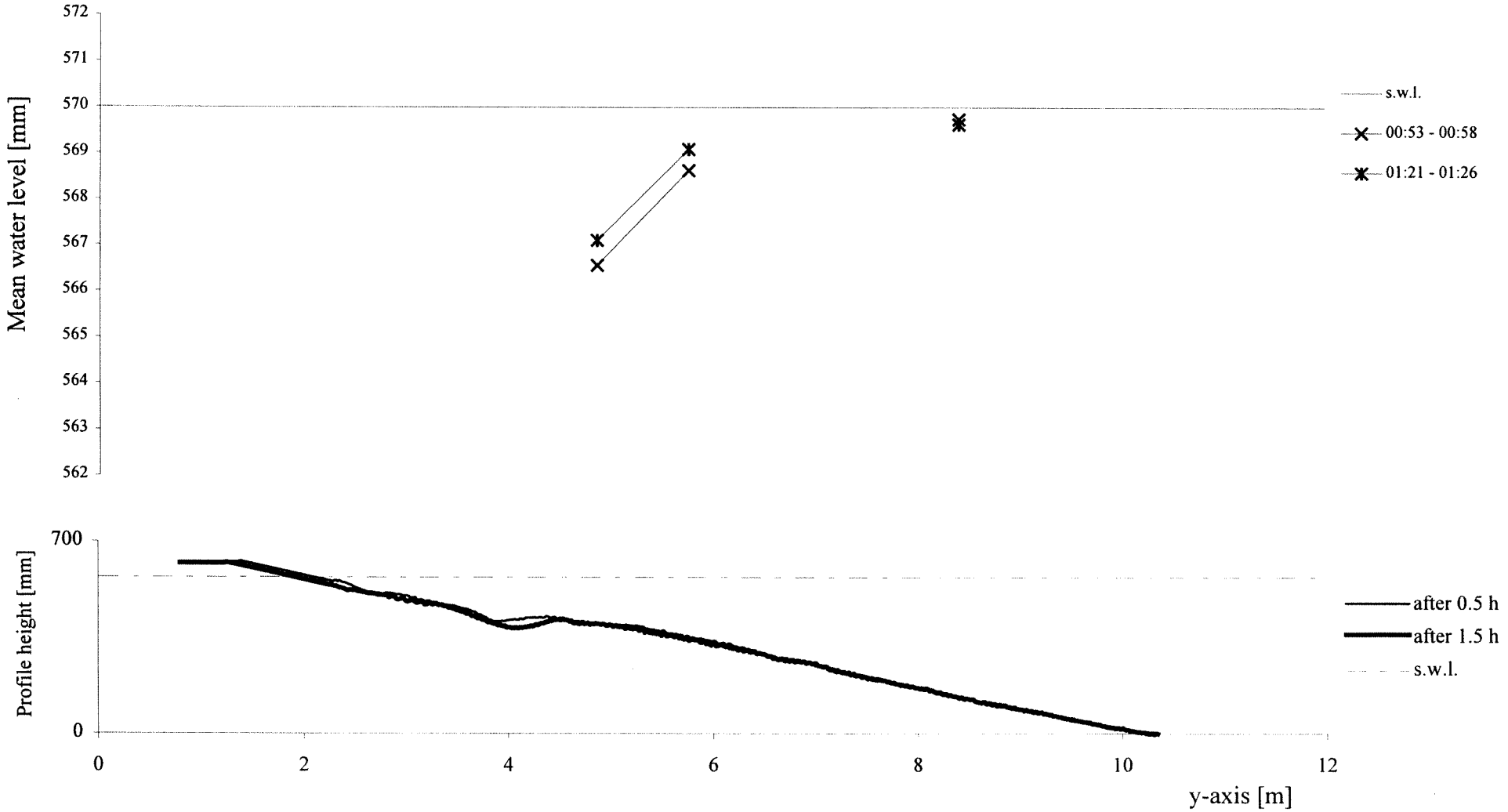

TEST D1 - cross-section x=12.5 m - interval 01:30 - 03:30

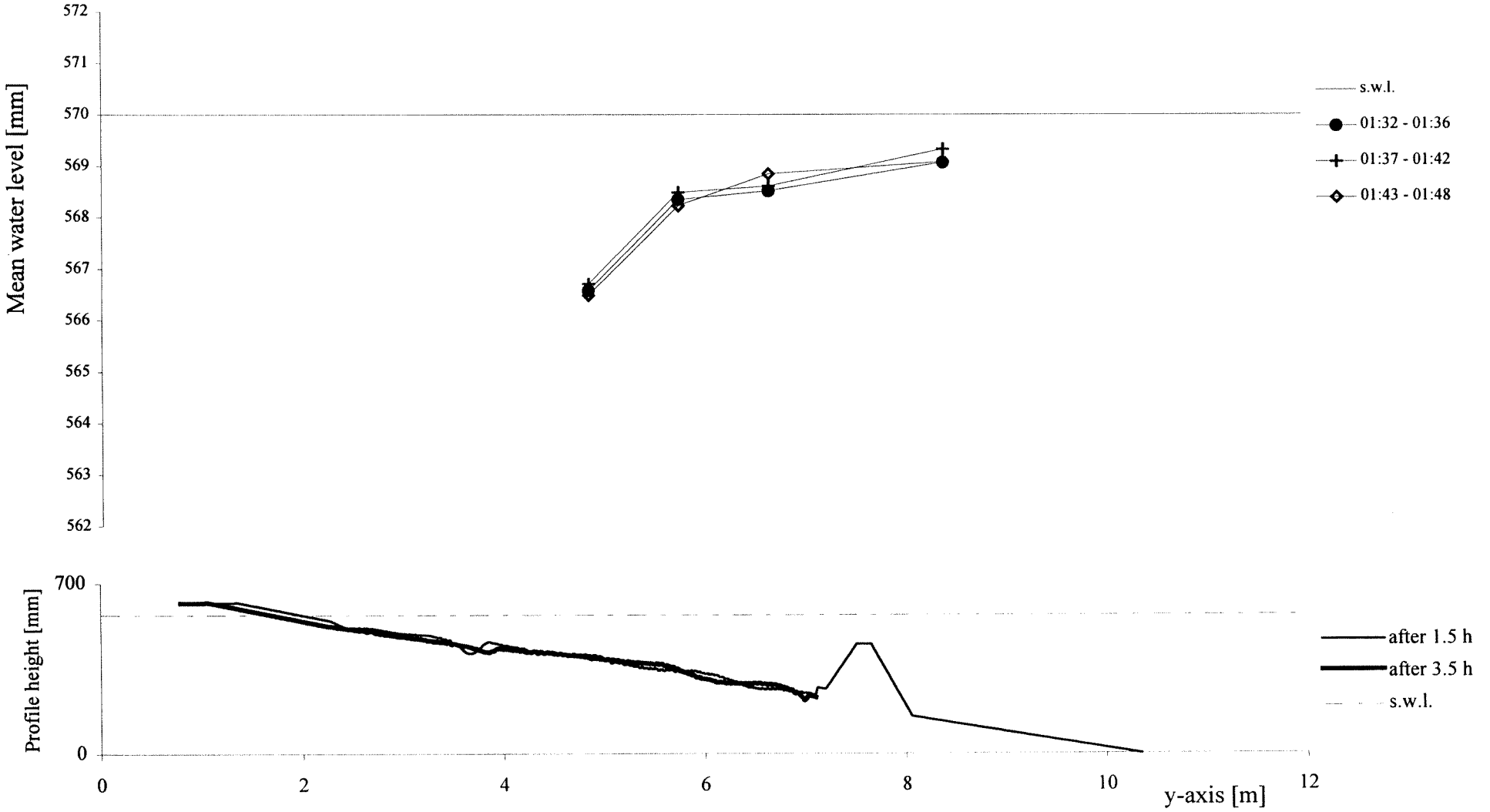

TEST D1 - cross-section x=14 m - interval 01:30 - 03:30

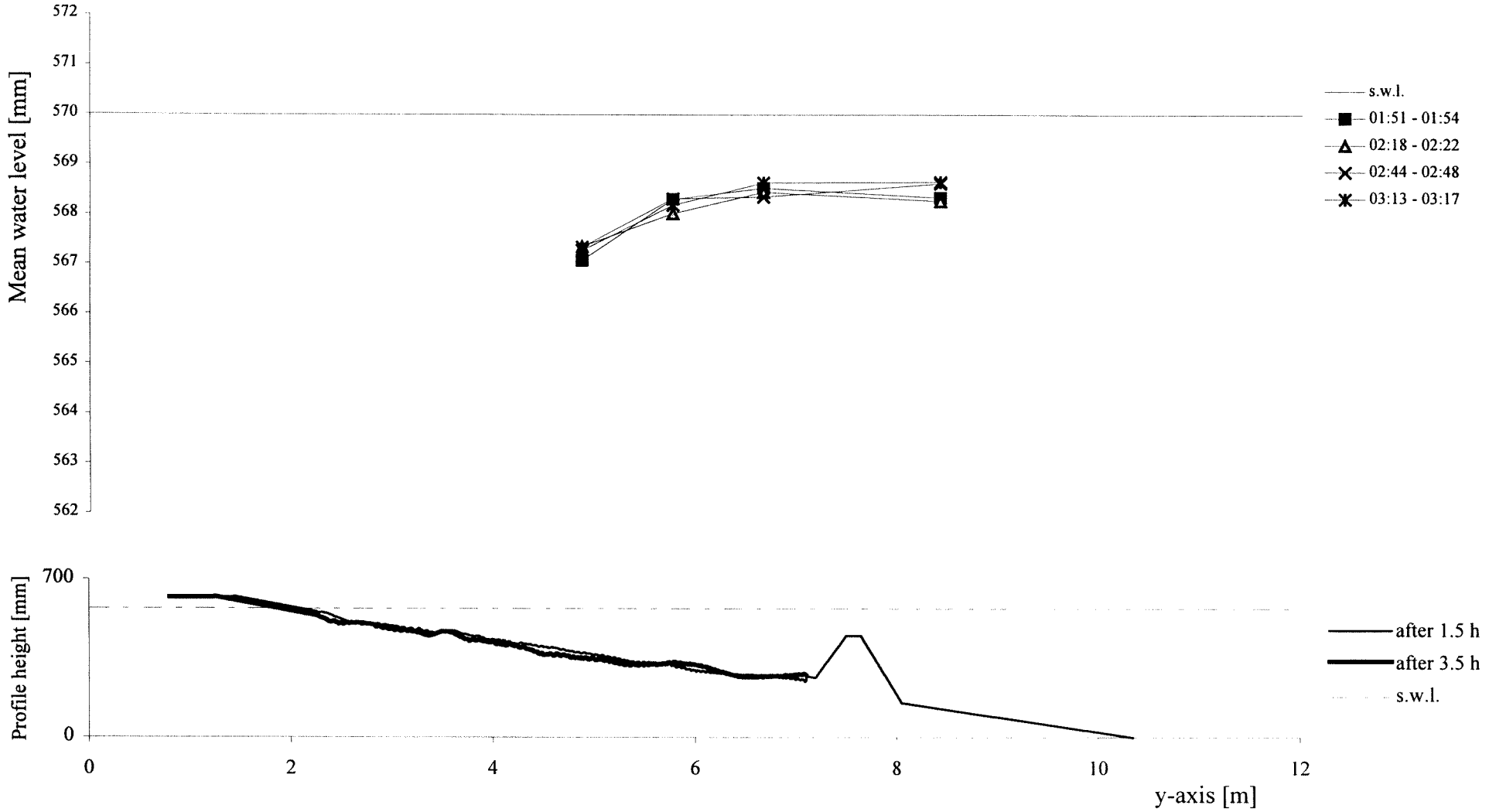

TEST D1 - cross-section x=15.5 m - interval 01:30 - 03:30

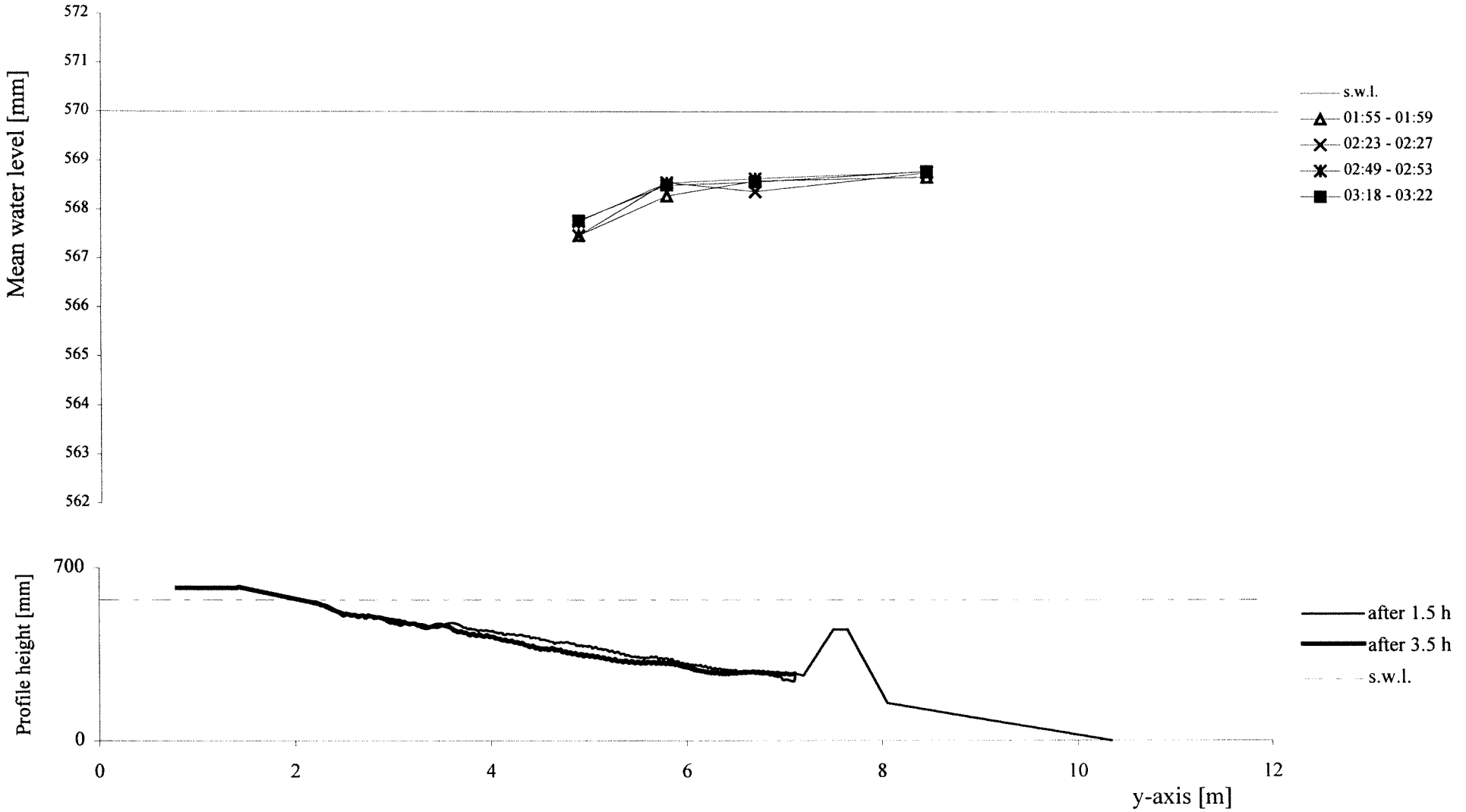

TEST D1 - cross-section x=17 m - interval 01:30 - 03:30

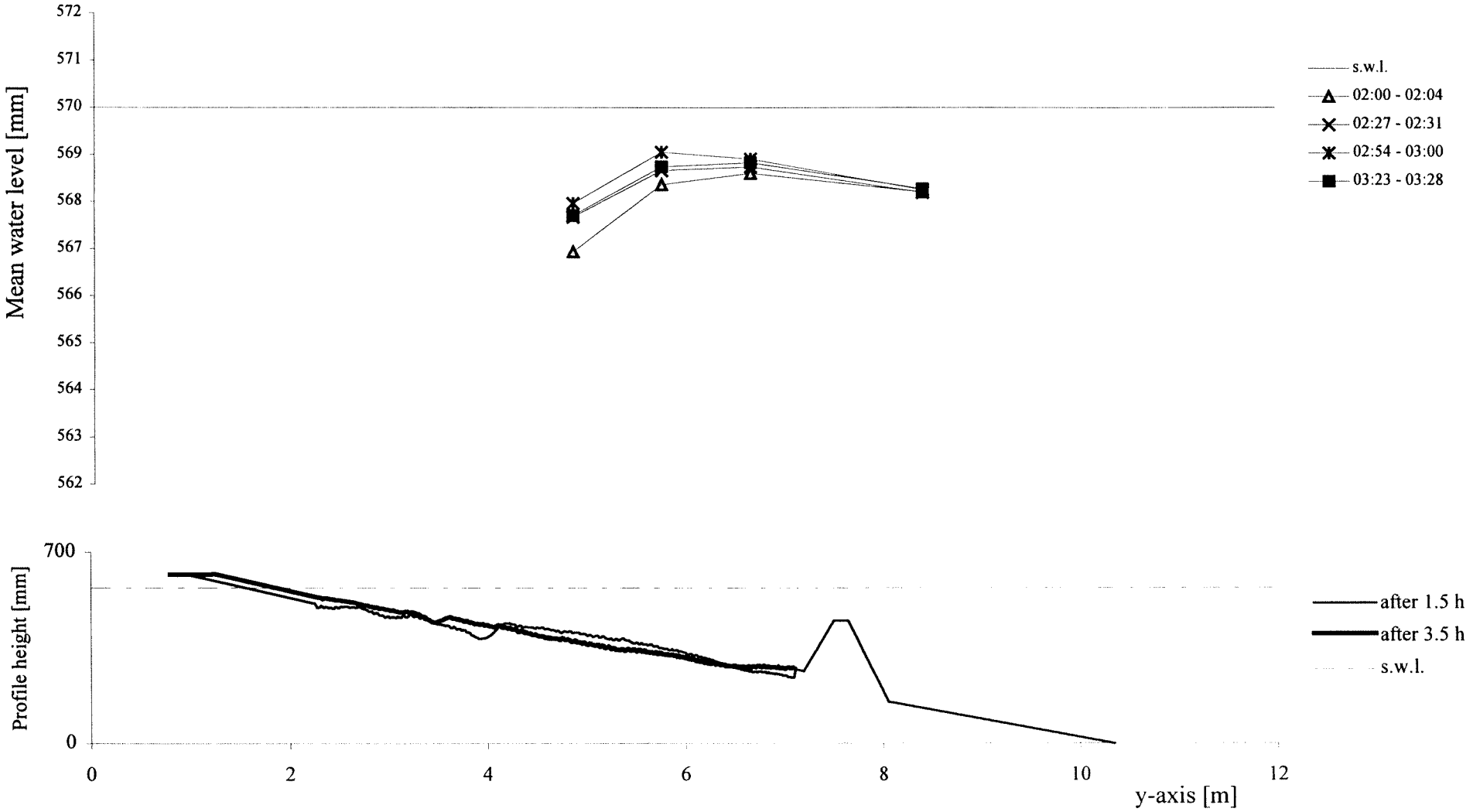

TEST D1 - cross-section x=18.5 m - interval 01:30 - 03:30

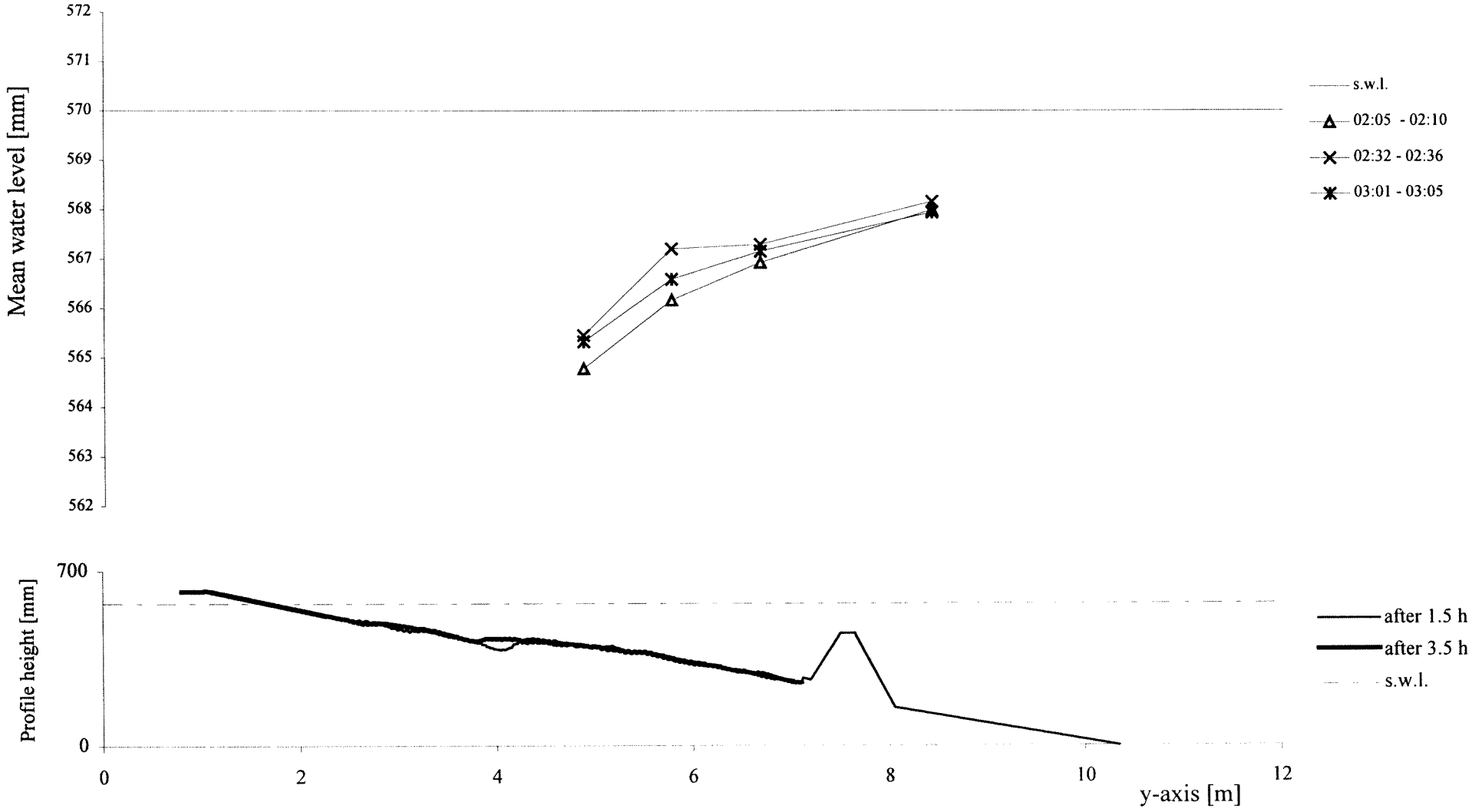

TEST D1 - cross-section x=20 m - interval 01:30 - 03:30

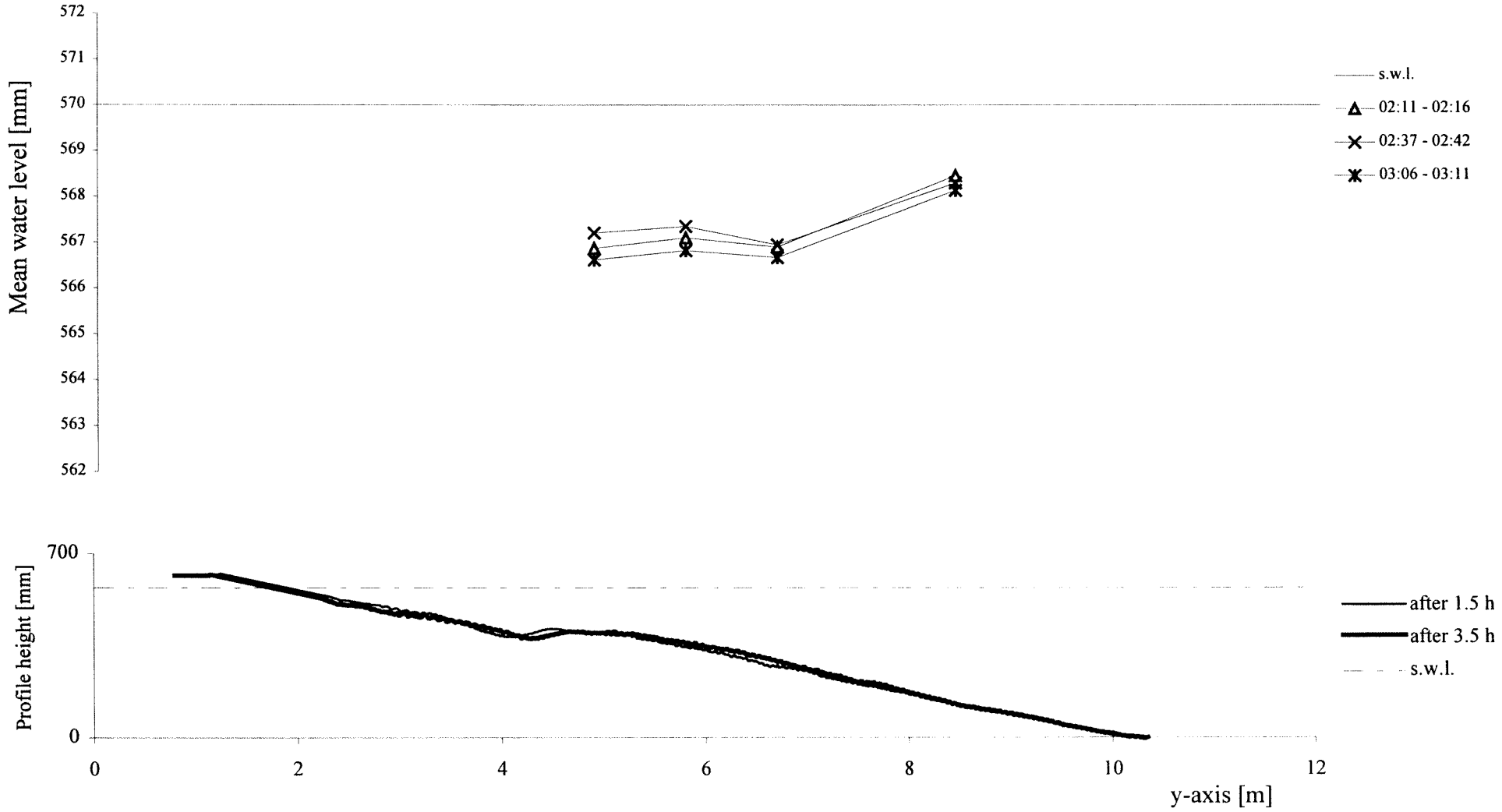

TEST D1 - cross-section x=12.5 m - interval 03:30 - 07:30

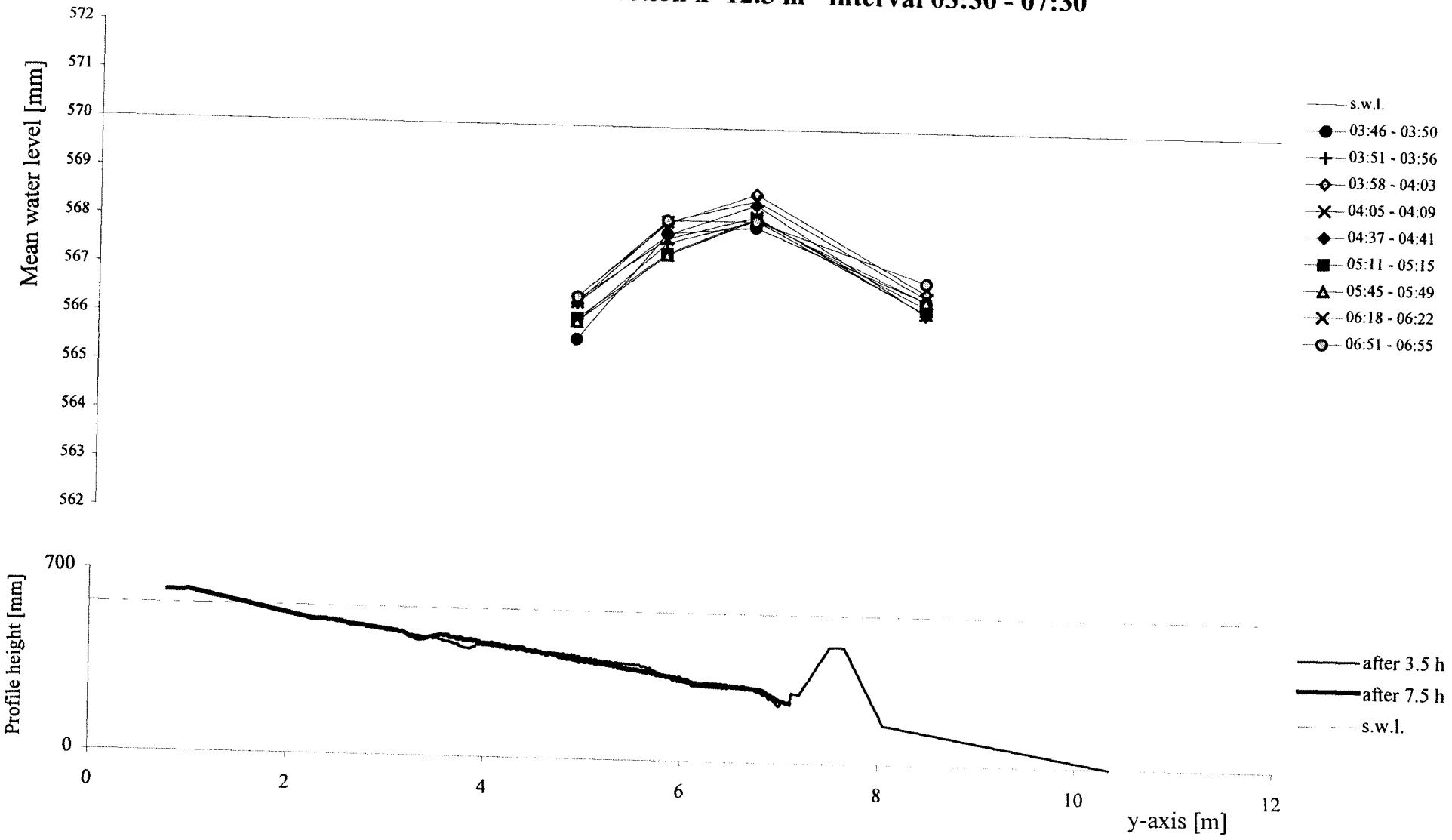

TEST D1 - cross-section x=14 m - interval 03:30 - 07:30

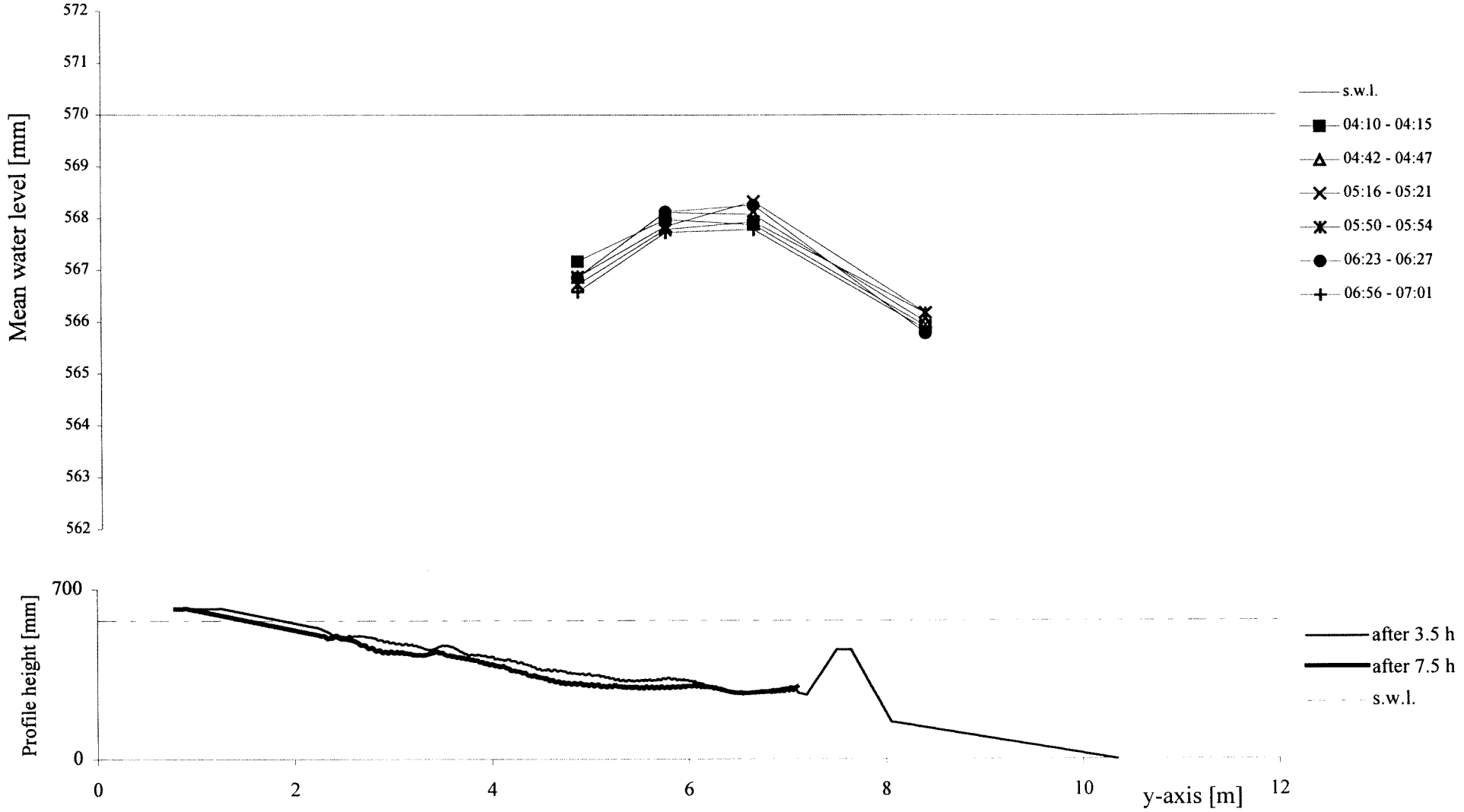

TEST D1 - cross-section x=15.5 m - interval 03:30 - 07:30

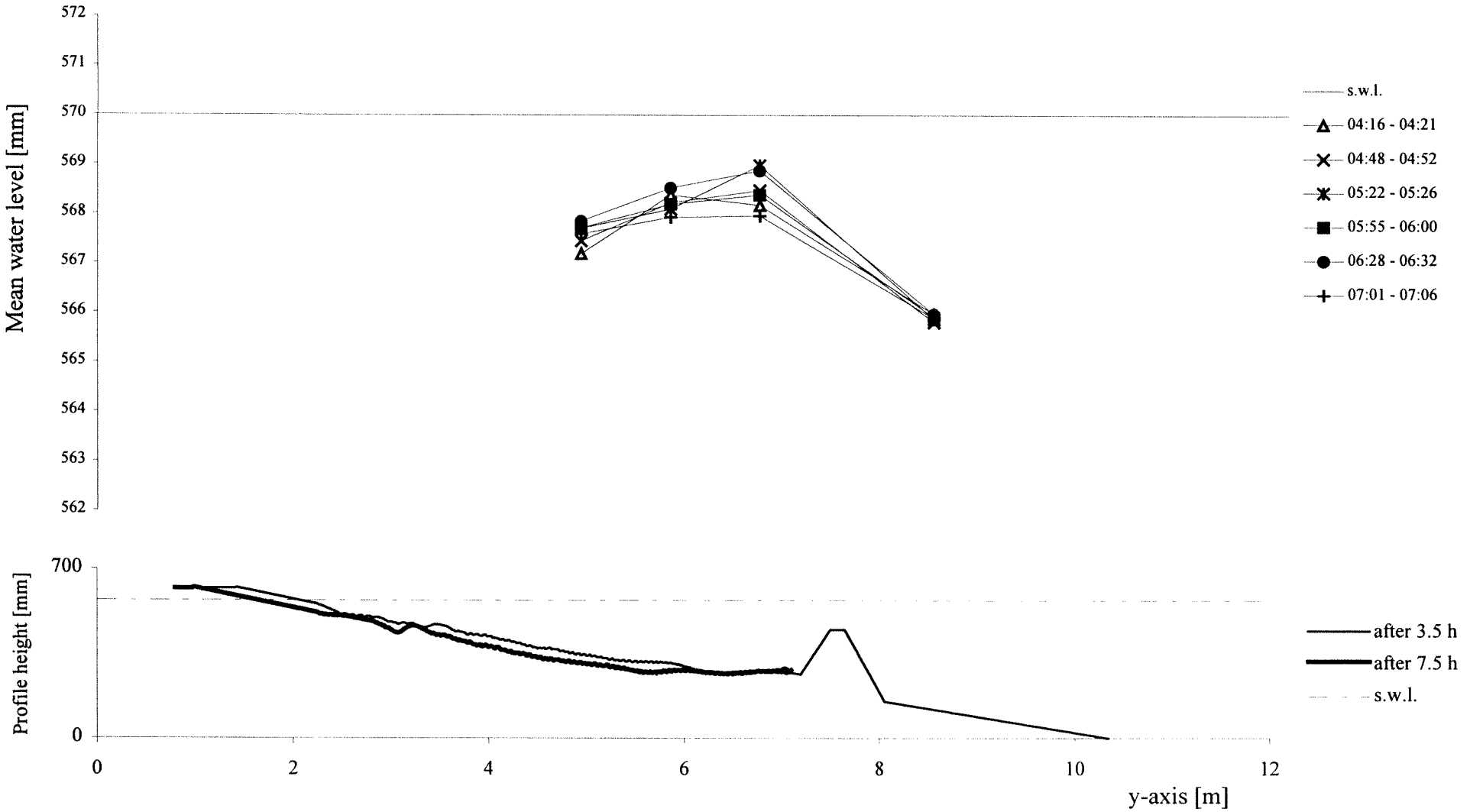

TEST D1 - cross-section x=17 m - interval 03:30 - 07:30

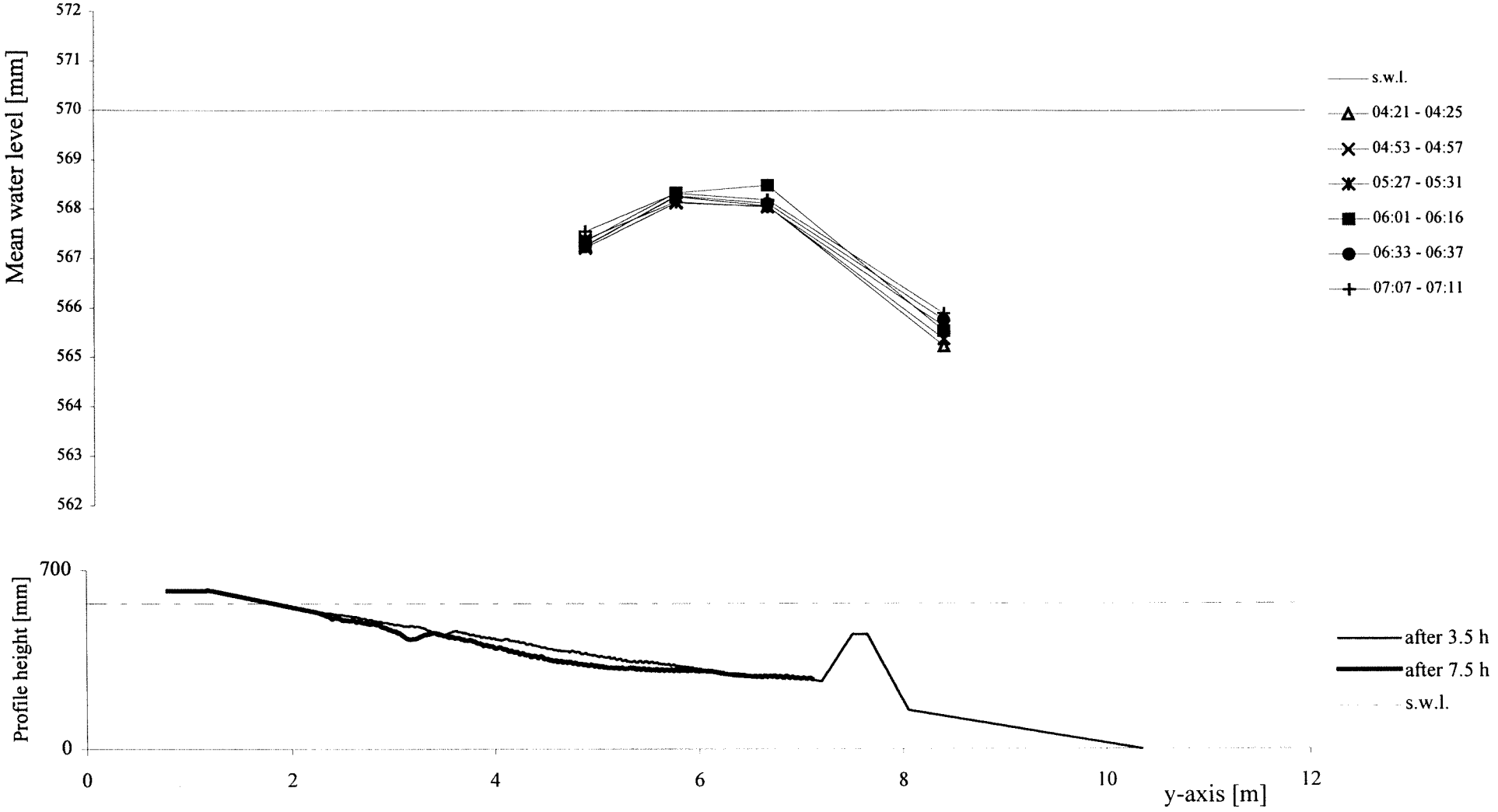

TEST D1 - cross-section x=18.5 m - interval 03:30 - 07:30

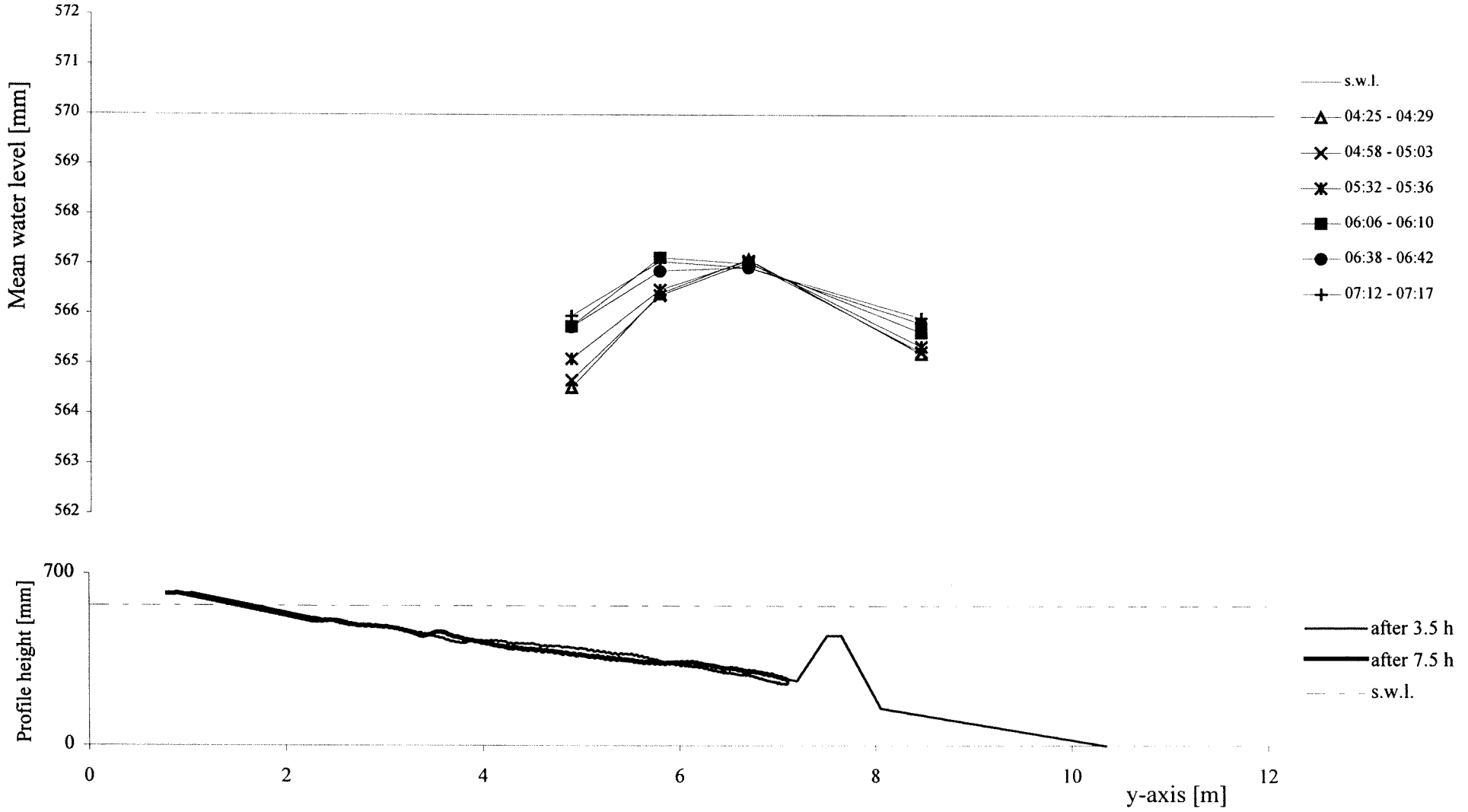

TEST D1 - cross-section x=20 m - interval 03:30 - 07:30

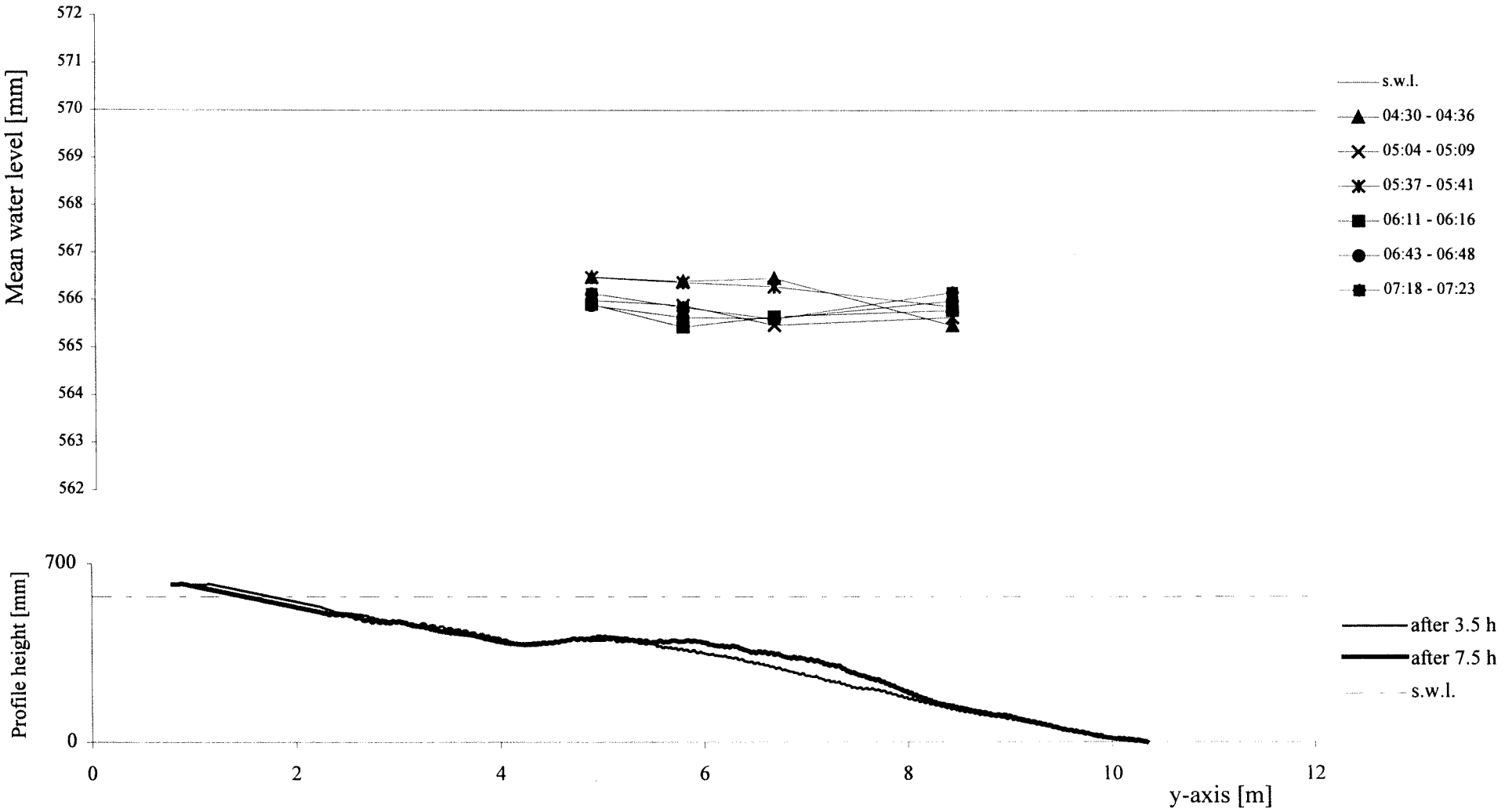

Appendix C2. Graphics TEST D2 - Average Water Level

TEST D2 - cross-section x=12.5 m - interval 00:00 - 00:30

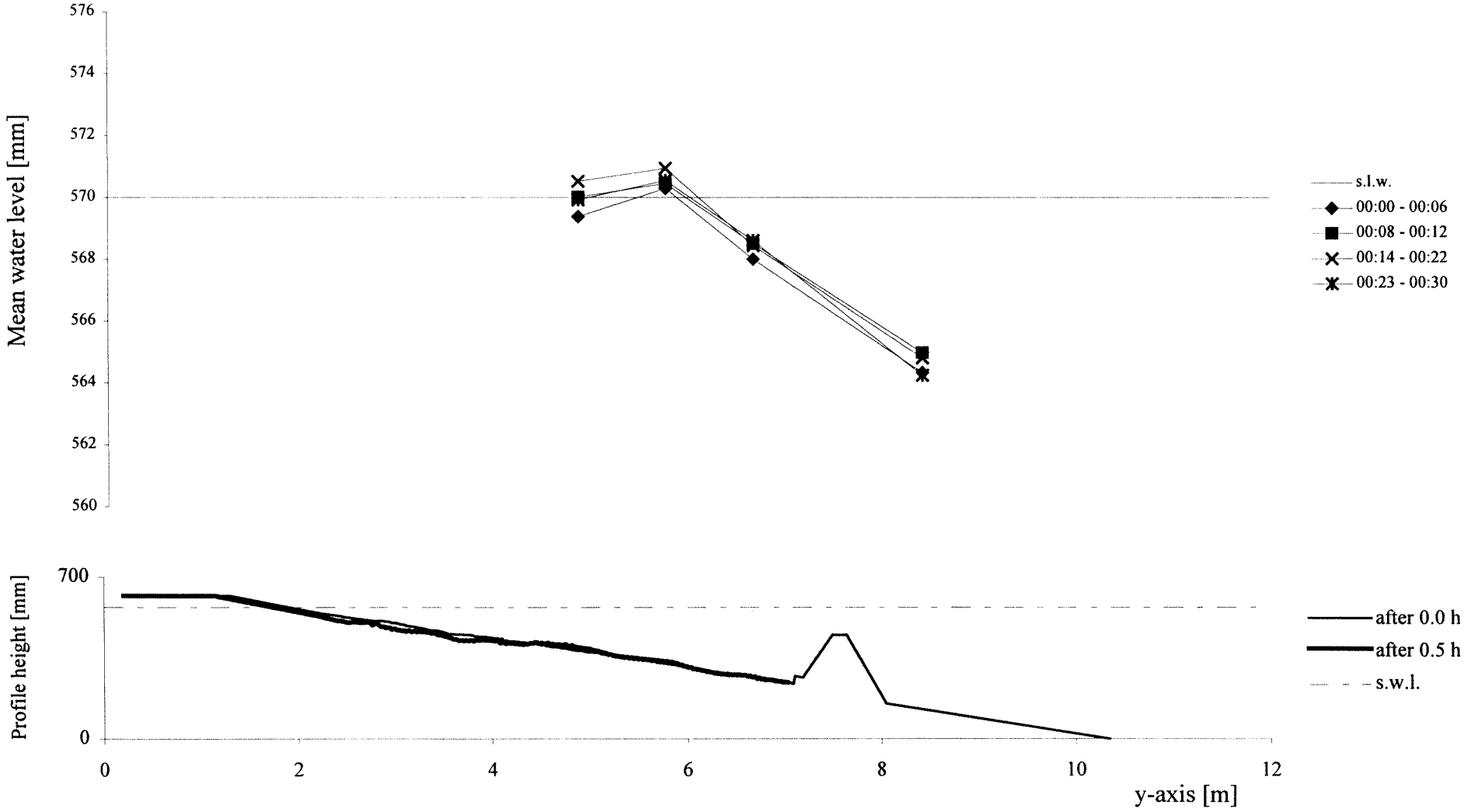

TEST D2 - cross-section x=14 m - interval 00:30 - 01:30

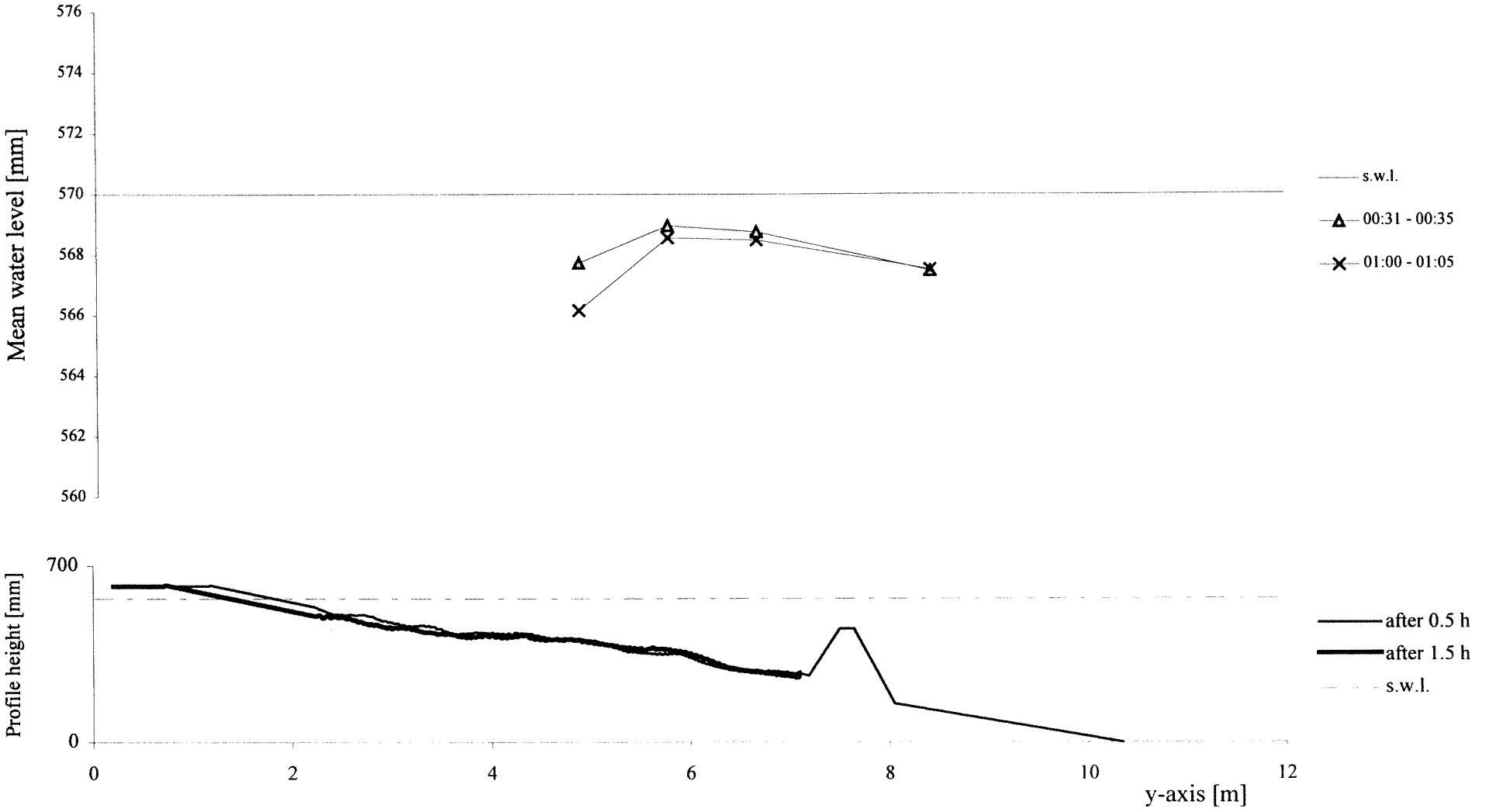

TEST D2 - cross-section x=15.5 m - interval 00:30 - 01:30

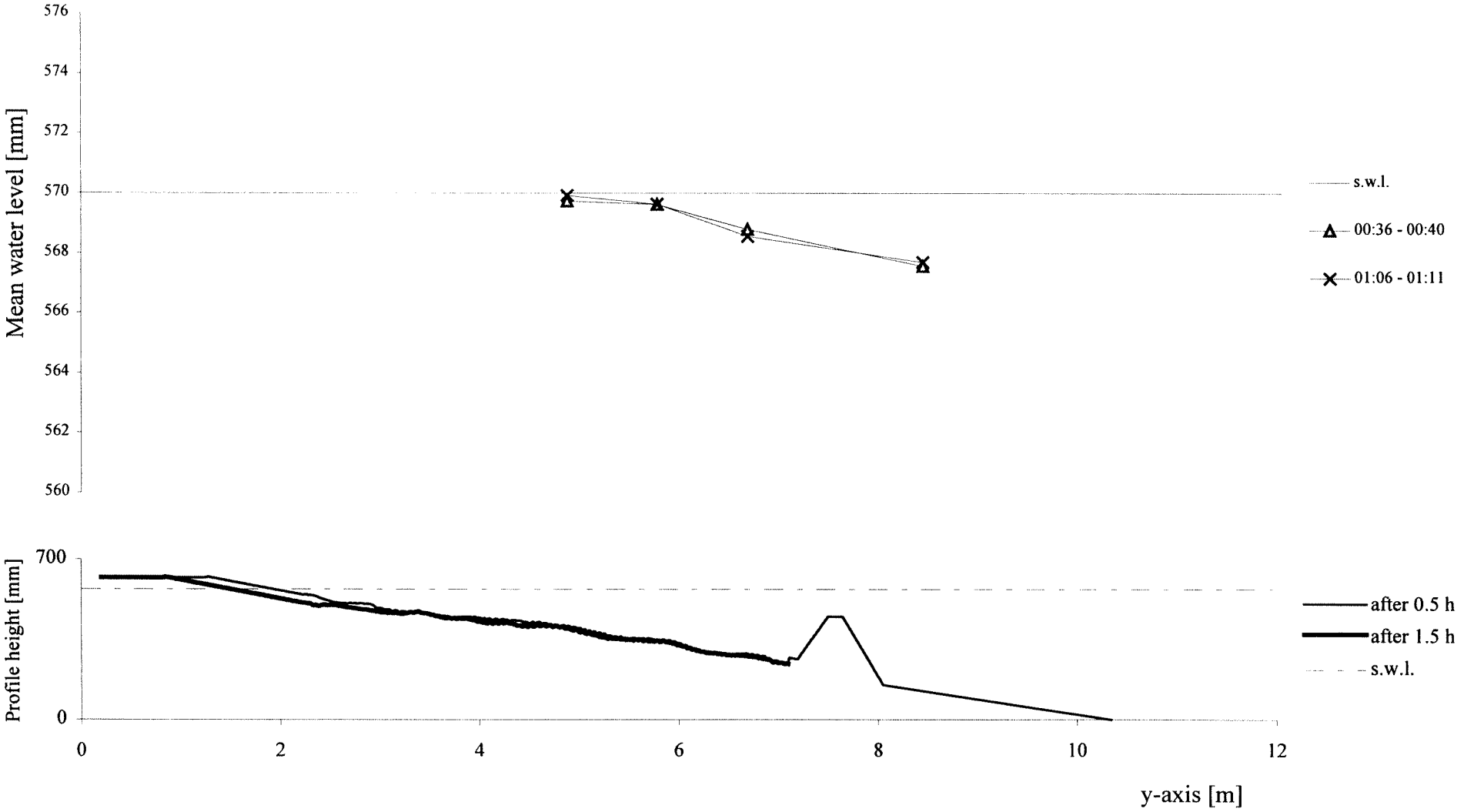

TEST D2 - cross-section x=17 m - interval 00:30 - 01:30

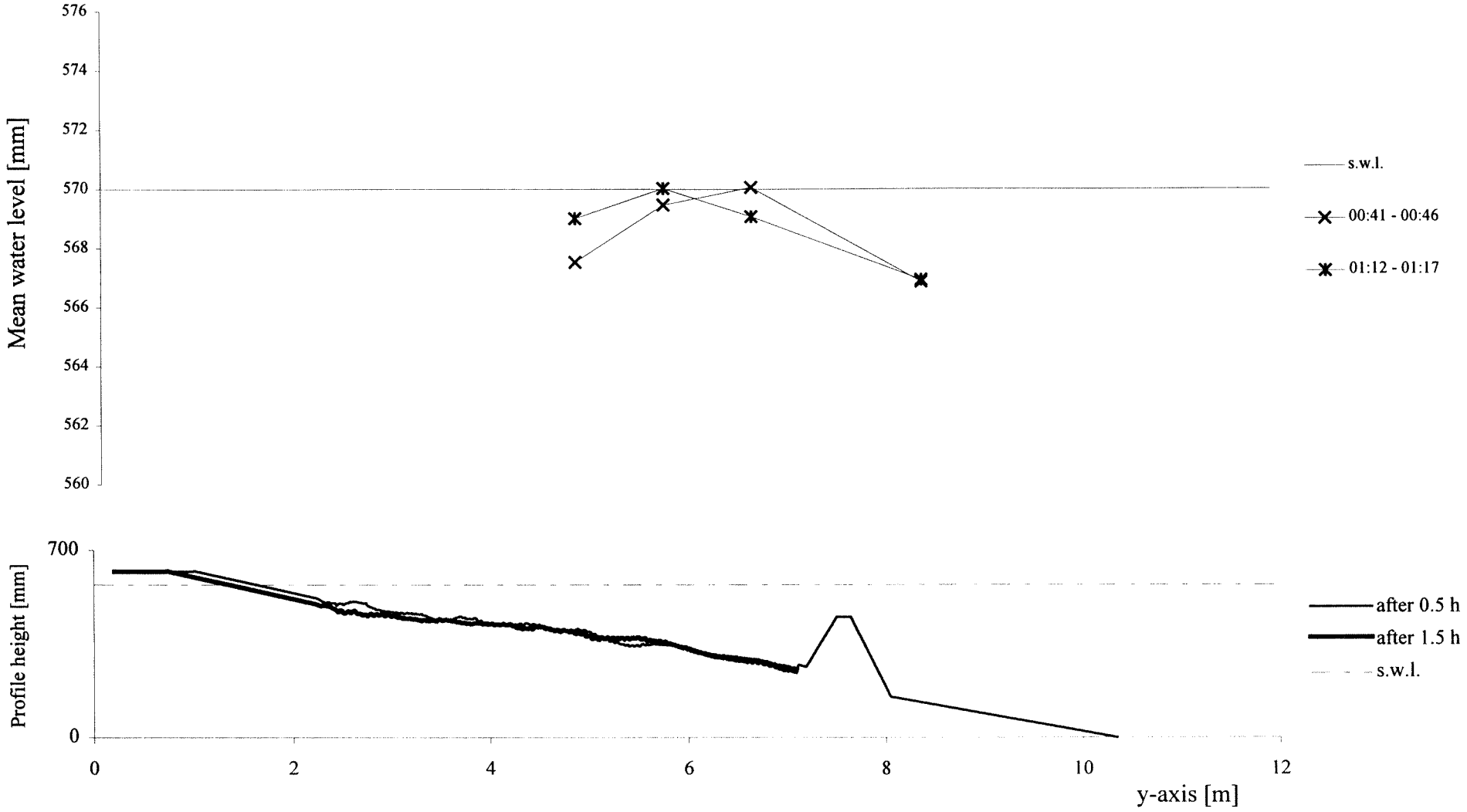

TEST D2 - cross-section x=18.5 m - interval 00:30 - 01:30

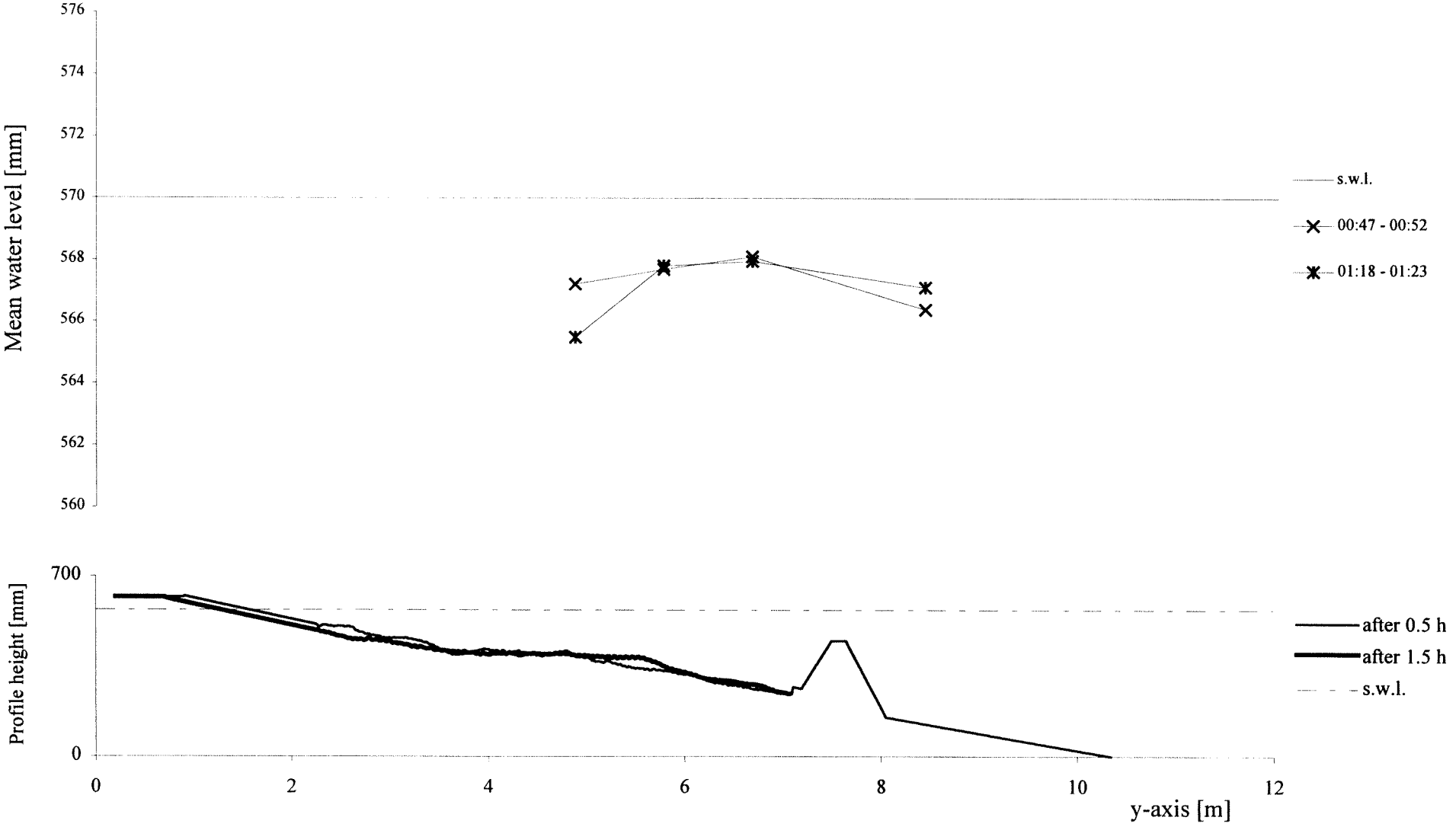

TEST D2 - cross-section x=20 m - interval 00:30 - 01:30

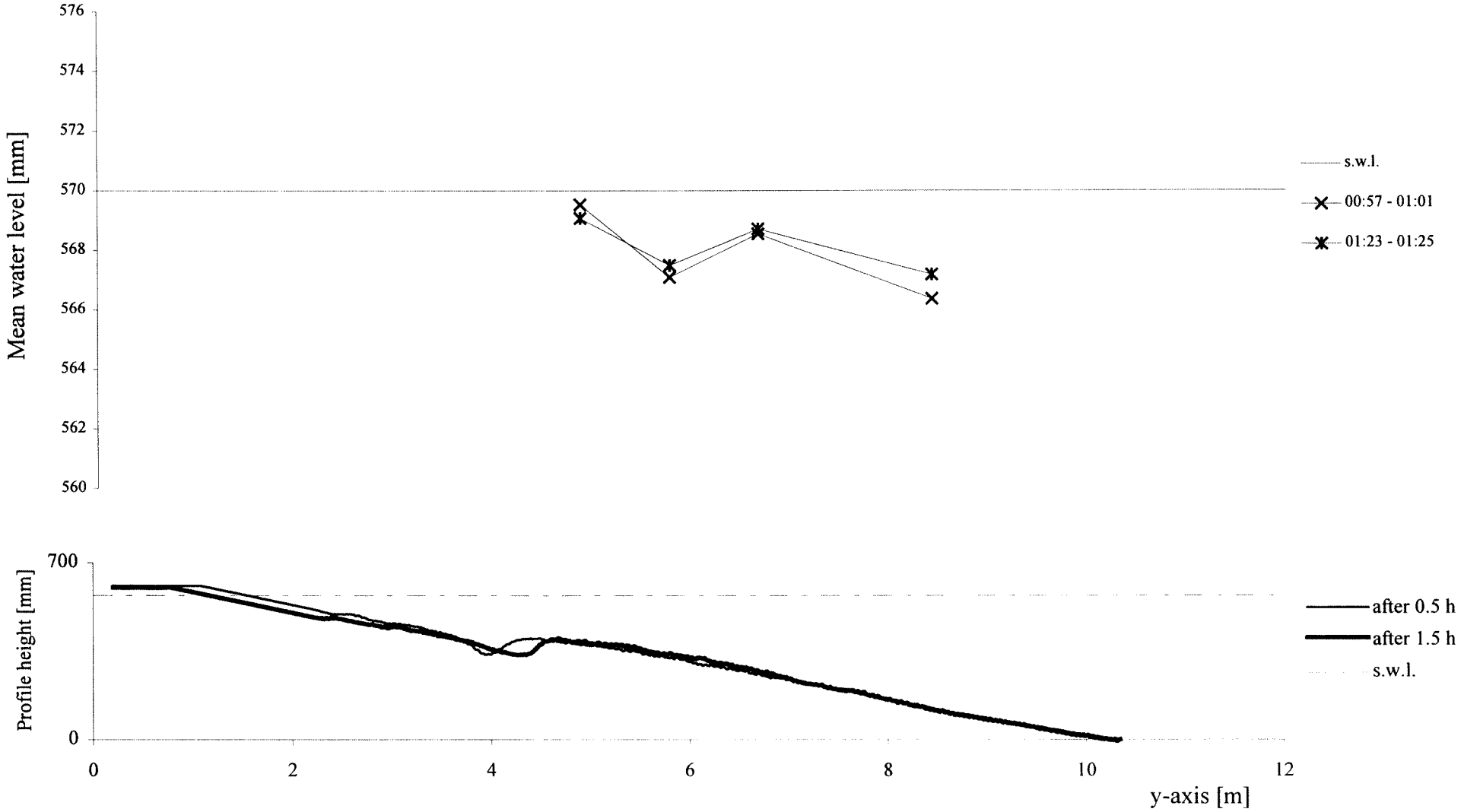

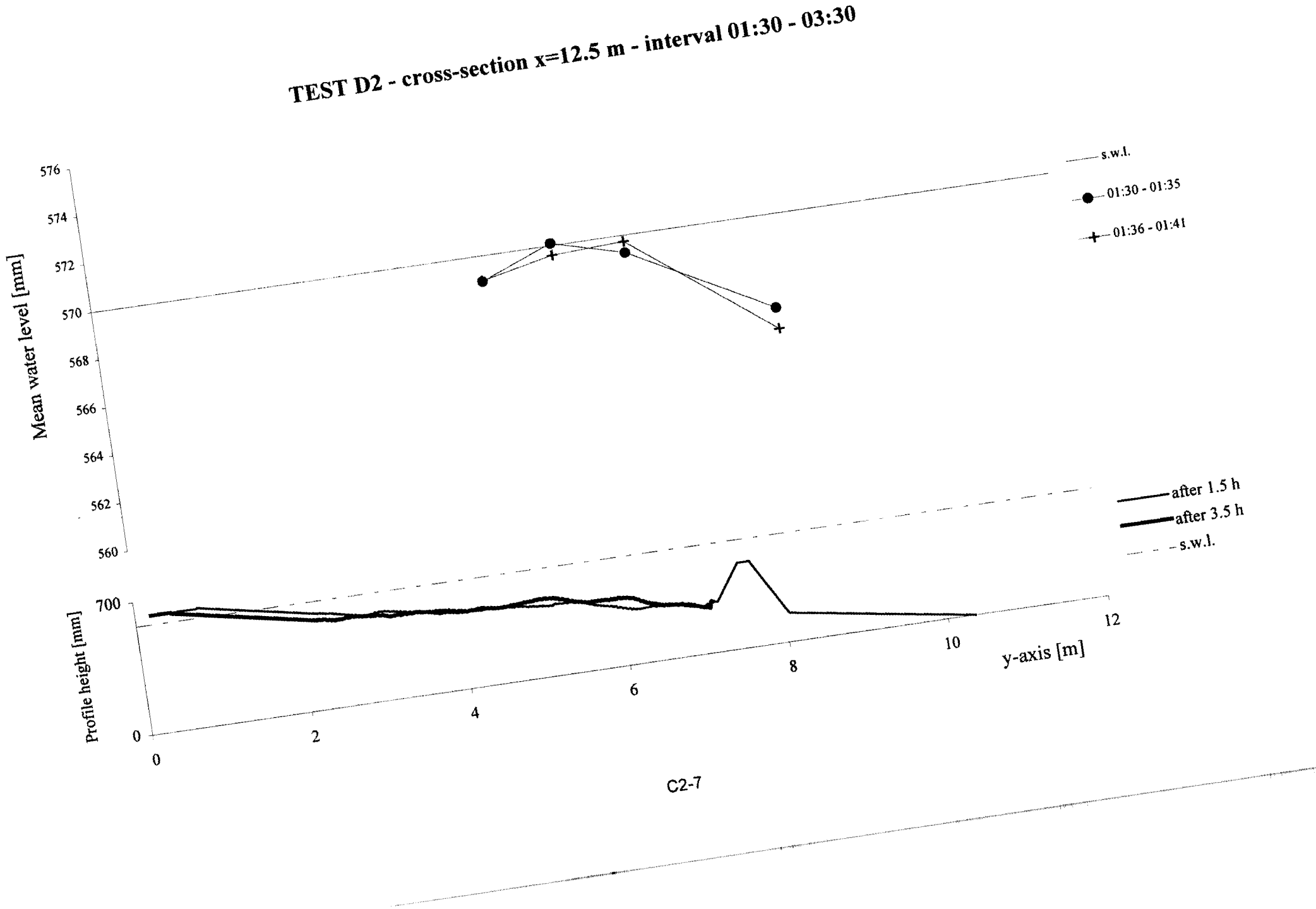
TEST D2 - cross-section x=12.5 m - interval 01:30 - 03:30
Mean water level [mm]
576
574
572
570
568
566
564
562
560
s.w.l.
01:30 - 01:35
01:36 - 01:41
after 1.5 h
after 3.5 h
s.w.l.
Profile height [mm]
700
0
0
2
4
6
8
10
12
y-axis [m]
C2-7

TEST D2 - cross-section x=14 m - interval 01:30 - 03:30

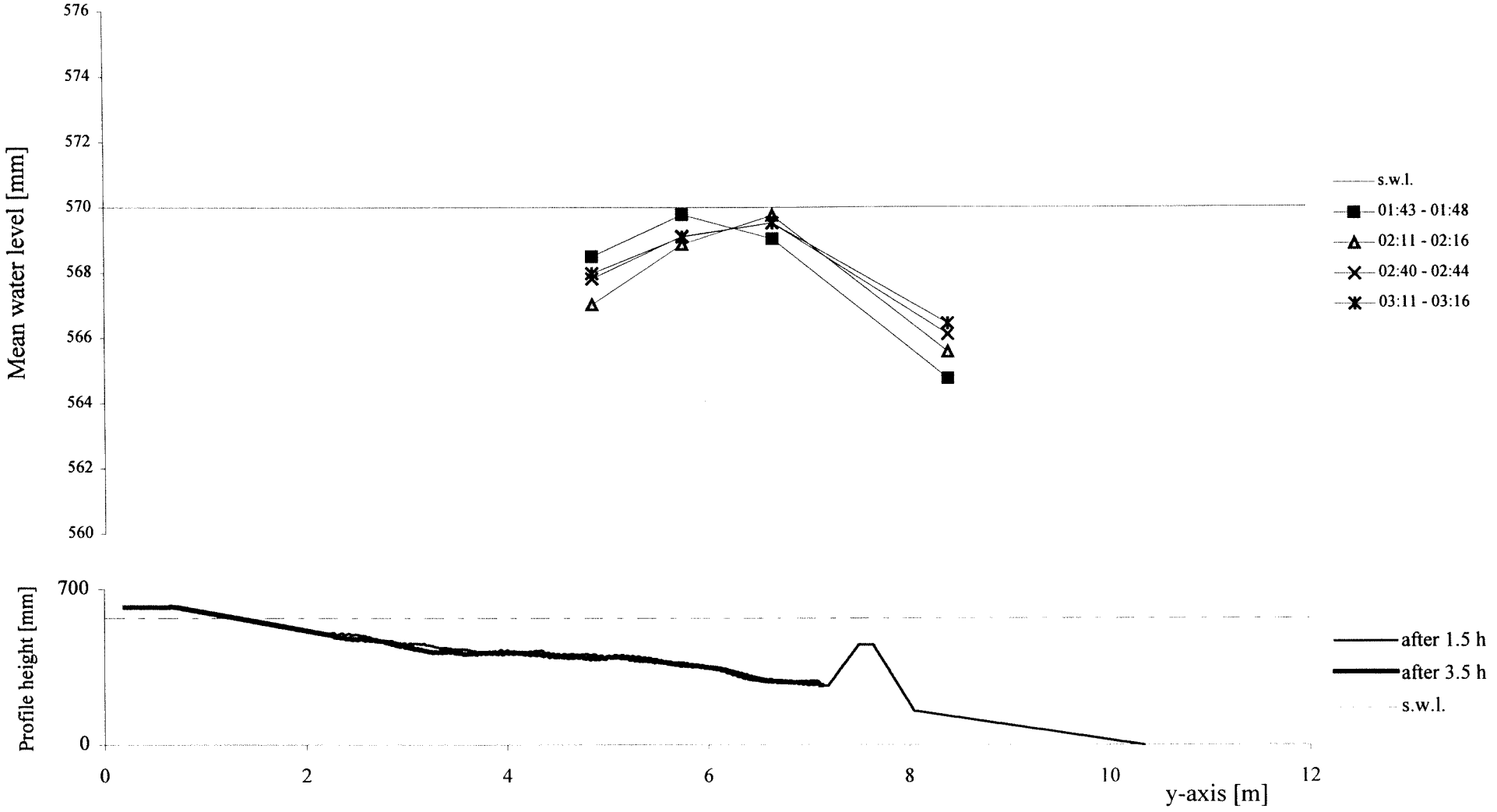

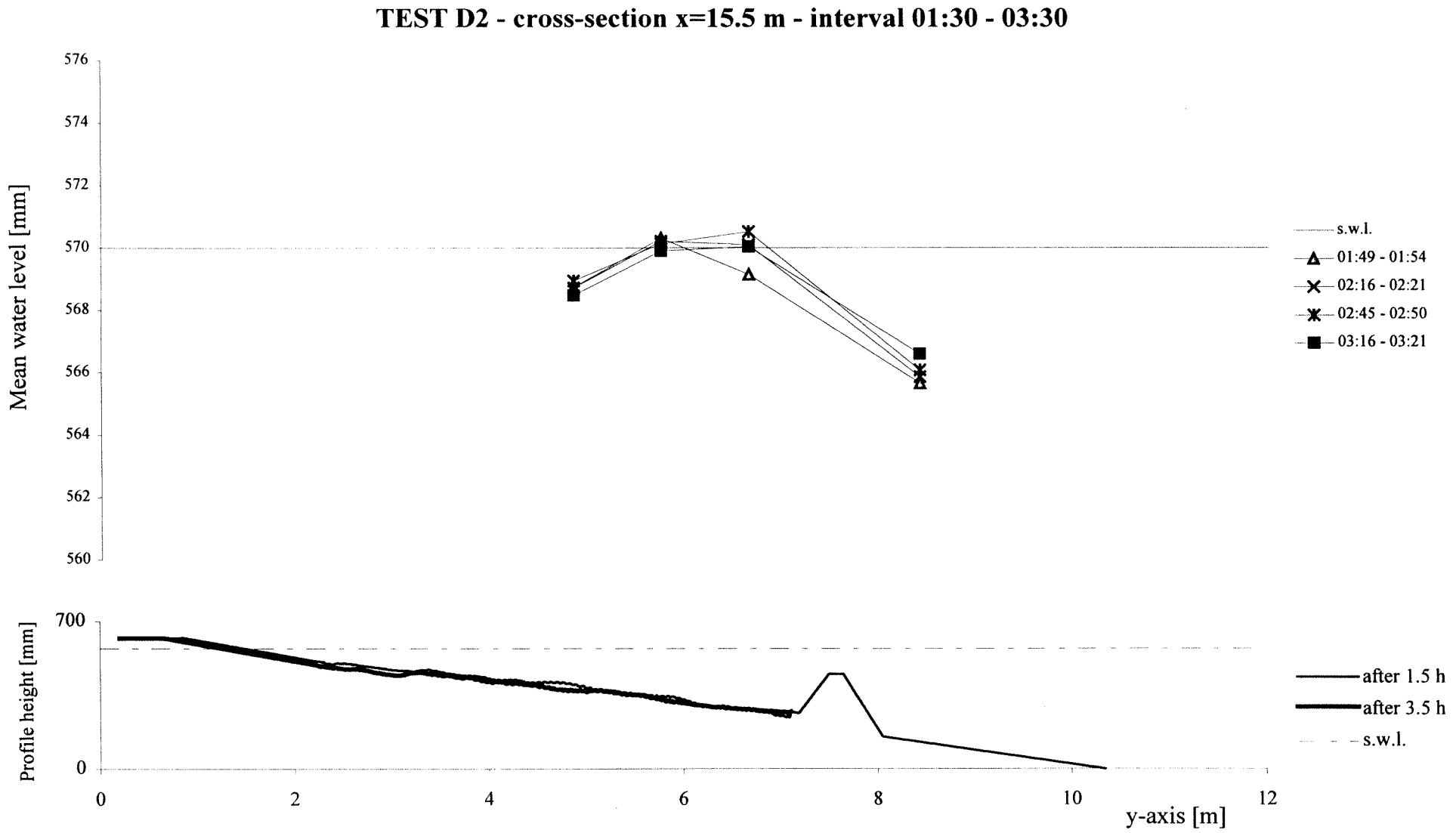
TEST D2 - cross-section x=15.5 m - interval 01:30 - 03:30
Mean water level [mm]
576
574
572
570
568
566
564
562
560
s.w.l.
01:49 - 01:54
02:16 - 02:21
02:45 - 02:50
03:16 - 03:21
Profile height [mm]
700
0
0
2
4
6
8
10
12
y-axis [m]
after 1.5 h
after 3.5 h
s.w.l.

TEST D2 - cross-section x=17 m - interval 01:30 - 03:30

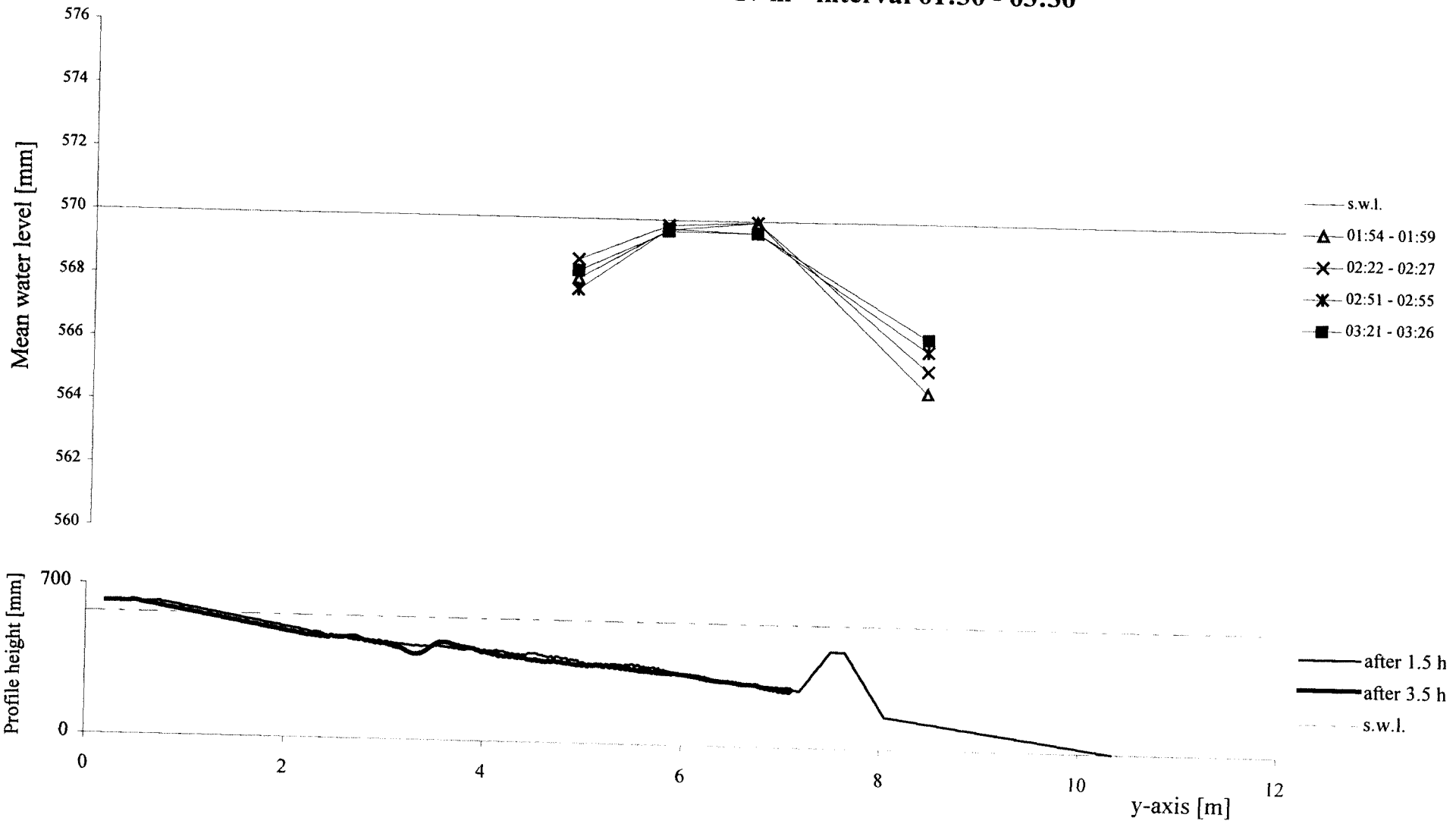

TEST D2 - cross-section x=18.5 m - interval 01:30 - 03:30

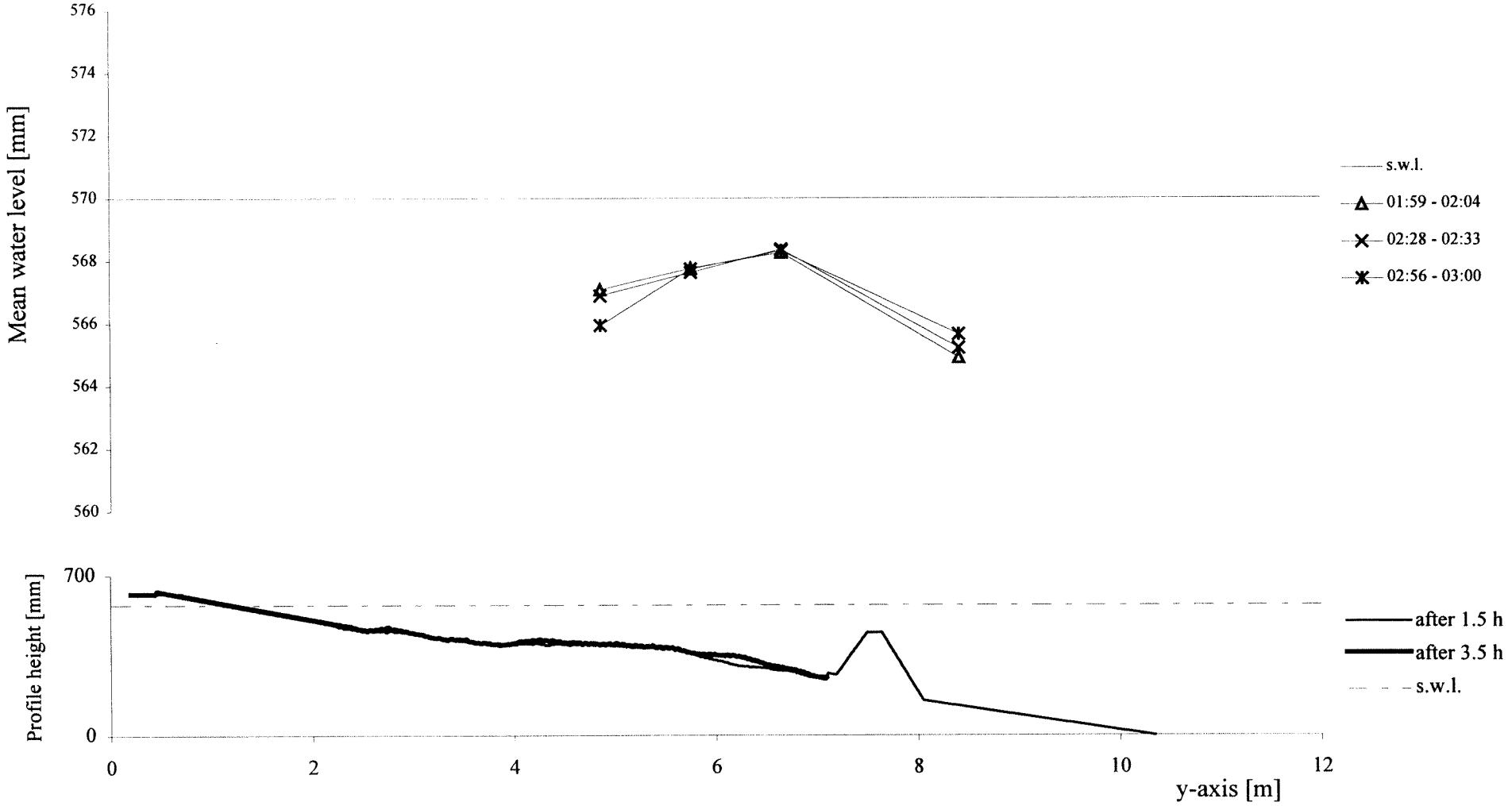

TEST D2 - cross-section x=20 m - interval 01:30 - 03:30

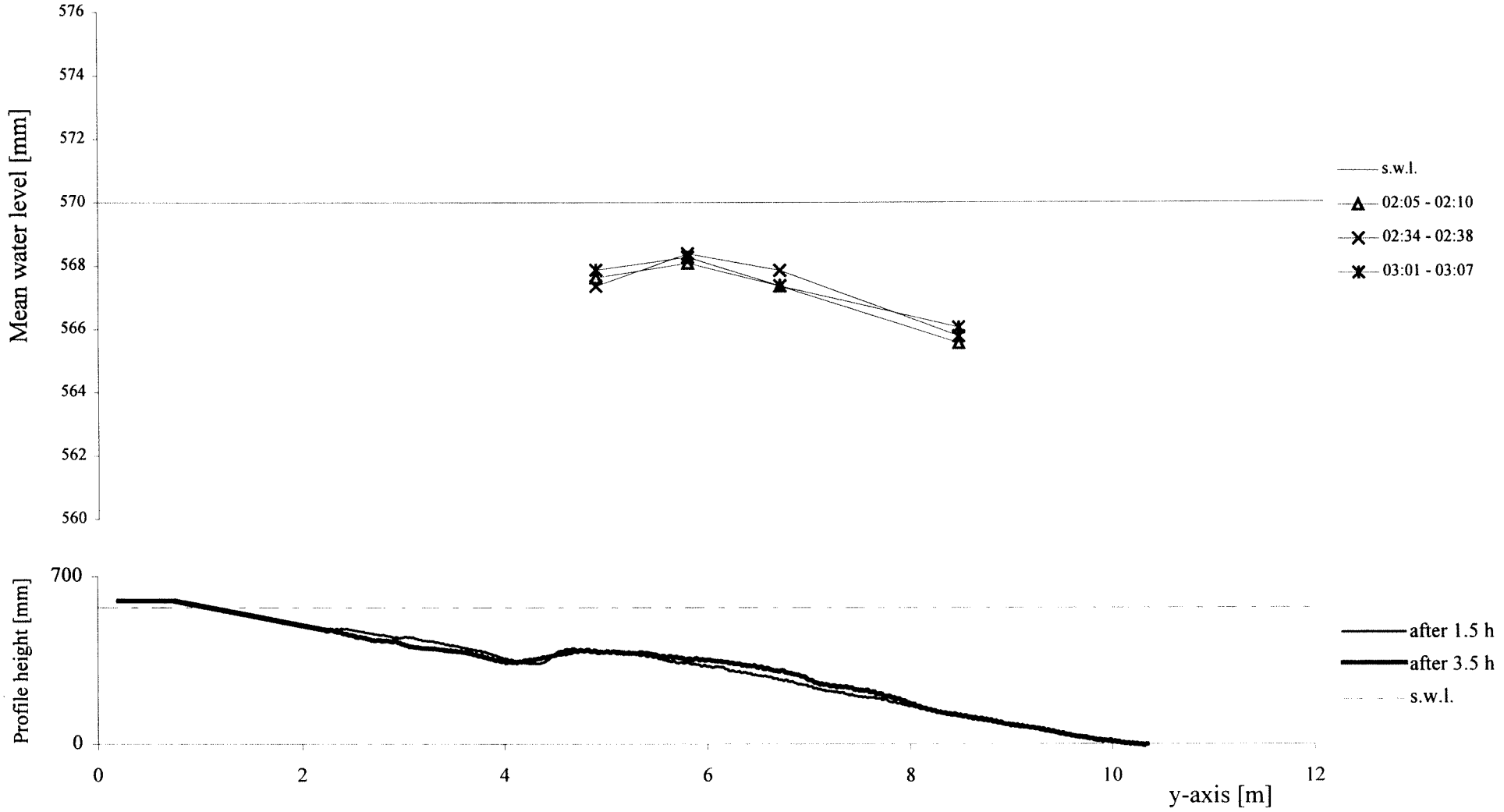

TEST D2 - cross-section x=12.5 m - interval 03:30 - 07:30

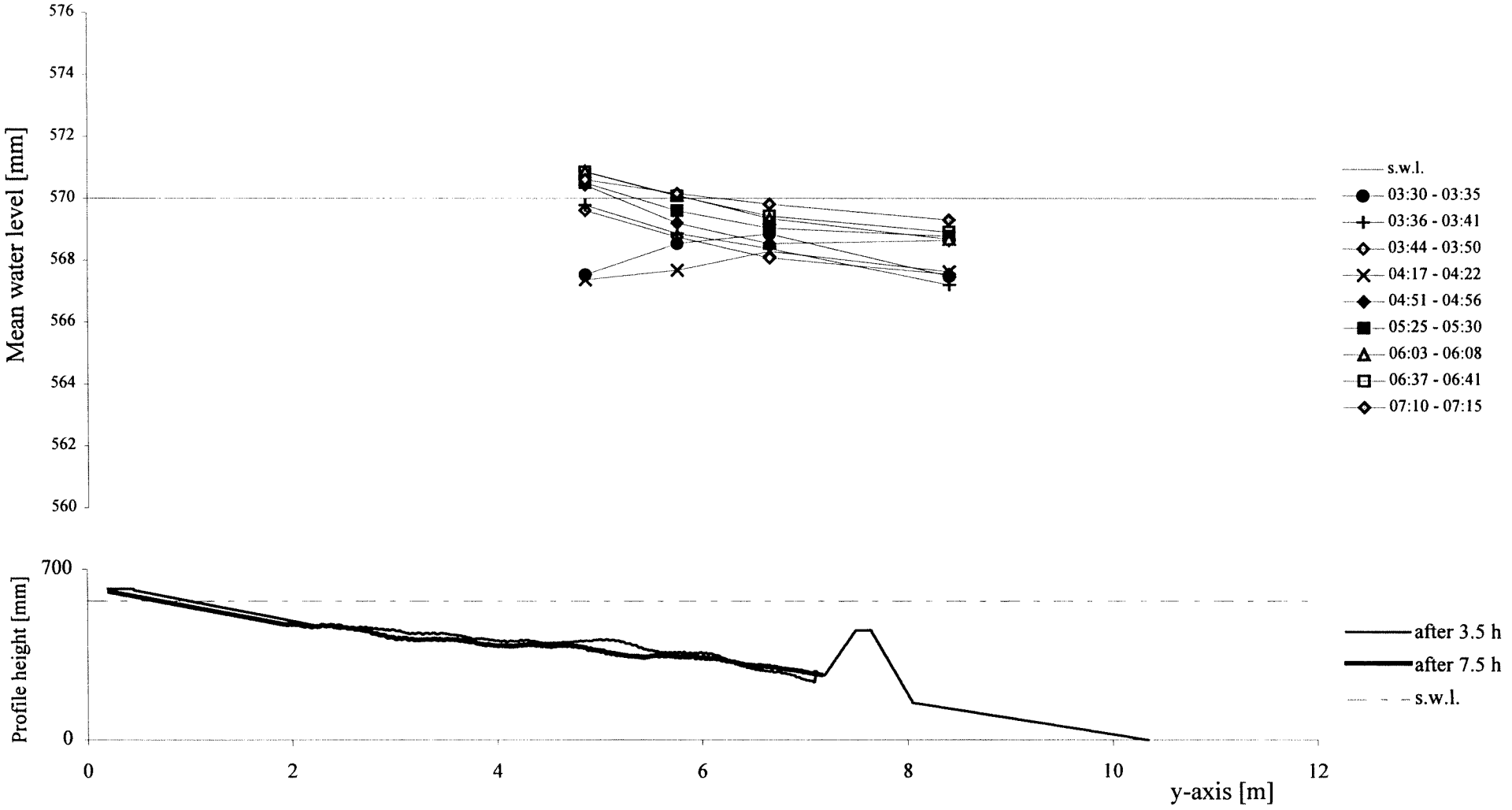

TEST D2 - cross-section x=14 m - interval 03:30 - 07:30

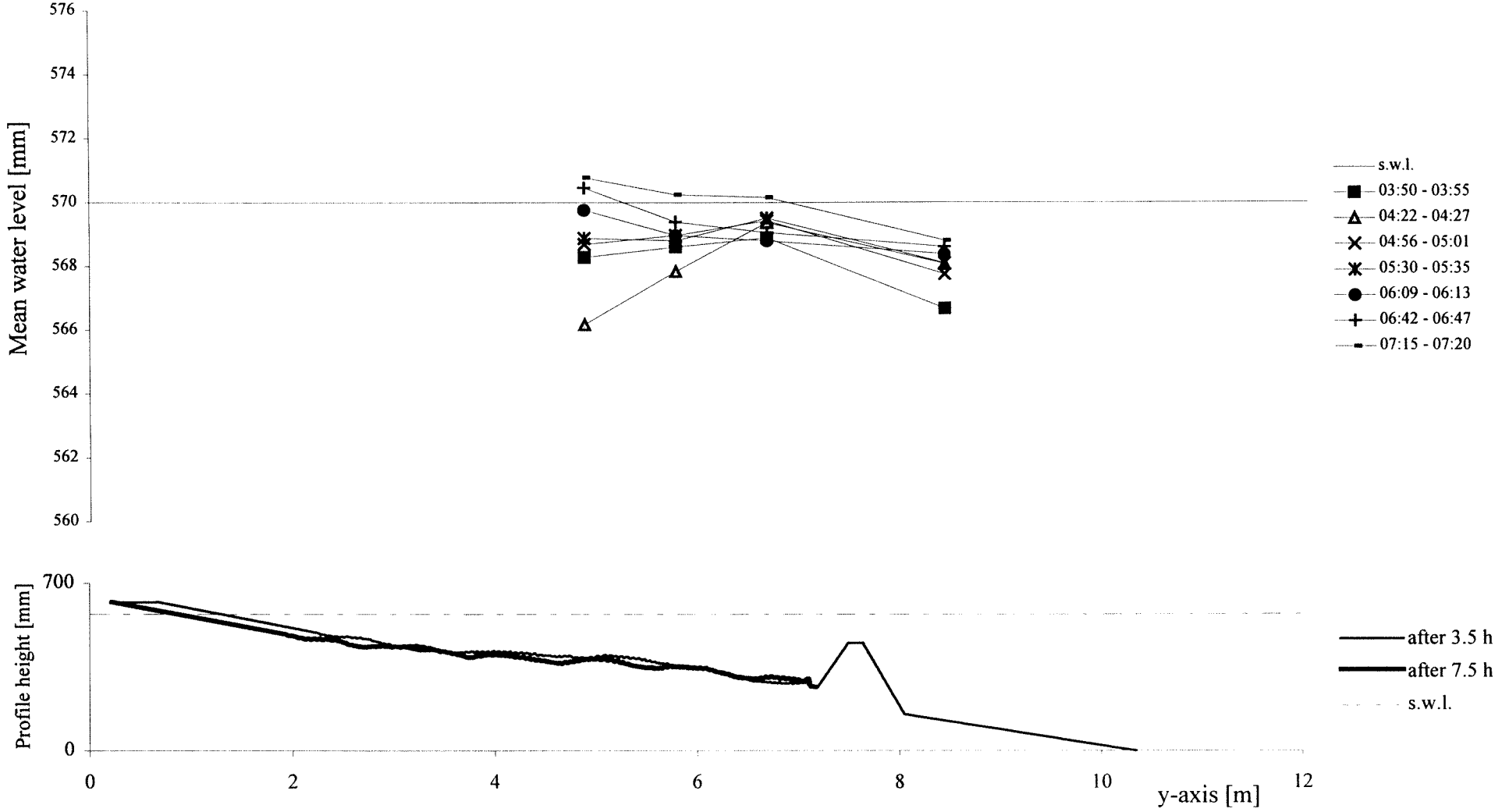

TEST D2 - cross-section x=15.5 m - interval 03:30 - 07:30

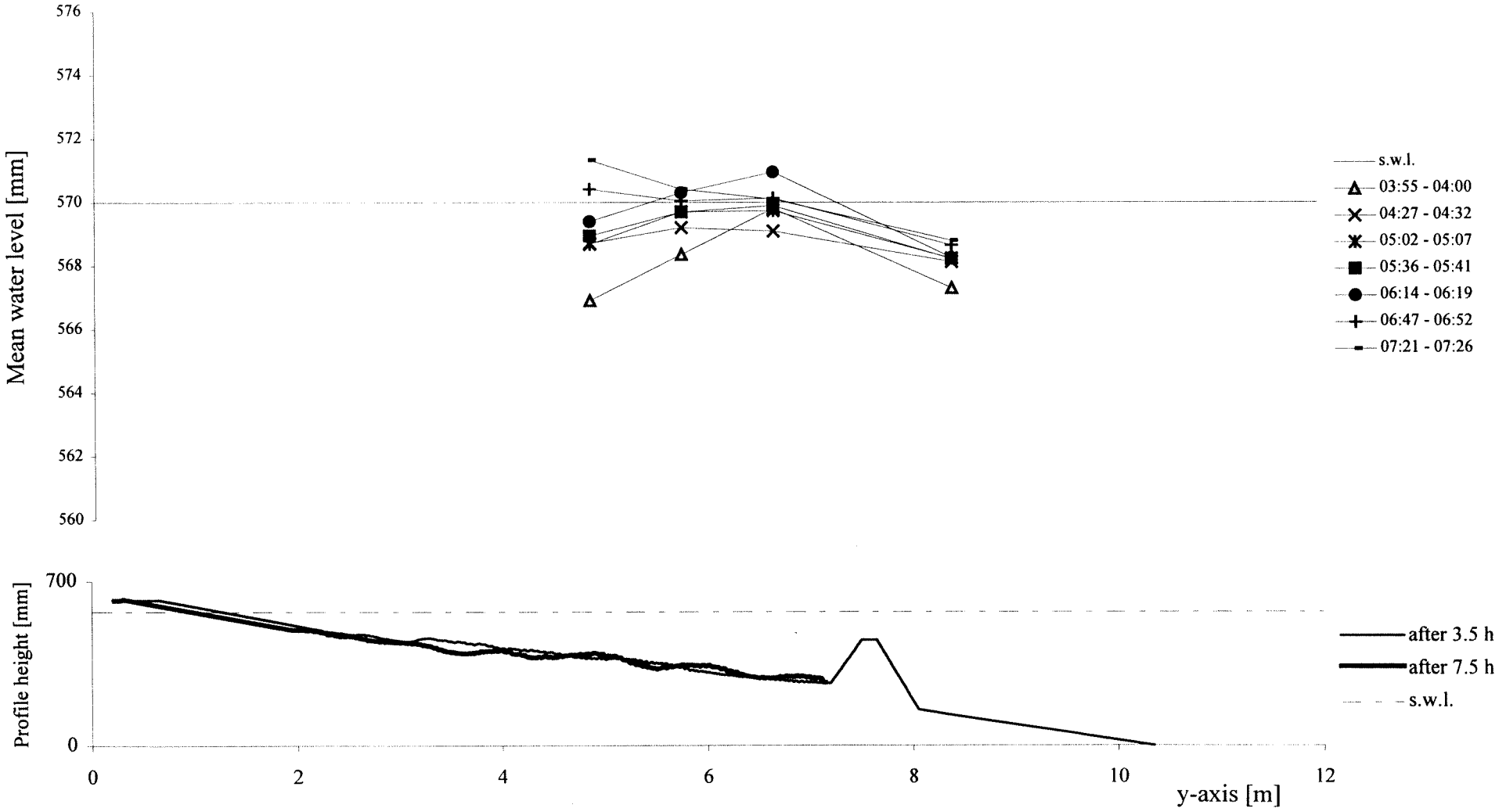

TEST D2 - cross-section x=17 m - interval 03:30 - 07:30

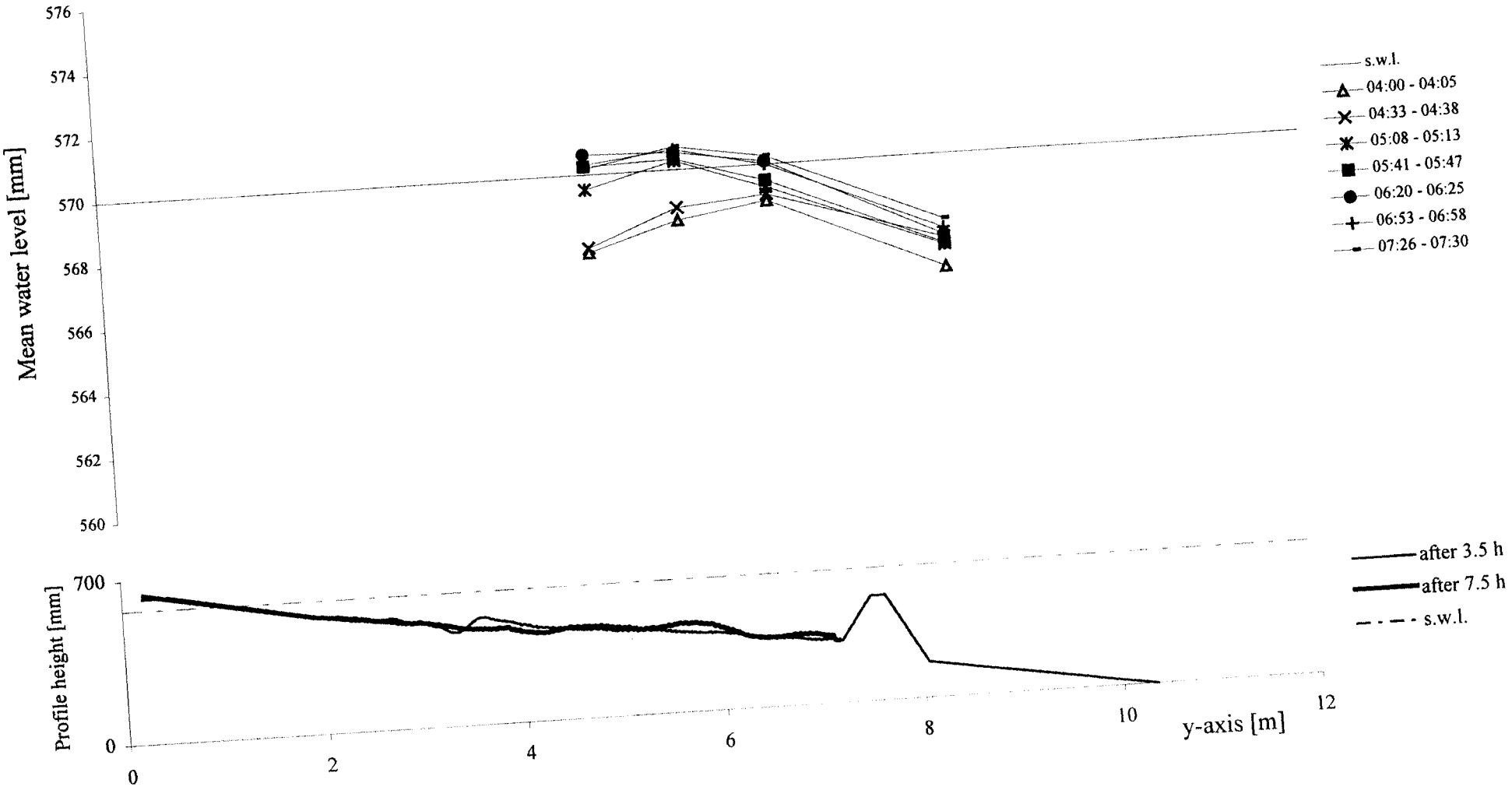

TEST D2 - cross-section x=18.5 m - interval 03:30 - 07:30

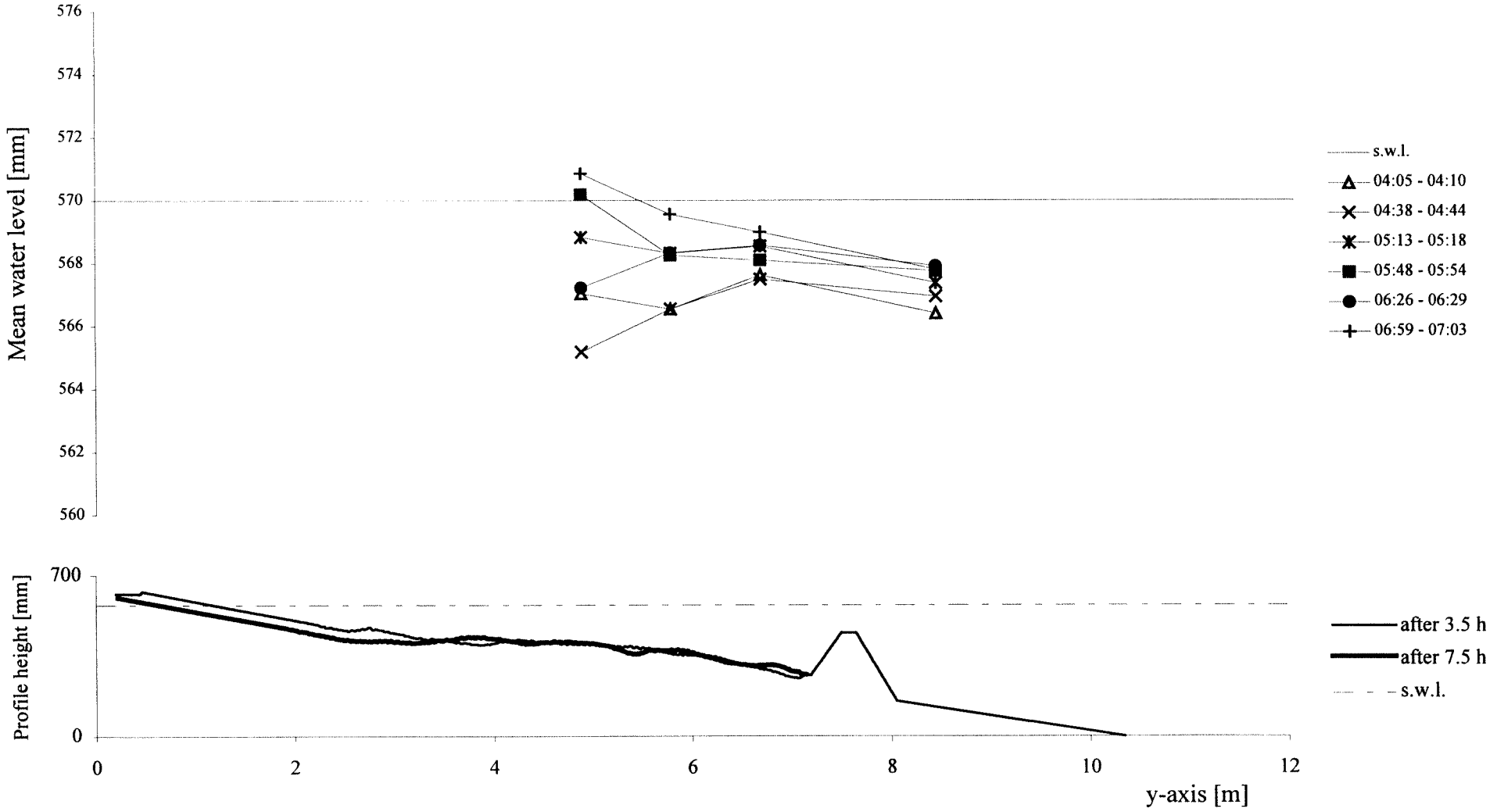

TEST D2 - cross-section x=20 m - interval 03:30 - 07:30

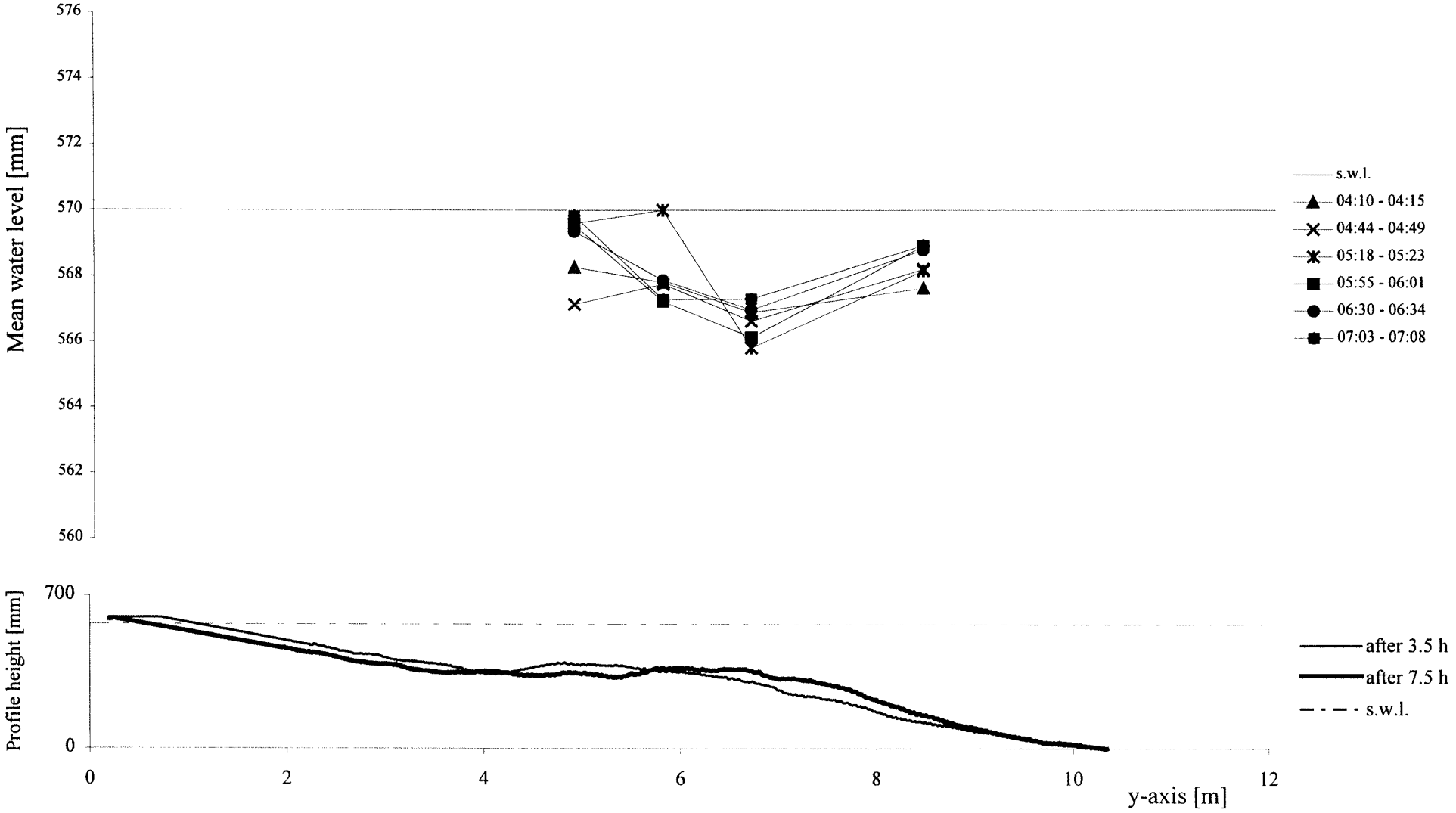

Appendix C3. Graphics TEST D3 - Average Water Level

TEST D3 - cross-section x=12.5 m - interval 00:00 - 00:30

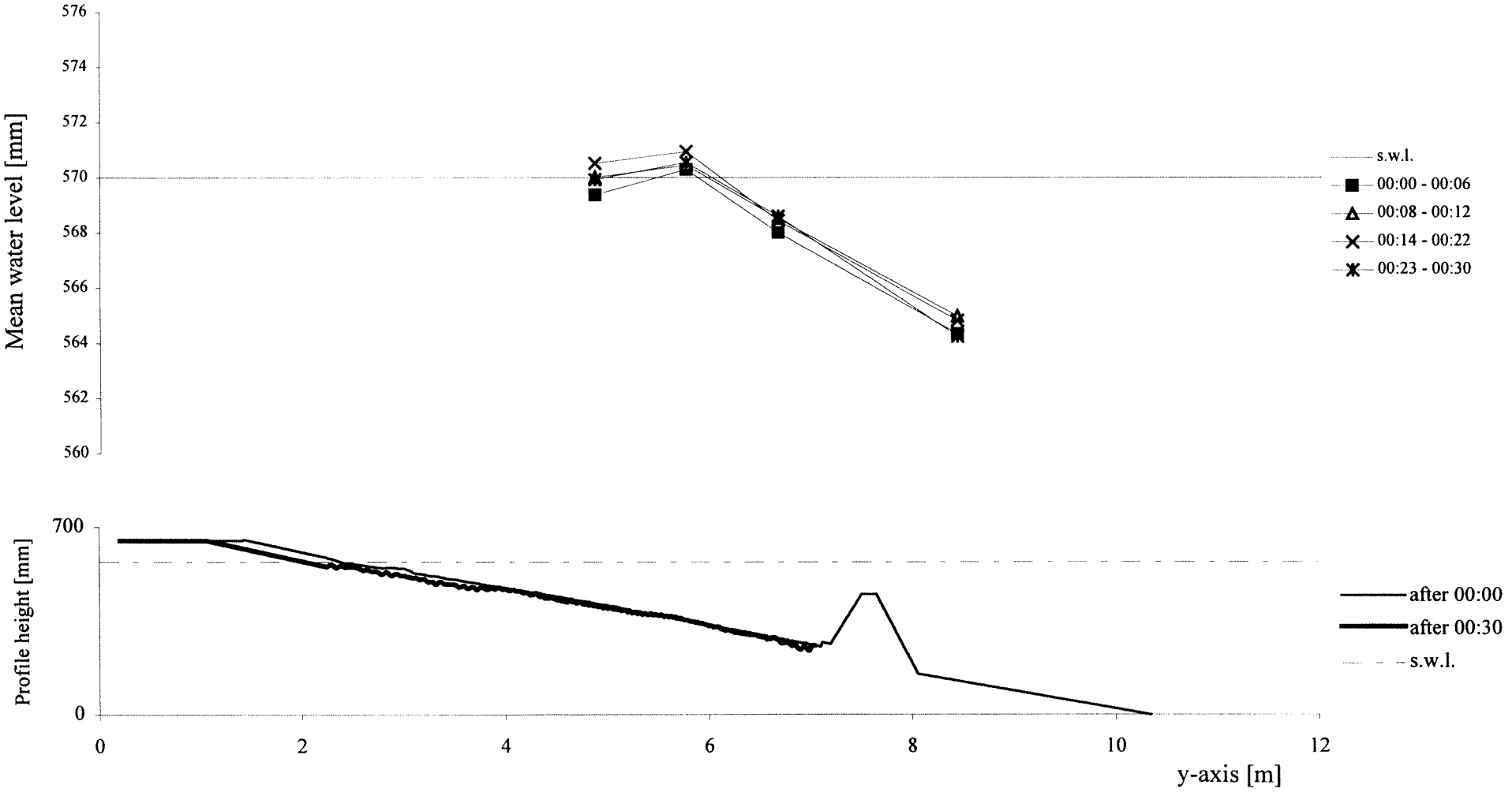

TEST D3 - cross-section x=12.5 m - interval 00:30 - 01:30

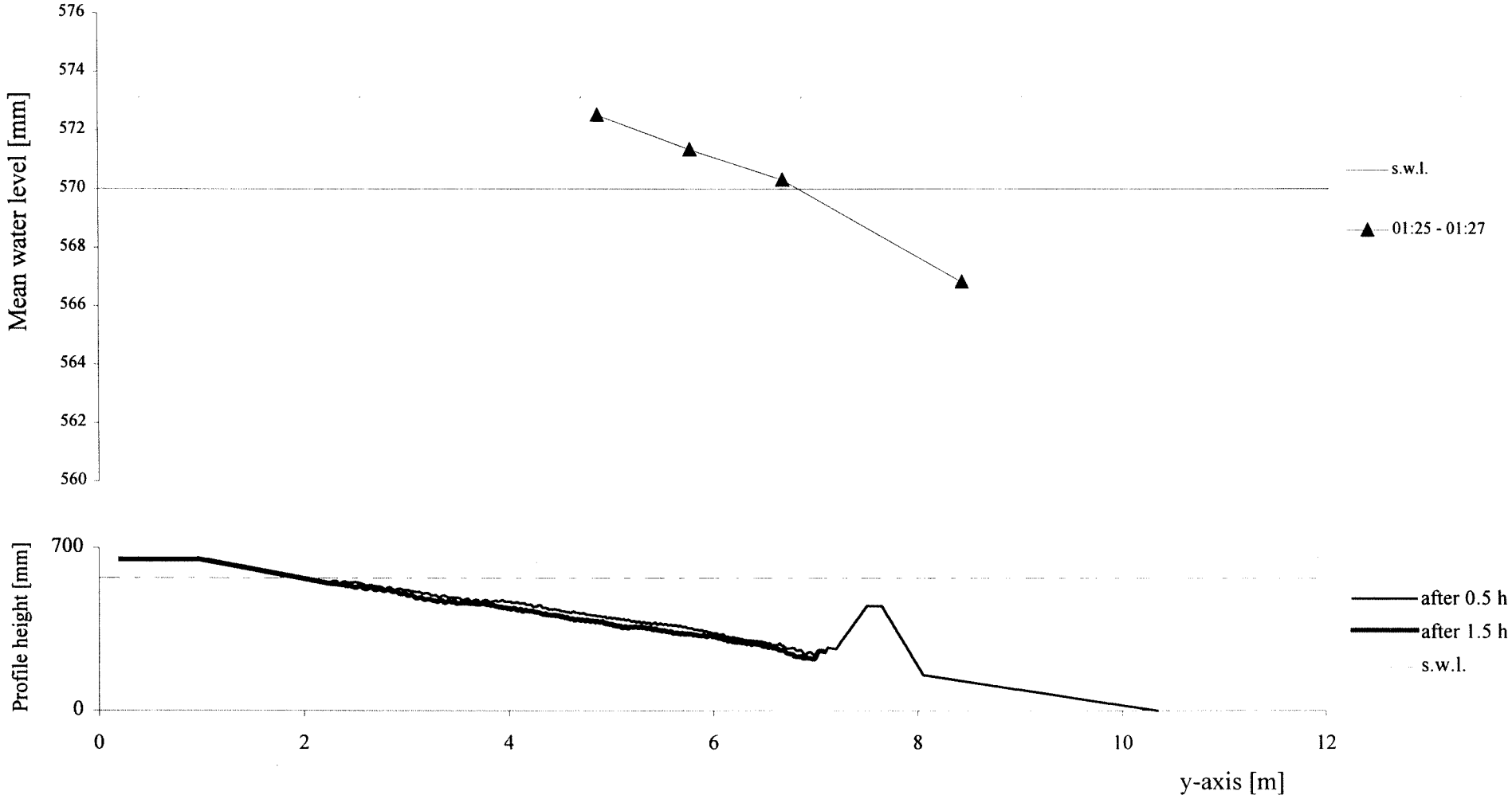

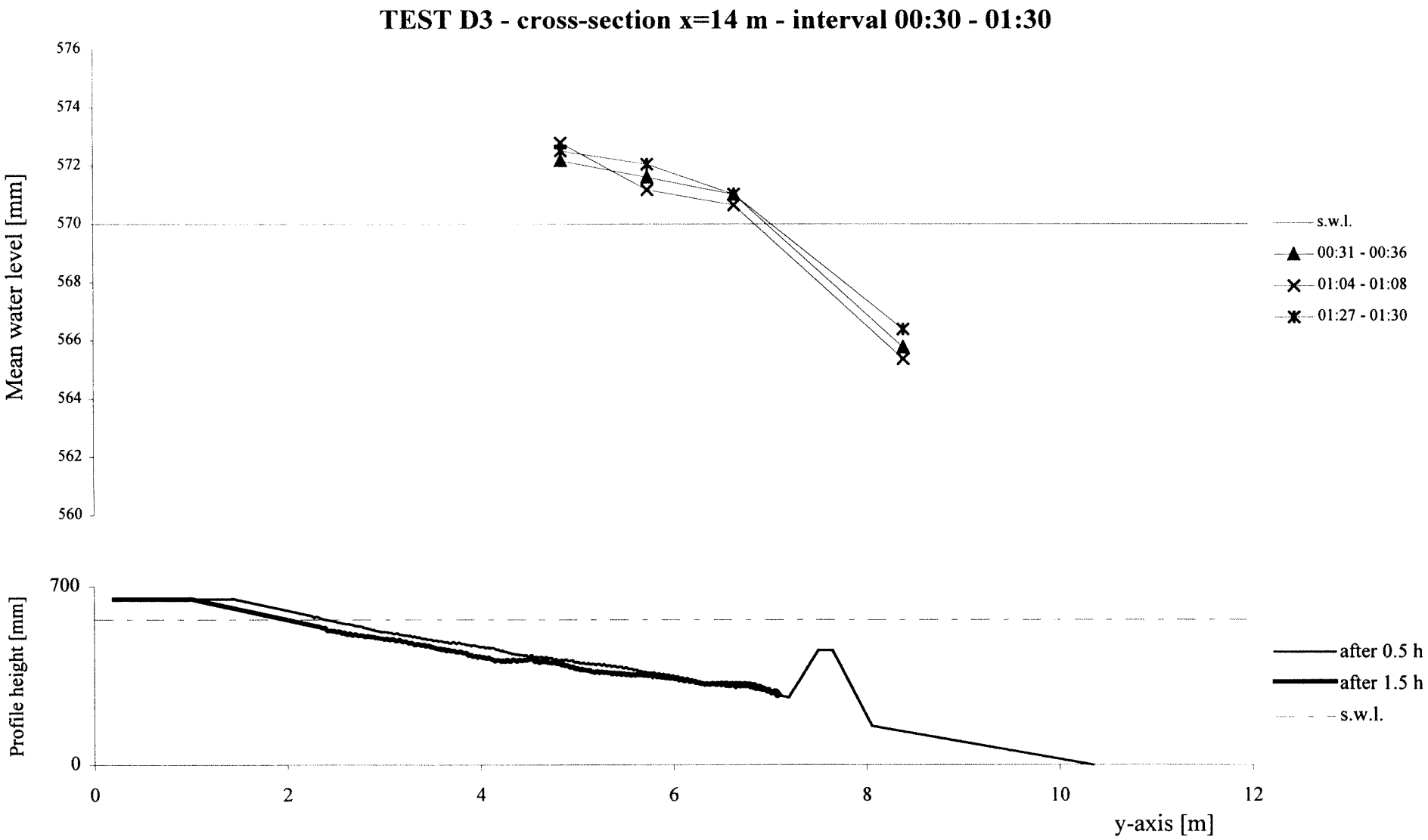
TEST D3 - cross-section x=14 m - interval 00:30 - 01:30
Mean water level [mm]
576
574
572
570
568
566
564
562
560
s.w.l.
00:31 - 00:36
01:04 - 01:08
01:27 - 01:30
Profile height [mm]
700
0
0
2
4
6
8
10
12
y-axis [m]
after 0.5 h
after 1.5 h
s.w.l.

TEST D3 - cross-section x=15.5 m - interval 00:30 - 01:30

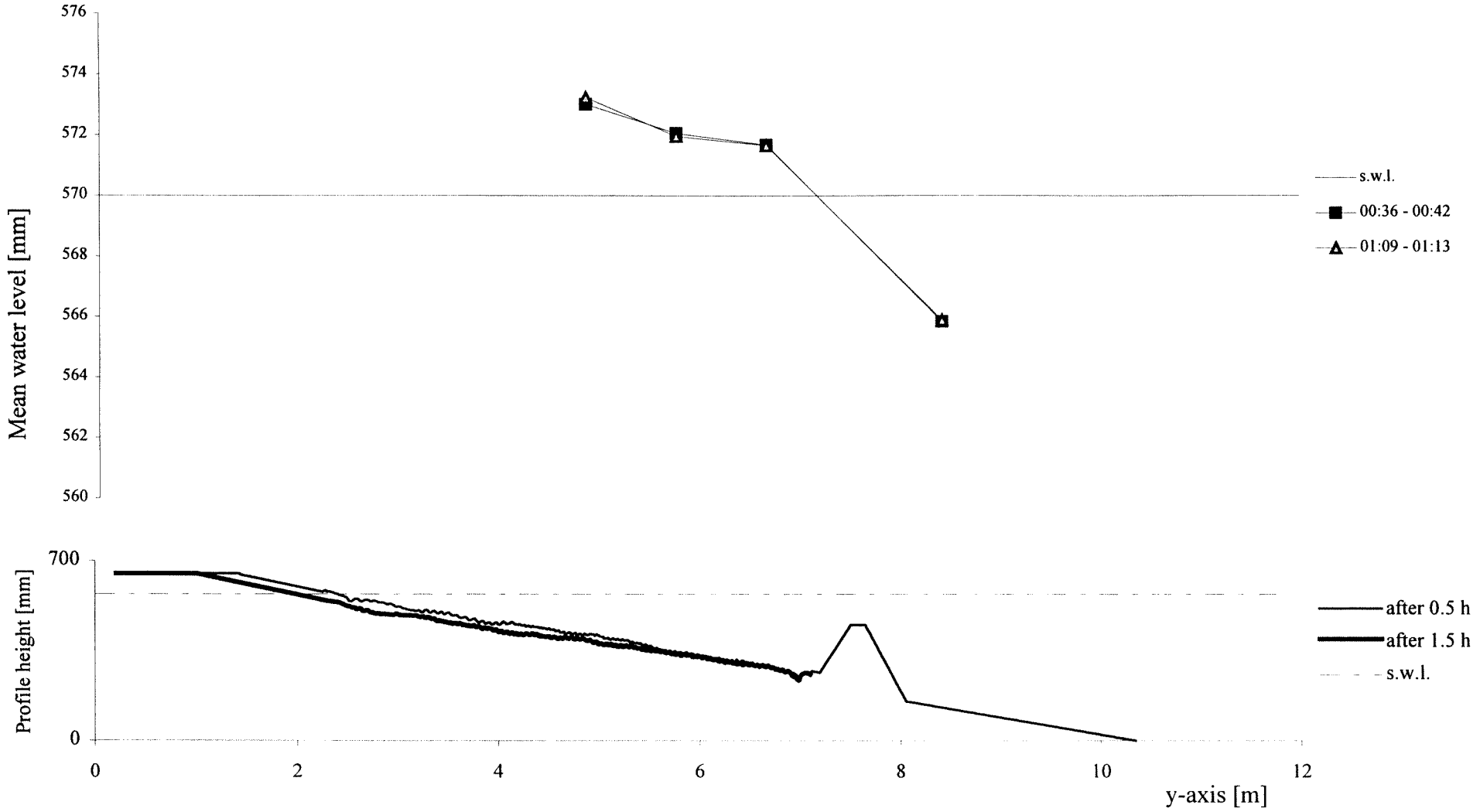

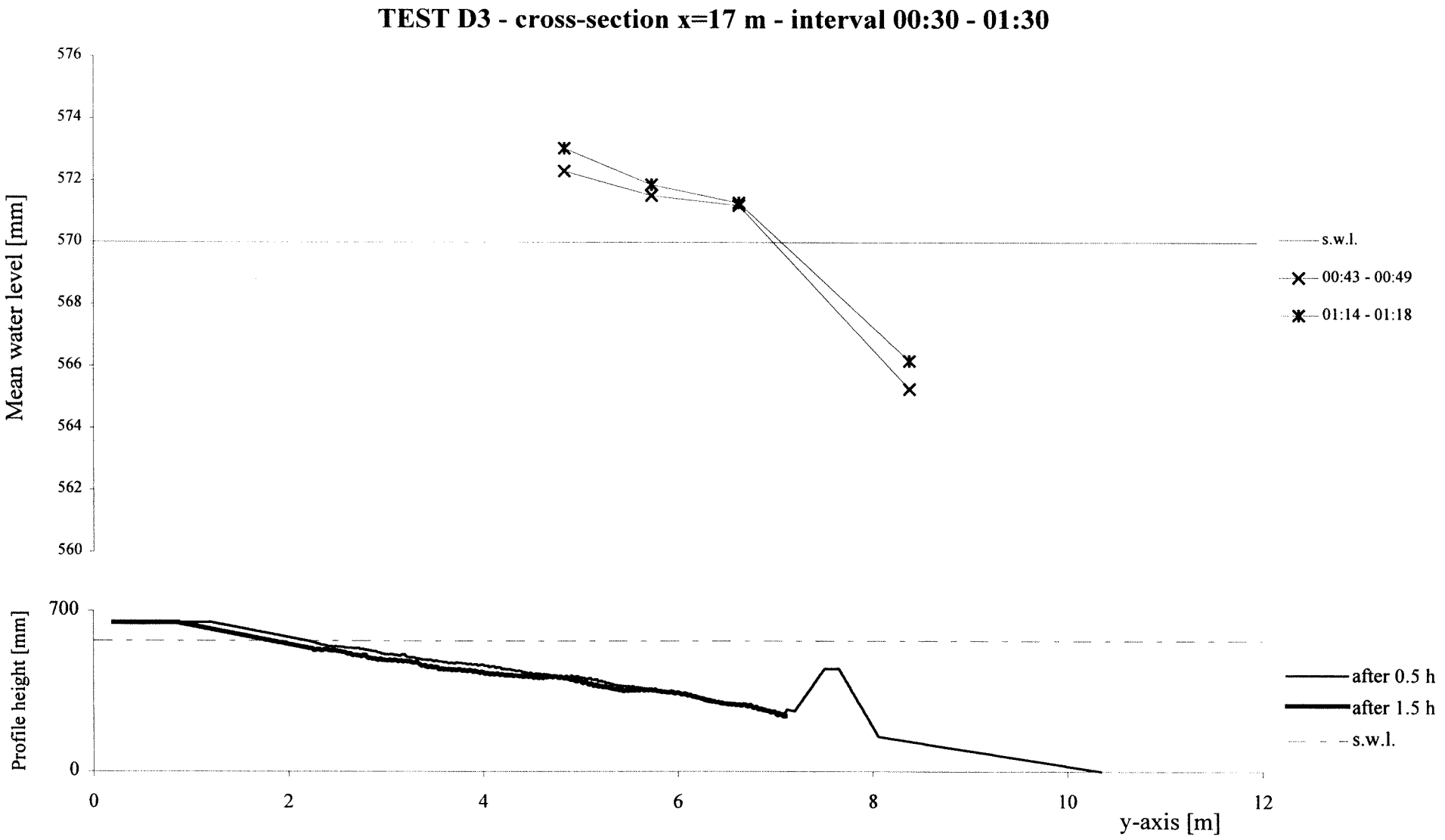
TEST D3 - cross-section x=17 m - interval 00:30 - 01:30
Mean water level [mm]
576
574
572
570
568
566
564
562
560
s.w.l.
00:43 - 00:49
01:14 - 01:18
Profile height [mm]
700
0
0
2
4
6
8
10
12
y-axis [m]
after 0.5 h
after 1.5 h
s.w.l.

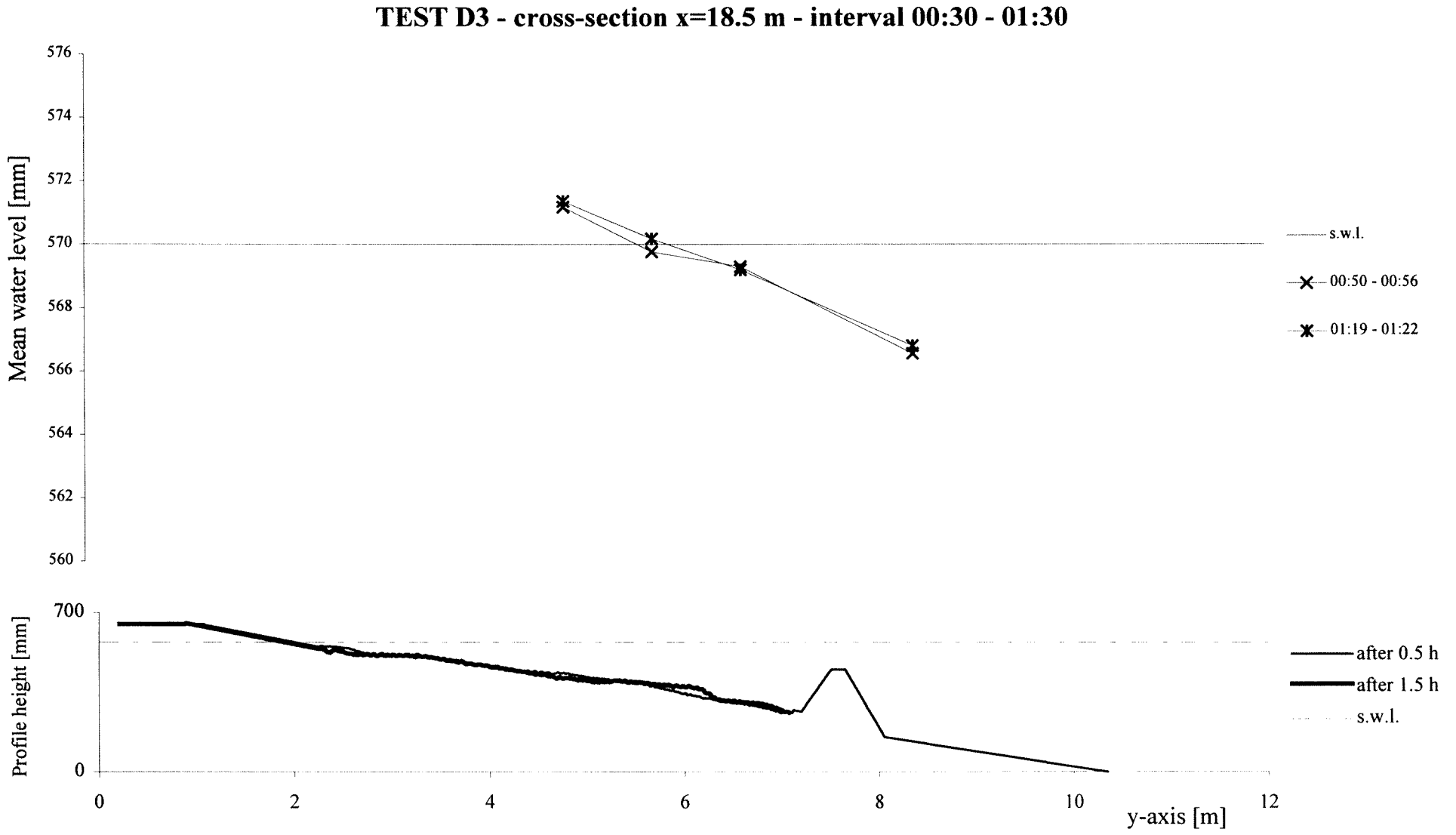
TEST D3 - cross-section x=18.5 m - interval 00:30 - 01:30
Mean water level [mm]
576
574
572
570
568
566
564
562
560
s.w.l.
00:50 - 00:56
01:19 - 01:22
Profile height [mm]
700
0
after 0.5 h
after 1.5 h
s.w.l.
0
2
4
6
8
10
12
y-axis [m]

TEST D3 - cross-section x=20 m - interval 00:30 - 01:30

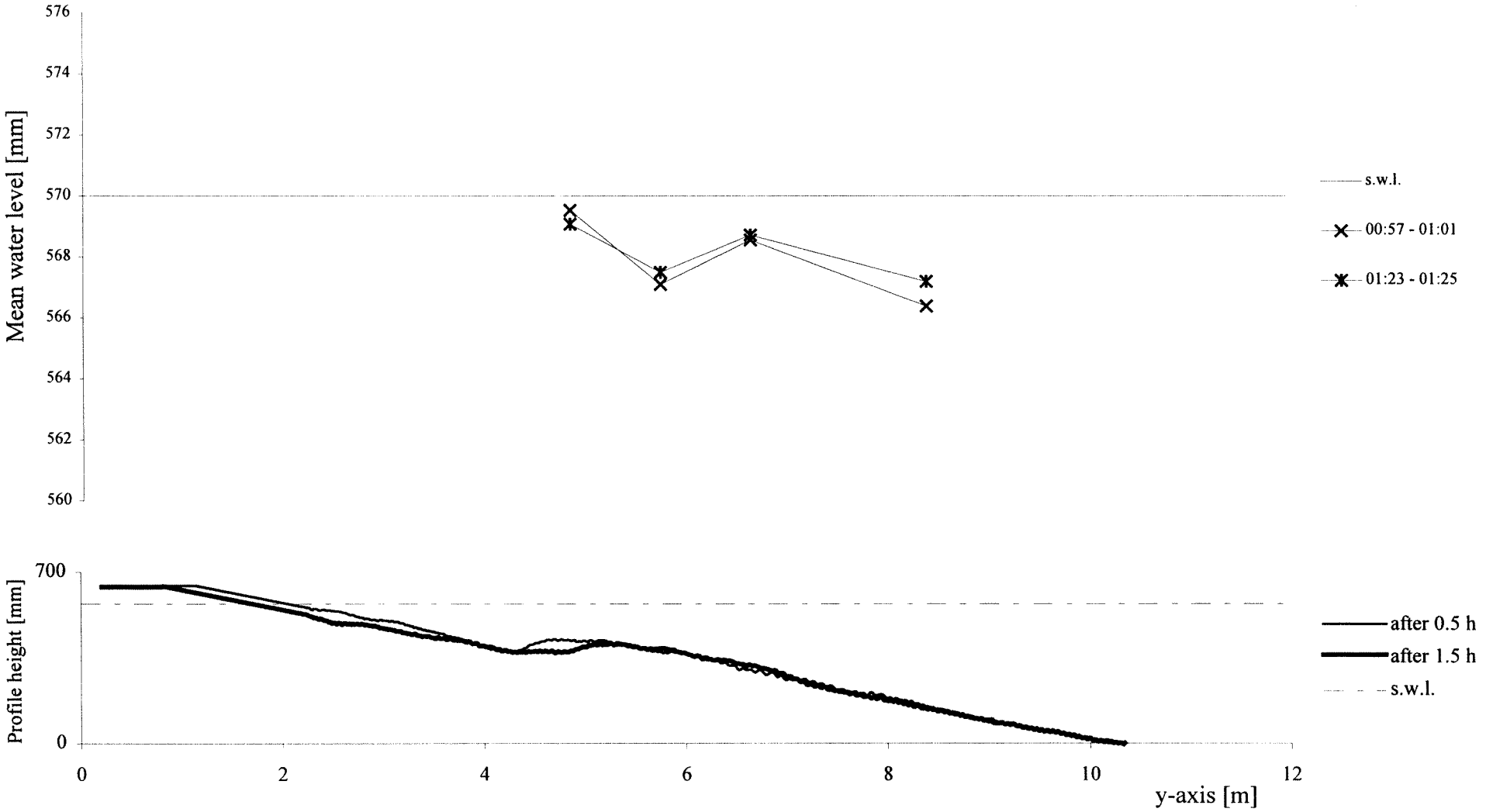

TEST D3 - cross-section x=12.5 m - interval 01:30 - 03:30

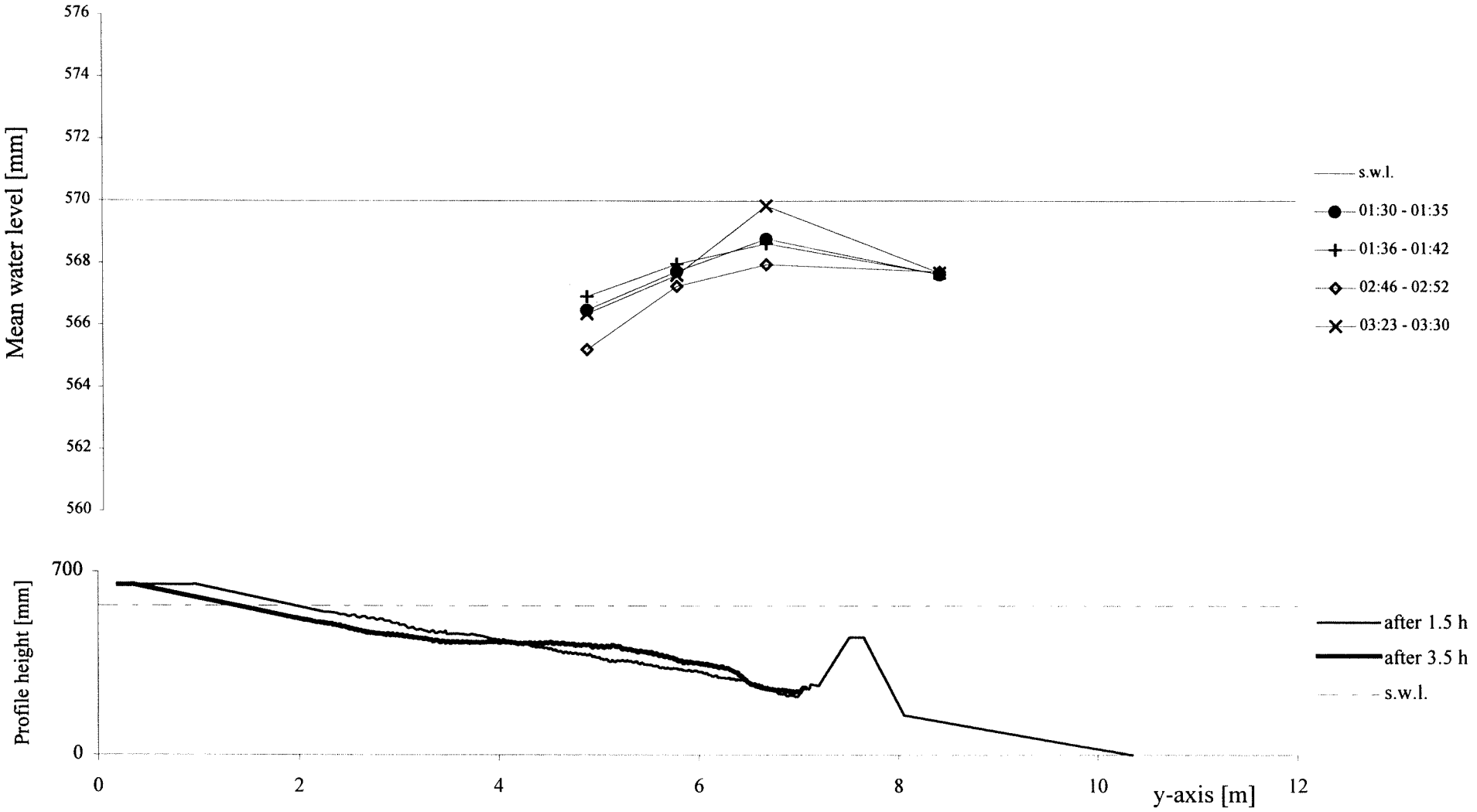

TEST D3 - cross-section x=14 m - interval 01:30 - 03:30

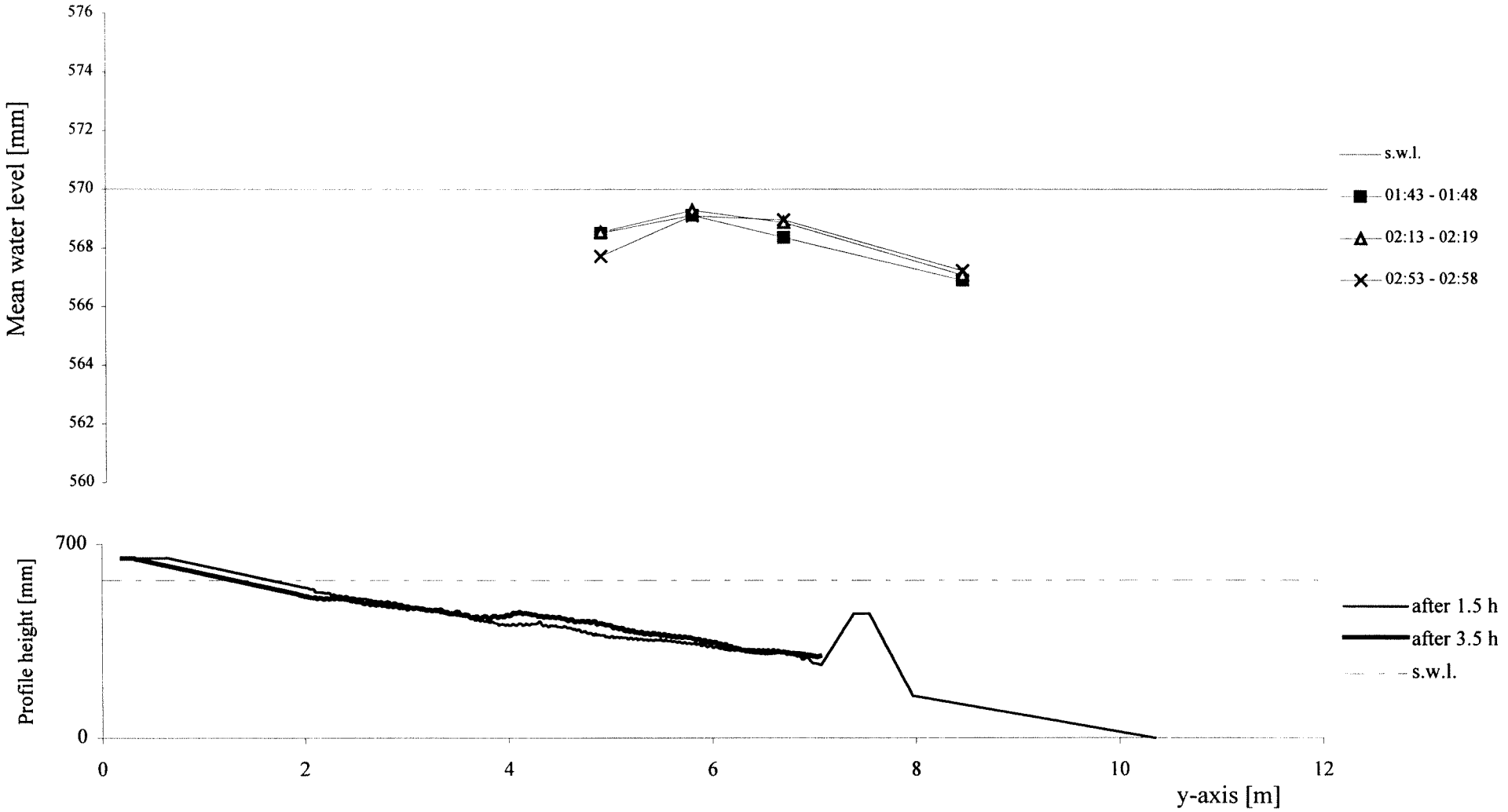

TEST D3 - cross-section x=15.5 m - interval 01:30 - 03:30

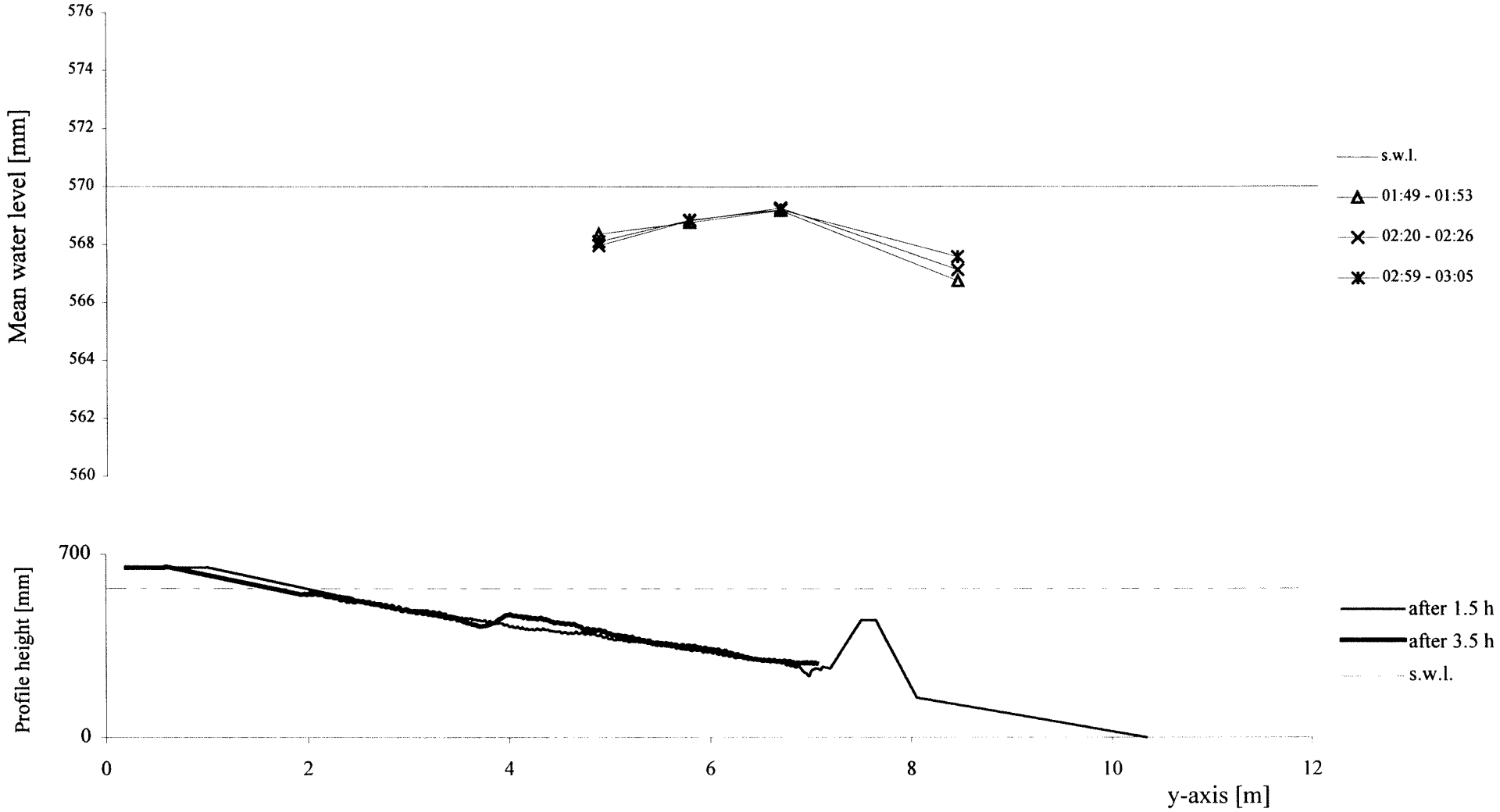

TEST D3 - cross-section x=17 m - interval 01:30 - 03:30

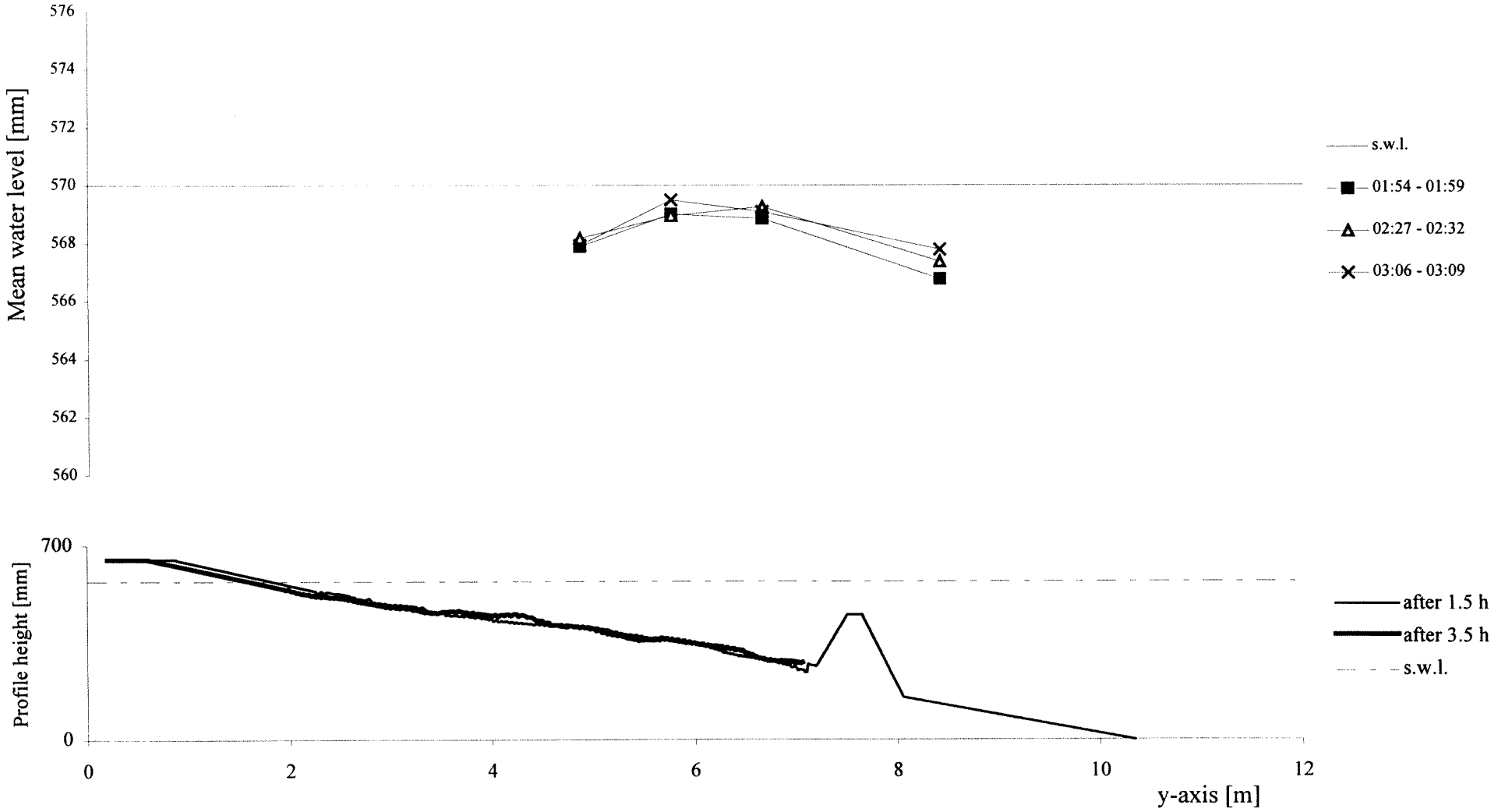

TEST D3 - cross-section x=18.5 m - interval 01:30 - 03:30

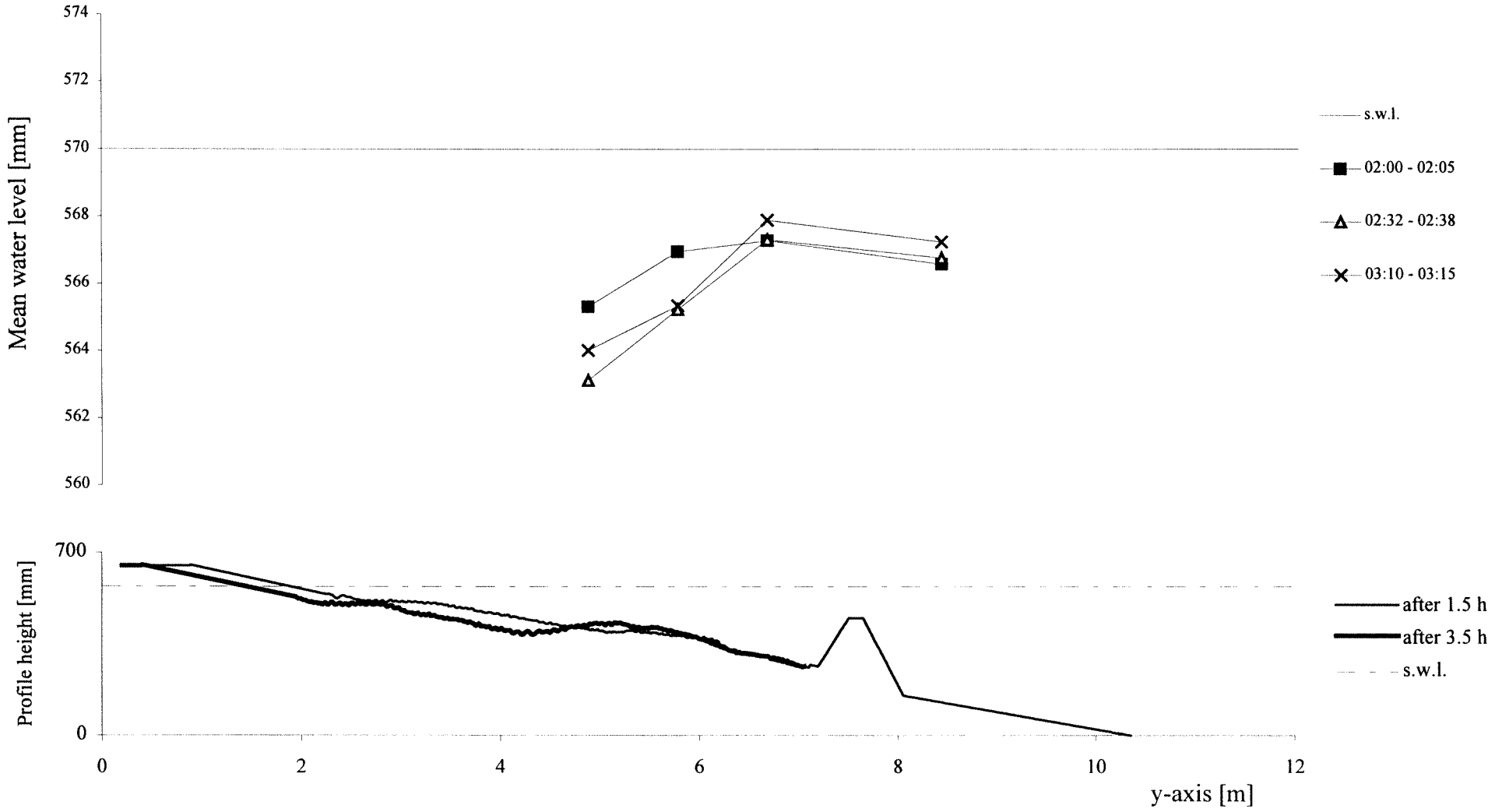

TEST D3 - cross-section x=20 m - interval 01:30 - 03:30

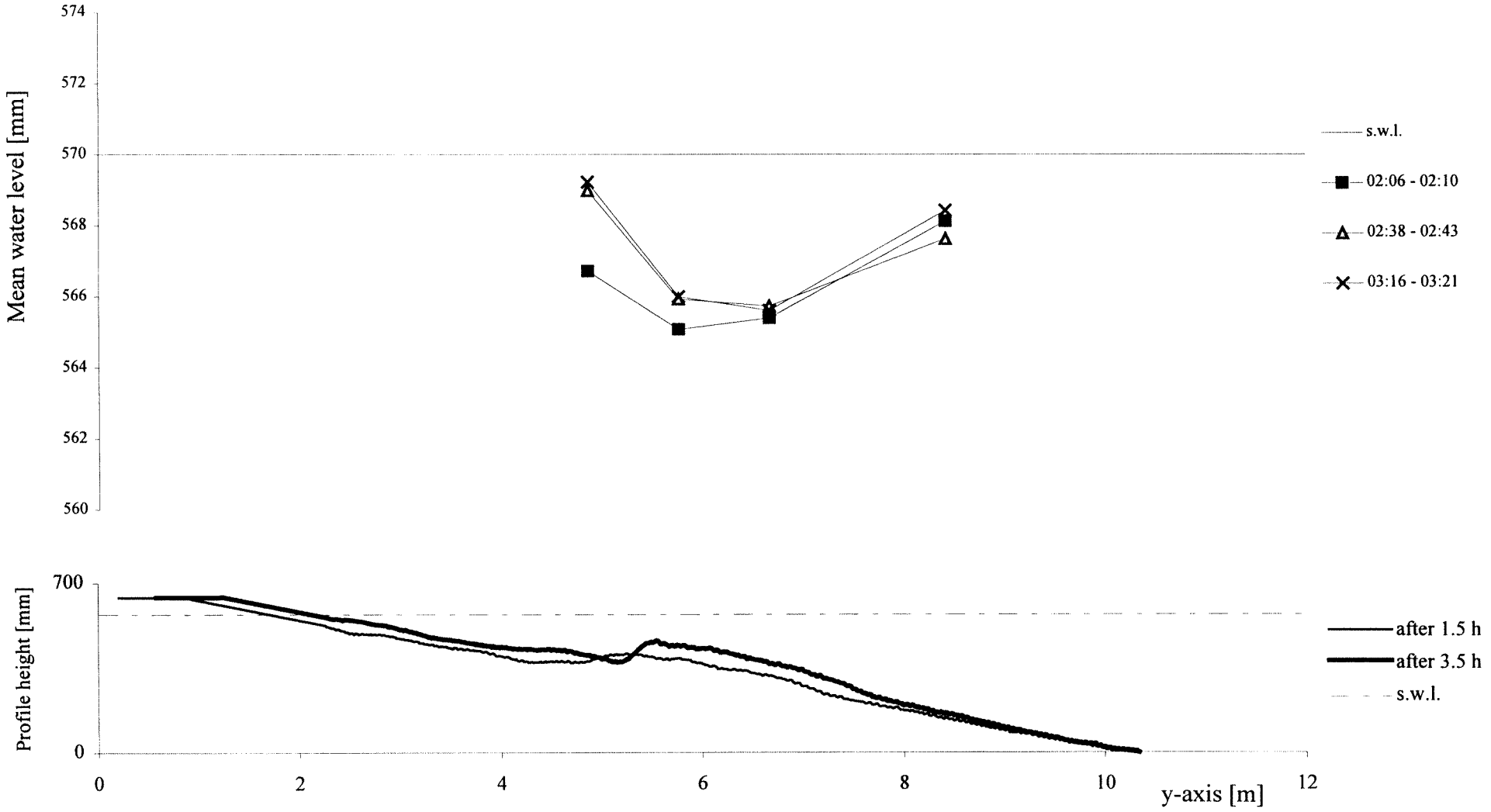

TEST D3 - cross-section x=12.5 m - interval 03:30 - 07:30

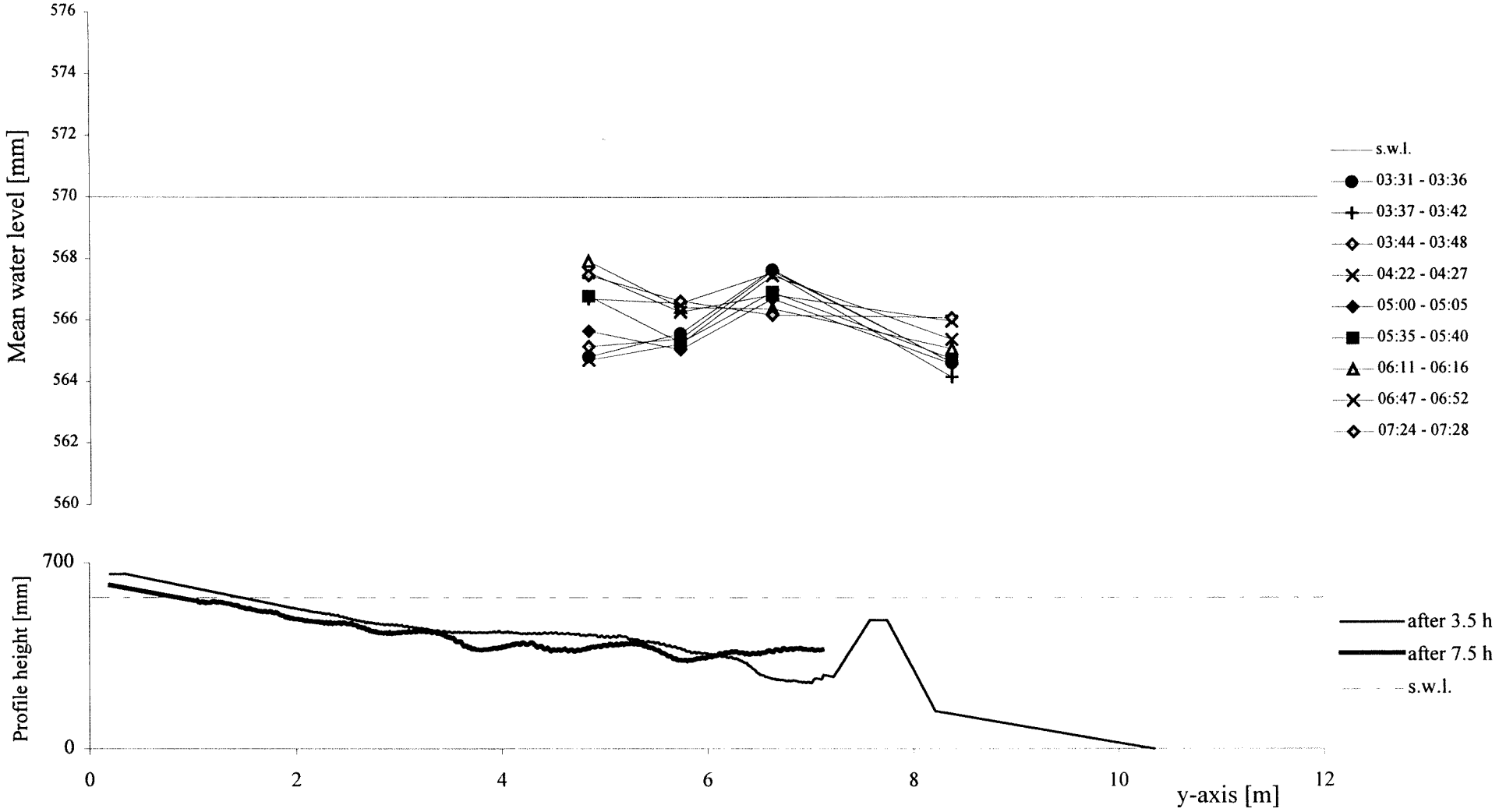

TEST D3 - cross-section x=14 m - interval 03:30 - 07:30

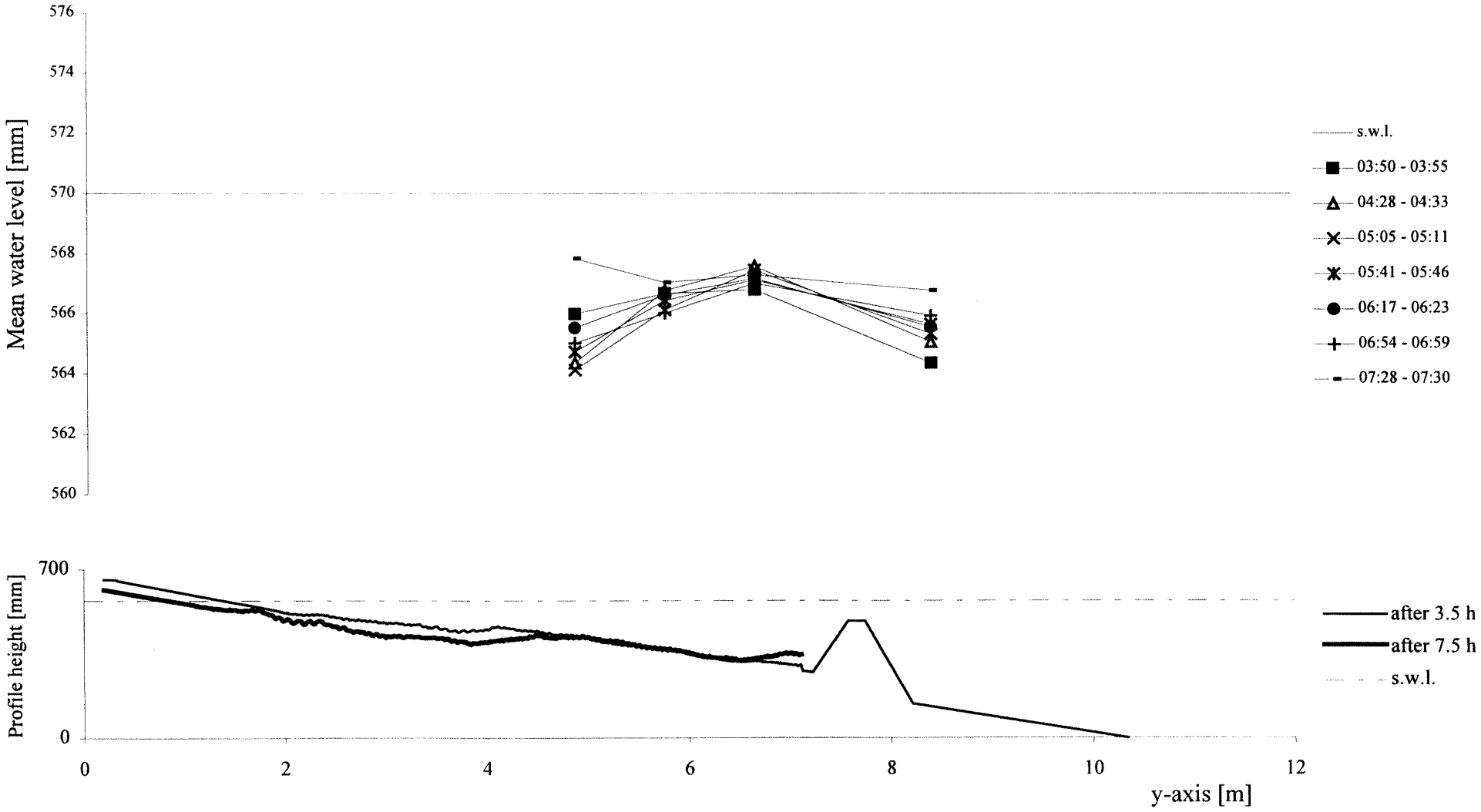

TEST D3 - cross-section x=15.5 m - interval 03:30 - 07:30

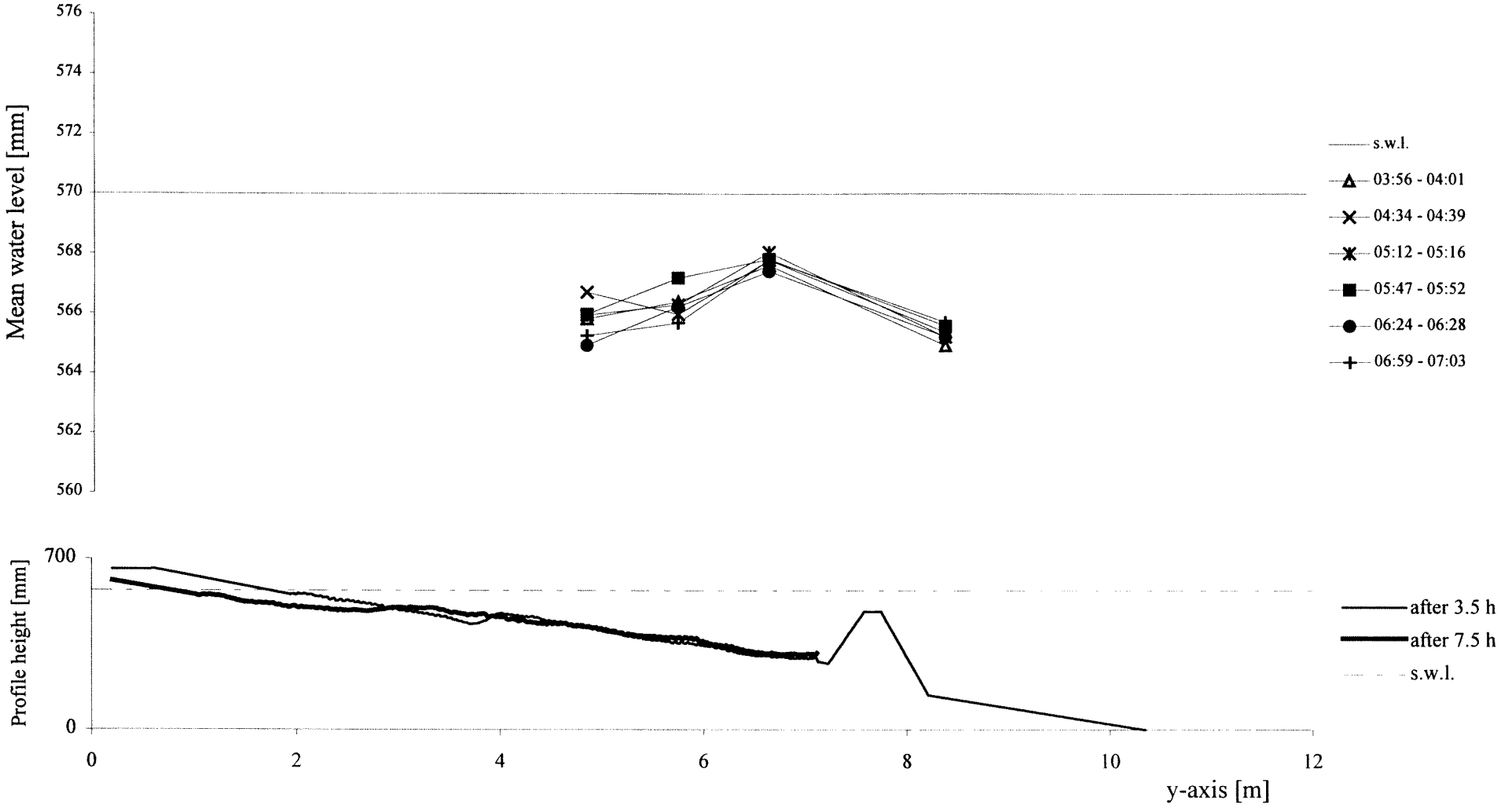

TEST D3 - cross-section x=17 m - interval 03:30 - 07:30

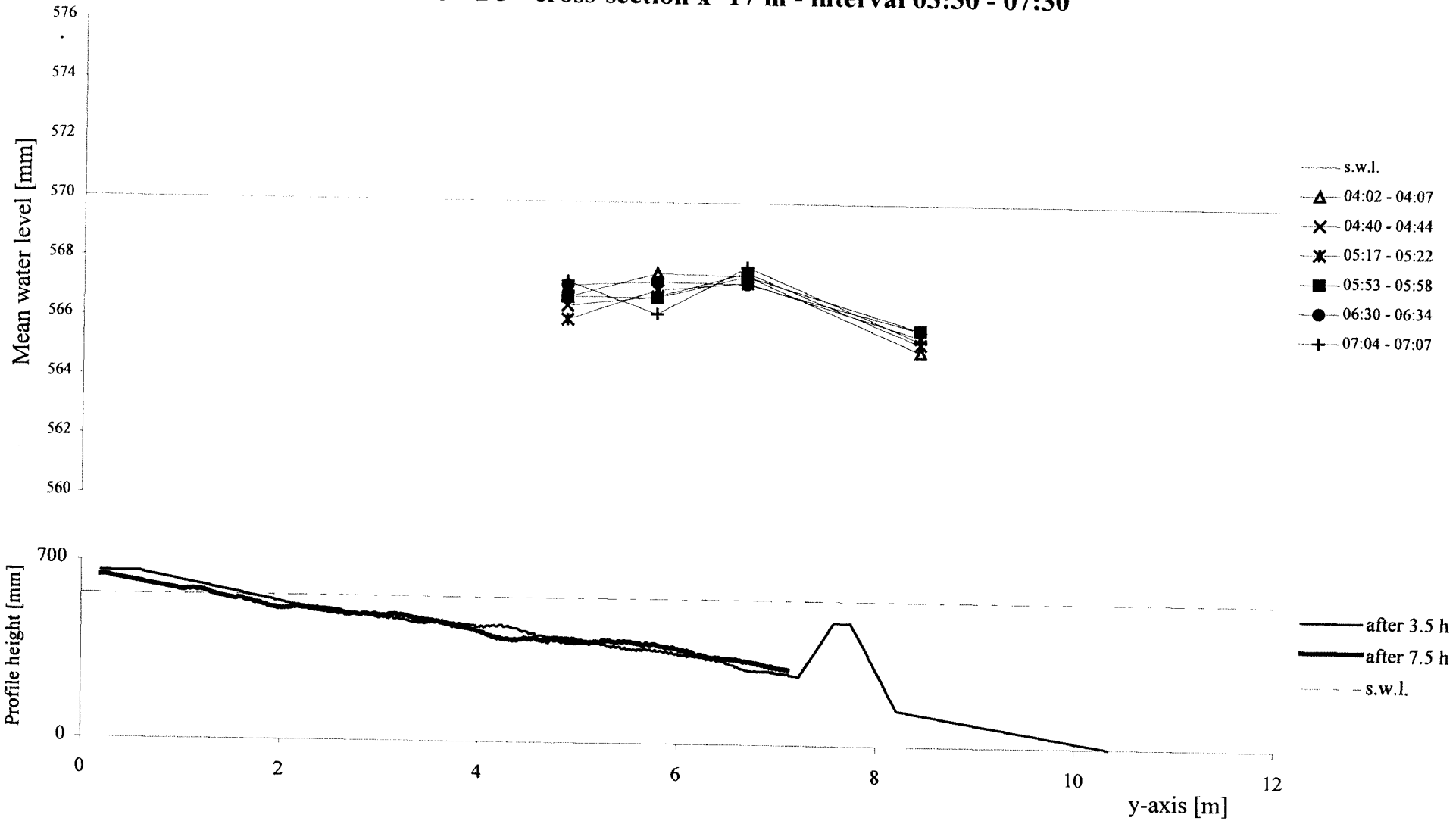

TEST D3 - cross-section x=18.5 m - interval 03:30 - 07:30

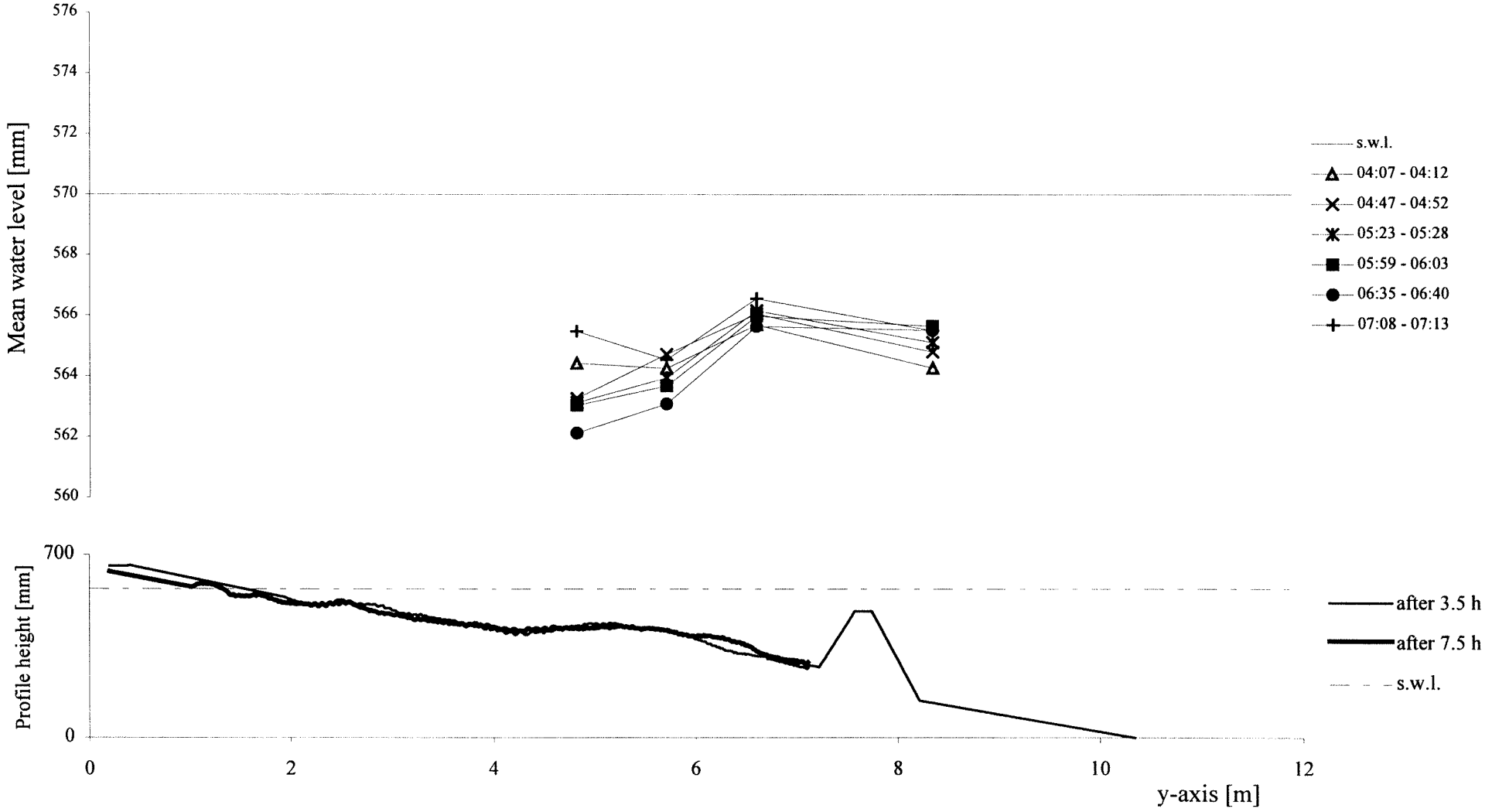

TEST D3 - cross-section x=20 m - interval 03:30 - 07:30